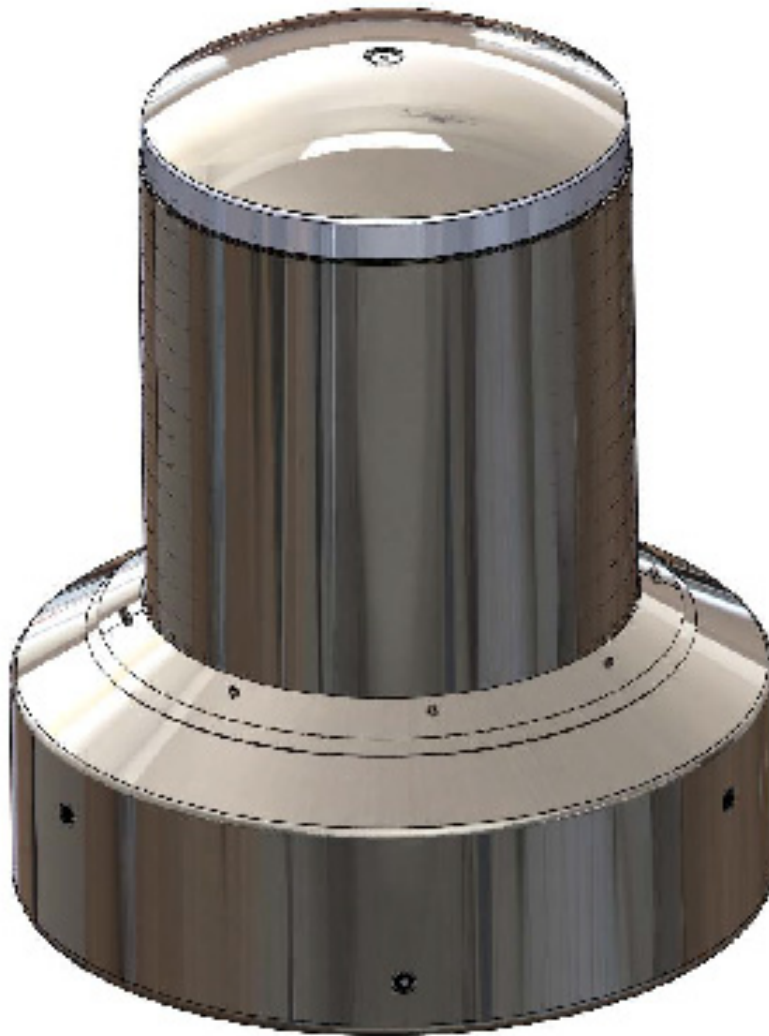




DOCKET 71-9379

1105-SD

TRANSPORT PACKAGE



Safety Analysis Report

Orano Federal Services LLC

Revision 0
August 2018

TABLE OF CONTENTS

1.0 GENERAL INFORMATION.....	1.1-1
1.1 Introduction	1.1-1
1.2 Package Description	1.2-1
1.2.1 Packaging	1.2-1
1.2.2 Contents.....	1.2-7
1.2.3 Special Requirements for Plutonium.....	1.2-8
1.2.4 Operational Features.....	1.2-8
1.3 Appendices	1.3-1
1.3.1 References	1.3-1
1.3.2 Glossary of Terms and Acronyms.....	1.3-2
1.3.3 Packaging General Arrangement Drawings	1.3-4
2.0 STRUCTURAL EVALUATION.....	2.1-1
2.1 Structural Design.....	2.1-1
2.1.1 Discussion	2.1-1
2.1.2 Design Criteria	2.1-2
2.1.3 Weights and Centers of Gravity	2.1-6
2.1.4 Identification of Codes and Standards for Package Design	2.1-6
2.2 Materials.....	2.2-1
2.2.1 Material Properties and Specifications	2.2-1
2.2.2 Chemical, Galvanic, or Other Reactions	2.2-1
2.2.3 Effects of Radiation on Materials.....	2.2-2
2.3 Fabrication and Examination.....	2.3-1
2.3.1 Fabrication.....	2.3-1
2.3.2 Examination.....	2.3-1
2.4 General Standards for All Packages.....	2.4-1
2.4.1 Minimum Package Size.....	2.4-1
2.4.2 Tamper-Indicating Feature	2.4-1
2.4.3 Positive Closure.....	2.4-1
2.4.4 Valves	2.4-1
2.4.5 Package Design	2.4-1
2.4.6 External Temperatures	2.4-1
2.4.7 Venting	2.4-1

2.5	Lifting and Tie-down Standards for All Packages	2.5-1
2.5.1	Lifting Devices	2.5-1
2.5.2	Tie-down Devices	2.5-1
2.6	Normal Conditions of Transport	2.6-1
2.6.1	Heat	2.6-1
2.6.2	Cold	2.6-5
2.6.3	Reduced External Pressure	2.6-5
2.6.4	Increased External Pressure	2.6-6
2.6.5	Vibration	2.6-6
2.6.6	Water Spray	2.6-7
2.6.7	Free Drop	2.6-8
2.6.8	Corner Drop	2.6-8
2.6.9	Compression	2.6-8
2.6.10	Penetration	2.6-8
2.7	Hypothetical Accident Conditions	2.7-1
2.7.1	Free Drop	2.7-1
2.7.2	Crush	2.7-9
2.7.3	Puncture	2.7-9
2.7.4	Thermal	2.7-11
2.7.5	Immersion – Fissile	2.7-15
2.7.6	Immersion – All Packages	2.7-15
2.7.7	Deep Water Immersion Test	2.7-16
2.7.8	Summary of Damage	2.7-17
2.8	Accident Conditions for Air Transport of Plutonium	2.8-1
2.9	Accident Conditions for Fissile Material Packages for Air Transport	2.9-1
2.10	Special Form	2.10-1
2.11	Fuel Rods	2.11-1
2.12	Appendices	2.12-1
2.12.1	References	2.12.1-1
2.12.2	Certification Test Plan	2.12.2-1
2.12.3	Certification Test Results	2.12.3-1
2.12.4	Finite Element Analysis	2.12.4-1
2.12.5	Seal Performance Tests	2.12.5-1

3.0 THERMAL EVALUATION.....	3.1-1
3.1 Description of Thermal Design	3.1-1
3.1.1 Design Features	3.1-1
3.1.2 Content's Decay Heat.....	3.1-5
3.1.3 Summary Tables of Temperatures	3.1-5
3.1.4 Summary Tables of Maximum Pressures.....	3.1-5
3.2 Material Properties and Component Specifications	3.2-1
3.2.1 Material Properties	3.2-1
3.2.2 Component Specifications.....	3.2-3
3.3 Thermal Evaluation for Normal Conditions of Transport.....	3.3-1
3.3.1 Heat and Cold.....	3.3-1
3.3.2 Maximum Normal Operating Pressure.....	3.3-3
3.4 Thermal Evaluation for Hypothetical Accident Conditions.....	3.4-1
3.4.1 Initial Conditions.....	3.4-1
3.4.2 Fire Test Conditions	3.4-2
3.4.3 Maximum Temperatures and Pressure	3.4-2
3.4.4 Maximum Thermal Stresses.....	3.4-10
3.5 Appendices	3.5-1
3.5.1 References	3.5-2
3.5.2 Computer Analysis Results	3.5-5
3.5.3 Analytical Thermal Model	3.5-5
3.5.4 'Last-A-Foam' Response under HAC Conditions	3.5-33
4.0 CONTAINMENT	4.1-1
4.1 Description of the Containment System.....	4.1-1
4.1.1 Containment Boundary.....	4.1-1
4.1.2 Containment Penetrations.....	4.1-1
4.1.3 Seals.....	4.1-1
4.1.4 Welds.....	4.1-3
4.1.5 Closure.....	4.1-3
4.2 Containment Under Normal Conditions of Transport.....	4.2-1
4.3 Containment Under Hypothetical Accident Conditions.....	4.3-1
4.4 Leakage Rate Tests for Type B Packages	4.4-1
4.4.1 Fabrication Leakage Rate Tests	4.4-1
4.4.2 Maintenance/Periodic Leakage Rate Tests.....	4.4-1

4.4.3	Preshipment Leakage Rate Tests.....	4.4-1
4.5	Appendix	4.5-1
4.5.1	References	4.5-1
5.0	SHIELDING EVALUATION.....	5.1-1
5.1	Description of Shielding Design	5.1-1
5.1.1	Design Features	5.1-1
5.1.2	Summary Table of Maximum Radiation Levels	5.1-1
5.2	Source Specification	5.2-1
5.2.1	Gamma Source	5.2-1
5.2.2	Neutron Source.....	5.2-3
5.3	Shielding Model	5.3-1
5.3.1	Configuration of Source and Shielding	5.3-1
5.3.2	Material Properties	5.3-3
5.4	Shielding Evaluation	5.4-1
5.4.1	Methods	5.4-1
5.4.2	Input and Output Data	5.4-2
5.4.3	Flux-to-Dose Rate Conversion	5.4-3
5.4.4	External Radiation Levels	5.4-3
5.4.5	LTSS Loading Methodology.....	5.4-4
5.5	Appendices	5.5-1
5.5.1	References	5.5.1-1
5.5.2	Sample Input Files for LTSS Evaluation	5.5.2-1
5.5.3	Shielded Device Evaluation	5.5.3-1
6.0	CRITICALITY EVALUATION	6.1-1
6.1	References	6.1-1
7.0	PACKAGE OPERATIONS.....	7.1-1
7.1	Procedures for Loading the Package.....	7.1-1
7.1.1	General Lifting and Handling.....	7.1-1
7.1.2	Loading of Contents	7.1-1
7.1.3	Preparation of the 1105-SD Package for Transport	7.1-8
7.1.4	Loading and Preparing the LTSS for Transport.....	7.1-8
7.2	Procedures for Unloading the Package	7.2-1
7.2.1	Removal of Contents	7.2-1

7.3	Preparation of an Empty Package for Transport	7.3-1
7.4	Preshipment Leakage Rate Test	7.4-1
7.4.1	Gas Pressure Rise Leakage Rate Test Acceptance Criteria.....	7.4-1
7.4.2	Determining the Test Volume and Test Time	7.4-1
7.4.3	Performing the Gas Pressure Rise Leakage Rate Test	7.4-1
7.4.4	Optional Preshipment Leakage Rate Test	7.4-2
7.5	Appendix	7.5-1
7.5.1	LTSS Loading Examples.....	7.5-1
7.5.2	References	7.5-2
8.0	ACCEPTANCE TESTS AND MAINTENANCE PROGRAM.....	8.1-1
8.1	Acceptance Tests.....	8.1-1
8.1.1	Visual Inspection and Measurements	8.1-1
8.1.2	Weld Examinations	8.1-1
8.1.3	Structural and Pressure Tests	8.1-1
8.1.4	Fabrication Leakage Rate Tests	8.1-2
8.1.5	Component and Material Tests.....	8.1-4
8.1.6	Shielding Integrity Tests	8.1-10
8.1.7	Thermal Tests	8.1-11
8.2	Maintenance Program	8.2-1
8.2.1	Structural and Pressure Tests	8.2-1
8.2.2	Maintenance/Periodic Leakage Rate Tests.....	8.2-1
8.2.3	Component and Material Tests.....	8.2-2
8.2.4	Thermal Tests	8.2-3
8.3	Appendix	8.3-1
8.3.1	References	8.3-1

This page left intentionally blank.

1.0 GENERAL INFORMATION

This section presents a general introduction and description of the 1105-SD package. The 1105-SD package is used to transport radioactive sources in the Long Term Storage Shield (LTSS) or shielded devices containing their sources. This application seeks authorization of the 1105-SD package as a Type B(U)–96 shipping container in accordance with the provisions of Title 10, Part 71 of the Code of Federal Regulations [1]. The packaging also meets the requirements of SSR-6 [2].

The major components comprising the package are discussed in Section 1.2.1, *Packaging*, and illustrated in Figure 1.2-1 through Figure 1.2-8. A glossary of terms is presented in Appendix 1.3.2, *Glossary of Terms and Acronyms*. Detailed drawings of the package design are presented in Appendix 1.3.3, *Packaging General Arrangement Drawings*.

1.1 Introduction

The **Model 1105-SD** package has been developed to transport radioactive sealed sources in the LTSS, as well as shielded irradiation devices (shielded devices) containing sources. The LTSS may transport gamma sources (the majority of sources in the LTSS), beta sources, and very small neutron sources. Fissile materials such as Pu-239 are limited to quantities of less than 15 grams. Thus the payload is fissile exempt per the provisions of §71.15(b) [1]. All shielded devices contain gamma sources only. The 1105-SD package does not supply significant biological shielding. The primary shielding is provided by the lead shielding in the LTSS or in the shielded devices. All sources are sealed. The 1105-SD package provides leaktight containment of the radioactive contents under all NCT and HAC.¹

The packaging consists of a base, a bell cover which is bolted to the base, and an internal lodgment which supports the LTSS. Shielded devices are placed in an inner container for shipment. The package uses conventional materials and metalworking techniques. When loaded and prepared for transport, the 1105-SD package is 83 inches tall, 70 inches in diameter (over the lower impact limiter), and weighs a maximum of 10,100 lb. The package is designed to be transported singly, with its longitudinal axis vertical, by ground, air, or by water in non-exclusive use.

Since all payloads transported in the 1105-SD are either non-fissile or fissile-exempt, the criticality safety index does not apply.

An isometric view of the 1105-SD packaging is shown in Figure 1.1-1. Cross sectional views of the package configured with a LTSS payload and a shielded device payload are shown in Figure 1.1-2 and 1.1-3, respectively.

¹ Leaktight is defined as a maximum of 1×10^{-7} reference-cm³/sec, air leakage per ANSI N14.5–2014 [3].

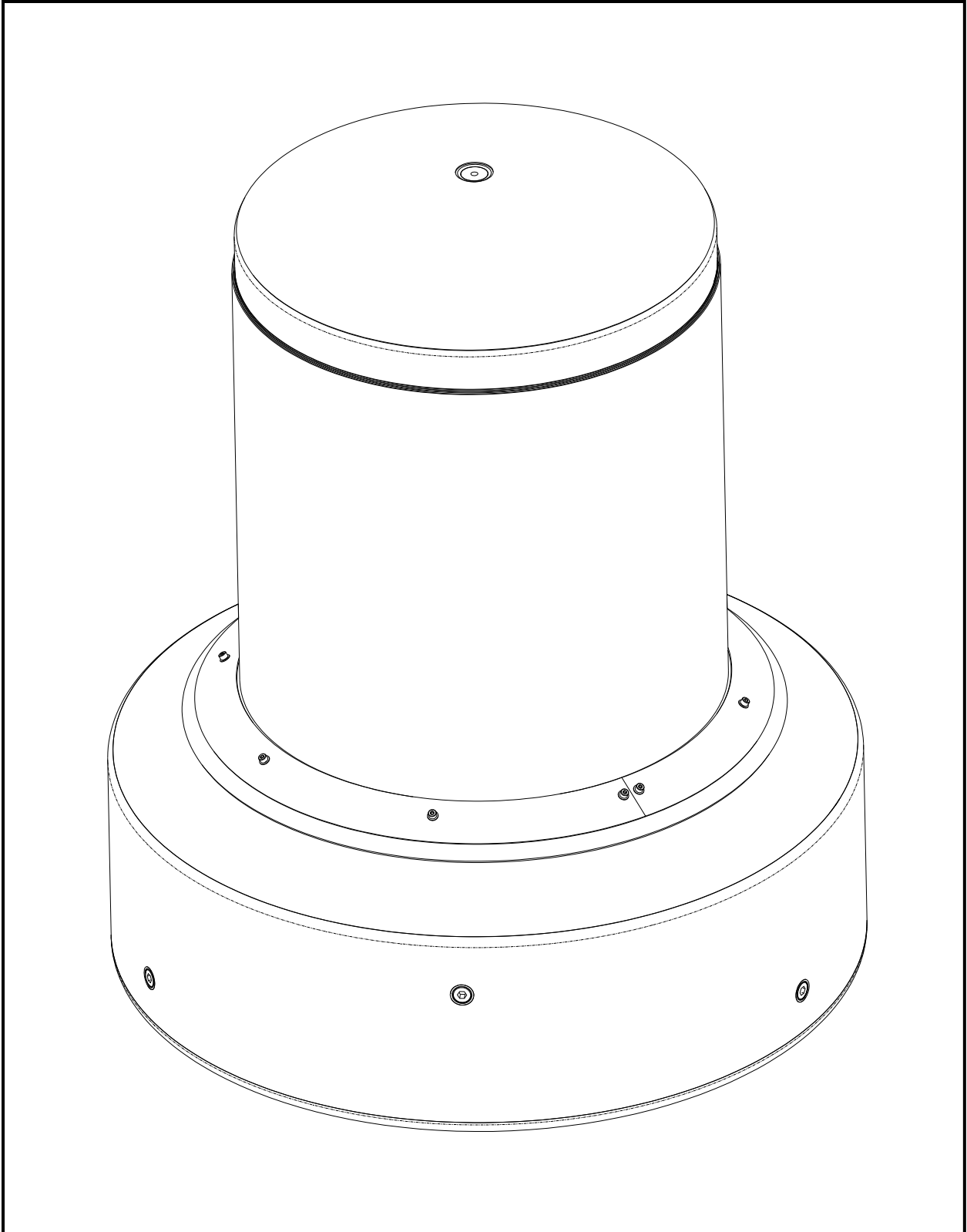


Figure 1.1-1 – 1105-SD Packaging

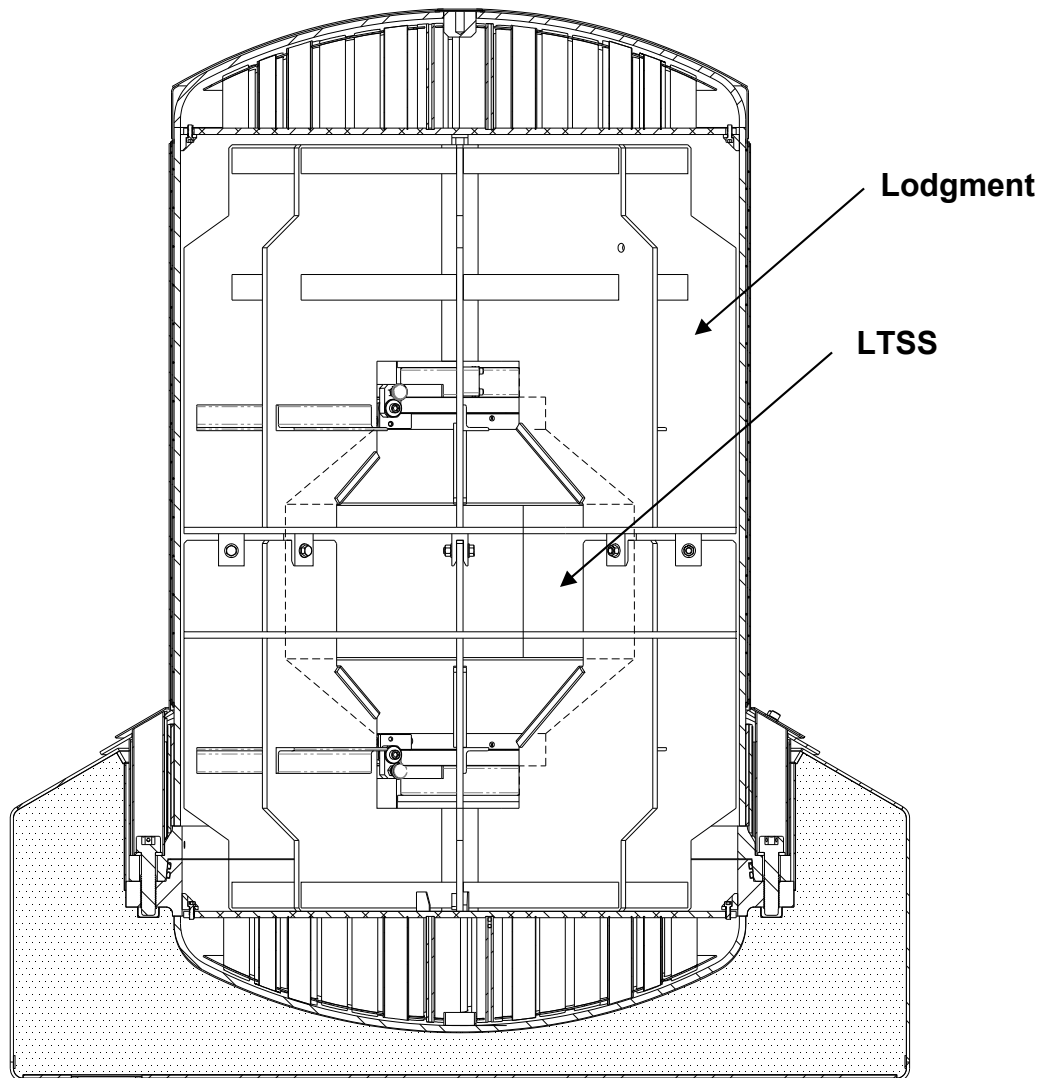


Figure 1.1-2 – 1105-SD Package With LTSS

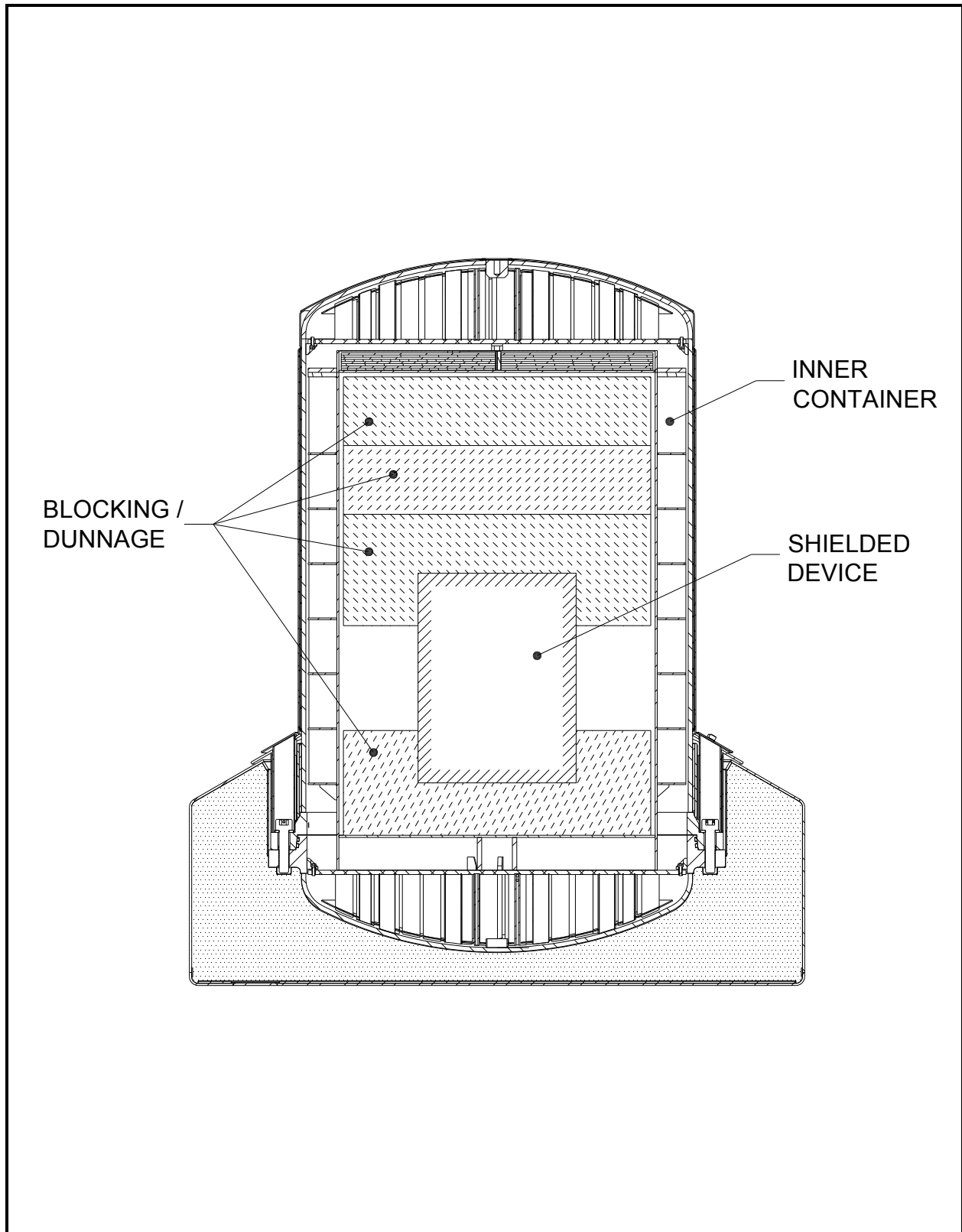


Figure 1.1-3 – 1105-SD Package With Shielded Device

1.2 Package Description

This section presents a basic description of the 1105-SD package components and construction. In the following, drawing references are to the general arrangement drawings provided in Appendix 1.3.3, *Packaging General Arrangement Drawings*.

1.2.1 Packaging

The 1105-SD package (drawing 3021717-SAR) consists of a lower body assembly or base, including the impact limiter containing polyurethane foam, an upper body assembly or bell, two internal impact limiter assemblies, 24 closure bolts, the LTSS payload with a lodgment (drawing 3021718-SAR) to support the LTSS within the package, or a shielded device payload inside an inner container (drawing 3021719-SAR). The package is primarily of welded construction, using Type 304 austenitic stainless steel. The lodgment is made from welded structural aluminum. The LTSS is made from Type 304 stainless steel and lead. The inner container is made of Type 304 stainless steel. These components will now be discussed in detail.

1.2.1.1 Containment Vessel

The 1105-SD containment vessel consists of a cylindrical body shell with an inner diameter of 43.5 inches and two torispherical heads, all $\frac{1}{2}$ inches thick. The torispherical inner radius is equal to 43.5 inches, and the knuckle radius is equal to 3.5 inches. The vessel is made from ASTM Type 304 stainless steel and includes a brass vent port plug. The upper and lower portions of the vessel connect at a heavy flange joint, located at the lower end of the cylindrical shell. The flanges are 2 inches thick and are connected using 24, 1-1/4-7 UNC bolts made of ASTM A320, L43 material. Each of these components (not including the bolts) may be made from separate pieces of material and joined using full penetration welds. All butt welds in the containment boundary are full-penetration and radiograph inspected.

The closure seal is a 3/8-inch cross-sectional diameter O-ring made of butyl rubber. A vent port, sealed with a butyl sealing washer and threaded brass plug, is located in a block welded to the upper flange (see Section M-M on sheet 6). The block is attached using a circumferential 3/16-inch (non-containment) fillet weld, and the containment is made by a circumferential 1/8-inch fillet weld. The machined opening on the lower flange face (containment) is closed using a full depth groove weld of minimum 0.25-inch thickness. Both of these containment welds are liquid penetrant inspected on the final pass. The seal test port block (not part of containment) is identically configured. The elastomer material of the containment seal and test seal O-rings, and the vent port and seal test port sealing washers, is made from Rainier Rubber R-0405-70, and subject to the tests given in Section 8.1.5.2, *Butyl Rubber O-rings*. The 1105-SD containment boundary consists of the following components:

- The upper torispherical head and upper body assembly lifting boss
- The cylindrical side shell
- The upper flange (attached to the upper body assembly)
- The lower flange (attached to the lower body assembly)
- The lower torispherical head
- The containment elastomer O-ring seal

- The vent port block in the upper flange including brass plug and elastomer sealing washer

A sketch of the containment vessel is shown in Figure 1.2-1. Additional detail on the containment vessel and other packaging components is given below, and depicted in Figure 1.2-2 through Figure 1.2-7.

1.2.1.2 Lower Body Assembly (Base)

The lower body assembly consists of the lower torispherical head, lower flange, lower internal impact limiter, and integral external impact limiter, and is depicted as Assembly A2 on drawing 3021717-SAR. All material conforms to ASTM A240, Type 304 stainless steel unless otherwise specified.

The lower torispherical head is formed from ½-inch thick plate, and is connected to the lower flange using a full penetration weld. The lower flange is made from ASTM A182, Grade F304 forging, or ASTM A240, Type 304 plate material. The flange has an inner diameter of 43-1/4 inches, an outer diameter of 52.0 inches, and is 2.0 inches thick. An extension of the flange supports the containment closure and test O-ring grooves. The O-rings are arranged on a 5° taper, are bore-type seals, and interface with a recess in the upper flange.

The external impact limiter is integral with, and permanently connected to the lower body. The inner cylindrical shell of the impact limiter is 0.12 inches thick and is welded to the outer edge of the lower flange. The outer shell (tapered top, outer cylinder, and flat bottom) is ¼ inches thick. The top plate of the impact limiter is tapered at 30° from the horizontal, and includes a short lead-in chamfer to guide the upper body assembly into place. The outer cylindrical shell is 70 inches in diameter and approximately 21 inches tall and features six fire-consumable plastic plugs designed to relieve pressure in the HAC fire event. The inside surface of the bottom shell is covered with a ¼-inch thick layer of refractory insulation paper to reduce heat flow into the flat bottom from the HAC fire event. The cavity of the limiter is filled with 15 lb/ft³ polyurethane foam. The foam is rigid, closed-cell, and is poured in place.

The lower flange features threaded holes for the closure bolts and two alignment pins. These holes may be optionally fitted with alloy steel thread inserts or helically coiled stainless steel thread inserts. On the underside (foam side) of the flange, each hole is covered with a thin cross-section stainless steel cup, tack welded in place and sealed using RTV sealant. The cups provide clearance for the ends of the closure bolts and seal the foam cavity.

The lower internal impact limiter is described in Section 1.2.1.4, *Internal Impact Limiters*.

1.2.1.3 Upper Body Assembly (Bell)

The upper body assembly consists of the upper torispherical head, cylindrical shell, upper flange, vent and test port blocks, upper internal impact limiter, dual side thermal shield, head thermal shield, and the closure bolt access tube structure, and is depicted as Assembly A3 on drawing 3021717-SAR. All material conforms to ASTM A240, Type 304 stainless steel unless otherwise specified.

The upper torispherical head and cylindrical shell are formed from ½-inch thick plate, having a minimum yield strength of 40 ksi and a minimum ultimate tensile strength of 80 ksi. The upper flange is made from ASTM A182, Grade F304 forging, or ASTM A240, Type 304 plate material. The flange has an inner diameter of 43-1/4 inches, an outer diameter of 51.5 inches, and is 2.0 inches thick. The inner diameter of the cylindrical shell is 43.5 inches. A 2.5-inch diameter, 2-inch thick

lifting boss, containing a 3/4-10 UNC threaded hole, is located in the center of the torispherical head. This hole may be optionally fitted with an alloy steel thread insert or with a helically coiled stainless steel thread insert. The head, lifting boss, cylindrical shell, and flange are connected using full penetration welds. The vent and test port blocks are made from A276 or A479, Type 304 stainless steel. Their configuration is discussed in Section 1.2.1.1, *Containment Vessel*.

At the lower end of the upper body assembly is a structure consisting of tubes and shells which provides access to the closure bolts and the vent port and seal test port while also protecting these components from HAC puncture bar impact or excessive heat input from the HAC fire event. A detail view of this area is shown in Detail D, Section B-B, and Section C-C on sheet 6. An isometric cut-away view is given on sheet 7. There are 24 evenly spaced, 2.5-inch O.D. × 0.12-inch wall thickness bolt access tubes made from ASTM A249 or A269, Type TP304 stainless steel. In addition, there are two more tubes, 90° apart, and located halfway between bolt access tubes, which provide access to the vent port and seal test port. Both ports are closed with threaded plugs made of ASTM B16 brass and sealed with butyl rubber sealing washers. A port insulation cylinder (Assembly A5 on sheet 6) is used in each port access tube to prevent excessive heat input from the HAC fire event. The port insulation cylinder is made from a 2-inch diameter, 0.06-inch wall thickness stainless steel tube, closed at both ends with a 0.06-inch thick disk of stainless steel, and filled with mineral wool. Each disk is attached using a 1/16-inch all-around fillet weld. A 1/8-inch diameter wire loop is fillet welded to the top disk for handling. Detail views of the vent port and test port are given in Section M-M and Section N-N, respectively, on sheet 6.

The top ends of the tubes are held in place by a 1/4-inch thick tube sheet, oriented at a slope to match the upper surface of the external impact limiter. The outside edge of the tube sheet forms a skirt to cover the gap between the upper and lower body assemblies. This prevents the entry of precipitation and, in the HAC fire event, the entry of excessive heat. The tubes pass through the tube sheet and are fillet welded to the sheet all around each tube. The lower ends of the tubes are partially welded to the flange, and the remaining joint which is inaccessible for welding is sealed with RTV sealant. The upper end of the sloped tube sheet is connected to the cylindrical side wall of the package using a partial penetration weld as shown in Detail U on sheet 5. The outer shell of the tube region consists of a 0.12-inch thick sheet, welded to the outer top edge of the flange on the lower end, and to the underside of the tube sheet on the upper end. The area of the containment wall adjacent to the tubes is covered with two, 1/4-inch thick layers of refractory insulation paper. The paper is retained using a formed sheet of 0.048-inch thick stainless steel, which is held in place using tack welds. Machined blocks of 30 lb/ft³ polyurethane foam are located between the tubes.

The top openings of the tubes are covered by a 0.12-inch thick stainless steel rain shield cover. The rain shield is formed in two halves and attached to bolting bosses located in the tube sheet using 5, 1/2-13 UNC stainless steel bolts (total of 10 bolts). These holes may be optionally fitted with alloy steel thread inserts or helically coiled stainless steel thread inserts. The rain shield also retains the port insulation cylinders used in the vent and seal test ports.

Between the top of the tube sheet and approximately the location of the weld between the torispherical head and sidewall, is located a dual side thermal shield consisting of two gaps and two sheets, as depicted in Detail R and Detail U on sheet 5. The inner sheet is 0.060 inches thick, and the outer sheet is 0.105 inches thick. The gaps are formed by a spiral wrap of stainless steel wire, 0.105 inches in nominal diameter, wrapped on a 3-inch pitch and tack welded in place. At each end of the shield, small spacer strips are used to locate the sheets, which are fully welded in place to seal the gaps. Covering the upper torispherical head is a single thermal shield, 0.105 inches thick, using

1105-SD Package Safety Analysis Report

0.105-inch nominal diameter wire, spiral wrapped on a 3-inch pitch, as depicted in Detail T on sheet 6. The inner edge of the head thermal shield is welded to a circular spacer strip, and the lower edge is welded to the top end of the side shield. In order to maintain a low thermal emissivity across the shields, the outer surface of the ½-inch thick containment shell, the inner and outer faces of the 0.060-inch thick sheet, and the inner surface of the 0.105-inch thick sheet are brightened per flag note 42 on sheet 2.

The upper body and lower body assemblies are connected using 24, 1-1/4-7 UNC bolts made of ASTM A320, L43 material, with hardened stainless steel washers. The bolts are plated with electroless nickel per SAE-AMS 2404, Revision F, Class 1, or MIL-DTL-26074 Rev. F Class 1 Grade B, and tightened to a torque of 300 ± 30 ft-lb.

The upper internal impact limiter is described in Section 1.2.1.4, *Internal Impact Limiters*.

1.2.1.4 Internal Impact Limiters

The internal impact limiters located at each end of the payload cavity are depicted as Assembly A4 on drawing 3021717-SAR, sheet 7. They are made from an array of 130, 2-inch diameter \times 0.035-inch wall thickness, ASTM A249 or A269, Type TP304 stainless steel tubes. The limiters are curved on one side to match the inside of the torispherical head, and flat on the other, so that when fully assembled, the payload cavity is a right circular cylinder 60.3 inches long.

The flat side of the impact limiters is made from a ½-inch thick, ASTM B209, 6061-T6 aluminum plate. The tubes are located in shallow grooves machined into one side of the plate, which stabilizes one end of the tubes. The other end of the tubes is stabilized by passing through a 0.105-inch thick stainless steel tube stabilizer sheet which is spherically curved to match the torispherical heads. Each of the 130 tubes is tack welded in three places to the tube sheet. The tube array is bolted to the aluminum plate using 10, 1/4-20 stainless steel bolts as shown in Section Y-Y on sheet 7. The limiters absorb energy in an impact by crippling deformation in an axial direction. The aluminum plate of the lower impact limiter has protrusions on the top surface that aid in proper placement of the payload during package use.

The internal impact limiters are held in place using four stainless steel clips welded to the inner surface of the containment boundary in the lower and upper position. There are four square notches in the 1/2-inch thick aluminum plate that match the four clips, which allow the limiter to pass beyond the clips. Then the limiter is turned about the package axis approximately 22.5° until smaller notches in the aluminum plate align with any two opposite (180° apart) clips. A 3/8-16 UNC, ASTM A574 bolt is installed in the two clips, which prevents the limiter from rotating. The lower internal impact limiter rests directly on the lower torispherical head, and the load path of the payload is directly into the head, not the clips. To ensure stability in normal use, the load path for the payload goes through a single row of tubes. The fifth concentric row of tubes (consisting of 22 tubes at a radius of 12.5 inches) extends slightly above the adjacent rows of tubes, thus supporting the entire load under normal operation. The upper internal impact limiter rests on the upper clips.

1.2.1.5 Lodgment

The lodgment is designed to maintain the position of the LTSS within the package payload cavity during NCT and HAC, and is depicted as Assembly A1 on sheet 2 of drawing 3021718-SAR. It is a weldment made from ASTM B209 or B221, 6061-T6 aluminum alloy. The LTSS is transported

with its axis vertical and its lower end approximately 8 inches above the bottom surface of the lodgment. The main structural components of the lodgment are 8 equally spaced ribs running longitudinally and two circumferential ribs going around the body of the LTSS. All ribs are $\frac{1}{2}$ inches thick. At the center of the longitudinal ribs is a "hub" made from MIL-P25995, 6061-T6, 4-inch, schedule 40 pipe. The longitudinal ribs are spaced and stiffened by 2-in. \times 2-in. \times $\frac{1}{4}$ -in. thick angles made from ASTM B308, 6061-T6.

The lodgment is constructed with a lower half and an upper half. The two halves are connected using 8, $\frac{1}{2}$ -13 UNC bolts and nuts in double shear. When assembled, the lodgment is 42.75 inches in diameter and 59.5 inches tall. The LTSS rests on a $\frac{1}{2}$ -inch thick plate covered with a $\frac{1}{2}$ -inch thick layer of neoprene rubber, which is attached to the plate using four, $\frac{1}{4}$ -inch diameter screws. There is nominally no contact between lodgment ribs and the LTSS. The neoprene rubber has no safety function. The top end of the LTSS is stabilized for transport using three toggle clamps which are bolted to three ribs. The lodgment is lifted using two opposite ribs. The lifting shackles may be placed in storage positions on the lodgment for transport.

1.2.1.6 LTSS

The LTSS consists of a central steel magazine, or barrel, surrounded by thick lead encased in a steel shell. All of the steel used in the LTSS is ASTM type 304 stainless steel. The barrel contains four longitudinal holes, each of which can accommodate one drawer assembly. The barrel is maintained axially in position using a support plate on each end, which is 20 mm thick and attached to the main body of the LTSS using eight, M10 socket head cap screws. A non-structural plate is attached to each support plate. Each end of the LTSS is closed using a lead-filled, hinged door which is attached using eight, M16 socket head cap screws. Four lift lugs are attached to the top lateral side for use in transporting the LTSS horizontally in a facility. On one end are located two threaded lifting blocks for upending and for transporting the LTSS with the axis vertical. Except for some minor operational differences in the support plates and index pins, and except for the axial lifting blocks, the LTSS is essentially radially symmetric and identical at each end. The LTSS is depicted in Figure 1.2-8 and Figure 1.2-9.

The drawer assemblies are 548 mm long and 63 mm in diameter. There are two types of drawer assembly. The Large Source Drawer has a cavity 508 mm long and a wall thickness of 5 mm. It contains the NLM-52 source capsule, which has an outer diameter of 52 mm, and two end shields made of tungsten having a minimum density of 17 g/cm³. There are five different lengths of the NLM-52, as shown in the following table:

Capsule ID	Capsule Length, mm
NLM 52-74	74
NLM 52-150	150
NLM 52-200	200
NLM 52-250	250
NLM 52-325	325

Each NLM-52 source capsule may contain one or more sealed sources as described in Section 1.2.2, *Contents*. Other special form or non-special form capsules may be used that have the same length, diameter, and at least as much radiation attenuation as the NLM-52 capsule series. The Large Source Drawer is depicted in Figure 1.2-10.

The other drawer type is the T80/T780. The T80 and T780 drawers are dimensionally identical. Like the large source drawer, they are 21.5 inches long and 2.5 inches in diameter. In the center is a 1.1-inch diameter cross-drilled hole which accepts a source capsule. The drawers are made of brass with a wall thickness of 0.2 inches and a stainless steel end thickness of 0.8 inches. For the T80 drawer, the shielding on each side of the source is 9.2 inches of lead. For the T780 drawer, the shielding may be either lead, tungsten, or depleted uranium. The T80/780 drawer is depicted in Figure 1.2-11.

1.2.1.7 Inner Container

The inner container (IC) is designed to hold a shielded device and provide support for the device and the blocking materials during transport. It is depicted as Assembly A1 on sheet 2 of drawing 3021719-SAR. The IC is 59.5 inches tall and 42.75 inches in outer diameter, with an interior cavity of 36.0 inches in diameter and 53.0 inches long. The IC is a weldment made from ASTM A240, Type 304 stainless steel. The lid is attached using six, 1-8UNC hex bolts with flat washers and nuts. The shell, the base, and the inner sheet of the lid are made from 1/4-inch thick material; the bolting flanges, of 1/2-inch thick material; and the grid pattern of stiffening and energy-absorbing ribs on the outside are made from 3/16-inch thick material. The base structure is 4.0 inches high and is stiffened by 8 ribs made from 1/4-inch thick material. The lid is 2.5 inches thick, with three, 1/4-inch thick ribs and three threaded blocks near the outer diameter for lifting the entire IC. The open space in the lid is filled with eight layers of 1/4-inch thick refractory insulation paper. The top of the lid is sealed with 16 GA (0.06-inch thick) sheet metal. The outer rim of the lid features three breathers to equalize the pressure in the lid cavity.

1.2.1.8 Gross Weight

The gross weight of the 1105-SD package, including the empty packaging, and lodgment and LTSS or inner container and shielded device, is 10,100 lb. The empty weight is 4,940 lb. A summary of overall component weights is shown in Table 2.1-2 and discussed in Section 2.1.3, *Weights and Centers of Gravity*.

1.2.1.9 Neutron Moderation and Absorption

Since the 1105-SD package transports material which is either non-fissile or fissile exempt, no moderation or absorption of neutrons is necessary to control criticality.

1.2.1.10 Receptacles, Valves, Testing and Sampling Ports

The 1105-SD package upper body assembly contains a vent port and a containment seal test port. There are no valves or receptacles used in the 1105-SD package.

1.2.1.11 Heat Dissipation

The dissipation of heat from the 1105-SD package is entirely passive. A thermal shield is used on the upper body assembly and upper head to limit the heat flux into the package in the HAC

fire event. A more detailed description of the package thermal design is given in Chapter 3, *Thermal Evaluation*.

1.2.1.12 Lifting and Tie-down Devices

The 1105-SD is lifted using a shipping skid and a fork lift truck. The threaded hole on the top of the upper package assembly is used only to lift the upper package assembly component. The package is tied down using straps or hold-down structures placed over the top of the impact limiter, and which are fastened to the shipping skid or to the conveyance. Thus, there are no lifting or tie-down devices that are a structural part of the package.

1.2.1.13 Pressure Relief System

There is no pressure relief system in the 1105-SD package.

1.2.1.14 Shielding

Biological shielding of gamma radiation is provided by lead located in the LTSS or in the shielded devices. No other components whose primary purpose is shielding are included in the 1105-SD. Details of the gamma shielding in the LTSS are provided in Section 1.2.1.6, *LTSS*. Gamma shielding in the shielded devices is described and evaluated in Chapter 5, *Shielding Evaluation*.

1.2.2 Contents

The 1105-SD package contains two payload types: the LTSS and shielded devices. The contents of the LTSS are subdivided into Content 1 and Content 2. The shielded device category is subdivided into Group 1 and Group 3 devices.

1.2.2.1 LTSS Contents

The LTSS contains sealed sources taken from shielded devices such as industrial irradiators, medical equipment, or research facilities. The sources are sealed and may be in special form, and may be present in the T80/T780 source drawer. Content 1 and Content 2 are defined in Section 7.1.4.1, *Qualifying a Payload for Transport*. The nuclides that will be transported in the LTSS are listed in Table 1.2-1. The maximum decay heat in the package is 200W or less. The quantity of Pu-239 is less than 15g. No other fissile isotopes are transported. Fissile exemption of the payload is discussed in Chapter 6, *Criticality Evaluation*. The 1105-SD, when containing isotopes of plutonium or americium, will not be offered for transport by air. Allowable combinations of nuclides within a single LTSS is discussed in Chapter 5, *Shielding Evaluation*.

1.2.2.2 Shielded Devices

Shielded devices are units which were designed and manufactured to provide a safe source of radiation for industrial, medical, or research purposes. Each such device includes a sealed source (or a group of sources), shielding material, and a steel shell to surround the shielding material and provide structure (a limited portion of the GC-40 shell includes cast iron). All devices transported in the 1105-SD are found in the NRC Sealed Source Device Registry (SSDR). Each device was engineered to be safely used in a normally occupied environment (i.e., not requiring a hot cell environment), and was repeatedly surveyed for radiation dose over its lifetime.

Conservatively, prior to transport, each device will be surveyed, with a surface dose rate limit of 200 mrem/hr and a dose rate at a distance of one meter from the surface of 10 mrem/hr. As noted in the SSDRs, the actual measured dose rate is as much as two orders of magnitude lower than this.

All shielded devices are placed into the inner container for shipment in the 1105-SD, described in Section 1.2.1.7, *Inner Container*, and blocked in position using dunnage materials. Blocking/dunnage materials are metallic structures or polymeric foam, and are described in Section 7.1.2.2, *Loading the Inner Container (IC)*. The blocking/dunnage is used to prevent unwanted motion during normal transport, and does not provide a safety function. Cabinets, stands, or unnecessary appurtenances are not transported. Prior to loading, movable sources are placed in the safe shipping position, the structural integrity is evaluated, and a radiation survey is performed. More information is provided in Section 7.1.2.2, *Loading the Inner Container (IC)*.

Group 1 shielded devices were manufactured by Radiation Machinery Corporation, Isomedix, Atomic Energy of Canada Limited, MDS Nordion, and Best Theratronics. All of the Group 1 devices feature a fixed-source design, that is, the source capsule(s) are located in a fixed position within the device, and the sample was moved (typically rotated) into or out of position using a shielded specimen holder. All Group 1 devices use Cs-137, with a maximum activity of 3,840 Ci and have a weight of approximately 3,300 lb. All of the devices are shielded with lead, which is contained within a thick steel shell weldment. The model types included in Group 1 are listed in Table 1.2-2. Photographs of the Group 1 devices are provided in Figure 1.2-12 through Figure 1.2-15.

Group 3 consists of the Gammacell-40 (a.k.a. GC-40 and Exactor), formerly manufactured by Atomic Energy of Canada Limited and MDS Nordion, and currently by Best Theratronics. The GC-40 features a telescoping source design, in which the source is contained in a source drawer which is moved along its axis through the shield. In the active position, the source is exposed to a lateral opening in the shield. In the storage position, the source is located near the center of the shield. The drawer contains shielding on each end of the source. All shielding material is lead. The GC-40 has two essentially identical shielded units (upper and lower). Each unit is transported singly. The maximum activity in any one unit is 2,250 Ci of Cs-137. The weight is approximately 2,650 lb. A figure of the GC-40 is provided in Figure 1.2-16.

1.2.3 Special Requirement for Plutonium

The 1105-SD package may contain plutonium in excess of 20 Ci, which is in solid form.

1.2.4 Operational Features

The 1105-SD package is of conventional design and is not complex to operate. Operational features are depicted on the drawings provided in Appendix 1.3.3, *Packaging General Arrangement Drawings*. Operating procedures and instructions for loading, unloading, and preparing an empty package for transport are provided in Chapter 7, *Package Operations*.

Table 1.2-1 – LTSS Payload Source Nuclides

Nuclide	Maximum Activity
Co-60	12,970 Ci
Cs-137	14,000 Ci
Sr-90	1,000 Ci
Am-241 (no Be) ^⑥	1000 Ci
Am-241Be ^⑥	6.6 Ci
Pu-238 (no Be) ^⑦	75 g Pu
Pu-239 (no Be) ^⑦	15 g Pu
Pu-239Be ^⑦	15 g Pu
Ir-192	200 Ci
Se-75	80 Ci

Notes:

1. Physical form of all nuclides is solid material in a sealed capsule.
2. The maximum decay heat limit for the 1105-SD package is 200W.
3. The maximum activity listed is the maximum for a single nuclide in the LTSS. For combinations of different nuclides, lower activity limits apply as discussed in Chapter 5, *Shielding Evaluation*.
4. The total activity in this table is 86,732 A₂. This value exceeds the maximum number of A₂ that could be transported.
5. Not used.
6. Impurities may include oxygen and chlorine.
7. Impurities may include oxygen.

Table 1.2-2 – Shielded Devices

Model Name/Type	Maximum Activity, Ci	Weight, lb	SSDR No. ^③
<i>Group 1 Devices</i>			
Gammator 50B, B, B34, G-50-B	420	1800	NR-0880-D-802-S
Gammator M34	1,920	1,850	NR-0880-D-806-S
Gammator M38	3,840	2,250	NR-0880-D-806-S
Gammacell 1000 (GC-1000) -Models A through D -Elite A through D, Type I and Type II	3,840 (bounding value)	2,800	NR-0880-D-808-S, NR-1307-D-102-S
Gammacell 3000 (GC-3000) -Elan A through C, Type I and Type II ^②	3,048	3,300	NR-1307-D-102-S
<i>Group 3 Devices</i>			
Gammacell-40 (GC-40, Exactor)	2,250 ^④	2,650	NR-1307-D-101-S

Notes:

1. Radionuclide in all cases is Cs-137.
2. Gammacell 3000 external secondary shielding is not credited in the shielding analysis.
3. Consult SSDR for design and safety features of each model.
4. Gammacell-40 activity is given for one of the two device components that make up a complete Gammacell-40. Only one device component may be shipped at one time.

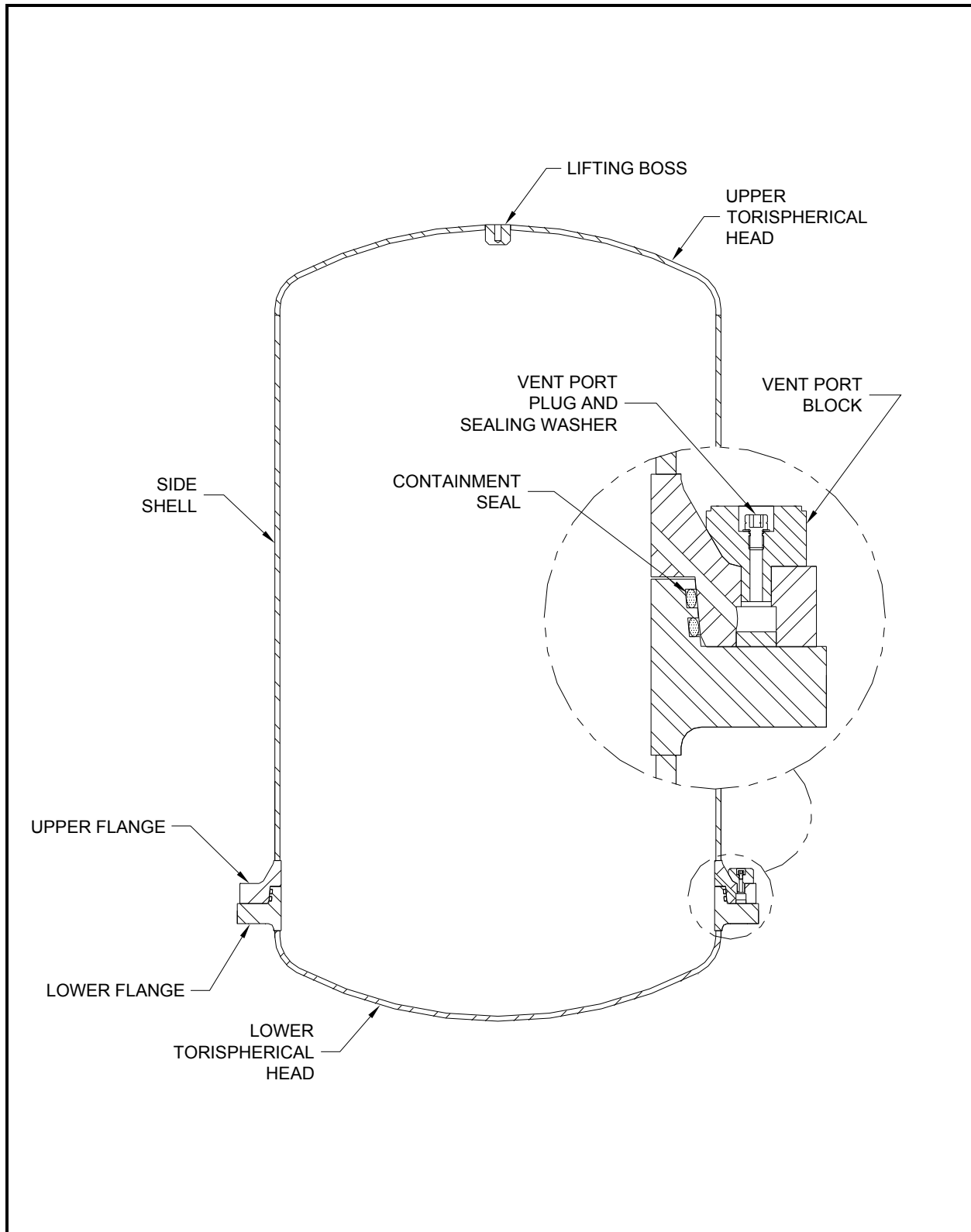
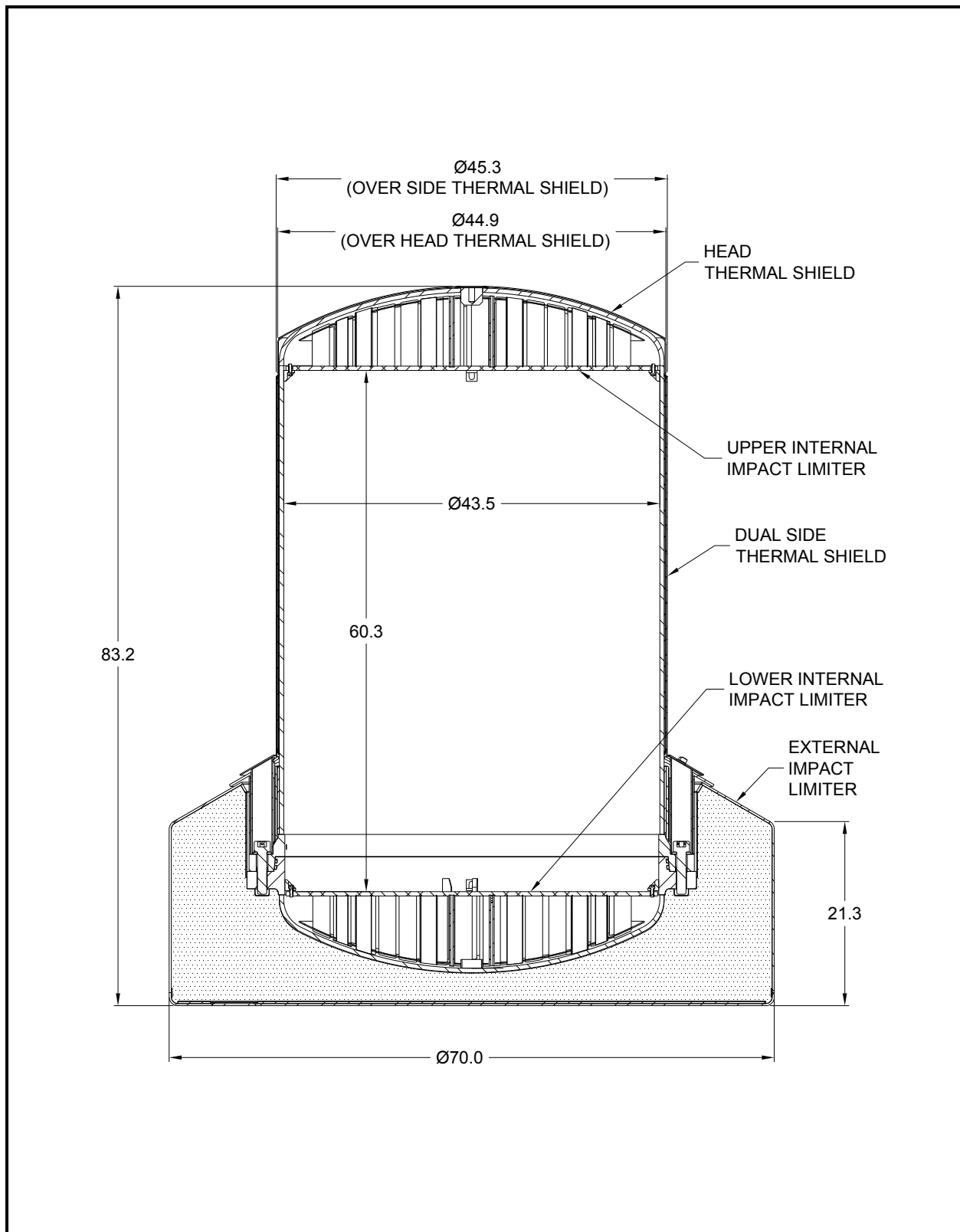


Figure 1.2-1 – 1105-SD Containment Boundary

**Figure 1.2-2 – 1105-SD Cross Sectional View**

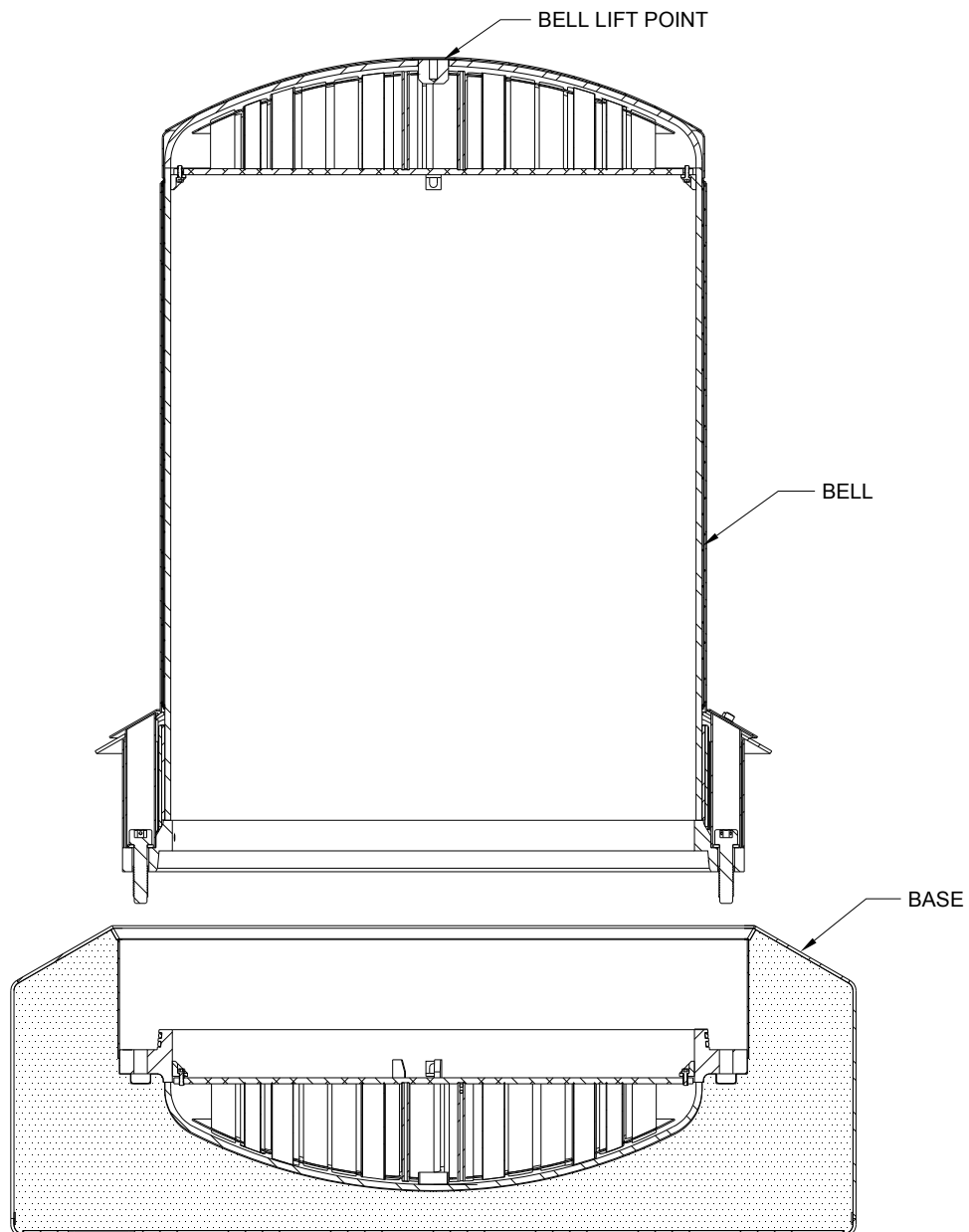


Figure 1.2-3 – Exploded View

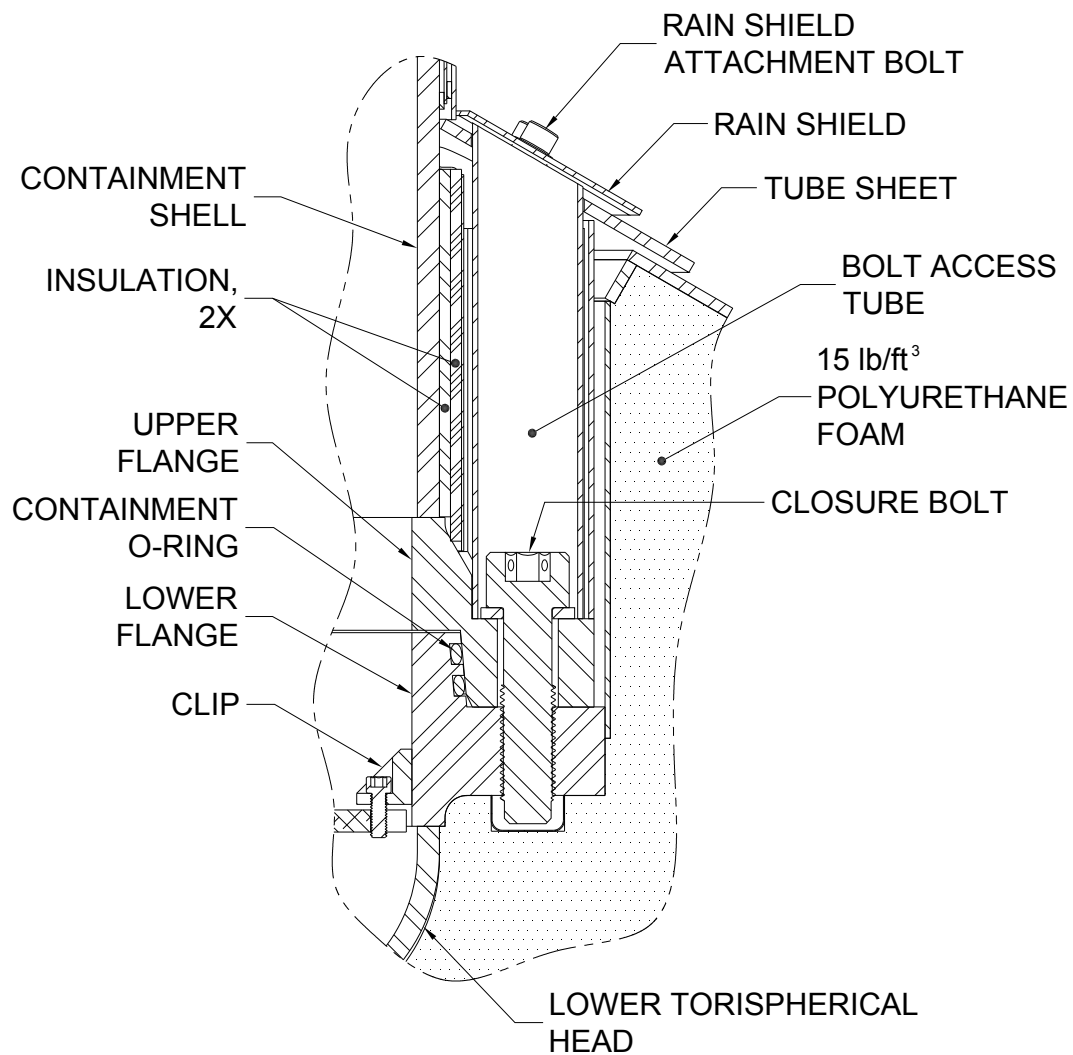


Figure 1.2-4 – Detail View of Flange Area

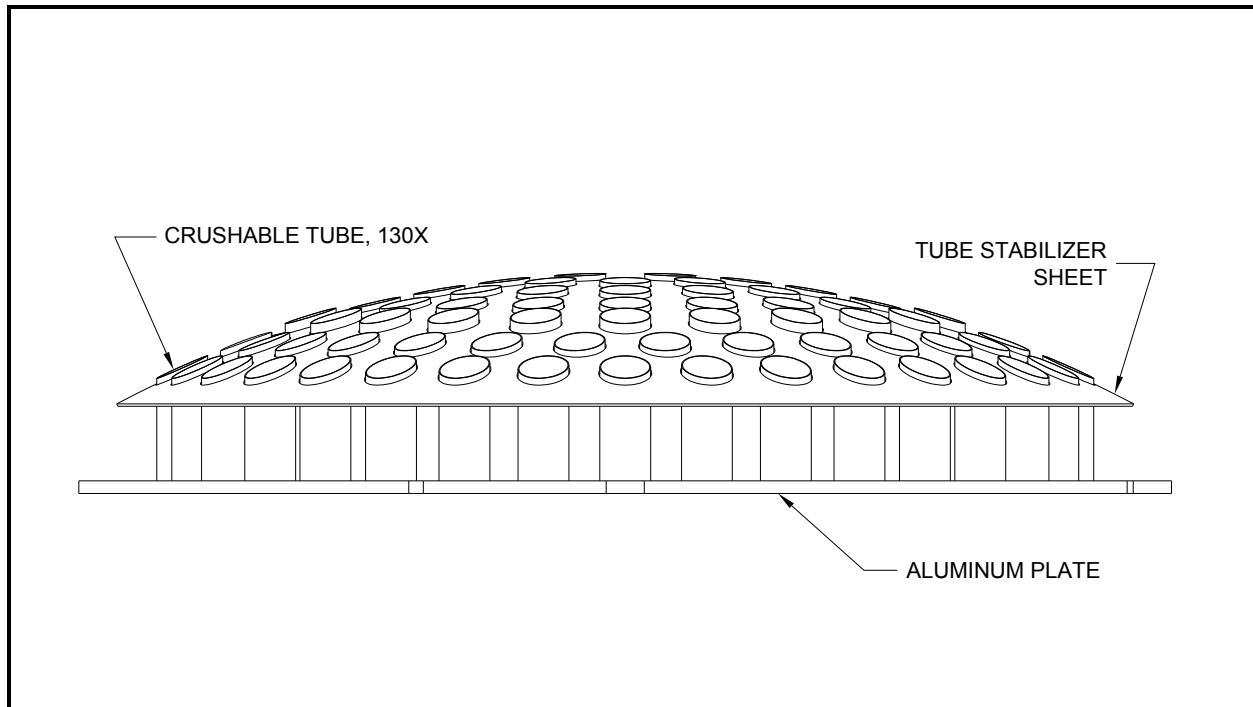


Figure 1.2-5 –Internal Impact Limiter

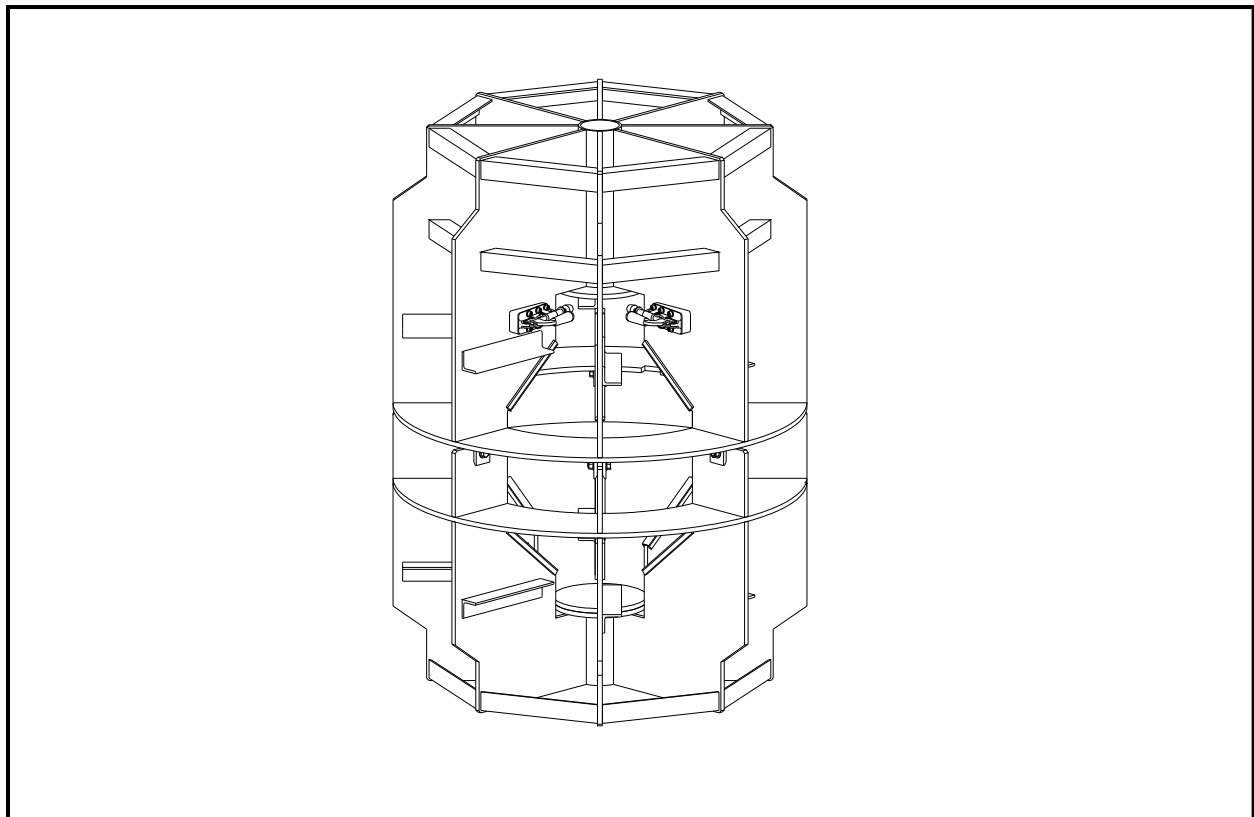


Figure 1.2-6 – LTSS Lodgment

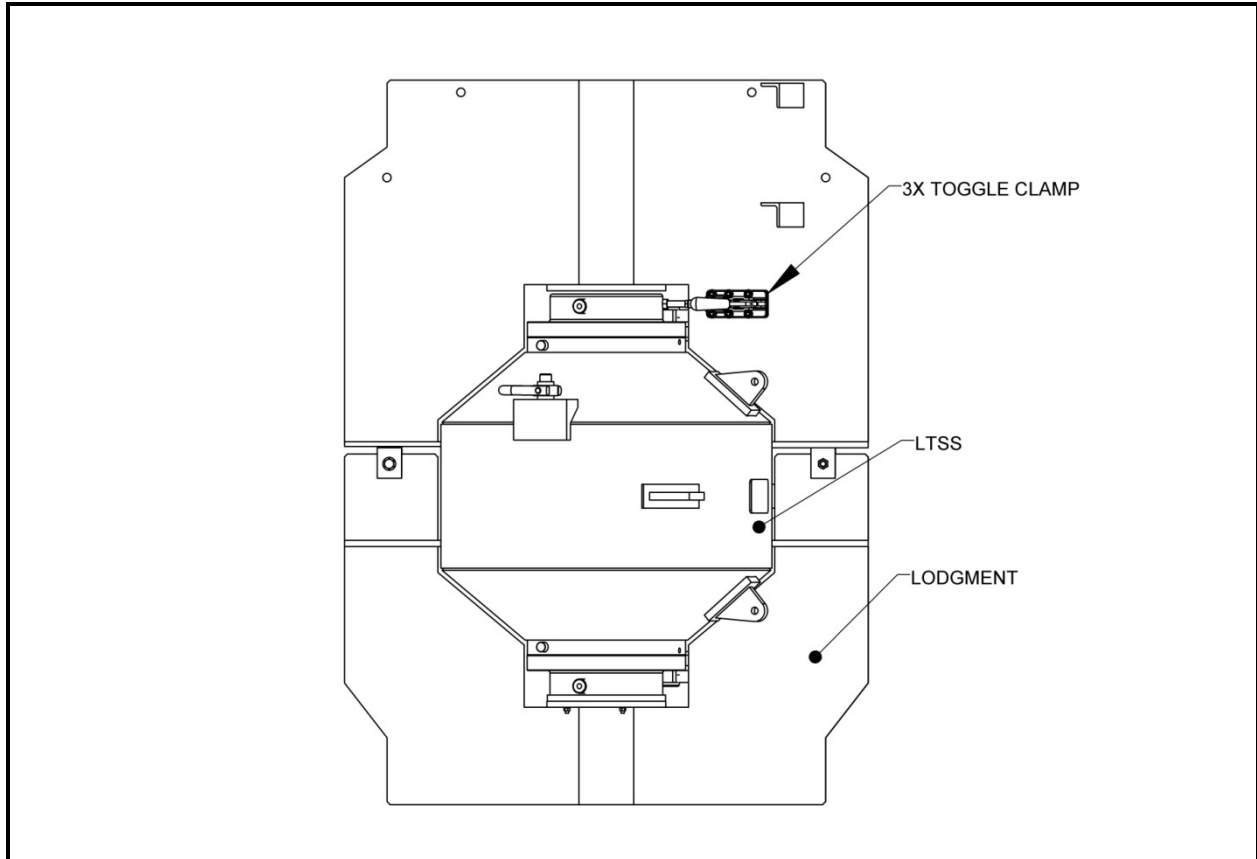


Figure 1.2-6a – LTSS Placed in Lodgment

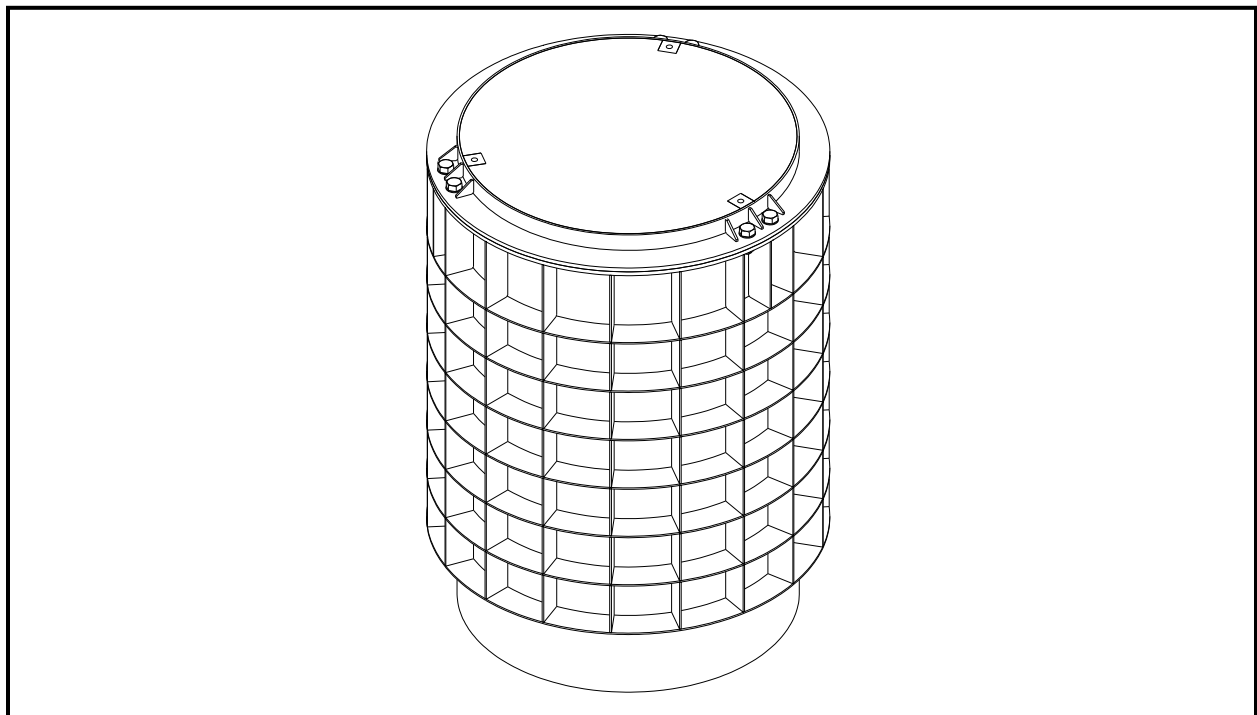
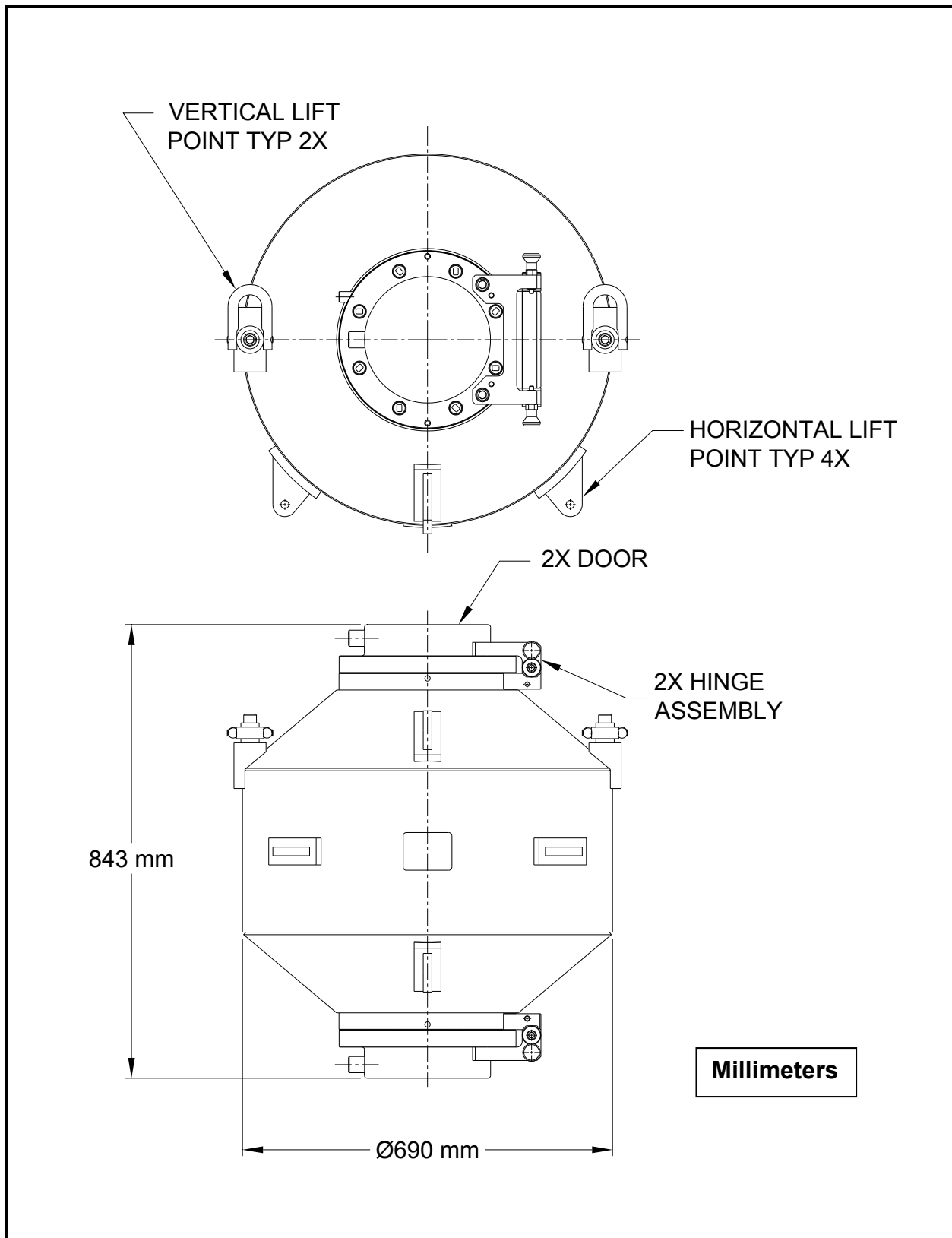


Figure 1.2-7 – Inner Container

**Figure 1.2-8 – LTSS Overview**

**Security-Related Information
Figure Withheld Under
10 CFR 2.390**

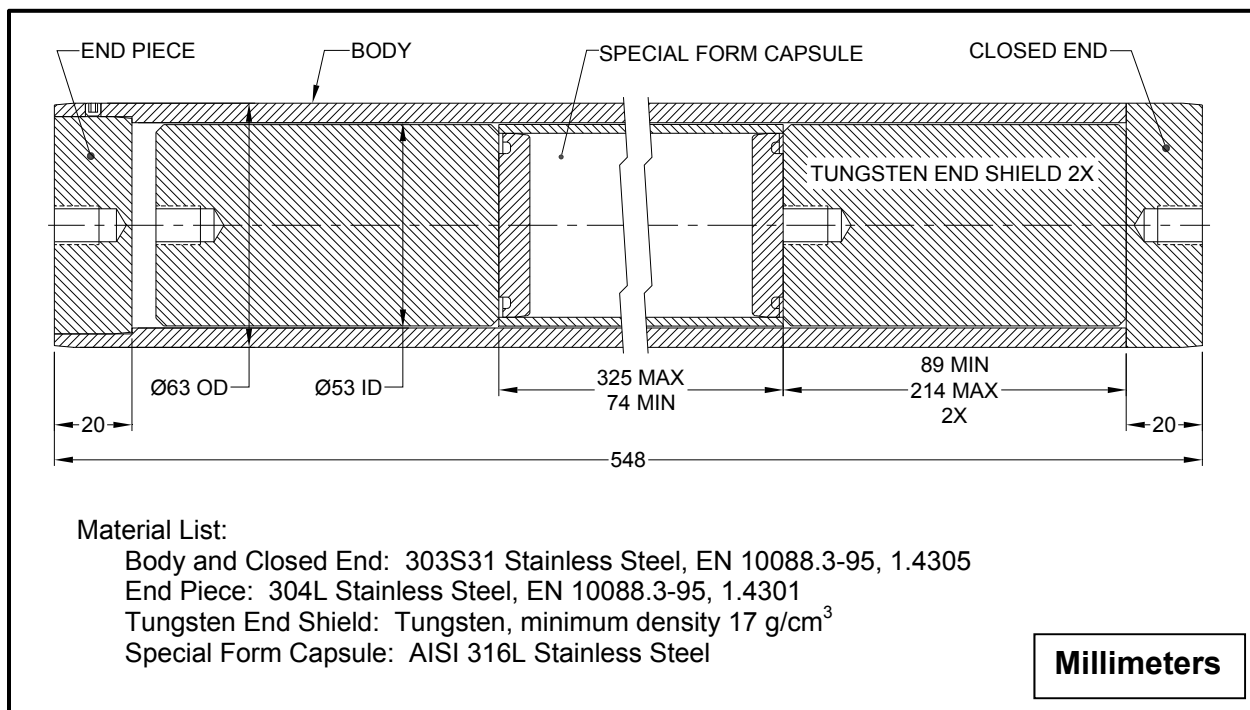


Figure 1.2-10 – LTSS Large Source Drawer

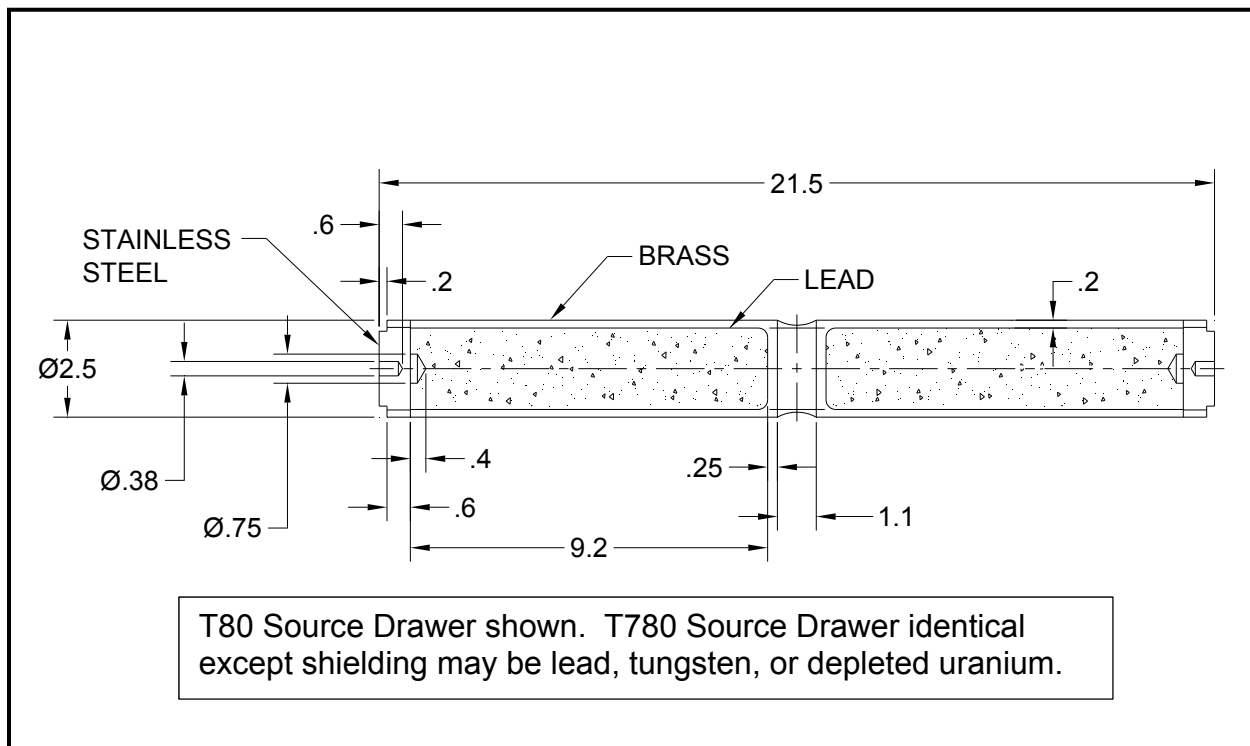


Figure 1.2-11 – T80/780 Source Drawer (inches)



Figure 1.2-12 – Gammator G-50-B Shielded Device



Figure 1.2-13 – Gammator M38 Shielded Device



Figure 1.2-14 – Gammacell 1000 Shielded Device



Figure 1.2-15 – Gammacell 3000 Shielded Device



Figure 1.2-16 – Gammacell-40 Shielded Device (Upper Head Shown)

1.3 Appendices

1.3.1 References

1. Title 10, Code of Federal Regulations, Part 71 (10 CFR 71), *Packaging and Transportation of Radioactive Material*, 01–01–18 Edition.
2. International Atomic Energy Agency, *Regulations for the Safe Transport of Radioactive Material*, SSR-6, 2012 Edition.
3. ANSI N14.5–2014, *American National Standard for Radioactive Materials – Leakage Tests on Packages for Shipment*, American National Standards Institute (ANSI), Inc.

1.3.2 Glossary of Terms and Acronyms

ANSI –	American National Standards Institute.
ASME B&PV Code –	American Society of Mechanical Engineers Boiler and Pressure Vessel Code.
ASTM –	American Society for Testing and Materials.
AWS –	American Welding Society.
Base –	See <i>Lower Body Assembly</i> .
Bell –	See <i>Upper Body Assembly</i> .
Clip –	Eight brackets (four top and four bottom), welded to the inside of the containment boundary, supports and retains the <i>Internal Impact Limiters</i> in place.
Closure Bolts –	Fasteners that secure the <i>Upper Body Assembly</i> to the <i>Lower Body Assembly</i> . Includes washers.
Closure Bolt Access Tube –	24, 2-¼ -inch inner diameter tubes that permit access to the <i>Closure Bolt</i> heads. See also <i>Port Access Tube</i> .
Containment O-ring Seal –	Upper elastomeric seal, retained by the lower flange, which forms part of the containment boundary.
Crush Tubes –	Tubes used with the <i>Internal Impact Limiter</i> to absorb free drop energy.
HAC –	Hypothetical Accident Conditions.
Head Thermal Shield –	Assembly of a sheet and a wire wrap attached to the outside of the upper torispherical head, forming a thin air gap that inhibits heat transfer into the package during the HAC fire event.
Inner Container –	Steel container with a bolted lid used to house <i>Shielded Devices</i> , interfaces with the 1105-SD payload cavity.
Internal Impact Limiter –	An energy absorbing component that is placed into each torispherical head. Forms flat ends for the payload cavity and absorbs payload kinetic energy in end drops.
Large Source Drawer –	Shielded drawer used with the <i>LTSS</i> .
Lodgment –	Aluminum weldment used to hold the <i>LTSS</i> inside the payload cavity.
Lower Body Assembly (Base) –	Lower part of packaging, includes the lower torispherical head, lower flange, <i>Internal Impact Limiter</i> , and external impact limiter. Interfaces with the <i>Upper Body Assembly</i> .
Long Term Storage Shield (LTSS) –	Lead-shielded container which holds source capsules.
MNOP –	Maximum Normal Operating Pressure.
NCT –	Normal Conditions of Transport.

Port Access Tube –	Two, 2- $\frac{1}{4}$ -inch inner diameter tubes that permit access to the <i>Vent Port</i> and <i>Seal Test Port</i> plugs. Holds the <i>Port Insulation Cylinder</i> . See also <i>Closure Bolt Access Tube</i> .
Port Insulation Cylinder –	An insulated tube that fits within each <i>Port Access Tube</i> to provide additional thermal insulation for the port <i>Sealing Washers</i> .
Rain Shield –	Sheet, 0.120-inch thick, which covers the open ends of the <i>Closure Bolt Access Tubes</i> and <i>Port Access Tubes</i> .
Seal Test Port –	Opening located in a block welded to the upper flange, used to test the leakage rate of the <i>Containment O-ring Seal</i> . Closed with the <i>Seal Test Port</i> plug.
Sealed Source –	Sealed capsule containing source material.
Sealing Washers –	Integrated metal and elastomer seals that are used with the <i>Vent Port</i> and <i>Seal Test Ports</i> .
Side Thermal Shield –	Assembly of sheets and wire wraps attached to the outside of the outer shell, forming two thin air gaps that inhibit heat transfer into the package during the HAC fire event.
Shielded Device –	Industrial, medical, or research device for use in irradiating samples. Contains the source, shielding, and surrounding structure.
Special Form Capsule –	NLM 52, a welded capsule used in the <i>Large Source Drawer</i> .
T80/T780 Drawers –	Shielded source drawers used with the <i>LTSS</i> .
Test O-ring Seal –	Lower elastomeric O-ring seal, retained by the lower flange, used to allow leakage rate testing of the <i>Containment O-ring Seal</i> .
Tube Sheet –	The $\frac{1}{4}$ -inch thick plate, inclined at 30° to the horizontal, that holds the upper end of the <i>Closure Bolt Access Tubes</i> in place.
Tube Stabilizer Sheet –	Bowl-shaped, 0.105-inch thick sheet that stabilizes the <i>Internal Impact Limiter</i> tubes.
Upper Body Assembly (Bell) –	Upper part of packaging, includes the upper torispherical head, cylindrical shell, upper flange, lifting boss, bolt tube structures, vent and test port blocks, access to closure bolts, and upper inner impact limiter. Interfaces with the <i>Lower Body Assembly</i> .
Vent Port –	Opening located in a block welded to the upper flange, used to vent the cavity and to introduce helium for leakage rate testing during operations. Closed with the vent port plug.

1.3.3 Packaging General Arrangement Drawings

The packaging general arrangement drawings consist of:

- 3021717-SAR, 1105-SD Package Assembly SAR Drawing, 7 sheets
- 3021718-SAR, 1105-SD LTSS Lodgment SAR Drawing, 2 sheets
- 3021719-SAR, 1105-SD Inner Container SAR Drawing, 2 sheets

Security-Related Information
Figure Withheld Under
10 CFR 2.390

Security-Related Information
Figure Withheld Under
10 CFR 2.390

**Security-Related Information
Figure Withheld Under
10 CFR 2.390**

Security-Related Information
Figure Withheld Under
10 CFR 2.390

Security-Related Information
Figure Withheld Under
10 CFR 2.390

**Security-Related Information
Figure Withheld Under
10 CFR 2.390**

Security-Related Information
Figure Withheld Under
10 CFR 2.390

**Security-Related Information
Figure Withheld Under
10 CFR 2.390**

**Security-Related Information
Figure Withheld Under
10 CFR 2.390**

**Security-Related Information
Figure Withheld Under
10 CFR 2.390**

**Security-Related Information
Figure Withheld Under
10 CFR 2.390**

2.0 STRUCTURAL EVALUATION

This section presents evaluations demonstrating that the 1105-SD package meets all applicable structural criteria. The 1105-SD package, consisting of a lower and upper body assembly and lodgment or inner container, is evaluated and shown to provide adequate protection for the LTSS or shielded device payloads. Normal conditions of transport (NCT) and hypothetical accident condition (HAC) evaluations are performed to address 10 CFR 71 [1] performance requirements. The primary method of performance demonstration is by full-scale test. When analysis is used, demonstration techniques comply with the methodology presented in NRC Regulatory Guides 7.6 [2] and 7.8 [3]. NCT free drop and HAC free drop and puncture performance is evaluated by means of three full scale test units. A discussion of the tests performed is given in Appendix 2.12.2, *Certification Test Plan*, and results of the certification tests are provided in Appendix 2.12.3, *Certification Test Results*.

2.1 Structural Design

2.1.1 Discussion

The 1105-SD package is designed to transport radioactive sources contained in the LTSS or in shielded devices. An isometric view of the package is shown in Figure 1.1-1, with cross-sections of the package with the two payload types shown in Figure 1.1-2 and Figure 1.1-3. Other views of the packaging and of its internal components are shown Figure 1.2-1 through Figure 1.2-7. The 1105-SD package consists of a lower body assembly, an upper body assembly, two internal impact limiters, and a lodgment or an inner container (IC). The payload cavity is 43.5 inches in diameter and 60.3 inches long. Shielding of the radioactive sources is provided by the thick lead body of the LTSS or of the shielded devices. The 1105-SD containment boundary consists of ½-inch thick Type 304 stainless steel, and includes a cylindrical body, two torispherical ends, and heavy bolting flanges. A quantity of 24, 1-1/4-inch diameter alloy steel bolts are used to fasten the upper and lower assemblies together. The containment closure seal is a 3/8-inch cross-sectional diameter butyl O-ring seal. A test O-ring seal is used to provide a cavity for helium leak testing of the containment seal. Vent and test ports are located adjacent to the upper flange. A dual thermal shield is attached to the outside of the cylindrical shell and a single thermal shield is attached to the upper torispherical head.

An external impact limiter is located at the lower end of the package to protect the closure from impact loads and HAC fire heat. The impact limiter shell is ¼ inches thick and envelops nominally 15 lb/ft³ polyurethane foam impact absorbing material. The impact limiter is integrally attached to the lower body assembly by welds. Two internal impact limiters, which absorb the energy of the payload using the crippling deformation of steel tubes, are used at each end of the payload cavity.

A lodgment consisting of an aluminum alloy weldment is used to maintain the LTSS in position. An inner container with internal blocking is used to hold the shielded devices. A comprehensive discussion of the 1105-SD package design and configuration is provided in Section 1.2, *Package Description*.

2.1.2 Design Criteria

Proof of performance for the 1105-SD package is achieved by a combination of full scale certification testing and analysis. The acceptance criteria for analytic assessments are in accordance with Regulatory Guide 7.6. The acceptance criterion for certification testing is a demonstration that the containment boundary remains leaktight [4] following the imposed loading conditions. Additionally, package deformations obtained from testing must be such that deformed geometry assumptions used in subsequent thermal evaluation is validated. These design criteria meet the following safety requirements of 10 CFR §71.51:

1. For normal conditions of transport, there shall be no loss or dispersal of radioactive contents, as demonstrated to a sensitivity of 10^{-6} A₂ per hour, no significant increase in external radiation levels, and no substantial reduction in the effectiveness of the packaging.
2. For hypothetical accident conditions, there shall be no escape of radioactive material exceeding a total amount A₂ in one week, and no external radiation dose rate exceeding one rem per hour at one meter from the external surface of the package.

The 1105-SD package qualifies as a Category I container, which is the highest and most stringent category [5]. Per NUREG/CR-3019 [6] and NUREG/CR-3854 [7], the cask components are classified as follows:

- Containment components are classified as ASME Code, Section III, Subsection NB [8].
- Non-containment structures such as the thermal shields, impact limiter shells, and internal impact limiter components are classified as ASME Code, Section III, Subsection NF [9].
- Lodgment and IC components are classified as ASME Code, Section III, Subsection ND [25].

The remainder of this section presents the detailed acceptance criteria used for analytic structural assessments of the 1105-SD package.

2.1.2.1 Containment Structures

A summary of allowable stresses used for containment structures is presented in Table 2.1-1. Containment structures include the cylindrical shell, the torispherical heads, and the flanges. The allowable stresses shown in Table 2.1-1 are consistent with Regulatory Guide 7.6, and the ASME Code, Section III, Subsection NB, and Appendix F [32]. Peak stresses are further discussed in Section 2.1.2.3.2, *Fatigue Assessment*, and buckling in Section 2.1.2.3.3, *Buckling Assessment*. Closure bolts are evaluated using the guidance of NUREG/CR-6007 [10]. Furthermore, stress intensity in the flanges which could affect compression of the containment O-ring seal is limited to the lesser of the value shown in Table 2.1-1, or the yield strength.

2.1.2.2 Other Structures

The external impact limiter, including the steel shells and energy-absorbing foam, is expected to permanently deform under NCT and HAC. The performance criteria are:

- Limit impact magnitude such that package component stress and deflection criteria are met.
- Prevent "hard" contact of a rigid part of the cask with the ground due to excessive deformation of the foam.

- Maintain sufficient structural integrity subsequent to the HAC free drop and puncture drop events that the containment O-ring seal is protected from excessive temperature in the subsequent HAC fire event.

The internal impact limiters contribute significantly to the absorption of the payload energy in a free drop event. They must limit the relative motion of the payload such that package component stress and deflection criteria are met.

The performance of the packaging is discussed in Sections 2.6, *Normal Conditions of Transport*, and 2.7, *Hypothetical Accident Conditions of Transport*. The thermal performance of the packaging is evaluated in Chapter 3, *Thermal Evaluation*.

Since the 1105-SD package is not lifted using any structural part of the package, lifting structural criteria are not required. Furthermore, since the 1105-SD package is not attached to the conveyance using any structural part of the package, tiedown structural criteria are not required.

2.1.2.3 Miscellaneous Structural Failure Modes

2.1.2.3.1 Brittle Fracture

With the exception of the closure bolts, all structural components of the 1105-SD package are fabricated of austenitic stainless steel or aluminum. These materials do not undergo a ductile-to-brittle transition in the temperature range of interest (i.e., down to -40 °F), and thus do not need to be evaluated for brittle fracture. The closure bolts are fabricated from ASTM A320, Grade L43 alloy steel bolting material. This material is specifically intended for low temperature service. In addition, per Section 5 of NUREG/CR-1815 [11], bolts are not considered as fracture-critical components because multiple load paths exist and bolting systems are generally redundant, as is the case with the 1105-SD package. Therefore, brittle fracture is not a failure mode of concern.

2.1.2.3.2 Fatigue Assessment

2.1.2.3.2.1 Normal Operating Cycles

Normal operating cycles do not present a fatigue concern for the 1105-SD package components over its service life. The basis for this conclusion is reached using the six criteria of Article NB-3222.4(d) of the ASME Boiler and Pressure Vessel Code. A summary of the six criteria and their application are discussed below. The service life of the package is 25 years with up to 50 shipments per year for a maximum of 1,250 shipments in the service life.

(1) Atmospheric to Service Pressure Cycle: The total number of atmospheric-to-operating pressure cycles during normal operations does not exceed the number of cycles on the fatigue curve corresponding to a value of $S_a = 3S_m$ for Type 304 stainless steel. From Section 2.2.1, *Material Properties and Specifications* at a bounding temperature of 200 °F per Section 2.6.1.1, *Summary of Pressures and Temperatures*, the S_m value for Type 304 stainless steel is 20 ksi, which corresponds to an alternating stress value of $S_a = 3S_m = 60$ ksi. The corresponding number of cycles for a value of $S_a = 60$ ksi is greater than 6,000 from Figure I-9.2 and Table I-9.2 of the ASME Code [12]. The package undergoes one atmospheric-to-operating pressure cycle per shipment, therefore the package will experience 1,250 atmospheric-to-operating pressure cycles in its life. Since the allowable number of cycles is greater than the maximum expected number of cycles, the first criterion is satisfied.

(2) Normal Service Pressure Fluctuation: The specified full range of pressure fluctuations during normal service does not exceed the quantity $1/3 \times \text{Design Pressure} \times (S_a/S_m)$, where the Design Pressure is 25 psi, S_a is the value obtained from the Type 304 stainless steel design fatigue curve for the total specified number of significant pressure fluctuations (SPF), and S_m is the allowable stress intensity for the material at the service temperature. The total number of service cycles is based on the fill gas extreme temperature range as stated below. Conservatively, two complete temperature cycles are assumed to occur for each of the 1,250 lifetime shipments for a total quantity of 2,500 pressure fluctuation cycles. From Table I-9.2, $S_a = 80,140$ psi for 2,500 cycles. The value of S_m was defined above as 20 ksi at service temperature. The limiting full range of pressure fluctuation (FRF) becomes:

$$\text{FRF}_{\text{LIMIT}} = 1/3 \times \text{Design Pressure} \times (S_a/S_m) = 33.4 \text{ psi}$$

Next, the maximum pressure fluctuations in the package will be determined. Of note, the maximum pressure fluctuations will be conservatively assumed to be above the significance level, and therefore the value SPF does not need to be computed. The bulk average fill gas temperature varies between the extremes of $T_1 = -40$ °F and a conservative bounding temperature of $T_2 = 200$ °F. The maximum pressure (conservatively assuming that atmospheric pressure corresponds to -40 °F) is:

$$\frac{P_2}{P_1} = \frac{T_2}{T_1} \Rightarrow P_2 = P_1 \left(\frac{T_2}{T_1} \right) = 14.7 \left(\frac{200 + 460}{-40 + 460} \right) = 23.1 \text{ psia}$$

The resulting pressure fluctuation is $\text{FRF} = 23.1 - 14.7 = 8.4$ psi, which is less than $\text{FRF}_{\text{LIMIT}} = 33.4$ psi presented above and therefore, the second criterion is satisfied.

(3) Temperature Difference — Startup and Shutdown: The temperature between adjacent points of a package component during normal service does not exceed $1/2(S_a/E\alpha)$, where S_a is the design fatigue curve value taken from Table I-9.2 for the total specified number of temperature difference fluctuations, E is the modulus of elasticity, and α is the mean coefficient of thermal expansion, all evaluated at temperature. The total number of temperature fluctuations will not exceed the number of uses of the package, which is 1,250 as calculated above. It will be conservative to use the value of S_a from Table I-9.2 of the ASME Code for 2,500 cycles, which is 80,140 psi. From Section 2.2.1, *Material Properties and Specifications* at a bounding temperature of 200 °F, the value of the mean thermal expansion coefficient is $\alpha = 8.9(10^{-6})/\text{°F}$ and the modulus of elasticity, $E = 27.5(10^6)$ psi. Therefore, the value of $1/2(S_a/E\alpha) = 1/2(80,140/[27.5(10^6)8.9(10^{-6})]) = 164$ °F. Since the package design temperature is 200 °F under ambient conditions of 100 °F, the temperature difference between any two adjacent points cannot approach the 164 °F value. Thus, the third criterion is satisfied.

(4) Temperature Difference — Normal Service: The temperature difference between any two adjacent points does not change during normal service by more than the quantity $1/2(S_a/E\alpha)$, where S_a , E , and α are as defined above. However, normal operating temperatures of the containment boundary are largely determined by the steady heat load, and any changes in temperature due to changes in ambient conditions, warm-up, or cool-down will be relatively slow and even due to the large thermal mass of the package. Therefore, the fourth criterion is satisfied.

(5) Temperature Difference — Dissimilar Materials: The fifth criterion is concerned with dissimilar materials. The containment boundary is constructed of Type 304 stainless steel, and

includes a brass vent port plug. The ASTM B16 free-cutting brass used in the vent port plug has a coefficient of thermal expansion which is very similar to that of the stainless steel and the temperature of the plug and the surrounding steel is essentially identical. The plug is inspected at each use of the package, and is easily replaced if necessary. Alloy steel closure bolts are used to connect the two parts of the containment vessel. Consideration of the effect of temperature variation on the alloy steel closure bolts and stainless steel flanges is included in the closure bolt stress evaluation under criterion six below. Thus, dissimilar materials are not of concern and the fifth criterion is satisfied.

(6) Mechanical Loads: The specified full range of mechanical loads does not result in stresses whose range exceeds the S_a design fatigue curve for the total specified number of load fluctuations. The only repeating mechanical loads will be those associated with tightening of the closure bolts.

The maximum stress intensity developed in the closure bolts during normal operations, given in Section 2.6.1.5, *Closure Bolts*, is bounded by a value of $S_{max} = 38,000$ psi. This stress includes preload stress, thermal stress, and a conservative inclusion of 50% of the applied preload torque as a residual torsion stress. From Table 2.2-3, the ASME allowable stress for the bolting material, S_m , at 200 °F is 33,000 psi. As defined by Table I-9.0 of the ASME B&PV Code, the Maximum Nominal Stress (MNS) of 38,000 psi is less than $2.7S_m$ (i.e., $2.7(33,000) = 89,100$ psi). Per NB-3232.3(c), a stress concentration factor of four shall be applied to one-half the value of S_{max} , i.e., $4(0.5S_{max}) = 4 \times 0.5 \times 38,000 = 76,000$ psi. Per NB-3232.3(d), the alternating stress must be adjusted for the elastic modulus used in the fatigue curves. The modulus at a temperature of 200 °F is $27.1(10^6)$ psi and the modulus used for the fatigue curve in Figure I-9.4 is $30(10^6)$ psi. The adjusted alternating stress is:

$$S_{ALT} = \frac{30}{27.1} 76 = 84.1 \text{ ksi}$$

From Table I-9.0 for figure I-9.4, the conservative lower-bound service cycles allowed for a stress of 84.1 ksi is 1,400. Since closure bolts are tightened twice per package service cycle, the allowable number of package service cycles is half of this value. Therefore the closure bolts should be replaced every $1,400/2 = 700$ service cycles for the package, and the sixth criterion is satisfied.

Summary: The previous discussion verifies that fatigue failure of the packaging containment boundary due to normal operating cycles is not a concern, per Section III, Subsection NB, Article NB-3222.4(d) of the ASME Code. Therefore the resistance of the 1105-SD package to fatigue is adequate to ensure a minimum 25 year service life of up to 50 shipments per year.

2.1.2.3.2 Normal Vibration Over the Road

Fatigue associated with normal vibration over the road is addressed in Section 2.6.5, *Vibration*.

2.1.2.3.3 Buckling Assessment

Buckling, per Regulatory Guide 7.6, is an unacceptable failure mode for the containment vessel. The intent of this provision is to preclude large deformations that would compromise the validity of linear analysis assumptions and quasi-linear stress allowable limits, as given in Paragraph C.6 of Regulatory Guide 7.6.

Buckling investigations contained herein consider the cylindrical shell and torispherical heads of the 1105-SD package. The cylindrical shell buckling analysis is performed using the methodology of ASME B&PV Code Case N-284-2 [13]. Consistent with Regulatory Guide 7.6 philosophy, factors of safety corresponding to ASME B&PV Code, Level A and Level D service conditions are employed. For NCT (Service Level A), the factor of safety is 2.0, and for HAC (Service Level D), the factor of safety is 1.34. The torispherical head buckling analysis is performed using ASME B&PV Code, Section III, Subsection NE, Paragraph NE-3133.4(e). Buckling analysis details are provided in Section 2.6.4, *Increased External Pressure*, and Section 2.7.6, *Immersion – All Packages*. Buckling resistance to free drop impact loads is demonstrated by full scale certification test.

2.1.3 Weights and Centers of Gravity

The maximum gross weight of the 1105-SD package is 10,100 lb. The packaging component weights are summarized in Table 2.1-2. When transporting a LTSS, the center of gravity (CG) of the package is located 34.5 inches from the bottom outside surface of the external impact limiter. When transporting a shielded device, this dimension is 38.0 inches, assuming the shielded device is centered vertically inside the inner container. The mass moment of inertia of the cask about a transverse axis through the center of gravity is 7,370 in-lb-s² for LTSS transport, and 8,550 in-lb-s² for shielded device transport.

2.1.4 Identification of Codes and Standards for Package Design

The 1105-SD package is designated a Category I package. Per the guidance of NUREG/CR-3854, the appropriate design criteria for the containment is Section III, Subsection NB of the ASME B&PV Code. Consequently, the design of the containment boundary is based on the methodology of Regulatory Guide 7.6, and load cases are applied and combined according to Regulatory Guide 7.8. The closure bolts are designed using the guidance of NUREG/CR-6007.

The lodgment and the inner container are designated as "other safety" from Table 1.1 of [7], and the criteria is taken from Section III, Subsection ND of the ASME B&PV Code. For other structures such as the thermal shield, impact limiter shells, internal impact limiter components, the criteria is taken from Section III, Subsection NF of the ASME B&PV Code.

Table 2.1-1 – Containment Structure Allowable Stress Limits

Stress Category	NCT	HAC
General Primary Membrane Stress Intensity	S_m	Lesser of: $2.4S_m$ $0.7S_u$
Local Primary Membrane Stress Intensity	$1.5S_m$	Lesser of: $3.6S_m$ S_u
Primary Membrane + Bending Stress Intensity	$1.5S_m$	Lesser of: $3.6S_m$ S_u
Range of Primary + Secondary Stress Intensity	$3.0S_m$	Not Applicable
Pure Shear Stress	$0.6S_m$	$0.42S_u$
Peak	Per Section 2.1.2.3.2, <i>Fatigue Assessment</i>	
Buckling	Per Section 2.1.2.3.3, <i>Buckling Assessment</i>	
<i>Containment Fasteners:</i> ^①		
Average Tensile Stress Intensity	S_m ^②	Lesser of: S_y $0.7S_u$
Average Tensile + Average Shear + Bending + Residual Torsion Stress Intensity	$1.35S_m$ for $S_u > 100$ ksi	Not Applicable

Notes:

1. Containment fastener stress limits are in accordance with NUREG/CR-6007.
2. S_m is defined as $(2/3)S_y$ as recommended by NUREG/CR-6007.

Table 2.1-2 – 1105-SD Package Component Weights, pounds

Item	LTSS	Shielded Device
Lower body assembly (base)	2,270	2,270
Upper body assembly (bell)	2,670	2,670
Total empty package	4,940	4,940
Lodgment	500	---
LTSS	4,660	---
Inner Container + blocking	---	1,660
Shielded Device (maximum)	---	3,500
Total package (maximum)	10,100	10,100

2.2 Materials

The 1105-SD package structural components, including the external impact limiter shell and the deformable tubes of the internal impact limiters, are fabricated from Type 304 stainless steel in various product forms. The lodgment and the internal impact limiter load-bearing plates are fabricated from 6061-T6 aluminum. The inner container is fabricated from Type 304 stainless steel. Polyurethane foam is used for impact energy absorption. Other materials performing a structural function are ASTM B16 UNS C36000 brass alloy (for the test and vent port plugs), and ASTM A320, L43, alloy steel for the closure bolts. Alloy steel, stainless steel, or Nitronic 60 is used for the optional thread inserts used throughout the packaging components. The containment O-ring seal is made from butyl rubber. Plastic is used for the fire-consumable vent plugs in the foam cavities. The drawings presented in Appendix 1.3.3, *Packaging General Arrangement Drawings*, delineate the specific materials used for each 1105-SD package component.

2.2.1 Material Properties and Specifications

Table 2.2-1 through Table 2.2-6 present the mechanical properties for the structural materials used in the 1105-SD package. The density of stainless steel is 0.29 lb/in³, and Poisson's ratio is 0.31. Poisson's ratio for the alloy steel closure bolts is 0.30. The density of aluminum is 0.098 lb/in³, and Poisson's ratio is 0.33. Data is interpolated or extrapolated from the available data, as necessary, as noted in the tables.

Per drawing 3021717-SAR, Flag Note 12, the cylindrical side shell and the torispherical head of the upper body assembly are made from ASTM A240 Type 304 plate, having a minimum yield of 40 ksi and a minimum ultimate strength of 80 ksi, which are higher than the strengths shown in Table 2.2-1. The increased properties are used to develop the material model for the computer model described in Appendix 2.12.4, *Finite Element Analysis*.

The performance of the 1105-SD package in free drop and puncture events is partially dependent on the energy-absorbing performance of polyurethane foam. The foam is poured in place within the impact limiter steel shell. Nominally 15 lb/ft³ polyurethane foam is used. Section 8.1.5.1, *Polyurethane Foam* presents the details of acceptance tests for this material. The nominal, room-temperature crush properties of the polyurethane foam component are given in Table 2.2-6. Properties for both "parallel to rise" and "perpendicular to rise" are given. The "rise" direction is parallel to the force of gravity during solidification, and is oriented to be parallel to the cylindrical axis of the impact limiters.

2.2.2 Chemical, Galvanic, or Other Reactions

The materials of construction of the 1105-SD package will not have significant chemical, galvanic or other reactions in air or water environments. These materials have been previously used, without incident, in radioactive material packages for transport of similar payload materials such as the RH-TRU 72-B (NRC Docket 9212) and the BEA Research Reactor Cask (NRC Docket 9341). The polyurethane foam is fully enveloped by sheets of stainless steel and welded closed. The foam is a rigid, closed-cell (non-water absorbent) material that is free of halogens and chlorides, as discussed in Section 8.1.5.1, *Polyurethane Foam*. The lead gamma shielding in the LTSS or in the shielded devices is fully encased in a steel or stainless steel weldment and cannot be affected by water or atmospheric moisture.

The brass alloy vent port plug is very corrosion resistant. Any damage that could occur to the material is easily detectable since the fitting is handled each time the 1105-SD package is loaded and unloaded. Similarly, the alloy steel closure bolts, which are plated with corrosion-resistant nickel plating, can be readily inspected at each use for the presence of corrosion. The optional alloy steel thread inserts are plated for protection against corrosion.

The butyl elastomer that is used for the containment O-ring seals contains no corrosives that would react with or adversely affect the 1105-SD package. This material is organic in nature and noncorrosive to the stainless steel containment boundary of the 1105-SD package.

A successful RAM packaging history combined with successful use of these fabrication materials in similar industrial environments ensures that the integrity of the 1105-SD package will not be compromised by any chemical, galvanic or other reactions.

2.2.3 Effects of Radiation on Materials

The radiation associated with the source payload will have no effect on the containment or other safety components comprising the 1105-SD package. Since the payload of the 1105-SD package is heavily shielded, the radiation exposure of the package materials (including the butyl rubber containment seal) is negligible. For these reasons, there will be no deleterious radiation effects on the packaging, and the requirements of 10 CFR §71.43(d) are met.

Table 2.2-1 – Mechanical Properties of Wrought Type 304 Stainless Steel

Material Specification	Temperature (°F)	① Yield Strength, S_y (psi)	② Ultimate Strength, S_u (psi)	③ Allowable Strength, S_m (psi)	④ Elastic Modulus, E (×10⁶ psi)	⑤ Thermal Expansion Coefficient, α (×10⁻⁶ /°F)
ASTM A240 ASTM A249 ASTM A269 ASTM A276 ASTM A479 Type 304	-40	30,000	75,000	20,000	28.9	8.2
	-20	30,000	75,000	20,000	28.8	8.2
	70	30,000	75,000	20,000	28.3	8.5
	100	30,000	75,000	20,000	28.1	8.6
	200	25,000	71,000	20,000	27.5	8.9
	300	22,400	66,200	20,000	27.0	9.2
	400	20,700	64,000	18,600	26.4	9.5
	500	19,400	63,400	17,500	25.9	9.7
	600	18,400	63,400	16,600	25.3	9.9
	700	17,600	63,400	15,800	24.8	10.0
	800	16,900	62,800	15,200	24.1	10.1

Notes: ① ASME Code, Section II, Part D, Table Y-1. Value at -40 °F extrapolated using the values at -20 °F and 70 °F.

② ASME Code, Section II, Part D, Table U. Value at -40 °F extrapolated using the values at -20 °F and 70 °F.

③ ASME Code, Section II, Part D, Table 2A. Value at -40 °F extrapolated using the values at -20 °F and 70 °F.

④ ASME Code, Section II, Part D, Table TM-1, Material Group G. Values for -40 °F and -20 °F interpolated from 70 °F and -100 °F. Value at 100 °F interpolated using the values at 70 °F and 200 °F.

⑤ ASME Code, Section II, Part D, Table TE-1, Material Group 3, Mean Coefficient. Values for -40 °F and -20 °F extrapolated from 70 °F and 100 °F.

Table 2.2-2 – Mechanical Properties of Forged Type 304 Stainless Steel

Material Specification	Temperature (°F)	① Yield Strength, S_y (psi)	② Ultimate Strength, S_u (psi)	③ Allowable Strength, S_m (psi)	④ Elastic Modulus, E ($\times 10^6$ psi)	⑤ Thermal Expansion Coefficient, α ($\times 10^{-6}$ /°F)
ASTM A182 Type F304	-40	30,000	70,000	20,000	28.9	8.2
	-20	30,000	70,000	20,000	28.8	8.2
	70	30,000	70,000	20,000	28.3	8.5
	100	30,000	70,000	20,000	28.1	8.6
	200	25,000	66,300	20,000	27.5	8.9
	300	22,400	61,800	20,000	27.0	9.2
	400	20,700	59,700	18,600	26.4	9.5
	500	19,400	59,200	17,500	25.9	9.7
	600	18,400	59,200	16,600	25.3	9.9
	700	17,600	59,200	15,800	24.8	10.0
	800	16,900	58,600	15,200	24.1	10.1

Notes: ① ASME Code, Section II, Part D, Table Y-1. Value at -40 °F extrapolated using the values at -20 °F and 70 °F.

② ASME Code, Section II, Part D, Table U. Value at -40 °F extrapolated using the values at -20 °F and 70 °F.

③ ASME Code, Section II, Part D, Table 2A. Value at -40 °F extrapolated using the values at -20 °F and 70 °F.

④ ASME Code, Section II, Part D, Table TM-1, Material Group G. Values for -40 °F and -20 °F interpolated from 70 °F and -100 °F. Value at 100 °F interpolated using the values at 70 °F and 200 °F.

⑤ ASME Code, Section II, Part D, Table TE-1, Material Group 3, Mean Coefficient. Values for -40 °F and -20 °F extrapolated from 70 °F and 100 °F.

Table 2.2-3 – Mechanical Properties of ASTM A320, Grade L43 Alloy Bolting Material

Material Specification	Temperature (°F)	① Yield Strength, S_y (psi)	② Ultimate Strength, S_u (psi)	③ Allowable Strength, S_m (psi)	④ Elastic Modulus, E ($\times 10^6$ psi)	⑤ Thermal Expansion Coefficient, α ($\times 10^{-6}$ /°F)
ASTM A320 Grade L43	-40	105,000	125,000	35,000	28.3	6.2
	-20	105,000	125,000	35,000	28.2	6.3
	70	105,000	125,000	35,000	27.8	6.4
	100	105,000	125,000	35,000	27.6	6.5
	200	99,000	125,000	33,000	27.1	6.7
	300	95,700	125,000	31,900	26.7	6.9
	400	91,800	125,000	30,600	26.2	7.1
	500	88,500	125,000	29,500	25.7	7.3
	600	84,300	125,000	28,100	25.1	7.4
	700	79,200	125,000	26,400	24.6	7.6

Notes: ① ASME Code, Section II, Part D, Table Y-1. Value at -40 °F extrapolated using the values at -20 °F and 70 °F.

② ASME Code, Section III, Code Case N-249-14, Table 5, for AISI 4340 bar stock having a minimum yield strength of 105 ksi. Values at -40 °F through 70 °F extrapolated using the values at 100 °F and 200 °F.

③ ASME Code, Section II, Part D, Table 4. Value at -40 °F extrapolated using the values at -20 °F and 70 °F.

④ ASME Code, Section II, Part D, Table TM-1, Material Group B. Values for -40 °F and -20 °F interpolated from 70 °F and -100 °F. Value at 100 °F interpolated using the values at 70 °F and 200 °F.

⑤ ASME Code, Section II, Part D, Table TE-1, Material Group 1, Mean Coefficient. Values for -40 °F and -20 °F extrapolated from 70 °F and 100 °F.

Table 2.2-4 – Mechanical Properties of 6061-T6^⑤ Aluminum Alloy

Material Specification	Temperature (°F)	① Tensile Yield Strength, S_y (psi)	② Tensile Ultimate Strength, S_u (psi)	③ Elastic Modulus, E ($\times 10^6$ psi)	④ Thermal Expansion Coefficient, α ($\times 10^{-6}$ /°F)
ASTM B209 6061-T6 ^⑤	-40	35,000	42,000	10.3	11.0
	-20	35,000	42,000	10.3	11.2
	70	35,000	42,000	10.0	12.1
	100	35,000	41,400	9.9	12.4
	200	33,700	39,400	9.6	13.0
	300	27,400	31,700	9.2	13.3
	400	13,300	17,700	8.7	13.6
	450	---	---	---	13.8

Notes: ① ASME Code, Section II, Part D, Table Y-1. Value at -40 °F extrapolated using the values at -20 °F and 70 °F.

② Based on *Engineering Data for Aluminum Structures*, Section 3 of the *Aluminum Construction Manual*, The Aluminum Association, Washington, D.C., 5th Edition, 1986. Typical data for ultimate strength at temperature ($S_{u\text{-typ}}$) taken from Table 8 and reduced to expected minimum values by the ratio $S_{u\text{-min}}/S_{u\text{-typ}} = (42/45.1)$, where $S_{u\text{-min}} = 42$ ksi from Table 3 of ASME Code, Section II, Part B, SB-209, and $S_{u\text{-typ}} = 45.1$ ksi at 70 °F by interpolation from Table 8 of *Engineering Data for Aluminum Structures*. For example, since $S_{u\text{-typ}} = 42.263$ ksi at 200 °F, then $S_{u\text{-min}} = 42.263 \times (42/45.1) = 39.358$ ksi \sim 39,400 psi.

③ ASME Code, Section II, Part D, Table TM-2. Values for -40 °F and -20 °F interpolated from 70 °F and -100 °F. Value at 100 °F interpolated using the values at 70 °F and 200 °F.

④ ASME Code, Section II, Part D, Table TE-2, Mean Coefficient. Values for -40 °F and -20 °F extrapolated from 70 °F and 100 °F.

⑤ Aluminum alloy 6061 tempers T651, T6510, or T6511 may be substituted for T6, when available.

Table 2.2-5 – Mechanical Properties of Brass Material

Material	Minimum Mechanical Properties
ASTM B16, UNS C36000, Temper H02	Yield Strength, $\sigma_y = 25,000$ psi Ultimate Strength, $\sigma_u = 55,000$ psi

Table 2.2-6 – Nominal Material Properties of 15 lb/ft³ Polyurethane Foam

Property	Direction	Room Temperature Value
Compressive Strength, S	Axial (Parallel-to-Rise)	629 psi @ 10% Strain 754 psi @ 40% Strain 2,645 psi @ 70% Strain
	Radial (Perpendicular-to-Rise)	603 psi @ 10% Strain 769 psi @ 40% Strain 2,691 psi @ 70% Strain

2.3 Fabrication and Examination

2.3.1 Fabrication

The 1105-SD package is fabricated using conventional metal forming and joining techniques. All welding procedures and welding personnel must be qualified in accordance with Section IX of the ASME Boiler and Pressure Vessel Code [14]. Containment boundary welds are full penetration joints. All non-containment joints are fabricated in accordance with the requirements delineated on the drawings in Appendix 1.3.3, *Packaging General Arrangement Drawings*. The containment shell fabrication complies with the tolerance requirements of the ASME Code, Subsection NE, Article NE-4220 [15]. Article NE-4220 is selected because the package cylindrical shells are verified for HAC buckling performance using the ASME Code Case N-284-2. This Code Case is for Section III, Division 1, Class MC construction, and is based on the fabrication requirements of NE-4222, as stated in Section 1120 of the Code Case. Therefore, it is appropriate to fabricate the 1105-SD package using shell tolerances from NE-4220, rather than NB-4220.

The polyurethane foam and butyl rubber O-rings are procured using written procedures. See Section 8.1.5, *Component and Material Tests*, for details of the fabrication and performance requirements of these components.

2.3.2 Examination

Each of the materials performing a significant safety function must meet the ASTM specifications delineated on the drawings in Appendix 1.3.3, *Packaging General Arrangement Drawings*. Safety-significant materials not having an ASTM designation are controlled by means of written procedures whose requirements are summarized in Section 8.1.5, *Component and Material Tests*.

Forgings are subject to ultrasonic and liquid penetrant inspection per the ASME Code, Subsection NB, Article NB-2540 [16]. All welds are subject to visual examination per AWS D1.6 [17]. The full penetration welds utilized in the containment boundary are subject to radiographic inspection in accordance with the ASME Code, Subsection NB, Article NB-5000, and Section V, Article 2 [18] and liquid penetrant inspection on the final pass in accordance with the ASME Code, Subsection NB, Article NB-5000, and Section V, Article 6 [19]. All other welds on the packaging except seal, tack, and intermittent welds are liquid penetrant inspected on the final pass in accordance with the ASME Code, Subsection NF, Article NF-5000, and Section V, Article 6 [20]. Welds on the lodgment are subject to visual examination per AWS D1.2 [26]. Welds on the inner container are subject to visual examination per [17] and, when specified, to liquid penetrant inspection in accordance with [20].

Each 1105-SD package will also be subjected to the following tests:

- An internal pressure test, in which the containment boundary is pressurized to 125% of the design pressure per the ASME Code [21], or 150% of the MNOP, per 10 CFR §71.85(b), whichever is greater. The pressure test requirements are described in Section 8.1.3.2, *Containment Boundary Pressure Testing*.
- Containment boundary leakage rate test, which includes helium leakage rate tests of the containment boundary, the main containment O-ring seal, and the vent port containment O-ring seal. The leakage rate test requirements are described in Section 8.1.4, *Fabrication Leakage Rate Tests*.

2.4 General Standards for All Packages

This section defines the general standards for all packages. The 1105-SD package meets all requirements delineated for this section.

2.4.1 Minimum Package Size

The minimum dimension of the 1105-SD package is approximately 45 inches (the upper torispherical head thermal shield outer diameter). Thus, the 4-in. minimum requirement of 10 CFR §71.43(a) is satisfied.

2.4.2 Tamper-Indicating Feature

A tamper-indicating seal is made by passing a lock wire through a hole in two adjacent rain shield retention bolts. The wire must be destroyed in order to remove the rain shield segment, which would be necessary to access the closure bolts beneath the rain shield. Destruction of the wire provides evidence of possible tampering. Thus, the requirement of 10 CFR §71.43(b) is satisfied.

2.4.3 Positive Closure

The 1105-SD package cannot be opened unintentionally. The two rain shield segments, which are each attached using ½-inch diameter bolts, blocks access to the closure bolts and to the vent and seal test ports. Thus, the requirements of 10 CFR §71.43(c) are satisfied.

2.4.4 Valves

The containment boundary of the 1105-SD package does not contain any valves. The upper flange contains one vent port which penetrates the containment boundary and which is closed with a brass port plug. The vent port is closed and tested during pre-shipment leak testing of the 1105-SD package. The port is protected from inadvertent use or from tampering by the rain shield as described above. Thus, the requirements of 10 CFR §71.43(e) are satisfied.

2.4.5 Package Design

As shown in Chapter 2.0, *Structural Evaluation*, Chapter 3.0, *Thermal Evaluation*, and Chapter 5.0, *Shielding Evaluation*, the structural, thermal, and shielding requirements, respectively, of 10 CFR §71.43(f) are satisfied for the 1105-SD package.

2.4.6 External Temperatures

As shown in Table 3.3-1 from Section 3.3, *Thermal Evaluation for Normal Conditions of Transport*, the maximum accessible surface temperature with maximum internal decay heat load and no insolation is bounded by 122 °F. This satisfies the limit of 10 CFR §71.43(g) for non-exclusive use shipments.

2.4.7 Venting

The 1105-SD package does not include any features intended to allow continuous venting of the containment boundary during transport. Thus, the requirements of 10 CFR §71.43(h) are satisfied.

2.5 Lifting and Tie-down Standards for All Packages

2.5.1 Lifting Devices

The 1105-SD package is only lifted by means of a pallet using a fork truck. The threaded hole in the center of the upper torispherical head is not used for lifting the package, and is labeled "Bell Lift Only" (i.e., upper body assembly lift only). Since there are no lifting attachments used to lift the package that are structural parts of the package, 10 CFR §71.45(a) does not apply to the 1105-SD.

2.5.2 Tie-down Devices

During transport, the 1105-SD package rests on a pallet, and is held down to the pallet by means of flexible straps which go over the top of the impact limiter and which fasten to the conveyance or the pallet. An optional tiedown method is by means of a metal frame or brackets, which bear against the top of the impact limiter and which is fastened to the conveyance or the pallet. In either case, the tiedown loads are applied to the package through the top slanted surface of the impact limiter as shown in Figure 2.5-1. Chocks are attached to the conveyance to react lateral loads through the pallet. In this configuration, the 1105-SD contacts only the pallet on the bottom and the flexible straps or metal frame/brackets on the top of the impact limiter, and therefore has no integral tie-down devices which are a structural part of the package. Therefore, per 10 CFR §71.45(b)(1), no evaluation of tie-down devices is required.

The threaded hole in the top of the package used for lifting the upper body assembly is covered by mechanical means, such as a bolt, during transport. Thus, 10 CFR §71.45(b)(2) is satisfied.

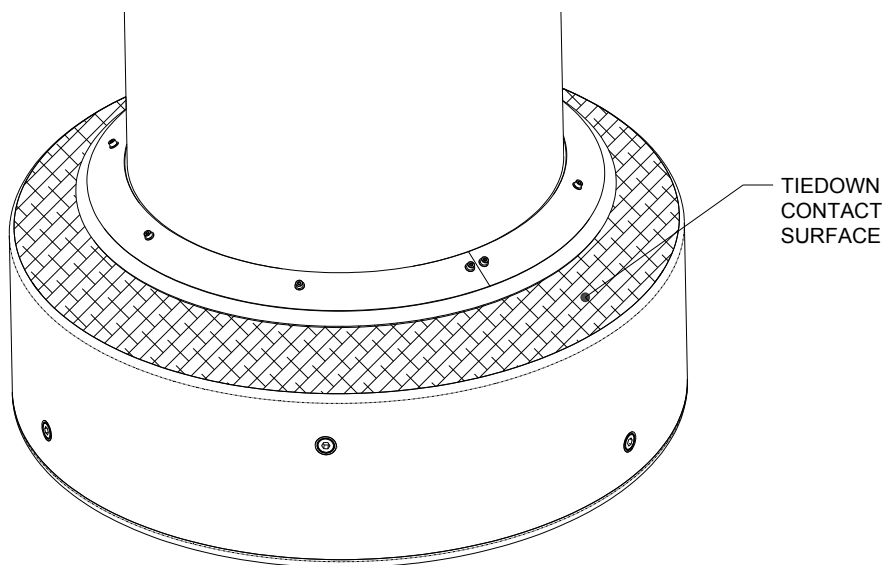


Figure 2.5-1 – 1105-SD Tiedown Contact Surface

2.6 Normal Conditions of Transport

When subjected to normal conditions of transport (NCT) as specified in 10 CFR §71.71, the 1105-SD package meets the performance requirements specified in Subpart E of 10 CFR 71. This is demonstrated in the following subsections where each NCT condition is addressed and shown to meet the applicable design criteria. Load combinations used in this section are consistent with Regulatory Guide 7.8.

2.6.1 Heat

The normal heat condition, as defined in 10 CFR §71.71(c)(1), is evaluated in Section 3.0, *Thermal Evaluation*. The bounding temperatures and pressures for use in structural analyses are summarized in the following section. Material properties and stress limits, consistent with the design criteria shown in Table 2.1-1, are summarized for the relevant bounding temperatures in Table 2.6-1.

2.6.1.1 Summary of Pressures and Temperatures

The bounding maximum temperatures for the 100 °F ambient NCT condition of the 1105-SD package are presented in Table 3.1-1 of Chapter 3, *Thermal Evaluation*. All components of the package, including the containment boundary, flanges, closure bolts, and elastomer seals, are bounded by a temperature of 200 °F. The lodgment, LTSS, inner container, and shielded device temperatures are also bounded by a value of 200 °F. The bulk average polyurethane foam in the impact limiter is bounded by a temperature of 150 °F.

The initial pressure in the package at assembly is ambient, i.e., 14.7 psia. As determined in Section 3.3.2, *Maximum Normal Operating Pressure*, the maximum normal operating pressure (MNOP) can be conservatively defined to be 5 psig. The design pressure of the 1105-SD package is 25 psig, which is significantly higher than the MNOP.

2.6.1.2 Differential Thermal Expansion

The following calculations demonstrate a positive clearance between the 1105-SD payload cavity and the lodgment, conservatively neglecting the expansion of the payload cavity itself. Since the coefficient of thermal expansion of aluminum (used for the lodgment) is significantly greater than that of stainless steel (used for the inner container), and since the lodgment and inner container have the same bounding dimensions and tolerances, the clearances applicable to the lodgment bound those that would occur when using the inner container.

The payload cavity has a nominal length of 60.30 inches with a tolerance of ± 0.25 inches, giving a minimum length of 60.05 inches. The lodgment has a nominal length of 59.50 inches with a tolerance of ± 0.25 inches, giving a maximum length of 59.75 inches, for a minimum room temperature axial clearance of 0.3 inches. The length of the lodgment at the NCT warm case temperature of 200 °F is:

$$L = 59.75[1 + \alpha(200 - 70)] = 59.85 \text{ inches}$$

where the coefficient of thermal expansion for the aluminum lodgment, $\alpha = 13.0(10^{-6})$ in/in/°F from Table 2.2-4, and the reference temperature is 70 °F. The increase in length of the lodgment

is therefore $59.85 - 59.75 = 0.1$ inches. The minimum axial clearance, conservatively neglecting any expansion of the payload cavity length, is:

$$CLR_{axial} = 0.3 - 0.1 = 0.2 \text{ inches}$$

The payload cavity has a nominal inner diameter of 43.5 inches with a tolerance of ± 0.3 inches, giving a minimum diameter of 43.2 inches. The lodgment has a nominal diameter of 42.75 inches with a tolerance of ± 0.12 inches, giving a maximum diameter of 42.87 inches, for a minimum room temperature diametral clearance of 0.33 inches. The diameter of the lodgment at the NCT warm case temperature of 200 °F is:

$$L = 42.87[1 + \alpha(200 - 70)] = 42.94 \text{ inches}$$

where α is defined above. The increase in diameter of the lodgment is therefore $42.94 - 42.87 = 0.07$ inches. The minimum diametral clearance, conservatively neglecting any expansion of the payload cavity diameter (which would be of a similar magnitude to that of the lodgment), is:

$$CLR_{diametral} = 0.33 - 0.07 = 0.26 \text{ inches}$$

Thus, clearance is maintained at the maximum NCT warm temperature.

2.6.1.3 Stress Calculations

2.6.1.3.1 Stresses Due to Pressure Loading

The stress in the torispherical heads due to the design pressure is found from the ASME Code, Section VIII, Subsection UG-32(e) [33]. This paragraph is applicable since $t/L = 0.011 > 0.002$, where the thickness of the head, $t = 0.5$ inches, and the inside crown radius, $L = 43.5$ inches. Further, the inside knuckle radius, $r = 3.5$ inches, is over 6% of the inside crown radius ($r/L \times 100 = 8.0\%$).

The formula given in the code is:

$$t = \frac{0.885PL}{SE - 0.1P}$$

where P is the internal design pressure, equal to 25 psi, E is the joint efficiency, which for a full penetration, radiographed joint as used in the containment of the 1105-SD is equal to unity as specified in Subsection UW-12, and S is the maximum allowable stress. Solving this relation for the stress:

$$S = \frac{P(0.885L + 0.1t)}{Et} = 1,927 \text{ psi}$$

For the cylindrical sidewall of the containment, the stress is:

$$S_c = \frac{Pr_{avg}}{t_c} = 1,100 \text{ psi}$$

where $r_{avg} = 22.0$ inches is the meridional radius of the shell, and $t_c = 0.5$ inches. The bounding stress in the containment is therefore 1,927 psi in the upper or lower torispherical head.

2.6.1.3.2 Stresses Due to Thermal Loading

Since the 1105-SD package has a simple pressure vessel design, having relatively modest temperature gradients (see Figure 3.3-1 and Figure 3.3-3) and no significant restraints against thermal expansion, the thermal stresses due to NCT temperatures will not be significant, and are not specifically evaluated.

2.6.1.4 Comparison with Allowable Stresses

The bounding stress in the torispherical head determined above will be conservatively compared to the minimum, i.e., the membrane allowable stress. From Table 2.1-1, the limit on primary membrane stress is S_m . At the bounding temperature of 200 °F given in Section 2.6.1.1, *Summary of Pressures and Temperatures*, the value of S_m for Type 304 is 20,000 psi from Table 2.6-1. Applying this limit to the bounding stress intensity of 1,927 psi calculated for the torispherical head, the margin of safety is:

$$MS = \frac{20,000}{1,927} - 1 = +9.4$$

Thus, the margin of safety for the NCT warm condition is large.

2.6.1.5 Closure Bolts

Twenty-four closure bolts attach the upper body assembly to the lower body assembly. The closure joint is sized such that support against lateral loads (i.e., loads in the plane of the joint) is obtained from the radial bearing between the flanges, thus preventing any shear loading of the closure bolts.

The closure bolts are tightened to 300 ± 30 ft-lb of torque, or a maximum of 330 ft-lb. From Section 4.2 of [10], the maximum non-prying tensile force per bolt due to the preload, F_{a_max} , is found from:

$$F_{a_max} = \frac{Q_{max}}{(K)(D_b)} = 21,120 \text{ lb}$$

where $Q_{max} = 330 \times 12 = 3,960$ in-lb is the maximum bolt torque, $K = 0.15$ is the nut factor for a lubricated bolt (approximately equal to the average of the values for lubricated surfaces in Table 4.1 of [10]), and $D_b = 1.25$ inches is the nominal diameter of the closure bolt. The maximum residual torsion is 50% of the applied torsion, or:

$$M_{tr} = 0.5(Q_{max}) = 1,980 \text{ in} - \text{lb}$$

From Section 4.4 of [10], the maximum non-prying tensile force per bolt, F_{a_max} , due to pressure loads are:

$$F_{a_max} = \frac{\pi D_l g^2 (P_{li} - P_{lo})}{4 N_b} = 2,787 \text{ lb}$$

where $D_l g = 48.5$ inches is the diameter of the pressure boundary, which for convenience is conservatively taken as equal to the bolt circle, $P_{li} = 25 \text{ psig} + 14.7 \text{ psia} = 39.7 \text{ psia}$ is the internal pressure, $P_{lo} = 3.5 \text{ psia}$ is the NCT cold external reduced pressure from Section 2.6.3, *Reduced External Pressure*, and $N_b = 24$ is the quantity of closure bolts. From this it is clear that the preload force is governing over the pressure force.

Even though the temperatures of the closure joint and the bolts are the same, a thermally induced loading is applied to the closure bolts due to the difference in thermal expansion coefficient between the ASTM A320 L43 alloy steel closure bolts and the Type 304 stainless steel closure flange. From Section 4.5 of [10], the maximum non-prying tensile force due to thermal expansion effects is:

$$F_a = \frac{\pi}{4} D_b^2 (E_b) [a_l(T_l) - a_b(T_b)] = 9,511 \text{ lb}$$

where the modulus of elasticity of the bolt, $E_b = 27.1(10^6)$ psi, the thermal expansion coefficient of the closure joint, $a_l = 8.9(10^{-6})$ in/in/°F, and the thermal expansion coefficient of the bolt, $a_b = 6.7(10^{-6})$ in/in/°F, all from Table 2.6-1. The change in temperature of both components, $T_l = T_b = (200 - 70) = 130$ °F, where the bounding temperature of the components is 200 °F, and the ambient temperature is 70 °F.

The maximum stress in the bolt occurs in the shank, which is necked down to a value of 1.09 inches (slightly below the thread root diameter). The area of the shank is:

$$A_{sh} = \frac{\pi}{4} (1.09^2) = 0.933 \text{ in}^2$$

The average axial bolt stress corresponding to these loadings is:

$$S_{ba} = \frac{(21,120 + 9,511)}{A_{sh}} = 32,831 \text{ psi}$$

where the load term in the numerator is the sum of the preload and thermal loads. The residual torsional stress is:

$$S_{bt} = \frac{(M_{tr})c}{J} = 7,763 \text{ psi}$$

where J is the torsional moment of inertia and c is the shank radius, equal to:

$$J = \frac{\pi(1.09^4)}{32} = 0.139 \text{ in}^4 \quad c = 1.09/2 = 0.545 \text{ in}$$

From Table 2.1-1, for NCT the allowable average tensile stress is $S_m = (2/3)S_y$, which from Table 2.6-1 is equal to 66,000 psi at the NCT hot temperature of 200 °F. The margin of safety is:

$$MS_{S_{ba}} = \frac{66,000}{S_{ba}} - 1 = +1.01$$

Combining the axial and residual torsional shear stresses, the maximum closure bolt stress intensity is:

$$S_{bi} = \sqrt{S_{ba}^2 + 4S_{bt}^2} = 36,317 \text{ psi}$$

From Table 2.1-1, the allowable stress intensity is $1.35S_m$ for cases where S_y is greater than 100 ksi. The margin of safety is:

$$MS_{S_{bi}} = \frac{1.35(66,000)}{S_{bi}} - 1 = +1.45$$

Thus the closure bolts are not of concern for the NCT warm condition, including the reduced external pressure load case.

2.6.2 Cold

For the cold condition, a -40 °F steady state ambient temperature is utilized per Regulatory Guide 7.8 [3], with zero insolation and zero decay heat. This results in a uniform temperature of -40 °F throughout the cask. The materials of construction for the 1105-SD package are not adversely affected by the -40 °F condition, including brittle fracture, which is evaluated in Section 2.1.2.3.1, *Brittle Fracture*.

Since the coefficient of thermal expansion of the flange material is slightly larger than that of the bolting material, a reduction in closure bolt preload will occur at the NCT cold condition. Using the terminology of [10], the reduction in preload is:

$$F_a = \frac{\pi}{4} D_b^2 (E_b) [a_f(T_f) - a_b(T_b)] = -7,640 \text{ lb}$$

where the bolt nominal diameter, $D_b = 1.25$ inches, the bolt modulus of elasticity, $E_b = 28.3(10^6)$ psi, the coefficient of thermal expansion of the flange material, $a_f = 8.2(10^{-6})$ in/in/°F for Type 304 stainless steel, the coefficient of thermal expansion of the bolt material, $a_b = 6.2(10^{-6})$ in/in/°F for A320 L43 alloy steel, and $T_f = T_b = -40 - 70 = -110$ °F. The material properties are taken from Table 2.6-1. The minimum bolt preload torque is 300 ft-lb minus 30 ft-lb, or $Q_{\min} = 3,240$ in-lb. The minimum bolt preload force is:

$$F_{a_min} = \frac{Q_{\min}}{K(D_b)} = 17,280 \text{ lb}$$

where D_b is defined above and $K = 0.15$, consistent with the definition in Section 2.6.1.5, *Closure Bolts*. Accounting for differential thermal expansion, the remaining preload is $17,280 - 7,640 = 9,640$ lb.

As shown in Section 2.6.5, *Vibration*, a loading in the vertical (i.e., axial) direction of $\pm 2g$ can result from transportation vibration. From Table 2.1-2, the weight of the upper body assembly (bell) is 2,670 lb. Thus, to keep the bell seated on the lower flange (and the containment seal properly compressed), the sum of preload forces in the closure bolts must be at least equal to the upward vertical vibration load on the bell of $2,670 \times 2 = 5,340$ lb. Since there are 24 closure bolts, each bolt needs to have a minimum preload of $5,340 / 24 = 222.5$ lb. Since the remaining preload in the -40 °F case is 9,640 lb per bolt, the margin of safety is:

$$MS = \frac{9,640}{222.5} - 1 = +42.3$$

Thus the remaining preload force per bolt is adequate to maintain the joint and containment seal in a closed and leak tight configuration for the 10 CFR §71.71(c)(2) Cold condition.

2.6.3 Reduced External Pressure

The effect of reduced external pressure of 3.5 psia, per 10 CFR §71.71(c)(3), is considered negligible for the 1105-SD package compared to other design loadings. This conclusion is based on the NCT structural analyses presented in Section 2.6.1, *Heat*, demonstrating the structural

integrity for a 25 psig internal design pressure. Based on the Maximum Normal Operating Pressure (MNOP) of 5 psig, the reduced external pressure conditions would cause a pressure of 16.2 psig. Therefore, the 25 psig internal design pressure analysis is conservatively bounding for the reduced external pressure case.

2.6.4 Increased External Pressure

The effect of an increased external pressure of 20 psia, per 10 CFR §71.71(c)(4), is acceptable for the 1105-SD package. Consistent with Regulatory Guide 7.8, this loading corresponds to an ambient temperature of -20 °F, no insolation, no decay heat, and minimum internal pressure.

As stated in Chapter 7, *Package Operations*, at the time of shipment, the package cavity is backfilled to a pressure of approximately one atmosphere, or 14.7 psia. Since the cask is closed under ambient conditions, the internal pressure in the cask at a temperature of -20 °F is

$$p_i = p_{amb} \frac{(-20 + 460)}{(70 + 460)} = 12.2 \text{ psia}$$

where p_{amb} is 14.7 psia. Therefore the net external differential gas pressure $p_o = 20 - 12.2 = 7.8$ psi. The compressive hoop stress is:

$$\sigma_\theta = p_o \frac{r_{avg}}{t} = 343 \text{ psi}$$

where the meridional radius, $r_{avg} = 22.0$ inches and the wall thickness, $t = 0.5$ inches. It is evident from this small resultant that a significant state of stress will not occur from the increased external pressure case. In addition, the package is subjected to an external pressure differential of a full atmosphere (14.7 psi) during the fabrication verification leakage rate testing (see Section 8.1.4, *Fabrication Leakage Rate Tests*) and at maintenance intervals (see Section 8.2.2, *Maintenance/Periodic Leakage Rate Tests*), without evidence of buckling or distortion. The factor of safety on buckling is therefore at least equal to $14.7/7.8 = 1.9$. The actual factor of safety is much higher than 2.0 since the package is routinely subjected to a full vacuum without imminent risk of buckling. This is consistent with the factor of safety recommended in [13] for NCT. Thus, the increased external pressure load case is not of concern for the 1105-SD package.

2.6.5 Vibration

The effects of vibration normally incident to transport are shown to be insignificant. Draft ANSI Standard N14.23 [23] identifies peak truck trailer vibration inputs. Table 2 of [23] shows peak vibration accelerations of a trailer bed as a function of package and tiedown system natural frequency. For the frequency range 0 to 5 Hz, and conservatively assuming a light package, Table 2 gives peak accelerations (99% level) of 2g in the vertical direction, and 0.1g in both the lateral and longitudinal directions. All other frequency ranges give significantly lower acceleration levels. Due to cask symmetry, the vertical load of $\pm 2g$ governs the $\pm 0.1g$ in the lateral and longitudinal directions.

Design fatigue curves are taken from Figure I-9.2 and Table I-9.2 of [12] for the Type 304 stainless steel cask material, from which the allowable amplitude, S_a , of the alternating stress component (1/2 of the alternating stress range) as a function of number of loading cycles may be obtained. The allowable amplitude, S_a at the fatigue limit, which is used in the fatigue

1105-SD Package Safety Analysis Report

assessment of transportation vibration, is 13,600 psi from Table I-9.2 for Type 304 stainless steel cask material at 10^{11} cycles. This value is adjusted based on the ratio of room temperature elastic modulus of $28.3(10)^6$ psi, which is the basis for Table I-9.2, and the elastic modulus at NCT maximum temperature, as follows:

$$S_a = 13,600 \left[\frac{27.5(10^6)}{28.3(10^6)} \right] = 13,216 \text{ psi}$$

where $27.5(10^6)$ psi is the elastic modulus at the bounding temperature of 200 °F from Table 2.6-1.

The 1105-SD package is transported vertically. In this orientation, the upper torispherical head experiences the $\pm 2g$ loading as a transverse load (i.e., along the package axis). Conservatively, the head will be evaluated as a simply supported flat plate having the same mass. This representation has much less transverse stiffness and results in larger vibrational stress than would occur in the actual head. The weight of the head, including the crown, knuckle, and lifting boss, is bounded by $W = 310$ lb. The diameter of the plate is equal to the outside diameter of the head skirt of 44.5 inches, or $a = 44.5/2 = 22.25$ inches. The projected area of the plate is thus

$$A = \pi a^2 = 1,555.3 \text{ in}^2$$

Under a load of $2g$, the maximum bending moment in the plate (at the center) is found from Table 24, Case 10a of [24], and is:

$$M = 2K_M q a^2 = 40.8 \text{ in} - \text{lb} / \text{in}$$

where the factor 2 is the vibrational load, $K_M = 0.20625$ for $r_o = 0$ from [24], the plate radius, a , is defined above, and q is the 1-g plate loading, equivalent to a pressure, found from:

$$q = \frac{W}{A} = 0.2 \text{ psi}$$

where W and A are defined above. The stress in the flat head is:

$$\sigma = \frac{6M}{t^2} = 979.2 \text{ psi}$$

where the thickness of the head, $t = 0.5$ inches. For the allowable amplitude, S_a , found above, equal to 13,216 psi, the margin of safety against fatigue of the torispherical head due to vibration is:

$$MS = \frac{13,216}{979.2} - 1 = +12.5$$

Therefore, fatigue of the 1105-SD package due to transportation vibration is not of concern.

2.6.6 Water Spray

The materials of construction used in the 1105-SD package are not affected by the water spray test identified in 10 CFR §71.71(c)(6).

2.6.7 Free Drop

Section 10 CFR §71.71(c)(7) specifies a free drop from a height of 4 ft for a package weight less than 11,000 lb. As discussed in Appendix 2.12.2, *Certification Test Plan*, each HAC, 30-ft free drop was preceded by a NCT, 4-ft free drop in the same orientation and impact location, and performed at the same worst-case temperatures as the HAC free drop. Because the NCT and HAC free drops were identical (except for the drop height), the damage resulting from any NCT free drop was similar to the corresponding HAC damage, except having a significantly lesser magnitude. The damage resulting from the bounding HAC free drops is described and illustrated by photographs in Appendix 2.12.3, *Certification Test Results*. The impact magnitudes of the NCT and HAC free drops, as recorded by active accelerometers, is given in Appendix 2.12.3. Since the packaging containment was leaktight per the requirements of [3] after each full sequence of NCT free drop, HAC free drop, and HAC puncture drop, then the packaging was leaktight following all NCT free drops. Thus, the effects of the damage resulting from the NCT free drop is demonstrated not to affect the ability of the 1105-SD package to meet the HAC requirements of 10 CFR §71.73.

2.6.8 Corner Drop

The 1105-SD package is not required to be evaluated for the corner drop condition, since 10 CFR §71.71(c)(8) applies only to rectangular fiberboard or wood packages weighing less than 110 lb or to cylindrical fiberboard or wood packages weighing less than 220 lb. The weight of the 1105-SD package exceeds these limits and therefore does not need to be evaluated for the NCT corner drop.

2.6.9 Compression

Section 10 CFR §71.71(c)(9) specifies, for packages weighing up to 11,000 lb, a compression loading equal to the greater of the equivalent of five times the package weight or 2 lb/in^2 over the package projected area. Since the 1105-SD weighs 10,100 lb, five times the package weight is $W = 50,500 \text{ lb}$. The projected area of the head thermal shield, having an outer diameter of 44.9 inches, is $A = 1,583 \text{ in}^2$. The resulting pressure, $W/A = 31.9 \text{ psi}$. This is greater than 2 psi and is thus required to be used for this evaluation.

As shown in Section 2.7.6, *Immersion – All Packages*, the maximum pressure loading which may be applied to the head per ASME B&PV Code, Section III, Subsection NE-3133.4(e) (before application of the factor of 1.5 for HAC) is 92.0 psi. Since this pressure is nearly three times the bounding compression loading determined above, the compression load on the 1105-SD package is not of concern.

2.6.10 Penetration

Section 10 CFR §71.71(c)(10) requires the impact of the hemispherical end of a vertical steel cylinder having a 1.25-inch diameter and 13 lb mass, dropped from a height of 40 inches onto the exposed surface of the package that is expected to be most vulnerable to puncture. This test was not performed in lieu of the much more demanding HAC puncture tests which were performed as documented in Appendix 2.12.3, *Certification Test Results*. In the HAC puncture tests, a far greater amount of energy was applied to the package, based on the package weight compared to the 13 lb cylinder. The radius of the HAC puncture bar (0.25 inches maximum) is also significantly more damaging than the 0.63-inch radius of the penetration test bar. As

documented in Appendix 2.12.3, HAC puncture tests were performed on the package side, the package upper head, the impact limiter shell, and on the rain shield. Subsequent to all of these tests, the containment boundary was shown by test to remain leak tight per ANSI N14.5. The penetration bar of 10 CFR §71.71(c)(10) could impart only a very small fraction of the damage that was imparted by the HAC puncture test. This same demonstration approach has been used in other safety analysis reports, including the TRUPACT-II (NRC Docket 71-9218) and the MFFP (NRC Docket 71-9295). Therefore, the penetration test has no significant effect on the package.

Table 2.6-1 – Summary of NCT Design Parameters

Parameter	Containment (Type 304)	Closure Bolts (A320, Grade L43)
NCT Hot Bounding Temperature, °F	200	200
Coefficient of Thermal Expansion, α , (in/in/°F)	8.9×10^{-6}	6.7×10^{-6}
Elastic Modulus, psi	27.5×10^6	27.1×10^6
Design Stress, S_m , psi	20,000	66,000
Yield Stress, S_y , psi	25,000	99,000
Primary Membrane Stress Intensity (P_m), psi	$S_m = 20,000$	n/a*
Primary Membrane + Bending Stress Intensity ($P_m + P_b$), psi	$1.5S_m = 30,000$	n/a*
Primary Membrane + Bending + Secondary Stress Intensity ($P_m + P_b + Q$), psi	$3.0S_m = 60,000$	n/a*
NCT Cold Bounding Temperature, °F	-40	-40
Coefficient of Thermal Expansion, α , (in/in/°F)	8.2×10^{-6}	6.2×10^{-6}
Elastic Modulus, psi	28.9×10^6	28.3×10^6

* Bolting allowable stresses are discussed in the sections where they are used.

2.7 Hypothetical Accident Conditions

When subjected to the hypothetical accident conditions (HAC) as specified in 10 CFR §71.73 [1], the 1105-SD package meets the performance requirements specified in Subpart E of 10 CFR 71. The method of demonstration is primarily by full-scale test of the 435-B package (see Section 2.7.1.2, *Certification Test Units and Test Conditions*.) Analysis is used for all NCT except the NCT free drop, for the HAC immersion case, and to evaluate free drop orientations not tested. Three certification test units (CTUs) were used to perform a total of six, NCT 4-ft free drops, six, HAC 30-ft free drops, and seven, HAC puncture drops. The test program confirms that the 1105-SD containment boundary remains leaktight following a worst case HAC sequence. Deformations that could affect thermal performance are included in Chapter 3, *Thermal Analysis*. Detailed information is provided in Appendix 2.12.3, *Certification Test Results* and summarized in Section 2.7.8, *Summary of Damage*. A detailed discussion of the basis of the structural certification testing performed is provided in Appendix 2.12.2, *Certification Test Plan*.

2.7.1 Free Drop

Subpart F of 10 CFR 71 requires that a 30 ft free drop be considered. The free drop is to occur onto a flat, essentially unyielding, horizontal surface, and the cask is to strike the surface in an orientation for which maximum damage is expected. Several impact orientations and bounding ambient environments are considered. Because the NCT free drop height of 4 ft is over 13% of the HAC free drop height of 30 ft, the damage caused by the NCT free drop is explicitly considered. To maximize the accumulation of damage between the NCT and HAC free drops, each HAC free drop was preceded by a NCT free drop using the same orientation and impact location.

2.7.1.1 Technical Basis for the Free Drops

In order to determine the worst case free drop orientation, a consideration of the features of the package that could be vulnerable to damage in a free drop event was made. Components of the packaging could experience potentially significant damage as follows:

1. Closure joint, including structural deformation making the O-ring ineffective as well as impact limiter damage leading to excessive O-ring temperature in the fire.

Free drop impact could impart significant structural loading to the closure joint bolts. Local puncture deformation could cause leakage of the joint. Inside-out deformation from a failure of the lodgment to control the LTSS (or a failure of the inner container to control the shielded device) could cause deformation in the joint. Puncture bar damage near the joint could lead to excessive O-ring temperatures in the fire event.
2. Containment boundary, either from excessive strains in the free drop impact or from the subsequent puncture.
3. Lodgment, whether from a failure to keep the LTSS from gross movement or from causing internal damage to the containment.
4. LTSS (or shielded device), by suffering damage from interaction with the lodgment (or inner container) that could reduce its shielding function.

5. Inner container, from a failure to keep the dummy device from causing internal damage to the containment.

Computer modeling is used to guide the selection of worst-case orientations. As shown in Appendix 2.12.4, *Finite Element Analysis*, and in Figure 2.12.4-43 for impact results, Figure 2.12.4-45 for foam crush results, and Figure 2.12.4-46 for containment boundary strain results, the worst case free drop orientations are as follows:

- The highest overall impact load is for the bottom-down orientation. This impact orientation applies bounding loads in the axial direction to the closure flange, to the attachment between the impact limiter and the lower flange, and to the LTSS and lodgment or to the shielded device and inner container.
- The highest lateral impact load is for the side orientation (simultaneous at each end). This impact orientation applies bounding loads in the lateral direction to the closure and to the LTSS and lodgment or to the shielded device and inner container.
- The minimum remaining polyurethane foam after crush deformation is for the side orientation. When combined with a puncture drop, this represents a possible governing case for the HAC fire event.
- The largest value of strain in the containment boundary material is essentially for the CG over knuckle orientation (head down, 63° from horizontal). It is noted from Figure 2.12.4-46 that the 70° from horizontal case exhibits slightly more strain than the CG over knuckle (32.3% vs. 31.0%). However, this difference ($\Delta 1.3\%$ strain) is very small, and the CG over knuckle orientation will apply the full drop energy into the package as a whole. Furthermore, the strain will be maximized by applying a puncture drop in the same location.

A more detailed discussion of the free drop orientations which were considered, including orientations that are not governing, is given in Section 2.12.2.3.1, *Free Drops*. The free drops actually performed were distributed across the three CTUs to avoid overtesting a single test unit. The tests performed and the justification for choosing them is detailed in Section 2.12.2.4, *Summary of Certification Tests*, summarized in Table 2.12.2-1, and depicted in Figure 2.12.2-1.

2.7.1.2 Certification Test Units and Test Conditions

The 1105-SD packaging is identical to the 435-B packaging documented in 435-B SAR Revision 4.3 (corresponding to NRC CoC USA/9355/B(U)-96, Revision 2). Thus, results obtained from the testing of the 435-B are fully applicable to the 1105-SD. Each of the CTUs was an essentially prototypic representation, in full scale, of the 435-B packaging. Any differences between them and the drawings of the 1105-SD packaging in Appendix 1.3.3, *Packaging General Arrangement Drawings*, are not material, and are discussed and justified in Section 2.12.3.3, *Certification Test Unit Configuration*. CTU #1 and #2 contained a prototypic representation of the LTSS and lodgment, and CTU #3 contained an inner container and blocking, and a simulated, representative shielded device called the dummy payload. CTU #1 was tested with the polyurethane foam energy-absorbing material at cold temperature, in order to evaluate the effects of the maximum impact magnitude on the packaging and on the LTSS and lodgment. CTU #3 was also tested at cold temperature to evaluate the effects of the maximum impact magnitude on the ability of the inner container to control and protect the shielded device. One test sequence on CTU #2 was tested with the polyurethane foam at warm temperature, in

order to evaluate the maximum crush deformation and the related thermal consequences, and the other test sequence on CTU #2 was performed at ambient temperature, since foam was not relevant to that test. The cold test foam, at a temperature of 0 °F or below, accurately simulated the stress-strain behavior of the prototypic foam at a temperature of -40 °F, as described in Section 2.12.3.3, *Certification Test Unit Configuration*. The low temperature of -40 °F was chosen instead of the less conservative temperature of -20 °F in order to establish the compliance of the tests with the cold environment temperature required by [27]. The warm test foam, at a temperature of 110 °F or above, approached the stress-strain behavior of the prototypic foam at the bulk average NCT hot temperature of 150 °F. Since the test foam at the test temperature was slightly stronger than the minimum-strength prototypic foam, a small adjustment to the maximum test crush deformation is made in Section 2.7.1.5, *Results of Free Drops Evaluated by Finite Element Analysis*. Each free drop test was instrumented with active accelerometers. Refer to Section 2.12.3.2, *Test Facilities and Instrumentation*, for further detail.

2.7.1.3 Acceptance Criteria

The acceptance criteria for the free drop tests (including the subsequent puncture drop tests) is given in Section 2.12.2.5, *Acceptance Criteria*. Discussion of the test results relative to the acceptance criteria is given in Section 2.7.8, *Summary of Damage*.

2.7.1.4 Summary of the Results of the Free Drop Tests

The damage resulting from the free drop tests is summarized below, with further details and photographs given in Appendix 2.12.3, *Certification Test Results*. The principal test criterion is that, after the worst-case sequence of NCT free drop, HAC free drop, and puncture drop, the containment boundary is leaktight per the requirements of [4]. After each test sequence (or pair of test sequences), a helium leakage rate test was performed on the containment boundary penetrations, i.e., on the containment O-ring seal and on the vent port sealing washer. In each case, the seals were leak tight. At the conclusion of all testing, each containment boundary was helium leakage rate tested, and the results were leak tight.

The lodgment holding the LTSS suffered negligible damage from any of the free drops, and the position of the LTSS inside the package was essentially unchanged. The LTSS did not experience any lead slump or damage to the closure doors, thus ensuring that the radioactive sources will stay in position relative to the lead shielding.

A discussion of the shielded device payload and the inner container is given in Section 2.7.1.6, *Structural Evaluation of the Shielded Devices*.

2.7.1.4.1 Test Series D1 (Free Drops D1N and D1H)

Test Series D1 was performed on CTU #1 and consisted of a free drop in the bottom-down orientation, with the axis vertical, followed by an oblique puncture drop test (P1) on the flat bottom of the impact limiter. The polyurethane foam was chilled to a temperature of approximately -10 °F. The averaged impact acceleration is given in Table 2.7-1. Deformation of the external packaging structures from either of these tests was negligible. Internally, the lower internal impact limiter crushed approximately 1.43 inches (total from both drops). The weld connecting the impact limiter to the lower flange showed no cracking or failure. Other than some damage to the toggle clamps that secure the LTSS in position, there was no material

damage to the lodgment. There was no apparent damage to the LTSS. More detail is given in Section 2.12.3.4.1, *Test Series D1*.

2.7.1.4.2 Test Series D2 (Free Drops D2N and D2H)

Test Series D2 was performed on CTU #1 and consisted of a free drop on the side of the package, with the upper torispherical knuckle and the top edge of the impact limiter contacting the ground simultaneously, followed by a puncture near to the upper knuckle free drop damage (P2). The test reused all of the same components from Test Series D1. The polyurethane foam was chilled to a temperature of approximately -9 °F. The averaged impact acceleration is given in Table 2.7-1. The deformation consisted of flat spots on the knuckle and on the impact limiter. The foam impact limiter crush equaled 4.27 inches perpendicular to the ground. The internal impact limiters did not crush significantly. The upper internal limiter aluminum plate was somewhat buckled due to the deformation that occurred in the knuckle region. There was further damage to the toggle clamps, but the lodgment damage was negligible, and the LTSS was still in its original location. The only change to the LTSS configuration was faintly visible deformations on the impact side, approximately 1/8 inches deep, that corresponded to the circular rings of the lodgment. (Since the shielding analysis conservatively considers a 0.3-inch gap between the LTSS steel shell and the lead, this dent has no effect on the calculated dose rate). The containment wall was also deformed locally approximately 1/8 inches toward the ground due to the weight of the payload in the impact. More detail is given in Section 2.12.3.4.3, *Test Series D2*.

2.7.1.4.3 Test Series D3 (Free Drops D3N and D3H)

Test Series D3 was performed on CTU #2 and consisted of a free drop in the CG-over-top knuckle orientation, followed by a puncture on the damage, in the same orientation (P3). The test used a new lodgment, but the same LTSS. The polyurethane foam did not participate in the impact and was therefore left at ambient temperature. The averaged impact acceleration is given in Table 2.7-1. The deformation consisted of a flat on the top end, biased toward one side. The package was not opened until following Test Series D4. Discussion of the internal configuration will be deferred to the following section. More detail is given in Section 2.12.3.4.4, *Test Series D3*.

2.7.1.4.4 Test Series D4 (Free Drops D4N and D4H)

Test Series D4 was performed on CTU #2 and consisted of a simultaneous side drop (the same as Test Series D2), followed by a puncture drop on the foam impact limiter deformed surface (P4). For D4, the vent port was located nearest the ground. The polyurethane foam was warmed to a core temperature of approximately 117 °F. The averaged impact acceleration is given in Table 2.7-1. The deformation consisted of flat spots on the knuckle and on the impact limiter. The foam impact limiter crush equaled 4.68 inches perpendicular to the ground. The upper internal impact limiter was crushed in the region of the D3 free drops, but the lodgment did not move significantly in an axial direction. The lodgment plates that were nearest to the D3 impact showed some very local buckling, but global damage to the lodgment was negligible, and the LTSS remained in its original position. Further damage to the LTSS was negligible. Note that the LTSS experienced four complete test series without material damage. More detail is given in Section 2.12.3.4.6, *Test Series D4*.

2.7.1.4.5 Test Series D5 (Free Drops D5N and D5H)

Test Series D5 was performed on CTU #3 and consisted of a free drop in the bottom-down orientation, with the axis vertical (identical to Test Series D1), followed by an oblique puncture drop test (P6) on the flat bottom of the impact limiter. The polyurethane foam was chilled to a temperature of approximately -5 °F. The averaged impact acceleration is given in Table 2.7-1. Deformation of the external packaging structures from either of these tests, as for the case of Test Series D1, was negligible. Crush of the lower internal impact limiter was limited. The bottom structure of the inner container deformed downward 0.9 inches. The wood dunnage inside the inner container crushed by the dummy payload. More detail is given in Section 2.12.3.4.2, *Test Series D5*.

2.7.1.4.6 Test Series D6 (Free Drops D6N and D6H)

Test Series D6 was performed on CTU #3 and consisted of a simultaneous side drop (the same as Test Series D2), followed by a puncture drop on the prototypic side thermal shield (P7) and a second puncture drop on the rain shield/tube sheet region (P5). The polyurethane foam was chilled to a temperature of approximately -3 °F. The averaged impact acceleration is given in Table 2.7-1. The deformation consisted of flat spots on the knuckle and on the impact limiter. The foam impact limiter crush equaled 3.04 inches perpendicular to the ground. The damage to the package was very similar to that sustained by CTU #1 from Test Series D2. More detail is given in Section 2.12.3.4.5, *Test Series D6*.

2.7.1.5 Results of Free Drops Evaluated by Finite Element Analysis

As discussed in Appendix 2.12.4, *Finite Element Analysis*, The results of the certification tests were used to benchmark the LS-Dyna finite element model that had been developed during the test planning stage. The benchmarking criteria were primarily measured impact acceleration and deformation. Subsequently, the model was used to perform structural evaluations that were not part of the certification testing.

2.7.1.5.1 Maximum Closure Bolt Stress

As shown in Section 2.12.4.5.2, *Slapdown Free Drop Results*, the maximum load in any closure bolt occurs for the near-vertical, bottom-down drop orientation with the cask axis at an angle of 75° from the horizontal. This orientation was not tested and is consequently evaluated using the benchmarked finite element analysis model. The resulting bolt load depends on the location of the CG of the payload. Of the two payload types (LTSS/lodgment or inner container/shielded device), the CG is highest for the inner container, since the CG of the LTSS is located below the mid-height of the lodgment, whereas the device CG may be located at the mid-height of the inner container. When loaded with a device weighing 3,500 lb located at the mid-height of the cavity and using dunnage weighing 500 lb, the center of gravity of the loaded inner container is located 30.1 inches above the outside bottom of the inner container. When inserted into the finite element model upside-down, the lodgment/LTSS CG is located 33.5 inches from the lower end (the normal top surface) of the lodgment. Therefore, using the lodgment upside-down in the analysis model will result in a conservatively bounding maximum bolt load in the worst-case free drop impact. To further maximize the bolt load, the lodgment was placed at the top of the 1105-SD cavity in the model, leaving a gap of 0.67 inches at the bottom at the moment of impact. The

resulting maximum bolt load is 35,774 lb. (Since the maximum bolt load with the gap omitted was 33,373 lb, it can be seen that the effect of the gap is relatively small.)

From [10], the load per bolt due to the design pressure is found from:

$$F_{a_max} = \frac{\pi Dlg^2(P_{li} - P_{lo})}{4Nb} = 1,924 \text{ lb}$$

where the pressure diameter, Dlg is taken for convenience as equal to the bolt circle of 48.5 inches, the number of bolts, $Nb = 24$, the internal design gage pressure, $P_{li} = 25$ psi, and the external gage pressure, $P_{lo} = 0$ psi. The maximum load on a closure bolt under HAC is therefore $35,774 + 1,924 = 37,698$ lb, which exceeds the preload and is conservatively bounded by a value of $F_{a_max} = 40,000$ lb. The average tensile stress is:

$$S_{ba} = \frac{F_{a_max}}{A_{sh}} = 42,872 \text{ psi}$$

where A_{sh} was calculated to be equal to 0.933 in^2 in Section 2.6.1.5, *Closure Bolts*. From Table 2.1-1, the allowable average stress intensity for HAC is equal to the lesser of $0.7S_u$ or S_y , which for the ASTM A320 L43 bolting material is $0.7S_u = 87,500$ psi at 200 °F. The margin of safety is:

$$MS = \frac{87,500}{42,872} - 1 = +1.04$$

Thus, the closure bolt stress in the worst-case HAC free drop impact is not of concern.

2.7.1.5.2 Maximum Impact Limiter Crush Deformation

As shown in Figure 2.12.4-1, the strength of the polyurethane foam in the external impact limiter in the warm test (D4) was slightly stronger than the minimum strength of the prototype, 15 lb/ft^3 foam at the bounding NCT warm environment temperature. Therefore, the maximum crush in the worst case (side-simultaneous orientation) will be slightly more than the amount measured in free drop test D4. Section 2.12.4.5.3, *Warm Free Drop Results*, describes a pair of finite element runs made to compare the foam crush from the two cases (test case, 14 lb/ft^3 density at 117 °F vs prototype case, 15 lb/ft^3 density at 150 °F). Note that the finite element runs are not intended to exactly duplicate the warm case results, but rather to determine a delta-crush amount that will be applied to the maximum certification test measurement. In the following, note that the nominal radial thickness of foam, based on the limiter OD of 70 inches, the shell thickness of $\frac{1}{4}$ inches, and the lower flange OD of 52 inches, is 8.75 inches.

For the finite element model using test conditions, the amount of foam remaining at the location of the lower flange after the impact is 2.5 inches. Since the original foam was 8.75 inches thick, the crush was $8.75 - 2.5 = 6.25$ inches. Similarly, for the prototype case, the amount of foam remaining in the model is 2.0 inches, and the crush was therefore 6.75 inches. As shown in Section 2.12.3.4.6, *Test Series D4*, and in Figure 2.12.3-48, the minimum measured amount of foam remaining after the warm test was 5.13 inches, giving a crush distance of 3.62 inches. The analytical test case crush result can then be benchmarked using the factor:

$$\frac{\text{Measured test result}}{\text{Calculated test result}} = \frac{3.62}{6.25} = 0.579$$

Consequently, the expected maximum crush using prototypic, 15 lb/ft³ foam under warm conditions is equal to $0.579 \times 6.75 = 3.91$ inches. The increase in crush due to the lower foam strength is $3.91 - 3.62 = 0.29$ inches. This value will be conservatively rounded up to 0.5 inches. Thus, the thickness of foam remaining in the worst case, based on certification test measurements and applicable to the thermal analysis, is $5.13 - 0.5 = 4.63$ inches.

2.7.1.6 Structural Evaluation of the Shielded Devices

The inner container will contain shielded devices from Group 1 and Group 3 as noted in Table 1.2-2. The devices contain the radioactive sources and provide shielding. The Sealed Source Device Registry (SSDR) number for each device is given in the table. Shielded devices are designed to be used in a normally occupied environment, and the external dose rates are small. The structural members of Group 1 shielded devices consist of carbon steel or stainless steel. For Group 3, the main structural members of the device (the cylindrical shell, flat ends, and outer conical section) are made from carbon steel. The inner conical shell is made from cast iron. If the radioactive source is movable, it is placed into the shielded transport position and secured. To ensure safe transport of the source, it must remain in a shielded position within the device under all NCT and HAC.

As shown in Appendix 2.12.3, *Certification Test Results*, the dummy shielded device was contained within the inner container and located using wood dunnage. In the free drop events, some of the energy of the dummy device was absorbed either by the crush of the wood dunnage (see Figure 2.12.3-15) or by deformation of the inner container (see Figure 2.12.3-37). Conversely, the lodgment and LTSS responded in a more rigid manner, having only negligible damage as shown in Figure 2.12.3-20 and Figure 2.12.3-21. For this reason, the calculated acceleration of the LTSS will bound the acceleration of the shielded device. As shown in Section 2.12.4.5.2, *Slapdown Free Drop Results*, the maximum acceleration of the LTSS is 206g in the bottom down orientation, and 228g in the side orientation. In the analyses which follow, a conservative bounding value of 300g is used. This value is valid for other kinds of dunnage such as rigid polymer foams or aluminum structures.

2.7.1.6.1 Group 1 Shielded Devices

Group 1 shielded devices have fixed, pencil-shaped sources that are held in position inside the shield by a shield plug which is welded to the outer shell. The devices are shipped with their axis vertical. Figure 2.7-1, which shows the GC-3000, illustrates the plug attachment. The plug is located in the upper right of the figure. A circular butt weld between the top plate of the plug and the outer shell of the device retains the plug in position. The plug is stepped, having a larger diameter equal to 5.75 inches and a smaller diameter equal to 4.5 inches. The overall depth of the plug is 3.5 inches. To calculate a bounding weight, it will be assumed to be of a single diameter equal to 6 inches and a depth of 4 inches, and the entire volume will be assumed to be lead (no steel). The weight of this cylinder, using a density of 0.41 lb/in³ for lead, is 46.4 lb. The source and holder can be bounded by a block of steel 13.25 inches long, 2.5 inches wide, and 0.9 inches thick, having a weight of 8.6 lb. With an impact of 300g, the force on the weld is $(46.4 + 8.6) \times 300 = 16,500$ lb. The circular weld has a 5.75-inch diameter on the GC-3000, but

will be conservatively represented by a 5.0-inch diameter weld. A conservatively low material yield strength of 25,000 psi is assumed. The shear yield strength is therefore $0.6 \times 25,000 = 15,000$ psi. If the depth of penetration of the weld is h and the weld stress is τ , then the shear stress in the weld can be written:

$$\tau = \frac{16,500}{5\pi h} = 15,000 \text{ psi}$$

This can be solved for h , which is the required minimum weld penetration of 0.07 inches. Since the material thickness of the shell and the top plate of the shield plug is 3/8 inches thick, a weld penetration of 0.07 inches will be assured. (Note: full depth penetration has been confirmed during numerous device disassembly operations by a DOE contractor.) Note also that weld yield shear strength has been conservatively used instead of the ultimate shear strength. Use of ultimate strength would be justified, since the source cannot be released until the weld completely fails. In a side drop, the plug is supported by the structure of the device and no load is applied to the weld. Thus, a conservative analysis shows that the source will be retained inside the Group 1 devices in the worst-case HAC impact event.

2.7.1.6.2 Group 3 Shielded Devices

Group 3 shielded devices have a sliding source drawer. For shipping, the drawer containing the source is moved all the way to the left in Figure 2.7-2, and a shipping spacer is placed in the remaining cavity. The drawer and spacer are retained in this position by shipping retainers on each end. The retainers are made of steel, nominally 1.5 inches thick, and are retained by four, 3/8-16 UNC socket head cap screws (SHCS). The shipping retainers interlock with the body of the device on each end by means of an approximately 0.1" deep step, which prevents shear loads from being applied to the bolts. In addition, the outer edge of the retainers have a virtually full-depth taper of approximately 45°, as shown in Figure 2.7-2. This feature prevents significant side loads from being applied to the shipping retainers.

An upper bound weight which would be applied to the shipping retainer SHCS on one side in the worst case HAC drop impact can be found by assuming that the drawer is made of solid lead, 2.5 inches in diameter and 16 inches long. The drawer weight is therefore bounded by 32.2 lb. The shipping spacer is a cylinder, 11.4 inches long, 2.5 inches O.D., and 1/4 inches thick, made of stainless steel. It weighs 5.8 lb. The shipping retainer can be modeled as a disk, 9 inches in diameter and 1.5 inches thick which has a bounding weight of 27.7 lb. With an impact of 300g, the load on one SHCS is:

$$F_b = 300(32.2 + 5.8 + 27.7)/4 = 4,928 \text{ lb}$$

The SHCS may be made of stainless steel or alloy steel. For stainless steel, ASTM standard F837 [28], Table 4, gives a minimum tensile strength for a 0.375-16 fastener made of stainless steel as 6,199 lb. For alloy steel, ASTM standard A574 [29], Table 4, gives a minimum tensile strength for the 0.375-16 fastener of 13,900 lb. The minimum margin of safety on the SHCS is for the stainless steel screw and is:

$$MS = \frac{6,199}{4,928} - 1 = +0.26$$

Thus, a conservative analysis shows that the source will be retained inside the Group 3 devices in the worst-case HAC impact event.

As noted in Section 1.2.2.2, a limited portion of the shell of the GC-40 is made from cast iron. With reference to Figure 2.7-2, the shells of the GC-40 consist of an outer cylindrical shell made of 0.38-inch thick carbon steel, two flat ends made of 1-inch thick carbon steel, and, on a transverse axis, inner and outer conical shells. The inner conical shell is clearly shown in Figure 2.7-2, and is cast in one piece with the large flange (shown in the figure as having a diameter of 24.7 inches). The outer conical shell is partially shown in Figure 2.7-2, but is more clearly shown in the photograph of Figure 1.2-16. The outer conical shell is made of 0.38-thick carbon steel. Thus, only the inner conical shell and associated flange are made of cast iron, and the rest is carbon steel. In the shipping position, the source is located in the cylindrical shell portion of the device. The device is well protected by the blocking/dunnage, the inner container, and the 1105-SD package. In the unlikely event of a non-ductile response of the cast portion of the shell to an HAC free drop, the carbon steel in the remainder of the shell will keep the device intact, and shielding of the source will be unaffected.

2.7.2 Crush

Since the weight of the 1105-SD package exceeds 1,100 lb, the crush test specified in 10 CFR §71.73(c)(2) does not apply.

2.7.3 Puncture

The 1105-SD package is evaluated for puncture resistance under HAC as defined in 10 CFR §71.73(c)(3). The puncture event is defined as a free drop from a height of 40 inches onto a vertical, cylindrical mild steel bar, 6 inches in diameter, in an orientation and in a location for which maximum damage is expected. The puncture event must occur subsequent to the free drop event. Seven different puncture tests were performed on the three CTUs.

2.7.3.1 Technical Basis for the Puncture Drops

Section 2.7.1.1, *Technical Basis for the Free Drops*, includes a list of the packaging components that are subject to possible damage in the HAC puncture drop event. The susceptibility of the 1105-SD package to puncture damage was considered and assumed to occur on undamaged areas as well as on prior free drop damage. As discussed in Section 2.12.2.3.2, *Puncture Drops*, the worst-case puncture drops are as follows (all punctures are through the CG, unless stated otherwise):

- A puncture directly on the prior CG-over-knuckle free drop damage would maximize the containment boundary strain, since it would add to the strain generated in the free drop.
- An oblique puncture on the bottom-down free drop damage could tear into the impact limiter shell and damage the lower torispherical head, or expose excessive amounts of polyurethane foam, with consequences for the containment seals in the HAC fire event.
- A puncture on the impact limiter side drop damage, generated in the warm side drop, would create the minimum remaining foam thickness (locally) and, if the shell tore, could expose excessive amounts of foam, with consequences for the containment seals in the HAC fire event.

- A puncture from the side on the rain shield/tube sheet region could impart enough deformation to compromise the vent port containment sealing washer, or make the rain shield unable to retain the port insulation cylinder. In order to place the puncture bar impact in the most damaging location and orientation, it may not be possible to aim the bar through the CG, however, the effect will be small.
- A puncture on the side drop damage to the knuckle would be similar to the puncture on the CG-over-corner damage to the knuckle, but in a different orientation. A puncture impact directly on the side drop knuckle damage would cause little damage, due to the geometric relationship of the CG to the damage. Therefore, an impact on the head, in the thinner knuckle region, adjacent to the side drop damage, would apply further strain deformation to the prior deformation of the containment boundary.
- A puncture on the side thermal shield could cause the relatively thinner thermal shield sheet(s) to rip and expose the inner shield sheet or even the containment boundary wall to the HAC fire heat.

A more detailed discussion of the puncture drop orientations which were considered, including orientations that are not governing, is given in Section 2.12.2.3.2, *Puncture Drops*. The seven puncture drops actually performed were distributed across the three CTUs to avoid overtesting a single test unit, and in most cases were applied on, or in relation to, prior free drop damage. The tests performed and the justification for choosing them is detailed in Section 2.12.2.4, *Summary of Certification Tests*, summarized in Table 2.12.2-1, and depicted in Figure 2.12.2-2.

2.7.3.2 Summary of the Results of the Puncture Drop Tests

The damage resulting from the puncture tests is summarized below, with further details and photographs given in Appendix 2.12.3, *Certification Test Results*. None of the puncture tests compromised the leak tight condition of the containment, nor caused exposure of excessive polyurethane foam (only one puncture test exposed any foam). There was no significant damage to either the rain shield or to the external thermal shield.

2.7.3.2.1 Puncture Drop Tests P1 and P6

Puncture tests P1 and P6 were identical tests performed on CTU #1 (subsequent to free drop test D1H) and CTU #3 (subsequent to free drop test D5H), respectively. For both tests, the package orientation, impact location, and prior free drop test were identical. CTU #1 was used to test the packaging and the lodgment/LTSS payload; CTU #3 was used to test the response of the packaging to the inner container/shielded device payload. The purpose of repeating the puncture test was to maintain consistency between the two test units. Puncture test P1 made a dent 3-1/8 inches deep, and partially cut through the impact limiter shell over a portion of the bar circumference, and exposed a segment of foam approximately 1.5 inches wide. As shown in Section 3.5.4, *'Last-A-Foam' Response under HAC Conditions*, the polyurethane foam used in the impact limiter forms a char in the hypothetical fire which will tend to block this opening from direct exposure to the flame, preventing significant local temperature peaks. Of note, no other puncture drop test exposed any foam. Puncture test P6 made a dent 1-9/16 inches deep, without cutting the shell. In neither case was any damage imparted to the lower torispherical head or lower flange. More detail is given in Section 2.12.3.4.1, *Test Series D1*, and Section 2.12.3.4.2, *Test Series D5*.

2.7.3.2.2 Puncture Drop Test P2

Puncture drop test P2 was performed on CTU #1 subsequent to free drop D2H. The bar struck the upper torispherical head adjacent to the side free drop damage to the knuckle, and left a dent approximately $\frac{3}{4}$ inches deep. There was no evidence of cracking of the containment boundary. Of note, this test was conservative because the 0.105-inch thick upper thermal shield was not present on CTU #1, which would have added to the resistance to this puncture. More detail is given in Section 2.12.3.4.3, *Test Series D2*.

2.7.3.2.3 Puncture Drop Test P3

Puncture drop test P3 was performed on CTU #2 subsequent to free drop D3H. The package orientation for the puncture drop was identical to that for the free drop. The bar struck the package at a location three inches radially inboard from the outside edge of the damaged knuckle region. The bar struck in a location such that it did not receive support from the lodgment ribs inside. The resulting dent was approximately 1-3/8 inches deep relative to the flat damaged area. More detail is given in Section 2.12.3.4.4, *Test Series D3*.

2.7.3.2.4 Puncture Drop Test P4

Puncture drop test P4 was performed on CTU #2 subsequent to free drop D4H. The bar struck the damaged impact limiter surface, through the CG, and left a dent approximately 1-1/2 inches deep. The bar did not cut the impact limiter shell. More detail is given in Section 2.12.3.4.6, *Test Series D4*.

2.7.3.2.5 Puncture Drop Test P5

Puncture drop test P5 was performed on CTU #3 subsequent to free drop D6H. The bar struck the tube sheet and deformed the edge of the sheet by approximately $\frac{1}{2}$ inches. Very slight deformation of the rain shield also occurred, but none of the rain shield attachment bolts were loosened, and the rain shield still covered the bolt tubes and the vent port and seal test port tubes. More detail is given in Section 2.12.3.4.5, *Test Series D6*.

2.7.3.2.6 Puncture Drop Test P7

Puncture drop test P7 was performed on CTU #3 subsequent to free drop D6H. The bar struck the side of the package on the dual thermal shield, aiming through the CG. The resulting dent was 1-7/8 inches deep. The outer, 0.105-inch thick thermal shield shell was not cut by the puncture bar. More detail is given in Section 2.12.3.4.5, *Test Series D6*.

2.7.4 Thermal

The 1105-SD package is designed to withstand the HAC 30 minute fire specified in 10 CFR §71.73(c)(4). The thermal evaluation is presented in Section 3.4, *Thermal Evaluation under Hypothetical Accident Conditions*.

2.7.4.1 Summary of Pressures and Temperatures

As shown in Table 3.1-3, the maximum internal pressure as a result of the HAC fire event is 9.4 psig. This is higher than the MNOP of 5 psig conservatively assumed in Section 2.6.1.1,

Summary of Pressures and Temperatures. A value of 10 psig will be utilized in the stress calculations which follow.

From Table 3.1-1, as a result of the HAC fire event, the maximum temperature of the containment boundary occurs in the upper torispherical head and is equal to 1,274 °F. This peak temperature occurs at the end of the fire and is located in a hypothetical puncture dent, which locally compresses the head thermal shield. A peak temperature of 1,164 °F occurs at the junction between the thermal shields on the head and bell where a narrow segment of the bell is directly exposed to ambient conditions. At an alternate puncture location just above the rain shield on the side of the package, the peak temperature is 1,132 °F (see Table 3.4-1). The peak temperatures at all of these locations represent temporary excursions which exceed the continuous-duty limit for Type 304 stainless steel of 800 °F for less than one hour. The peak temperatures of the closure flanges, closure bolts, and lower torispherical head are much lower. The peak temperature of the lodgment lower half is 464 °F and occurs at the location where the lodgment is touching the package shell at the location of the hypothetical puncture damage on the package side, as shown in Table 3.4-1 and Figure 3.4-5. At the end of the fire, this highly localized temperature rapidly falls as energy is distributed to the rest of the lodgment structure. The peak temperature of the lodgment upper half is 415 °F. The peak temperature of the inner container is 977 °F, which occurs in a single rib at the location of the hypothetical puncture damage on the package side, as shown in Table 3.4-3 and Figure 3.4-14. The peak temperature of the 1/4-inch thick cylindrical shell of the inner container, which controls the thermal expansion, is 445 °F, from Table 3.4-3.

2.7.4.2 Differential Thermal Expansion

The following calculations demonstrate a positive clearance under HAC between the 1105-SD payload cavity and the payload, consisting of the lodgment or inner container. The aluminum lodgment is governing due to its higher temperature (464 °F compared to 445 °F) and larger coefficient of thermal expansion. In addition, the hot rib of the inner container may locally deform under thermal expansion and have only a negligible effect on the overall length or diameter of the inner container. Thus, the clearances applicable to the lodgment bound those that would occur when using the inner container.

The payload cavity has a nominal length of 60.30 inches with a tolerance of ± 0.25 inches, giving a minimum length of 60.05 inches. The lodgment has a nominal length of 59.50 inches with a tolerance of ± 0.25 inches, giving a maximum length of 59.75 inches, for a minimum room temperature axial clearance of 0.30 inches. The maximum length of the lodgment is calculated using the average of the upper and lower lodgment peak temperatures. This is justified since the upper lodgment half (30.7 inches long) has very nearly the same length as the lower lodgment half (28.8 inches long). Added conservatism is afforded by the fact that the peak temperatures are highly localized. The average temperature at the end of the HAC fire is: $(464 + 415)/2 = 440$ °F. Conservatively, an average temperature of 450 °F will be assumed. The maximum length of the lodgment is:

$$L_L = 59.75[1 + \alpha(450 - 70)] = 60.06 \text{ inches}$$

where the coefficient of thermal expansion for the aluminum lodgment at 450 °F, $\alpha = 13.8(10^{-6})$ in/in/°F from Table 2.2-4, and the reference temperature is 70 °F. The temperature of the package shell is relatively hot, but is conservatively considered to be a minimum of 100 °F, since

the ambient temperature is 100 °F during the cool down period. The increased length of the package cavity is:

$$L_C = 60.05[1 + \alpha(100 - 70)] = 60.07 \text{ inches}$$

where the coefficient of thermal expansion for Type 304 at 100 °F, $\alpha = 8.6(10^{-6})$ in/in/°F from Table 2.2-1, and the reference temperature is 70 °F. The minimum axial clearance is:

$$CLR_{axial} = L_C - L_L = 0.01 \text{ inches}$$

As noted, this minimum clearance is conservatively calculated, since it considers that the localized peak temperature of the lodgment is uniform, and considers a relatively cool temperature for the package sidewall.

The payload cavity has a nominal inner diameter of 43.5 inches with a tolerance of ± 0.3 inches, giving a minimum diameter of $D_C = 43.2$ inches. The lodgment has a nominal diameter of 42.75 inches with a tolerance of ± 0.12 inches, giving a maximum diameter of 42.87 inches, for a minimum room temperature diametral clearance of 0.33 inches. From Figure 3.4-5, it is clear that a uniform temperature of 450 °F conservatively represents the equivalent uniform temperature of the lodgment lower half. The diametral expansion is bounded by:

$$D_L = 42.87[1 + \alpha(450 - 70)] = 43.09 \text{ inches}$$

where α is defined above. The minimum diametral clearance, conservatively neglecting any expansion of the payload cavity diameter, is:

$$CLR_{diametral} = D_C - D_L = 0.11 \text{ inches}$$

Thus, positive clearance is maintained under worst case HAC.

2.7.4.3 Stress Calculations

The 1105-SD containment boundary is designed as a pressure vessel. As shown in Section 2.6.1.3.1, *Stresses Due to Pressure Loading*, the stress generated in the material by internal pressure is relatively small. However, for the HAC fire event, some deformation of the structure may be present. The most penalizing damage would be for the top down free drop case, since it creates a quasi-flat end on the upper end of the package, which generates higher stress than the original torispherical shape. As shown in Figure 2.12.4-76, the top down drop creates a flat approximately 38 inches in diameter, with a smooth radius connecting it to the side wall. This will be conservatively modeled using a pressurized flat plate having the full package meridional diameter of 44 inches. From [24], Table 24, Case 10b for a fixed-edge plate, the maximum bending moment in the plate is:

$$M_{ra} = \frac{qa^2}{8} = 605 \text{ in} - \text{lb/in}$$

where the pressure, $q = 10$ psig, and the radius, $a = 22$ inches. The stress (located at the plate edge) is:

$$\sigma = \frac{6M_{ra}}{t^2} = 14,520 \text{ psi}$$

where the thickness, $t = 0.5$ inches. The stress evaluation method is found in [30]. The stress rupture value is taken from Table I-14.6A at a temperature of 1,300 °F and a duration of one hour, and is equal to 23 ksi. The allowable stress is 67% of this value, or $0.67 \times 23 = 15.4$ ksi. The stress from the flat plate evaluation is a bending stress, which may be designated P_b . From Article NH-3223(c), $K_t = 1.25$. Therefore:

$$P_L + P_b / K_t = 11,616 \text{ psi}$$

where $P_L = 0$, $P_b = 14,520$ psi, and K_t is defined above. The margin of safety is:

$$MS = \frac{15,400}{11,616} - 1 = +0.33$$

This evaluation is carried out with the following conservative assumptions:

1. The configuration considers a flat plate geometry which is larger than the worst case configuration calculated for the free drop impact damage. Since stress is proportional to diameter squared, this overestimates the stress by approximately 34%.
2. The rupture stress is taken at a conservative temperature (1,300 °F > 1,274 °F), which underestimates the rupture stress by approximately 8%.
3. The maximum temperature is assumed to remain constant for one hour. However, the transient temperature only peaks at 1,274 °F, and falls rapidly. In fact, the length of time for which the maximum temperature exceeds 800 °F is less than one hour.
4. The pressure of 10 psig exceeds the calculated maximum pressure of 9.4 psig, which overestimates the stress by approximately 6%. Furthermore, the peak pressure occurs at a later time than the peak temperature occurs.
5. The material of the head and sidewall of the package have a minimum yield strength of 40 ksi and minimum ultimate strength of 80 ksi, which is greater than the minimum values of 30 ksi and 75 ksi, respectively. The temperature and time to which the torispherical head is exposed is not sufficient to anneal the material (i.e., to reduce the strength to minimum). However, no adjustment was made to the ASME Code minimum rupture strength value.

Thus, it is evident that the true margin of safety is larger than 0.33. In addition, the stress must meet the Level D Service Limit in Section III, Appendix F, Article F-1331.1, of $1.5 \times 0.7 S_u = S_u$. Since S_u for Type 304 material at a temperature of 1,300 °F, from Table NH-3225-1, is 37.7 ksi, the margin of safety is:

$$MS = \frac{37,700}{14,520} - 1 = +1.60$$

Thus, stress in the HAC fire event is not of concern.

Per Regulatory Guide 7.6, paragraph C.7, the extreme range of stress must be considered. Of all the various allowable stresses corresponding to the different conditions evaluated (including fabrication stresses and normal conditions of transport), the largest allowable stress is equal to the material ultimate strength, S_u . It is therefore conservative to assume that S_u bounds all stresses actually developed in the structure. For Type 304 stainless steel, $S_u = 75,000$ psi at 70 °F. The maximum possible stress intensity range is twice this value, or 150,000 psi.

Applying a factor of four to account for possible stress concentrations at structural discontinuities gives a total elastic stress range of 600,000 psi. The alternating component is one-half of this value, or 300,000 psi. To account for temperature effects, this value of alternating stress is factored by the ratio of modulus of elasticity. This ratio is formed between the modulus of elasticity at room temperature (at which the test data applies directly) and the modulus of elasticity at the maximum temperature, conservatively bounded by a temperature of 1300 °F for the upper torispherical head in the HAC fire event. The adjusted stress is

$$S_{alt} = 300,000 \frac{E_{70^{\circ}\text{F}}}{E_{1300^{\circ}\text{F}}} = 418,227 \text{ psi}$$

where $E_{70^{\circ}\text{F}} = 28.3(10^6)$ psi and $E_{1300^{\circ}\text{F}} = 20.3(10^6)$ psi, from Table TM-1 of the ASME Code, for Material Group G. Per Figure I-9.2 and Table I-9.2 of the ASME Code [12], the allowable value for S_{alt} at 10 cycles is 870,000 psi. The margin of safety is

$$MS = \frac{870,000}{418,227} - 1 = +1.08$$

Considering the significant conservatism used in the underlying assumptions (e.g., use of allowable stress rather than smaller actual stresses, assuming worst case stresses are fully reversing, use of the maximum factor of stress concentration), it is apparent that the actual margin of safety is larger than 1.08. Thus, the requirement of paragraph C.7 of Regulatory Guide 7.6 is met.

2.7.5 Immersion – Fissile

An immersion test for fissile material packages is required by 10 CFR §71.73(c)(5). Since the 1105-SD package does not transport fissile materials, this requirement does not apply.

2.7.6 Immersion – All Packages

An immersion test for all packages is required by 10 CFR §71.73(c)(6), in which a separate, undamaged specimen must be subjected an equivalent pressure of 21.7 psig. The package will be evaluated for buckling resistance of the cylindrical portion of the containment boundary using Code Case N-284-2, and the torispherical heads using ASME B&PV Code, Section III, Subsection NE-3133.4(e). Although the immersion takes place in water, the maximum NCT warm temperature of 200 °F (see Section 2.6.1.1, *Summary of Pressures and Temperatures*) is conservatively utilized.

For the cylindrical side shell, the compressive hoop stress is:

$$\sigma_{\theta} = p_o \frac{r_{avg}}{t} = 954.8 \text{ psi}$$

where the pressure, $p_o = 21.7$ psig, the mean shell radius, $r_{avg} = 22.0$ inches, and the thickness, $t = 0.5$ inches. The compressive axial stress is:

$$\sigma_{\phi} = \frac{p_o \pi r_{skirt}^2}{2 \pi r_{avg} t} = 488.3 \text{ psi}$$

Where the pressure load is applied to the projected area of the top of the containment boundary, having an outer radius of $r_{skirt} = 44.5/2 = 22.25$ inches. Using Mohr's circle, the maximum shear stress is:

$$\sigma_{\phi\theta} = \frac{1}{2}(\sigma_{\theta} - \sigma_{\phi}) = 233.3 \text{ psi}$$

The possibility of buckling of the inner shell is evaluated using [13]. Consistent with Regulatory Guide 7.6, a factor of safety corresponding to ASME Code, Service Level D is employed. In this case, the applicable factor of safety is 1.34 for hypothetical accident conditions, as specified in [13]. The analysis used a modulus of elasticity of $27.5(10^6)$ psi, corresponding to 200 °F. Buckling analysis geometry and loading parameters are listed in Table 2.7-2 and results of the analysis in Table 2.7-3. As shown, all interaction parameters, including the maximum value of 0.0654, are less than unity, as required.

The buckling analysis of the torispherical head is evaluated using the technique outlined in [31]. The analysis for torispherical heads is the same as for ellipsoidal heads. Factor A is found as:

$$A = \frac{0.125}{R/T} = 0.00144$$

where the inside crown radius, $R = 43.5$ inches, and the head thickness, $T = 0.5$ inches. From ASME B&PV Code, Section II, Part D, Table HA-1, the corresponding value of factor B for a temperature of 200 °F is conservatively taken as $B = 8,000$. The maximum allowable external pressure is:

$$P_a = \frac{B}{(R/T)} = 92.0 \text{ psig}$$

Per Article NE-3222.2, a factor of 1.5 may be applied for Service Level D conditions, which are appropriate for HAC. The permissible external pressure is therefore $1.5 \times 92.0 = 138$ psig. For an external pressure of 21.7 psig, the factor of safety against buckling of the torispherical head is:

$$FS = \frac{138}{21.7} = 6.4$$

This value is significantly in excess of the minimum factor of 1.34 suggested by [13]. Therefore, the immersion test is not of concern.

2.7.7 Deep Water Immersion Test (for Type B Packages Containing More than $10^5 A_2$)

For Type B packages containing an activity of more than $10^5 A_2$, 10 CFR §71.61 requires that an undamaged containment system withstand an external pressure of $p_o = 290$ psig for a period of not less than one hour without collapse, buckling, or inleakage of water. As shown in Table 1.2-1, the payload represents a maximum activity of less than $10^5 A_2$. Therefore, this requirement does not apply to the 1105-SD package.

2.7.8 Summary of Damage

2.7.8.1 Summary of Certification Test Damage

From the discussions presented in the foregoing sections, it is shown that the hypothetical accident sequence does not result in any adverse structural damage to the 1105-SD package, and that the criteria established for hypothetical accident conditions in Section 2.1.2., Design Criteria, are satisfied. Full scale certification testing of free drop and puncture drop, including prior damage imposed by the NCT free drop, has demonstrated the resistance of the 1105-SD package to hypothetical accident conditions. A total of six potentially worst-case HAC sequences (consisting of a NCT free drop, followed by a HAC free drop followed by one or two puncture drops) were applied to three CTUs. After each test series (in one case, after a pair of test series), the main containment O-ring seal and the vent port sealing washer were leaktight to a level of 1×10^{-7} scc/sec, air, per [4]. After all testing was complete, the metallic containment boundary was leaktight as documented in Table 2.12.3-2. Deformations of the containment boundary were only observed in the upper half of the bell in connection with direct free drop or puncture impacts. No deformations were observed in the closure flanges or in the lower torispherical head, and gross buckling did not occur. None of the deformations compromised the leaktight barrier presented by the containment boundary.

The lodgment maintained the LTSS in essentially its original position in all cases. The LTSS did not experience any lead slump or deformations or other failures that could affect its ability to shield the radioactive sources transported. Since there were no loadings or evidence of damage to the LTSS end door closures, the radioactive sources within the LTSS could not change their position relative to the lead shielding. The inner container supported the shielded device and maintained it within the confines of the inner container. The inner container absorbed most of the potential energy of the device, and protected the packaging containment boundary, while absorbing some energy in the array of external ribs.

The fire analysis assumptions regarding the post-accident configuration of the packaging were supported. Particularly, the absence of significant exposure of foam and the integrity of the thermal shield shells was demonstrated. The vent port and seal test port insulation cylinders and the rain shield remained intact and in place, with no loosening of the rain shield attachment bolts.

2.7.8.2 Summary of Analytical Evaluation Results

Analytical evaluations support the conclusions stated above. The closure bolts, considering the worst case orientation and a conservative payload CG height and payload gap, have a margin of safety of 1.04. The retention of the radioactive source in the shielded position within the Group 1 or Group 3 shielded devices was demonstrated assuming conservatively bounding free drop accelerations. Utilizing a series of conservative assumptions, the stress in the containment boundary during and after the HAC fire event was demonstrated to have a minimum margin of safety of 0.33, and the range of stress, evaluated according to Reg. Guide 7.6, has a margin of safety of 1.08. The factor of safety for immersion of the package under water is 6.4.

Therefore, the 1105-SD satisfies all of the requirements of 10 CFR §71.73.

Table 2.7-1 – HAC Free Drop Impact Accelerations

Free Drop	Acceleration, g ^⓪		Comment ^⓪
D1H	768		Average of four accelerometer locations
D2H	466	249	Avg. of two upper locations/avg. of two lower locations
D3H	178		Average of four accelerometer locations
D4H	374	183	Avg. of two upper locations/avg. of two lower locations
D5H	812		Average of four accelerometer locations
D6H	411	173	Avg. of two upper locations/avg. of two lower locations

Notes:

1. Resolved perpendicular to the ground.
2. Accelerometer locations are described in Section 2.12.3.2.2, *Instrumentation*.

Table 2.7-2 – Immersion Test: Geometry and Loads

	Containment boundary shell dimensions, inches	Applied stress, psi	
Inner Dia.	43.5	σ_{ϕ}	954.8
Outer Dia.	44.5	σ_{θ}	488.3
Length (bounding)	60.0	$\sigma_{\phi\theta}$	233.3

Table 2.7-3 – Immersion Test: N-284-2 Results

Parameter	Value	Remarks
Capacity Reduction Factors (-1511)		
$\alpha_{\phi L} =$	0.2397	
$\alpha_{\theta L} =$	0.8000	
$\alpha_{\phi\theta L} =$	0.8000	
Plasticity Reduction Factors (-1610)		
$\eta_{\phi} =$	0.2534	
$\eta_{\theta} =$	0.7249	
$\eta_{\phi\theta} =$	0.1706	
Theoretical Buckling Values (-1712.1.1)		
$C_{\phi} =$	0.6050	
$\sigma_{\phi eL} =$	378,125 psi	
$C_{\theta r} =$	0.0544	
$\sigma_{\theta eL} = \sigma_{reL} =$	33,982 psi	
$C_{\theta h} =$	0.0527	
$\sigma_{\theta eL} = \sigma_{heL} =$	32,942 psi	
$C_{\phi\theta} =$	0.1758	
$\sigma_{\phi\theta eL} =$	109,882 psi	
Elastic Interaction Equations (-1713.1.1)		
$\sigma_{xa} =$	67,647 psi	
$\sigma_{ha} =$	19,667 psi	
$\sigma_{ra} =$	20,288 psi	
$\sigma_{\tau a} =$	65,601 psi	
Axial + Shear \Rightarrow Check (c):	0.0072	<1 \therefore OK (see note*)
Hoop + Shear \Rightarrow Check (d):	0.0471	<1 \therefore OK
Inelastic Interaction Equations (-1714.2.1)		
$\sigma_{xc} =$	17,142 psi	
$\sigma_{rc} =$	14,706 psi	
$\sigma_{\tau c} =$	11,194 psi	
Max(Axial,Hoop) \Rightarrow Check (a):	0.0649	<1 \therefore OK
Axial + Shear \Rightarrow Check (b):	0.0289	<1 \therefore OK
Hoop + Shear \Rightarrow Check (c):	0.0654	<1 \therefore OK

*Note: Elastic interaction checks (a), (b), (e), and (f) are not applicable.

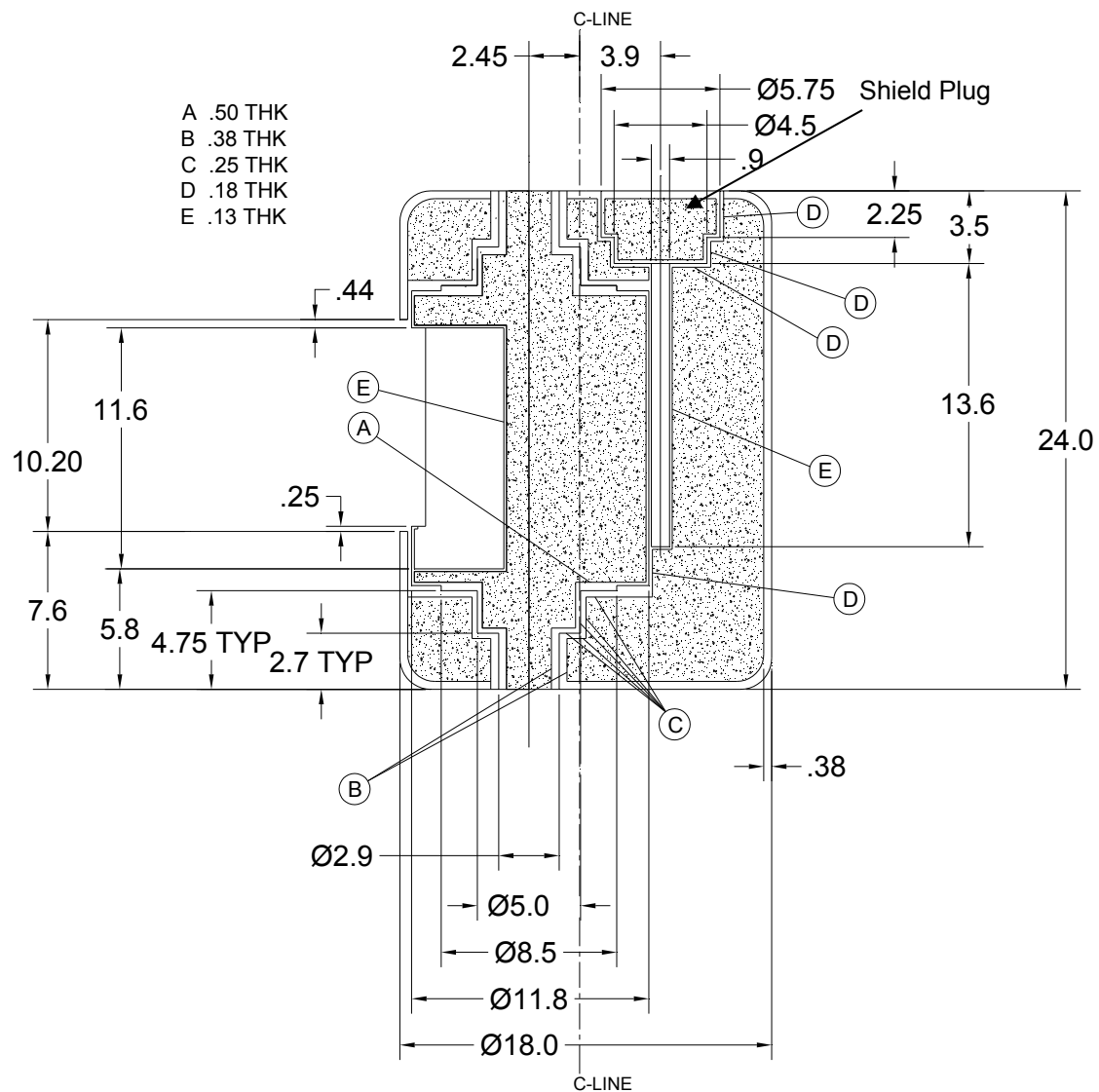


Figure 2.7-1 – Typical Shielded Device Group 1 Cross Section (Gammacell-3000)

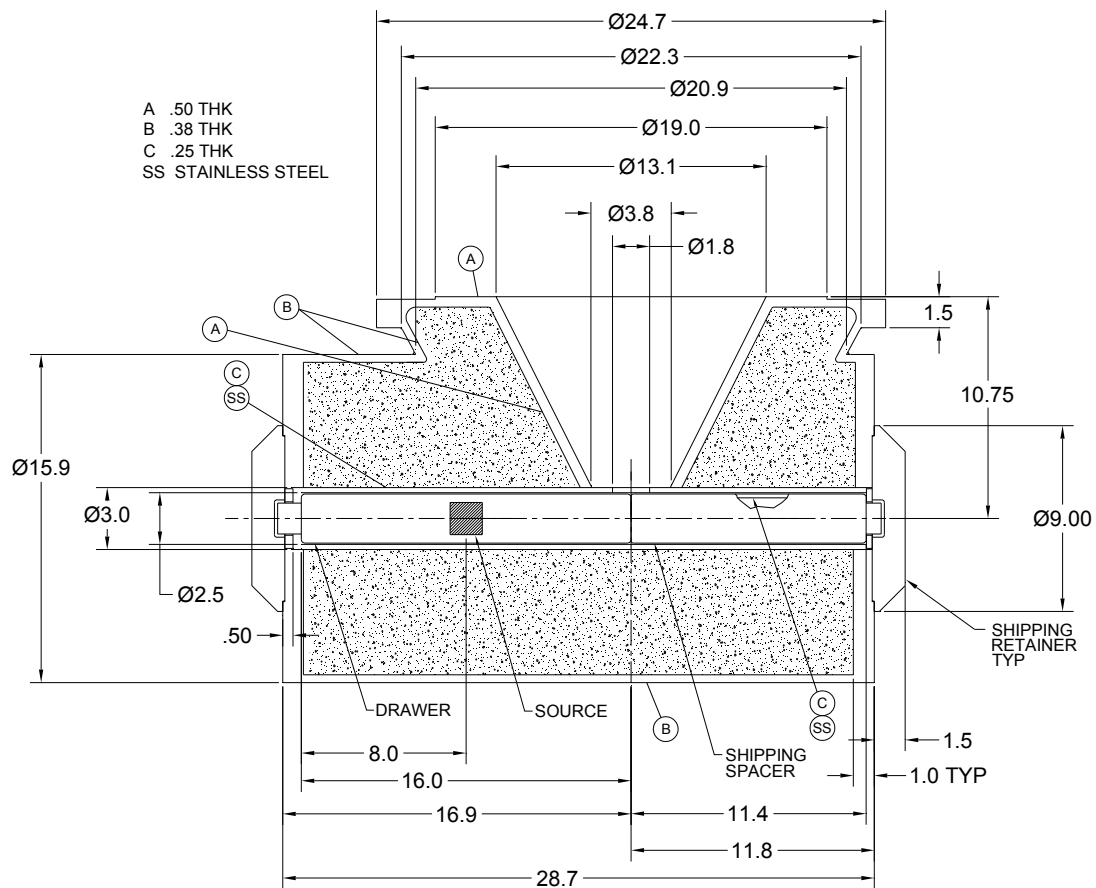


Figure 2.7-2 – Typical Shielded Device Group 3 Cross Section (GC-40)

2.8 Accident Conditions for Air Transport of Plutonium

This section does not apply, since air transport is not used for the 1105-SD package when transporting plutonium.

2.9 Accident Conditions for Fissile Material Packages for Air Transport

This section does not apply, since the contents of the 1105-SD package are fissile exempt as discussed in Chapter 6.0, *Criticality Evaluation*.

2.10 Special Form

This section does not apply, since special form is not claimed for the sources transported in the 1105-SD package. Most of the payloads placed into the LTSS will use special form capsules, however special form is not formally claimed for any payload.

2.11 Fuel Rods

This section does not apply, since fuel rods are not transported in the 1105-SD package.

2.12 Appendices

2.12.1 References

2.12.2 Certification Test Plan

2.12.3 Certification Test Results

2.12.4 Finite Element Analysis

2.12.5 Seal Performance Tests

2.12.1 References

1. Title 10, Code of Federal Regulations, Part 71 (10 CFR 71), *Packaging and Transportation of Radioactive Material*, 01-01-18 Edition.
2. U. S. Nuclear Regulatory Commission, Regulatory Guide 7.6, *Design Criteria for the Structural Analysis of Shipping Cask Containment Vessels*, Revision 1, March 1978.
3. U. S. Nuclear Regulatory Commission, Regulatory Guide 7.8, *Load Combinations for the Structural Analysis of Shipping Casks for Radioactive Material*, Revision 1, March 1989.
4. ANSI N14.5-1997, *American National Standard for Radioactive Materials – Leakage Tests on Packages for Shipment*, American National Standards Institute (ANSI), Inc.
5. U. S. Nuclear Regulatory Commission, Regulatory Guide 7.11, *Fracture Toughness Criteria of Base Material for Ferritic Steel Shipping Cask Containment Vessels with a Maximum Wall Thickness of 4 Inches (0.1 m)*, June 1991.
6. R. E. Monroe, H. H. Woo, and R. G. Sears, *Recommended Welding Criteria for Use in the Fabrication of Shipping Containers for Radioactive Materials*, NUREG/CR-3019, UCRL-53044, U.S. Nuclear Regulatory Commission, March 1985.
7. L. E. Fischer, W. Lai, *Fabrication Criteria for Shipping Containers*, NUREG/CR-3854, UCRL-53544, U.S. Nuclear Regulatory Commission, March 1985.
8. American Society of Mechanical Engineers (ASME) Boiler and Pressure Vessel Code, Section III, *Rules for Construction of Nuclear Facility Components*, Division 1 – Subsection NB, *Class 1 Components*, 2010 Edition.
9. American Society of Mechanical Engineers (ASME) Boiler and Pressure Vessel Code, Section III, *Rules for Construction of Nuclear Facility Components*, Division 1 – Subsection NF, *Supports*, 2010 Edition.
10. G.C. Mok, L.E. Fischer, S.T. Hsu, *Stress Analysis of Closure Bolts for Shipping Casks*, NUREG/CR-6007, UCRL-ID-110637, U.S. Nuclear Regulatory Commission, January 1993.
11. W.R. Holman, R. T. Langland, *Recommendations for Protecting Against Failure by Brittle Fracture in Ferritic Steel Shipping Containers Up to Four Inch Thick*, NUREG/CR-1815, UCRL-53013, U.S. Nuclear Regulatory Commission, August 1981.
12. American Society of Mechanical Engineers (ASME) Boiler and Pressure Vessel Code, Section III, *Rules for Construction of Nuclear Facility Components*, Appendix I, *Design Stress Intensity Values, Allowable Stresses, Material Properties, and Design Fatigue Curves*, 2010 Edition.
13. American Society of Mechanical Engineers (ASME) Boiler and Pressure Vessel Code, Section III, *Rules for Construction of Nuclear Power Plant Components*, Division 1, Class MC, Code Case N-284-2, *Metal Containment Shell Buckling Design Methods*, 2010 Edition.
14. American Society of Mechanical Engineers (ASME) Boiler and Pressure Vessel Code, Section IX, *Qualification Standard for Welding and Brazing Procedures, Welders, Brazers, and Welding and Brazing Operators*, 2010 Edition.

15. American Society of Mechanical Engineers (ASME) Boiler and Pressure Vessel Code, Section III, *Rules for Construction of Nuclear Facility Components*, Division 1 – Subsection NE, *Class MC Components*, Article NE-4220, 2010 Edition.
16. American Society of Mechanical Engineers (ASME) Boiler and Pressure Vessel Code, Section III, *Rules for Construction of Nuclear Facility Components*, Division 1 – Subsection NB, *Class 1 Components*, Article NB-2540, and Section V, *Nondestructive Examination*, Article 5, *Ultrasonic Examination Methods for Materials*, 2010 Edition.
17. ANSI/AWS D1.6/D1.6M:2007, *Structural Welding Code–Stainless Steel*, American Welding Society (AWS).
18. American Society of Mechanical Engineers (ASME) Boiler and Pressure Vessel Code, Section III, *Rules for Construction of Nuclear Facility Components*, Division 1 – Subsection NB, *Class 1 Components*, and Section V, *Nondestructive Examination*, Article 2, *Radiographic Examination*, 2010 Edition.
19. American Society of Mechanical Engineers (ASME) Boiler and Pressure Vessel Code, Section III, *Rules for Construction of Nuclear Facility Components*, Division 1 – Subsection NB, *Class 1 Components*, and Section V, *Nondestructive Examination*, Article 6, *Liquid Penetrant Examination*, 2010 Edition.
20. American Society of Mechanical Engineers (ASME) Boiler and Pressure Vessel Code, Section III, *Rules for Construction of Nuclear Facility Components*, Division 1 – Subsection NF, *Supports*, and Section V, *Nondestructive Examination*, Article 6, *Liquid Penetrant Examination*, 2010 Edition.
21. American Society of Mechanical Engineers (ASME) Boiler and Pressure Vessel Code, Section III, *Rules for Construction of Nuclear Facility Components*, Division 1 – Subsection NB, *Class 1 Components*, Article NB-6220, 2010 Edition.
22. Boucher, R. C., *Strength of Threads*, Product Engineering, November 27, 1961.
23. ANSI N14.23, *Design Basis for Resistance to Shock and Vibration of Radioactive Material Packages Greater Than One Ton in Truck Transport (DRAFT)*, 1980, American National Standards Institute, Inc, New York.
24. Roark's Formulas for Stress and Strain, Sixth Edition, McGraw–Hill, New York, 1989.
25. American Society of Mechanical Engineers (ASME) Boiler and Pressure Vessel Code, Section III, *Rules for Construction of Nuclear Facility Components*, Division 1 – Subsection ND, *Class 3 Components*, 2010 Edition.
26. ANSI/AWS D1.2/D1.2M:2008, *Structural Welding Code–Aluminum*, American Welding Society (AWS).
27. International Atomic Energy Agency, *Regulations for the Safe Transport of Radioactive Material*, SSR-6, 2012 Edition.
28. F837-08, *Standard Specification for Stainless Steel Socket Head Cap Screws*, American Society for Testing and Materials (ASTM).
29. A574-11, *Standard Specification for Alloy Steel Socket Head Cap Screws*, American Society for Testing and Materials (ASTM).

30. American Society of Mechanical Engineers (ASME) Boiler and Pressure Vessel Code, Section III, *Rules for Construction of Nuclear Facility Components*, Division 1 – Subsection NH, Class 1, *Components in Elevated Temperature Service*, Article NH-3225, 2010 Edition.
31. American Society of Mechanical Engineers (ASME) Boiler and Pressure Vessel Code, Section III, *Rules for Construction of Nuclear Facility Components*, Division 1 – Subsection NE, *Class MC Components*, Article NE-3133.4(e), 2010 Edition.
32. American Society of Mechanical Engineers (ASME) Boiler and Pressure Vessel Code, Section III, *Rules for Construction of Nuclear Facility Components*, Division 1 – Appendix F, *Rules for Evaluation of Service Loadings with Level D Service Limits*, 2010 Edition.
33. American Society of Mechanical Engineers (ASME) Boiler and Pressure Vessel Code, Section VIII, *Rules for Construction of Pressure Vessels*, Division 1 – Subsection A, *General Requirements*, 2010 Edition.

This page left intentionally blank.

2.12.2 Certification Test Plan

This appendix describes the certification tests that were performed on the 435-B package. The justification for choosing the specific tests performed is presented and discussed. Since this material served for test planning purposes, the future tense is used. The results of the tests are provided in Appendix 2.12.3, *Certification Test Results*.

The licensing basis for the package will be primarily by full-scale test of Hypothetical Accident Condition (HAC) free drop and puncture. Analysis will be used for all Normal Conditions of Transport (NCT), except the NCT free drop. Analysis will also be used to determine the worst-case orientations for test, to determine the performance in orientations not tested, and for the HAC fire event.

Test data will consist of measured accelerations, measurements of the damaged configuration, and helium leak testing of the containment boundary.

The 1105-SD packaging is identical to the 435-B packaging documented in 435-B SAR Revision 4.3 (corresponding to NRC CoC USA/9355/B(U)-96, Revision 2). Thus, results obtained from the testing of the 435-B are fully applicable to the 1105-SD.

2.12.2.1 Certification Objective

The objectives of the certification test program are to demonstrate the adequacy of the 1105-SD package and internal component design. Since the payloads provide the shielding function, they (or a generic representation) are included in the test program. The certification tests will demonstrate the performance of the package in both the NCT and HAC free drop and HAC puncture drop events. Although analysis will be used to direct the testing, primary emphasis will be placed on the test results. Free drop impact deformation and acceleration results will be used to benchmark the analysis model for use in non-tested orientations or conditions. The benchmarking analysis is provided in Appendix 2.12.4, *Finite Element Analysis*. Significant deformation or other damage to the LTSS will be used in the HAC shielding analysis. Since the LTSS has more weight and thinner outer steel shells than the shielded devices, any damage incurred by the LTSS is bounding for the devices.

The acceptance criteria for the tests is that, following the worst-case series of free drop and puncture drop events, the containment boundary and containment seals will be leaktight per the criterion of [1], i.e., a leakage rate of 1×10^{-7} scc/sec, air. In addition, the maximum combination of free drop and puncture drop deformation will be used in the thermal analysis to show that under these worst-case conditions, the elastomer O-ring seal temperature does not exceed safe limits during the HAC fire event. Finally, any deformations or damage occurring to the LTSS will not cause the HAC dose rate to exceed regulatory limits.

Several orientations will be tested to ensure that the worst-case series of free drop and puncture drop events has been considered. Due to the relative complexity of the package design and because the acceptance criteria is based on leakage rate, the certification test units will be fabricated in prototypic full-scale. Any differences which may exist between the Certification Test Units (CTUs) and a prototypic package will be described and justified in the test report.

2.12.2.2 Initial Test Conditions

2.12.2.2.1 Temperature and Pressure

For free drops where maximum impact is desired, the foam behavior must correspond to the minimum temperature of the packaging. Of the two regulations considered [2, 3], the bounding minimum temperature is -40 °F as found in [3]. At this temperature, the polyurethane foam will exhibit its maximum crush resistance and generate the maximum impact in the given orientation. Since the foam-filled impact limiter is integral with the package, the entire CTU would need to be chilled and held at this temperature for each of the relevant free drops. To avoid the need to chill such a large package to a uniform temperature of -40 °F, an equivalent foam strength may be used. The equivalent foam must exhibit essentially the same stress-strain curve as the prototypic foam, but at a somewhat higher temperature which can be achieved in certification testing. In this way, the impact obtained will be essentially the same as the impact that would be obtained using the prototypic foam at -40 °F. A foam density of 16 lb/ft³ at a temperature of zero °F will be used. (See Section 2.12.3.3, *Certification Test Unit Configuration*, for the comparison between the strength of the foam actually used in the CTUs at the cold temperature achieved in the test, vs the maximum strength of the prototypic, 15 lb/ft³ foam at -40 °F.)

For free drops where maximum foam crush deformation is desired, the foam behavior must correspond to the NCT warm temperature of the packaging. From preliminary thermal analysis, the bulk average foam temperature under maximum heat conditions is bounded by a temperature of 150 °F. To avoid the need to heat the package to this temperature, an equivalent foam strength may be used. The equivalent foam must exhibit essentially the same stress-strain curve as the prototypic foam, at a somewhat lower temperature. In this way, the crush deformation obtained will be essentially the same as the deformation that would be obtained using the prototypic foam at 150 °F. A foam density of 14 lb/ft³ at a temperature of 110 °F will be used. (See Section 2.12.3.3, *Certification Test Unit Configuration*, for the comparison between the strength of the foam actually used in the CTUs at the warm temperature achieved in the test, vs the minimum strength of the prototypic, 15 lb/ft³ foam at 150 °F.)

Since the strength of the steel will not vary greatly with temperature, any free drop tests that do not depend on foam performance, and all puncture tests, will be performed at the prevailing temperature at the time of the test.

Since the maximum normal operating pressure (MNOP) of the 1105-SD package is 5 psig, the hoop stress in the shell will be 220 psi. This value will not have a significant effect on the test results, and therefore the test units will not be pressurized during the tests.

2.12.2.2.2 Test Facilities and Instrumentation

The certification drop and puncture testing will be conducted using a drop pad having a mass of at least 10 times the weight of the CTU. The top of the pad must be covered by an embedded steel plate of adequate thickness such that the drop pad will represent an essentially unyielding surface. The puncture bar must be a 6-in diameter bar of mild steel, mounted perpendicular to the drop pad, and having an edge radius not exceeding 1/4-inch. The bar will be reinforced by gussets at its base and fastened securely to the pad. The length of the bar must permit the bar to do maximum damage before the package becomes supported by the drop pad, and it must be at least 8 inches long. More than one length of bar may be used. Puncture bars will not be reinforced beyond what is necessary to provide rigidity at the baseplate joint.

CTU temperature will be measured by means of thermocouples embedded in the foam. As a minimum, the region of foam expected to undergo crush deformation will be monitored.

The primary means of recording the results of the certification testing will be physical measurements and observations of the CTU before and after testing. In addition, each free drop impact (both NCT and HAC) will be recorded using active accelerometers. Since puncture drops are not governing for impact, puncture drops do not need to be instrumented.

Prior to beginning testing, during testing (if the containment seal must be disturbed), and at the end of testing of each CTU, a helium leak test will be performed on the closure containment seal, and on the vent port containment seal. At the conclusion of all tests, a helium leakage rate test will be performed on the remainder of the containment boundary. Intermediate vacuum tests on the seals may be performed to ensure continued integrity.

2.12.2.2.3 Certification Test Unit Configuration

All of the CTU components (packaging, lodgment, inner container (IC), and LTSS) will be fabricated in prototypic full-scale. The shielded device payload will be simulated by a dummy shielded device which will feature the maximum device weight and typical device dimensions. Some features of the prototypic design may be modified or omitted. Any modification or omission shall be stated and justified in the test report. Some features may be added specifically to facilitate testing, such as an auxiliary vent port, accelerometer blocks welded to the containment shell, or special lifting lugs. Care shall be exercised to prevent such modifications from affecting the outcome of the tests.

2.12.2.3 Identification of Worst-Case Test Orientations

The objectives of the certification test program are:

1. To demonstrate that the 1105-SD package is leaktight following the worst-case series of free drop and puncture.
2. To quantify the worst-case damage for the HAC fire event thermal analysis.
3. To support benchmarking of the computer structural model, in order to validate calculations for orientations not tested.
4. To demonstrate the general structural integrity of the lodgment. The lodgment must prevent uncontrolled movement of the LTSS in the various impact events, such that the LTSS is not free to damage the containment boundary or incur damage from the lodgment.
5. To demonstrate the general structural integrity of the LTSS. Any non-negligible damage will be accounted for in the shielding analysis.
6. To demonstrate the general structural integrity of the IC. The IC must prevent damage to the containment boundary by the shielded device.

Components of the packaging could experience potentially significant damage as follows:

1. Closure joint, including structural deformation making the O-ring ineffective as well as limiter damage leading to excessive O-ring temperature in the fire.

Free drop impact could impart significant structural loading to the closure joint bolts.
Local puncture deformation could cause leakage of the joint. Inside-out deformation

from a failure of the lodgment to control the LTSS (or a failure of the IC to control the dummy device) could cause deformation in the joint. Puncture bar damage near the joint could lead to excessive O-ring temperatures in the fire event.

2. Containment boundary, either from excessive strains in the free drop impact or from the subsequent puncture.
3. Lodgment, whether from a failure to keep the LTSS from gross movement or from causing internal damage to the containment.
4. LTSS, by suffering damage from interaction with the lodgment that could reduce its shielding function.
5. IC, from a failure to keep the dummy device from causing internal damage to the containment.

Computer modeling is used to guide the selection of worst-case orientations. Preliminary runs of the type provided in Appendix 2.12.4, *Finite Element Analysis*, are used for this purpose. Only the final runs are reproduced in this SAR. In the following discussion, refer to Figure 2.12.4-43 for impact results, Figure 2.12.4-45 for foam crush results, and Figure 2.12.4-46 for containment boundary strain results.

2.12.2.3.1 Free Drops

Using the guidance of the FEA model results, the following tests are considered significant. Since the NCT drop height of four feet is over 13% of the HAC drop height of 30 feet, a NCT free drop will precede each HAC free drop, and be applied in the same orientation in order to maximize damage accumulation in the series.

Bottom down. Due to the large diameter of the flat bottom, energy can only be absorbed in the impact limiter at a relatively high force level. This drop consequently represents the largest overall impact of the package, as well as the largest impact along the lodgment or IC axis. This drop also challenges the attachment of the impact limiter to the lower flange. To obtain the maximum impact, it must be done at cold temperature. The impact of the payload will be less than that of the cask, due to the action of the internal absorber. The lodgment or IC must prevent the LTSS or dummy device from possibly damaging the containment boundary or sealing areas. This drop will be performed.

Side, cold (simultaneous head/limiter). As shown in Figure 2.12.4-43, the maximum lateral impact occurs in the simultaneous impact of the knuckle and impact limiter in the cold condition. This represents the largest impact perpendicular to the package axis. The lodgment or IC must prevent the LTSS or dummy device from possibly damaging the containment boundary or sealing areas. This drop will be performed.

CG over knuckle. Several orientations (top down, CG over knuckle, and knuckle-primary slapdowns) will require the upper torispherical head and side to absorb impact energy. The CG over knuckle orientation will require all of the drop energy to be absorbed by the head knuckle region. When combined with a puncture drop, it will produce the greatest plastic strain in the containment boundary. This drop does not have bounding impact, and interaction with the lodgment or IC is expected to be minimal. This drop will be performed.

Side, warm (simultaneous head/limiter). Figure 2.12.4-45 shows that the maximum foam crush occurs for the simultaneous side drop orientation. Under warm conditions, the foam crush would

be greater than shown in the figure. This type of damage, when combined with puncture damage, will potentially represent the worst case for the subsequent HAC fire event. There is also the potential for compromise of containment if the free drop or puncture forces cause deformation of the closure joint flanges. This drop will be performed.

Free drops that will not be tested are discussed below.

CG over bottom corner. As shown in Figure 2.12.4-47, the maximum closure bolt loading occurs for the near-vertical orientation in the cold condition. This is due to the lateral action of the payload acting against the inside of the upper body. The maximum bolt load is determined by analysis in Section 2.7.1.5.1, *Maximum Closure Bolt Stress*, using the benchmarked finite element model. Therefore, this orientation does not need to be tested.

Top down. The top down orientation does not generate bounding strains or impacts. The strain in the upper torispherical head is bounded by the CG over knuckle orientation. The axial impact on the package and on the payload is bounded by the bottom down orientation. This drop does not challenge the impact limiter or containment seal. The effect of internal pressure on the deformed head in the fire event is evaluated analytically in Section 2.7.4, *Thermal*, using the benchmarked finite element model. Therefore, the vertical top down free drop does not need to be tested.

Slapdown. As shown in Figure 2.12.4-43, Figure 2.12.4-45, and Figure 2.12.4-46, no slapdown drops (either knuckle primary or impact limiter primary) represent bounding impact, foam crush, or containment boundary strain. Therefore, no slapdown drops need to be performed.

2.12.2.3.2 Puncture Drops

The spectrum of possible punctures will include impacts on prior free drop damage and on undamaged areas. The temperature of all puncture tests will be the prevailing temperature at the time of the test.

On CG over knuckle damage. As discussed above, the maximum strain in the containment boundary will occur due to a puncture impact on the upper torispherical head damage caused by the CG over knuckle drop. The puncture drop orientation of the package would be the same as for the free drop, and be directed through the CG. Since the knuckle area is somewhat thinner than the base material due to the forming process used to fabricate the torispherical head, the edge of the bar should strike just inboard of the fold to maximize the shear strain in a slightly thinner region. To demonstrate the integrity of the containment boundary under conditions of maximum strain, this puncture drop will be performed.

Oblique on bottom down damage. Puncture could occur on the bottom of the package, where the foam is relatively thin, and may be somewhat thinner due to bottom down drop deformation. Although the foam is thinnest on the package axis, a greater risk of perforation of the impact limiter shell will occur with an angled puncture orientation. Such an orientation would also bring the puncture damage closer to the thermally sensitive flange area. This puncture drop will be performed.

On side drop (warm) damage – IL shell. Puncture could occur on the side drop impact limiter warm damage area. The minimum remaining foam thickness will result from the warm side drop case. The worst case puncture would be aimed approximately at the closure flange, through the package CG, with an oblique angle impact for the greatest opportunity of perforation of the

impact limiter shell. This puncture test could create damage relevant to the thermal analysis, as well as challenge the integrity of the closure flanges. This puncture drop will be performed.

Side puncture on the tube sheet region. Puncture could occur on the region around the top of the bolt tubes, tube sheet, and rain shield. The bar will be aimed at right angles to the package axis, within a small distance to the CG. An attempt to aim at the CG would require inclination of the package axis and render the target area too small to hit with adequate certainty in the actual test. The difference in damage will be small since the offset of the puncture axis from the CG will be approximately only six inches. The puncture will primarily impact the outer edge of the tube sheet and rain shield. The damage may show the maximum package side wall deformation, the ability of the rain shield to remain largely intact (i.e., limit the damage to a small region), and may produce damage relevant to the thermal analysis. This puncture drop will be performed.

On the side drop damage to the knuckle. Puncture could occur on the damage to the top head knuckle from the side drop. The bar will be aimed to strike on the top side of the damage with the bar axis through the CG. This puncture drop will be performed.

On the side thermal shield. A puncture could occur on the side thermal shield area and cause damage local to the puncture. The bar will be aimed through the CG with an oblique angle to the surface to increase the chance of ripping into the shield, which could produce damage relevant to the thermal analysis. This puncture drop will be performed.

Other possible punctures are as follows:

On the impact limiter, not on prior damage. Since the puncture bar will advance nearest the flange and seals when applied on prior damage as discussed above, puncture drops not on prior damage are not governing and do not need to be performed.

On the bolt tube area, puncture bar directed toward the bottom of the package. A puncture drop impact could be applied, either parallel to and adjacent to the package side onto the rain shield, or onto the rain shield perpendicular to the 30° inclined top surface of the impact limiter. However, the line of force would be directed mainly toward the package bottom, and thus substantially away from the package CG, and damage from this orientation is likely to be minimal. Therefore, this test does not need to be performed.

Adjacent to the lifting boss. Due to the strength of the torispherical head design, no significant damage is expected from a puncture drop adjacent to the lifting boss. Therefore this test does not need to be performed.

2.12.2.4 Summary of Certification Tests

Based on the discussions in Section 2.12.2.3, *Identification of Worst Case Orientations*, the planned certification tests for the 1105-SD package are summarized below and in Table 2.12.2-1. Free drops are depicted in Figure 2.12.2-1 and puncture drops in Figure 2.12.2-2.

The test sequence utilizes three separate CTUs, designated CTU #1, CTU #2, and CTU #3. All three CTUs are identical except for payload, polyurethane foam, and thermal shield configuration. CTU #1 and #2 contain a lodgment and LTSS (one LTSS test model will be re-used for both units). CTU #1 and #2 feature a simplified rather than a prototypic side thermal shield since no tests performed on these units will affect the side thermal shield. CTU #2 includes a head thermal shield, since the CG-over-knuckle drop and a subsequent puncture drop test occurs on the region covered by the head thermal shield. CTU #3 contains an IC and

dummy payload with wood blocking. CTU #3 includes a prototypic side thermal shield, but no head thermal shield. A summary of the configuration of the thermal shields on the test units is given in Table 2.12.2-2. Each test unit will be tested in two free drop orientations and two or three puncture orientations. The complete test series consists of six, 4-foot NCT free drops, six, 30-foot HAC free drops (in the same orientation as the NCT drops), and seven, 40-inch puncture drops.

The free drops and punctures may be performed in the order given in Table 2.12.2-1 or a different order if necessary. All free drops on CTU #1 and #3 shall be performed with the bulk average temperature of the equivalent (16 lb/ft³) foam at approximately zero °F or less. The side drop on CTU #2 shall be performed with the bulk average temperature of the equivalent (14 lb/ft³) foam at approximately 110 °F or greater, per the discussion given in Section 2.12.2.1, *Temperature and Pressure*. Interference of damage between test series is expected to be negligible. The temperature of CTU #2 for the CG over knuckle drop does not need to be controlled.

2.12.2.4.1 Tests on CTU #1

Two free drop orientations and two puncture drop orientations will be performed on CTU #1.

Free Drop, Flat Bottom Down (D1N and D1H on CTU #1). CTU #1 will be tested in the bottom end drop orientation at cold temperature. The purpose of this test is to demonstrate:

- The attachment of the impact limiter to the lower flange
- The ability of the internal absorber to absorb most of the payload energy
- The ability of the lodgment to prevent excessive movement of the LTSS

Expected results: Very modest deformation of the foam below the containment vessel, and significant deformation of the internal absorber. The LTSS will retain its general position, and damage to the lodgment will be acceptable. The impact limiter will remain attached to the lower flange, with no distortion of the flange sealing area. Containment will be leaktight.

Puncture on the bottom down impact damage from D1 (P1 on CTU #1). This puncture will occur on the bottom face of the impact limiter with the package axis inclined approximately 30° from the vertical. The purpose is to demonstrate acceptability of potentially bounding, thermally-relevant impact limiter damage. Azimuth is not important.

Expected results: The ¼-inch shell represents essentially 100% of the Bechtel TOP-9A [4] recommendation. Experience with other puncture tests on foam impact limiters shows that perforation is unlikely at this thickness level, and none is expected.

Open the package after completing tests D1N, D1H, and P1, and evaluate the need to replace the lower absorber with a new component. Evaluate the ability of the lodgment to sustain a governing side impact and repair or replace as necessary, before proceeding to test series D2.

Free Drop, Side (D2N and D2H on CTU #1). CTU #1 will be tested in the orientation where the knuckle and impact limiter contact the ground simultaneously, at cold temperature. The azimuth orientation will be with the vent port at the top (i.e., impact is 180° from the vent port) which will place lodgment ribs equally straddling the impact point. The purpose of this test is to demonstrate:

- Acceptable behavior of the impact limiter and containment under maximum lateral impact
- The ability of the lodgment to prevent excessive movement of the LTSS

Expected results: Lateral deformation of both the knuckle and the impact limiter, and possible outward deformation of the sidewall. The LTSS will retain its general position, and damage to the lodgment will be acceptable. Containment will be leaktight.

Puncture on the knuckle damage from D2 (P2 on CTU #1). This puncture will occur with the puncture bar axis through the CG, and placed to impact on the top side of the head adjacent to the damage (which is on the side of the knuckle) as shown in Figure 2.12.2-2. The azimuth location will be the same as the side drop (D2).

Expected results: A dent approximately 1 – 2 inches deep. Little or no payload interaction. Containment will be leaktight.

Tests on CTU #1 are complete.

2.12.2.4.2 Tests on CTU #2

Two free drop orientations and two puncture drop orientations will be performed on CTU #2.

Free Drop, CG over Top Knuckle (D3N and D3H on CTU #2). CTU #2 will be tested with the CG over the upper knuckle at prevailing temperature. The purpose is to impart the maximum bending strain in the knuckle region for subsequent puncture, which could affect containment. In addition, it will demonstrate the ability of the head thermal shield to maintain sufficient integrity for thermal performance in the HAC fire. The azimuth orientation (point of first contact) should be opposite to the vent port, which places it halfway between lodgment ribs. Since this impact does not include foam, the temperature of the foam is not important.

Expected results: A large flat on the top end, biased toward one side with a significant buckle in the knuckle region. The head thermal shield will not be ripped open or torn off. The internal absorber will crush locally, but the lodgment will not move significantly relative to the package interior. This will represent the maximum bending strain in the containment due to free drop. Containment will be leaktight.

Free Drop, Side (D4N and D4H on CTU #2). CTU #2 will be tested in the orientation where the knuckle and impact limiter contact the ground simultaneously, identical to tests D2N and D2H on CTU #1. This test shall be done at warm temperature, with the azimuth orientation having the vent port at the bottom. The lodgment ribs will be equally straddling the impact point. The purpose of this test is to create the maximum strain in the foam, which occurs near to the closure joint flanges. The maximum damage will also occur right at the vent port.

Expected results: Maximum foam strain will occur from this impact, which will be combined with puncture for maximum potential damage. Containment will be leaktight.

Puncture on the CG over top knuckle impact damage from D3 (P3 on CTU #2). This puncture will nominally occur in the same orientation as the associated free drop, with the puncture axis through the CG of CTU #2. The purpose is to demonstrate that the containment can sustain the worst case plastic strain and remain leak tight, and demonstrate the ability of the head thermal shield to maintain sufficient integrity for thermal performance in the HAC fire. The location of the impact should be approximately 2 – 3 inches from the outside edge of the

larger fold as shown in Figure 2.12.2-3, so as to maximize local shear loading and maximum strain. Optionally, this test could be performed immediately after test D3H.

Expected results: A dent approximately 1 – 2 inches deep. Little or no payload interaction. The head thermal shield may locally shear through but will not be torn off. Containment will be leaktight.

Puncture on the impact limiter side damage from D4 (P4 on CTU #2). This puncture will occur on the side drop crush damage on the impact limiter with the puncture bar aimed at the flange and the package CG. The angle of the package axis to the horizontal is approximately 35°. The azimuth will be the same as free drop D4. The purpose of this test is to demonstrate:

- Acceptability of potentially bounding, thermally-relevant impact limiter damage
- Containment is maintained following the worst case puncture near the closure flange

Expected results: A dent will occur at the puncture site, but no perforation of the shell is expected. The damage will be compared to other cases for thermal consequences and the worst case will be included in the thermal analysis. Containment will be leaktight.

Tests on CTU #2 are complete.

2.12.2.4.3 Tests on CTU #3

Two free drop orientations and three puncture drop orientations will be performed on CTU #3. The purpose of CTU #3 is to test the behavior of the IC with the dummy payload and blocking. The governing drops for the payload will be the maximum impact, which are the same ones that were used for the lodgment/LTSS tests in CTU #1. Therefore, the free drop orientations will be the same as for CTU #1.

Free Drop, Flat Bottom Down (D5N and D5H on CTU #3). CTU #3 will be tested in the bottom end drop orientation at cold temperature. The purpose of this test is to demonstrate the ability of the IC to adequately control the dummy device.

Expected results: The same package responses as for D1N and D1H on CTU #1. The dummy device may change position, but no unacceptable damage to the package will occur. The package will be leaktight.

Puncture on the bottom down impact damage from D5 (P6 on CTU #3). This puncture will be identical to puncture P1 on CTU #1. The results will be the same.

Open the package after completing tests D5N, D5H, and P6, and evaluate the need to replace the lower absorber, the IC, or the blocking with new components before proceeding to test series D6.

Free Drop, Side (D6N and D6H on CTU #3). CTU #3 will be tested in the orientation where the knuckle and impact limiter contact the ground simultaneously, at cold temperature. The azimuth orientation will be with the vent port at the top. The purpose of this test is to demonstrate the ability of the IC to adequately control the dummy device.

Expected results: The same package responses as for CTU #1. The dummy device may change position, but no unacceptable damage to the package will occur. The package will be leaktight.

Puncture on package side on the tube sheet (P5 on CTU #3). This puncture will occur with the puncture bar perpendicular to the package axis, and placed essentially centered on the tube sheet and rain shield region as shown in Figure 2.12.2-4. The bar will be directed as near as

practical to the CG. (Trying to aim directly at the CG may invalidate the test because a slight error in the impact point could cause the puncture bar to miss the tube sheet altogether.) The azimuth location will be at the vent port.

Expected Results: The tube sheet and adjacent bolt tubes will be crushed. The rain shield will be locally deformed, but will remain globally in proper position. The vent port shield will be trapped in its tube. The side wall may deform inward. Containment will be leaktight.

Puncture on the thermal shield (P7 on CTU #3). This puncture will occur with the puncture bar axis through the CG with the package axis at 30° to the horizontal, head down, as shown in Figure 2.12.2-2. The azimuth is not important.

Expected results: A dent approximately 1 – 2 inches deep. Some tearing of the outer or inner thermal shields is possible. Containment will be leaktight.

Tests on CTU #3 are complete.

2.12.2.5 Acceptance Criteria

The following are the acceptance criteria for certification testing of the 1105-SD package:

1. Each CTU, at the conclusion of all drop and puncture testing, shall remain leaktight per [1], as demonstrated by helium leakage rate testing.
2. The maximum damage to the package from the single worst-case free drop and puncture test sequence must fall within the bounding assumptions used in the HAC fire thermal analysis. Alternatively, the worst post-test configuration will form the basis for a conservative thermal analysis.
3. After all testing, including the worst-case puncture onto the rain shield/bolt tube region, the vent port insulation cylinder must be retained either by the rain shield or by other deformation, such as deformation of the vent port tube.
4. The lodgment shall control the displacement of the LTSS, and the IC must control the dummy device, such that the CTU remains leaktight.
5. The LTSS must remain intact, and deformations must be negligible relative to the shielding function. Alternatively, the LTSS damage, including lead slump if any, will form the basis for a conservative shielding analysis.

Table 2.12.2-1 – Summary of Certification Tests

No.	Test Description	CTU/Payload	Foam Density & Temperature	Purpose of Test & Expected Damage
D1N D1H	Bottom end drop	#1 (LTSS)	16 lb/ft ³ , Cold	Maximum end impact, internal absorber crush, lodgment performance
D2N D2H	Side (simultaneous)	#1 (LTSS)	16 lb/ft ³ , Cold	Maximum lateral impact, impact limiter, lodgment performance
D3N D3H	CG over knuckle	#2 (LTSS)	Not controlled	Plastic strain, challenge to containment
D4N D4H	Side (simultaneous)	#2 (LTSS)	14 lb/ft ³ , Warm	Maximum foam crush, combine with worst case puncture
D5N D5H	Bottom end drop	#3 (IC)	16 lb/ft ³ , Cold	Maximum axial impact for payload
D6N D6H	Side (simultaneous)	#3 (IC)	16 lb/ft ³ , Cold	Maximum lateral impact for payload
P1	On bottom end drop (D1) damage	#1 (LTSS)	Not controlled	Possible governing thermal damage
P2	On side knuckle (D2) damage	#1 (LTSS)	Not controlled	Plastic strain, challenge to containment
P3	On CG over knuckle (D3) damage	#2 (LTSS)	Not controlled	Plastic strain, challenge to containment
P4	On side drop (D4) damage	#2 (LTSS)	Not controlled	Possible governing thermal damage, challenge to containment
P5	On rain shield/tube sheet region	#3 (IC)	Not controlled	Deformation of tube sheet, rain shield, and side wall, possible governing thermal damage
P6	On bottom end drop (D5) damage	#3 (IC)	Not controlled	Possible governing thermal damage
P7	On side thermal shield	#3 (IC)	Not controlled	Obtain bounding damage to shield for thermal analysis

Table 2.12.2-2 – Summary of Certification Test Unit Thermal Shield Configuration

CTU	Thermal Shields	Comments
1	Simulated side shield, no head shield	Neither type of thermal shield is relevant to the tests performed on this unit.
2	Simulated side shield, prototypic head shield	CG-over-knuckle free drop and related puncture will test the prototypic head thermal shield.
3	Prototypic side shield, no head shield	Puncture on side of package tests the prototypic side thermal shields.

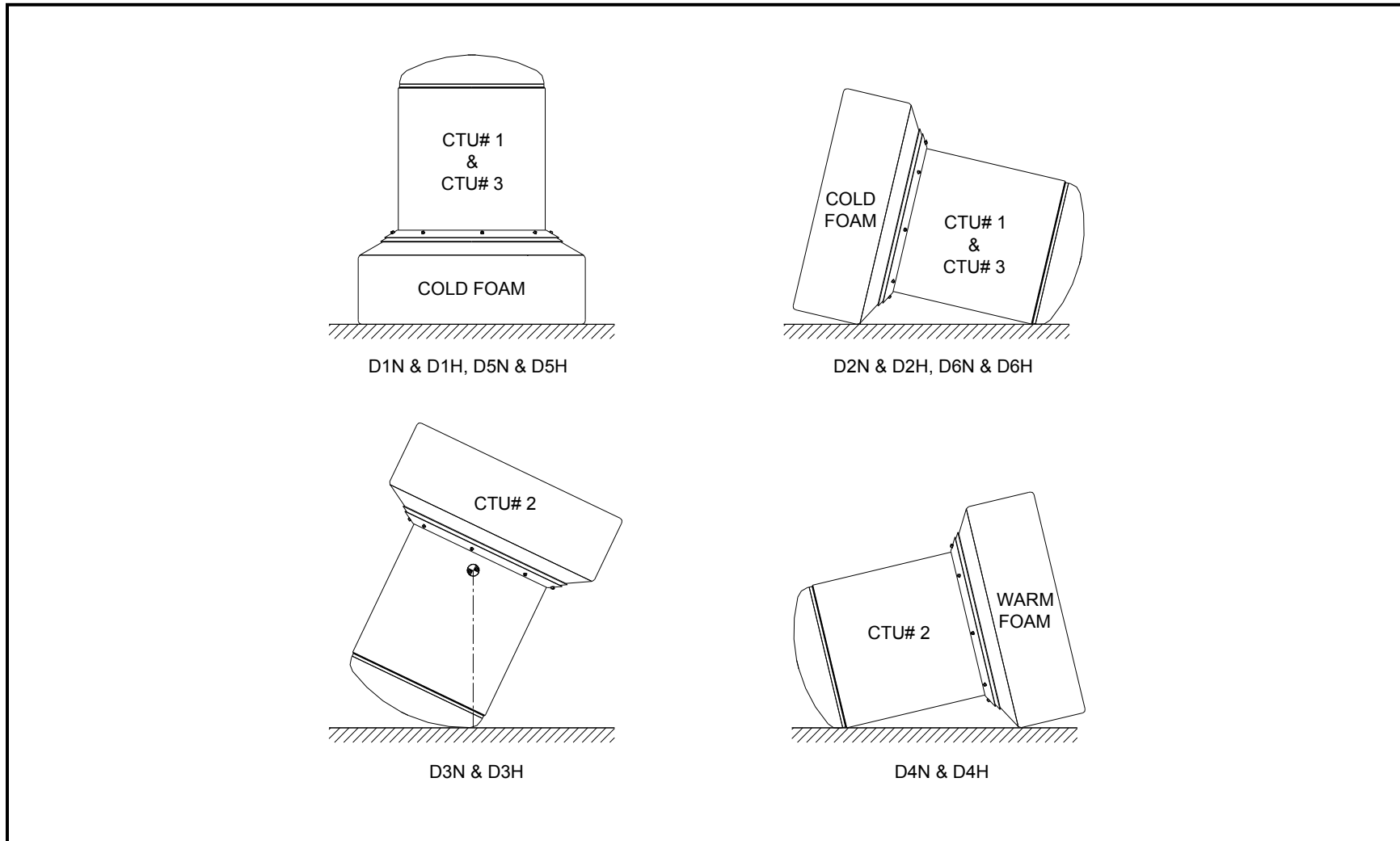


Figure 2.12.2-1 – 1105-SD Free Drop Orientations

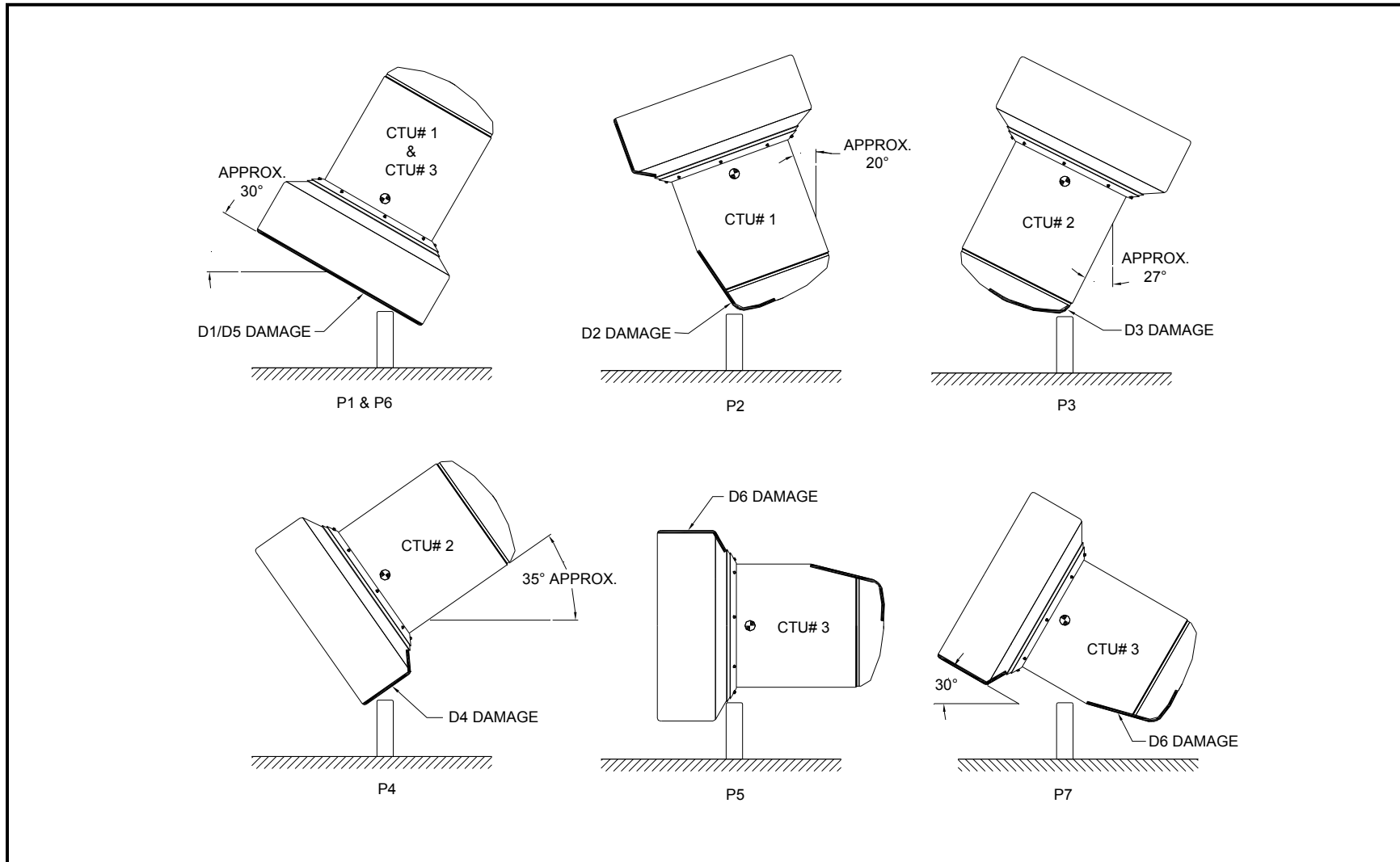


Figure 2.12.2-2 – 1105-SD Puncture Drop Orientations

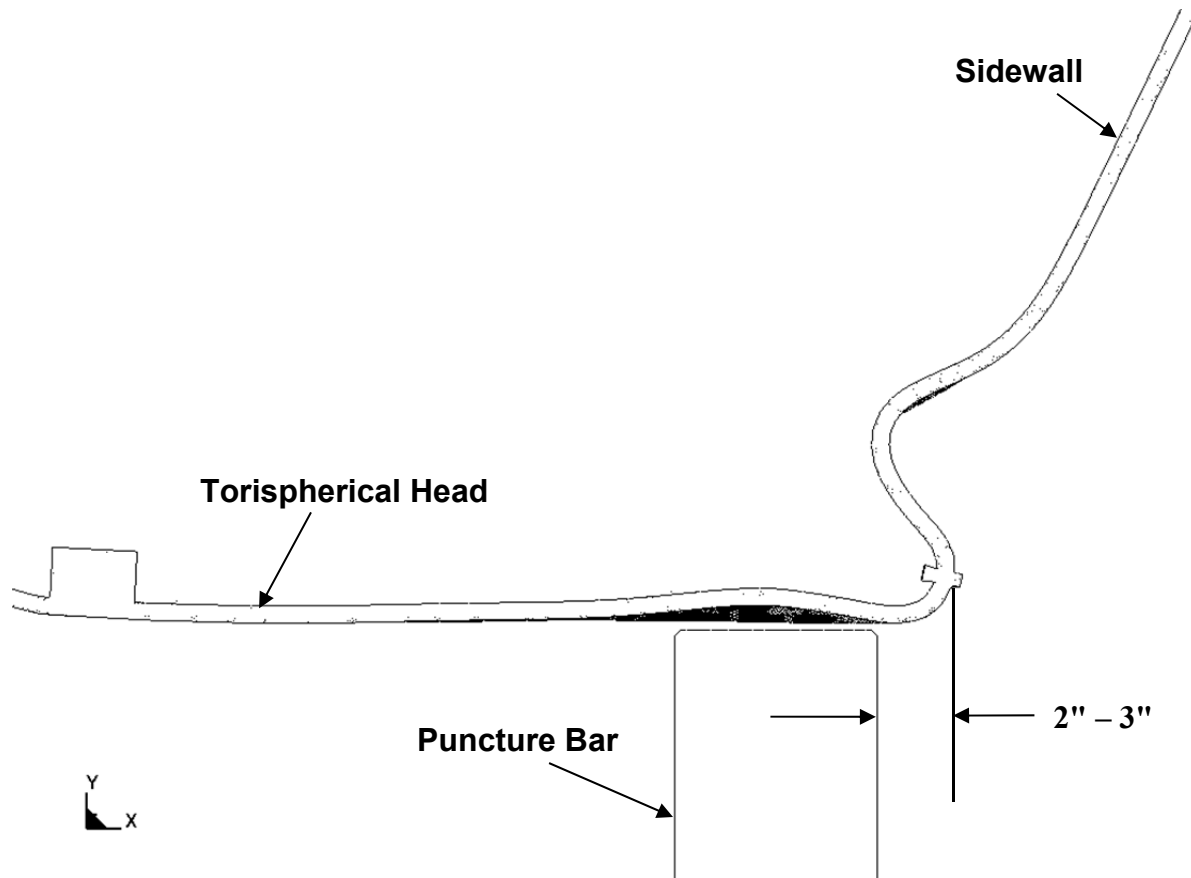


Figure 2.12.2-3 - Puncture Drop Orientation Detail for P3

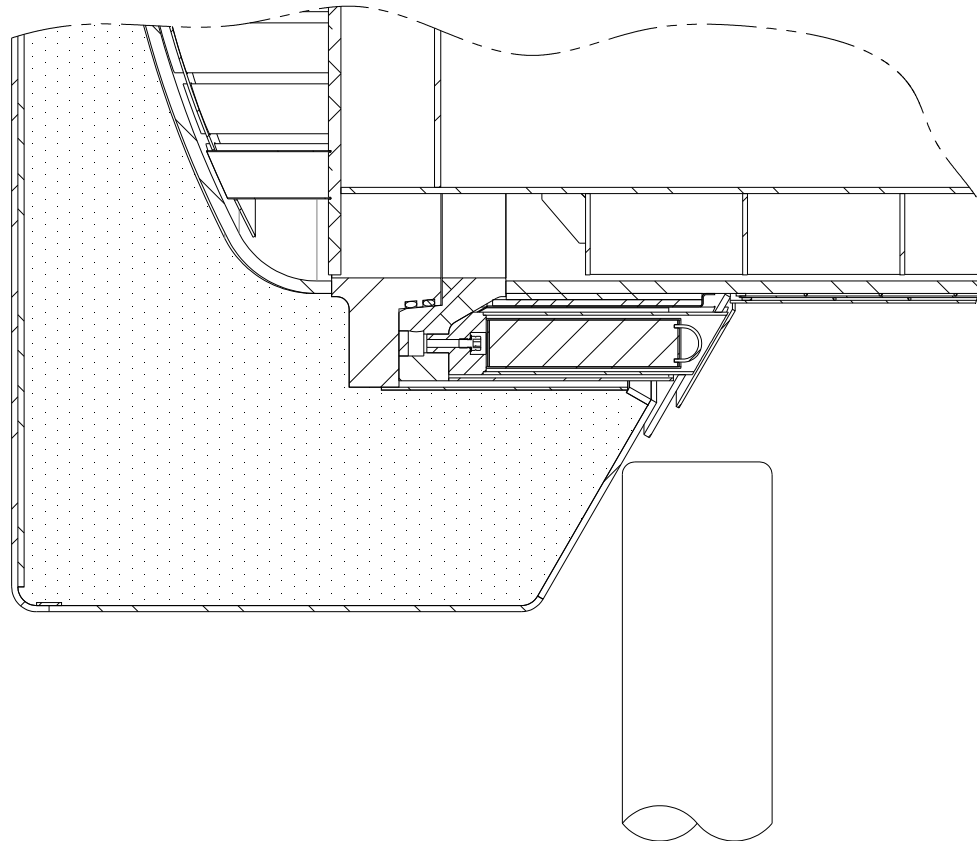


Figure 2.12.2-4 - Puncture Drop Orientation Detail for P5

2.12.2.6 References

1. ANSI N14.5-1997, *American National Standard for Radioactive Materials – Leakage Tests on Packages for Shipment*, American National Standards Institute (ANSI), Inc.
2. Title 10, Code of Federal Regulations, Part 71 (10 CFR Part 71), *Packaging and Transportation of Radioactive Material*, 01-01-18 Edition.
3. International Atomic Energy Agency, *Regulations for the Safe Transport of Radioactive Material*, SSR-6, 2012 Edition.
4. Bechtel Power Corporation, *Design of Structures for Missile Impact*, BC-TOP-9A, Rev. 2, 9/1974.

This page left intentionally blank.

2.12.3 Certification Test Results

This appendix presents the results of the certification testing of the 435-B package that addresses the performance requirements of 10 CFR 71 [1]. This material summarizes the information presented in the certification test report [2]. The 1105-SD packaging is identical to the 435-B packaging documented in 435-B SAR Revision 4.3 (corresponding to NRC CoC USA/9355/B(U)-96, Revision 2). Thus, results obtained from the testing of the 435-B are fully applicable to the 1105-SD.

2.12.3.1 Introduction

Demonstration of the compliance of the design of the 1105-SD package with the requirements of 10 CFR §71.73 was primarily achieved using formal certification testing. Analysis was used for all NCT events except the free drop, and for the HAC thermal case. Analysis using a model benchmarked against test results was also used to evaluate certain orientations that were not tested. The NCT and HAC free drop events and HAC puncture event were demonstrated by testing. This appendix describes the results of the free drop and puncture testing, including post-test measurements and evaluations. The testing utilized three, full-scale certification test units (CTUs). Testing was performed to a written procedure which was based on the test plan presented in Appendix 2.12.2, *Certification Test Plan*. A total of six NCT free drops, six HAC free drops, and seven HAC puncture drop tests were performed on the units. The primary success criterion was that, subsequent to all free drop and puncture testing, the CTU containment boundary, including the main containment seal and vent port seal, be leaktight per ANSI N14.5 [3]. Other supporting data, including accelerations and physical measurements, was collected as described herein.

2.12.3.2 Test Facilities and Instrumentation

2.12.3.2.1 Test Facilities

Testing was performed at Lampson International LLC in Pasco, Washington, beginning November 28, 2011. The drop pad weighed approximately 110,000 lb, including a 2-inch thick, embedded steel plate impact surface. The pad therefore represented an essentially unyielding surface for the CTUs, which weighed between approximately 9,650 and 9,775 lb. The puncture bar assembly was made of ASTM A36 steel, 6 inches in diameter, 24 inches long, with an edge radius of 0.22 to 0.25 inches. The bar was affixed to a steel baseplate and welded to the drop pad for puncture drop testing.

Eight free drops were performed with the impact limiter polyurethane foam in the cold condition. A refrigerated trailer was present onsite to chill the CTUs prior to testing. Thermocouples were inserted in 1/4-inch diameter holes in each CTU, 9 inches deep, through the plastic plugs on the side of the CTUs. Three thermocouples were used for each test article, located 120° apart. Two free drops were performed with the impact limiter foam at warm temperature. A combination of heating blankets and warm ambient air inside an enclosure were used to warm the foam. Two free drops were performed using the prevailing temperature of the CTU. All puncture tests used prevailing temperature.

2.12.3.2.2 Instrumentation

Accelerometers were used to record the impact of each free drop. Accelerations of the puncture drops were not recorded. For axial or near-axial drop orientations, the measurement axis of the accelerometers was axial. For the near-horizontal side drops, the measurement axis was transverse to the cask axis.

Two axial and two transverse mounting positions were provided at each end of the cask. The measurement axes were as close to the cask surface as possible, and the mounting blocks were rigidly welded to the cask. The mounting location and orientation of each accelerometer is shown in Figure 2.12.3-1. The transverse accelerometers at each end were all mounted on the same axial plane with their axes parallel. The two accelerometers located at the azimuth of the seal test port were designated T/U (at test port, upper location) and T/L (at test port, lower location). The two accelerometers located 180° away from the first set were designated OT/U and OT/L, where the 'O' indicates 'opposite', i.e., 180° away from the first set.

The raw data was conditioned and low-pass filtered at a cutoff frequency of 500 Hz. Per the guidance given in TS-G-1.1, *Advisory Material for the IAEA Regulations for the Safe Transport of Radioactive Material*, an appropriate cutoff frequency range is found from:

$$f_c = [100 \text{ to } 200] \times \left(\frac{100}{m} \right)^{\frac{1}{3}} = 280 \text{ to } 560 \text{ Hz}$$

Where m is the mass of the package in metric tonnes (10,100 lb equals 4.59 metric tonnes). From this, a reasonable cutoff frequency of 500 Hz is chosen. Further reduction of accelerometer data is discussed in Section 2.12.3.4, *Free Drop and Puncture Drop Test Results*.

2.12.3.3 Certification Test Unit Configuration

The three CTUs were fabricated in full scale in accordance with the SAR drawings in Appendix 1.3.3, *Packaging General Arrangement Drawings*, except as noted and justified below. CTU #1 used a dummy LTSS payload and lodgment #1. CTU #2 used the same LTSS payload and lodgment #2. The two lodgments were identical and are shown on drawing 3021718-SAR. CTU #3 used an Inner Container (IC), shown on drawing 3021719-SAR, and a dummy shielded device payload. The details of the CTU configurations are given in Table 2.12.3-1 and depicted in Figure 2.12.3.3-1 through Figure 2.12.3.3-5. A number of features are common to all of the CTUs, and these are listed at the beginning of Table 2.12.3-1 and depicted in Figure 2.12.3.3-1. Features specific to each individual CTU are then detailed in the remainder of the table and in Figure 2.12.3.3-2 through Figure 2.12.3.3-5. In each case, the differences between the CTU and the SAR drawings are justified in the numbered paragraphs of this section and indexed in the table and on the figures. The weights of the CTUs are given in Table 2.12.3-2. The dummy LTSS is shown in Figure 2.12.3.3-6 and the dummy shielded device is shown in Figure 2.12.3.3-7. The specific features of the CTUs are identified and justified as follows.

1. CTU #1 and CTU #3 had slightly higher density (nominally 16 lb/ft³) polyurethane foam installed in the impact limiter compared to the production foam density (nominally 15 lb/ft³). The higher density foam, when chilled to a temperature of 0 °F as discussed in Section 2.12.2.2, *Initial Test Conditions*, has crush properties essentially equal to those of the production foam at a temperature of -40 °F. The temperature of -40 °F is conservatively below the cold environment temperature of -20 °F found in [1], and corresponds to the

minimum environment temperature found in [4]. In this way, the crush strength of the foam in CTUs #1 and #3 at the target test temperature of 0 °F would accurately simulate the higher strength of the production foam at a temperature of -40 °F. The comparison of the stress-strain curves for the two foam densities at cold temperature is given in Figure 2.12.3-2. The production foam (15 lb/ft³) is shown for -40 °F and includes a +10% manufacturing strength tolerance and a dynamic adjustment. The test foam (16 lb/ft³) is shown for the actual manufactured strength, the actual test temperature of -10 °F, and a dynamic adjustment. The properties of the production foam are developed in Appendix 2.12.4, *Finite Element Analysis*.

2. CTU #2 had slightly lower density (nominally 14 lb/ft³) polyurethane foam installed in the impact limiter compared to the production foam density (nominally 15 lb/ft³). The lower density foam, when heated to a temperature of 110 °F as discussed in Section 2.12.2.2, *Initial Test Conditions*, has crush properties essentially equal to those of the production foam at a temperature of 150 °F. The temperature of 150 °F is slightly above the foam bulk average temperature under the hot environment conditions presented in Chapter 3, *Thermal Evaluation*. In this way, the crush strength of the foam in CTU #2 at the target test temperature of 110 °F accurately simulated the lower strength of the production foam at a temperature of 150 °F. The comparison of the stress-strain curves for the two foam densities at elevated temperature is given in Figure 2.12.3-2. The production foam (15 lb/ft³) is shown for 150 °F and includes a -10% manufacturing strength tolerance and a dynamic adjustment. The test foam (14 lb/ft³) is shown for the actual manufactured strength, the actual test temperature of 117 °F, and a dynamic adjustment. The properties of the production foam are developed in Appendix 2.12.4, *Finite Element Analysis*.
3. CTU #1 and CTU #2 had simulated thermal shields installed on the side of the packages instead of production thermal shields. A production thermal shield on the cylindrical side (shown in Detail R on sheet 5 of drawing 3021717-SAR) was installed on CTU #3, since a puncture test was performed directly on the shield of that unit in order to test its integrity. But since the presence of a thermal shield on the side of CTUs #1 and #2 did not have any significant effect on the tests performed on those units, it was not necessary to include production thermal shields. The simulated thermal shields consisted of a single layer of 0.105-inch thick stainless steel, essentially the full length of the side shield region, without stand-off wires, in order to partially make up the weight of the full shield. It was welded using intermittent welds to the cask shell, and its vertical seam was a lap joint using intermittent welds, as detailed in Figure 2.12.3.3-5. As such, it represented less structural strength than a production shield, which has uninterrupted welds to the body and a full bevel weld vertical seam. Note also that the inner, 0.060" thick thermal shield was conservatively not included with the simulated thermal shields. To account for the effect of the stack-up of steel strips that is used at the top end of the production thermal shield (an area which was deformed in the side drop events), an equivalent strip of 5/16-inch thick stainless steel was welded to the location of the top and lower ends of the production shield. Thus, the simulated thermal shields on CTUs #1 and #2 represented a package having somewhat less structural strength on the side than the production model, while including the hard point that could increase containment boundary strain in a side impact.
4. CTU #1 and CTU #3 did not have a thermal shield on the upper torispherical head. A production head thermal shield (as shown in Detail T on sheet 6 of drawing 3021717-SAR)

was installed on CTU #2, since the tests on that unit included the free drop and puncture drop impact on the head. Since the thermal shield provides added structure to the torispherical head of the package, the effect of the absence of the head shield on CTUs #1 and #3 is conservative. Since the weight of the head thermal shield is relatively small (~ 67 lb), it was not necessary to make up the weight of the missing shield.

5. Because the testing performed on the CTUs was structural and not thermal, it was not necessary to provide a production finish to the internal surfaces of the production thermal shields used on CTU #2 (top head shield) and #3 (side shield). The finishes specified for the production package (see flag note 42 on sheet 2 of drawing 3021717-SAR) are provided only to reduce heat transfer by radiation. The surface finish used on the CTUs was as-received.
6. To facilitate leak testing during the certification test series, an auxiliary vent port was placed in each CTU on the side near the top head joint, in an azimuth location that prevented significant damage to the 1-inch NPT hole. The presence of the hole did not have a significant effect on any of the tests.
7. In order to facilitate rigging and lifting the CTUs, the threaded hole on the top of the upper head was increased to 1-8 UNC thread and a correspondingly large swivel hoist ring was used. The production hole is 3/4-10 UNC, and is used only to lift the top assembly (the bell). The larger hole and hoist ring allowed for safe lifting of the entire package. This difference had no effect on any tests. To further facilitate rigging, carbon steel plates having a threaded hole were attached by welding to the lower sides of the impact limiter. These plates are depicted in Figure 2.12.3.3-1 and are shown in numerous photographs, such as in the lower right-hand corner of Figure 2.12.3-17. These plates were distant from the deformation of the impact limiter in each case, and had no effect on any tests.
8. To record impact accelerations of the free drops, four accelerometers were used with each drop. To mount the accelerometers, Type 304 stainless steel blocks, 1-inch cubic in size, were mounted to the package as shown in Figure 2.12.3-1. The mounting locations required small cutouts to be made in the production (CTU #3) and simulated (CTU #1 and #2) side thermal shields. The blocks and cutouts had no effect on any of the tests.
9. To record the temperature of the polyurethane foam, three thermocouple wires were used in holes that were placed in the three plastic melt-out plugs on the side of the impact limiter. The holes were 9 inches deep and 1/4 inches in diameter. This depth placed the thermocouples at essentially the volumetric center of the foam body. Two additional holes were placed through the impact limiter steel shell, at the same height, on CTU #2. These holes did not have a significant effect on the crush behavior of the impact limiters in any drop or puncture event.
10. Due to flange distortion during fabrication, the vent and test ports became misaligned to the package axis. They were repaired by placing new ports in a block welded to the flange. The production design uses the same welded block, except the block is configured such that no flange counter bore is necessary. In addition, the production design has a 50% larger vent hole diameter, a different configuration in the flange, and an additional weld. Because both designs depend for strength on the same 3/16-inch all-around fillet weld between the block and the flange, they have the same resistance to damage. The as-tested and production designs are compared in Figure 2.12.3-3. The production designs are formally detailed in Section M-M and Section N-N of sheet 6 of drawing 3021717-SAR. Furthermore, during

testing, no significant loadings were transmitted to the vent or test port regions, as demonstrated by the relatively large distance between the port areas and external damage areas. Therefore the difference in the port designs had no effect on the test results.

11. To ensure that the lodgment was azimuthally oriented properly for the worst-case damage to occur, two aluminum tabs were welded to the lower internal impact limiter assemblies at a distance of 14 inches from the center of the plate. The tabs are shown in Figure 2.12.3-8 in the 6 o'clock position. The tabs are not used on the production package. Since their purpose was to ensure the test damage was maximized, their presence in the test units was conservative.
12. The lid of the IC features three radial ribs. In the production design, the ribs are welded to the inner sheet of the lid using intermittent fillet welds as shown in Section B-B on sheet 2 of drawing 3021719-SAR. Instead, a continuous fillet weld was used on the test articles. The performance of the 1105-SD does not depend on the IC lid. The IC lid is a relatively thin structure that simply transmits any impact loading from inside the IC to the upper internal impact limiter. The IC lid is not designed to resist loads using the rib-to-inner sheet welds. Therefore, the performance of the 1105-SD would be the same whether the welds were intermittent or continuous.
13. The CTUs did not have any caps over the guide pin holes in the upper flange. The caps in the production design keep the region surrounding the bolt access tubes closed to the environment, and are shown in Section F-F on sheet 4 of drawing 3021717-SAR. The lack of these caps (two) had no effect on the test results.
14. The CTUs did not have a lead-in chamfer on the bell opening, which is depicted in Detail AA on Sheet 6 of drawing 3021717-SAR. This had no effect on the test results.
15. The CTU used three melt-out plugs on the outer circumference of the external impact limiter. The production quantity is six melt-out plugs. This difference had no effect on the test results.
16. The diameter of the containment and test O-rings was 44.6 inches for CTU #1 and #3, and 44.1 inches for CTU #2. The production diameter is 44.1 inches. The small difference in diameter (0.5 inches for CTU #1 and #3) had no effect on the test results.
17. The outer diameter of the lodgment and IC used in the CTUs was nominally 43.0 inches. The production nominal diameter is 42.75 inches, or a difference of 0.25 inches. In addition, the height of the lower corner of the lodgment was nominally 8.0 inches from the base. The production nominal dimension is 10.0 inches, as shown in View B-B on sheet 2 of drawing 3021718-SAR. These small differences did not have a significant effect on the test results.
18. The adjustment bolt used with the toggle clamps attached to the lodgment for CTU #1 and CTU #2 was made from alloy steel. The production adjustment bolt is made from bronze. The toggle clamp and adjustment bolt is shown in Zone D/6-7 on sheet 2 of drawing 3021718-SAR and in Figure 1.2-6a. The three toggle clamps apply a lateral stabilizing force to the top end of the LTSS to prevent unwanted motion during routine transport. The bronze adjustment bolts are chosen to reduce the possibility of marring of the LTSS surface by the adjustment bolt heads in normal use. Of note, the toggle clamps do not perform a safety function. The LTSS is fully controlled by the structure of the lodgment. Bending of the steel adjustment bolts and unlatching of the toggle clamps occurred during the free drop testing of

the CTUs, and is acceptable. The LTSS was not damaged by the toggle clamp bolts. The bronze production bolts will not change the performance of the 1105-SD package or the LTSS under NCT or HAC.

The dummy LTSS was used for test in CTU #1 and CTU #2, and is shown in Figure 2.12.3.3-6 and Figure 2.12.3-21. It was constructed using the same bounding outer dimensions as the production LTSS. It included all of the same external steel shells, protrusions, welds, and lead fill. The dummy LTSS used a solid steel central barrel, without any longitudinal holes or drawers. The dummy LTSS did not have operating hinges for the end doors, having instead welded steel blocks that simulated the size, shape, attachment, and location of the production hinges. The internal security plates were installed loose instead of bolted in place. The dummy LTSS weighed 4,460 lb from Table 2.12.3-2, which is within the 4.3% of the weight of the production LTSS which weighs nominally 4,660 lb from Table 2.1-2. These differences were not material to the test

The dummy shielded device was used for tests in CTU #3 and is shown in Figure 2.12.3.3-7 and Figure 2.12.3-39. It was designed to simulate the weight of a generic shielded device. The body is a pipe, 20 inches in diameter, filled with lead, and closed with rigid steel ends. The overall length is 34 inches. It had a weight of 3,570 lb, essentially equal to the maximum device weight limit of 3,500 lb. It was held in place within the IC using wood dunnage. The dunnage was of two kinds: pallets and end caps. The pallets were made from 4×4 lumber attached to a disc of ½-inch thick plywood. The end caps were made of 1-1/8-inch thick plywood sheets. One end cap (with test damage) is shown in Figure 2.12.3-38.

2.12.3.4 Free Drop and Puncture Drop Test Results

Results of the free drop and puncture drop tests are given below. Tests on the three CTUs were arranged in six series of two on each CTU, consisting of one, 4-ft NCT free drop followed by one, 30-ft HAC free drop, and concluded by at least one, 40-inch puncture drop test. Thus there were a total of six, 4-ft NCT free drop tests, six, 30-ft HAC free drop tests and seven 40-inch puncture drop tests. The test series were performed in the order D1 (D1N, D1H, & P1), D5 (D5N, D5H, & P6), D2 (D2N, D2H, & P2), D3 (D3N, D3H, & P3), D6 (D6N, D6H, P5 & P7), and D4 (D4N, D4H, & P4). The tests are depicted in Figure 2.12.2-1 and Figure 2.12.2-2 and summarized in Table 2.12.2-1 from Appendix 2.12.2, *Certification Test Plan*. Photographs of each test, including post-test examinations, are given in Figure 2.12.3-4 through Figure 2.12.3-49. Low pass filtered accelerometer time histories are given below in Section 2.12.3.6, *Filtered Accelerometer Time Histories*. The acceleration peak values are then resolved to a value that is perpendicular to the ground. Due to the necessity of mounting some accelerometers with their mounting threads facing upwards and others with the threads facing downwards, both positive and negative signals were recorded. However, all results shown in the following summaries are given as positive. Since the data was collected orthogonal to the cask axes, the resultant of the average of the peak acceleration data in the oblique impact cases is as follows.

For free drop tests D1 and D5, which were vertical bottom-down drops, the accelerometers were mounted with their measurement axes parallel to the impact direction. Therefore, the accelerometer readings require no adjustment.

For tests D2, D4, and D6, which were identical side drops in which the upper knuckle and impact limiter corner contacted the pad simultaneously, the cask axis was inclined at an angle of 13° to

the ground. The accelerometers were mounted with their measuring axes transverse to the cask axis. The accelerometer reading is divided by the cosine of 13° to obtain the impact which occurred perpendicular to the ground.

For test D3, which was the c.g.-over-knuckle free drop, the accelerometers were mounted with their measurement axes parallel to the cask axis. The accelerometer reading is divided by the cosine of 27°, which corresponds to the recorded angle between the cask axis and the vertical, to obtain the impact perpendicular to the ground.

All puncture drop tests were performed from a height of 40 inches above the top of the 24-inch long puncture bar. The bar remained securely attached to the drop pad during the test, and was not observed to experience permanent deformation. The radius became damaged from contact with the CTUs and was re-dressed prior to further use.

For each test, the temperature of the polyurethane foam (for test D3, the exposed steel surface on the top) was recorded, depending on which was relevant to the test impact. As discussed in Section 2.12.3.3, *Certification Test Unit Configuration*, the cold temperature target for the bulk of the polyurethane foam was 0 °F, and the warm temperature target was 110 °F. The temperature of the steel and of the foam for puncture drops was accepted at the prevailing temperature and recorded at the time of the test.

After the completion of each series of 4-ft, 30-ft, and puncture drop tests (with the single exception of the D3 series), the CTUs were opened for internal inspection. Each time this was done, a helium leakage rate test with a criteria of leak tight per [3] was performed to test the integrity of the main containment O-ring seal and vent port containment sealing washer. (All leakage rate tests mentioned in this SAR used the same leak tight criteria from [3].) This was followed by a measurement of the removal torque of the closure bolts and inspections of the internal components. Removal torque was measured using a dial-type torque wrench loaded in the counter-clockwise direction. Loading was manually increased until the reversal torque reached a maximum, which was recorded. The torque was not removed from any bolt until all of the bolts had been checked. Note that, due to the inclined angle of the threads, the removal torque is somewhat less than the application torque. Trials have shown that bolt removal torque will be between 2/3 and 3/4 of the application torque for joints that have not undergone drop testing. Thus an even lower value would be expected from impact tested joints. It was noted during removal that some of the bolt washers were scored. Subsequently, care was taken to lubricate not only the threads but also the washers during reassembly. Prior to resuming tests (if any), the components of the CTU were cleaned, reassembled according to drawing requirements, and leakage rate tested.

At the conclusion of all free drop and puncture testing, each CTU was subjected to a helium leakage rate test of the containment boundary. All surface obstructions, such as, for example, the head thermal shield, or the sheet enclosing the bolt tube region, were removed or cut open to ensure free access of helium to the entire bell and upper heavy flange surface. On the base, the impact limiter foam was not removed before leakage rate testing. Since the base containment boundary (consisting of the lower torispherical head and lower heavy flange) did not experience any recorded deformations, and in light of the fact that the material (ASTM Type 304 stainless steel) is capable of very large strains before fracture and is not subject to low-strain cracking, the presence of a crack or fissure resulting from any of the tests is not credible. Therefore testing

with the polyurethane foam in place was acceptable. The integrated leak rates for each containment boundary are summarized in Table 2.12.3-3.

2.12.3.4.1 Test Series D1

Test series D1 was performed on CTU #1 and consisted of a 4-ft NCT and a 30-ft HAC free drop in the bottom-down orientation, with the axis vertical, followed by a puncture drop test on the flat bottom of the impact limiter, with the cask axis inclined at 30° from the vertical. The tests were designated D1N, D1H, and P1 for the 4-ft, 30-ft, and puncture drops, respectively. The free drop orientation (identical for D1N and D1H) is shown in Figure 2.12.3-4. The polyurethane foam temperature readings for test D1N were -10.0 °F, -11.3 °F, and -11.2 °F, and for test D1H, -9.0 °F, -9.5 °F, and -10.4 °F. Accelerometer results are shown in the table below.

Accelerations, Free Drop Test D1					
Location	T/U	T/L	OT/U	OT/L	Avg. \perp
Test D1N	316g	315g	353g	330g	329g
Test D1H	856g	815g	696g	705g	768g

Both of these impacts imparted no visible damage to the CTU. The only external measurement taken at the time of the drops was the overall height. The height after D1N was 83-7/16 inches, compared to an as-fabricated height of 83-3/4 inches, for an apparent decrease of 5/16 inches. The same measurement taken after the D1H drop was the same as for the D1N drop, seeming to indicate no further compression of the impact limiter. It appears anomalous that a small drop height would produce more deformation than a larger one. In fact, the actual changes in overall height of the package were probably too small to be accurately measured using the techniques used. In any case, the external deformation was negligible. As discussed below, energy was absorbed internally.

After the D1H free drop, a 1/4-inch diameter hole was drilled at the center of the bottom sheet of the impact limiter and through the foam to the lowest point on the lower torispherical head. After subtracting a total of 0.66 inches for the steel shell, the insulating paper, and an observed gap, the thickness of the foam was measured to be 3.9 inches. Since a pre-test measurement of this dimension was not made, the post-test result must be compared to the fabricated nominal dimension, which was 3.4 inches. Since this value is less than the post-test result, it is postulated that an unobserved gap was created between the torispherical head lower surface and the inner surface of foam by the impact. In any case, it appears that the crush of foam in the free drop events was very small. The package after the D1H drop is shown in Figure 2.12.3-5.

The puncture drop P1 orientation is shown in Figure 2.12.3-6. The axis of the puncture bar was directed through the c.g. at an oblique angle of 29.5° to the bottom surface. The temperatures of the foam were 12.1 °F, 12.7 °F, and 15.2 °F. The bar made a dent 3-1/8 inches deep and cut a small, approximately 1.5-inch wide perforation in the bottom sheet. (This was, incidentally, the only exposure of polyurethane foam from any of the drops or puncture tests.) The puncture damage is shown in Figure 2.12.3-7.

After Test Series D1 was complete, CTU #1 was disassembled for inspection. Prior to disassembly, a leak test was performed on the containment closure and vent port seals as discussed above. The results showed no detectable leak. The average removal torque of the

closure bolts was 150 ft-lb, with a low value of 60 ft-lb and a high of 230 ft-lb. Initial installation torque was 300 ft-lb.

There was no sign of any weld failure or distress of the welds connecting the impact limiter to the lower flange. The only deformation of the lodgment was a slight bowing of the angle segments connecting the bottom ribs, caused by contact with the deformed plate of the lower internal impact limiter. The lodgment was still flat on the bottom. The total deformation of the lower internal impact limiter tubes, based on measurements of the lodgment relative to the lower brackets, was 1.43 inches downward, achieved by buckling of the tubes. The lower internal impact limiter top view is shown in Figure 2.12.3-8 and the underside view, showing the buckling of the tubes, in Figure 2.12.3-9. The upper internal impact limiter was not significantly damaged. Two of the lodgment toggle clamps became unclamped, and one was damaged. The LTSS was not damaged or deformed.

After Test Series D1 inspection was complete, CTU #1 was reassembled using all the same components. The closure bolts were tightened to drawing requirements and leakage rate tested.

2.12.3.4.2 Test Series D5

Test series D5 was performed on CTU #3 and consisted of a 4-ft NCT and a 30-ft HAC free drop in the bottom-down orientation, with the axis vertical, followed by a puncture drop test on the flat bottom of the impact limiter, with the cask axis inclined at 30° from the vertical. (Note: the D5 series was identical to the D1 series.) The tests were designated D5N, D5H, and P6 for the 4-ft, 30-ft, and puncture drops, respectively. The free drop orientation (identical for D5N and D5H) is shown in Figure 2.12.3-10. The polyurethane foam temperature readings for test D5N were -5.3 °F, -4.5 °F, and -6.5 °F, and for test D5H, -2.9 °F, -2.1 °F, and -3.0 °F. Accelerometer results are shown in the table below.

Accelerations, Free Drop Test D5					
Location	T/U	T/L	OT/U	OT/L	Avg. \perp
Test D5N	256g	256g	206g	203g	230g
Test D5H	797g	794g	855g	802g	812g

Like the D1 series, neither of these impacts imparted any visible damage to the CTU. The only external measurement taken at the time of the drops was the overall height. The height after D5N was 83-15/32 inches, compared to an as-fabricated height of 83-1/2 inches, for an apparent decrease of 1/32 inches. The same measurement taken after the D5H drop was 83-5/16 inches, for a further apparent decrease of 5/32 inches. The actual changes in overall height of the package were probably too small to be accurately measured using the techniques used. In any case, the external deformation was negligible. As discussed below, energy was absorbed internally.

After the D5H free drop, a 1/4-inch diameter hole was drilled at the center of the bottom sheet of the impact limiter and through the foam to the lowest point on the lower torispherical head. After subtracting a total of 0.54 inches for the steel shell, the insulating paper, and an observed gap, the thickness of the foam was measured to be 4.0 inches. Since a pre-test measurement of this dimension was not made, the post-test result must be compared to the fabricated nominal dimension, which was 3.4 inches. Since this value is less than the post-test result, it is postulated

that an unobserved gap was created by the impact between the torispherical head lower surface and the inner surface of foam. In any case, it appears that the crush of foam in the free drop events was very small. The package after the D5H drop is shown in Figure 2.12.3-11.

The puncture drop P6 orientation is shown in Figure 2.12.3-12. The axis of the puncture bar was directed through the c.g. at an oblique angle of 30.0° to the bottom surface. The temperatures of the foam were +1 °F and -1 °F, with one thermocouple not reading. The bar made a dent 1-9/16 inches deep without perforating the impact limiter shell or exposing any foam. The puncture damage is shown in Figure 2.12.3-13.

After Test Series D5 was complete, CTU #3 was disassembled for inspection. Prior to disassembly, a leak test was performed on the containment closure and vent port seals as discussed above. The results showed no detectable leak. The average removal torque of the closure bolts was 138 ft-lb, with a low value of 80 ft-lb and a high of 190 ft-lb.

There was no sign of any weld failure or distress of the welds connecting the impact limiter to the lower flange. The IC showed a downward deformation of the bottom structure by approximately 0.9 inches, along with some dents in the IC sidewall from impact with the dummy payload. Inside the IC, the lower wood dunnage was significantly crushed. The upper dunnage was not crushed, but the 'donut' section of the dunnage became unattached from the 'disk' portion. Two views of the damaged lower dunnage are given in Figure 2.12.3-14 and Figure 2.12.3-15. The dummy payload was not damaged. The IC rested firmly on the bottom internal impact limiter. The deformation of the lower internal impact limiter tubes was considerably less than in the D1 (lodgment) case, since there was significant energy absorption in the wood dunnage and some further deformation in the bottom structure of the IC. The upper internal impact limiter was not significantly damaged.

After Test Series D1 inspection was complete, CTU #3 was reassembled using a new IC, dunnage, and dummy payload, but using the same internal impact limiters. The closure bolts were tightened to drawing requirements and leakage rate tested.

2.12.3.4.3 Test Series D2

Test Series D2 was performed on CTU #1 and consisted of a 4-ft NCT and a 30-ft HAC free drop in the side orientation (where the impact limiter corner and the knuckle contacted simultaneously), followed by a puncture drop test on the knuckle in the region damaged by the free drop tests. The tests were designated D2N, D2H, and P2 for the 4-ft, 30-ft, and puncture drops, respectively. The free drop orientation (approximately 13° from horizontal, and identical for D2N and D2H) is shown in Figure 2.12.3-16. The free drop impact occurred on the opposite side of the package from the vent port. The polyurethane foam temperature readings for test D2N were -9.0 °F, -9.4 °F, and -9.5 °F. Due to the short time interval between tests D2N and D2H, and to the cold ambient temperature, the foam temperatures for test D2H were negligibly different from those recorded for test D2N, and well below the target value of 0 °F.

Accelerometer results are shown in the table below.

Accelerations, Free Drop Test D2								
Location	T/U	T/L	OT/U	OT/L	Avg. Upper	Avg. Lower	Resolved \perp Upper	Resolved \perp Lower
Test D2N	154g	84g	154g	110g	154g	97g	158g	100g
Test D2H	449g	225g	459g	260g	454g	243g	466g	249g

The damage consisted of flat spots on the impact limiter and knuckle. After the D2H drop, the combined damage from both the NCT and HAC drops were as follows: the impact limiter flat was 25-1/4 inches long (along cask axis) and 33-1/4 inches wide (orthogonal). The knuckle flat was 12 inches long and 18 inches wide. At the height of the weld seam at the top of the cylindrical side of the impact limiter (essentially the lower impact point), the radial crush distance was 4-3/8 inches, using measurements based on the cask body O.D. Since the crush occurred with the cask axis at an angle of 13° to the ground, the crush in the direction of impact was $4\text{-}3/8 \times \cos(13) = 4.27$ inches. (The crush at the knuckle was significantly less). An approximation of the amount of foam remaining was obtained by drilling a hole perpendicular to the flat damage surface, 17.5 inches from the bottom of the limiter. The bottom of the hole was approximately at the nearest point of hard flange material to the impact. The distance of foam, less the 1/4-inch thick shell, was $5.94 - 0.25 = 5.69$ inches. It was noted that all of the rain shield bolts were snug. The package after the D2H drop is shown in Figure 2.12.3-17.

Puncture drop P2 orientation is shown in Figure 2.12.3-18. The package was suspended essentially upside down over the puncture bar. The axis of the puncture bar was aimed at the knuckle at the location of the free drop damage and directed at the c.g. of the package. The temperature of the steel surface near the impact point was 31.4 °F. The puncture bar left a six-inch diameter impression at impact, the center of which was approximately 16 inches radially from the package centerline. The dent was 3/4-inches deep. There was no evidence of cracking in the containment boundary material. Note that this test was conservative since the 0.105-inch thick head thermal shield was not present. The puncture damage is shown in Figure 2.12.3-19.

After Test Series D2 was complete, CTU #1 was disassembled for inspection. Prior to disassembly, a leak test was performed on the containment closure and vent port seals as discussed above. The results showed no detectable leak. The average removal torque of the closure bolts was 154 ft-lb, with a low value of 50 ft-lb and a high of 250 ft-lb.

The upper internal impact limiter was not crushed significantly, but the aluminum plate was somewhat buckled in the region of impact. The lower internal impact limiter, somewhat crushed in test series D1, did not experience significant additional damage. One guide pin in the base, located at the impact point, was slightly bent. Since the flange was not deformed, this likely occurred due to a misalignment between the bell and base during final disassembly. The side impact caused some minor radial deformations of the bell side wall of 1/8 inches maximum at locations which corresponded to the main structural members of the lodgment.

The lodgment was not significantly damaged, and the LTSS was essentially still in the original location. One toggle clamp was broken. The eight clevises connecting the two halves of the lodgment were intact. All eight bolts were slightly bent, occurring most likely during the D1 end impact. The LTSS was essentially undamaged, showing some surface waviness of approximately 1/8 inches on the impact side, corresponding to the main structural members of the lodgment. Internal damage from the D2 series is shown in Figure 2.12.3-20 and Figure

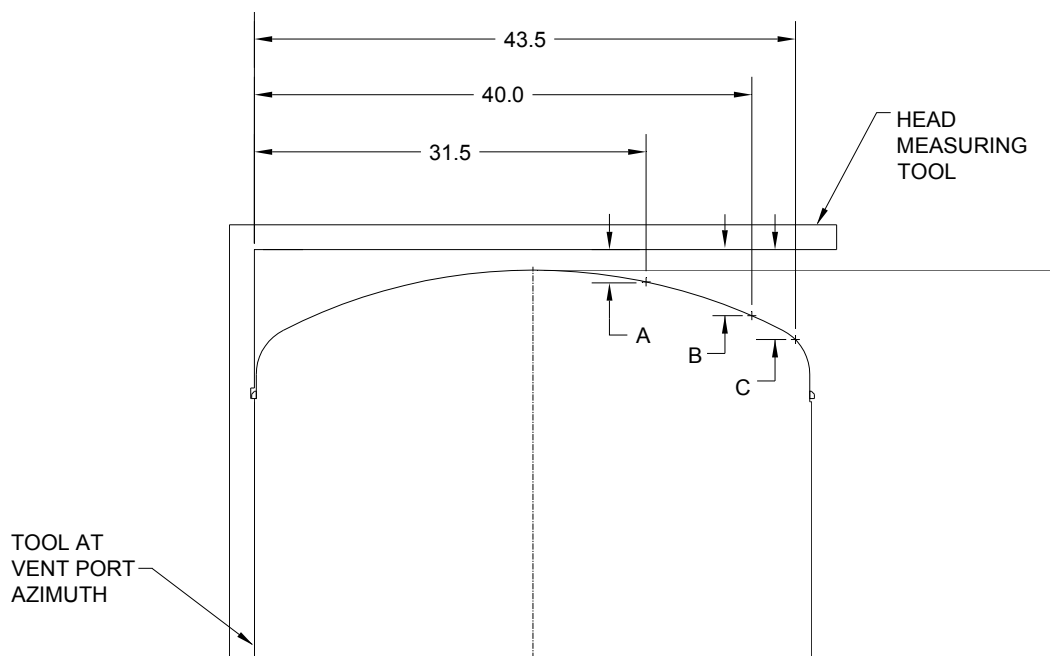
2.12.3-21. After all testing and disassembly, the containment boundary of CTU #1 was helium leakage rate tested. The maximum leakage rate was $2.9(10^{-8})$ He-cc/sec against a criteria of $2.2(10^{-7})$ He-cc/sec. Thus the package, after two complete series of free drop and puncture tests, was leaktight.

2.12.3.4.4 Test Series D3

Test series D3 was performed on CTU #2 and consisted of a 4-ft NCT and a 30-ft HAC free drop in the c.g.-over-top knuckle orientation, followed by a puncture drop through the c.g., directly on the free drop damage. The tests were designated D3N, D3H, and P3 for the 4-ft, 30-ft, and puncture drops, respectively. The free drop orientation (identical for both D3N and D3H) is shown in Figure 2.12.3-22. The package was oriented 27° from the vertical as shown. CTU #2 had the thermal shield installed on the upper torispherical head. The temperature of the outer shield shell was approximately 50°F , based on the overnight environment temperature, the relatively short exposure to the cold ambient, and the thermal delay caused by the head shield. Accelerometer results are shown in the table below.

Accelerations, Free Drop Test D3						
Location	T/U	T/L	OT/U	OT/L	Avg.	Resolved \perp
Test D3N	108g	No signal	106g	113g	109g	122g
Test D3H	162g	No signal	164g	152g	159g	178g

The damage consisted of a flat spot on the torispherical head, offset towards one side. After the D3H drop, the combined damage from both the NCT and HAC drops was a flat spot 21 inches long in the radial direction and 33-1/2 inches long in the circumferential direction. Another characterization showed the change in vertical location of the surface, illustrated in the figure below. Results are provided in the table below.



Location	Axial measurement, inches (after D3H)		
	Pre-test	Post-test	Change (deformation)
A	2-7/8	4.0	1-1/8
B	5-3/8	9-13/16	4-7/16
C	6-15/16	11-1/4	4-5/16

The package after the D3H drop is shown in Figure 2.12.3-23.

The puncture drop P3 orientation is shown in Figure 2.12.3-24. The axis of the puncture bar was directed through the c.g. of the package with the impact point (outermost edge) of the bar located at 3 inches from the outer edge of the buckle as shown in Figure 2.12.3-25. The package was oriented at the same angle as for the free drops. The internal lodgment ribs were placed to straddle the puncture impact, thus minimum support to puncture was afforded by internal structures. The bar made a dent approximately 1-3/8 inches deep, based on a straight edge laid across the entire damaged surface. The thermal shield shell did not tear or perforate, and there were no weld failures of the shield. The nominally 0.102-inch diameter wires in the puncture damage were somewhat flattened by the impact. Some of the intermittent welds attaching the simulated side thermal shield cracked, but the simulated shield was not displaced. The puncture damage is shown in Figure 2.12.3-25 and Figure 2.12.3-26. After the D3 test series, a vacuum was placed on the containment seal in the test annulus in lieu of a full helium leakage rate test, according to the test procedure. A vacuum of $7.5(10^{-4})$ Torr was sustained, indicating a leaktight containment seal. A full helium leakage rate test of the containment and vent port seals was performed following Test Series D4. The closure bolts were not retightened or nor was the vent port disturbed between the D3 and D4 series of tests.

2.12.3.4.5 Test Series D6

Test Series D6 was performed on CTU #3 and consisted of a 4-ft NCT and a 30-ft HAC free drop in the side orientation (identical to the free drop orientation of Series D2), followed by two puncture drop tests: one on the side on the production side thermal shield, and one on the side on the bolt tube/rain shield region. The tests were designated D6N, D6H, P7 and P5 for the 4-ft, 30-ft, thermal shield puncture drop, and bolt tube puncture drops, respectively. The free drop orientation (approximately 13° from horizontal, and identical for D6N and D6H) is shown in Figure 2.12.3-27. The free drop impact occurred on the opposite side of the package from the vent port. The polyurethane foam temperature readings for test D6N were -3.5 °F, -4.0 °F, and -3.0 °F. Due to the short time interval between tests D6N and D6H, and to the cold ambient temperature, the foam temperatures for test D6H were negligibly different from those recorded for test D6N, and were thus below the target temperature of 0 °F. Accelerometer results are shown in the table below.

Accelerations, Free Drop Test D6								
Location	T/U	T/L	OT/U	OT/L	Avg. Upper	Avg. Lower	Resolved \perp Upper	Resolved \perp Lower
Test D6N	158g	75g	166g	78g	162g	77g	166g	79g
Test D6H	395g	159g	404g	178g	400g	169g	411g	173g

Like Test Series D2, the damage consisted of flat spots on the impact limiter and knuckle. After the D6H drop, the combined damage from both the NCT and HAC drops were as follows: the impact limiter flat was 21-3/4 inches long (along cask axis) and 30 inches wide (orthogonal). The knuckle flat was 11-1/4 inches long and 14-1/2 inches wide. At the height of the weld seam at the top of the cylindrical side of the impact limiter (essentially the lower impact point), the radial crush distance was 3-1/8 inches, using measurements based on the cask body O.D. Since the crush occurred with the cask axis at an angle of 13° to the ground, the crush in the direction of impact was $3\text{-}1/8 \times \cos(13) = 3.04$ inches. (The crush at the knuckle was significantly less). An approximation of the amount of foam remaining was obtained by drilling a hole perpendicular to the flat damage surface, 17.5 inches from the bottom of the limiter. The bottom of the hole was approximately at the nearest point of hard flange material to the impact. The distance of foam, less the 1/4-inch thick shell, was $7.0 - 0.25 = 6.75$ inches. (This measurement was essentially confirmed after dissecting the impact limiter). It was noted that all of the rain shield bolts were snug. The package after the D6H drop is shown in Figure 2.12.3-28.

Puncture drop P7 orientation is shown in Figure 2.12.3-29. It occurred at the same azimuth as the free drops, i.e., opposite the vent port. The package was suspended over the puncture bar with the axis inclined at 30° , impact limiter up, and the axis of the puncture bar was aimed through the c.g. of the package. The temperature of the outermost thermal shield steel surface was 21.5°F . The puncture bar struck the package approximately halfway up the cylindrical side and left an oblique dent 1-7/8 inches deep (measured on the outside). The 0.105-inch thick, outermost thermal shield was not ripped by the puncture bar, and there was no exposure of the inner thermal shield. The P7 puncture damage is shown in Figure 2.12.3-30.

Puncture drop P5 orientation is shown in Figure 2.12.3-31. It occurred at the azimuth of the vent port. The package was suspended essentially horizontally, with the puncture bar axis aiming perpendicularly to the package axis, slightly towards the bottom end from the c.g. This orientation was chosen to ensure that the puncture bar impact would occur on the tube sheet/rain shield region. Due to the difficulty in achieving a perfect impact location, trying to aim at the c.g. would present too large a risk of missing the desired impact point, given that the angle between the puncture bar and impact limiter slanted top surface was a very small acute angle. It was therefore judged that a horizontal package orientation represented the best choice for maximum damage. The puncture bar hit the slanted top of the impact limiter, and skidded up until it struck the tube sheet, which it deformed radially by 1/2-inches. The buckling of the 1/4-inch thick tube sheet essentially stopped the impact progress, until the package bounced off of the bar and a secondary impact with the side thermal shield occurred. The rain shield was locally very slightly bent. The deformation of the top of the limiter caused the vent port tube opening to collapse onto the vent port insulation cylinder, which needed to be pried out. The P5 puncture damage is shown in Figure 2.12.3-32 and Figure 2.12.3-33. The dent in the vent port tube that

trapped the vent port cylinder is shown in Figure 2.12.3-34. The vent port insulation cylinder was held securely in position by both the fully intact rain shield as well as the collapsed tube.

After Test Series D6 was complete, CTU #3 was disassembled for inspection. Prior to disassembly, a leak test was performed on the containment closure and vent port seals as discussed above. The results showed no detectable leak. The average removal torque of the closure bolts was 157 ft-lb, with a low value of 40 ft-lb and a high of 290 ft-lb.

The upper internal impact limiter was not crushed significantly, but the aluminum plate was somewhat buckled in the region of impact. The lower internal impact limiter was not significantly damaged. The P7 puncture dent, measured radially from the inside, was 1-1/2 inches high. An internal view of the dent is shown in Figure 2.12.3-35. A slightly different view is given in Figure 2.12.3-36, which shows the impression made on the inner surface of the containment boundary by the IC ribs, demonstrating that the puncture bar struck just adjacent to the ribs. Thus the bar was not supported by the IC ribs. The damage caused by the secondary bounce onto the bar in test P5, measured radially from the inside, was 9/16 inches high.

Since the IC was locked into the CTU #3 bell by the puncture sidewall damage, it was necessary to cut the bottom out and remove the IC wall by piecemeal cutting. The dummy payload cut through the IC wall somewhat in one location in the side drop (see Figure 2.12.3-37), but any buckling of the egg-crate reinforcements of the outside of the IC were minimal. The dummy payload did not engage more than one or two of the plywood sheets in the dunnage (top and bottom), and these sheets were significantly damaged in the side drop (see Figure 2.12.3-38). The balance of the dunnage was undamaged. The dummy payload was undamaged as shown in Figure 2.12.3-39. Two of the six bolts holding on the IC lid sheared off.

After all testing and disassembly, the containment boundary of CTU #3 was helium leakage rate tested. The maximum leakage rate was $1.9(10^{-7})$ He-cc/sec against a criteria of $2.2(10^{-7})$ He-cc/sec. Thus the package, after two complete series of free drop and puncture tests, was leaktight.

2.12.3.4.6 Test Series D4

Test Series D4 was performed on CTU #2 and consisted of a 4-ft NCT and a 30-ft HAC free drop in the side orientation (identical to the free drop orientations of Series D2 and D6), followed by a puncture drop test on the cylindrical side of the impact limiter through the c.g. The tests were designated D4N, D4H, and P4 for the 4-ft, 30-ft, and puncture drop, respectively. The free drop orientation (approximately 13° from horizontal, and identical for D4N and D4H) is shown in Figure 2.12.3-40. The free drop impact occurred at the vent port. The polyurethane foam temperature readings for test D4N were 118 °F and 120 °F. In contrast to the cold test cases, these readings were taken approximately 12 inches on either side of the impact point, at the regular depth of 9 inches. At a depth of 4.5 inches, the D4N temperatures were 112 and 120 °F. For test D4H, the corresponding temperatures at 9 inches were 116 and 119 °F, and at 4.5 inches, 90 and 116 °F. (The 90 °F temperature reading is doubtful.) Accelerometer results are shown in the table below.

Accelerations, Free Drop Test D4								
Location	T/U	T/L	OT/U	OT/L	Avg. Upper	Avg. Lower	Resolved \perp Upper	Resolved \perp Lower
Test D4N	144g	74g	130g	82g	137g	78g	141g	80g
Test D4H	356g	168g	372g	187g	364g	178g	374g	183g

Like Test Series D2 and D6, the damage consisted of flat spots on the impact limiter and knuckle. After the D4H drop, the combined damage from both the NCT and HAC drops were as follows: the impact limiter flat was 25-1/2 inches long (along cask axis) and 33 inches wide (orthogonal). The knuckle flat was 11-1/2 inches long and 18-1/2 inches wide. At the height of the weld seam at the top of the cylindrical side of the impact limiter (essentially the lower impact point), the radial crush distance was 4-13/16 inches, using measurements based on the cask body O.D. Since the crush occurred with the cask axis at an angle of 13° to the ground, the crush in the direction of impact was $4-13/16 \times \cos(13) = 4.68$ inches. (The crush at the knuckle was significantly less). A measure of the amount of foam remaining was not obtained until after the puncture drop was complete. It was noted that all of the rain shield bolts were snug. The package after the D4H drop is shown in Figure 2.12.3-41.

Puncture drop P4 orientation is shown in Figure 2.12.3-42. It occurred on the free drop damage on the impact limiter (thus, at the vent port azimuth) with the bar aimed through the c.g. of the package. The measured angle of the package axis was 36° to the horizontal. The polyurethane foam temperature was 114°F at 9 inches deep, and 99°F at 4.5 inches deep. The puncture bar struck the package approximately 7-1/2 inches up the side from the flat bottom and skidded approximately 3-1/2 inches before stopping. There was no fissure or perforation of the impact limiter shell and no exposure of foam. The maximum depth of the puncture dent was 1-1/2 inches. The P4 puncture damage is shown in Figure 2.12.3-43.

After Test Series D4 was complete, CTU #2 was disassembled for inspection. Prior to disassembly, a leak test was performed on the containment closure and vent port seals as discussed above. The results showed no detectable leak. The average removal torque of the closure bolts was 101 ft-lb, with a low value of 0 ft-lb (found on two adjacent bolts) and a high of 270 ft-lb. Note that the closure bolts were not re-tightened between Test Series D3 and D4, and therefore these residual torques resulted from two complete test series.

Upon disassembly, the test O-ring seal was observed to be cut over an approximately 3-inch length. Since the leakage rate test was successful, it is presumed that this cut occurred during removal of the bell from the base. Since the bell and base were difficult to separate, the bell was not drawn off slowly but fell, with a sudden misalignment of the base to the bell, at which time the seal likely became cut by the sharp edge of the bell.

As expected, the tubes located at the impact of test D3 were crushed flat, and the plate of the upper internal impact limiter was buckled from both the D3 and D4 impacts. The pattern of tube crushing is shown in Figure 2.12.3-44. The deformation of the package due to Test Series D3 is shown in Figure 2.12.3-45 and Figure 2.12.3-46, where the head thermal shield has been locally cut away to expose the containment boundary. The lower internal impact limiter had little damage. The lodgment showed some buckling of the radial plate adjacent to the impact of the D3 test, but little other damage (see Figure 2.12.3-47). The LTSS was supported in essentially its original position. Note that the LTSS was thoroughly tested in Test Series D1 and D2. The

only additional damage to the LTSS from Test Series D3 and D4 was some shallow deformations (approximately 1/8 inches or less) due to support from the lodgment's circular plates in the side (D4) free drops.

In the region of the D4 and P4 damage, the impact limiter was cut away on the plane of the free drop and puncture drop and measurements of the foam thickness made. The minimum depth of foam (not including the shell and gap), measured perpendicular to the outer surface of the foam to the hard flange upper corner, was 5-1/8 inches, and is shown in Figure 2.12.3-48. The distance from the bottom of the P4 puncture damage to the hard flange lower corner was 6-1/4 inches, and is shown in Figure 2.12.3-49.

After all testing and disassembly, the containment boundary of CTU #2 was helium leakage rate tested. The maximum leakage rate was $1.1(10^{-7})$ He-cc/sec against a criteria of $2.2(10^{-7})$ He-cc/sec. Thus the package, after two complete series of free drop and puncture tests, was leaktight.

2.12.3.5 Summary of Test Results

Certification testing was performed on the 1105-SD packaging design using three full scale CTUs. A total of six, 4-ft NCT free drops, six, 30-ft HAC free drops, and seven puncture drops were performed on the test units. After all tests, the CTUs were helium leaktight. Free drop accelerations were recorded for use in finite element model benchmarking and other structural analyses. The deformations of the packaging that could have an effect on performance in the HAC fire event were recorded. The deformations of the LTSS or the dummy shielded device were negligible, such that no change in the shielding performance is expected.

Table 2.12.3-1 – Certification Test Unit Configuration

CTU Configuration	SAR Production Unit Configuration	Justified in Section 2.12.3.3 paragraph number
<i>Configuration Common to All CTUs (1, 2, and 3)</i>		
Auxiliary vent port in sidewall	No vent port in sidewall	6
Threaded hole top of bell 1-8 UNC	Threaded hole top of bell 3/4-10 UNC	7
Lifting plates on impact limiter	No plates	7
Accelerometer mounting blocks	No blocks	8
Thermocouple wire holes in melt-out plugs and foam	No holes	9
Vent and test port repair configuration shown in Figure 2.12.3-3	Configuration shown on 3021717-SAR, sheet 6, Section M-M and Section N-N	10
Payload orienting tabs	No tabs	11
No caps over guide pin holes	Caps as shown on 3021717-SAR sheet 4, Section F-F	13
No lead-in chamfer on bell opening	Lead-in chamfer as shown on 3021717-SAR sheet 6, Detail AA	14
Three melt-out plugs equally spaced on impact limiter OD	Six plugs equally spaced	15
<i>Additional Configuration Information for CTU #1</i>		
Payload: Dummy LTSS in lodgment #1		
Impact limiter foam was 16 lb/ft ³	15 lb/ft ³ per 3021717-SAR list of materials, I/N 19	1
Simulated thermal shield on side as shown in Figure 2.12.3.3-5	Full side thermal shield shown on 3021717-SAR sheet 5, Detail R	3
No thermal shield on upper torispherical head	Full head thermal shield shown on 3021717-SAR sheet 6, Detail T	4
Containment and Test O-ring diameter 44.6 inches	Diameter 44.1 inches	16
Lodgment OD 43 inches and lower corner 8 inches from base	Lodgment OD 42.75 inches and lower corner 10 inches from base	17
Alloy steel toggle clamp adjustment bolts	Bronze toggle clamp adjustment bolts	18

Table 2.12.3-1, continued

CTU Configuration	SAR Production Unit Configuration	Justified in Section 2.12.3.3 paragraph number
<i>Additional Configuration Information for CTU #2</i>		
Payload: Dummy LTSS in lodgment #2		
Impact limiter foam was 14 lb/ft ³	15 lb/ft ³ per 3021717-SAR list of materials, I/N 19	2
Simulated thermal shield on side as shown in Figure 2.12.3.3-5	Full side thermal shield shown on 3021717-SAR sheet 5, Detail R	3
Full head thermal shield shown on 3021717-SAR sheet 6, Detail T	Full head thermal shield shown on 3021717-SAR sheet 6, Detail T	4
Thermal shield interior surface finish not maintained	Interior surfaces of thermal shield finished per 3021717-SAR, flag note 42	5
Containment and Test O-ring diameter 44.1 inches	Diameter 44.1 inches (i.e., same)	16
Lodgment OD 43 inches and lower corner 8 inches from base	Lodgment OD 42.75 inches and lower corner 10 inches from base	17
Alloy steel toggle clamp adjustment bolts	Bronze toggle clamp adjustment bolts	18
<i>Additional Configuration Information for CTU #3</i>		
Payload: IC with dummy device and dunnage		
Impact limiter foam was 16 lb/ft ³	15 lb/ft ³ per 3021717-SAR list of materials, I/N 19	1
Full side thermal shield shown on 3021717-SAR sheet 5, Detail R	Full side thermal shield shown on 3021717-SAR sheet 5, Detail R	3
No thermal shield on upper head	Full head thermal shield shown on 3021717-SAR sheet 6, Detail T	4
Thermal shield interior surface finish not maintained	Interior surfaces of thermal shield finished per 3021717-SAR, flag note 42	5
IC lid rib continuous weld	Intermittent weld per 3021719-SAR, sheet 2	12
Containment and Test O-ring diameter 44.6 inches	Diameter 44.1 inches	16
IC OD 43 inches	IC OD 42.75 inches	17

Table 2.12.3-2 – Certification Test Unit Weight, lb

	CTU #1	CTU #2	CTU #3
Base	2,280	2,216	2,285
Bell	2,315	2,394	2,435
Lodgment	512	508	1,110 ^②
LTSS	4,460	4,460	3,870 ^③
Total^①	9,642	9,653	9,775

Notes:

1. Total weight includes 75 lb for closure bolts, washers, and rain shields.
2. Weight of inner container (IC).
3. CTU #3 used a dummy device weighing 3,570 lb and wood blocking weighing 300 lb. Tests D5N, D5H, and P6 used IC #1, and tests D6N, D6H, P5, and P7 used IC #2. Both ICs, when fully assembled, weighed the same.

Table 2.12.3-3 – Summary of Containment Boundary Integrated Leakage Rate Tests^②

Test Unit	Leakage Rate, He-cc/sec^①	Pass/Fail
CTU #1	2.9(10 ⁻⁸)	Pass
CTU #2	1.1(10 ⁻⁷)	Pass
CTU #3	1.9(10 ⁻⁷)	Pass

Notes:

1. Leak tight criteria is 2.2(10⁻⁷) He-cc/sec, which is equivalent to 1.0(10⁻⁷) std-cc/sec, air.
2. Containment seal and vent port seals were leak tight whenever checked (prior to each test series and after test series D1, D2, D4, D5, and D6). After test series D3, a hard vacuum was sustained in lieu of a helium leakage rate test. The containment and vent port seals were not disturbed until after the next drop test series (D4) and subsequent helium leakage rate test had been successfully performed, thus assuring helium leaktightness after test series D3.

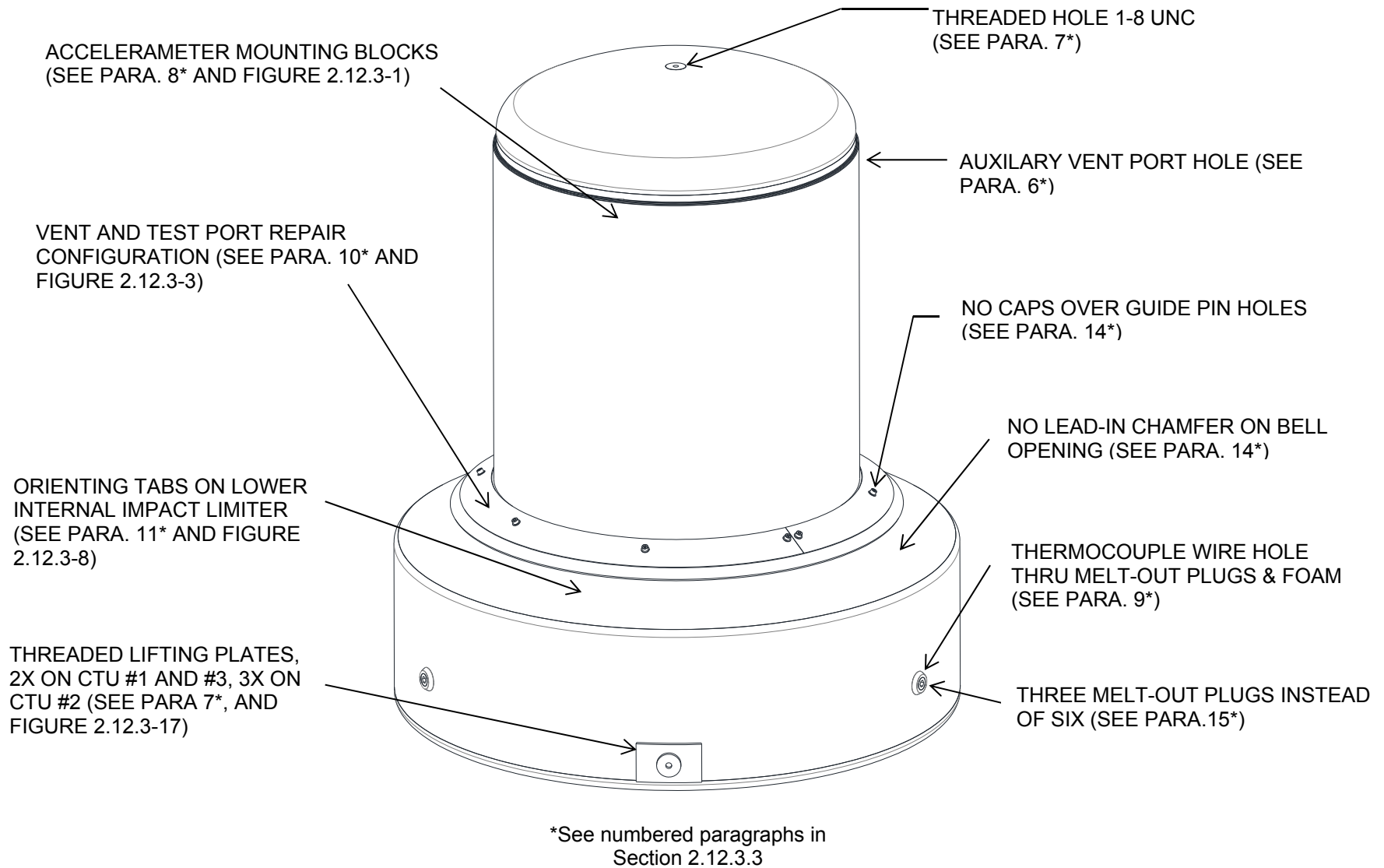
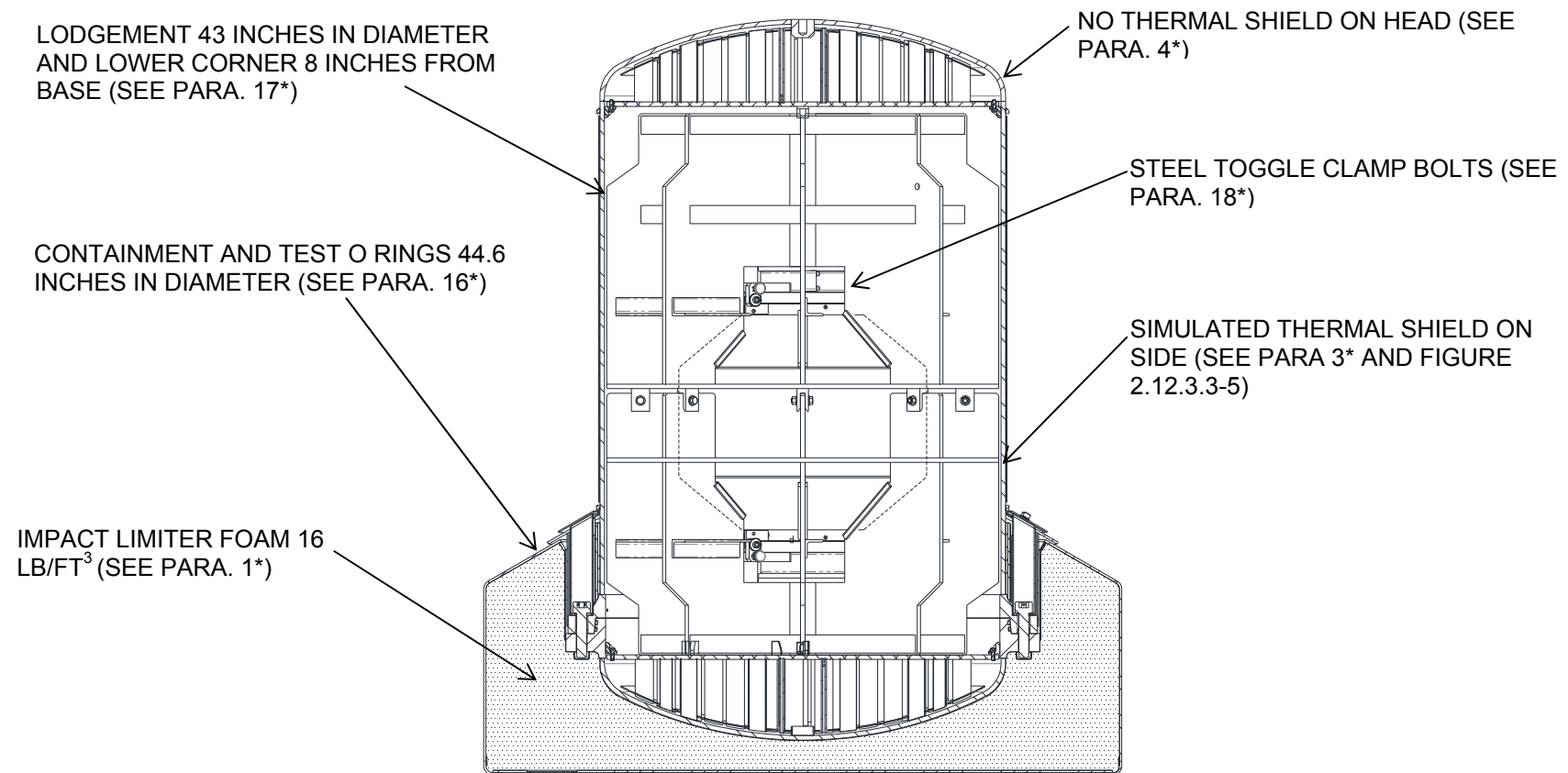


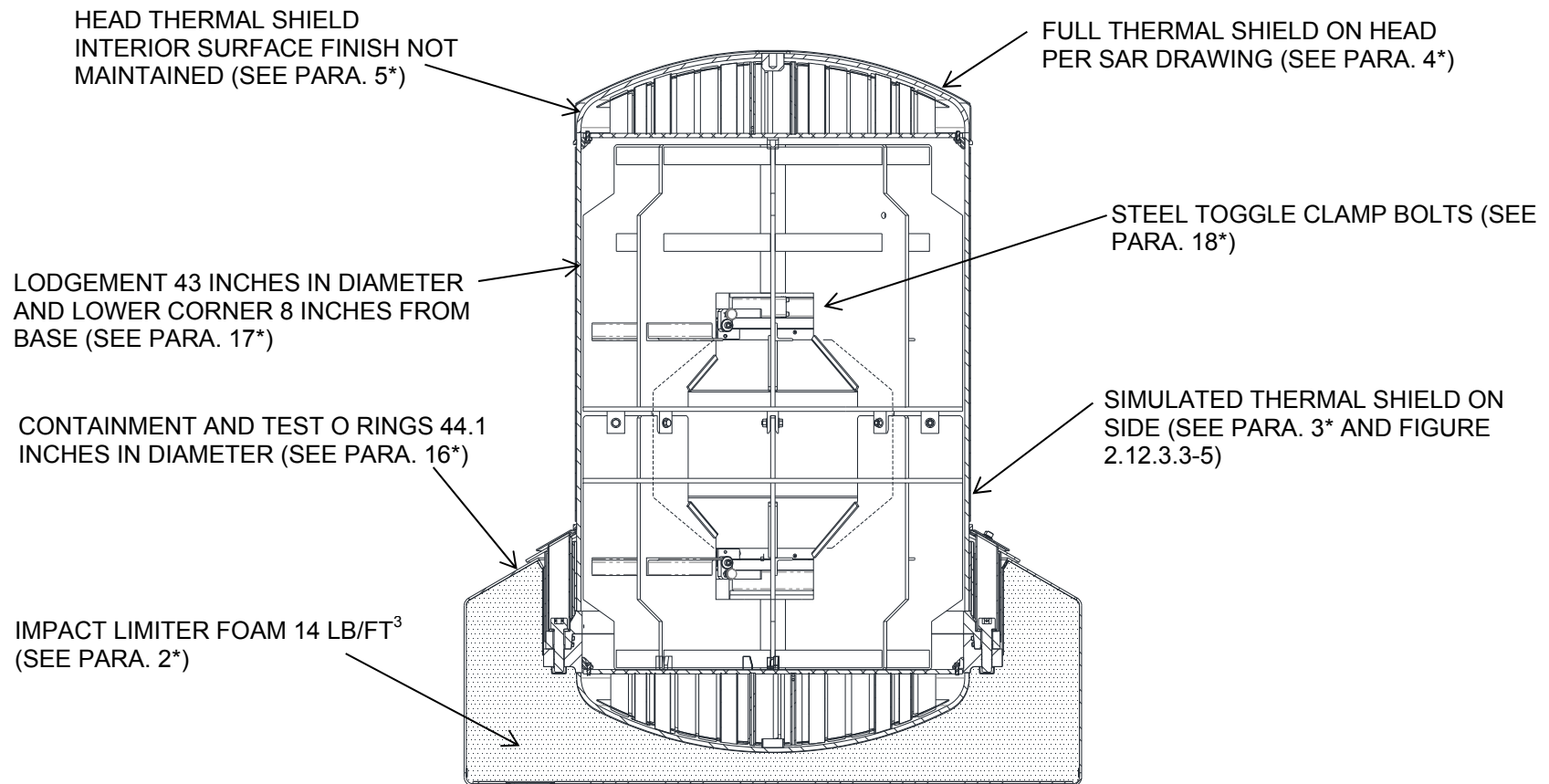
Figure 2.12.3.3-1 – CTU Common Configuration (Applies to CTU 1, 2, and 3)



Payload: Lodgment and Dummy LTSS

*See numbered paragraphs in
Section 2.12.3.3

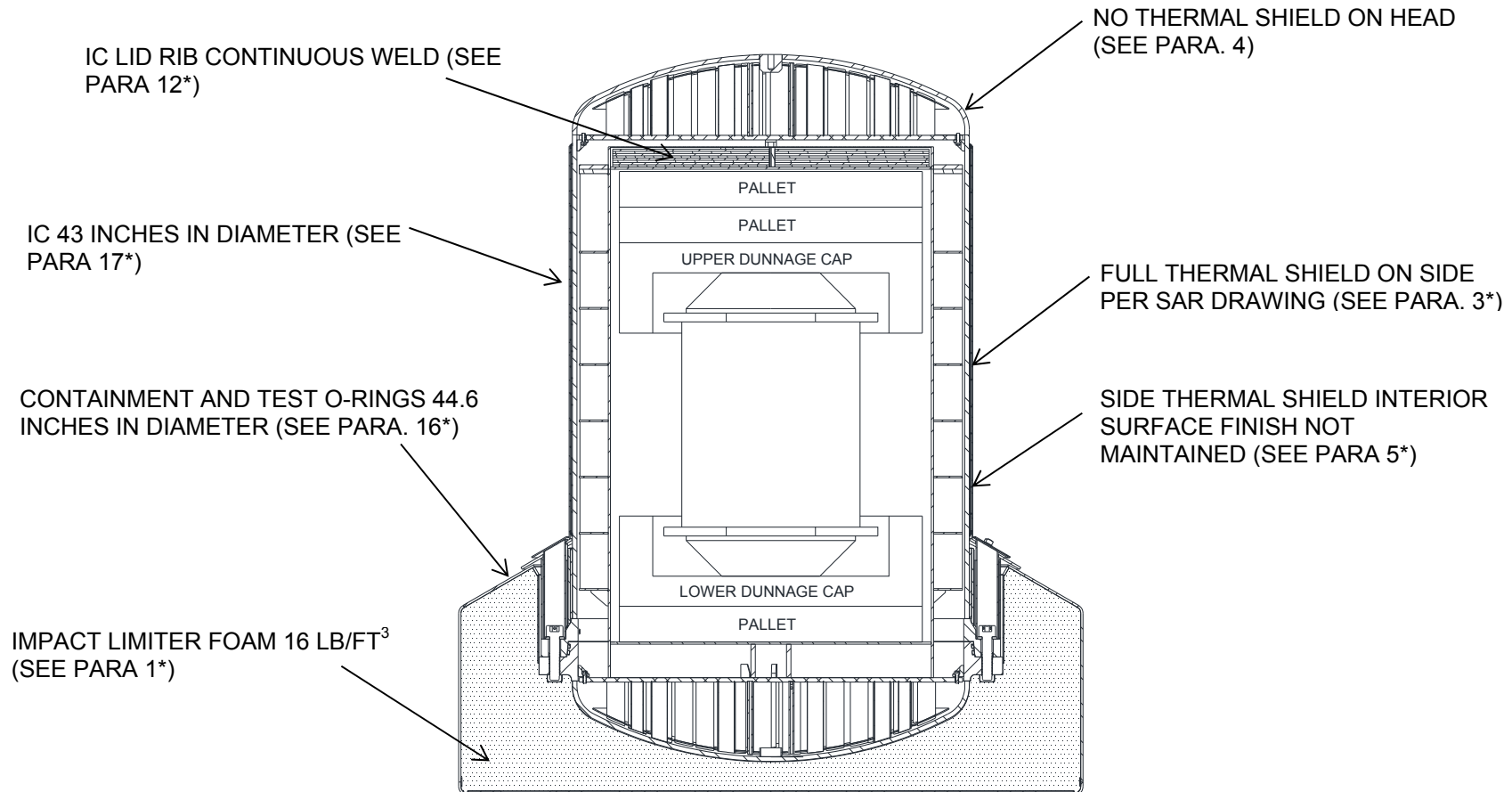
Figure 2.12.3.3-2 – Additional Configuration Information for CTU #1 (All ‘Common Configuration’ Notations in Figure 2.12.3.3-1 Apply)



*See numbered paragraphs in
Section 2.12.3.3

Payload: Lodgment and Dummy LTSS

Figure 2.12.3.3-3 – Additional Configuration Information for CTU #2 (All ‘Common Configuration’
Notations in Figure 2.12.3.3-1 Apply)



*See numbered paragraphs in
Section 2.12.3.3

Payload: Inner Container (IC with Dummy Device and Dunnage)

Figure 2.12.3.3-4 – Additional Configuration Information for CTU #3 (All ‘Common Configuration’ Notions in Figure 2.12.3.3-1 Apply)

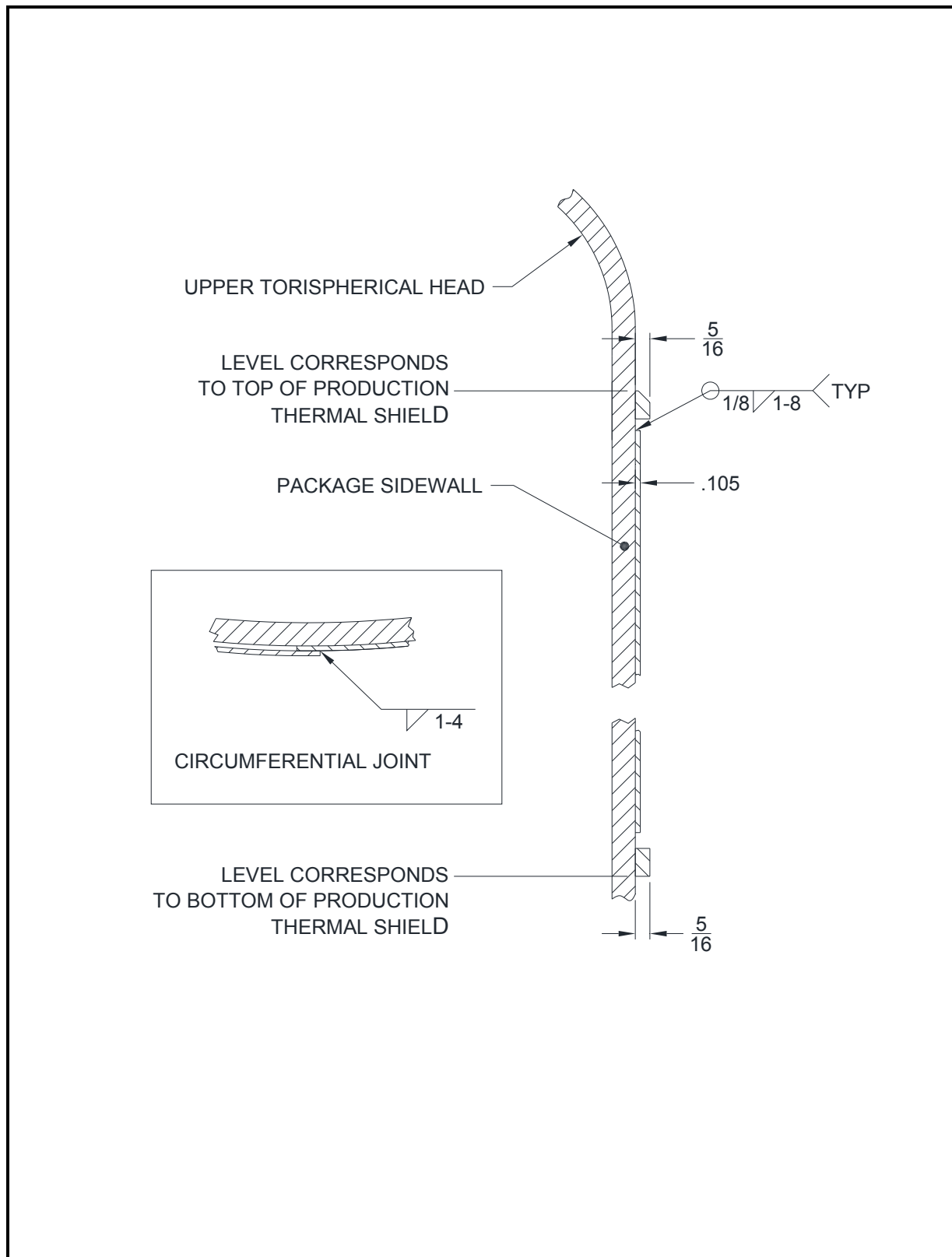


Figure 2.12.3.3-5 – Simulated Side Thermal Shield Detail (CTU #1 and CTU #2)

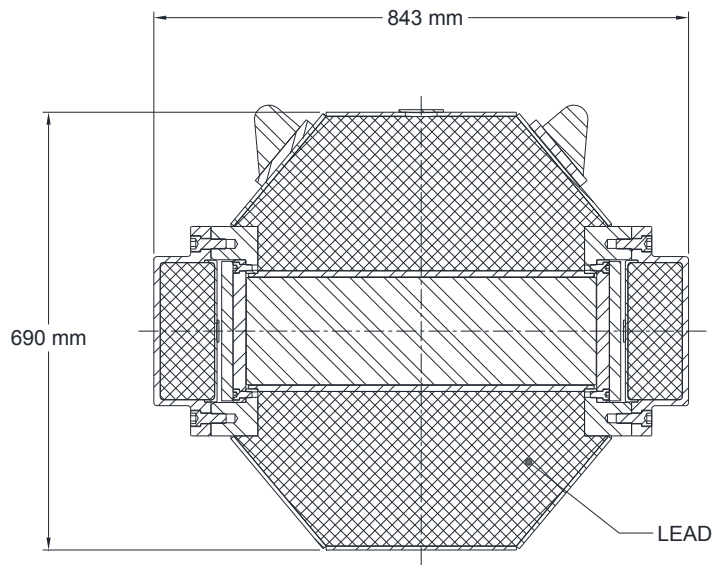


Figure 2.12.3.3-6 – Dummy LTSS

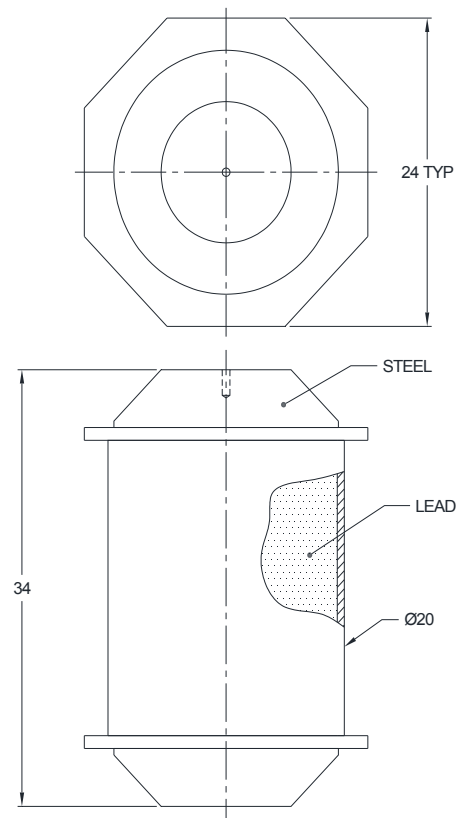


Figure 2.12.3.3-7 – Dummy Shielded Device

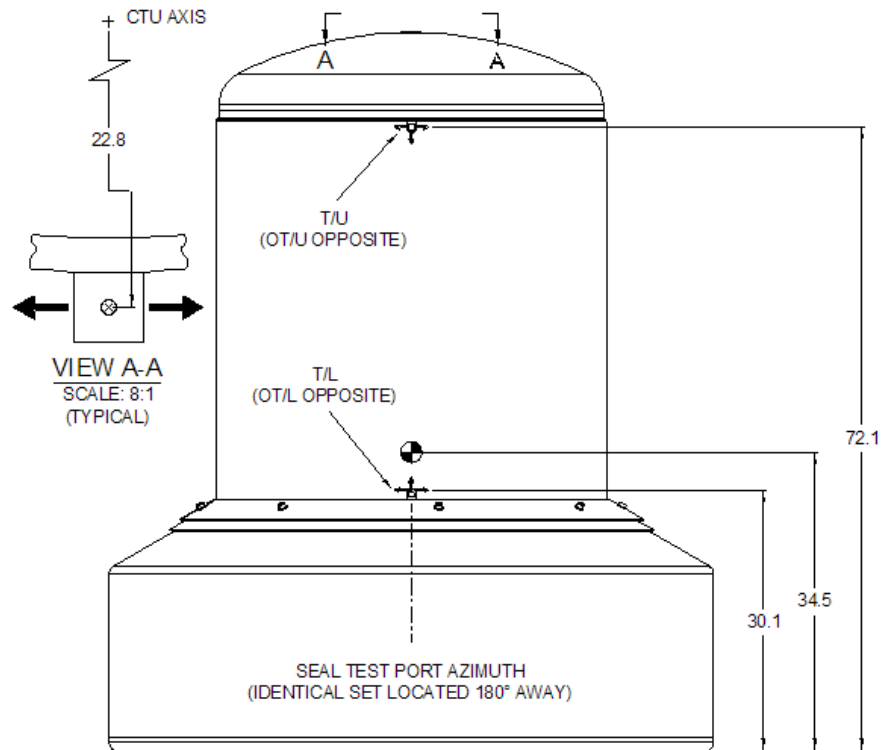


Figure 2.12.3-1 – Accelerometer Mounting

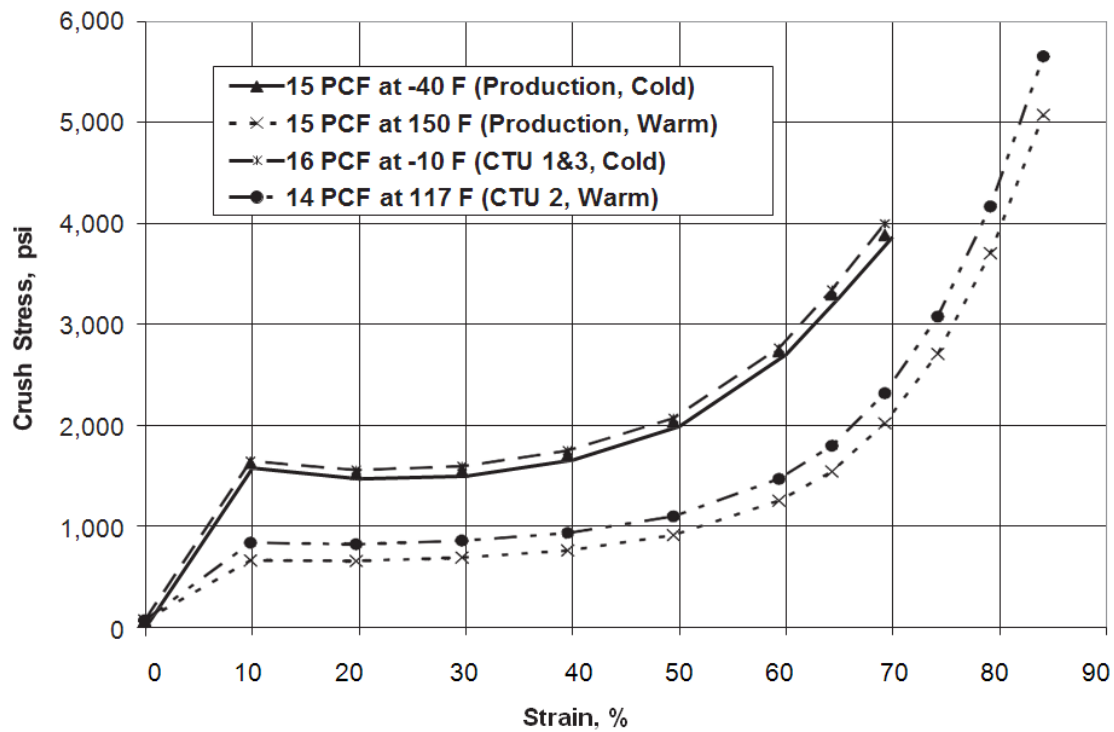


Figure 2.12.3-2 – Comparison of Foam Stress-Strain at Cold and Warm Conditions

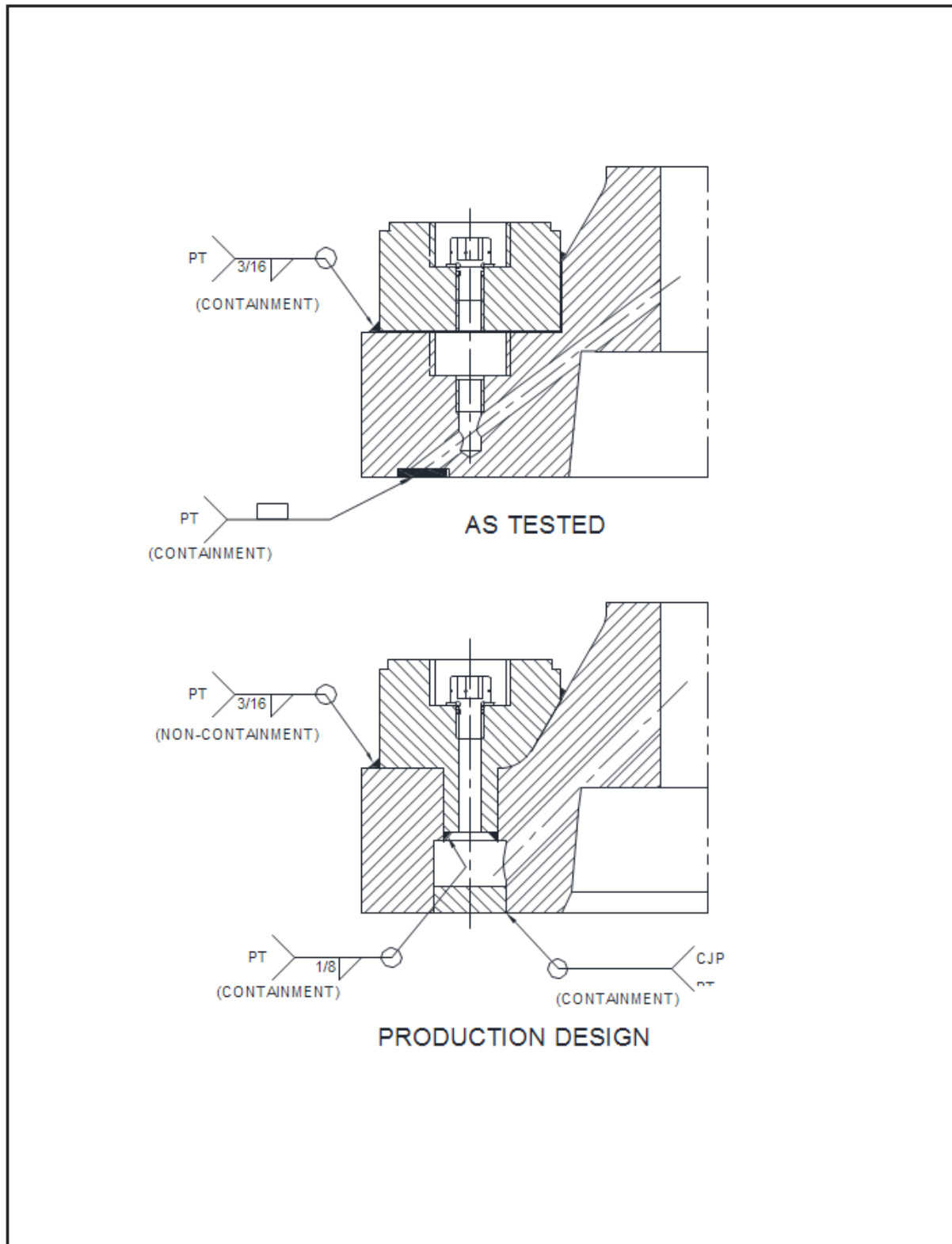


Figure 2.12.3-3 – Vent/Test Port Configuration Differences (Vent Port Shown)



Figure 2.12.3-4 – Free Drop Test D1N/D1H Orientation



Figure 2.12.3-5 – CTU #1 Condition After Free Drop Test D1H



Figure 2.12.3-6 – Puncture Drop Test P1 Orientation



Figure 2.12.3-7 – Damage to Impact Limiter Bottom Due to Puncture Drop Test P1

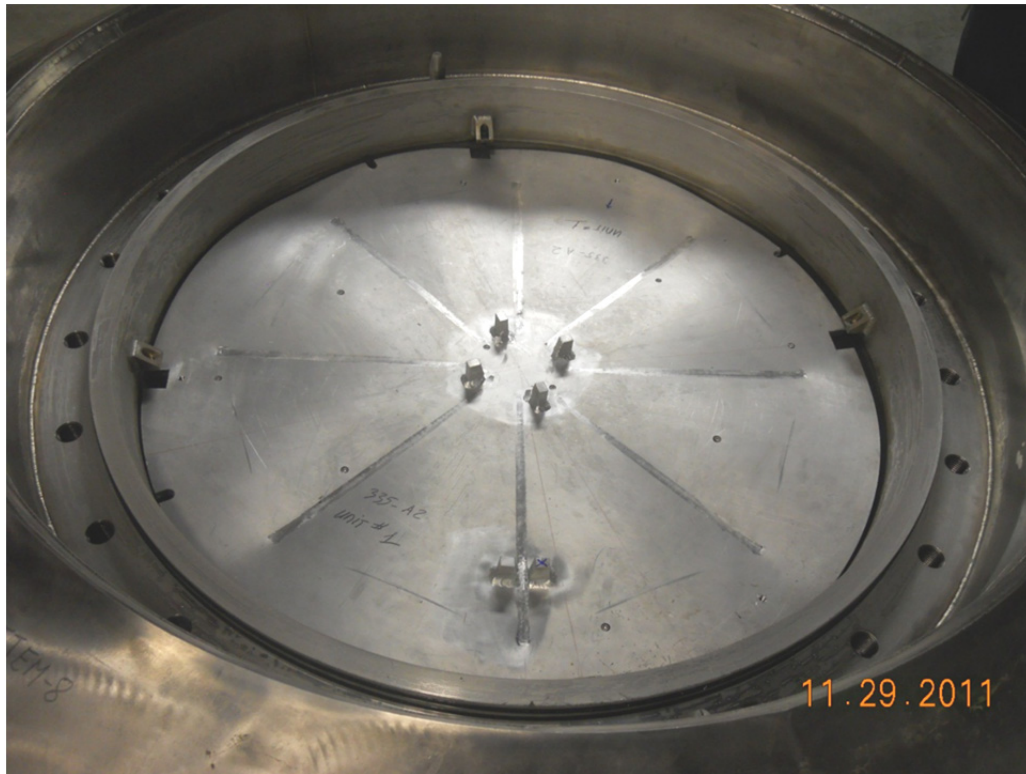


Figure 2.12.3-8 – Lower internal impact limiter, After D1 Series



Figure 2.12.3-9 – Lower internal impact limiter, View From Beneath, After D1 Test Series



Figure 2.12.3-10 – Free Drop Test D5N/D5H Orientation



Figure 2.12.3-11 – CTU #3 Condition After Free Drop Test D5H



Figure 2.12.3-12 – Puncture Drop Test P6 Orientation



Figure 2.12.3-13 – Damage to Impact Limiter Bottom Due to Puncture Drop Test P6



Figure 2.12.3-14 – Inner Container Lower Dunnage After D5 Test Series



Figure 2.12.3-15 – Detail of Lower Dunnage Damage After D5 Test Series

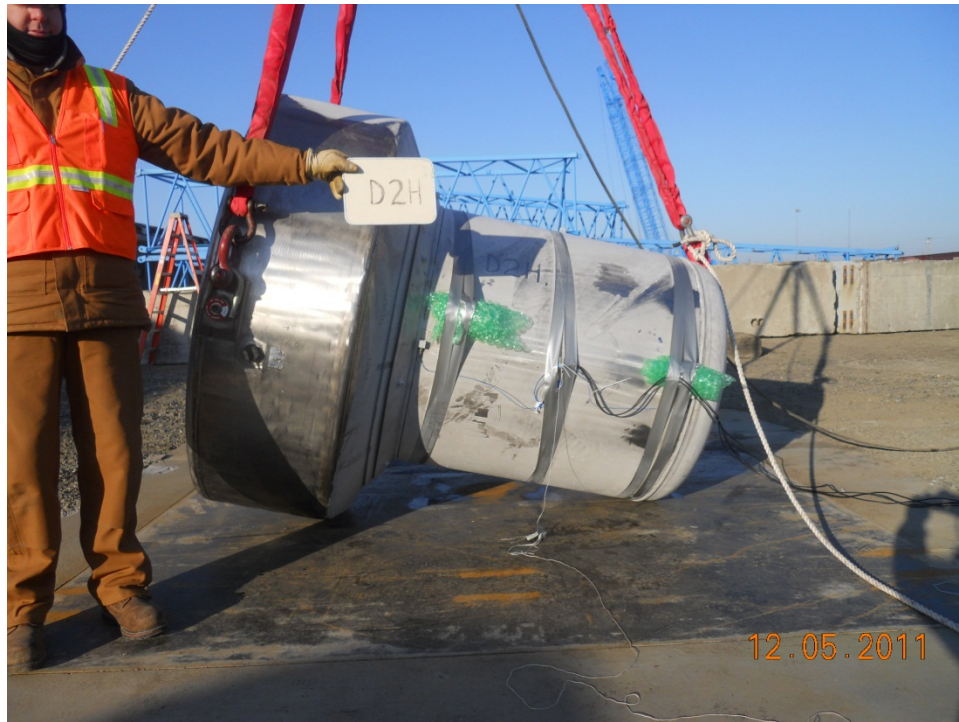


Figure 2.12.3-16 – Free Drop Test D2N/D2H Orientation



Figure 2.12.3-17 – CTU #1 Condition After Free Drop Test D2H



Figure 2.12.3-18 – Puncture Drop Test P2 Orientation



Figure 2.12.3-19 – Damage to Package Top Due to Puncture Drop Test P2



Figure 2.12.3-20 – General Condition of Lodgment & LTSS After D1 and D2 Test Series



Figure 2.12.3-21 – Condition of LTSS After D1 and D2 Test Series



Figure 2.12.3-22 – Free Drop Test D3N/D3H Orientation



Figure 2.12.3-23 – CTU #2 Condition After Free Drop Test D3H



Figure 2.12.3-24 – Puncture Drop Test P3 Orientation

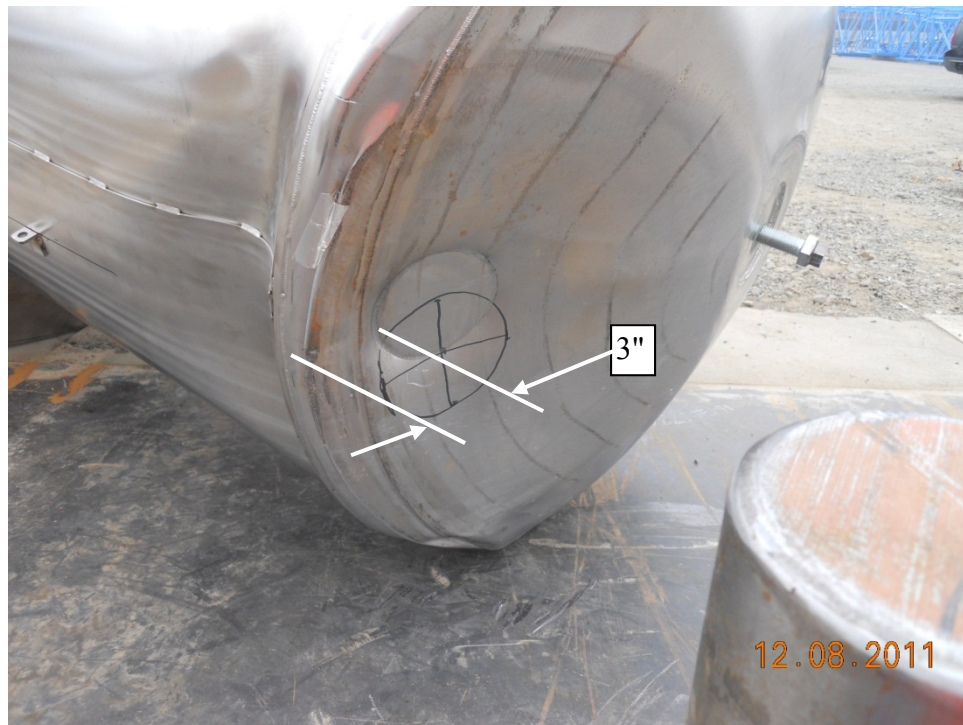


Figure 2.12.3-25 – Damage to Package Top Due to Puncture Drop Test P3



Figure 2.12.3-26 – Detail of Puncture Test P3 Damage



Figure 2.12.3-27 – Free Drop Test D6N/D6H Orientation



Figure 2.12.3-28 – CTU #3 Condition After Free Drop Test D6H (Also Showing P7)



Figure 2.12.3-29 – Puncture Drop Test P7 Orientation



Figure 2.12.3-30 – Damage to Package Side Due to Puncture Drop Test P7



Figure 2.12.3-31 – Puncture Drop Test P5 Orientation



Figure 2.12.3-32 – Damage to Package Side Due to Puncture Drop Test P5



Figure 2.12.3-33 – Detail of Puncture Test P5 Damage (Rain Shield Removed)

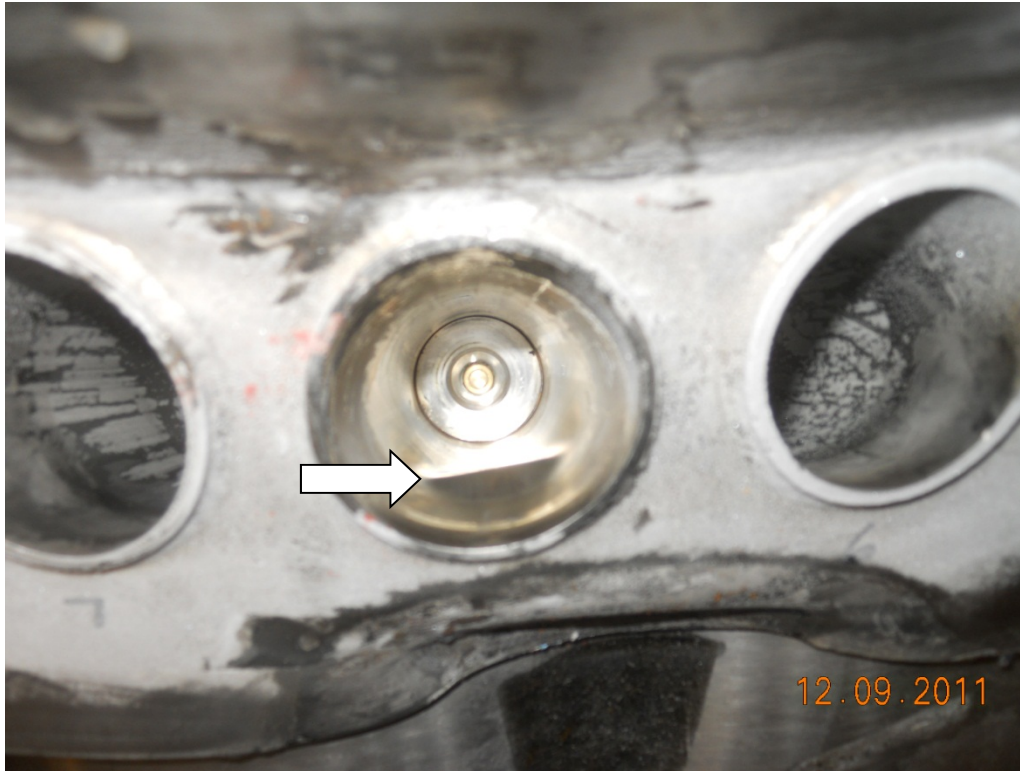


Figure 2.12.3-34 – Puncture Test P5 Damage Showing Internal Dent in Vent Port Tube



Figure 2.12.3-35 – Internal View of Damage from Puncture Test P7



Figure 2.12.3-36 – Internal View of Damage from Puncture Test P7, Detail

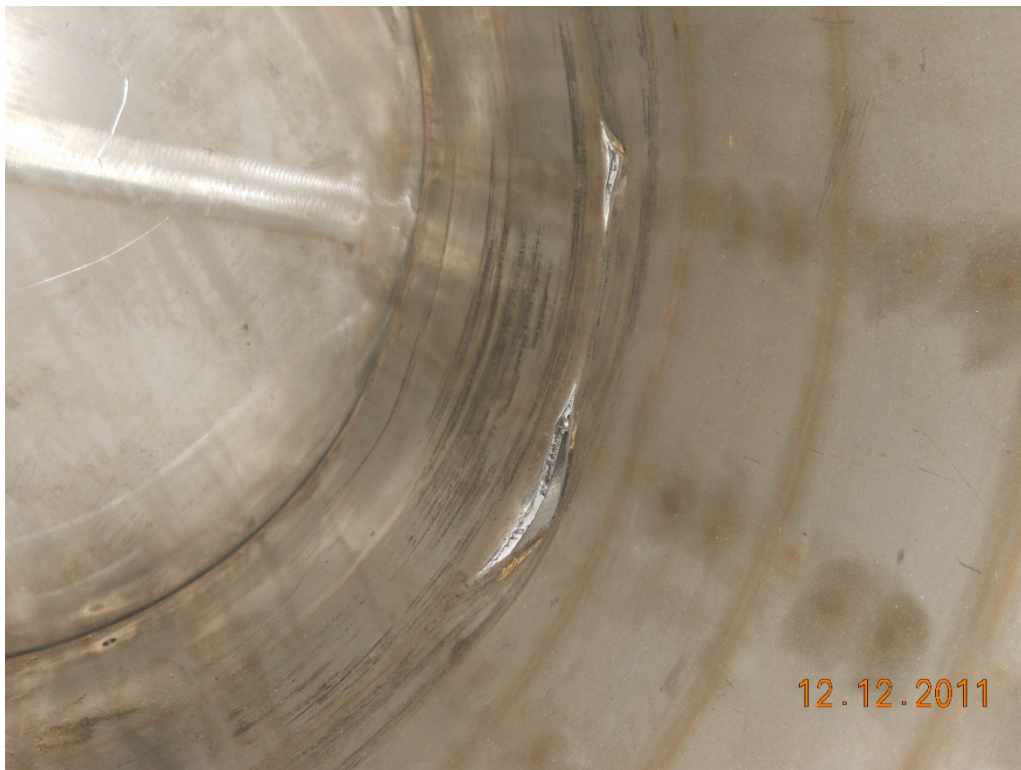


Figure 2.12.3-37 – Cut in Inner Container (IC) Wall Due to Dummy Payload Side Impact



Figure 2.12.3-38 – Dunnage After D6 Test Series



Figure 2.12.3-39 – Dummy Payload After D6 Test Series

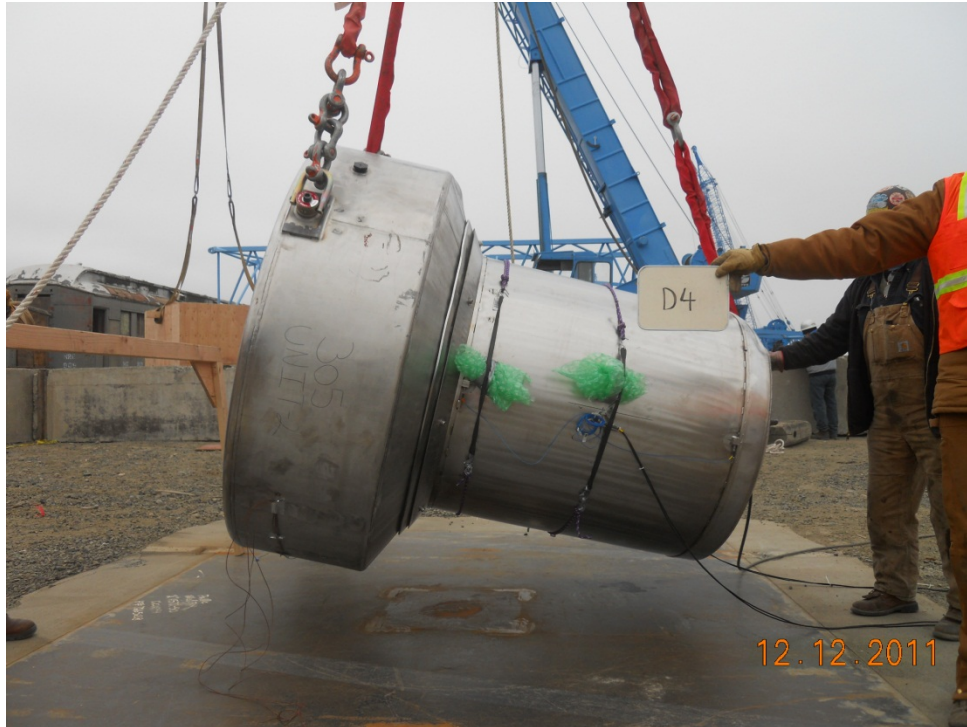


Figure 2.12.3-40 – Free Drop Test D4N/D4H Orientation



Figure 2.12.3-41 – CTU #2 Condition After Free Drop Test D4H (Also Showing P4)



Figure 2.12.3-42 – Puncture Drop Test P4 Orientation



Figure 2.12.3-43 – Damage to Impact Limiter Side Due to Puncture Drop Test P4



Figure 2.12.3-44 – Crushed Internal impact limiter Tubes (Upper) Due to Free Drop D3

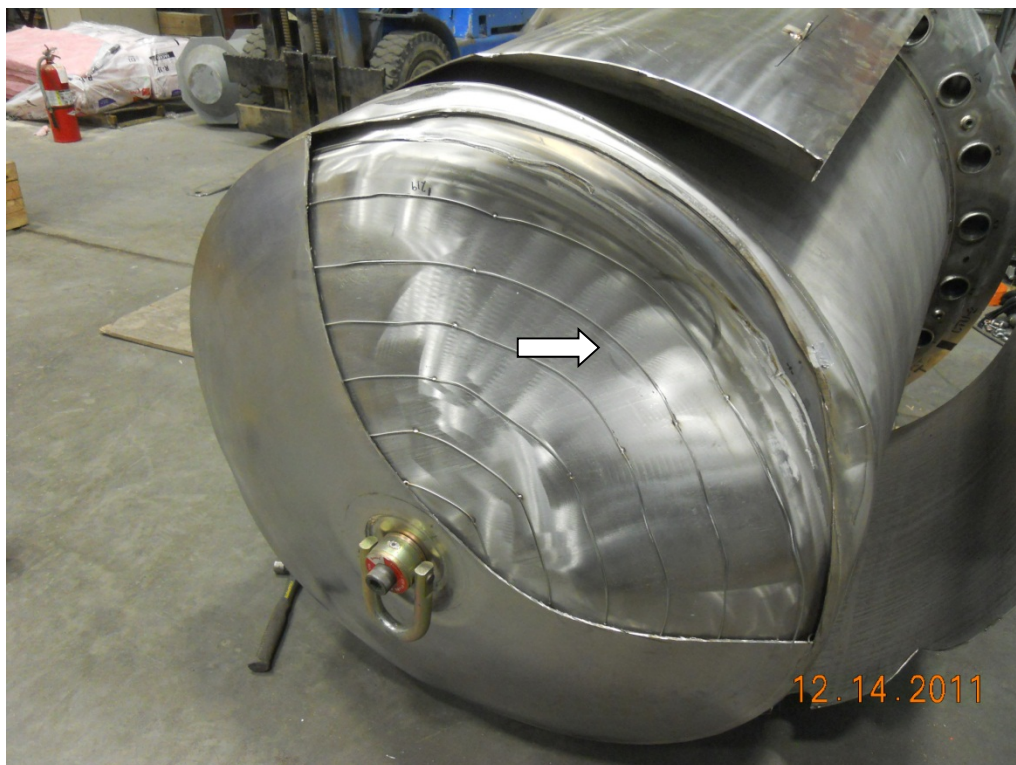


Figure 2.12.3-45 – View of Damage Due to Test Series D3, Head Shield Cut Away (arrow indicates puncture bar impact location)



Figure 2.12.3-46 – View of Damage Due to Test Series D3



Figure 2.12.3-47 – Damage to Lodgment After Test Series D3 and D4



Figure 2.12.3-48 – Minimum Foam Remaining After Free Drop D4H

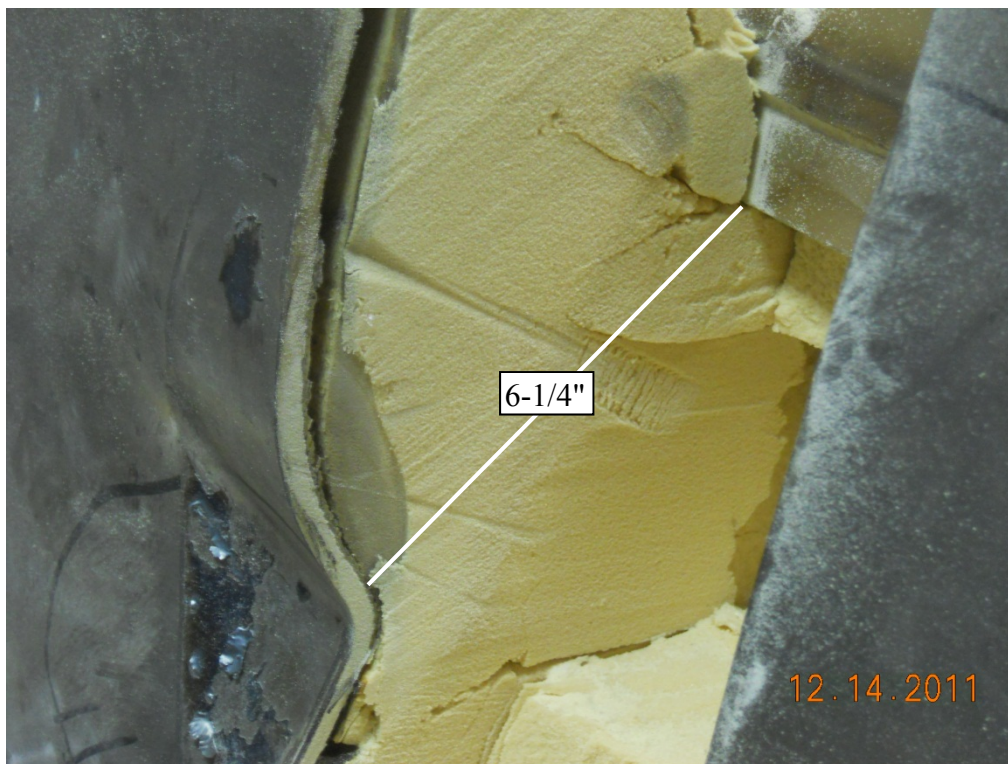
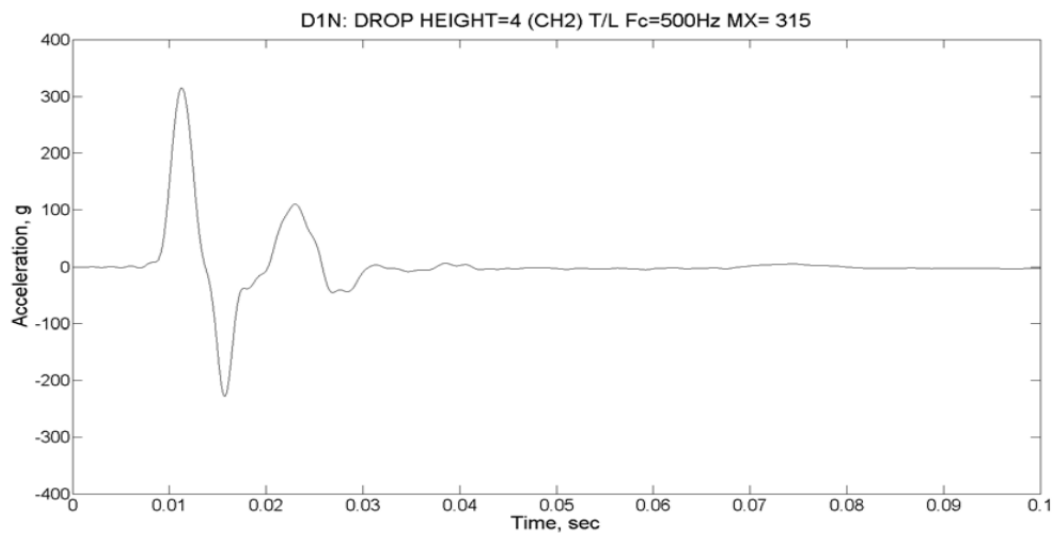
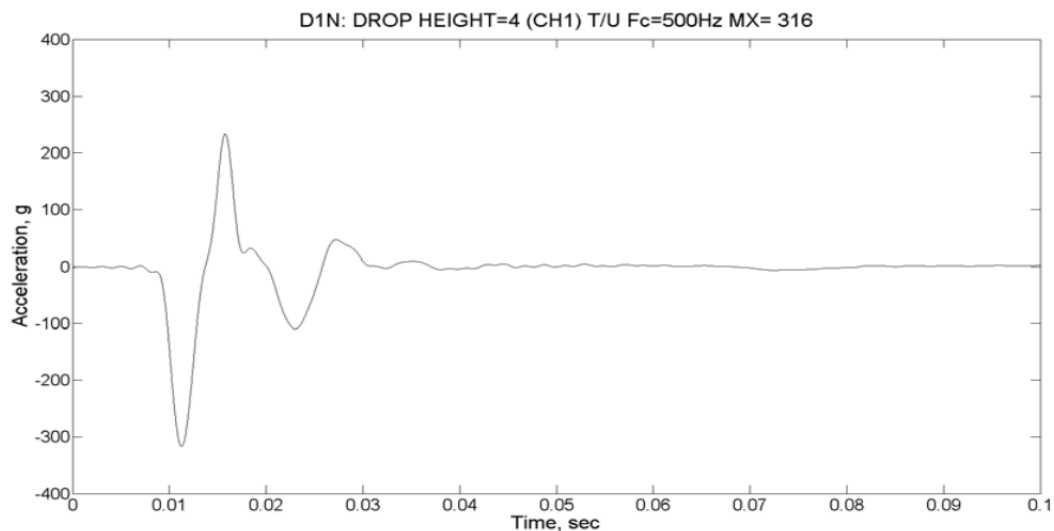
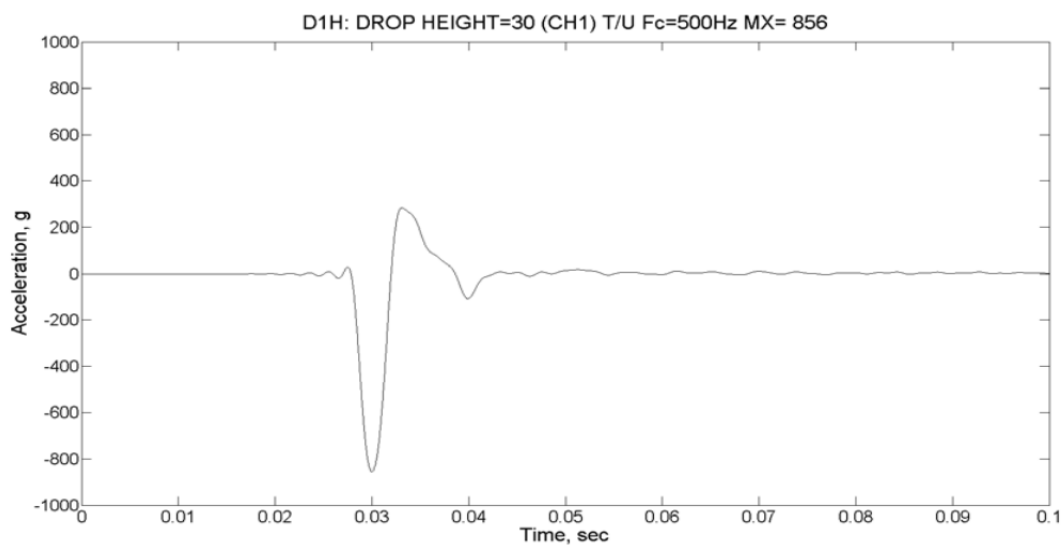
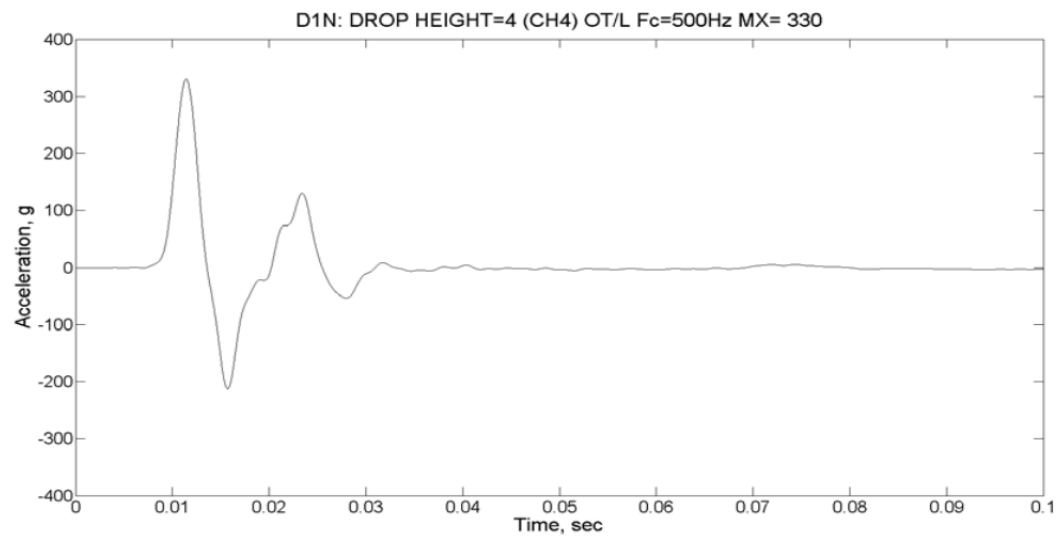
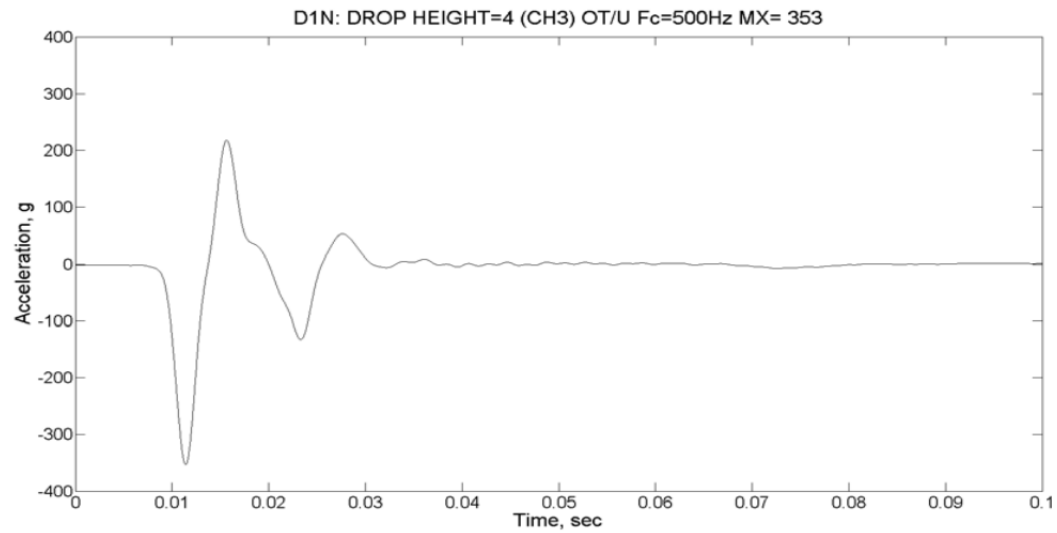


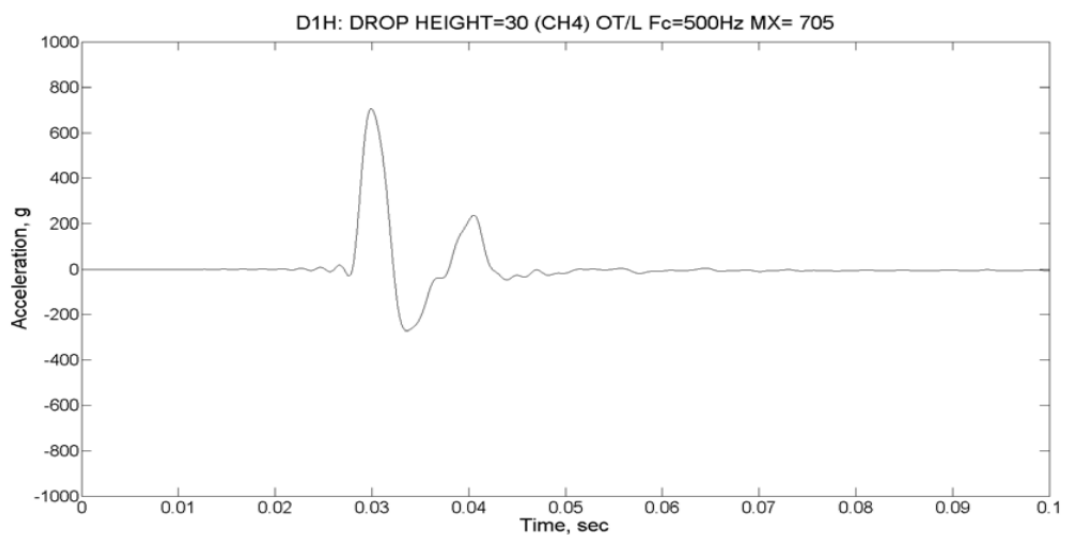
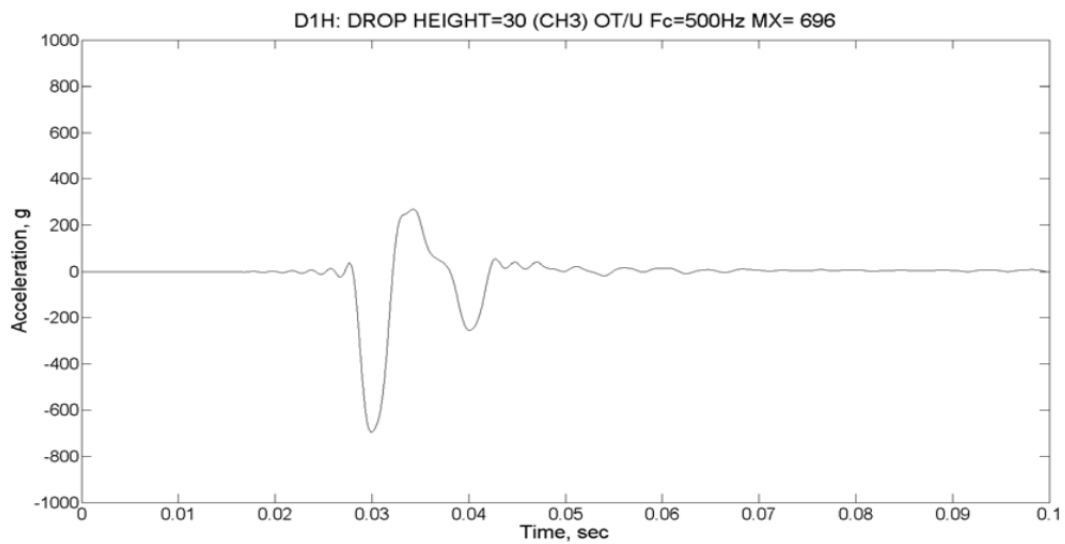
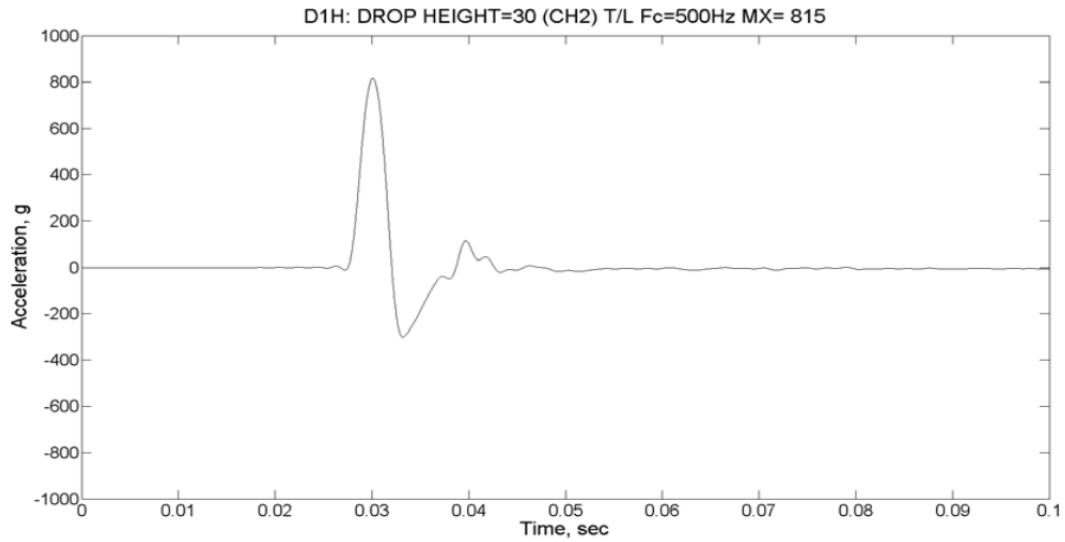
Figure 2.12.3-49 – Minimum Foam Remaining After Puncture P4

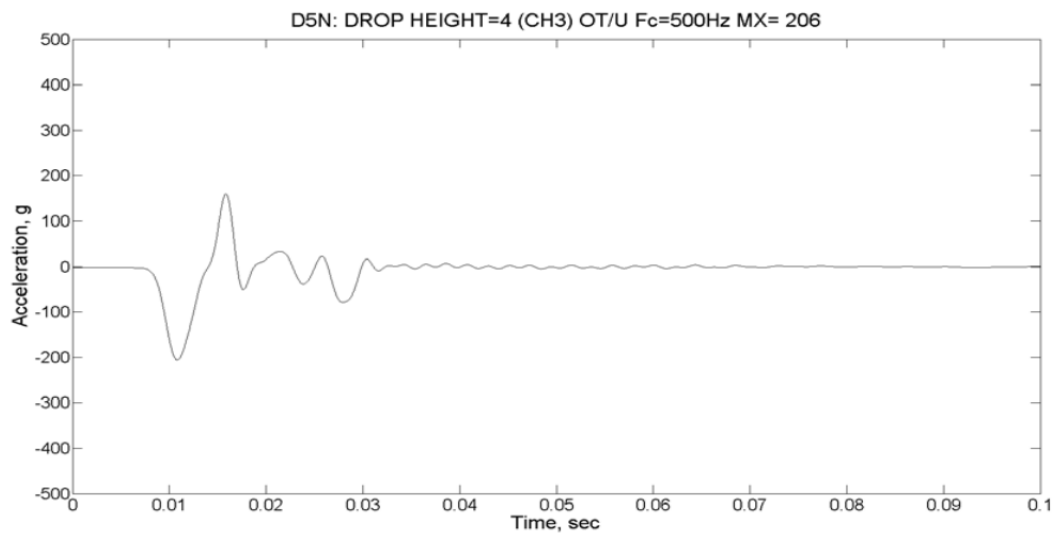
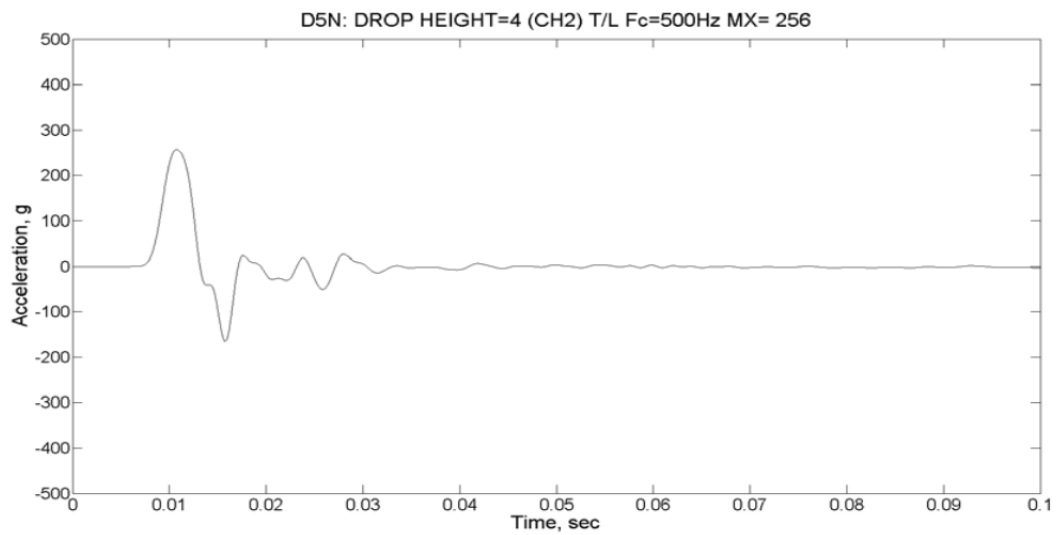
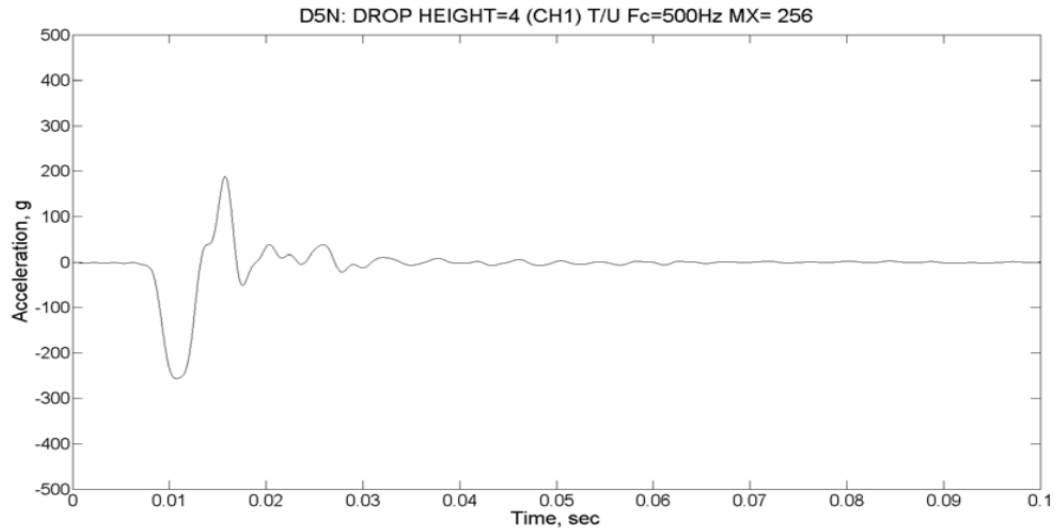
2.12.3.6 Filtered Accelerometer Time Histories

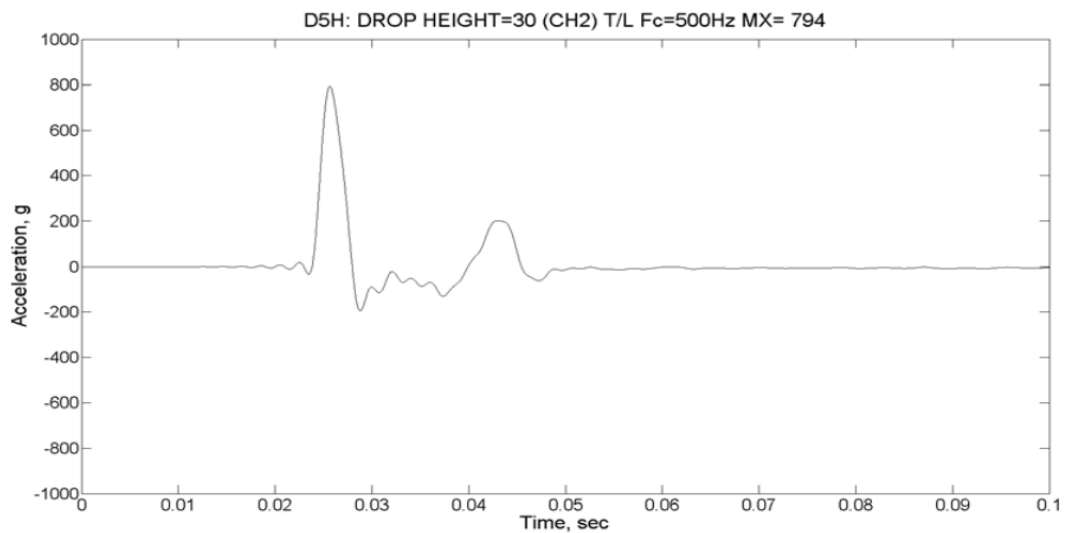
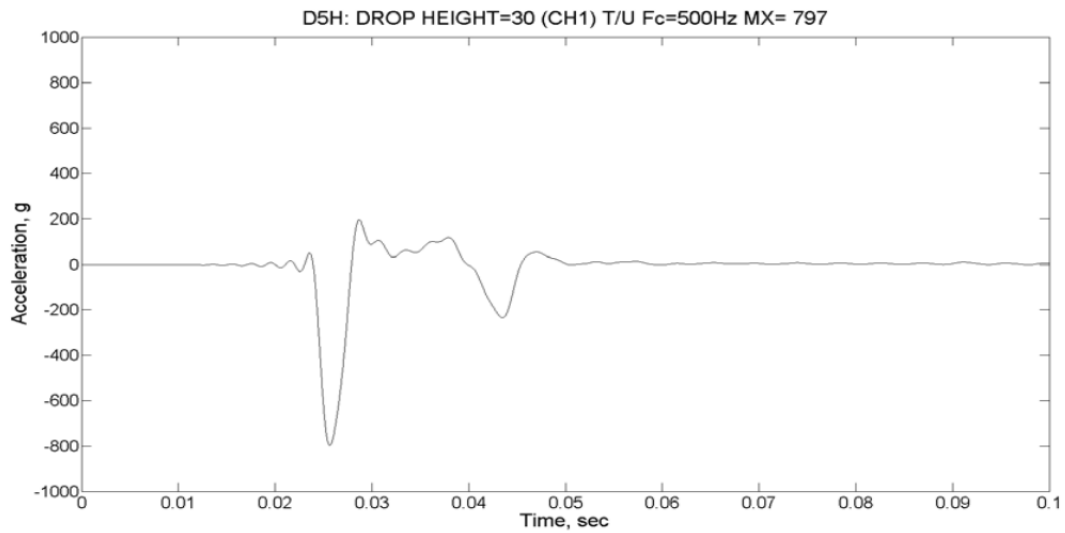
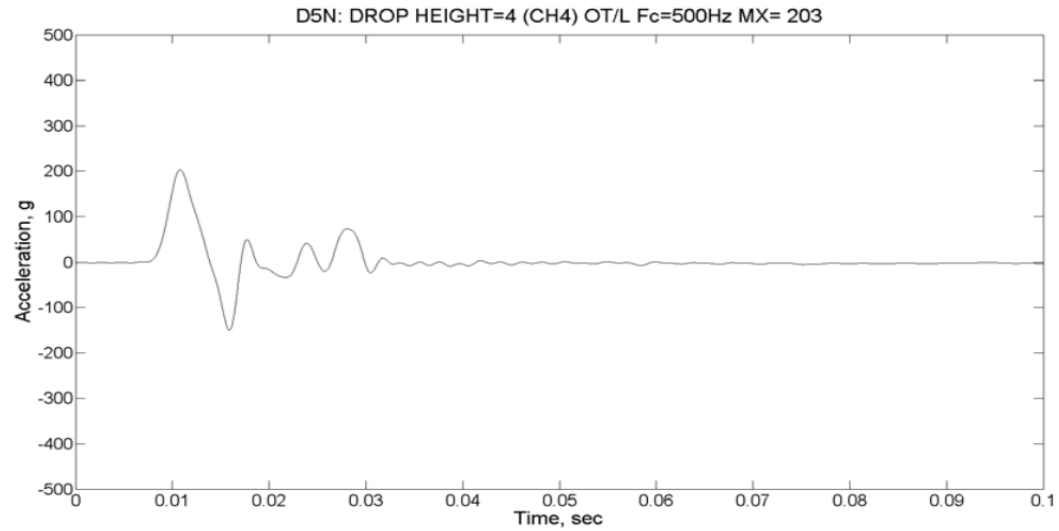
Accelerometer time history plots are provided below. Information identifying each plot is given above the figure as: drop test I.D.; drop height in ft; channel no.; location on CTU (see Section 2.12.3.2.2, *Instrumentation*, for description); filter cutoff frequency (500 Hz in all cases); and peak value, g.

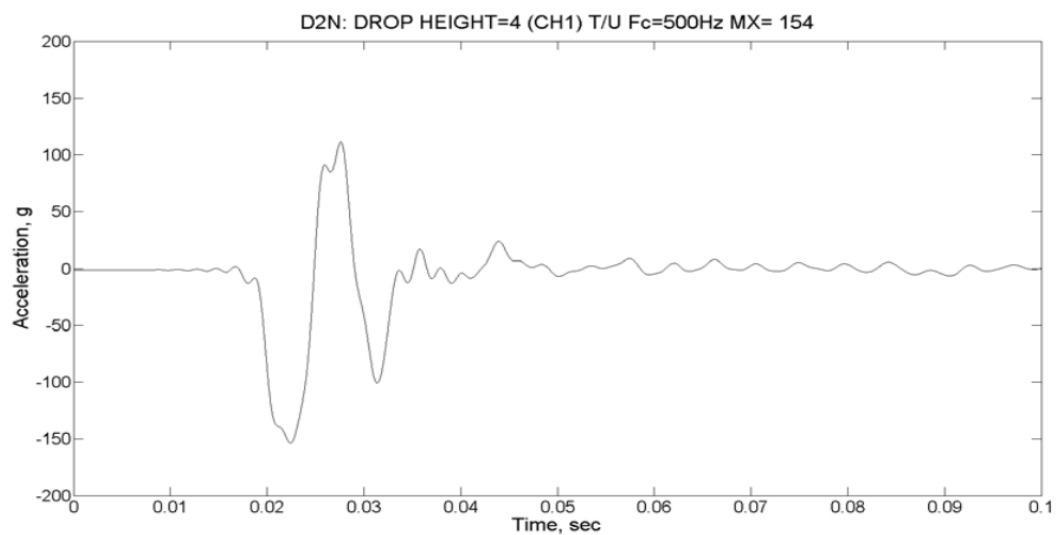
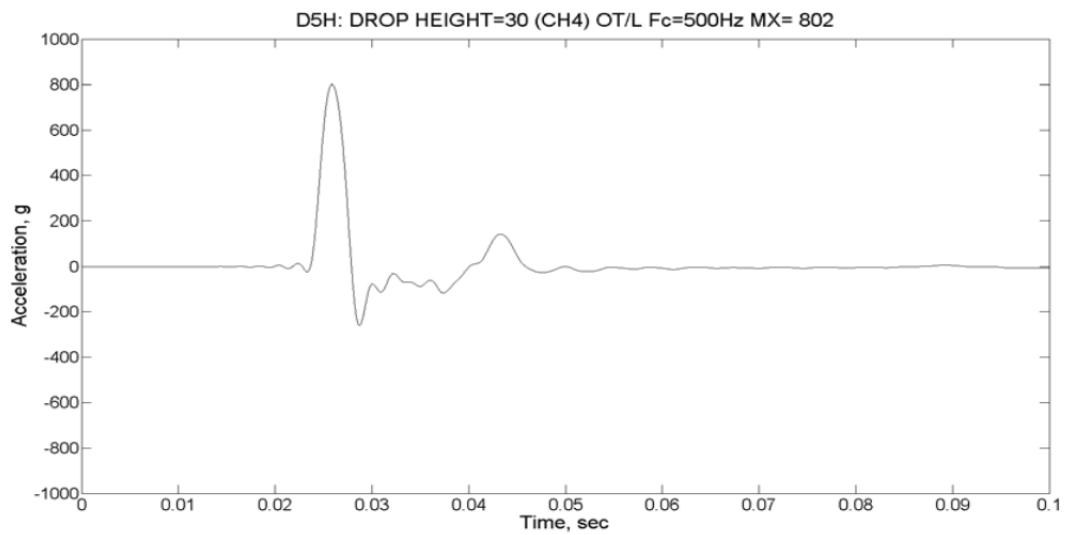
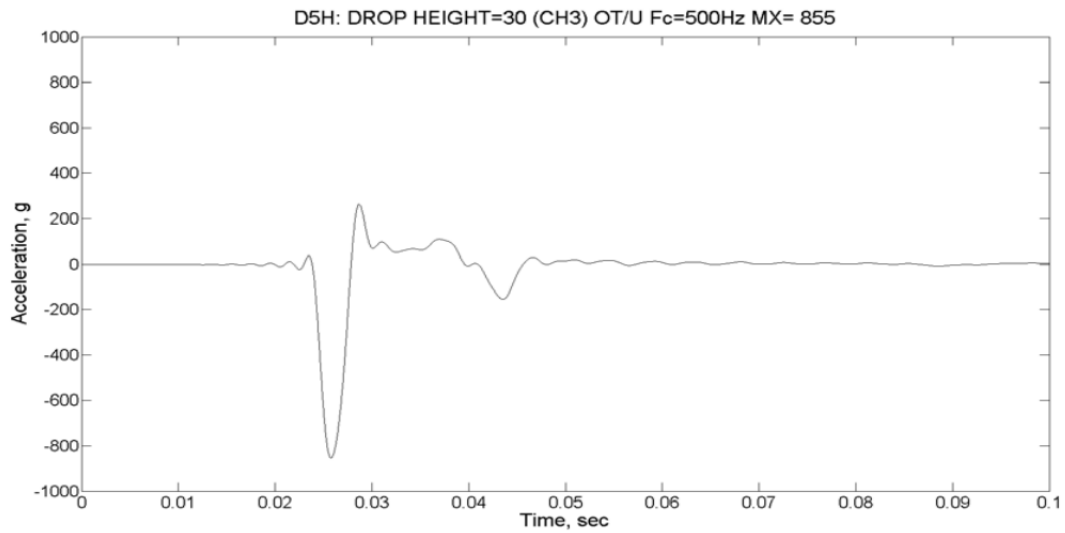


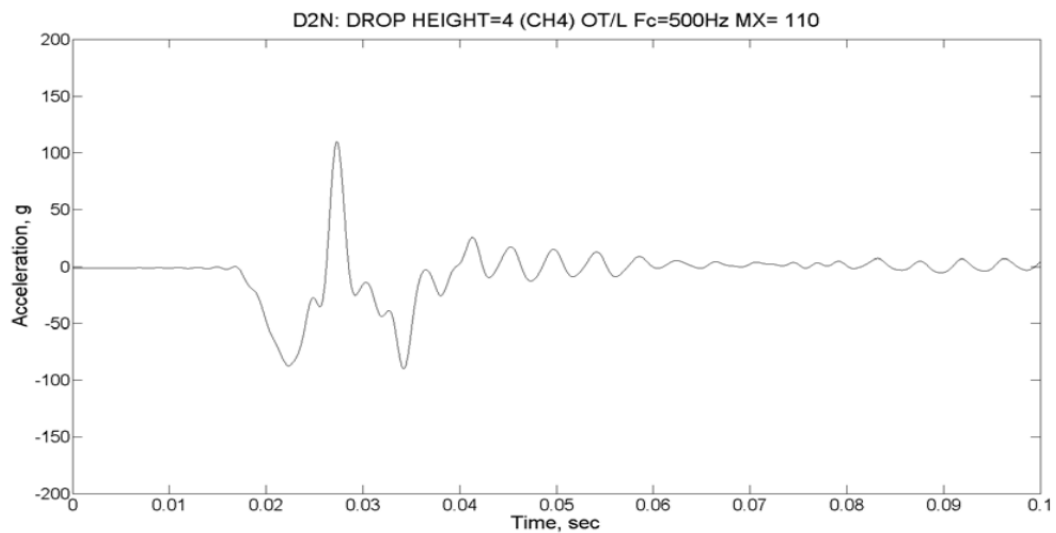
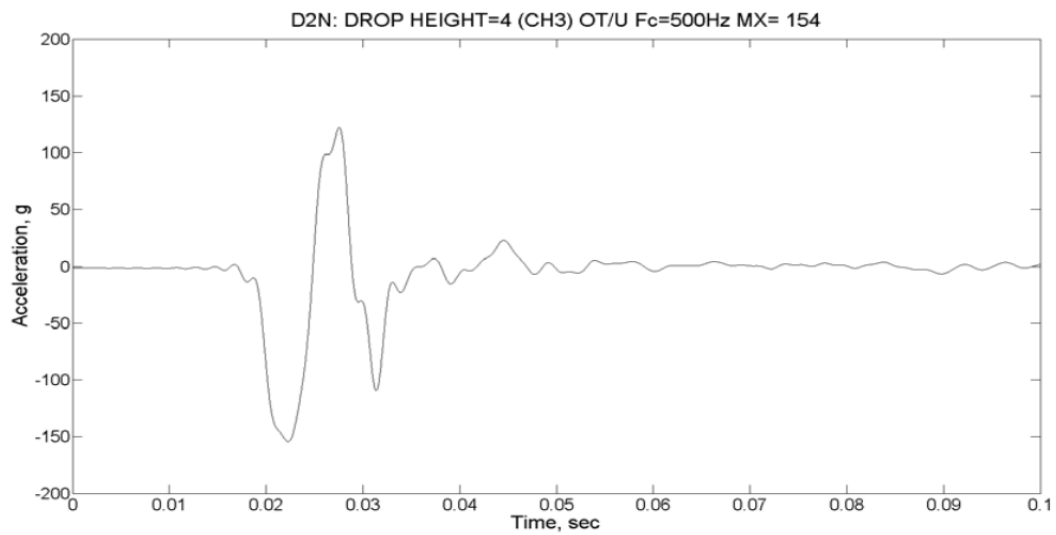
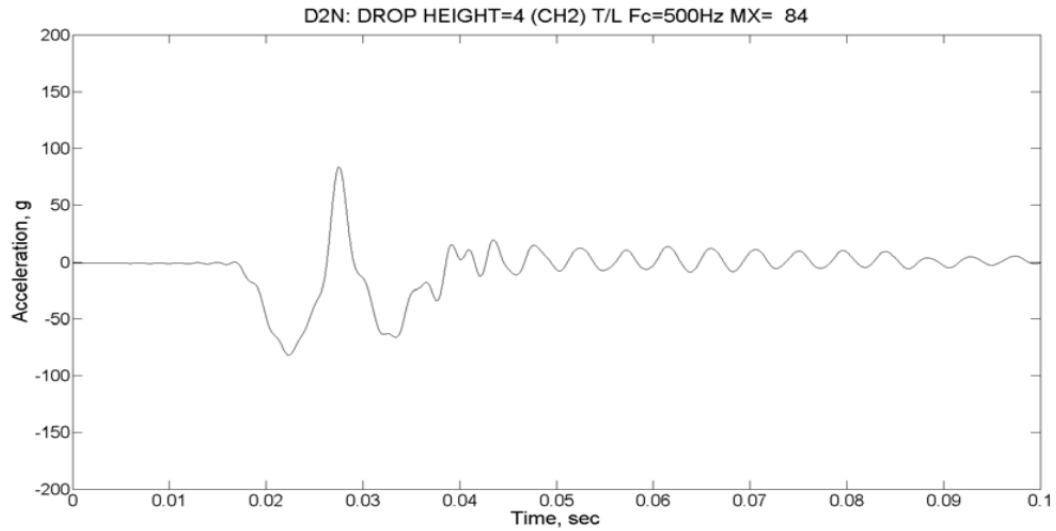


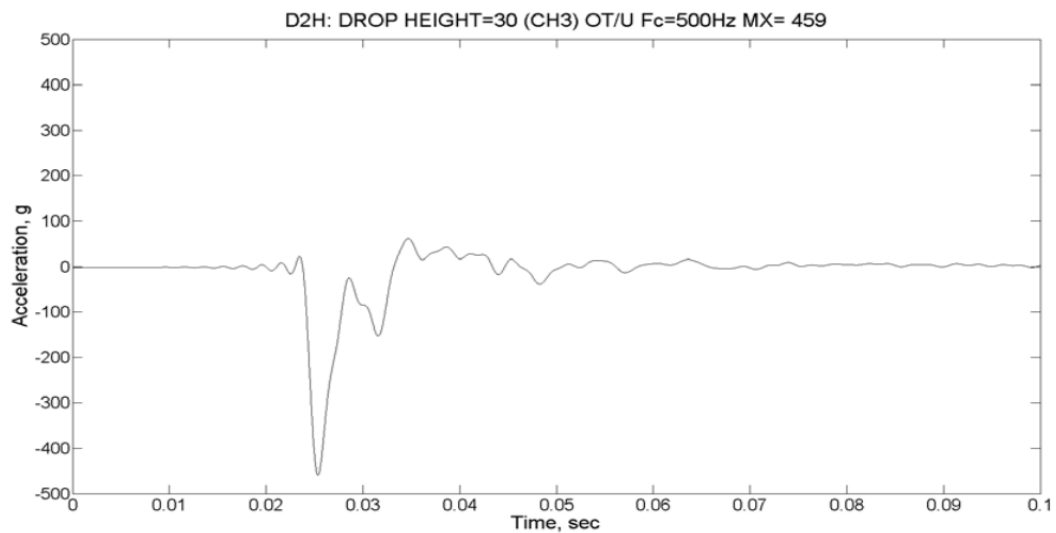
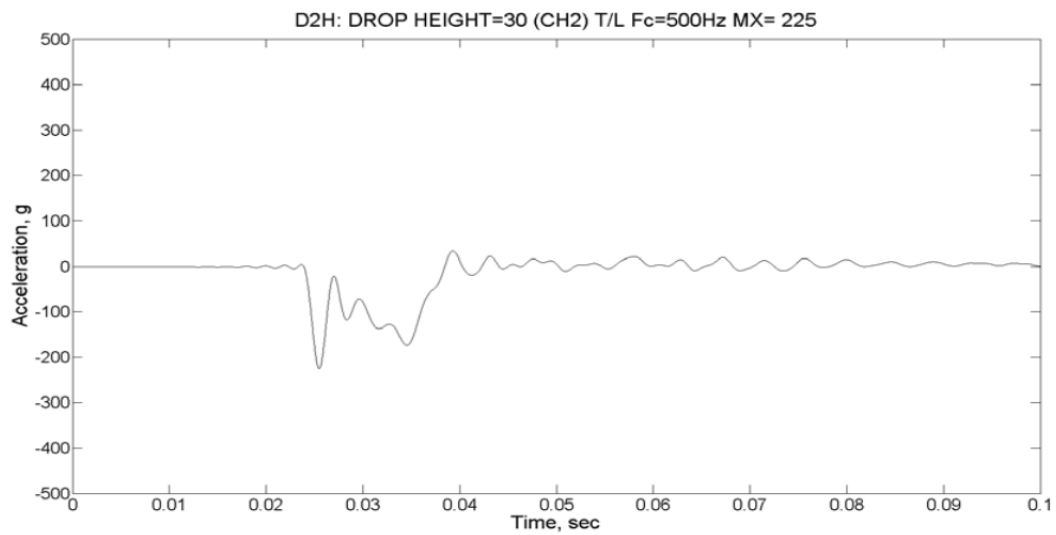
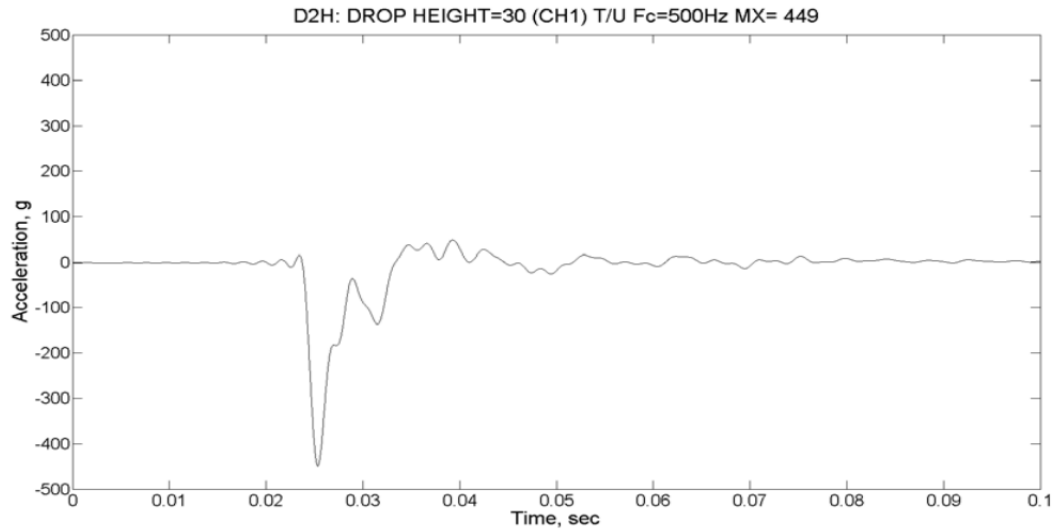


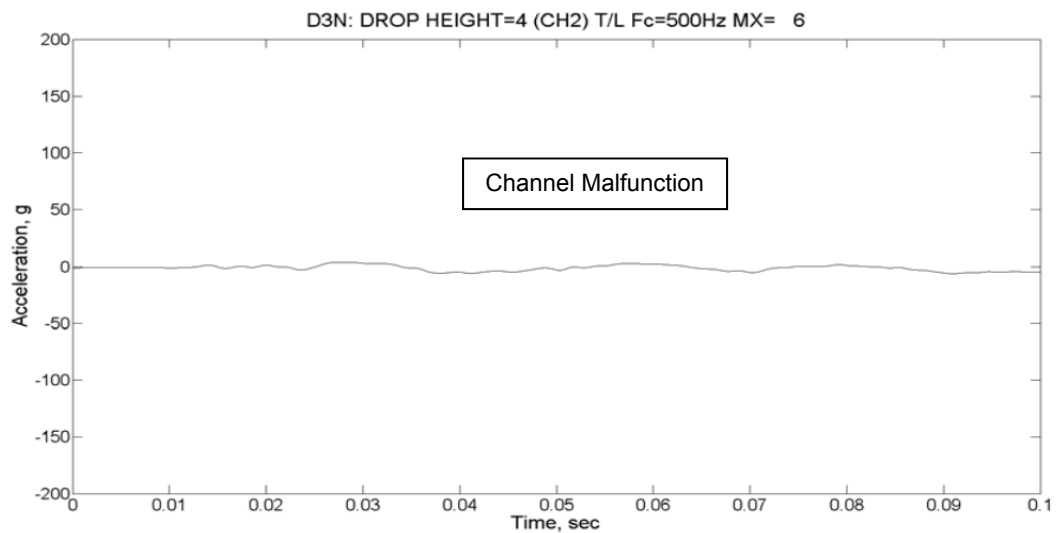
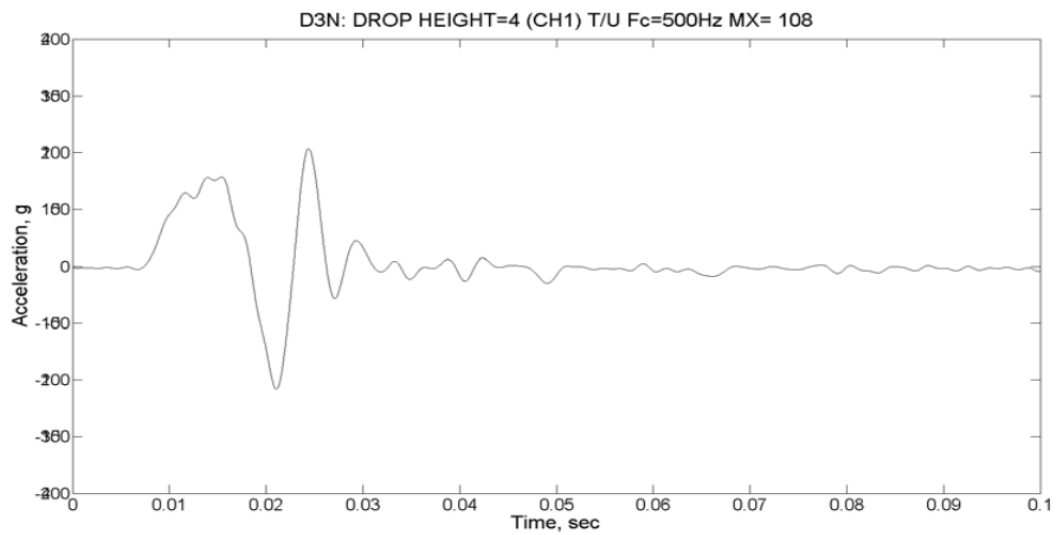
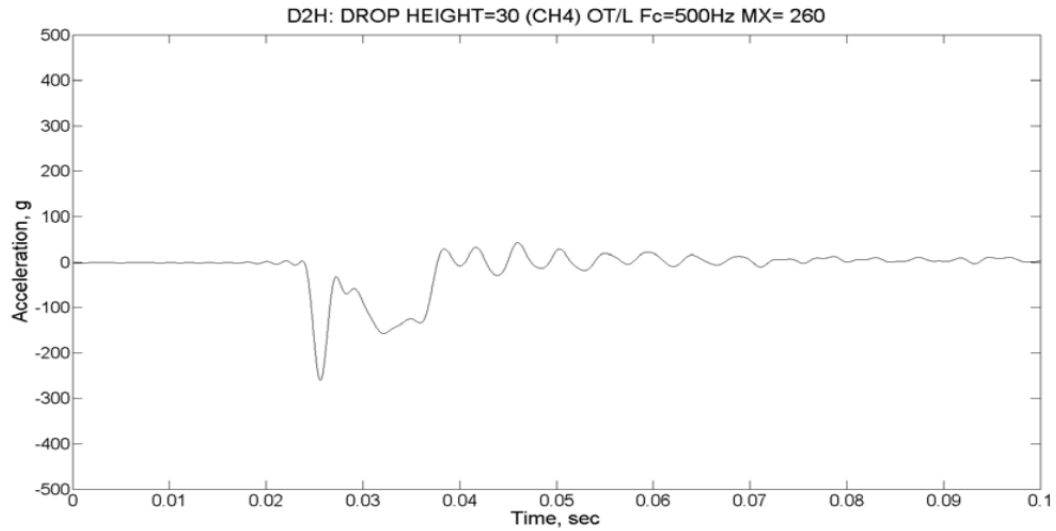


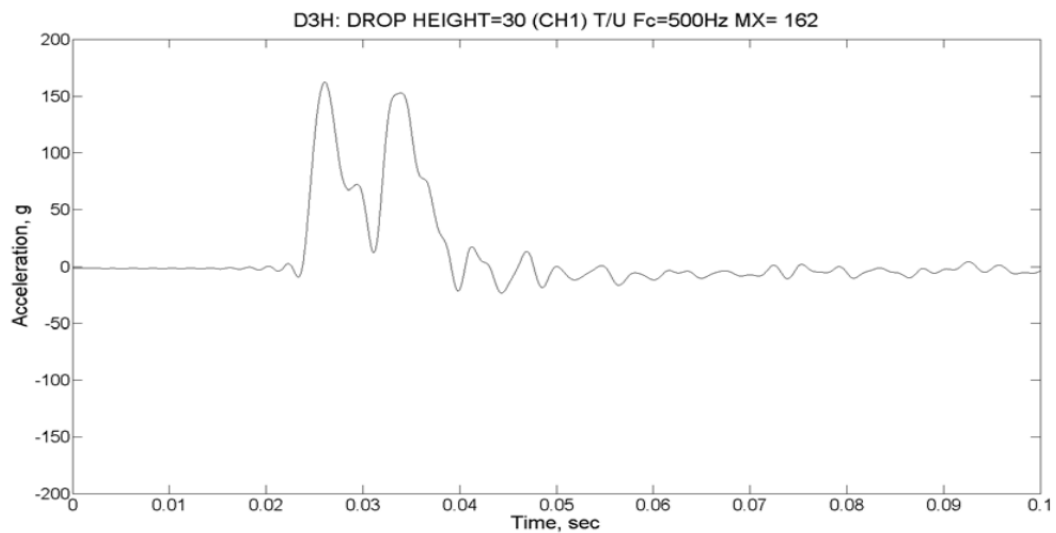
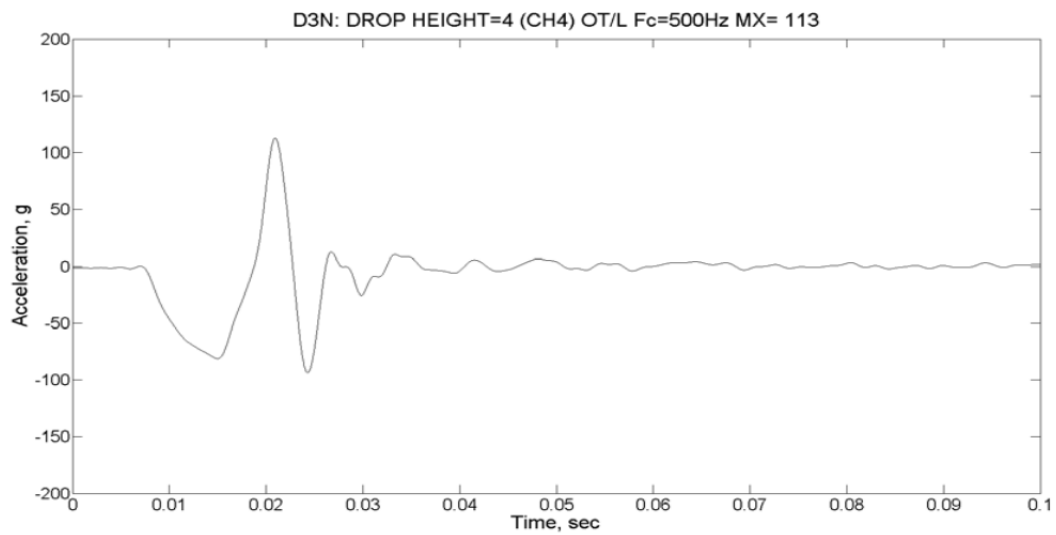
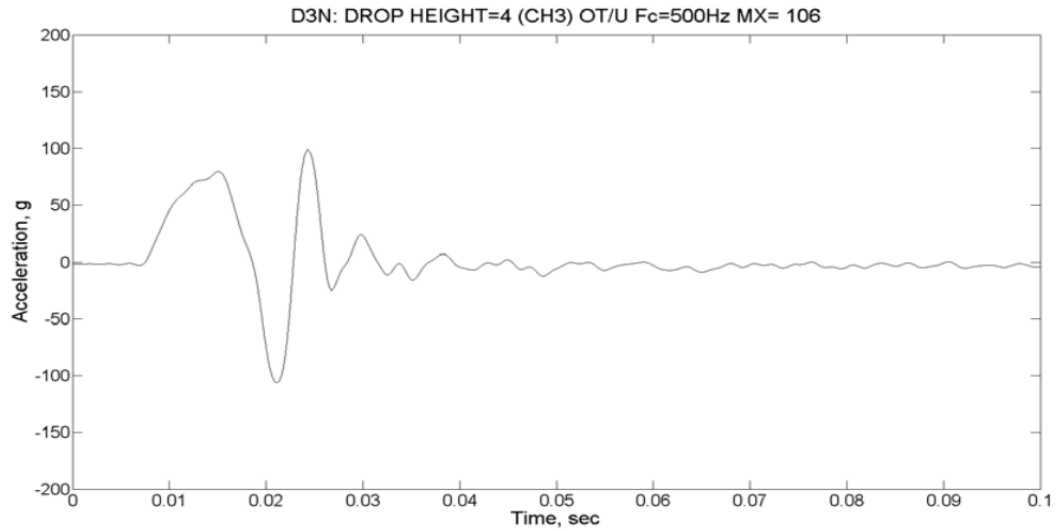


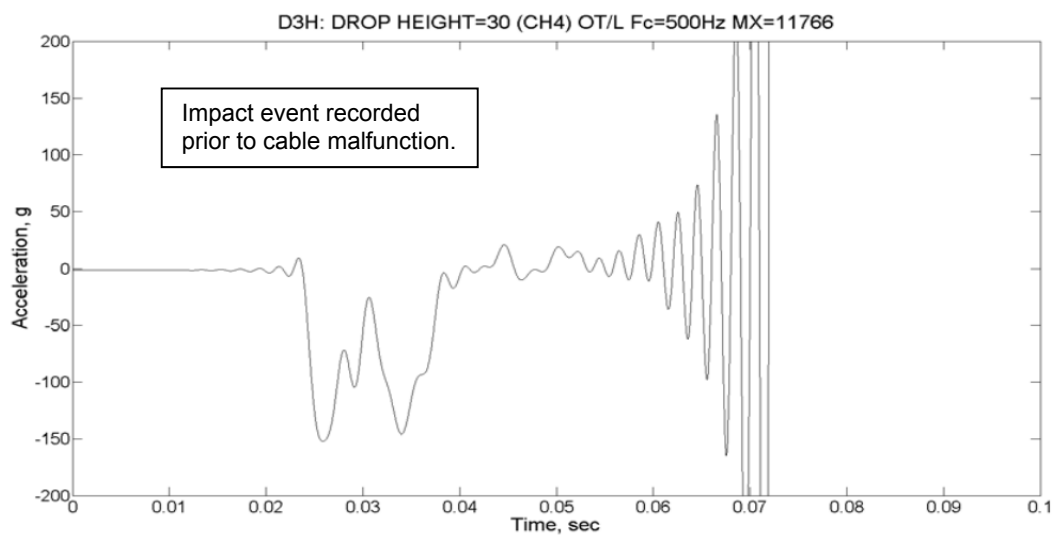
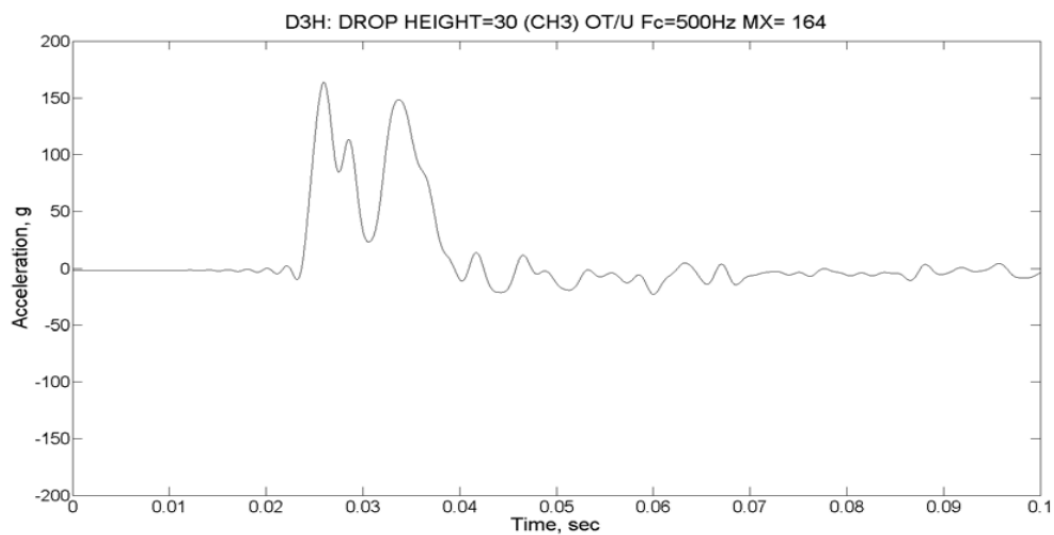
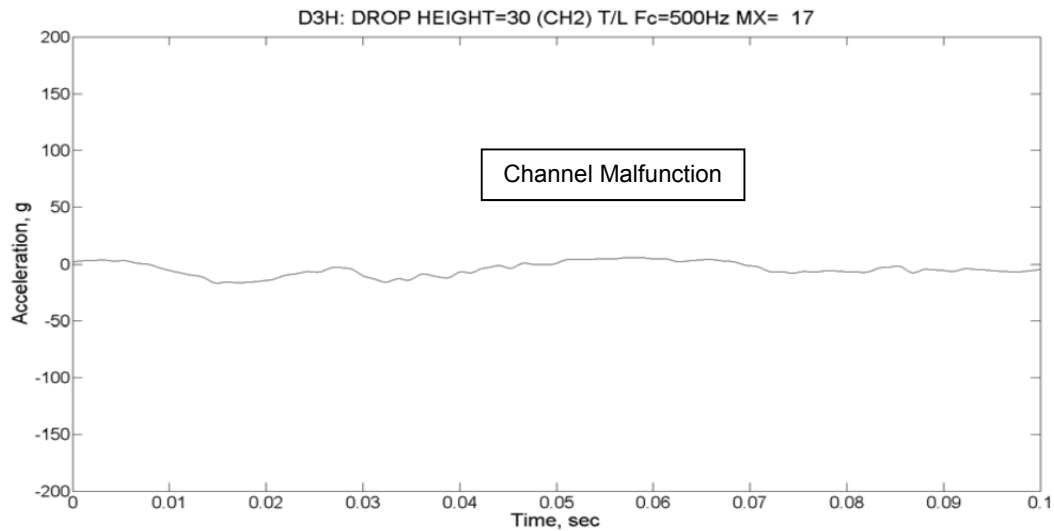


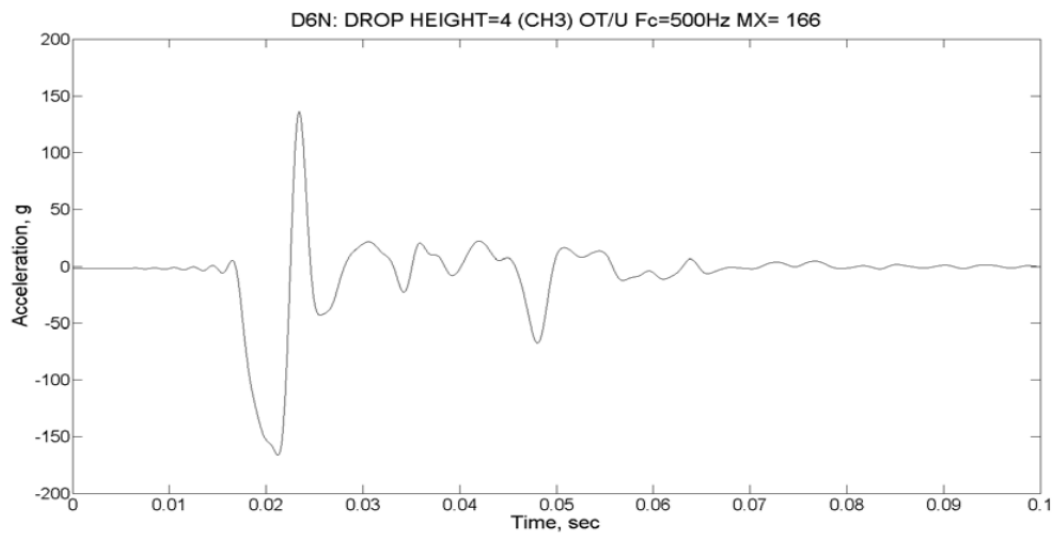
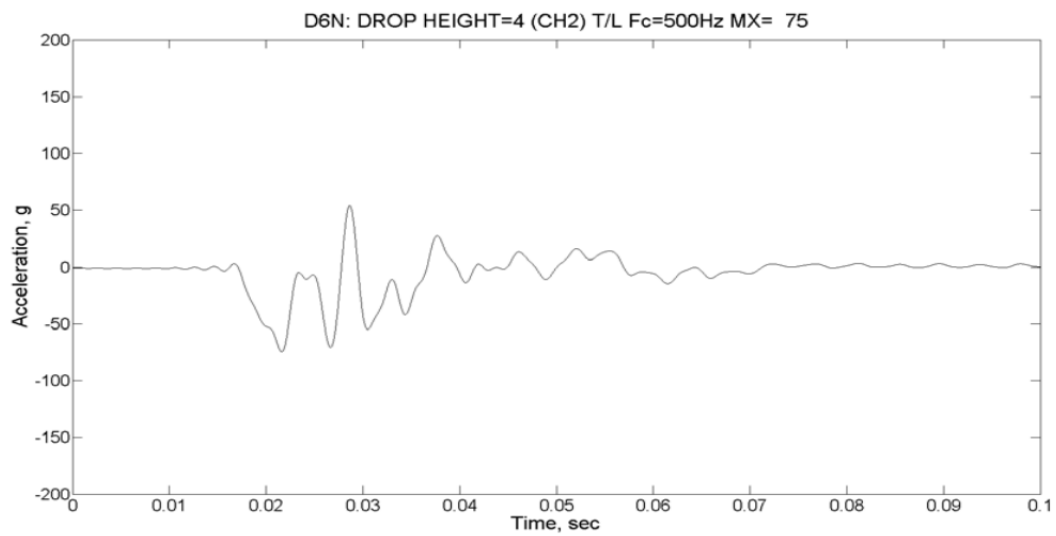
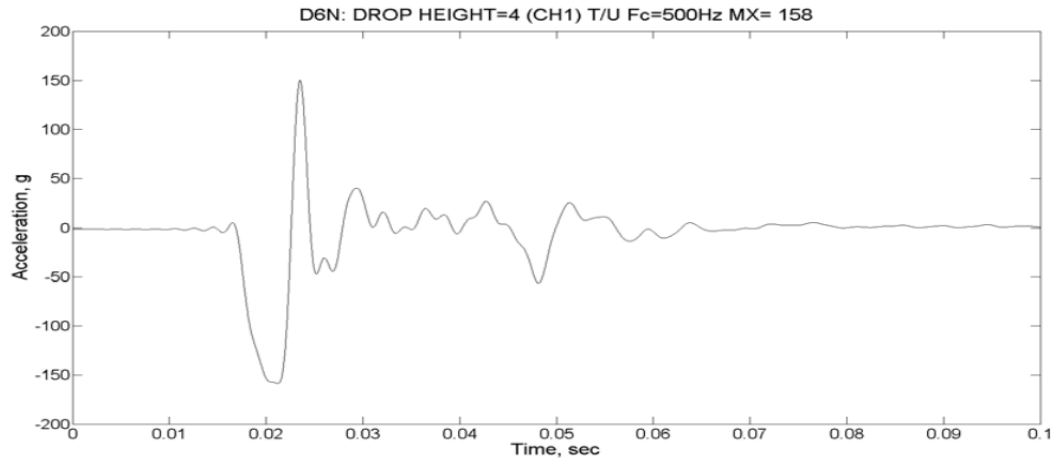


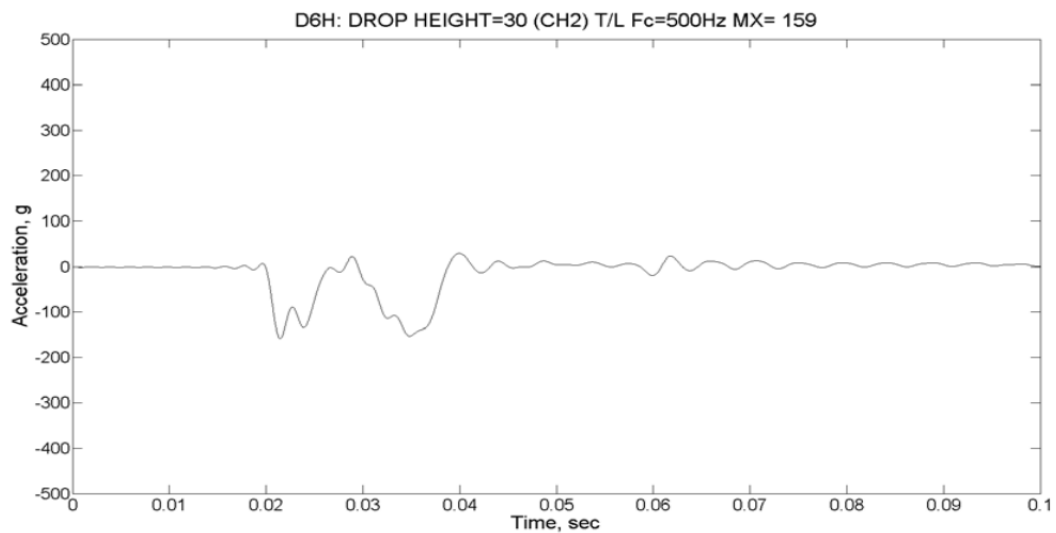
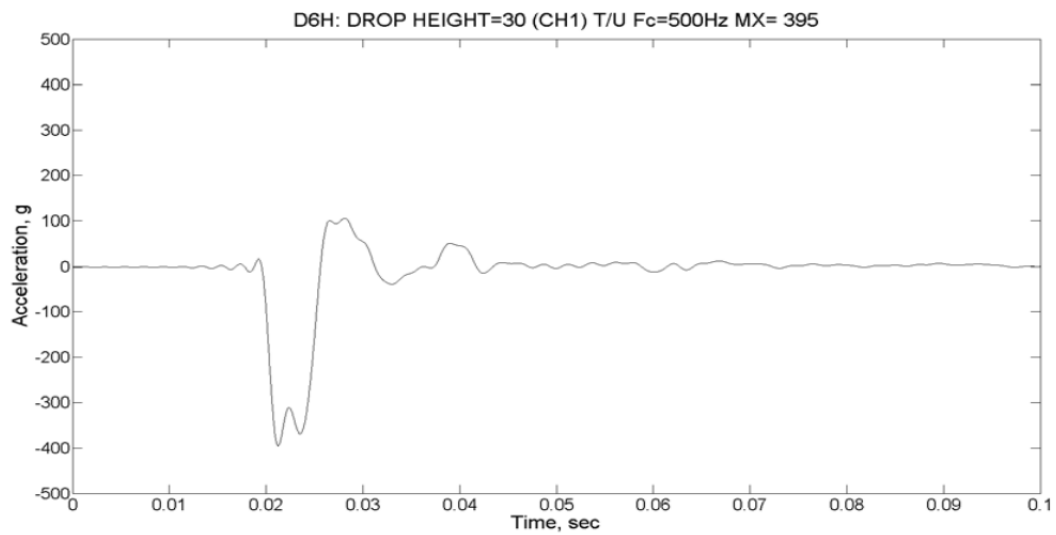
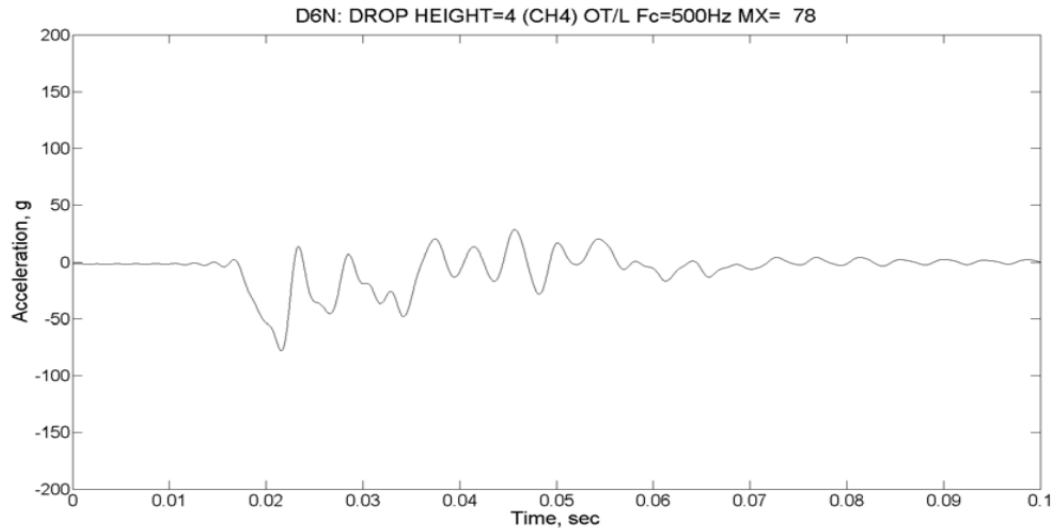


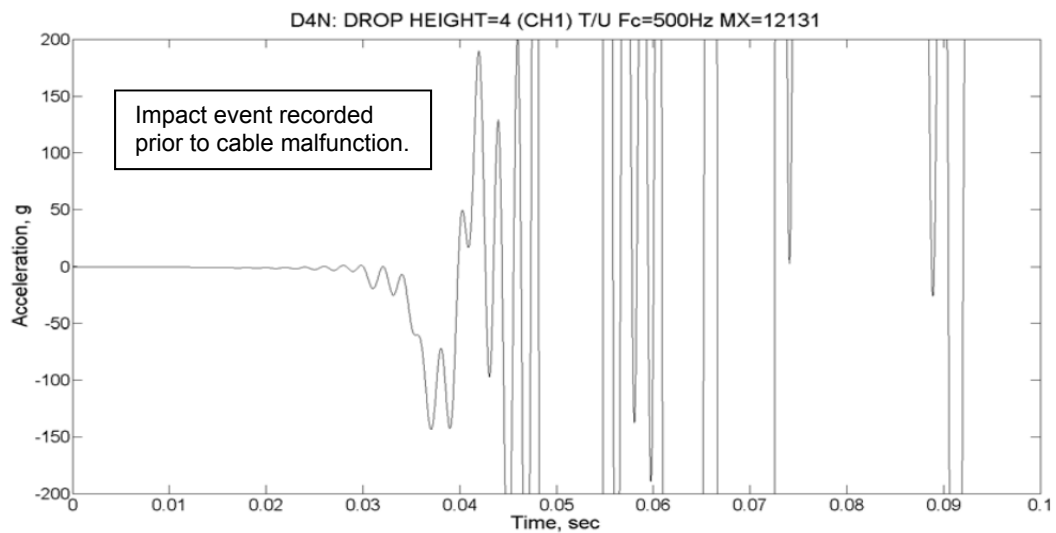
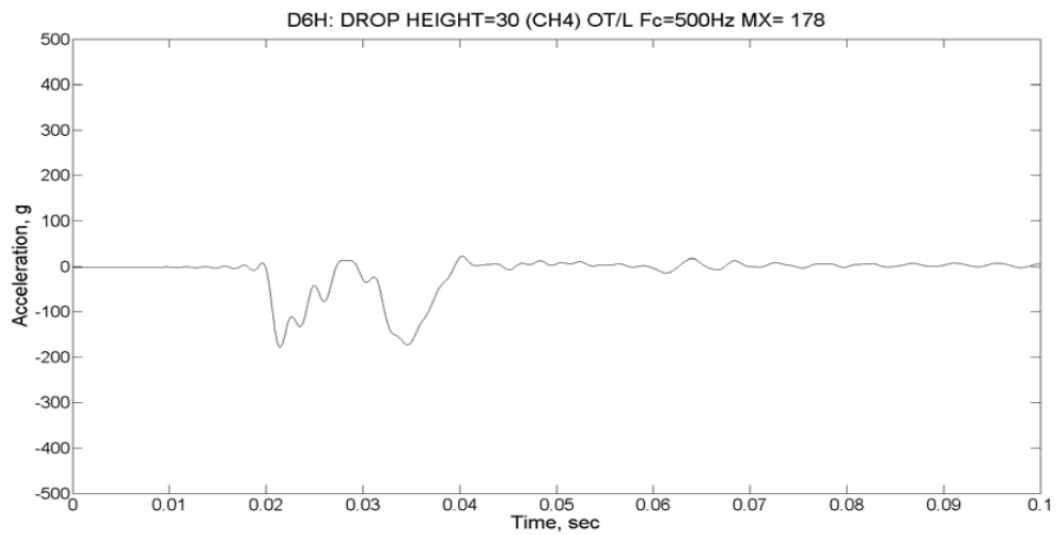
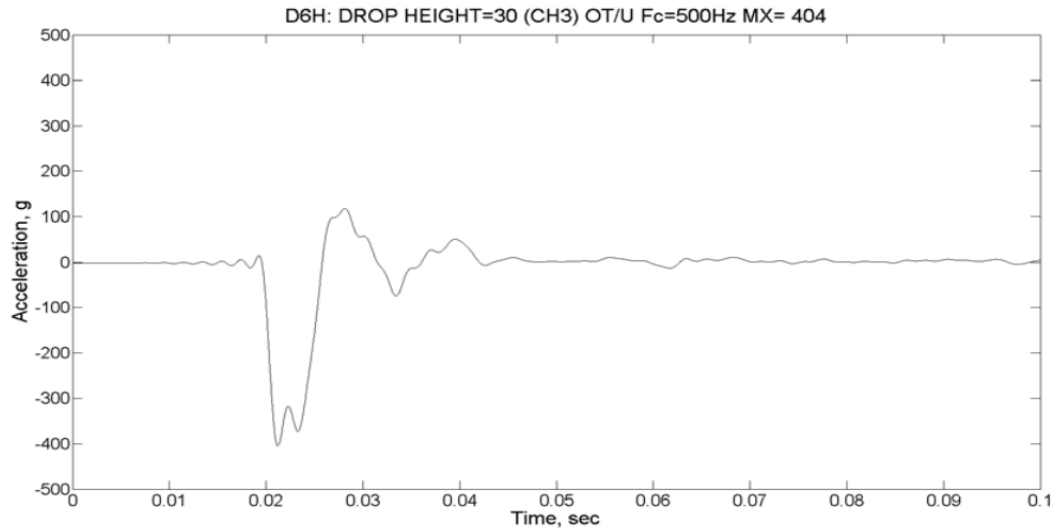


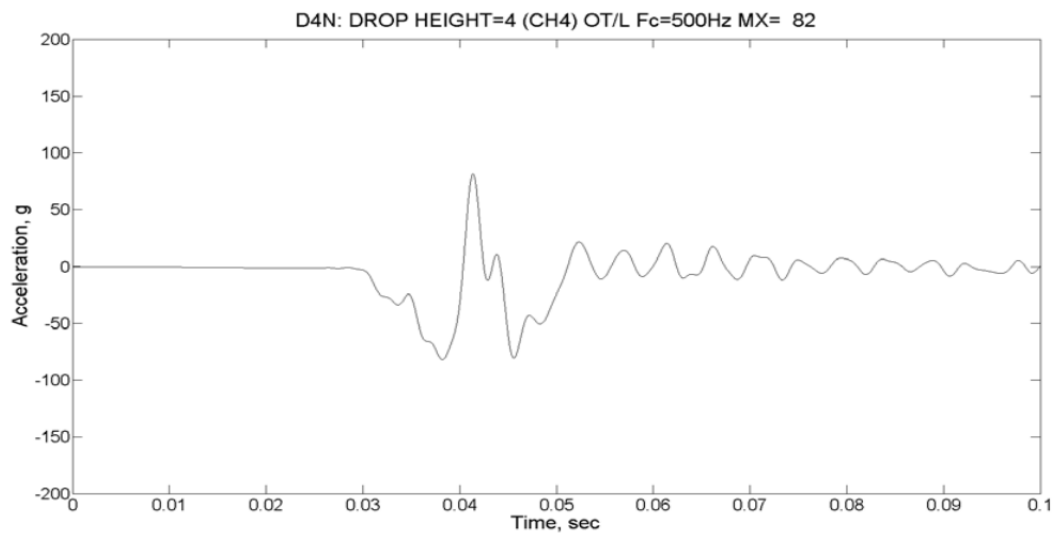
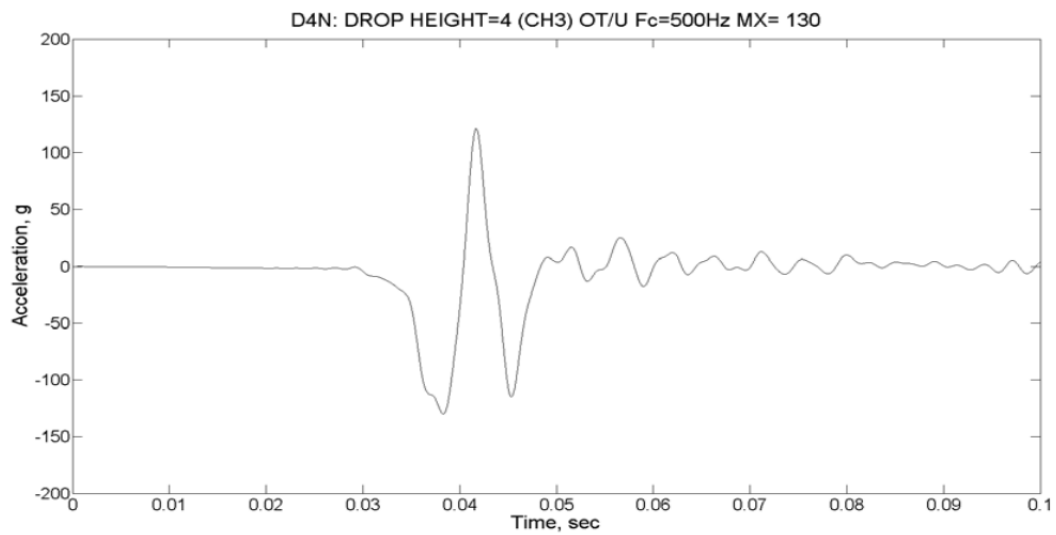
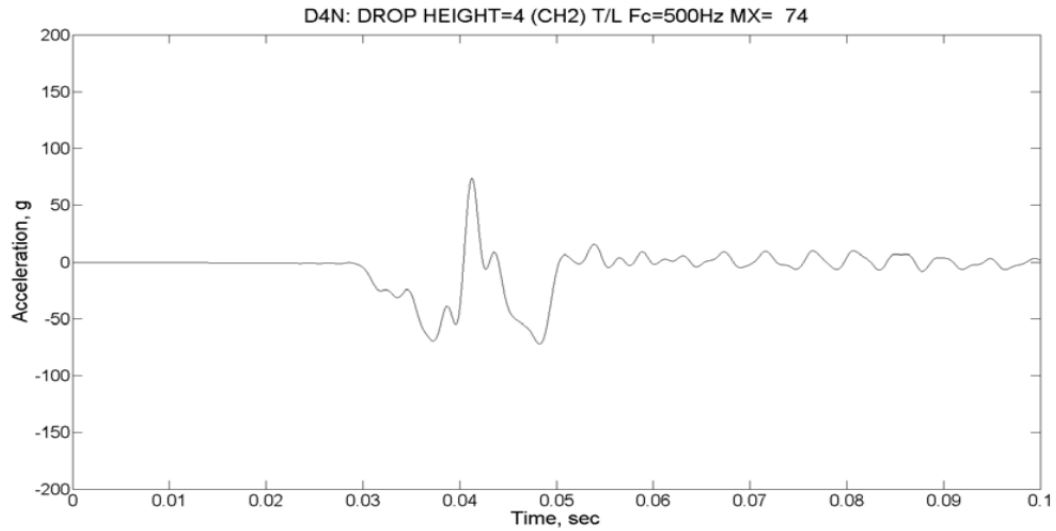


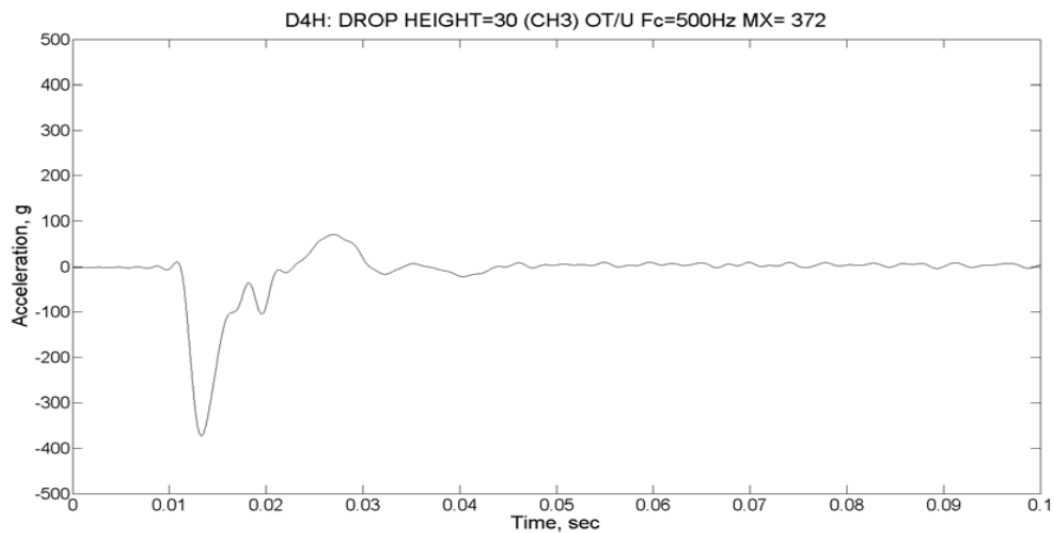
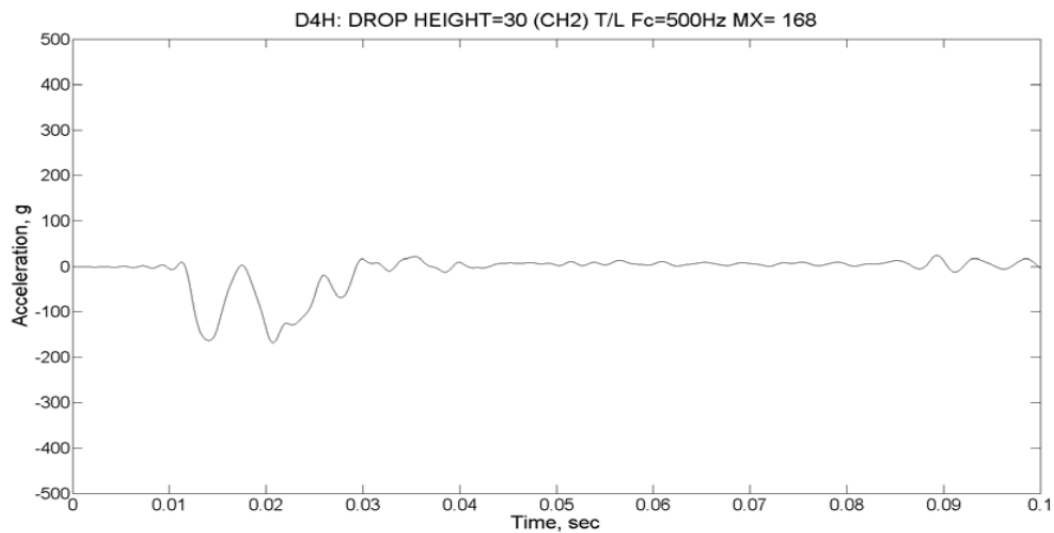
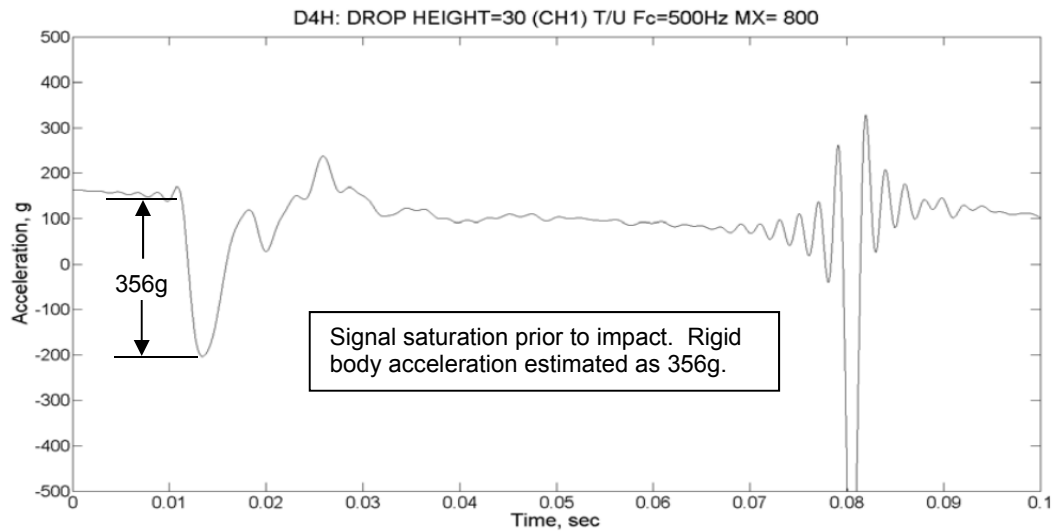


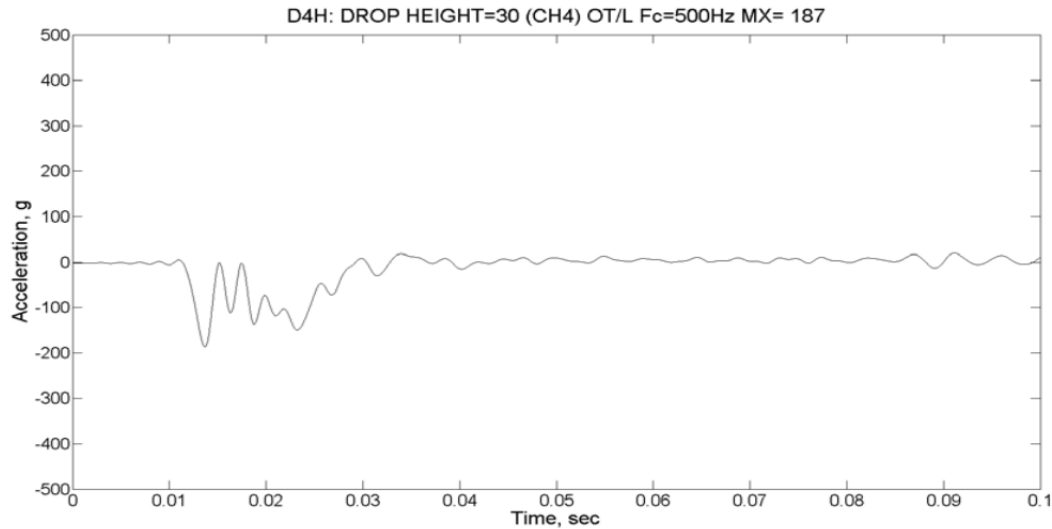












2.12.3.7 References

1. Title 10, Code of Federal Regulations, Part 71 (10 CFR Part 71), *Packaging and Transportation of Radioactive Material*, 01-01-18 Edition.
2. 435-B Certification Test Report, PKG-TR-SPC-011, AREVA Federal Services LLC.
3. ANSI N14.5-1997, *American National Standard for Radioactive Materials – Leakage Tests on Packages for Shipment*, American National Standards Institute (ANSI), Inc.
4. International Atomic Energy Agency, *Regulations for the Safe Transport of Radioactive Material*, SSR-6, 2012 Edition.

2.12.4 Finite Element Analysis

This appendix provides supporting drop simulation data for the certification testing performed on the 435-B package. This material summarizes the information presented in the drop analysis [1].

2.12.4.1 Introduction

The primary method of demonstration of the 1105-SD is certification test of the 435-B. Finite element analysis is used to:

- Demonstrate that the bounding drop orientations were chosen for the certification testing.
- Calculate the maximum closure bolt stress (not generated by any certification tests).
- Calculate the maximum warm case crush (since the warm foam used in the certification test was not bounding).

The Finite Element Analysis (FEA) simulations performed in this appendix are for supporting the selection of worst-case orientations tested, and to determine the performance in orientations not tested. The FEA simulations include benchmark orientations that are compared directly to the certification test results. Free drop impact deformation and acceleration results are used to benchmark the finite element analysis model for use in non-tested orientations and conditions. The non-tested orientations are slapdown free drops with both the base impact limiter primary and the bell (lid) torispherical head primary in a wide range of angles. The slapdown free drops are considered drop orientations where a primary impact occurs with the drop pad inducing significant rotation of the package such that a secondary and potentially bounding impact occurs. Most drops for which the center of gravity was over the impact were physically tested as documented in Appendix 2.13.3, *Certification Test Results*.

The simulations must demonstrate the bounding certification test orientations were performed and the simulations should also corroborate the certification test results. Simulations are performed using the explicit finite element software LS-DYNA [6], version ls971s R4.2.1, 53450 from Livermore Software Technology Corporation (LSTC).

2.12.4.2 Design Input

2.12.4.2.1 Conditions

The certification test conditions are defined by Appendix 2.12.2, *Certification Test Plan*, and are documented by Appendix 2.12.3, *Certification Test Results*. The benchmarked free drops include the end drop, D1 series on CTU #1, side drop, D2 series on CTU #1, and the cg-over-top knuckle, D3 series on CTU #2. These orientations are chosen for benchmarking because they encompass the maximum axial impact (end drop), maximum transverse impact (side drop), and maximum containment boundary deformation (cg-over-top knuckle).

Numerous slapdown free drop orientations, which are not included in certification testing, are simulated with the benchmarked finite element model. The slapdown free drop simulation results are compared with certification test simulation results to demonstrate the bounding attributes of the certification test orientations.

2.12.4.2.2 Geometry

The 435-B Certification Test Unit (CTU) packaging is defined by the drawings in Appendix 1.3.3, *Packaging General Arrangement Drawings*, except as discussed in Section 2.12.3.3, *Certification Test Unit Configuration*. The finite element model is based on the test unit drawings and as-tested configuration. The inner container (IC) is not included in these simulations because the packaging deformations observed in certification testing with the IC are less than those observed when tested with the lodgment and LTSS. Therefore, certification testing and simulations performed with the lodgment and LTSS are bounding with respect to packaging deformations and payload accelerations.

2.12.4.2.3 Material Properties

The benchmarking and other simulations are performed at cold temperatures. Properties at elevated temperatures are not needed except as discussed in following paragraphs for the polyurethane foam crush strength.

The 1105-SD base, thermal shield(s), miscellaneous components, and LTSS are designed utilizing Type 304 stainless steel, predominately ASTM A240, A276, and A479. The minimum material yield strength is 30,000 psi and the minimum material ultimate strength is 75,000 psi from Table 2.2-1. The Modulus of Elasticity is 28.3×10^6 psi per Table 2.2-1, and Poisson's ratio is 0.31 from Section 2.2.1, *Material Properties and Specifications*.

The cylindrical side shell of the bell, including the torispherical head and welded hoist ring boss, are designed with Type 304 stainless steel and specified to have a minimum material yield strength of 40 ksi and minimum material ultimate strength of 80 ksi, which is above the minimum material specifications for ASTM Type 304 stainless steel.

The closure bolts are ASTM A320 Grade L43 where the minimum material yield strength is 105,000 psi and the minimum material ultimate strength is 125,000 psi from Table 2.2-3. The Modulus of Elasticity is 27.8×10^6 psi per Table 2.2-3, and Poisson's ratio is 0.30 from Section 2.2.1, *Material Properties and Specifications*.

The base weldment is filled with General Plastics FR-3700 series polyurethane foam. The prototypic foam density is 15 pounds per cubic foot (pcf). The certification test units had 16 pcf (Units 1 & 3) and 14 pcf (Unit 2).

The lodgment is designed with aluminum material, 6061-T6, predominantly ASTM B209, B221, and B308. The material yield strength is 35,000 psi for B209, B221, and B308 for 6061-T6 aluminum per Table 2.2-4. The material ultimate strength is 42,000 psi for 6061-T6 per Table 2.2-4. The Modulus of Elasticity is 10.0×10^6 psi per Table 2.2-4, and Poisson's ratio is 0.33 from Section 2.2.1, *Material Properties and Specifications*. The bolts used to secure the upper and lower halves of the lodgment together are ASTM A193 Grade B8 that has a yield strength of 30,000 psi and ultimate strength of 75,000 psi.

The material models used in the simulations are described in the following sub-sections.

2.12.4.2.3.1 Type 304 Stainless Steel (*mat_plastic_kinematic)

The base flange and lower torispherical head weldment, upper flange, internal impact limiter stabilizer (dome) sheets, and lower center tube are modeled with a Type 304 stainless steel

plastic kinematic material for all simulations. This is LS-DYNA material model 3. The following properties are discussed above and converted to true stress-strain. The elongation below is taken as ultimate elongation from ASME Section II, Part A.

- Stainless Steel SA-240 Type 304 at -20 to 100F
- $E = 28,300 \text{ ksi}$, $S_y = 30.0 \text{ ksi}$, $S_u = 75.0 \text{ ksi}$, elongation = 0.40, density = 0.290 lb/in³
- True Yield Stress: $S_{yt} = S_y(1+(S_y/E+0.002)) = 30.1 \text{ ksi}$
- True Ultimate Stress: $S_{ut} = S_u(1+eu) = 105.0 \text{ ksi}$
- True Yield Strain: $\epsilon_{yt} = \ln(1+e_y) = 0.00306$
- True Ultimate Strain: $\epsilon_{ut} = \ln(1+eu) = 0.336$
- True Tangent Modulus: $E_{tant} = (S_{ut}-S_{yt})/(\epsilon_{ut}-\epsilon_{yt}) = 225.0 \text{ ksi}$

Where e_y is the engineering yield strain ($S_y/E+0.002$), and eu is the engineering ultimate strain (elongation = 0.40).

2.12.4.2.3.2 Type 304 Stainless Steel (*mat_piecewise_linear plasticity)

The outer shell and upper torispherical head (bell), thermal shields, bell skin (enclosing the bolt tubes and foam blocks), bolt tubes, base skin (external impact limiter shell), internal impact limiter clips (base blocks), and internal impact limiter tubes are modeled with a Type 304 stainless steel elastic-plastic material. This is LS-DYNA material model 24. The material properties of Type 304 stainless steel are obtained from Section 2.2, *Materials* as shown above, and actual Certified Material Test Reports (CMTRs) from the certification test units.

The true stress-strain behavior of Type 304 stainless steel is presented in Table 2.12.4-1. From [5], stainless steel is modeled using a power-law hardening material model. This model treats the material as elastic up to the limit of proportionality and captures the plasticity by the equation:

$$\sigma = \sigma_p + A \langle \epsilon_p - \epsilon_l \rangle^n$$

Where σ is the true stress, σ_p is the stress at the limit of proportionality (taken as the true yield strength), A is the hardening constant, ϵ_p is the true equivalent plastic strain, ϵ_l is the Luder's strain (zero for stainless steel), $\langle \rangle$ indicates the Heaviside function where the expression enclosed in the brackets is unchanged when positive and equal to zero when negative and n is the hardening exponent. Note that the values from the above equation correspond to room temperature. From [5], the parameters for 304L stainless steel are $\sigma_p = 28 \text{ ksi}$, $A = 192.746 \text{ ksi}$, $\epsilon_l = 0$ and $n = 0.74819$.

To use this equation for Type 304 at temperature, a conversion is necessary and is performed as follows. The mechanical and chemical properties of Type 304 and Type 304L are similar, so it is assumed that the stress-strain values obtained for Type 304L from [5] can be scaled to obtain Type 304 stress values at temperature. The stress values are scaled based on the scaling equation:

$$\sigma_{304} = \sigma_{304L} \frac{\sigma_{ty-304}}{\sigma_p}$$

where σ_{304} is the true stress for Type 304 stainless steel, σ_{304L} is the result of the power law equation above using the parameters from [5], σ_p equals 28,000, and σ_{ty-304} is the true yield stress for Type 304 at temperature. Engineering stresses and elastic moduli at temperature are taken from Section 2.2, *Materials* and CMTRs from the certification test units. Three material curves are generated using this method, material identities 15, 16, and 17.

Material ID 15 uses a yield strength of 40.0 ksi that comes from a minimum strength note on the drawings in Appendix 1.3.3, *Packaging General Arrangement Drawings*, for the bell outer shell and upper torispherical head. Material ID 15 is used for the bell skin (enclosing the bolt tubes and foam blocks), bolt tubes, base skin (external impact limiter shell), and internal impact limiter clips (base blocks) for all simulations. Material ID 15 is also used for the outer shell and upper torispherical head (bell), and shell side thermal shield for all the slapdown simulations. The shell side thermal shield also uses Material ID 15 for the D3 benchmark simulation.

Material ID 16 uses a yield strength of 51.5 ksi that comes from the average CMTR value of the internal impact limiter crush tubes. Material ID 16 is used for the internal impact limiter tubes and upper torispherical head thermal shield in all simulations.

Material ID 17 uses a yield strength of 45.0 ksi from the CMTR for the bell outer shell and upper torispherical head on CTUs 1 and 2. Material ID 17 is used exclusively for the outer shell and upper torispherical head (bell) in the benchmark simulations.

2.12.4.2.3.3 6061-T6 Aluminum (*mat_plastic_kinematic)

The flat plates of the internal impact limiters and the lodgment are modeled with a 6061-T6 aluminum plastic kinematic material. This is LS-DYNA material model 3. The following properties are from Section 2.2, *Materials* and converted to true stress-strain. This material model was used for all non-benchmark simulations. The elongation below is taken as ultimate elongation from ASME Section II, Part B.

- 6061-T6 Aluminum at -20 to 100F
- $E = 10,000$ ksi, $S_y = 35.0$ ksi, $S_u = 42.0$ ksi, elongation = 0.10, density = 0.098 lb/in³
- True Yield Stress: $S_{yt} = S_y(1+(S_y/E+0.002)) = 35.2$ ksi *
- True Ultimate Stress: $S_{ut} = S_u(1+eu) = 46.2$ ksi
- True Yield Strain: $eyt = \ln(1+ey) = 0.00548$
- True Ultimate Strain: $eut = \ln(1+eu) = 0.0953$
- True Tangent Modulus: $E_{tant} = (S_{ut}-S_{yt})/(eut-eyt) = 122.5$ ksi

Where ey is the engineering yield strain ($S_y/E+0.002$), and eu is the engineering ultimate strain (elongation = 0.10). * Note, 38.7 ksi was used in all non-benchmark simulations based on performance of the benchmarked CMTR value below, instead of 35.2 ksi.

The aluminum properties shown below for the benchmark simulations are from the CTU-1 CMTR.

1105-SD Package Safety Analysis Report

- 6061-T6 Aluminum at -20 to 100F
- $E = 10,000 \text{ ksi}$, $S_y = 38.7 \text{ ksi}$, $S_u = 43.7 \text{ ksi}$, $\text{elongation} = 0.16$, $\text{density} = 0.098 \text{ lb/in}^3$
- True Yield Stress: $S_{yt} = S_y(1+(S_y/E+0.002)) = 38.9 \text{ ksi}$
- True Ultimate Stress: $S_{ut} = S_u(1+e_u) = 50.7 \text{ ksi}$
- True Yield Strain: $e_{yt} = \ln(1+e_y) = 0.00585$
- True Ultimate Strain: $e_{ut} = \ln(1+e_u) = 0.148$
- True Tangent Modulus: $E_{tant} = (S_{ut}-S_{yt})/(e_{ut}-e_{yt}) = 83.0 \text{ ksi}$

Where e_y is the engineering yield strain ($S_y/E+0.002$), and e_u is the engineering ultimate strain (elongation = 0.16, from the CMTR).

2.12.4.2.3.4 Polyurethane Foam (*mat_crushable_foam)

The 1105-SD external impact limiter contains General Plastics FR-3700 series polyurethane foam that is modeled with a crushable foam material. This is LS-DYNA material model 63. The foam functions as an impact limiter around the bolted bell-to-base joint and as a thermal barrier reducing the heat input to the butyl rubber containment O-rings from the HAC fire case. The prototypic foam density is 15 pounds per cubic foot (pcf). Certification testing was performed with 16 pcf foam in CTU-1 and CTU-3, and 14 pcf foam in CTU-2. The minimum temperature requirement from SSR-6 [3] is -40 °F, and the maximum bulk average NCT temperature of the foam is bounded by 150 °F. Performing full scale certification testing at -40 °F and 150 °F is extremely challenging, therefore cold impact testing was performed at -10 °F with a harder density 16 pcf foam and the warm maximum crush testing was performed at 117 °F with a softer density 14 pcf foam. These two foam densities have very comparable crush strength properties to the prototypic 15 pcf foam at the respective -40 °F and 150 °F temperatures as shown in Figure 2.12.4-1. This method of testing equivalency is also discussed in the test plan, Section 2.12.2.2.1, *Temperature and Pressure* and test results, Section 2.12.3.3, *Certification Test Unit Configuration*. The crush strength properties are developed in the paragraphs below.

The foam has specific crush strength properties that are dependent on the foam density, temperature, orientation (parallel or perpendicular to foam rise), and dynamic factors. The foam design guide [7] has detailed descriptions and data for compensating the foam crush strength curve for these variables. The material property inputs required for performing the drop simulations are the foam crush strength curves. Four separate foam crush strength curves are generated for this purpose and are presented in Table 2.12.4-4. These four curves represent the bounding properties for the certification test units and prototypic packaging cases.

The actual static foam crush strength data at room temperature (~75 °F) for CTU-1 and CTU-2 is included in Table 2.12.4-2 from supplier test records. The static prototypic foam crush strength data is also included in Table 2.12.4-2. The prototypic 15 pcf foam, CTU-1 16 pcf foam, and CTU-2 14 pcf foam are adjusted for applicable test temperatures using the method and data from the foam design guide [7]. This includes multiplying the foam crush strength by the appropriate temperature correction factor, C_T , given in [7]. Crush strength curves at -20 °F, 100 °F, and 140 °F are created in a spreadsheet and then the values are interpolated or extrapolated to populate the crush strengths at the desired temperatures of -40 °F, 0 °F, 117 °F, and 150 °F. The prototypic (or production) foam is also conservatively compensated for a manufacturing

tolerance of $\pm 10\%$. The foam at cold temperature is tolerated to be stronger by 10% and the foam at warm temperature is tolerated to be weaker by 10%. The foam curves are then averaged between their orientation properties (parallel or perpendicular to foam rise) and listed in Table 2.12.4-3.

Lastly, the crush strengths are compensated for dynamic effects per the foam design guide [7] using the formula:

$$\sigma_{\text{Dynamic}} = Y_{\text{int}} (\sigma_{\text{Static}})^S$$

where Y_{int} and S are dynamic factors from Table 9 of [7], and σ_{Static} is the averaged and temperature adjusted static crush strength from Table 2.12.4-3. All the crush strength values above 70% strain are extrapolated in a spreadsheet, and shaded grey in Table 2.12.4-2 through Table 2.12.4-4.

The final foam crush strength curves are shown in Table 2.12.4-4 and Figure 2.12.4-1. The crush strength of 16 pcf at -10 °F is slightly harder than the crush strength of 15 pcf at -40 °F, and is therefore bounding with respect to the cold impacts. The crush strength of 15 pcf at 150 °F is slightly softer than the as-tested crush strength of 14 pcf at 117 °F. Therefore, the warm prototypic foam is not bounded by the as-tested warm CTU-2 foam and a relation must be developed to bound the maximum crush deformation for thermal performance consideration. See Section 2.7.1.5.2, *Maximum Impact Limiter Crush Deformation*.

For an example of how the foam crush strengths are calculated the following demonstration for 16 pcf foam at 40% strain is provided.

From Table 2.12.4-2 the actual static crush strength of 16 pcf foam at 40% strain and 75 °F is 930 psi parallel to rise, and 934 psi perpendicular to rise. From the foam design guide [7] the temperature correction factor, C_T , for -20 °F is 1.31 parallel to rise and 1.33 perpendicular to rise.

Parallel to Rise

$$\begin{aligned} \text{Crush strength of 16 pcf at 40\% strain and -20 °F} &= C_T \times \text{Actual Static at 75 °F} \\ &= 1.31 \times 930 = 1,218 \text{ psi} \end{aligned}$$

Perpendicular to Rise

$$\begin{aligned} \text{Crush strength of 16 pcf at 40\% strain and -20 °F} &= C_T \times \text{Actual Static at 75 °F} \\ &= 1.33 \times 934 = 1,242 \text{ psi} \end{aligned}$$

Then the crush strength values at 75 °F and -20 °F are used to linearly interpolate the crush strength at -10 °F, which for 16 pcf at 40% strain is 1,189 psi parallel to rise and 1,210 psi perpendicular to rise. These values are then averaged providing the 1,200 psi shown in Table 2.12.4-3. At this point, prototypic 15 pcf foam would be adjusted by a factor of 1.1 to account for manufacturing tolerance. It is not done in this example since it is for the actual foam test data from the CTU.

The dynamic factor is then applied per the equation discussed above.

$$\sigma_{\text{Dynamic}} = Y_{\text{int}} (\sigma_{\text{Static}})^S = 1.3887(1,200)^{1.0028} = 1,700 \text{ psi}$$

Where $Y_{int} = 1.3887$ and $S = 1.0028$ from [7]. This is the final crush strength value used in the simulations, and represented in Table 2.12.4-4 and Figure 2.12.4-1.

2.12.4.2.3.5 A320 Grade L43 (*mat_spotweld)

The closure bolts are 1 1/4 – 7UNC socket head bolts manufactured from ASTM A320 GR L43, LS-DYNA material model 100 is used with an elastic yield strength of 105 ksi.

2.12.4.2.3.6 Rigid LTSS and Drop Pad (*mat_rigid)

The LTSS and drop pad are modeled with LS-DYNA rigid material model 20. This material does not absorb energy and no stresses or strains are calculated. The density of the LTSS is controlled to model the gross weight of the prototypic LTSS and the as-tested LTSS. The elastic modulus and Poisson's ratio of steel are used, but only relevant to the contact algorithms.

2.12.4.3 Methodology

2.12.4.3.1 1105-SD FEA Model

2.12.4.3.1.1 Benchmark Model

The first phase of work in this calculation is to develop a FEA model and benchmark the simulation performance to the full-scale certification test results. The certification testing to be benchmarked includes three different free drop orientations and two CTUs. The results from Appendix 2.12.3, *Certification Test Results* to be used for benchmarking include: CTU #1 in test series D1 including bottom-down 4-ft NCT and 30-ft HAC free drops, CTU #1 in test series D2 including the side orientation (where the impact limiter corner and the knuckle contacted simultaneously) 4-ft NCT and 30-ft HAC free drops, and CTU #2 in test series D3 that consisted of 4-ft NCT and 30-ft HAC free drops in the c.g.-over-top knuckle orientation. There are two primary differences between CTU #1 and CTU #2. CTU #1 has cold 16 pcf foam, while CTU #2 has warm 14 pcf foam and a thermal shield on the upper torispherical head. CTU #3, which has 16 pcf foam and is loaded with an inner container was not benchmarked.

The benchmark model consists of four components; the 1105-SD packaging, the lodgment, the LTSS, and the impact surface. A total of 45 parts are defined in LS-DYNA for the benchmark, which includes approximately 800,000 nodes and 700,000 elements. The 1105-SD packaging is comprised of numerous parts utilizing solid, shell, and beam elements. The structural parts of the containment boundary including the upper and lower flanges, bell shell, upper and lower torispherical heads, and impact limiter clips (base blocks) are modeled with solid type 2, fully integrated selectively reduced elements. The shell, upper and lower torispherical heads are 1/2 inch thick type 304 stainless steel and have three elements through their thickness. The lower torispherical head, lower and upper flange use the plastic kinematic material in Section 2.12.4.2.3.1, *Type 304 Stainless Steel (*mat_plastic_kinematic)*. The bell shell, upper torispherical head, and impact limiter clips (base blocks) use the elastic-plastic material from Section 2.12.4.2.3.2, *Type 304 Stainless Steel (*mat_piecewise_linear_plasticity)*. The benchmark simulations use the 45 ksi yield strength, material ID 17 from Table 2.12.4-1 for bell shell and upper torispherical head. The internal impact limiter clips (base blocks) use the 40 ksi yield strength, material ID 15 from Table 2.12.4-1.

The polyurethane foam in the base is modeled with the default, solid type 1 constant stress elements with type 5 Flanagan-Belytschko hourglass control, which is a stiffness form with exact

volume integration for solid elements. The foam blocks in the bell that are between the closure bolt access tubes are modeled with the same element type and material as the base external impact limiter foam. The design calls for these foam blocks to be 30 pcf, however they are modeled with the same density (14 pcf, 15 pcf, or 16 pcf) as the base. Modeling the foam blocks with lighter density foam than specified in the design is conservative with respect to the possible incurred drop damage, and the accelerations near the base are not expected to be significantly affected because the foam properties are equivalent with the external base impact limiter. The crushable material for the foam is described in Section 2.12.4.2.3.4, *Polyurethane Foam* (*mat_crushable_foam).

The base skin (external impact limiter shell), bell skin (enclosing the bolt tubes and foam blocks), bolt tubes, tube sheet, thermal shields, and internal impact limiter assemblies use type 16 fully integrated shell elements with Lobatto integration and type 8 hourglass control. Activating the Lobatto integration style calculates the stresses of the outer integration points at the outer surface of the shell. The Type 8 hourglass control is applicable for type 16 fully integrated shell elements, which activates full projection warping stiffness for accurate solutions. All shell elements have a shear correction factor of 5/6, as recommended by [6]. All the shell elements less than 1/2 inch thick have 3 integration points through their thickness. The shell elements that are 1/2 inch thick, which includes the internal impact limiter aluminum base plates and the main lodgment plates, have 5 integration points through their thickness.

The closure bolts are modeled with beam elements that are the type 9 (spot weld) with the cross section type set to circular and the default integration rule of 2. The cross section diameter is 1.1108 inch, which is the mean thread diameter of the 1 1/4 - 7UNC bolts, using Table 8-2 from [10]. The model is half symmetrical with the symmetry plane cutting thru two of the closure bolts. The bolts on the symmetry plane have a reduced beam cross section of 0.7854 inch that produces an area equivalent to half of the full symmetry bolt stress area. Therefore, the model has two half symmetry bolts and eleven full symmetry bolts. The beam elements are defined as beam type 9 (spot weld) and used in conjunction with the material type *mat_spotweld from Section 2.12.4.2.3.5 for the purpose of enabling the command *initial_axial_force_beam. The command *initial_axial_force_beam is used to initialize the axial force resultant in beam elements that are used to model bolts. The preload force used for all the simulations is 19,200 lb for the full symmetry bolts, and 9,600 lb for the half symmetry bolts. The preload is determined by using $T = KF_d$, where the nominal bolt torque T is 300 ft-lb, K is an assumed torque (nut) factor of 0.15 from Section 2.6.1.5, *Closure Bolts*, and d is the bolt diameter of 1.25 inch.

The end drop (D1) and simultaneous side drop (D2) orientations are benchmarked without any thermal shields. CTU #1 does have a single thermal shield around the bell outer shell, however the thermal shield is not anticipated to significantly influence the drop results for the particular orientations benchmarked. The weight of the thermal shield is included in the model as an increased density factor across the other packaging components. The cg-over-top knuckle (D3) orientation benchmark does include the CTU side thermal shield and upper torispherical head thermal shield to be consistent with CTU #2, as this drop orientation may be affected by the strength of the thermal shields.

The lodgment is modeled entirely with shell elements, which have all the same attributes and features as described above for the bell, base, and internal impact limiter shells. The lodgment is an all aluminum structure that is modeled with plastic-kinematic properties as described in Section 2.12.4.2.3.3, *6061-T6 Aluminum* (*mat_plastic_kinematic). The lodgment has upper and

lower halves that are connected with constrained nodal rigid bodies. The constrained nodal rigid bodies connect the nodes around the perimeter of the u-bracket holes in the upper lodgment with the nodes around the perimeter of the mid-plates in the lower lodgment. The constrained nodal rigid body part numbers are 120, 121, 122, and 123. The lodgment design calls for 1/2 inch stainless steel bolts to join the upper and lower halves. The bolts performed well with no breakages in certification testing and are not specifically considered in the model. The lodgment is also modeled without consideration for fillet weld effective throat areas being less than joint minimum plate thicknesses or as-welded aluminum material properties. The lodgment is considered in the simulations to conservatively contribute to the impact accelerations of the LTSS for the different orientations and to conservatively interface with packaging containment boundary. The lodgment design is proven by certification testing that demonstrates under worst-case impacts, the lodgment joints do not fail. Therefore failure in the simulations does not need to be considered.

The impact surface of the benchmark model includes a 2 inch thick by 300 inch wide by 150 inch deep rigid drop pad. The drop pad is modeled with the default type 1 constant stress solid elements, however the material is completely rigid as described in Section 2.12.4.2.3.6, *Rigid LTSS and Drop Pad (*mat_rigid)*. All nodes on the bottom surface of the drop pad are fully constrained. The LTSS is modeled in general size, shape, and weight. However, like the drop pad it is modeled with rigid material. The LTSS performance is demonstrated by the certification testing and does not require stress-strain simulation data, therefore modeling with rigid material conservatively loads the 1105-SD packaging in the FEA simulations while reducing computation time.

The FEA model includes a wide array of structural interfaces and contacts. Structural interfaces are modeled with merged nodes, where permitted by the mesh generation, or by tied contact definitions. For instance, the interface between the upper flange and bell shell is a merged node interface, i.e., the mesh is continuous between the parts. In other areas, like the lodgment, all the parts are connected with tied contact definitions. Tied contact definitions are used where the mesh between parts is not similar or continuous. The FEA model also has numerous contacts between parts. The most common contact definition used is automatic surface to surface with the optional card A set with soft equal to 2 for segment-based contact and the depth equal to 5 for checking surface and edge to edge penetrations. Friction between the various parts is defined through the contact cards. The majority of contact interfaces have a coefficient of friction of 0. However, a significant number of contact interfaces have a coefficient of friction 0.40, such as all the contacts involving foam and internal impact limiters. Bonding between the foam and the external impact limiter has not been assumed. The coefficient of friction of 0.40 is used for both static and sliding conditions. The value is used in part by matching results between the benchmark simulations and certification testing. The value of 0.40 is also considered reasonable in comparison with a survey of dry sliding friction values in Table 3.2.4 of [9], where hard steel on hard steel is 0.42, mild steel on mild steel is 0.57, nickel on mild steel is 0.64, aluminum on mild steel is 0.47, and nickel on nickel is 0.53. The coefficient of friction used between the package and drop pad is 0.10, with two simulations using a value of 0 for demonstration purposes.

The benchmark model includes gravity as a body acceleration load of 386.4 in/sec^2 . The benchmark model also includes an initial velocity of 561.5 in/sec that is equivalent to a combined 4 ft NCT and 30 ft HAC drop. This initial velocity of 561.5 in/sec applies all the drop

energy of the 4 ft NCT and 30 ft HAC drops into one continuous impact simulation rather than two distinct drop events. The purpose of applying this simulation method is to limit the number of necessary simulations, thereby decreasing the total calculation computer run time, required data storage space, and post-processing labor while producing reasonable simulation results. The benchmark simulation results in Section 2.12.4.5.1, *Benchmark Results* justify the applicability of this method by comparison with the certification test results. Additionally, one benchmark orientation is simulated with sequential and cumulative, NCT and HAC drops for comparative information.

See Figure 2.12.4-2 through Figure 2.12.4-12 for the FEA model components and mesh. See Table 2.12.4-5 and Table 2.12.4-6 for a summary of the benchmark cases and their respective parameters.

2.12.4.3.1.2 Slapdown (Prototypic) Model

The second phase of the work in this calculation is to take the benchmarked FEA model and perform a series of slapdown free drops to demonstrate the certification test orientations are appropriate for the license application. The benchmark model is slightly adjusted for the slapdown simulations. The primary differences include 1) Weight. The benchmark model uses the as-tested LTSS weight of 4,460 lb, from Table 2.12.3-1, and the slapdown model uses the estimated design gross weight of 4,650 lb, essentially equal to the maximum weight of 4,660 lb from Table 2.1-2, 2) The bell shell and upper torispherical head strength. The benchmark model uses 45 ksi yield strength from the CTU CMTR, while the slapdown model uses 40 ksi yield strength from the SAR drawings in Appendix 1.3.3, *Packaging General Arrangement Drawings*, and 3) The aluminum plate thickness. The benchmark model uses 0.53 inch thick main lodgment plates and internal impact limiter base plates from the CTU fabrication, while the slapdown model uses 0.50 inch thick from the SAR drawings. All the slapdown simulations have the CTU side thermal shield and upper torispherical head thermal shield like the D3 benchmark simulation, i.e., D3_benchmark_302_6JN0.

The different FEA models are grouped in Table 2.12.4-7 with their respective component weights. Note that the “Loaded Package” weight for the slapdown simulations of 9,935 lb is only 1.6% less than the maximum weight of 10,100 lb given in Table 2.1-2. A complete summary of the FEA model components and descriptions is in Table 2.12.4-8, and a complete summary of the FEA model component parameters (material and thickness) is in Table 2.12.4-9. The material references in Table 2.12.4-9 are from Section 2.12.4.2.3, *Material Properties* where the ID # refers to the curves in Section 2.12.4.2.3.2, *Type 304 Stainless Steel* (*mat_piecewise_linear_plasticity) and 304 PK refers to the Plastic Kinematic material in Section 2.12.4.2.3.1, *Type 304 Stainless Steel* (*mat_plastic_kinematic). The foam densities refer to the material curves in Section 2.12.4.2.3.4, *Polyurethane Foam* (*mat_crushable_foam).

2.12.4.4 Acceptance Criteria

The objective of simulations performed in this calculation is to demonstrate that the certification test orientations performed are appropriate for the licensing basis. The primary method by which this will be demonstrated is comparison of the package free drop accelerations and package impact surface dimensions (“impact patch”) between the simulations and the certification test results. The certification test orientations are the worst case and conservatively demonstrate the structural NCT and HAC free drop safety effectiveness of the package. If a governing

performance parameter was not obtained from the certification testing, then the simulation results are utilized to obtain the required parameter.

2.12.4.5 Results

There are two primary groups of simulations. The benchmark simulations are developed for comparison with the certification test results. The prototypic (slapdown) simulations are developed for trending the effects of drop orientation, to confirm the certification test orientations represent the worst case. The differences between the two groups of simulations are not great. The benchmark simulations use as-tested material properties for the bell shell and upper torispherical head, and the as-tested LTSS weight as discussed in Section 2.12.4.3.1.2, *Slapdown (Prototypic) Model*. The prototypic (slapdown) simulations use design specified material properties for the bell shell and upper torispherical head, and the gross LTSS weight.

In all cases, the time history data obtained from the numerical simulation contains high frequency structural vibration and numerically-induced noises that are filtered out to provide an accurate assessment of the loadings on the package. In post-processing these analyses, the time history data is processed with a low-pass Butterworth filter. The cutoff frequency is 500Hz as referenced from Section 2.12.3.2.2, *Instrumentation* of the certification test results. The cutoff frequency was determined in Section 2.12.3.2.2 based on guidance given in Section 701.9 of TS-G-1.1 [8].

The CTUs were instrumented with accelerometers for the NCT and HAC certification free drops. The accelerometers were attached to the bell (lid) at four locations, two upper and two lower. The accelerometers were located at the azimuth of the seal test port and opposite the seal test port, as shown in Figure 2.12.3-1. To benchmark the FEA model and compare the CTU accelerations, the accelerations of the bell are processed at the approximate corresponding locations for the FEA model. The nodal accelerations are post-processed for 12 nodes at each upper and lower location. The 12 nodes at each location represent an area representative of the accelerometer blocks welded to the CTUs. The accelerations of the nodes are averaged and then filtered at 500Hz. See Figure 2.12.4-13 through Figure 2.12.4-15 for the FEA model nodes that are equivalent to the CTU accelerometer blocks.

The upper, lower, and average bell accelerations are the primary metric used to compare the FEA model results with certification testing, where the average is simply, (upper + lower) / 2. The impact patch dimensions including the circumferential width and axial height of the side drop and cg-over-top knuckle certification test damage are also used as a metric for comparison with the FEA model results. The impact patches are defined as the approximate region that contacts the drop pad surface. The CTU impact patches were measured by scuff marks (abrasions) indicating contact with the drop pad. The simulation impact patches are measured by observation of the time history animation to determine the extent of contact between the package and drop pad.

The upper, lower, and average bell accelerations are also the primary metric used to trend the simulation results for the severity of the various free drop orientations. Supplemental data used to trend the various free drop orientation severity includes the LTSS rigid body acceleration, maximum axial bolt force, containment boundary effective cumulative plastic strain, and minimum foam thickness near the seal region. In general, the benchmark simulations correlate well with the certification test results having accelerations and impact patch dimensions within

10%, and the slapdown free drop simulations demonstrate the worst case orientations were chosen for certification testing. Detailed comparison and evaluation of the benchmark simulations is discussed on Section 2.12.4.5.1, *Benchmark Results*. Detailed comparison and evaluation of the prototypic (slapdown) free drop simulations is discussed in Section 2.12.4.5.2, *Slapdown Free Drop Results* and warm simulation results are presented in Section 2.12.4.5.3, *Warm Free Drop Results*.

2.12.4.5.1 Benchmark Results

The FEA model is benchmarked with results from the full-scale certification testing. Three simulations are performed, including the D1 end drop, the D2 side drop (where the impact limiter and upper torispherical head contact the drop pad at the same time), and the D3 cg-over-knuckle drop. All the certification test results are referenced from Appendix 2.12.3, *Certification Test Results*. The certification testing included a 4 ft NCT drop followed by a 30 ft HAC drop to assess cumulative damage in the D1, D2, and D3 test orientations.

The FEA simulations are performed with a combined drop where the drop energy equivalent to 34 ft is applied in one continuous event. This combined drop height method is applicable based on comparison with a cumulative (rather than combined) test simulation and the certification test results. The D1 free drop orientation is simulated with a cumulative 4ft NCT and 30 ft HAC drop via a restart process and the results are compared to the certification testing and the combined drop simulations. The 30 ft HAC drop simulation with cumulative NCT drop damage produced an average bell acceleration of 804 g while the combined 34 ft drop simulation produced an average bell acceleration of 819 g. The 30 ft HAC certification drop, D1H, recorded an average bell acceleration of 768 g. The combined drop height simulation produced results that are conservative compared to the sequential drop simulation and to the drop test results. Therefore, a combined drop height of 34 ft was used for all benchmark and slapdown simulations. See all the results in Table 2.12.4-10 and Table 2.12.4-11 for the cumulative cases labeled D1_benchmark_NCT and D1_benchmark_HAC, and the equivalent combined case D1_benchmark302_6JN0.

All the benchmark results are presented in Table 2.12.4-12, where the acceleration results are compared with HAC certification test results from Appendix 2.12.3, and the impact patch dimensions (where deformation exists from contact with the drop pad), and internal impact limiter tube crush dimensions are compared with certification test measurements collected after each HAC event.

The effect of friction between the package and the drop pad is considered in the benchmark simulations. The benchmark simulations use a low coefficient of friction with the pad of 0.10, except for one test case that uses 0.0. See simulation results for D2_benchmark_309_6JN0 in Table 2.12.4-10 and Table 2.12.4-11 for 0.0 friction with the pad. The friction coefficient of 0.10 is used because of good correlation with the certification test results and because the 0.0 friction coefficient has tendency to produce an unrealistic slipping of the impact limiter in the shallow slapdown and side drop orientations, where the foam appears to squirt out the base of the package from between the impact limiter shell and base flange. This behavior was not observed in certification testing.

The benchmark simulation results are shown in Figure 2.12.4-16 through Figure 2.12.4-41, and are compared with the certification test results in Table 2.12.4-12. The impact g's of the benchmark simulations have a difference with the certification test data that ranges between

0.6% to 10.0%. The impact patches of the benchmark simulations range between 0.25 inches to 1.6 inches difference with the certification test data. The benchmark simulations show the FEA model produces results very similar to those seen in full-scale testing. These results demonstrate that the FEA model of the 1105-SD is capable of reliably predicting the behavior of the real package.

2.12.4.5.2 Slapdown Free Drop Results

The slapdown free drops are all the simulations in Table 2.12.4-13 and Table 2.12.4-14. These simulations include some orientations that do not physically slapdown. The slapdown connotation is used to separate this complete set of simulations from the benchmark simulations. The slapdown set of simulations includes 19 simulations that vary only by orientation, which ranges from end drop to bell drop. See Figure 2.12.4-42 for the drop orientation terminology. Four additional runs are included in this set to consider specific variables such as friction with the pad and elevation of the payload cg relative to the maximum bolt load.

Terminology of the drop simulation names is relative to these abbreviations: sar = safety analysis report, ilp = impact limiter primary, kp = knuckle (of upper torispherical head) primary, fr = coefficient with the drop pad, simu = simultaneous side drop, number = package angle in degrees. For example, sar_kp63 = safety analysis report, knuckle primary slapdown at 63 degrees. See Figure 2.12.4-69 for this orientation.

All the slapdown free drop simulation results are included in Table 2.12.4-13 and Table 2.12.4-14. The slapdown free drop simulation results are plotted versus drop orientation in Figure 2.12.4-43 through Figure 2.12.4-47. The maximum average bell (lid) acceleration of 797 g occurred in the end drop orientation, with the second highest average bell acceleration of 311 g occurring in the simultaneous side drop orientation, see Figure 2.12.4-43. The upper bell accelerations are predominantly higher than the lower bell accelerations, which is reasonable given the lower location is nearer the package CG and much closer to the foam impact limiter. The maximum impact at the upper bell, excluding the end drop, is 429 g for the impact limiter primary 0 degree slapdown (ILP0). Of note, an additional run is performed at ILP0, but using 0 friction with the drop pad. In this case, upper, lower, and LTSS accelerations are slightly less than the simulation with 0.10 friction although the containment boundary maximum cumulative effective plastic strain is slightly more. Since the change in results is less than 10% and no clear bounding condition exists that includes each evaluated characteristic the friction coefficient factor of 0.10 is used for all other cases.

The dip in the acceleration plot for the ILP-7 orientation appears to be a function of geometry. The package just slightly impacts the top edge of the base impact limiter, which does not induce the slapdown rotation like the ILP0 orientation or the blunt initial impact of the simultaneous side drop.

The simultaneous side orientation clearly produces the maximum LTSS impact, 228 g, as shown in Figure 2.12.4-44. This orientation produces a higher payload impact than the end drop, which is 206 g. The payload impact is mitigated in the end drop by the internal impact limiter. The simultaneous side drop orientation also causes the most impact limiter foam crush near the seal region. This is demonstrated in Figure 2.12.4-45 that shows the minimum remaining foam thickness versus drop orientation. The foam crush relative to the remaining foam thickness is important near the containment seal for thermal protection of the o-ring. Orientations, such as ILP45, that may have more foam crush than the simultaneous side drop are not checked for

minimum remaining foam because the crush region is not adjacent to the containment o-ring and the available foam thickness is large.

The maximum containment boundary cumulative effective plastic strain is demonstrated in Figure 2.12.4-46 to be caused by the cg-over-top knuckle orientation. The maximum containment boundary cumulative effective plastic strain occurs for a knuckle primary drop (onto the upper torispherical head) with an angle between 70° and 63°. The cumulative effective plastic strain for the knuckle primary 70° case is 32.3% and for the knuckle primary 63° case is 31.0%, as shown in Table 2.12.4-14. The difference in plastic strain between the 70° and 63° simulations is approximately 1.3%, which is negligible for austenitic stainless steel. Therefore, the D3 certification test at 63° is sufficiently bounding for containment boundary maximum strain.

The maximum bolt load is demonstrated in Figure 2.12.4-47 to be caused by the impact limiter primary 75° orientation. The maximum bolt load appears to be caused by the payload contacting the bell shell in near vertical end drop orientations. Three additional simulations are performed to evaluate the effect of the payload cg height on the maximum bolt load in this orientation. One simulation is performed at 75° with the payload elevated, (i.e., suspended and touching the top of the payload cavity prior to impact) and two simulations are performed with the payload upside down and elevated in the payload cavity at 68° and 75° orientations. The lodgment that controls the LTSS in the payload cavity is biased to keep the LTSS cg low in the payload cavity. Therefore, flipping the loaded lodgment upside down in the payload cavity and elevating it in the payload cavity prior to impact is a conservative simulation condition for determining the maximum bolt load. This is further discussed in Section 2.7.1.5.1, *Maximum Closure Bolt Stress*. Doing so generates a maximum bolt load of 35,774 lb in simulation sar_ilp68_udep, where udep = upside down elevated payload. This bolt load occurs for the maximum (cold) impact, with a payload gap at the bottom, and the maximum payload c.g. height. See the results summary in Table 2.12.4-13 and Table 2.12.4-14.

Figures for a sample of the simulation results used to create the data plots versus drop orientation are included in the following pages. For simulation sar_simu see Figure 2.12.4-48 through Figure 2.12.4-54. For simulation sar_ilp0 see Figure 2.12.4-55 through Figure 2.12.4-61. For simulation sar_ilp68_udep see Figure 2.12.4-62 through Figure 2.12.4-68. For simulation sar_kp63 see Figure 2.12.4-69 through Figure 2.12.4-75.

The deformation of the upper torispherical head for the top down drop simulation, sar_lid, is shown in Figure 2.12.4-76. The flat region created in the upper torispherical head by the top down drop has an approximate outer diameter of 38 inches, which is further considered for the HAC fire event in Section 2.7.4.3, *Stress Calculations*.

2.12.4.5.3 Warm Free Drop Results

The certification testing included a test series, D4, for determining the minimum remaining foam thickness near the seal region. The D4 test series was performed on CTU #2 with 14 pcf foam. The foam was heated and recorded to be approximately 117 °F before the HAC drop. The drop orientation was the simultaneous side drop, which has been shown to be the worst orientation for minimum foam thickness near the seal region.

The crush strength of the polyurethane foam is shown in Figure 2.12.4-1. The as-tested 14 pcf foam has a slightly higher crush strength at 117 °F than the prototypic 15 pcf foam has at the

NCT temperature of 150 °F. Therefore, two simulations are performed to determine the crush factor between the as-tested foam and prototypic foam. The actual remaining foam values from the simulations are not intended for use in the thermal evaluation, but only to adjust the measurements made on CTU #2. This is further discussed in Section 2.7.1.5.2, *Maximum Impact Limiter Crush Deformation*. The accelerations for the as-tested simulation compare well with the D4 drop results in Section 2.12.3.4.6, *Test Series D4*, lower bell accelerations of 186 g simulation and 183 g test, upper bell accelerations of 406 g simulation and 374 g test. However, the minimum remaining foam does not compare well being 2.5 inches simulation and 5.13 inches test. The certification test minimum remaining foam is shown to be 5.13 inches per Figure 2.12.3-48. The warm simulation results are shown in Table 2.12.4-15 and Table 2.12.4-16.

The objective of the two warm simulations is to determine the minimum remaining foam for each foam crush strength (14 pcf at 117 °F and 15 pcf at 150 °F), such that a comparative factor can be created to compensate the certification test result minimum remaining foam for the decreased prototypic foam crush strength. The compensated minimum remaining foam will then be considered in the thermal evaluation. For creating the comparative factor, the as-tested foam simulation has a minimum remaining foam thickness of 2.5 inches near the seal region, see Figure 2.12.4-77. Likewise, the prototypic foam simulation has a minimum remaining foam thickness of 2.0 inches near the seal region, see Figure 2.12.4-78. The comparative factor is calculated in Section 2.7.1.5.2, *Maximum Impact Limiter Crush Deformation*, and used in the thermal analysis in Chapter 3, *Thermal Analysis*.

2.12.4.6 FEA Summary

This document provides supporting drop simulation data for the certification testing performed on the 1105-SD package. The licensing basis for the package is primarily by full-scale test of Hypothetical Accident Condition (HAC) free drop and puncture. Analysis is used for all Normal Conditions of Transport (NCT), except the NCT free drop, to determine the worst-case orientations for test, to determine the performance in orientations not tested, and for the HAC fire event. The analysis performed in this calculation is for supporting the worst-case orientations tested, and to determine the performance in orientations not tested.

The primary method by which this will be demonstrated is comparison of the package free drop accelerations between the simulations and certification testing. The certification test orientations must be the worst case and conservatively demonstrate the structural NCT and HAC free drop safety effectiveness of the package. If a governing performance parameter was not obtained from the certification testing, then the simulation results are utilized to obtain the required parameter.

The FEA simulations performed in this calculation include benchmark orientations that are compared directly to the certification test results. Free drop impact deformation and acceleration results are used to benchmark the finite element analysis model for use in non-tested orientations and conditions. The non-tested orientations are slapdown free drops with both the base impact limiter primary and the bell (lid) torispherical head primary in a wide range of angles.

As discussed in Section 2.12.4.5, the simulation results compare well with the certification test results. The benchmark simulations show impact accelerations and impact patch sizes have a difference less than or equal to 10%. This is reasonable and useful, given the nature of variation

in physical testing, and that a simulations outcome is dependent on numerous inputs, modeling techniques, and code capabilities.

The slapdown series of simulations demonstrates that the appropriate certification test orientations were performed. The end drop has the highest average packaging impact with an acceleration of 797 g. The simultaneous side drop has the second highest average packaging impact with an acceleration of 311 g. This orientation is the highest impact perpendicular to the package axis. The simultaneous side drop also rivals the 0° slapdown for the highest upper bell acceleration (excluding the end drop), having a difference less than 3%. The simultaneous side orientation also produces the maximum LTSS acceleration, 228 g, and has the least amount of remaining foam near the seal region. Lastly, the cg-over-top knuckle drop generates the maximum cumulative effective plastic strain in the containment boundary. Therefore, all the certification tests are demonstrated by this calculation and the test plan, Appendix 2.12.2, *Certification Test Plan*, to be worst case, and appropriate for the license application. The only supplemental information necessary for the license application is the maximum bolt load (35,774 lb) from the simulations and the warm minimum remaining polyurethane foam comparative factor data.

Table 2.12.4-1 – True Plastic Stress-Strain Curves for Type 304 Stainless Steel at 70 °F

Strain (in/in)	Stress (psi)	Stress (psi)	Stress (psi)
	Material ID 15	Material ID 16	Material ID 17
0.000	40,137	51,697	45,192
0.002	42,779	55,100	48,167
0.004	44,575	57,414	50,189
0.006	46,148	59,440	51,961
0.008	47,592	61,300	53,586
0.010	48,947	63,044	55,112
0.020	54,935	70,757	61,854
0.030	60,180	77,513	67,759
0.040	64,993	83,713	73,179
0.050	69,510	89,530	78,264
0.060	73,803	95,059	83,098
0.070	77,918	100,360	87,732
0.080	81,888	105,473	92,202
0.090	85,734	110,427	96,532
0.100	89,474	115,244	100,743
0.150	106,960	137,766	120,431
0.200	123,008	158,437	138,501
0.250	138,066	177,832	155,455
0.300	152,378	196,267	171,570
0.350	166,100	213,940	187,020
0.400	179,334	230,987	201,921
0.500	204,627	263,563	230,399
0.600	228,667	294,528	257,468
0.700	251,715	324,214	283,418
0.800	273,945	352,847	308,448
0.900	295,484	380,590	332,700
1.000	316,428	407,566	356,282

Table 2.12.4-2 – Static Stress-Strain Curves for Polyurethane Foam

Strain (in/in)	Stress (psi)	Stress (psi)	Stress (psi)	Stress (psi)	Stress (psi)	Stress (psi)
	16 pcf at 75 °F	16 pcf at 75 °F	15 pcf at 75 °F	15 pcf at 75 °F	14 pcf at 75 °F	14 pcf at 75 °F
	CTU-1 Parallel	CTU-1 Perpendicular	Prototypic Parallel	Prototypic Perpendicular	CTU-2 Parallel	CTU-2 Perpendicular
0.00	0	0	0	0	0	0
0.10	755	741	629	603	606	607
0.20	769	770	630	625	615	627
0.30	822	824	668	670	656	668
0.40	930	934	754	769	737	749
0.50	1,176	1,175	964	977	917	927
0.60	1,727	1,727	1,436	1,445	1,326	1,338
0.65	2,263	2,272	1,886	1,903	1,728	1,750
0.70	3,185	3,212	2,645	2,691	2,421	2,456
0.75	4,273	4,328	3,551	3,629	3,231	3,287
0.80	5,803	5,902	4,819	4,952	4,365	4,453
0.85	7,880	8,048	6,540	6,758	5,898	6,033
	Actual Test Data		Nominal		Actual Test Data	

Table 2.12.4-3 – Averaged and Temperature Adjusted Static Stress-Strain Curves for Polyurethane Foam

Strain (in/in)	Stress (psi)	Stress (psi)	Stress (psi)	Stress (psi)
	16 pcf at -10 °F, no bias	15 pcf at -40 °F, +10% bias	14 pcf at 117 °F, no bias	15 pcf at 150 °F, -10% bias
	CTU-1	Prototypic Cold	CTU-2	Prototypic Warm
0.00	0	0	0	0
0.10	981	969	489	381
0.20	998	974	507	397
0.30	1,060	1,028	546	430
0.40	1,200	1,169	619	496
0.50	1,498	1,471	766	627
0.60	2,178	2,152	1,118	943
0.65	2,798	2,759	1,459	1,240
0.70	3,814	3,703	2,132	1,840
0.75	5,000	4,820	2,889	2,519
0.80	6,619	6,324	3,988	3,518
0.85	8,762	8,299	5,507	4,913

Table 2.12.4-4 – Dynamic Adjusted Stress-Strain Curves for Polyurethane Foam

Strain (in/in)	Stress (psi)	Stress (psi)	Stress (psi)	Stress (psi)
	16 pcf at -10 °F	15 pcf at -40 °F	14 pcf at 117 °F	15 pcf at 150 °F
	CTU-1	Prototypic Cold	CTU-2	Prototypic Warm
0.00	0	0	0	0
0.10	1,597	1,578	777	601
0.20	1,507	1,470	762	596
0.30	1,545	1,499	799	629
0.40	1,700	1,656	875	701
0.50	2,026	1,989	1,042	854
0.60	2,730	2,699	1,418	1,199
0.65	3,312	3,266	1,750	1,492
0.70	3,974	3,863	2,275	1,976
0.75	5,151	4,974	3,045	2,670
0.80	6,741	6,453	4,148	3,678
0.85	8,821	8,374	5,651	5,066

Table 2.12.4-5 – Benchmark Summary

CTU#	Certification Test Series	Simulation Test Description	Foam Type	Side Thermal Shield	Head Thermal Shield
1	D1	4-ft NCT, bottom down	cold 16 pcf	Single Wall (no mesh in model, mass added by density factor)	No
		30-ft HAC, bottom down			
		34-ft (NCT + HAC), bottom down			
	D2	34-ft (NCT + HAC) side orient			
		34-ft (NCT + HAC) side orient, zero friction			
2	D3	34-ft (NCT + HAC), c.g.-over-top knuckle	warm 14 pcf	Single Wall	Prototypic
	D4	Not benchmarked, side orientation			
3	D5	Not benchmarked, bottom down	cold 16 pcf	Prototypic	No
	D6	Not benchmarked, side orientation			

Table 2.12.4-6 – Benchmark Parameters

Computer Run	Initial Velocity	Orientation
D1_benchmark_302_6JN0	-561.5 (34 ft)	End 90°
D1_benchmark_HAC	-527.5 (30 ft)	End 90°
D1_benchmark_NCT	-192.6 (4ft)	End 90°
D2_benchmark_302_6JN0	-561.5 (34 ft)	Side - 13°
D2_benchmark_309_6JN0	-561.5 (34 ft)	Side - 13°
D3_benchmark_302_6JN0	-561.5 (34 ft)	Top - 63°

Table 2.12.4-7 – FEA Model Weights

Component	D1 & D2 Benchmarks	D3 Benchmark	Slapdown Simulations
	lb	lb	lb
Base Assembly	2,285	2,218	2,259
Lid Assembly	2,352	2,433	2,482
Empty Package	4,669	4,682	4,772
Lodgment	510	510	512
LTSS	4,460	4,460	4,651
Loaded Package	9,639	9,652	9,935

Table 2.12.4-8 – FEA Model Part Descriptions

Component Model Part #	Model Part Description
1	lid flange (lid is equivalent to bell)
2	lid shell (includes upper torispherical head)
3	lid skin 0.25 thk (angle tube sheet)
4	lid skin 0.12 thk (lid foam and bolt tube enclosure sheet)
5	lid aluminum plate 0.5 thk (of upper internal impact limiter)
7	lid foam (foam blocks between bolt access tubes)
9	bolt tubes (closure bolt access tubes)
10	impact limiter base blocks (internal impact limiter clips)
11	base flange (includes lower torispherical head)
12	base skin 0.25 thk (bottom and outer skin of impact limiter)
13	base skin 0.12 thk (inner skin of impact limiter by lid)
14	base aluminum plate 0.5 thk (of lower internal impact limiter)
16	base foam (base external impact limiter foam)
21	bolts (closure bolts)
22	symmetry bolts
25	bolt shell tops (rigid shells connecting bolt tops)
26	bolt shell bottoms (rigid shell connecting bolt bottoms)
48	ltss (Long Term Storage Shield)
71	upper tubes (upper internal impact limiter tubes)
72	upper support plate (upper internal impact limiter dome sheet)
73	lower tubes (lower internal impact limiter tubes)
74	lower support plate (lower internal impact limiter dome sheet)
75	lower center tube (centers the lower internal impact limiter)
80	knuckle thermal shield
81	head thermal shield
82	thermal shield spacer (on upper head near hoist ring boss)
83	side thermal shield (single layer side thermal shield)
100	Upper Lodgment Main Plates
101	Upper Lodgment Center Tube
102	Upper Lodgment Top Plate
103	Upper Lodgment Perim Plate (circular plate)
104	Upper Lodgment Top Angles
105	Upper Lodgment Mid Angles
106	Upper Lodgment Dbl Angles
107	Upper Lodgment Dbl Plates
108	Lower Lodgment Mid Plates
109	Lower Lodgment Main Plates
110	Lower Lodgment Center Tube
111	Lower Lodgment Bot Plate
112	Lower Lodgment Perim Plate (circular plate)
113	Lower Lodgment Bot Angles
114	Lower Lodgment Dbl Angles
115	Lower Lodgment Dbl Plates
116	Upper Lodgment U-Brackets

Table 2.12.4-9 – FEA Model Parameters

Component	D1 & D2 Benchmarks		D3 Benchmark		Slapdown Simulations		Warm		Warm Test	
Model Part #	Mat	Thk	Mat	Thk	Mat	Thk	Mat	Thk	Mat	Thk
1	304 PK	0.50	304 PK	0.50	304 PK	0.50	304 PK	0.50	304 PK	0.50
2	304 ID 17	0.50	304 ID 17	0.50	304 ID 15	0.50	304 ID 15	0.50	304 ID 15	0.50
3	304 ID 15	0.25	304 ID 15	0.25	304 ID 15	0.25	304 PK	0.25	304 PK	0.25
4	304 ID 15	0.12	304 ID 15	0.12	304 ID 15	0.12	304 PK	0.12	304 PK	0.12
5	6061-T6	0.53	6061-T6	0.53	6061-T6	0.50	6061-T6	0.50	6061-T6	0.50
7	16 pcf at -10°F		14 pcf at 117°F		16 pcf at -10°F		15 pcf at 150°F		14 pcf at 117°F	
9	304 ID 15	0.12	304 ID 15	0.12	304 ID 15	0.12	304 PK	0.12	304 PK	0.12
10	304 ID 15	1.25	304 ID 15	1.25	304 ID 15	1.25	304 ID 15	1.25	304 ID 15	1.25
11	304 PK	0.50	304 PK	0.50	304 PK	0.50	304 PK	0.50	304 PK	0.50
12	304 ID 15	0.25	304 ID 15	0.25	304 ID 15	0.25	304 PK	0.25	304 PK	0.25
13	304 ID 15	0.12	304 ID 15	0.12	304 ID 15	0.12	304 PK	0.12	304 PK	0.12
14	6061-T6	0.53	6061-T6	0.53	6061-T6	0.50	6061-T6	0.50	6061-T6	0.50
16	16 pcf at -10°F		14 pcf at 117°F		16 pcf at -10°F		15 pcf at 150°F		14 pcf at 117°F	
21	A320 L43	1.11	A320 L43	1.11	A320 L43	1.11	A320 L43	1.11	A320 L43	1.11
22	A320 L43	0.78	A320 L43	0.78	A320 L43	0.78	A320 L43	0.78	A320 L43	0.78
25	rigid	0.10	rigid	0.10	rigid	0.10	rigid	0.10	rigid	0.10
26	rigid	0.10	rigid	0.10	rigid	0.10	rigid	0.10	rigid	0.10
48	rigid 4,460 lb	na	rigid 4,460 lb	na	rigid 4,651 lb	na	rigid 4,651 lb	na	rigid 4,651 lb	na
71	304 ID 16	.035	304 ID 16	.035	304 ID 16	.035	304 ID 16	.035	304 ID 16	.035
72	304 PK	.105	304 PK	.105	304 PK	.105	304 PK	.105	304 PK	.105
73	304 ID 16	.035	304 ID 16	.035	304 ID 16	.035	304 ID 16	.035	304 ID 16	.035
74	304 PK	.105	304 PK	.105	304 PK	.105	304 PK	.105	304 PK	.105
75	304 PK	.049	304 PK	.049	304 PK	.049	304 PK	.049	304 PK	.049
80	-	-	304 ID 16	.105	304 ID 16	.105	304 PK	.105	304 PK	.105
81	-	-	304 ID 16	.105	304 ID 16	.105	304 PK	.105	304 PK	.105
82	-	-	304 ID 16	.105	304 ID 16	.105	304 PK	.105	304 PK	.105
83	-	-	304 ID 15	.105	304 ID 15	.105	304 PK	.105	304 PK	.105
100	6061-T6	0.53	6061-T6	0.53	6061-T6	0.50	6061-T6	0.50	6061-T6	0.50
101	6061-T6	0.24	6061-T6	0.24	6061-T6	0.24	6061-T6	0.24	6061-T6	0.24
102	6061-T6	0.53	6061-T6	0.53	6061-T6	0.50	6061-T6	0.50	6061-T6	0.50
103	6061-T6	0.53	6061-T6	0.53	6061-T6	0.50	6061-T6	0.50	6061-T6	0.50
104	6061-T6	0.25	6061-T6	0.25	6061-T6	0.25	6061-T6	0.25	6061-T6	0.25
105	6061-T6	0.25	6061-T6	0.25	6061-T6	0.25	6061-T6	0.25	6061-T6	0.25
106	6061-T6	0.25	6061-T6	0.25	6061-T6	0.25	6061-T6	0.25	6061-T6	0.25
107	6061-T6	0.25	6061-T6	0.25	6061-T6	0.25	6061-T6	0.25	6061-T6	0.25
108	6061-T6	0.53	6061-T6	0.53	6061-T6	0.50	6061-T6	0.50	6061-T6	0.50
109	6061-T6	0.53	6061-T6	0.53	6061-T6	0.50	6061-T6	0.50	6061-T6	0.50
110	6061-T6	0.24	6061-T6	0.24	6061-T6	0.24	6061-T6	0.24	6061-T6	0.24
111	6061-T6	0.53	6061-T6	0.53	6061-T6	0.50	6061-T6	0.50	6061-T6	0.50
112	6061-T6	0.53	6061-T6	0.53	6061-T6	0.50	6061-T6	0.50	6061-T6	0.50
113	6061-T6	0.25	6061-T6	0.25	6061-T6	0.25	6061-T6	0.25	6061-T6	0.25
114	6061-T6	0.25	6061-T6	0.25	6061-T6	0.25	6061-T6	0.25	6061-T6	0.25
115	6061-T6	0.25	6061-T6	0.25	6061-T6	0.25	6061-T6	0.25	6061-T6	0.25
116	6061-T6	0.35	6061-T6	0.35	6061-T6	0.35	6061-T6	0.35	6061-T6	0.35

Table 2.12.4-10 – Benchmark Simulation Acceleration Results Summary

Drop Simulation	Lower Bell Acceleration	Upper Bell Acceleration	Average Bell Acceleration	LTSS Acceleration
	Y-acceleration (g)	Y-acceleration (g)	Y-acceleration (g)	Resultant-acceleration (g)
D1_benchmark_302_6JN0	800	838	819	206
D2_benchmark_302_6JN0	224	445	335	256
D2_benchmark_309_6JN0 (0 Friction with Pad)	214	462	338	261
D3_benchmark_302_6JN0	172	195	184	216
D1_benchmark_NCT (4 ft)	313	338	326	167
D1_benchmark_HAC (30 ft) Cumulative	786	822	804	226

Table 2.12.4-11 – Benchmark Simulation Results Summary

Drop Simulation	Axial Bolt Force	Containment Boundary Plastic Strain	Minimum Foam Thickness
	Maximum for all Bolts (lb)	Cumulative Effective (%, inch/inch)	Near Seal (inch)
D1_benchmark_302_6JN0	21,648	5.6	
D2_benchmark_302_6JN0	25,012	23.4	4.3
D2_benchmark_309_6JN0 (0 Friction with Pad)	27,682	22.0	4.1
D3_benchmark_302_6JN0	21,798	28.9	
D1_benchmark_NCT (4 ft)	20,386	0.9	
D1_benchmark_HAC (30 ft) Cumulative	21,495	6.1	

Table 2.12.4-12 – Benchmark Simulation and CTU Results Comparison

Case ¹	Test Weight	Model Weight	Test Upper Impact	Model Upper Impact	Difference	Test Lower Impact	Model Lower Impact	Difference		
	lb	lb	g	g	$\Delta g, \%$	g	g	$\Delta g, \%$		
D1	9,642	9,639	776	838	+62, +8.0	760	800	+40, +5.3		
D2	9,642	9,639	466	445	-21, -4.5	249	224	-25, -10.0		
D3	9,653	9,652	183 ³	195	+12, +6.6	171 ³	172	+1, +0.6		
Case	Test Upper Patch Width	Model Upper Patch Width	Test Upper Patch Height	Model Upper Patch Height	Test Lower Patch Width	Model Lower Patch Width	Test Lower Patch Height	Model Lower Patch Height	Test ² Tube Crush	Model Tube Crush
	inch	inch	inch	inch	inch	inch	inch	inch	inch	inch
D1	NA	NA	NA	NA	NA	NA	NA	NA	1.43	2.0
D2	18.0	18.5	12.0	12.8	33.25	33.6	25.25	25.0	NA	NA
D3	33.5	33.1	21.0	22.6	NA	NA	NA	NA	NA	NA

Notes:

1. D1 is the End Drop orientation, D2 is the Side Drop orientation (where the base impact limiter and upper torispherical head knuckle contact the drop pad simultaneously), and D3 is the CG-Over-Top Knuckle orientation.
2. Axial crush of the lower internal impact limiter tubes. The CTU and model are measured for the change in length between the top of the lodgment and underside of the internal impact limiter clips (base blocks) to determine the tube crush.
3. The accelerations for D3 test data are from Appendix 2.12.3, *Certification Test Results*. The T/U and OT/U average and OT/L accelerations are resolved for comparison with the upper and lower model impact g's with the method discussed in Appendix 2.12.3, of dividing by the cosine of 27 degrees to resolve the average 159g to 178g for compensating the angle of the drop with the mounting orientation of the accelerometers.
4. The patch width and height are the respective packaging deformations in the circumferential and axial directions caused by impact with the drop pad surface.
5. Figure 2.12.4-16 through Figure 2.12.4-41 demonstrate the results summarized in Table 2.12.4-12 for the three benchmark simulations. All the results plots have been filtered at 500 Hz as discussed in Section 2.12.4.5, *Results*.

Table 2.12.4-13 – Slapdown Simulation Acceleration Results Summary

Drop Simulation	Lower Bell Acceleration	Upper Bell Acceleration	Average Bell Acceleration	LTSS Acceleration
	Y-acceleration (g)	Y-acceleration (g)	Y-acceleration (g)	Resultant-acceleration (g)
sar_end	787	806	797	206
sar_ilp83	198	203	201	188
sar_ilp75	197	194	196	139
sar_ilp75_ep (elevated payload)	148	158	153	142
sar_ilp75_udep (upside down elevated payload)	151	148	150	193
sar_ilp68	112	162	137	128
sar_ilp68_udep (upside down elevated payload)	129	166	148	182
sar_ilp60	116	156	136	133
sar_ilp45	138	157	148	148
sar_ilp30	134	96 (-117)	115	140
sar_ilp15	188	382	285	204
sar_ilp0	178	429	304	199
sar_ilp0_0fr (0 Friction with Pad)	160	419	290	189
sar_ilp-7	220	333	277	194
sar_simu	204	418	311	228
sar_kp20	203	326	265	192
sar_kp30	130	272	201	193
sar_kp45	139	227	183	185
sar_kp55	140	175	158	194
sar_kp63	158	167	163	188
sar_kp70	169	174	172	193
sar_kp75	179	185	182	180
sar_lid	154	165	160	139

Note:

Terminology of the drop simulation names is relative to these abbreviations: sar = safety analysis report, ilp = impact limiter primary, kp = knuckle (of upper torispherical head) primary, fr = coefficient with the drop pad, simu = simultaneous side drop, number = package angle in degrees. For example, sar_kp63 = safety analysis report, knuckle primary slapdown at 63 degrees.

Table 2.12.4-14 – Slapdown Simulation Results Summary

Drop Simulation	Axial Bolt Force	Containment Boundary Plastic Strain	Minimum Foam Thickness
	Maximum for all Bolts (lb)	Cumulative Effective (%, inch/inch)	Near Seal (inch)
sar_end	21,628	6.0	
sar_ilp83	29,703	4.6	
sar_ilp75	33,373	8.7 (minor area at hoist ring boss)	
sar_ilp75_ep (elevated payload)	34,871	4.8	
sar_ilp75_udep (upside down elevated payload)	35,693	5.3	
sar_ilp68	30,550	2.4	
sar_ilp68_udep (upside down elevated payload)	35,774	5.0	
sar_ilp60	26,692	2.3	
sar_ilp45	22,871	1.7	
sar_ilp30	19,735	2.3	
sar_ilp15	23,584	21.5	
sar_ilp0	22,228	24.6	5.5
sar_ilp0_0fr (0 Friction with Pad)	22,311	26.6	5.5
sar_ilp-7	22,510	25.8	5.2
sar_simu	25,451	23.8	4.2
sar_kp20	26,684	23.8	4.4
sar_kp30	23,557	24.1	5.1
sar_kp45	21,450	26.8	
sar_kp55	20,987	23.1	
sar_kp63	21,869	31.0	
sar_kp70	21,820	32.3	
sar_kp75	21,148	29.1	
sar_lid	19,928	6.0	

Note:

Terminology of the drop simulation names is relative to these abbreviations: sar = safety analysis report, ilp = impact limiter primary, kp = knuckle (of upper torispherical head) primary, fr = coefficient with the drop pad, simu = simultaneous side drop, number = package angle in degrees. For example, sar_kp63 = safety analysis report, knuckle primary slapdown at 63 degrees.

Table 2.12.4-15 – Warm Simulation Acceleration Results Summary

Drop Simulation	Lower Bell Acceleration	Upper Bell Acceleration	Average Bell Acceleration	LTSS Acceleration
	Y-acceleration (g)	Y-acceleration (g)	Y-acceleration (g)	Resultant-acceleration (g)
sar_warm_simu (15pcf @ 150F)	170	401	286	201
sar_warm_simu_test (14pcf @ 117F)	186	406	296	205

Table 2.12.4-16 – Warm Simulation Results Summary

Drop Simulation	Axial Bolt Force	Containment Boundary Plastic Strain	Minimum Foam Thickness
	Maximum for all Bolts (lb)	Cumulative Effective (% , inch/inch)	Near Seal (inch)
sar_warm_simu (15pcf @ 150F)	23,205	23.8	2.0
sar_warm_simu_test (14pcf @ 117F)	23,303	24.2	2.5

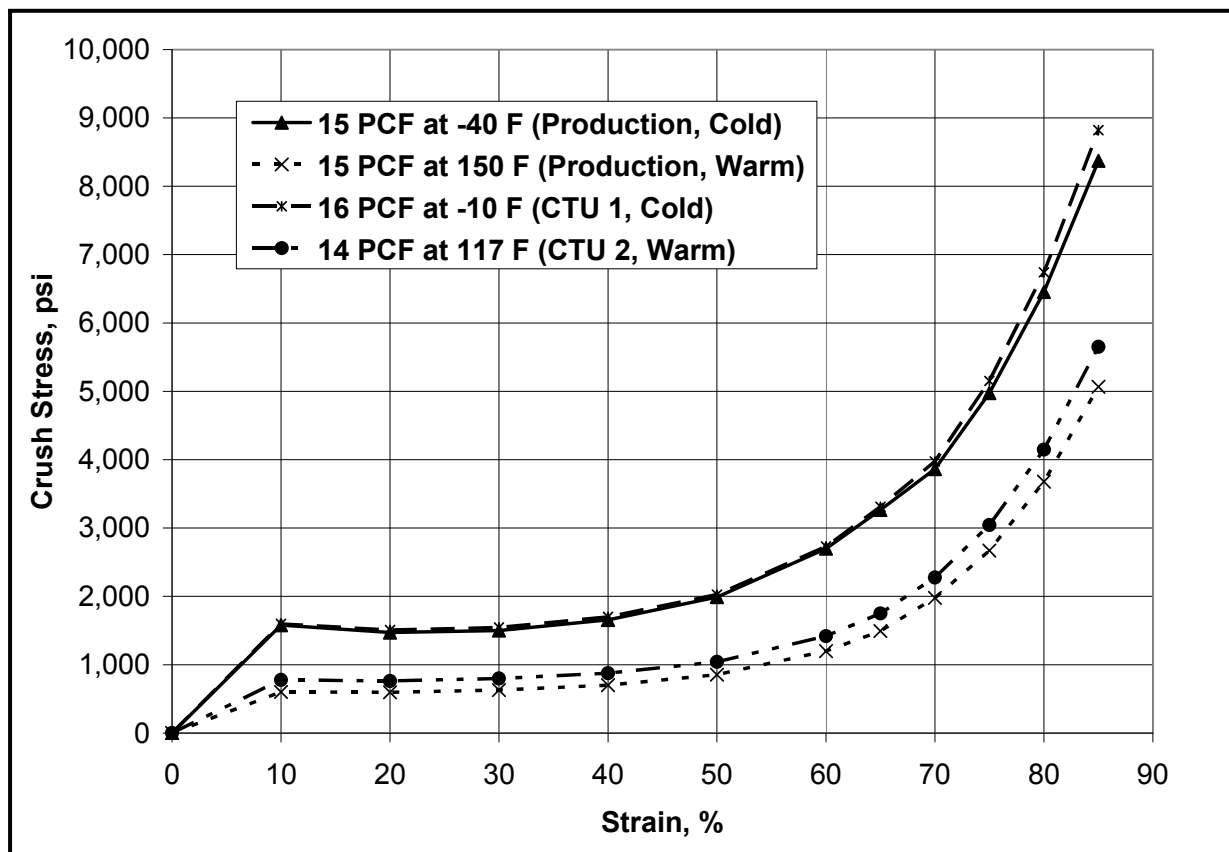


Figure 2.12.4-1 – Polyurethane Foam CTU and Prototypic (Production) Crush Strength Curves

Note: Many of the following figures are labeled internally with the notation '435-B'. The 1105-SD packaging is identical to the 435-B packaging documented in 435-B SAR Revision 4.3 (corresponding to NRC CoC USA/9355/B(U)-96, Revision 2). Thus these labels may be read as indicating, and equivalent to, '1105-SD'.

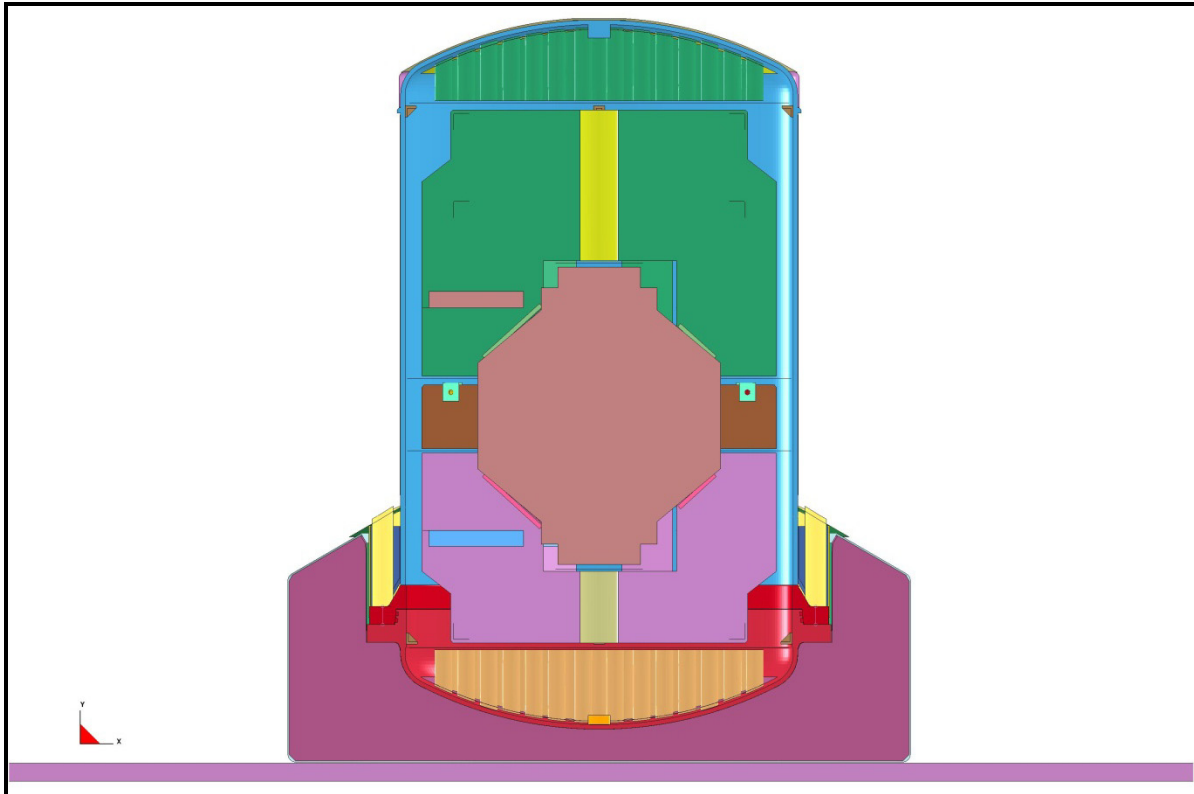


Figure 2.12.4-2 – 1105-SD FEA Model

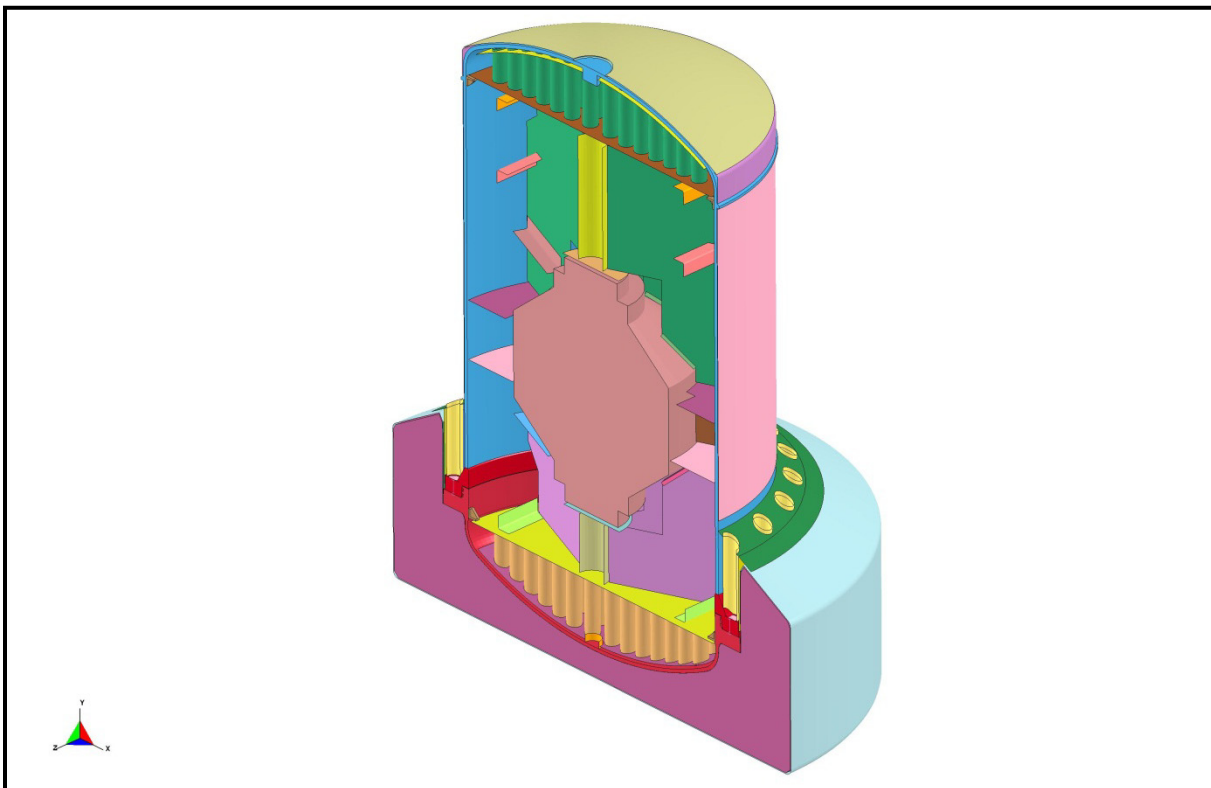


Figure 2.12.4-3 – 1105-SD FEA Model, Iso-View, Drop Pad Removed

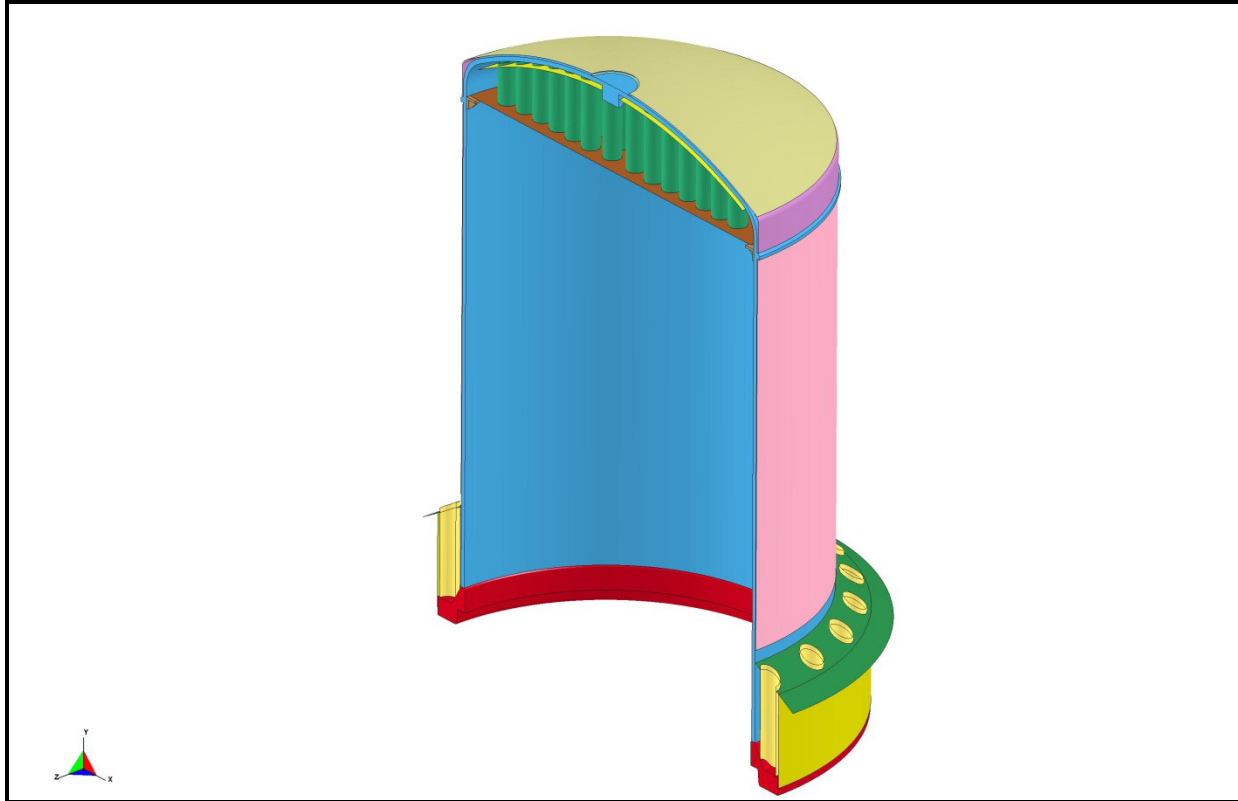


Figure 2.12.4-4 – 1105-SD FEA Model Bell (Lid)

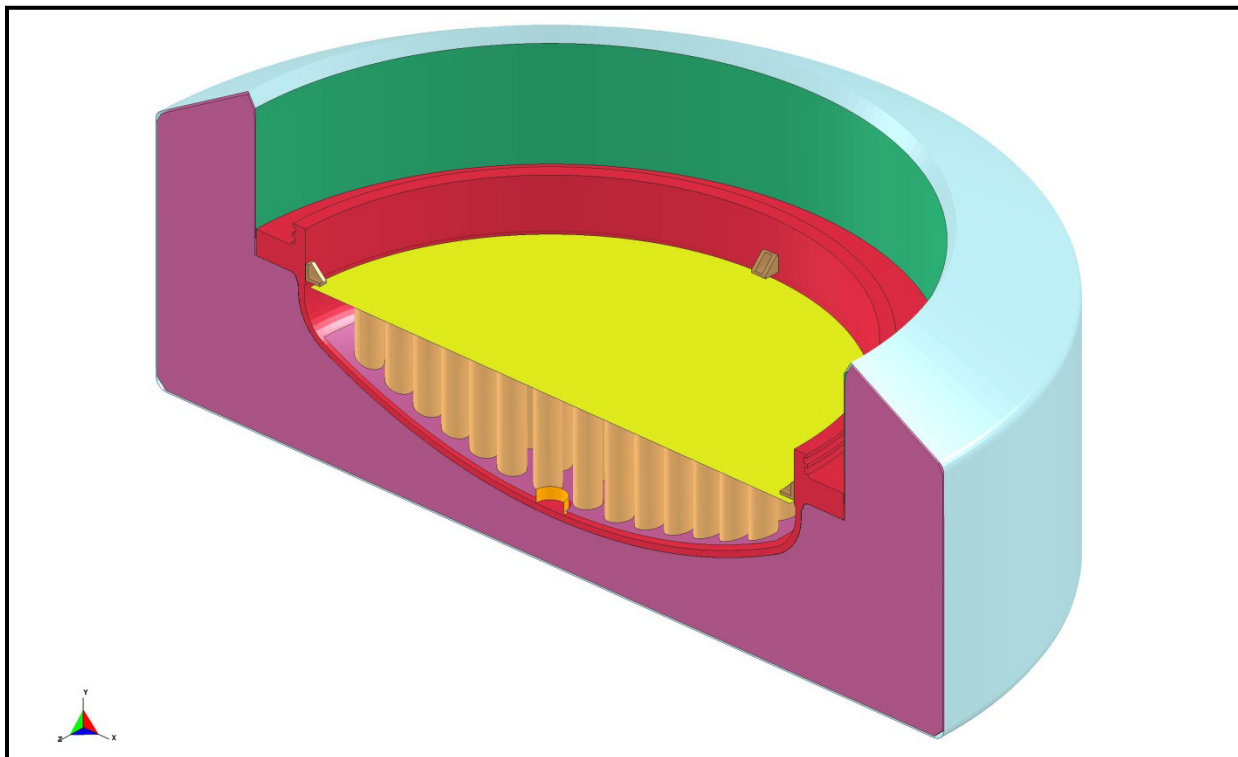


Figure 2.12.4-5 – 1105-SD FEA Model Base

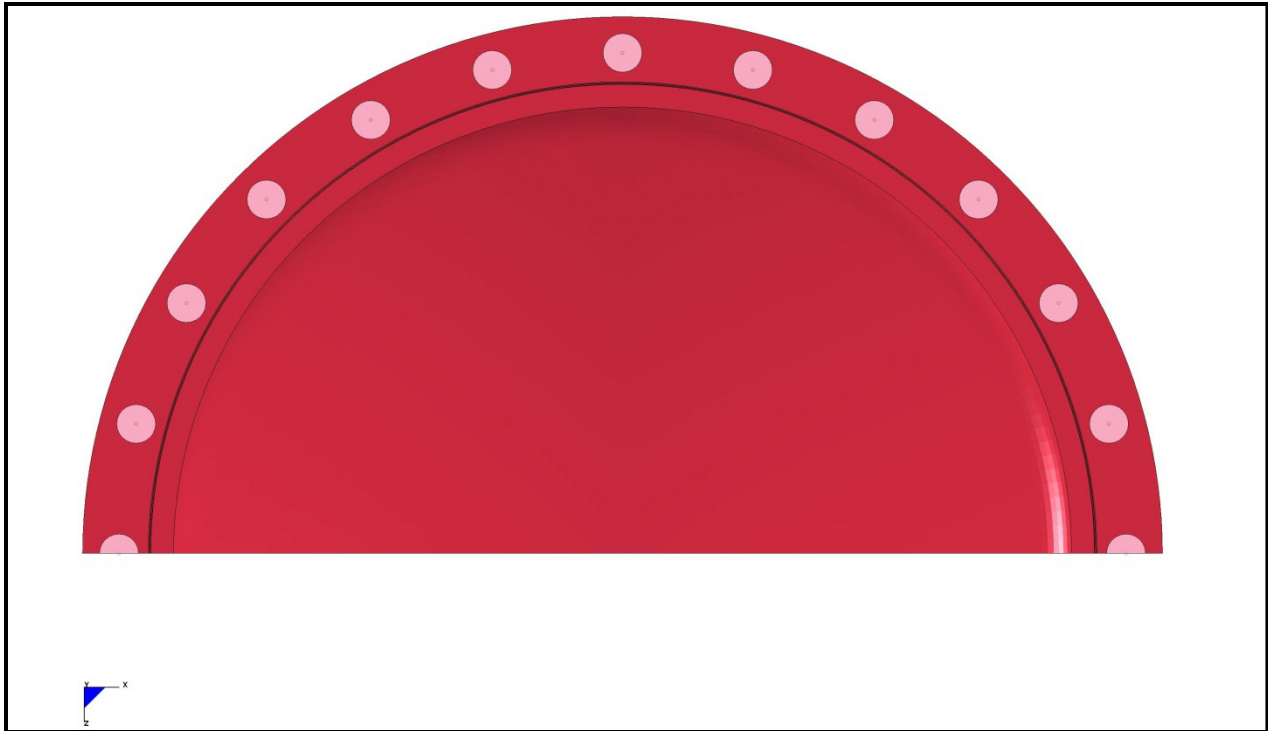


Figure 2.12.4-6 – 1105-SD FEA Model Closure Bolt Locations

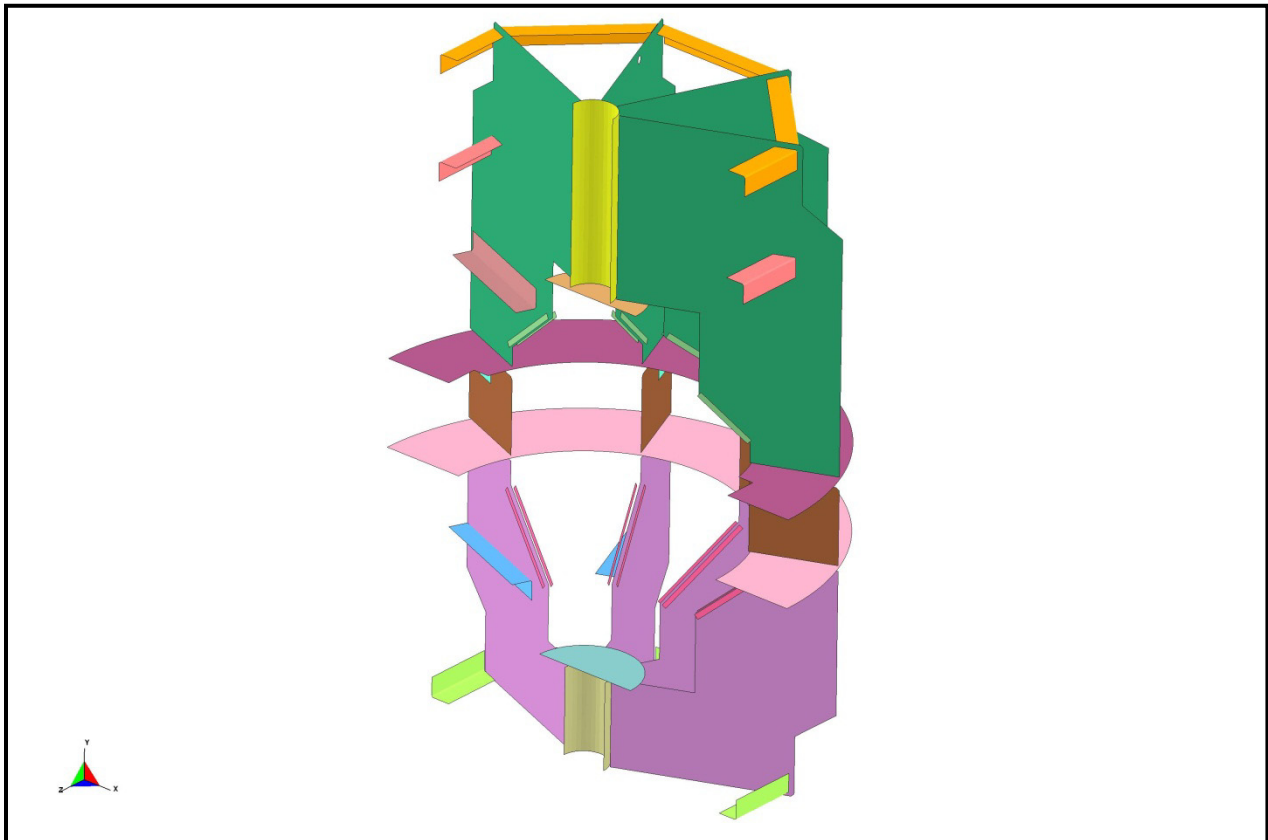


Figure 2.12.4-7 – 1105-SD FEA Model LTSS Lodgment

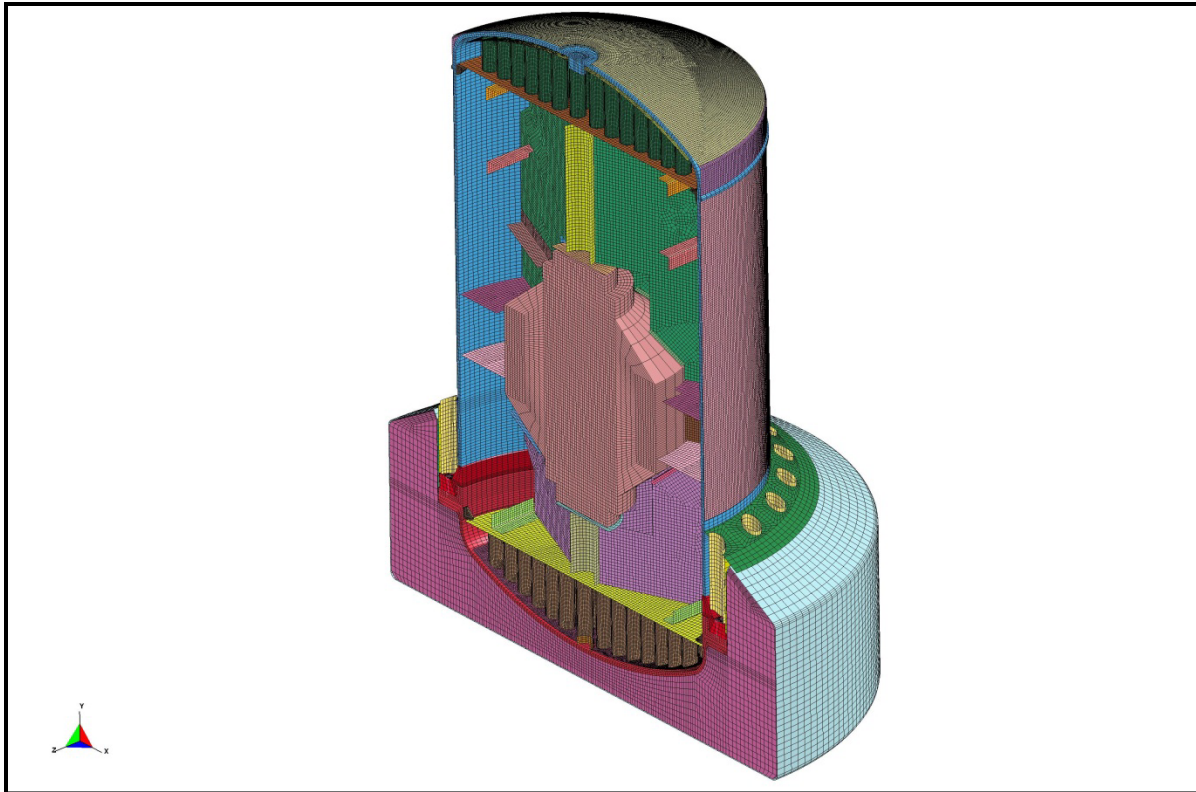


Figure 2.12.4-8 – 1105-SD FEA Model Mesh, Iso-View, Drop Pad Removed

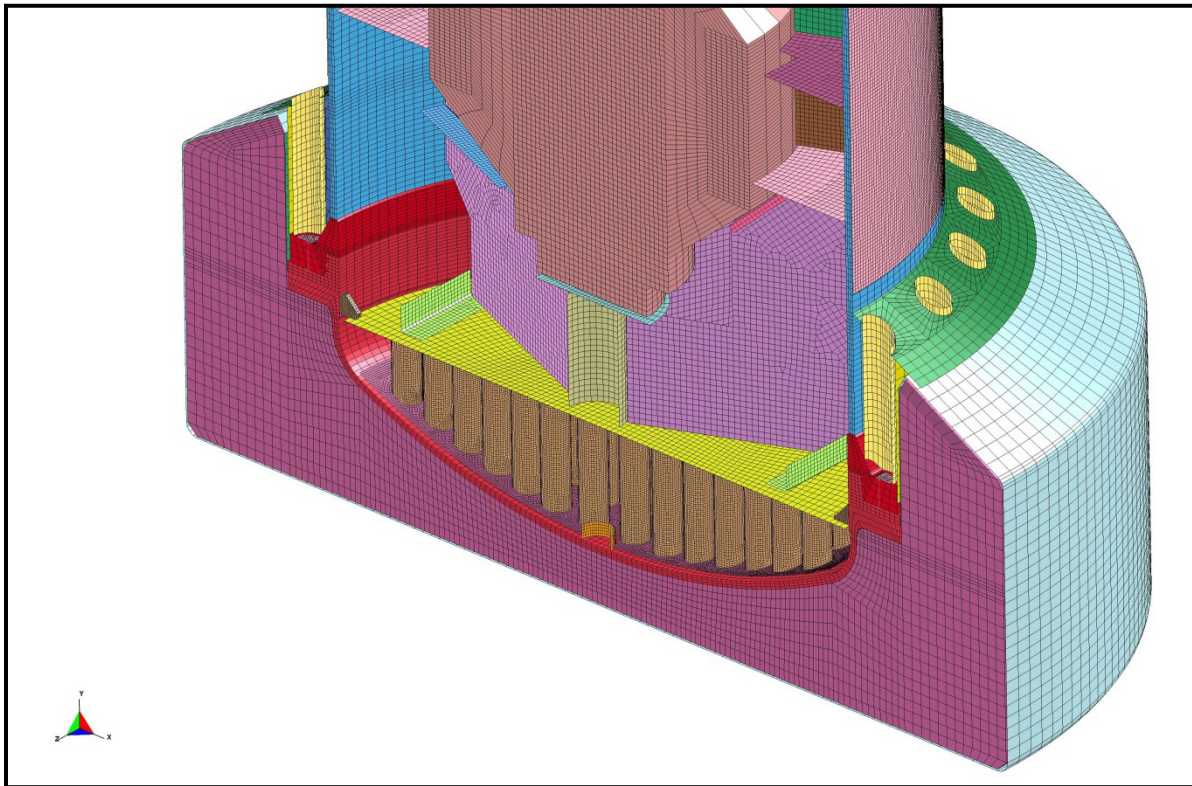


Figure 2.12.4-9 – 1105-SD FEA Model Mesh, Iso-View, Lower Half

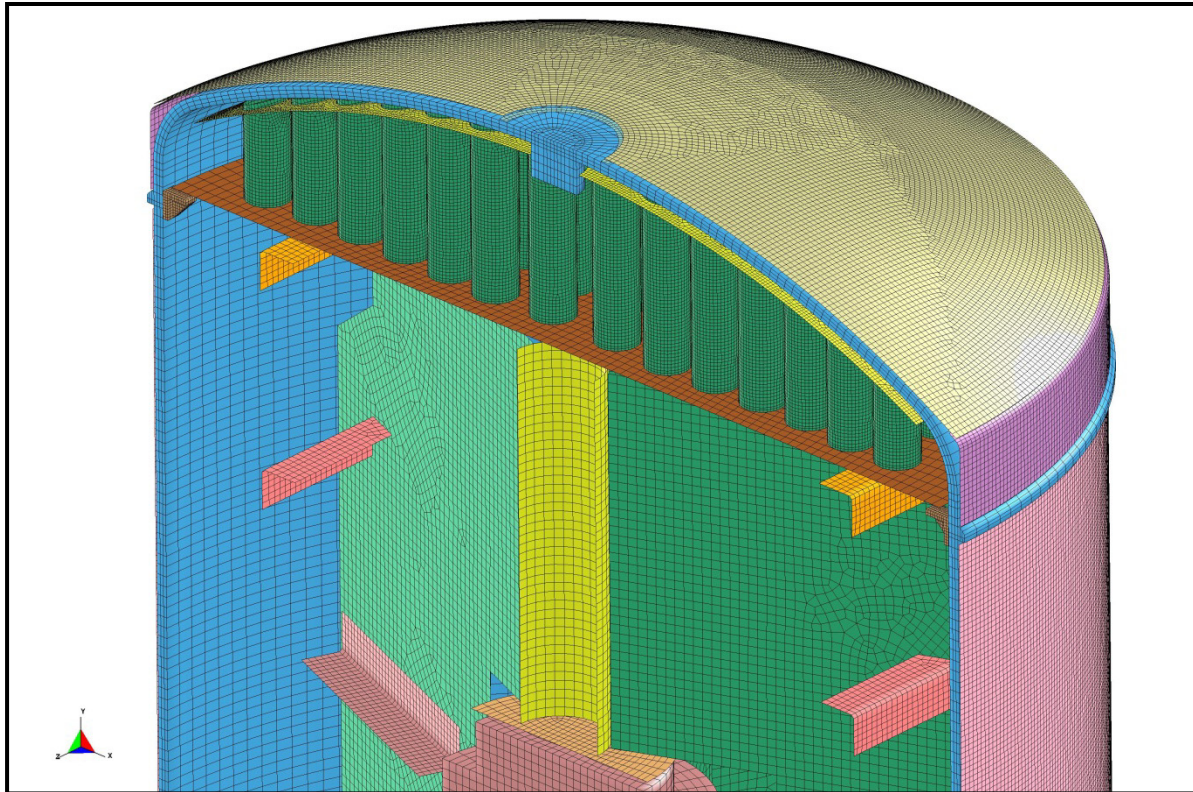


Figure 2.12.4-10 – 1105-SD FEA Model Mesh, Iso-View, Upper Half

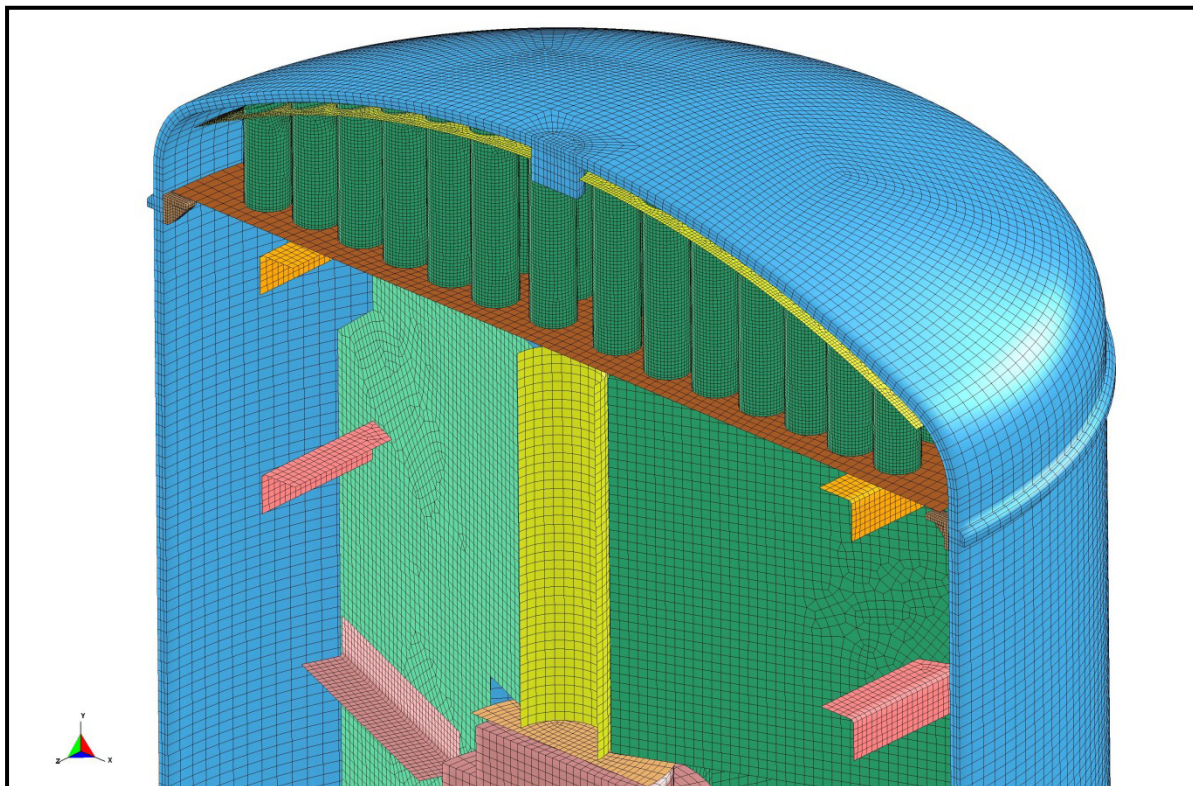


Figure 2.12.4-11 – 1105-SD FEA Model Mesh, Upper Half, Thermal Shields Removed

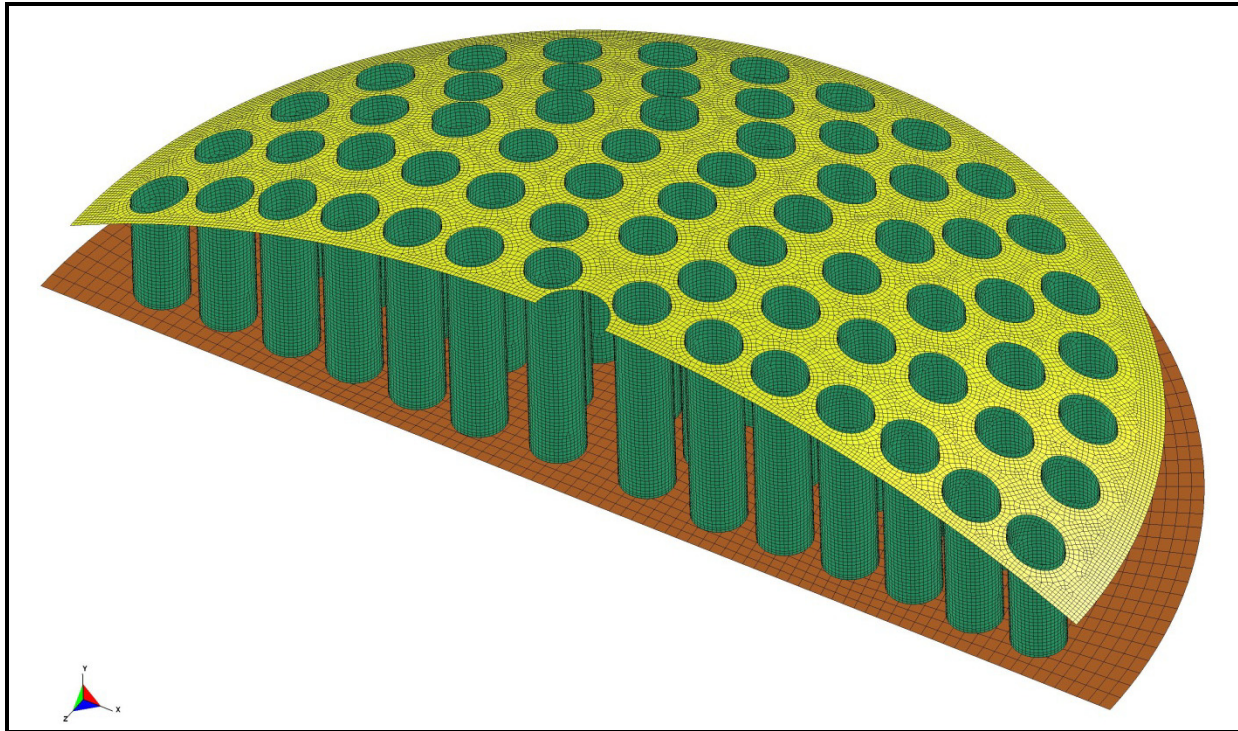


Figure 2.12.4-12 – 1105-SD FEA Model Mesh, Iso-View, Internal Impact Limiter

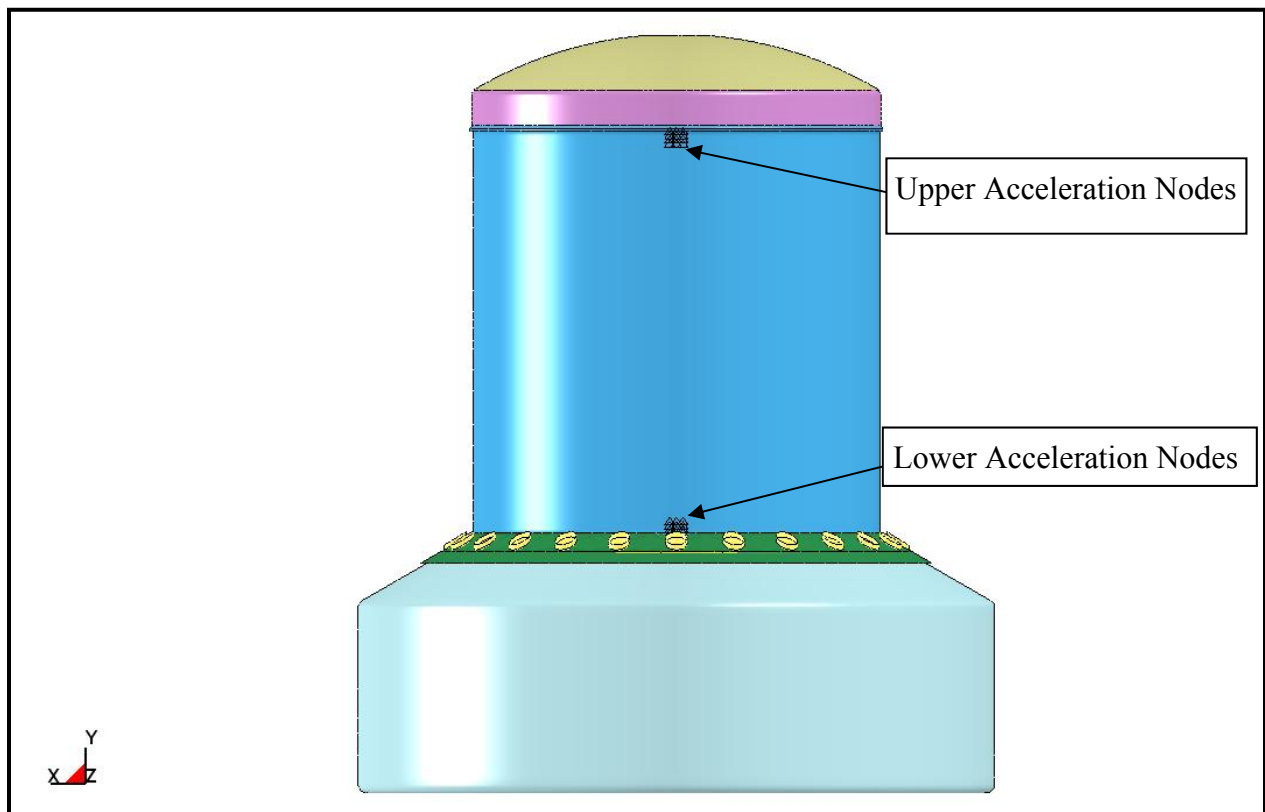


Figure 2.12.4-13 – FEA Model Nodes Equivalent to CTU Accelerometer Blocks

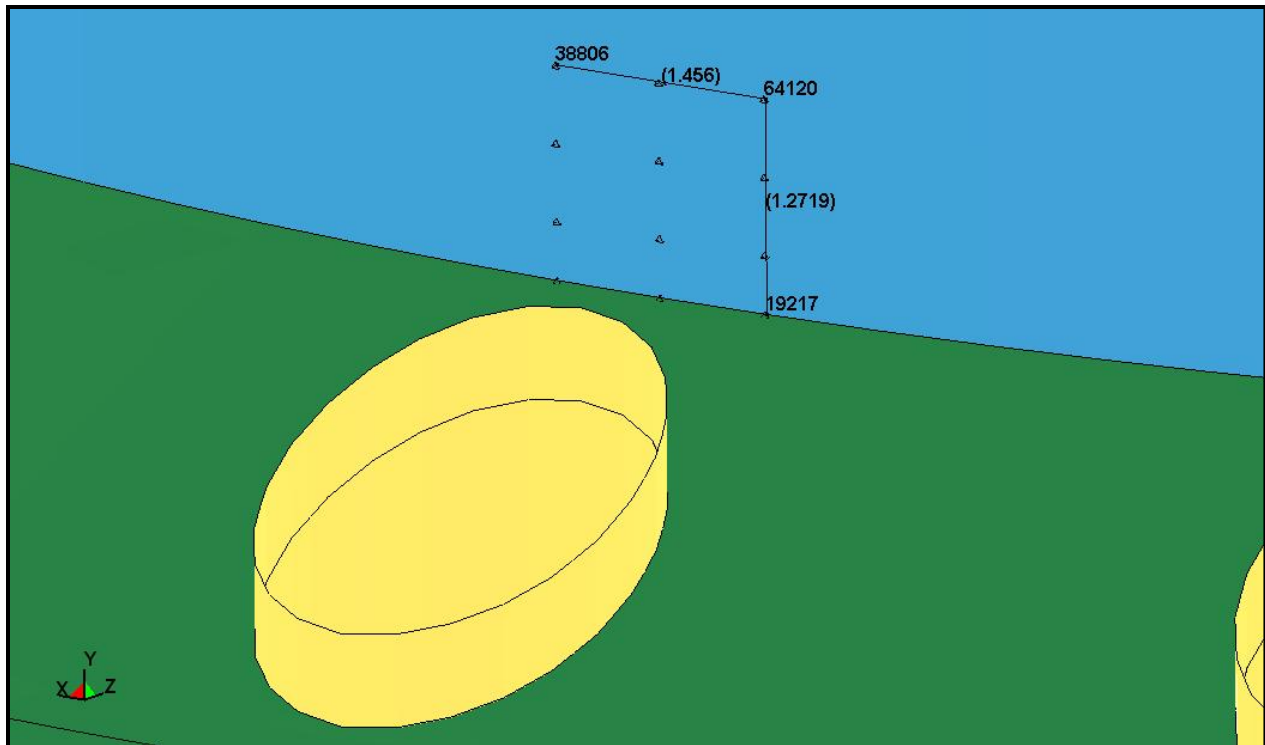


Figure 2.12.4-14 – FEA Model Nodes Equivalent to CTU Accelerometer Blocks (Lower)

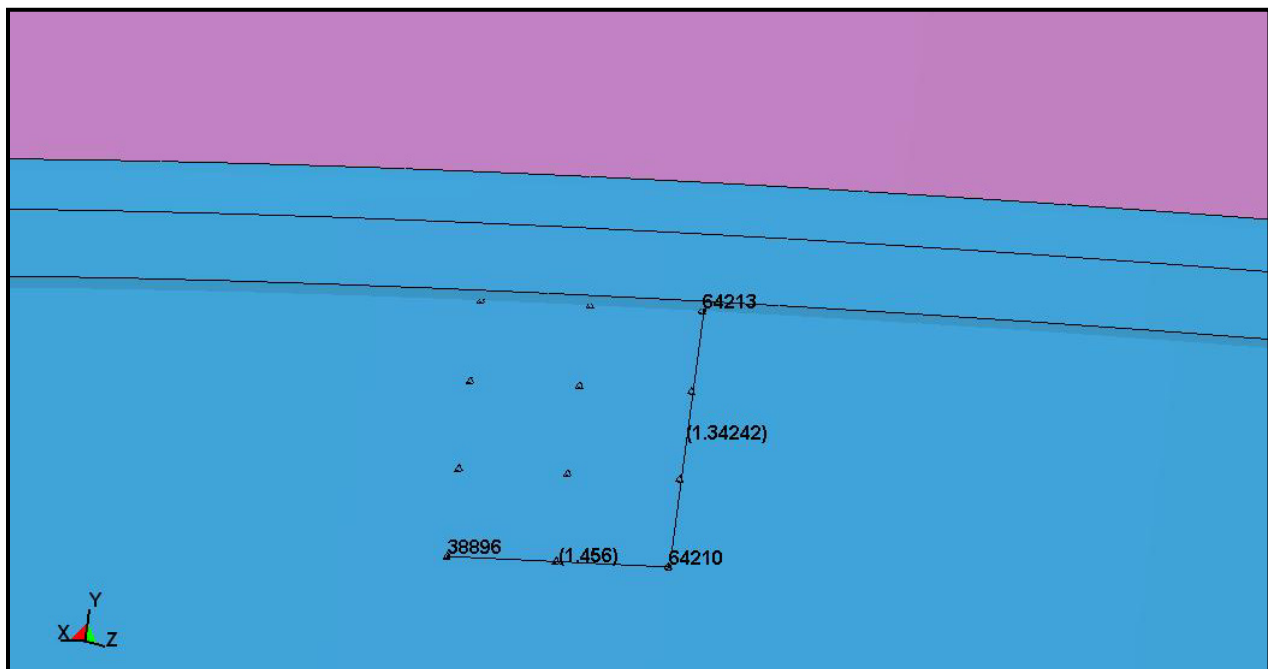


Figure 2.12.4-15 – FEA Model Nodes Equivalent to CTU Accelerometer Blocks (Upper)

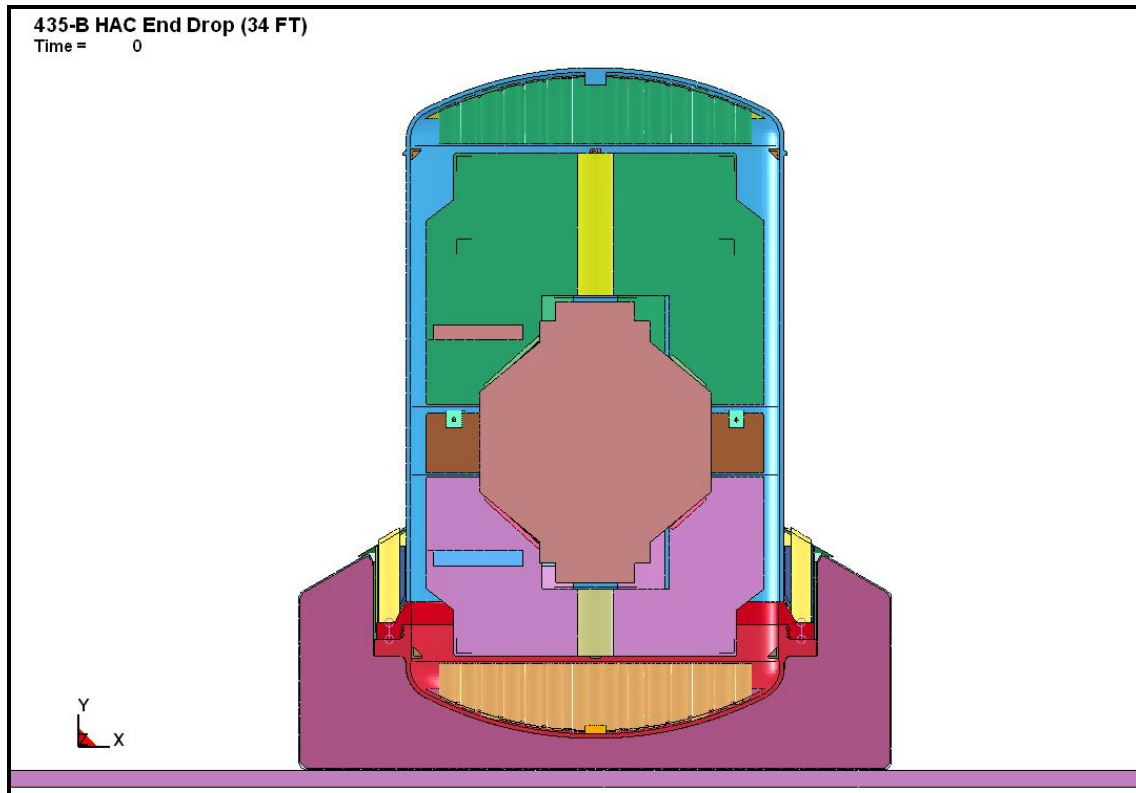


Figure 2.12.4-16 – D1 Benchmark Initial State

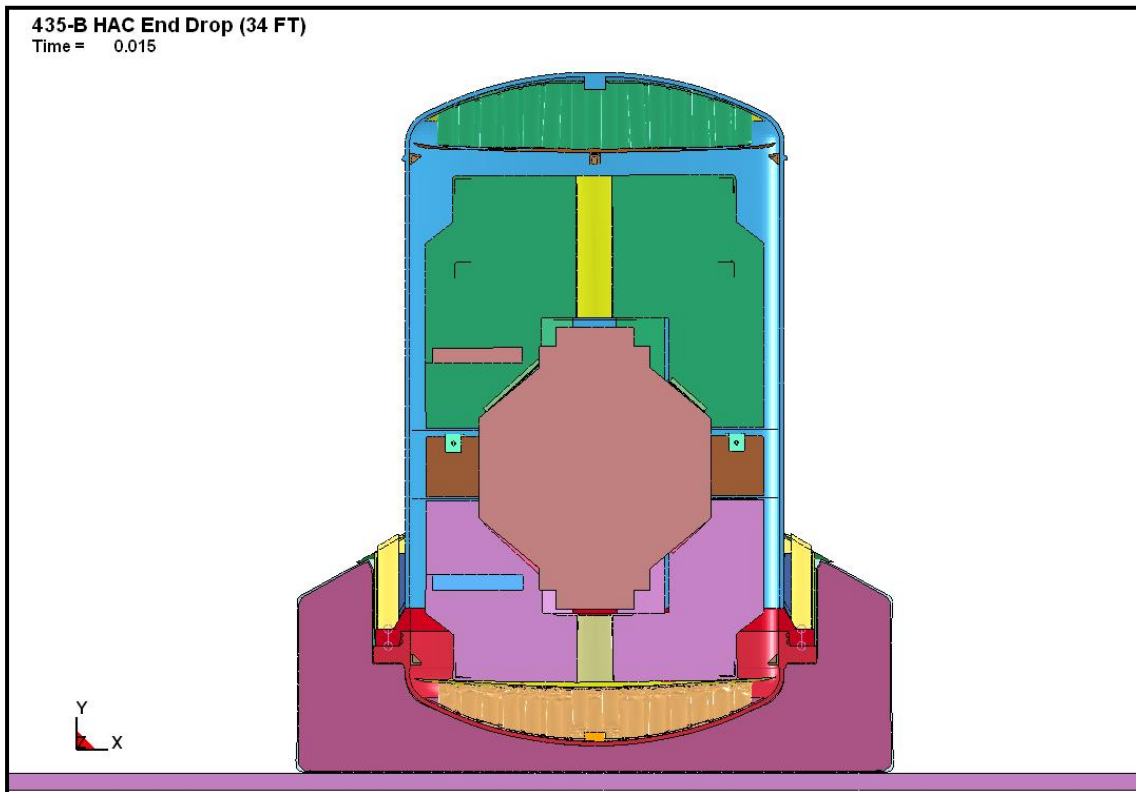
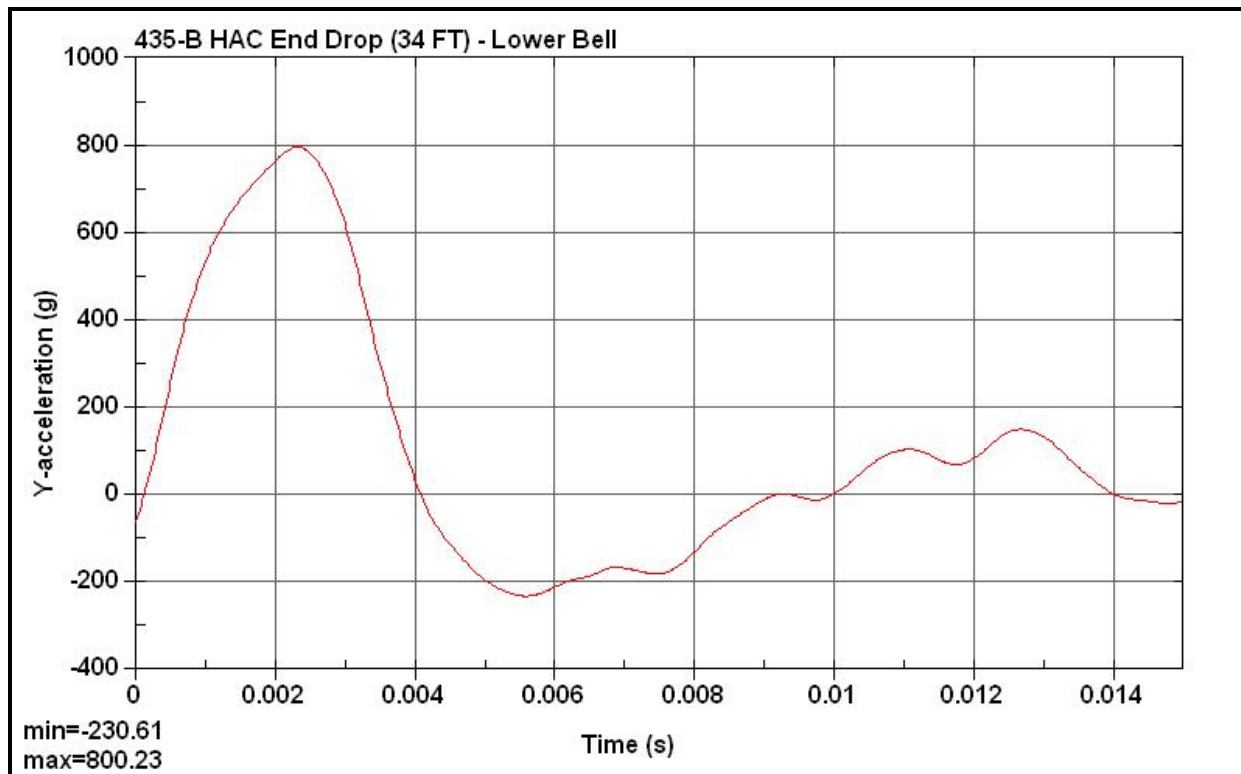
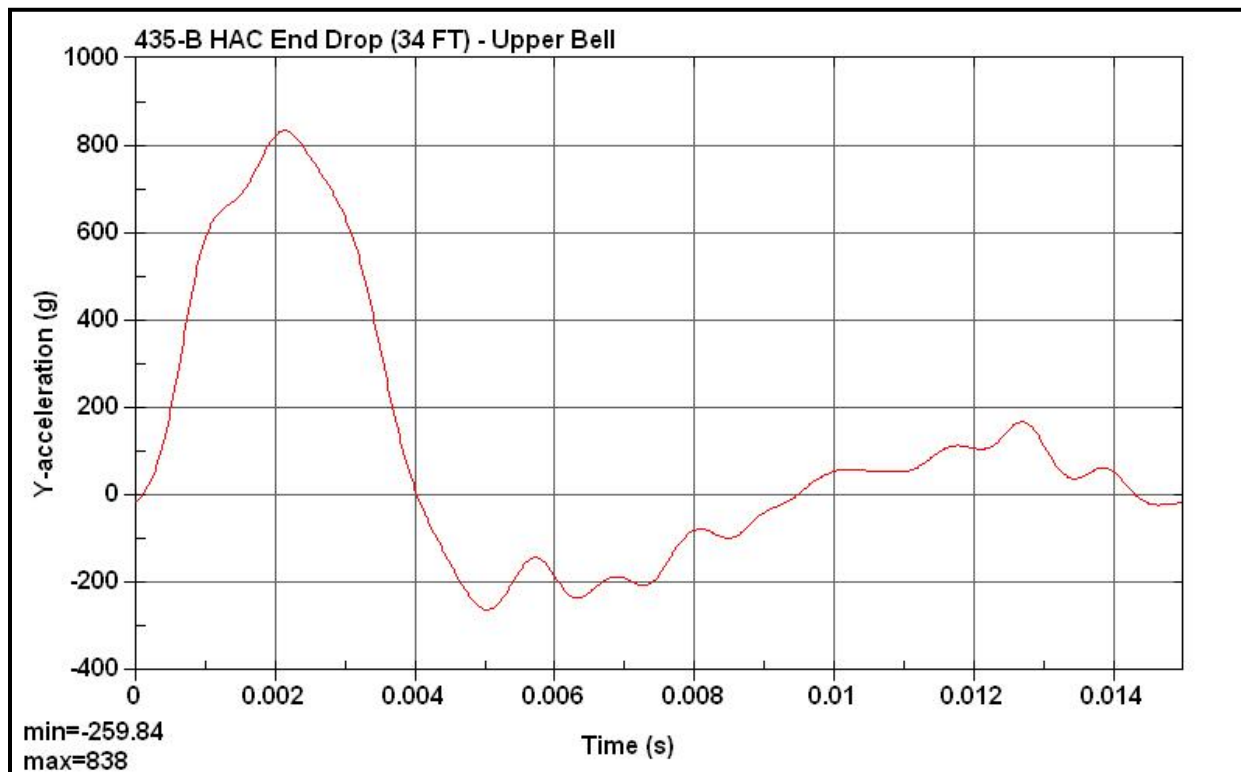
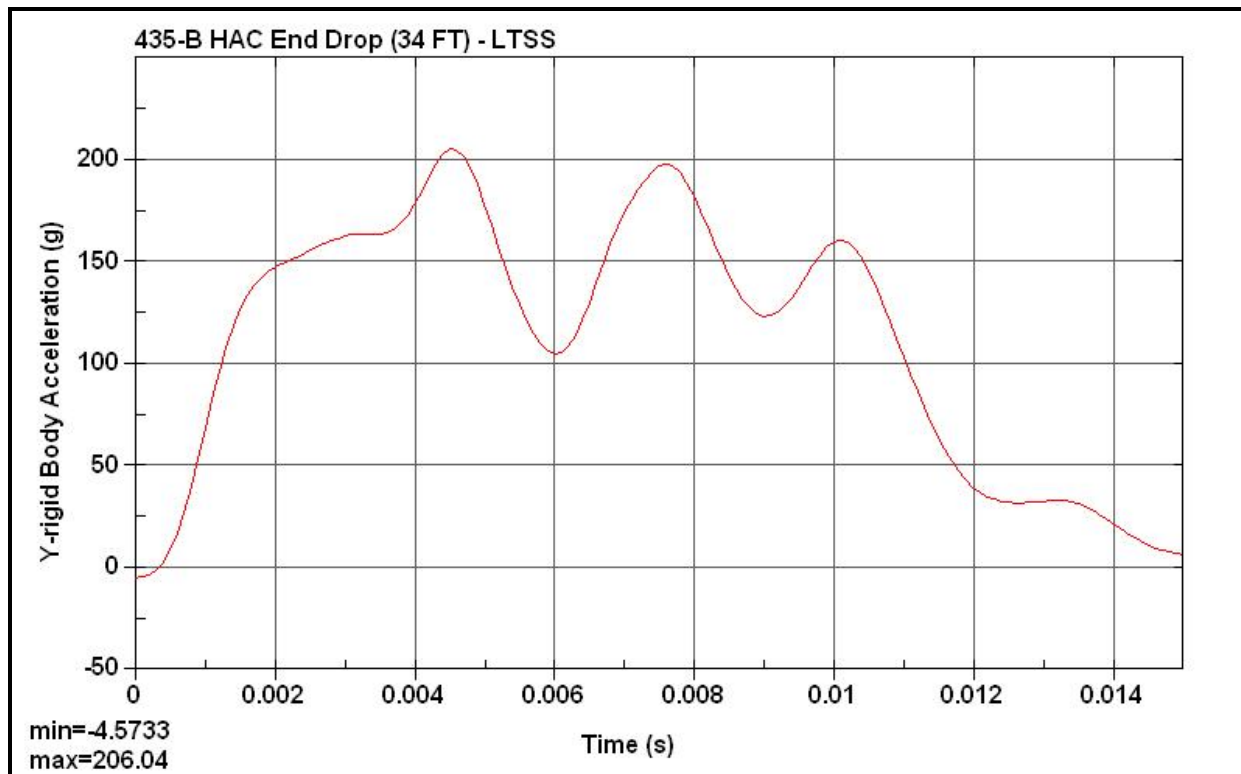
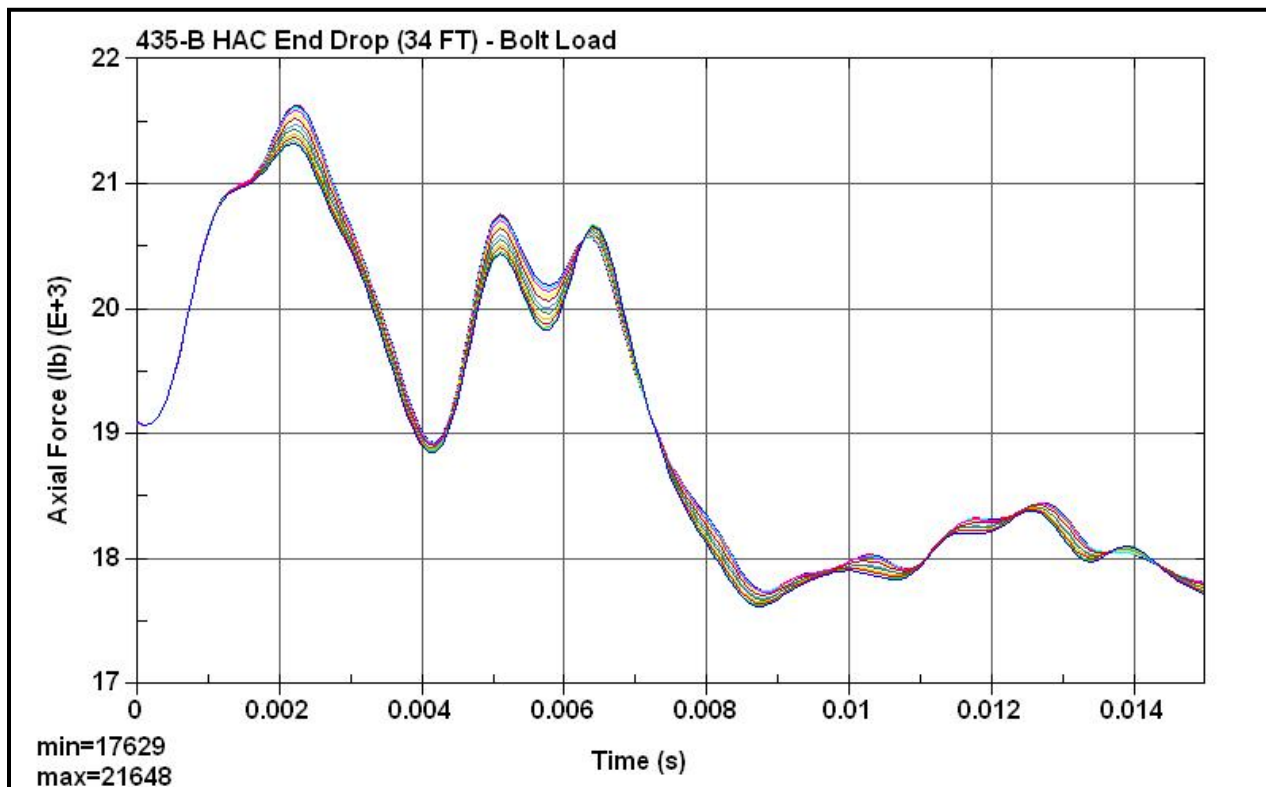


Figure 2.12.4-17 – D1 Benchmark Final State

**Figure 2.12.4-18 – D1 Benchmark Lower Bell Acceleration****Figure 2.12.4-19 – D1 Benchmark Upper Bell Acceleration**

**Figure 2.12.4-20 – D1 Benchmark LTSS Acceleration****Figure 2.12.4-21 – D1 Benchmark Axial Bolt Force**

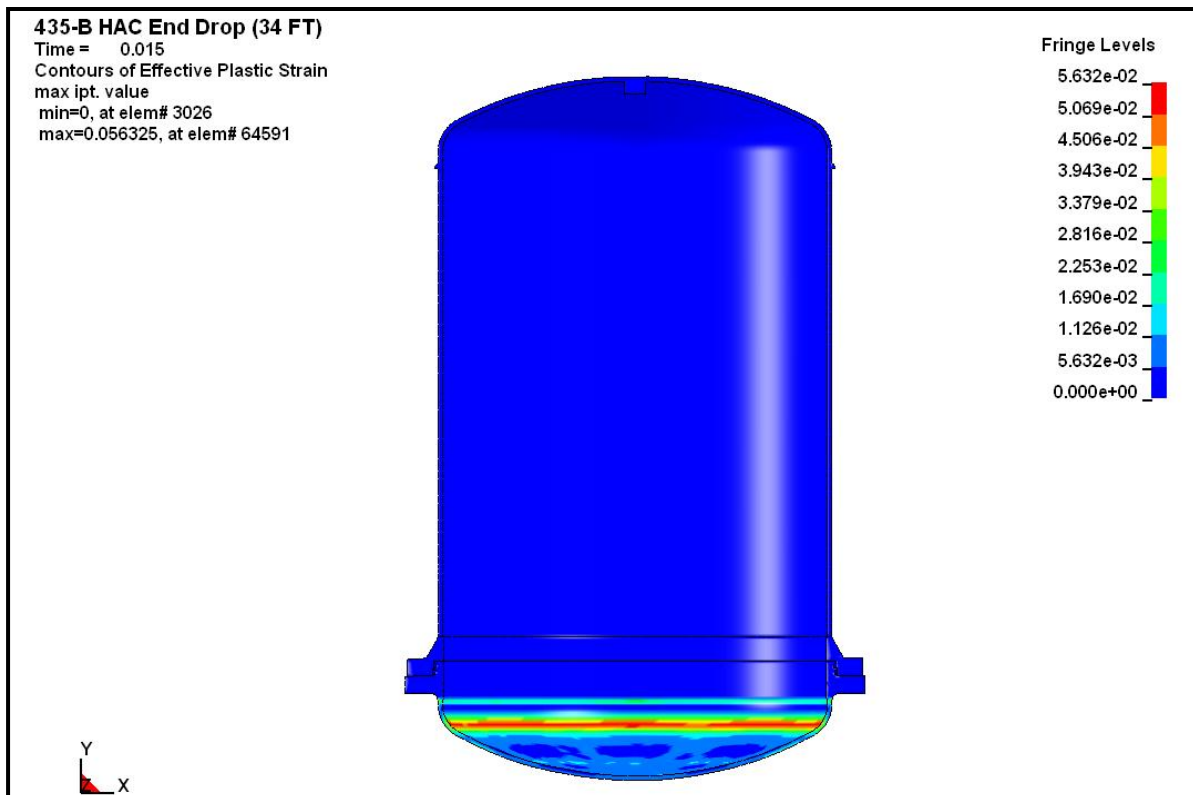


Figure 2.12.4-22 – D1 Benchmark Containment Boundary Cumulative Effective Plastic Strain

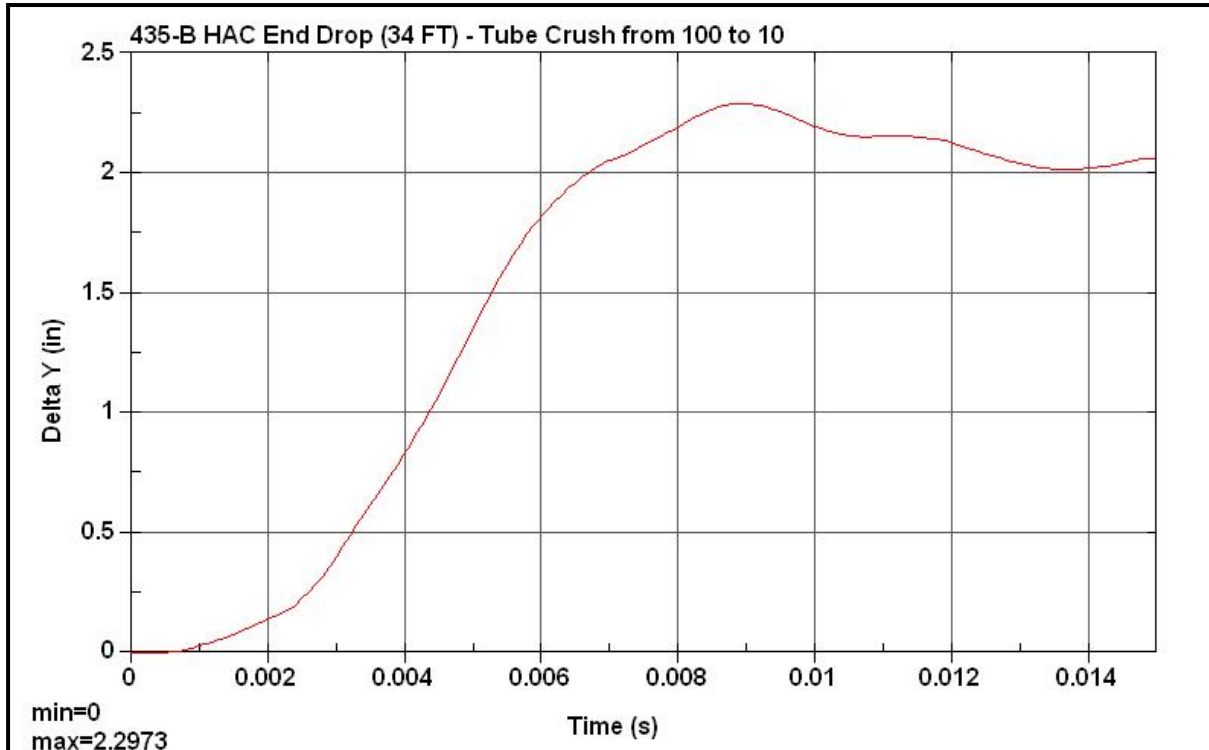
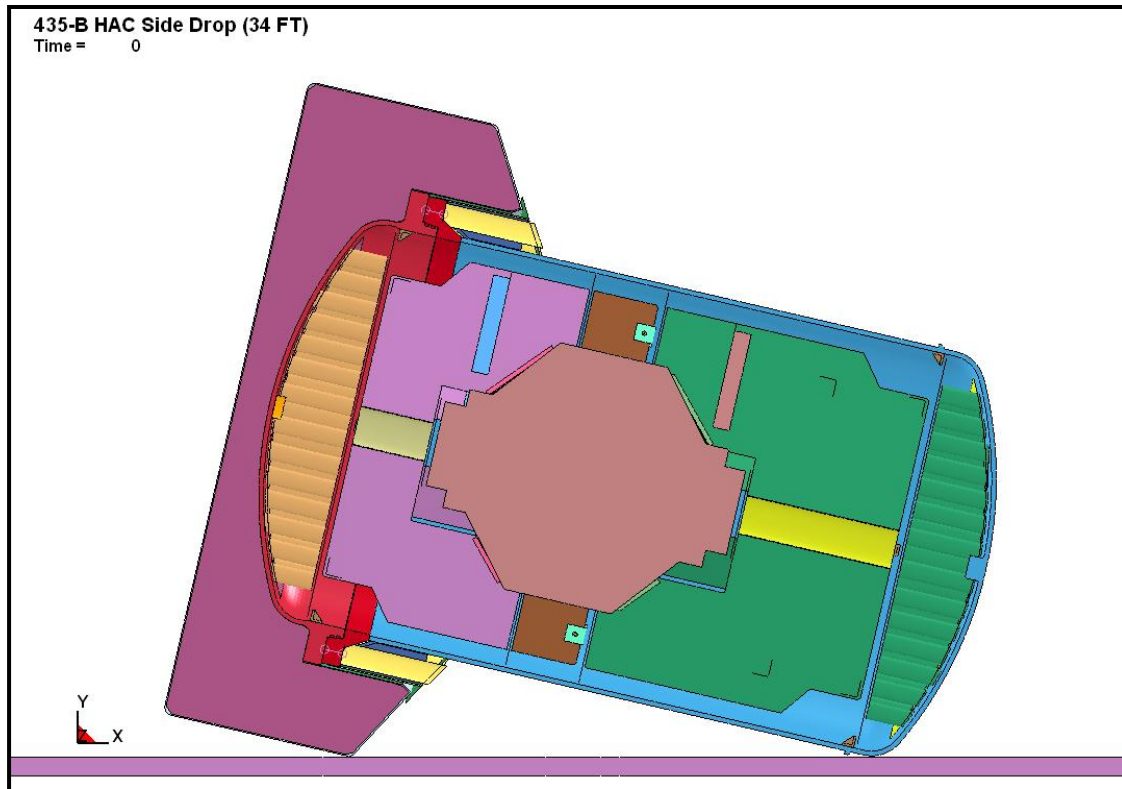
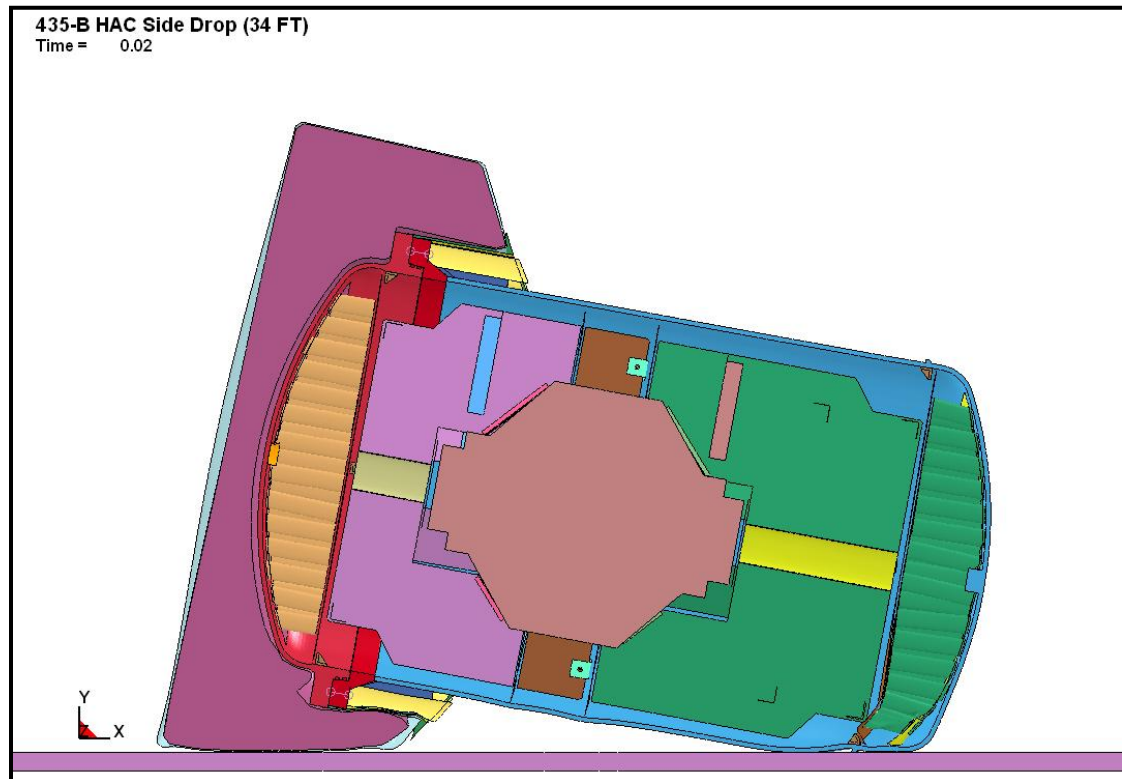
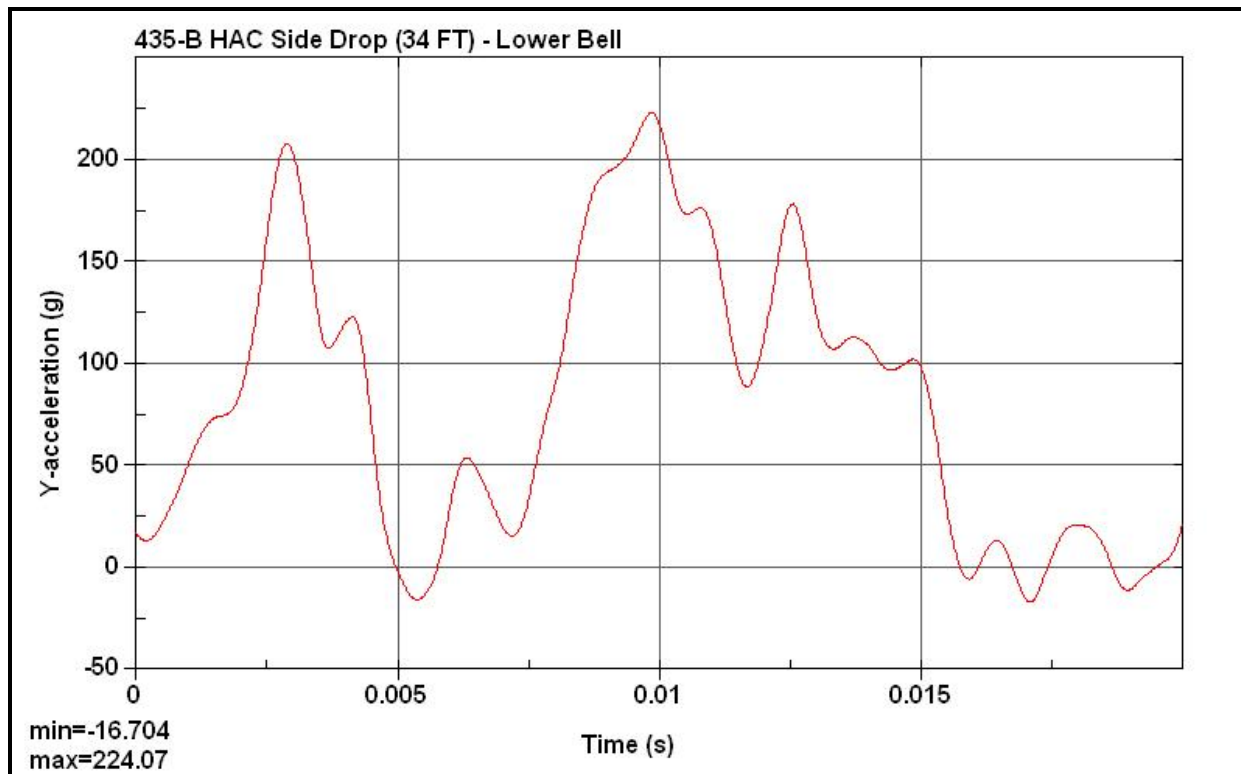
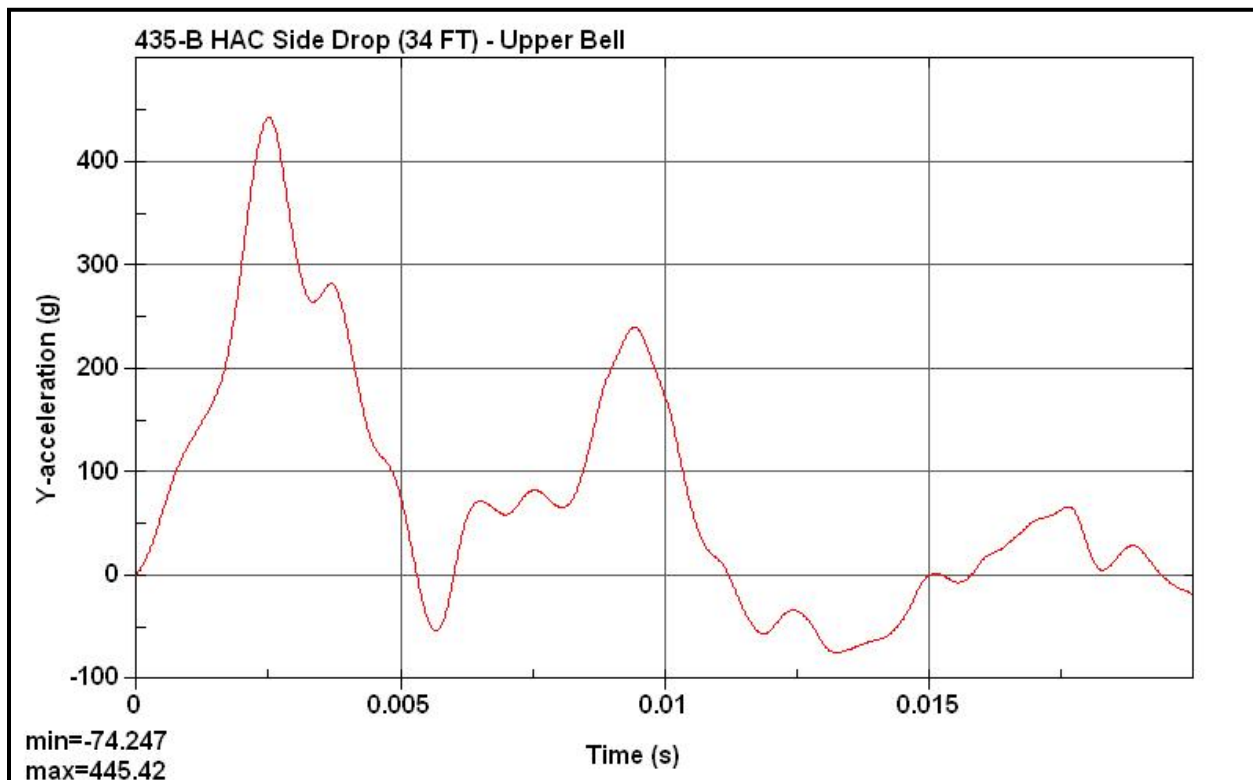
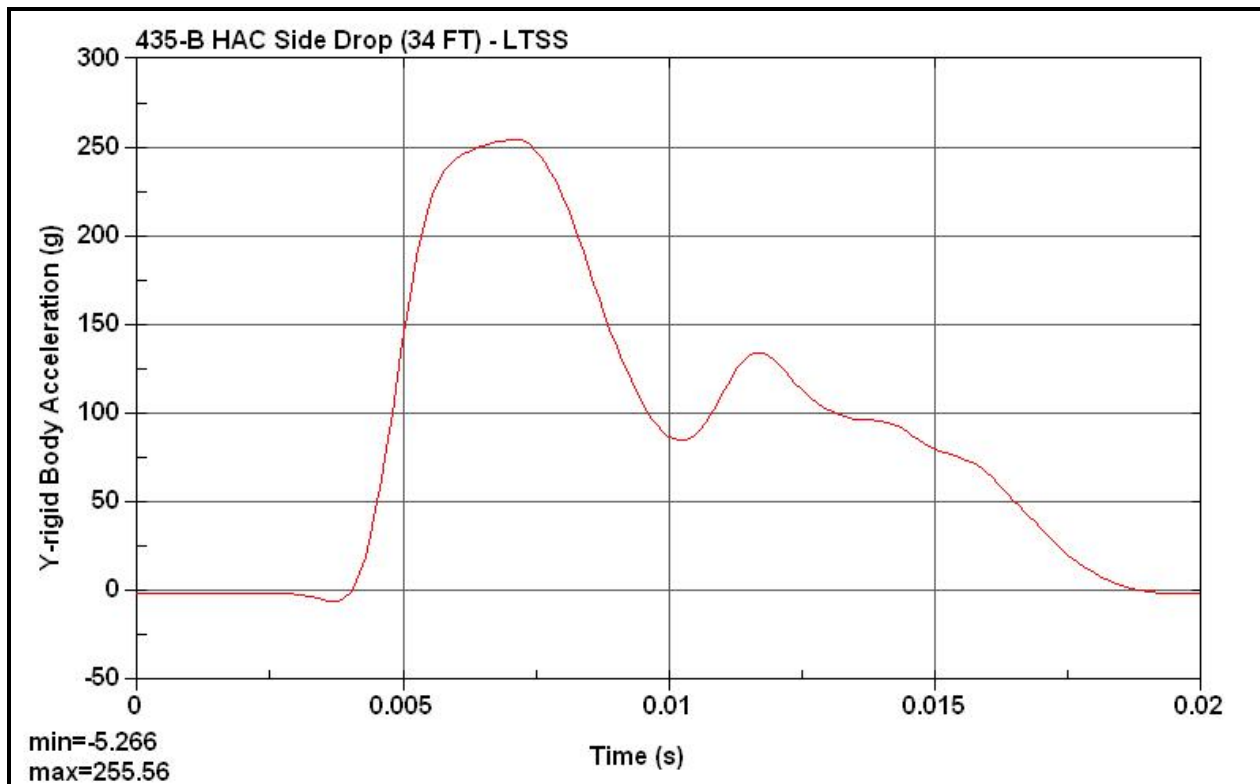
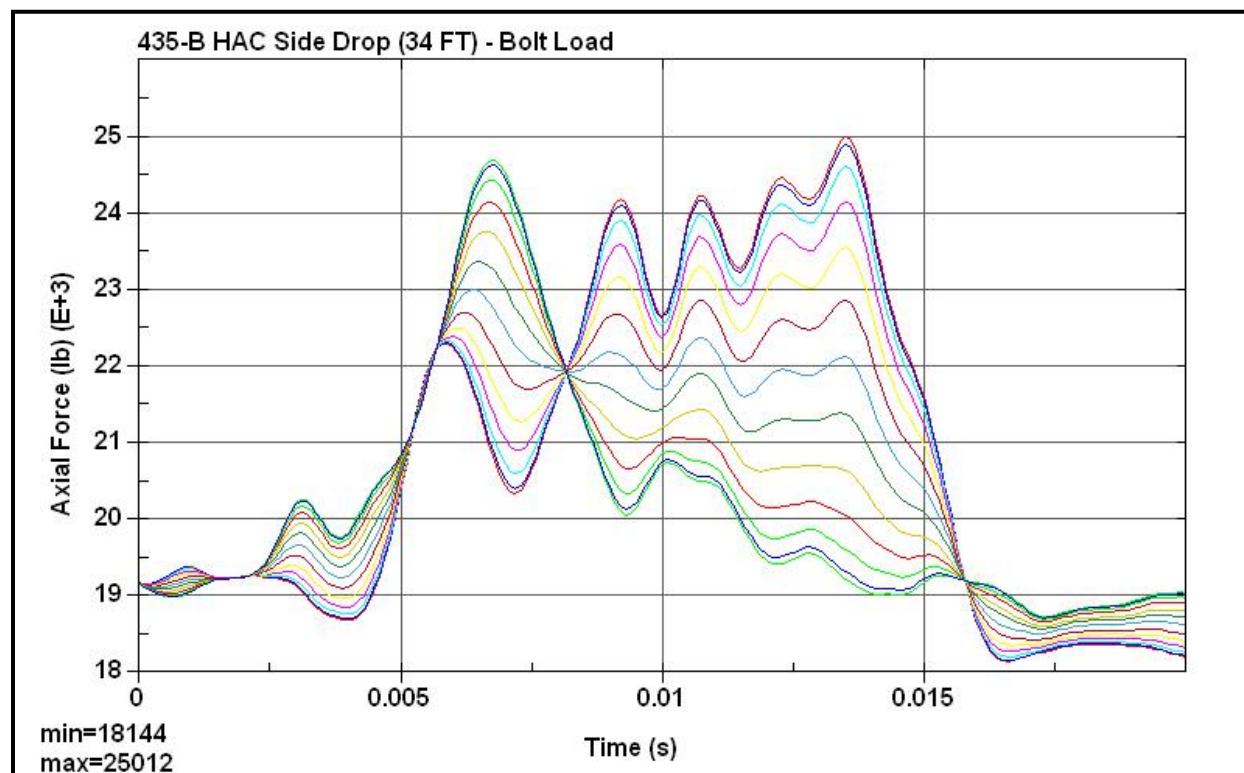
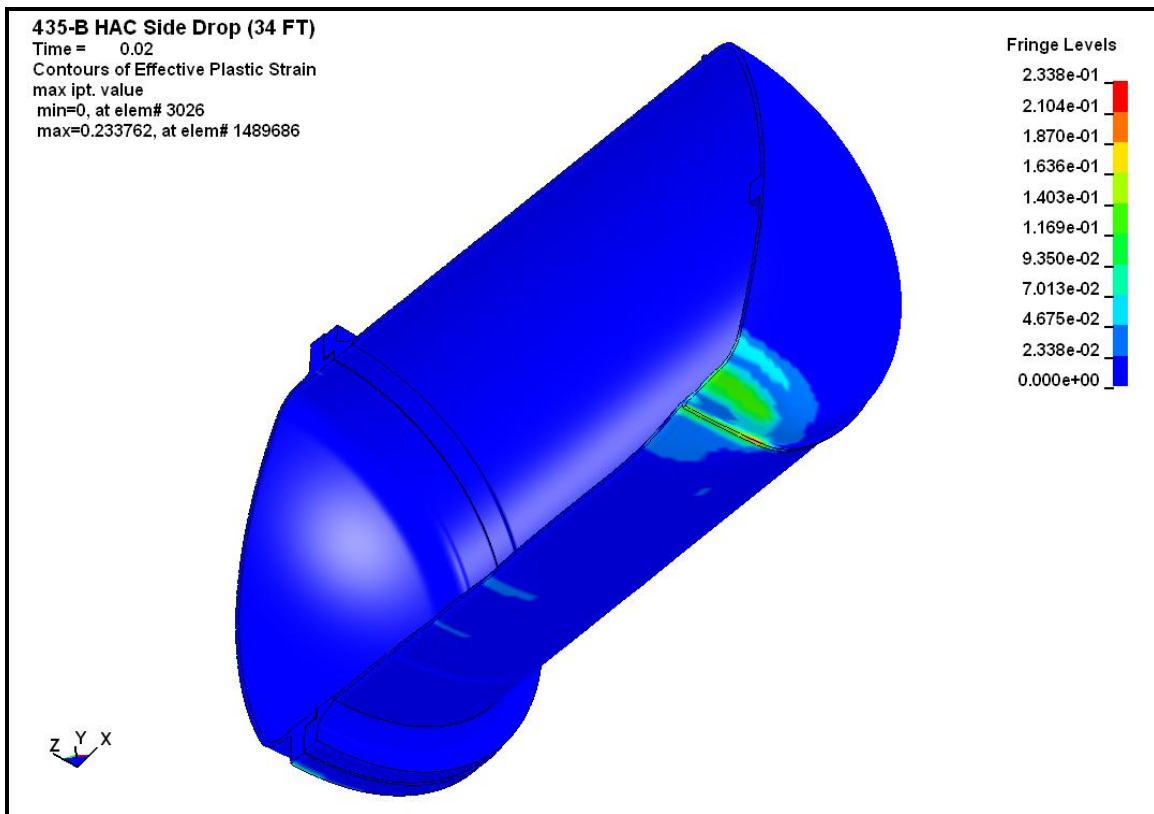
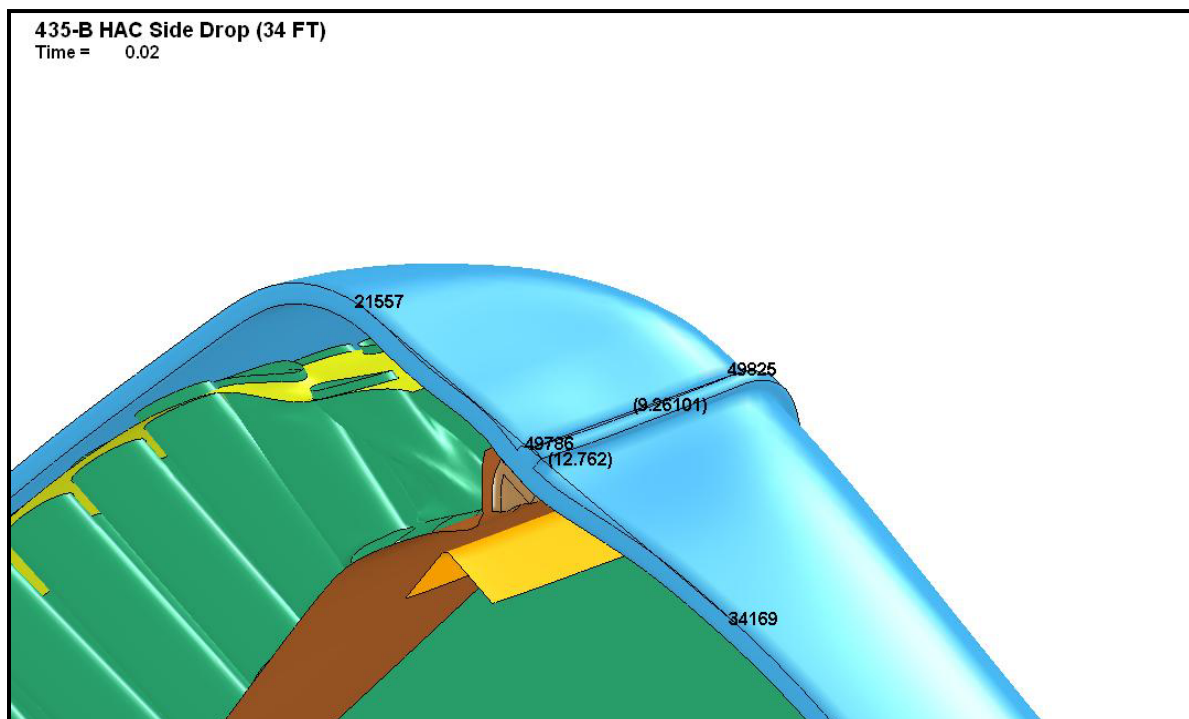


Figure 2.12.4-23 – D1 Benchmark Tube Crush from Lodgment (Part 100) to the Clips (Part 10)

**Figure 2.12.4-24 – D2 Benchmark Initial State****Figure 2.12.4-25 – D2 Benchmark Final State**

**Figure 2.12.4-26 – D2 Benchmark Lower Bell Acceleration****Figure 2.12.4-27 – D2 Benchmark Upper Bell Acceleration**

**Figure 2.12.4-28 – D2 Benchmark LTSS Acceleration****Figure 2.12.4-29 – D2 Benchmark Axial Bolt Force**

**Figure 2.12.4-30** – D2 Benchmark Containment Boundary Cumulative Effective Plastic Strain**Figure 2.12.4-31** – D2 Benchmark Upper Impact Patch

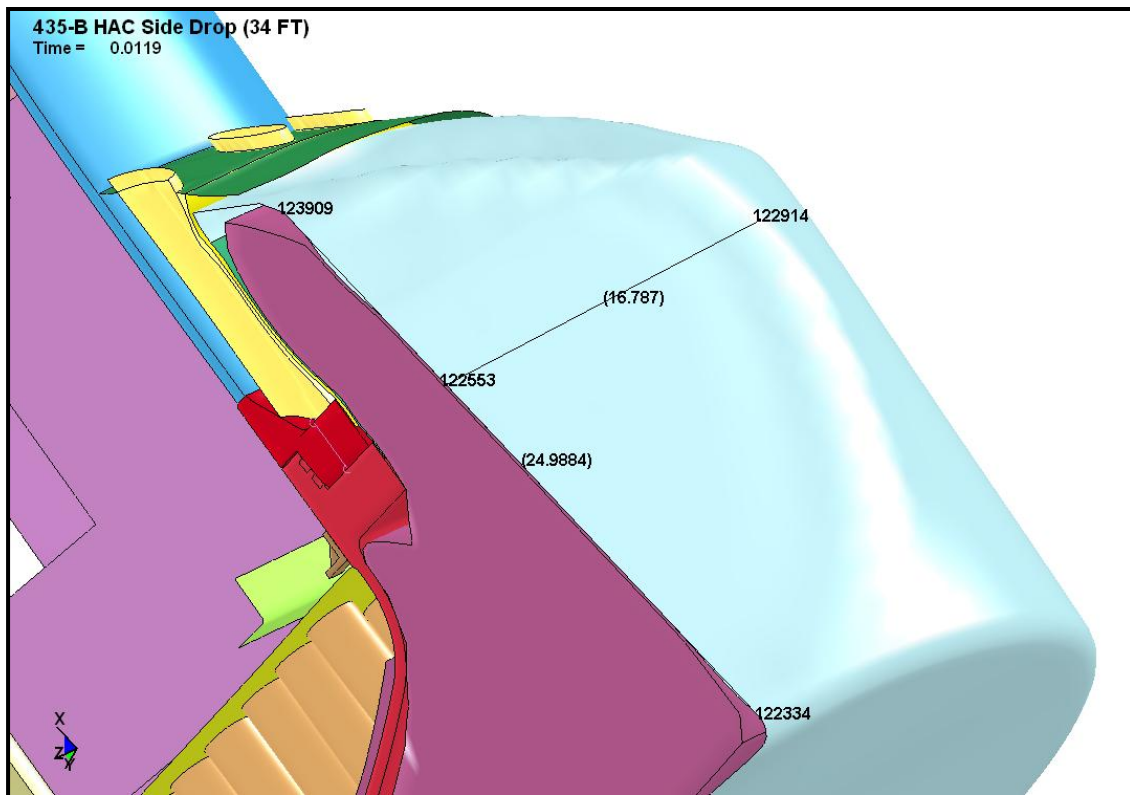


Figure 2.12.4-32 – D2 Benchmark Lower Impact Patch

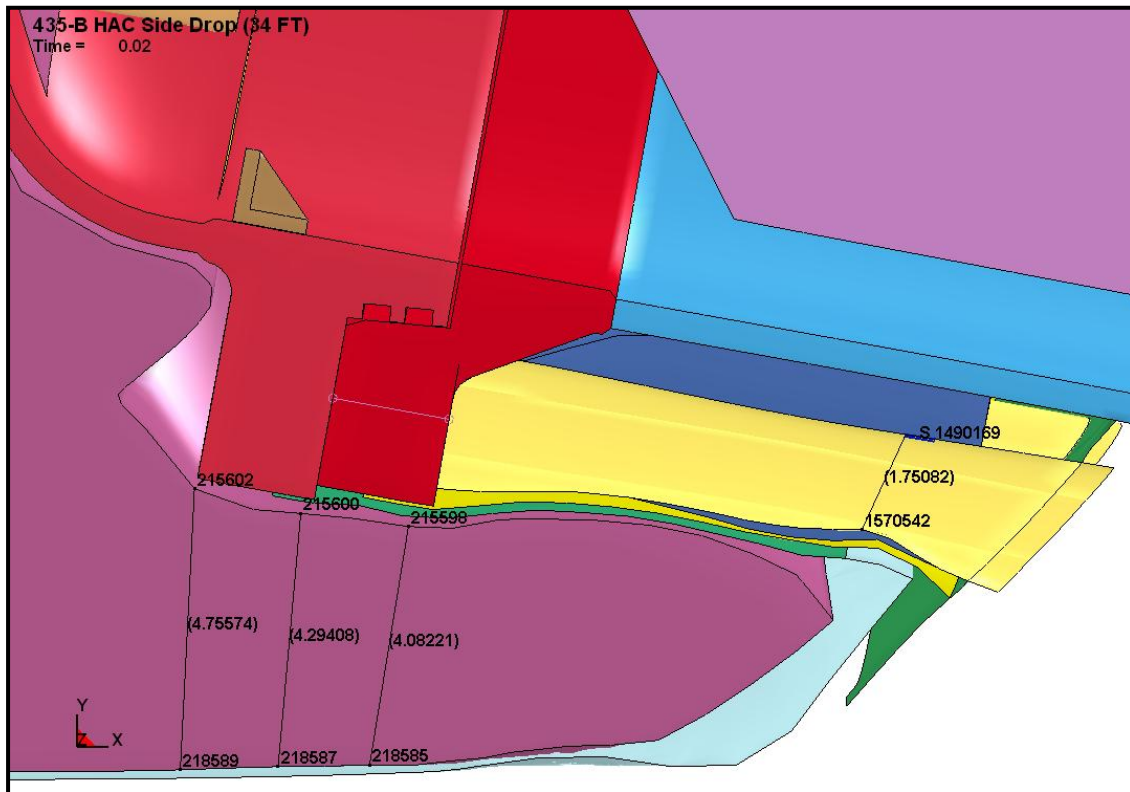


Figure 2.12.4-33 – D2 Benchmark Minimum Foam Near Seal

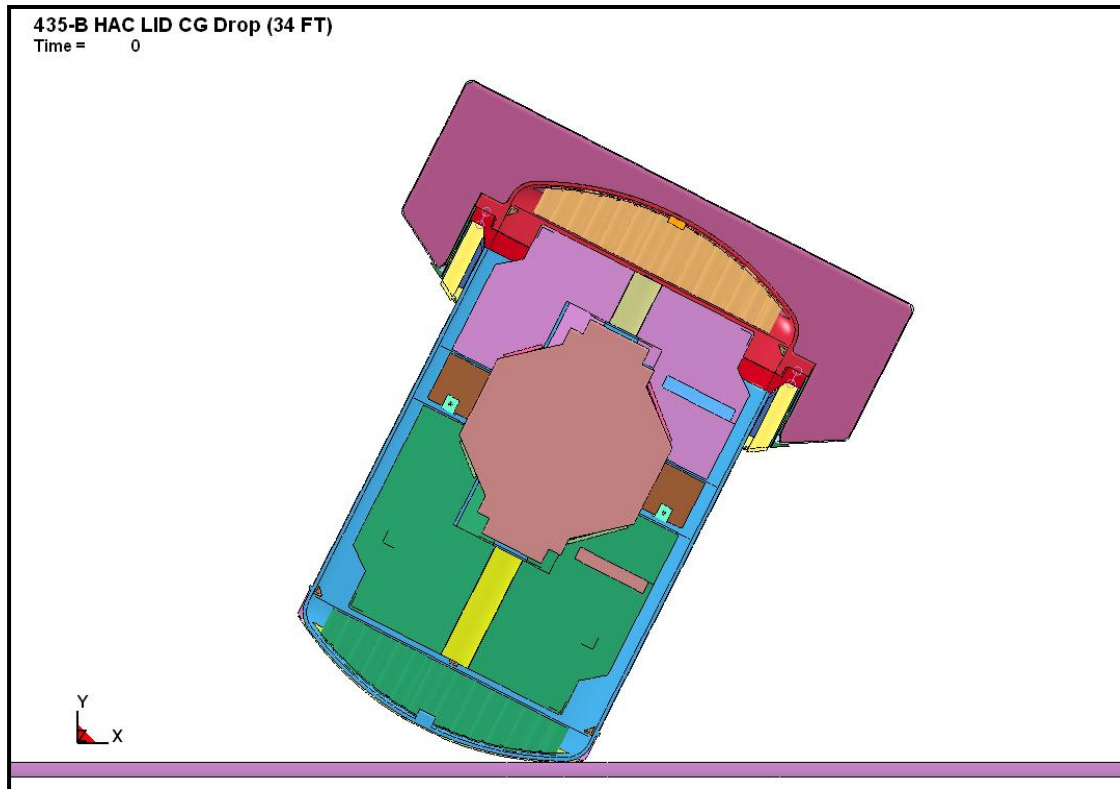


Figure 2.12.4-34 – D3 Benchmark Initial State

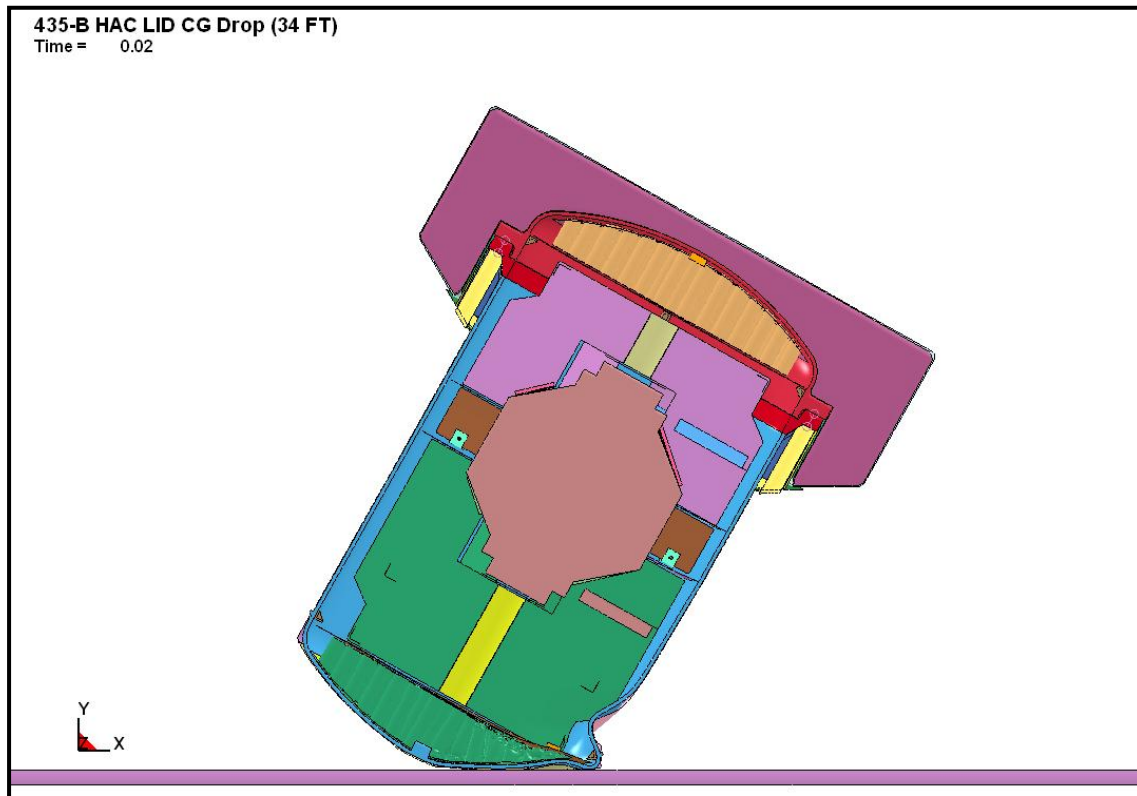
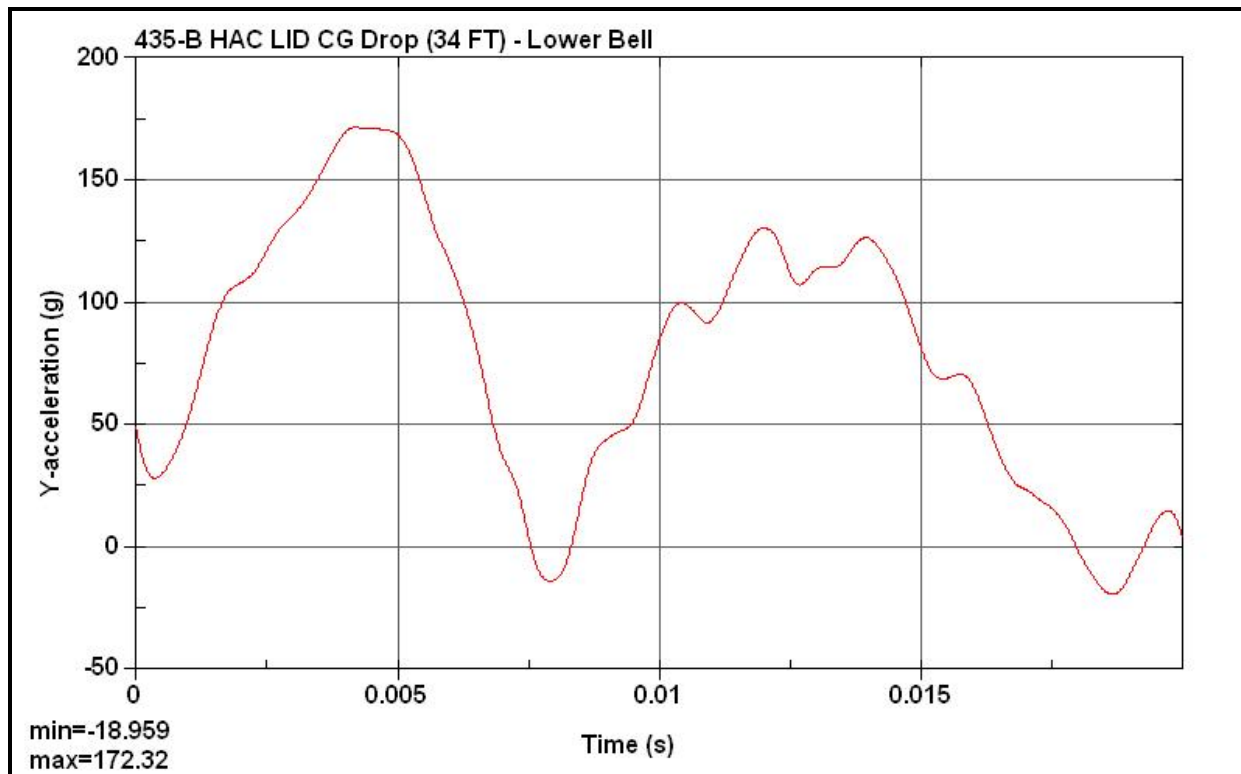
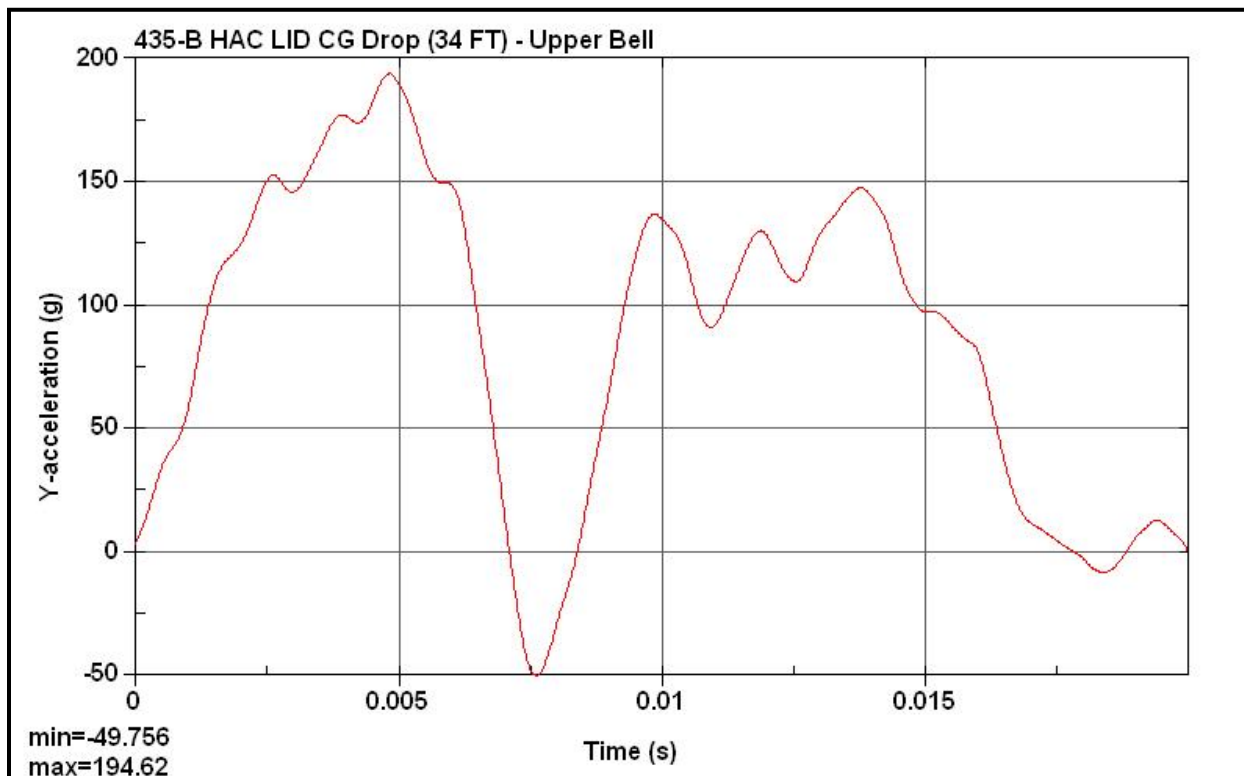
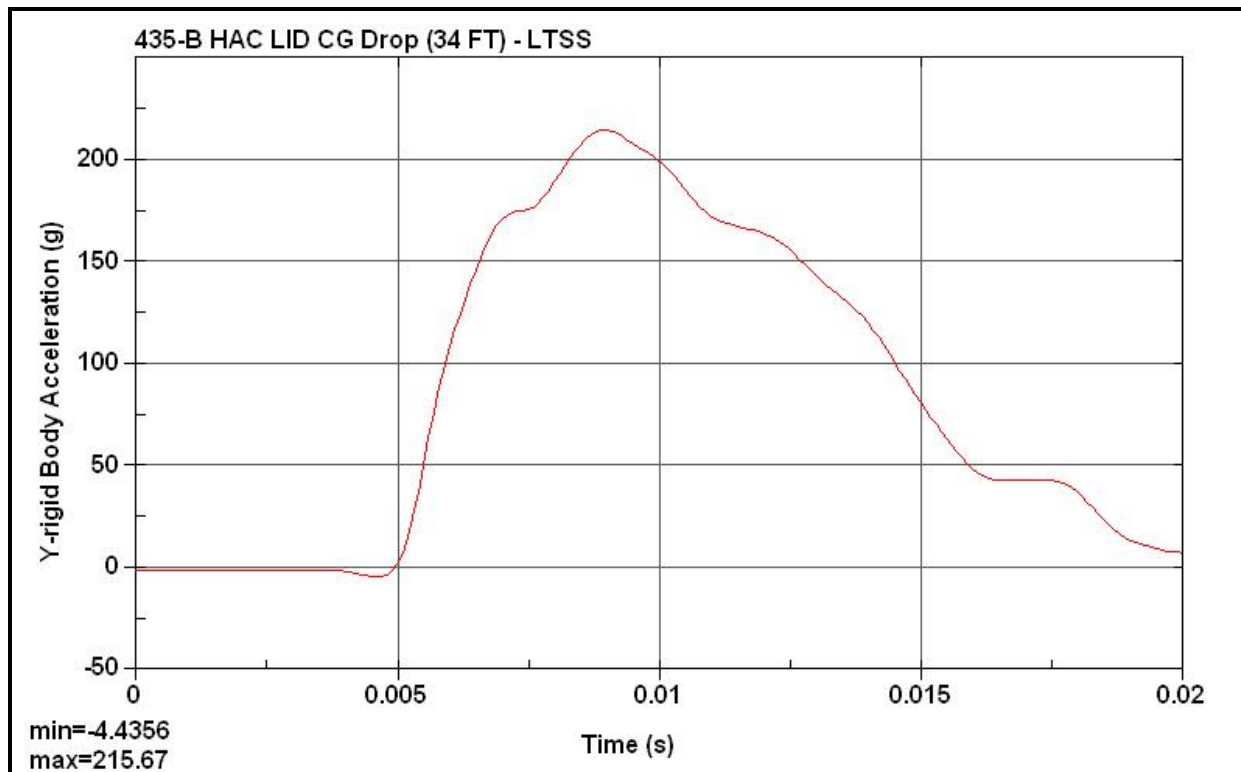
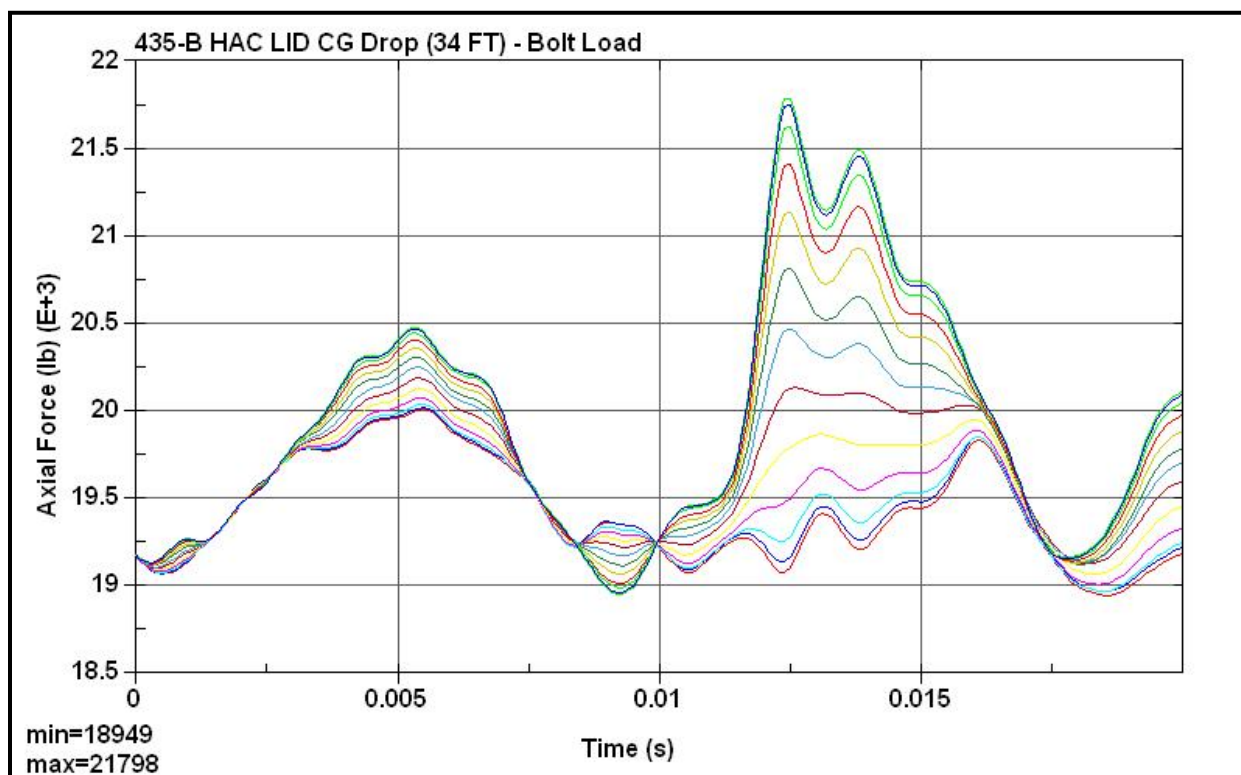


Figure 2.12.4-35 – D3 Benchmark Final State

**Figure 2.12.4-36 – D3 Benchmark Lower Bell Acceleration****Figure 2.12.4-37 – D3 Benchmark Upper Bell Acceleration**

**Figure 2.12.4-38 – D3 Benchmark LTSS Acceleration****Figure 2.12.4-39 – D3 Benchmark Axial Bolt Force**

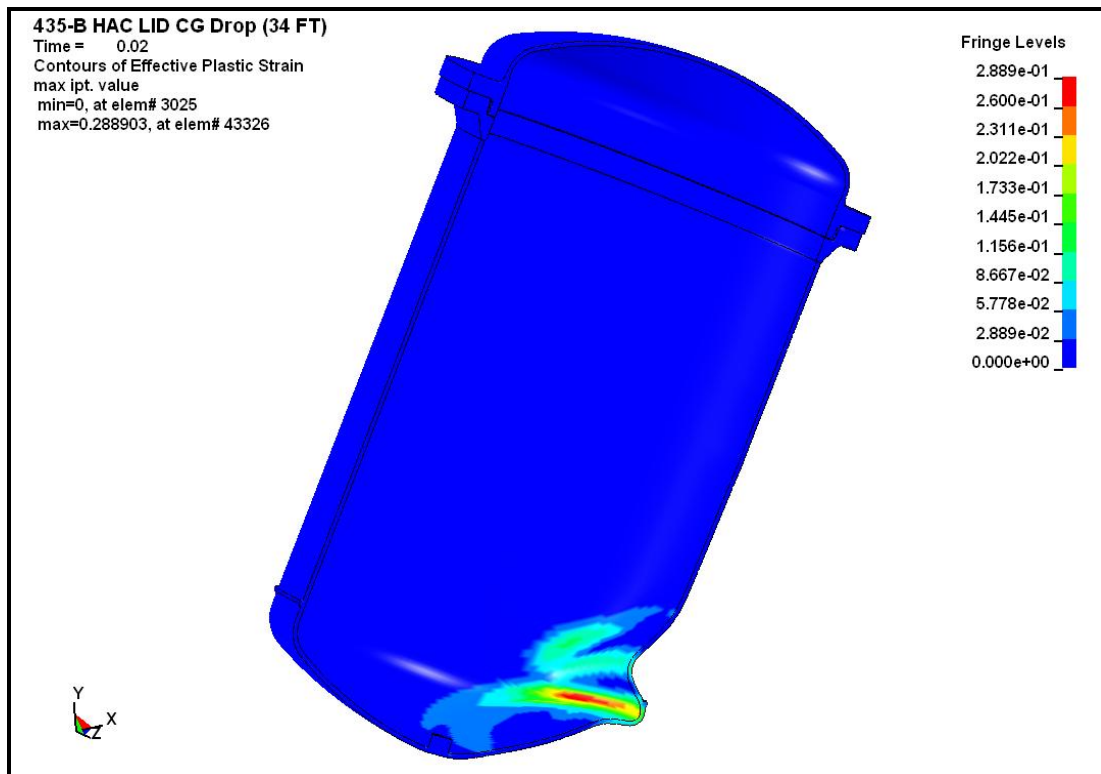


Figure 2.12.4-40 – D3 Benchmark Containment Boundary Cumulative Effective Plastic Strain

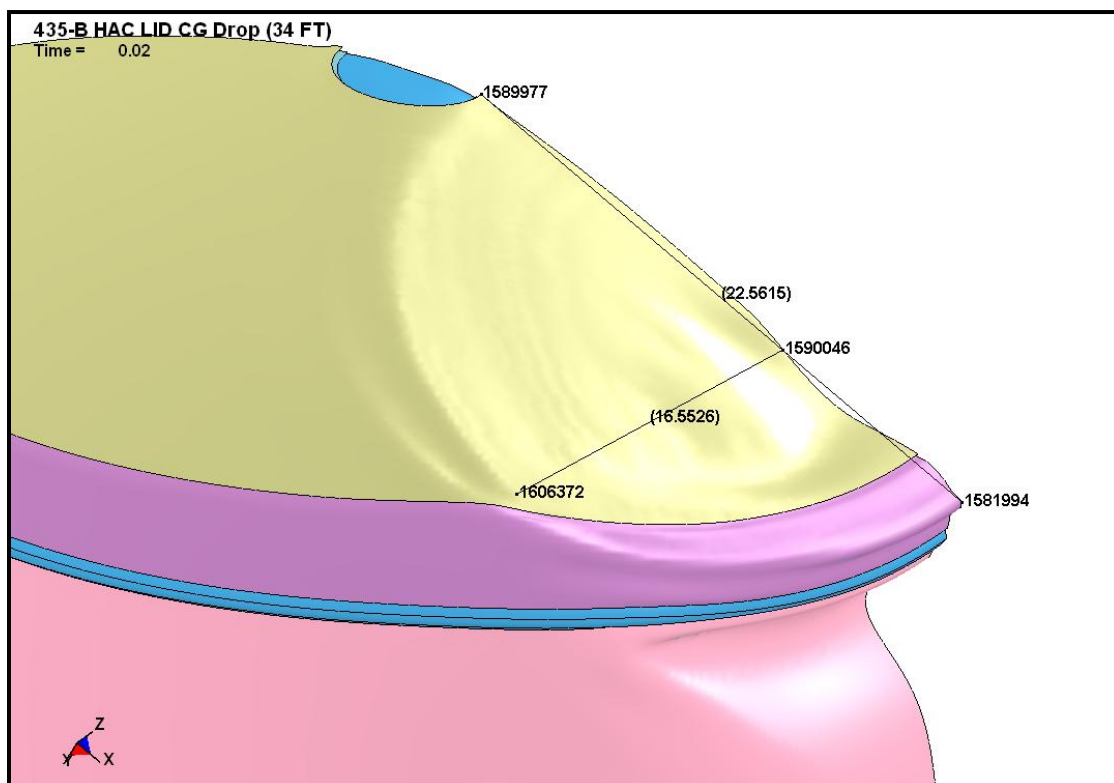


Figure 2.12.4-41 – D3 Benchmark Upper Impact Patch

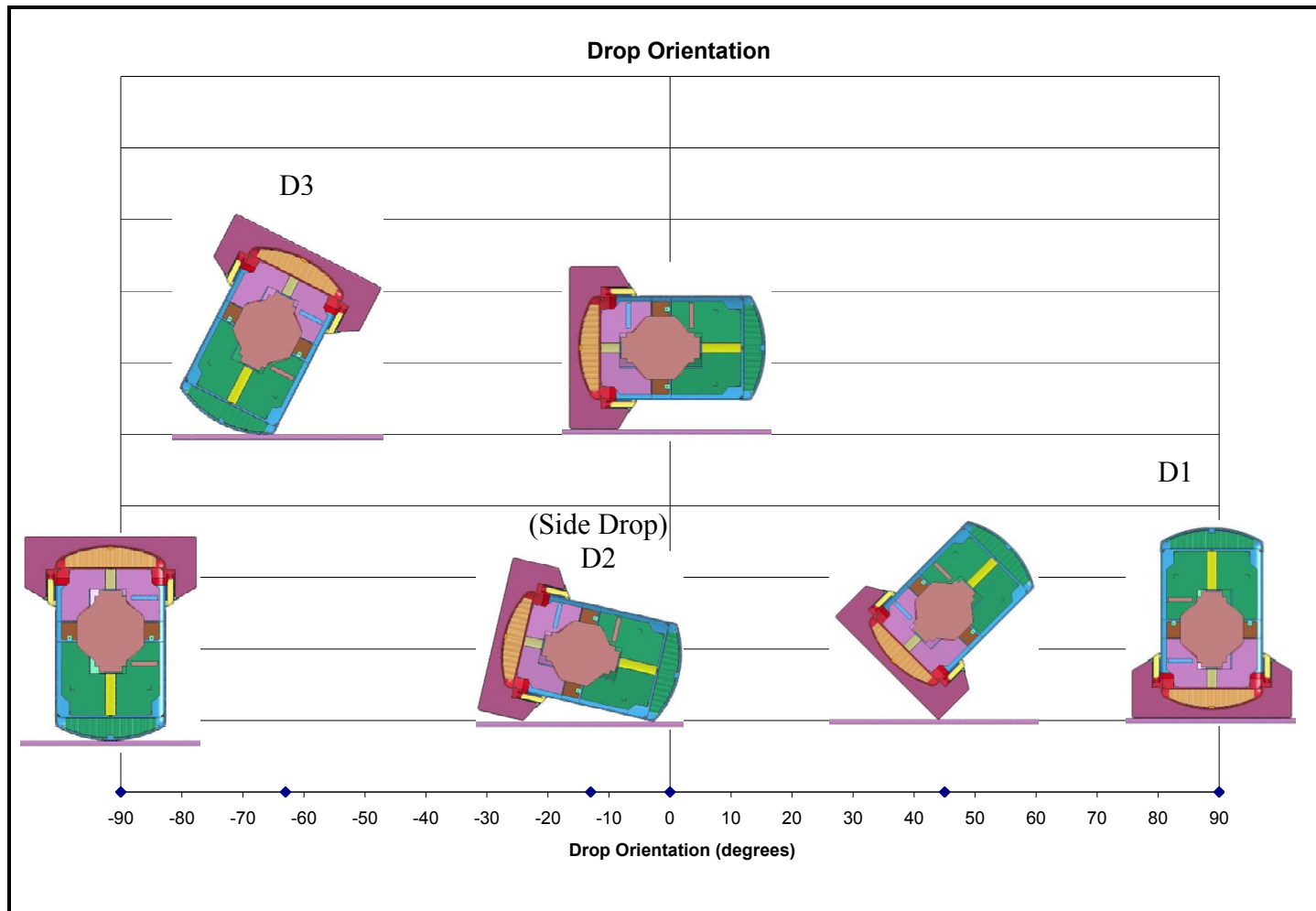


Figure 2.12.4-42 – Drop Orientation Terminology (Sampling of Orientations Only)

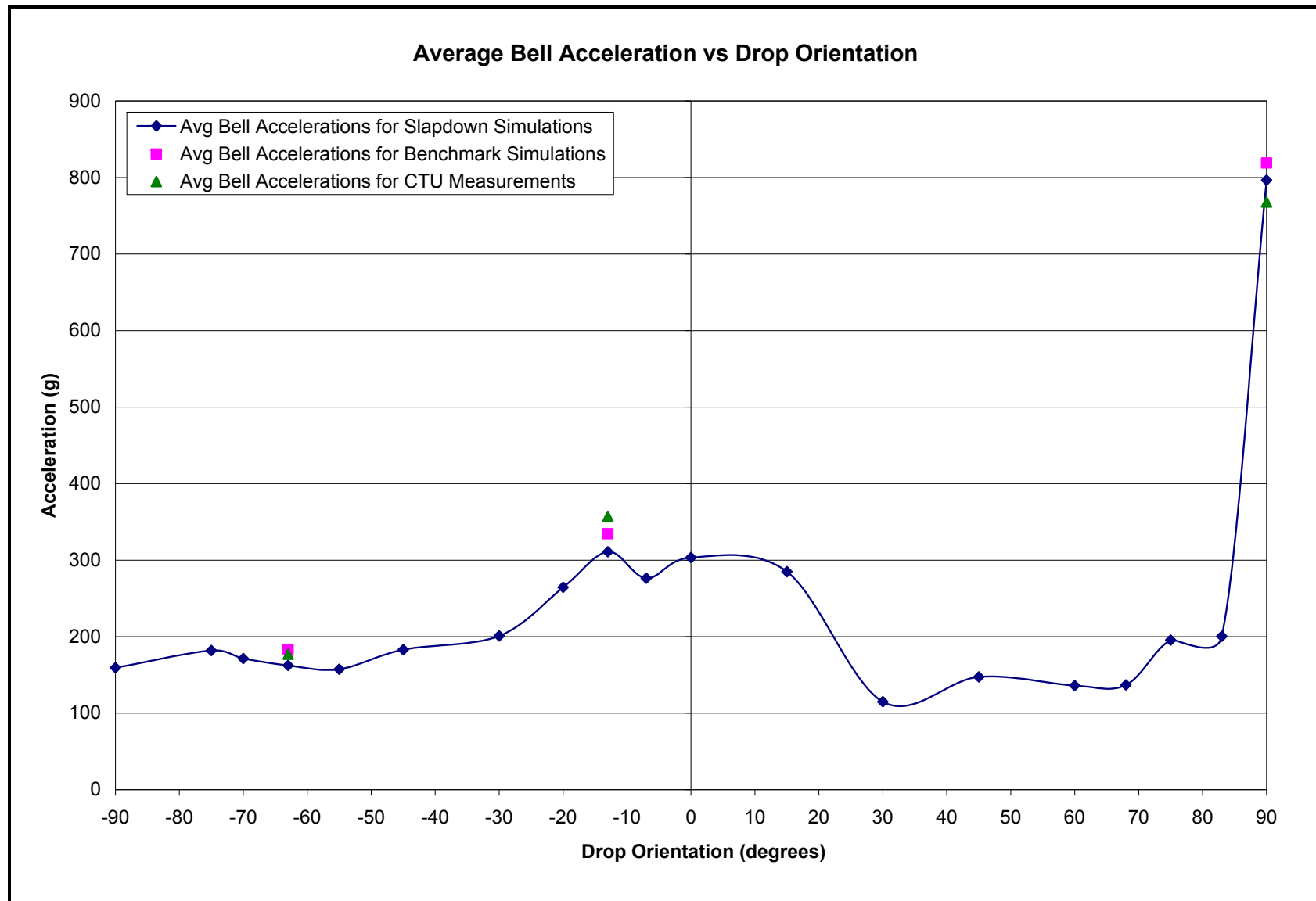
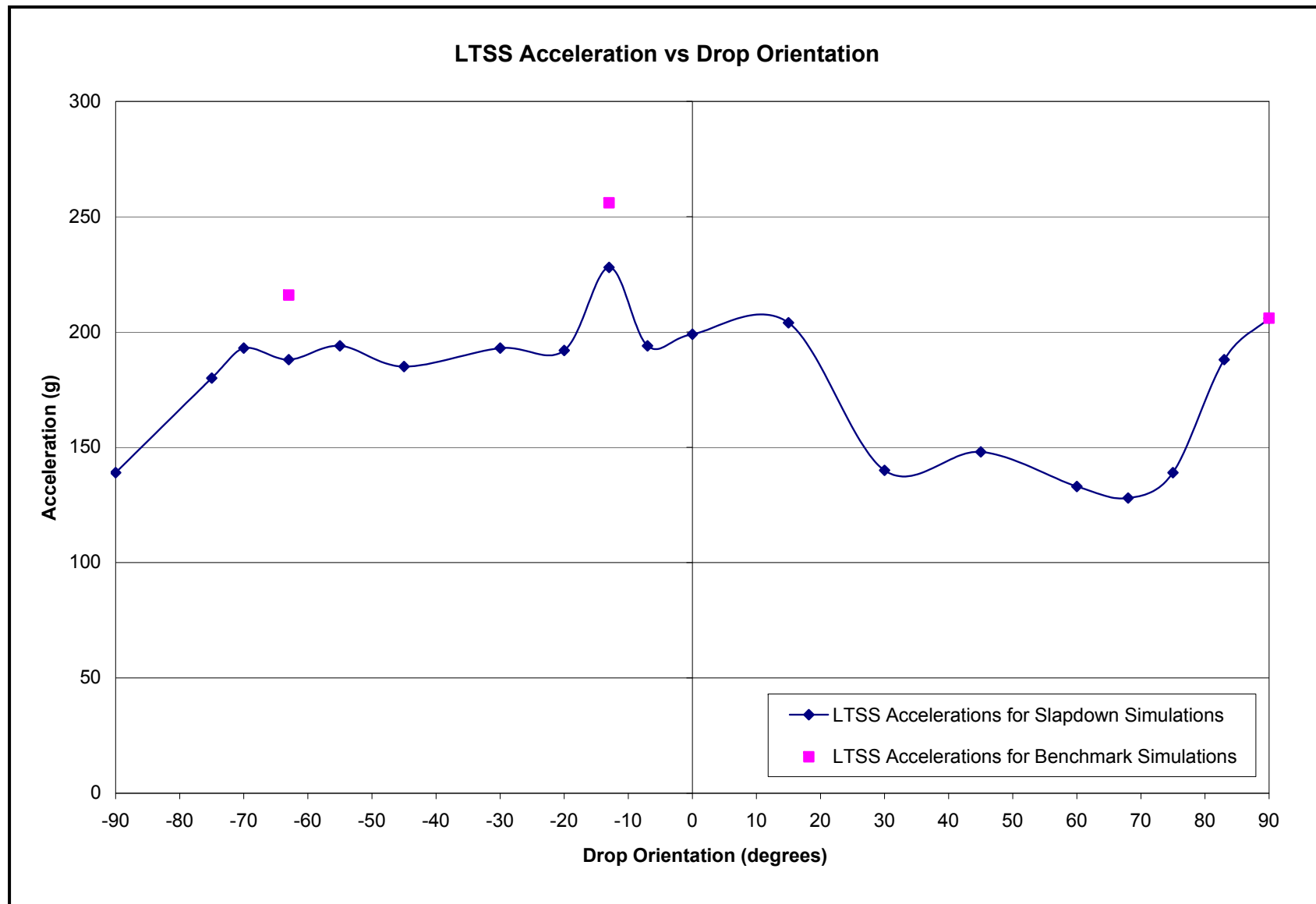


Figure 2.12.4-43 – Average Bell Acceleration vs Drop Orientation

**Figure 2.12.4-44** – LTSS Acceleration vs Drop Orientation

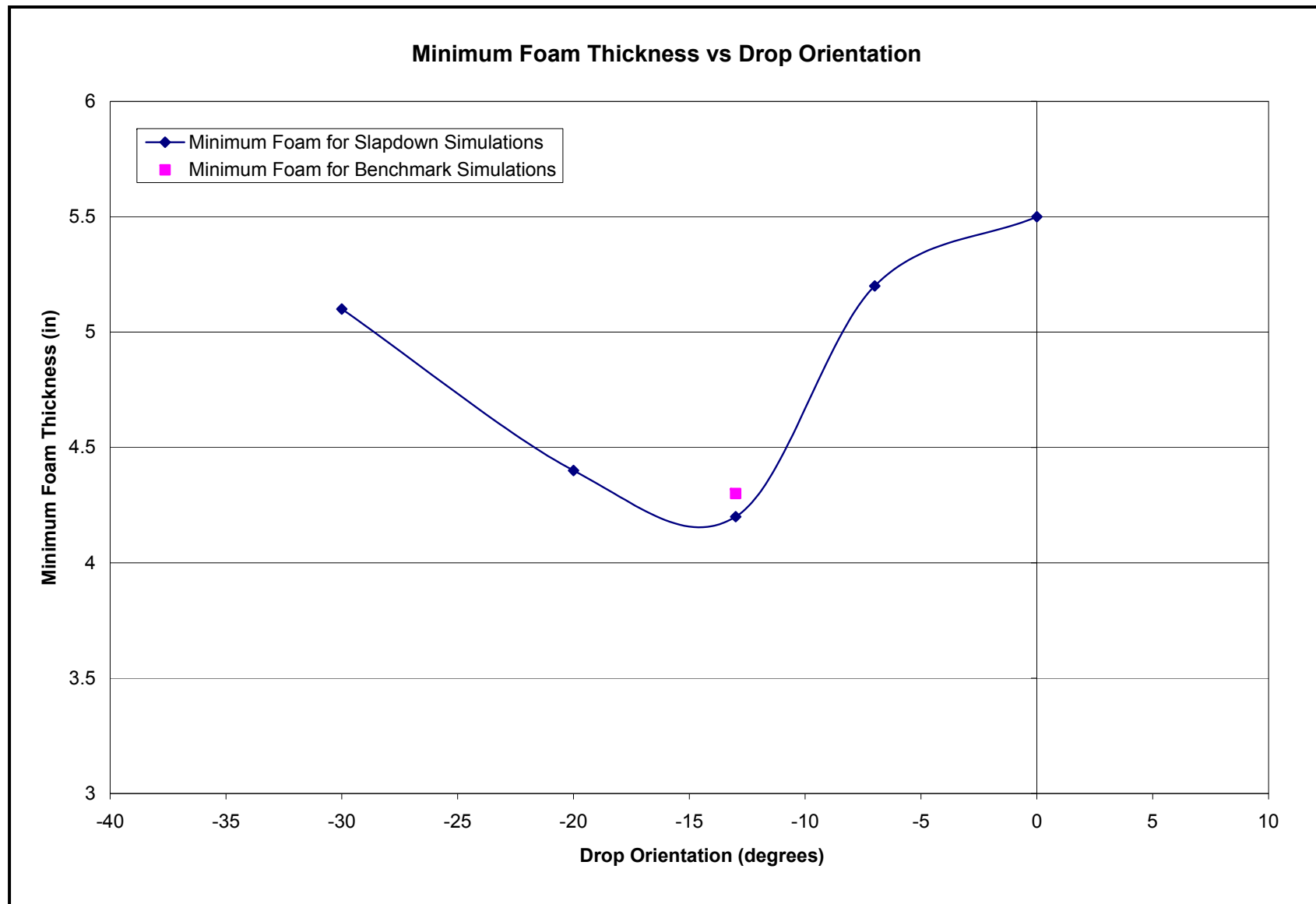


Figure 2.12.4-45 – Minimum Foam Thickness vs Drop Orientation

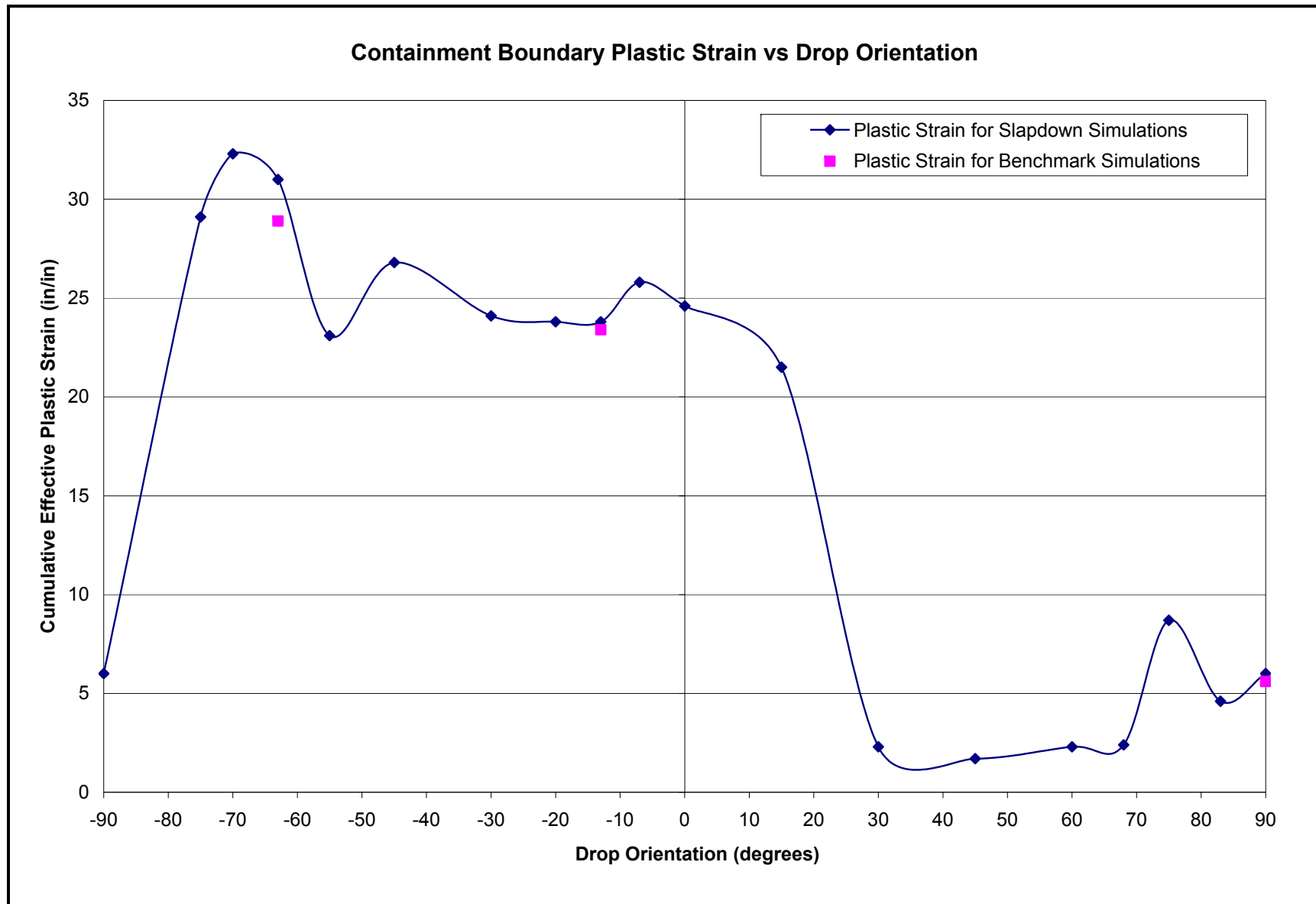


Figure 2.12.4-46 – Containment Boundary Plastic Strain vs Drop Orientation

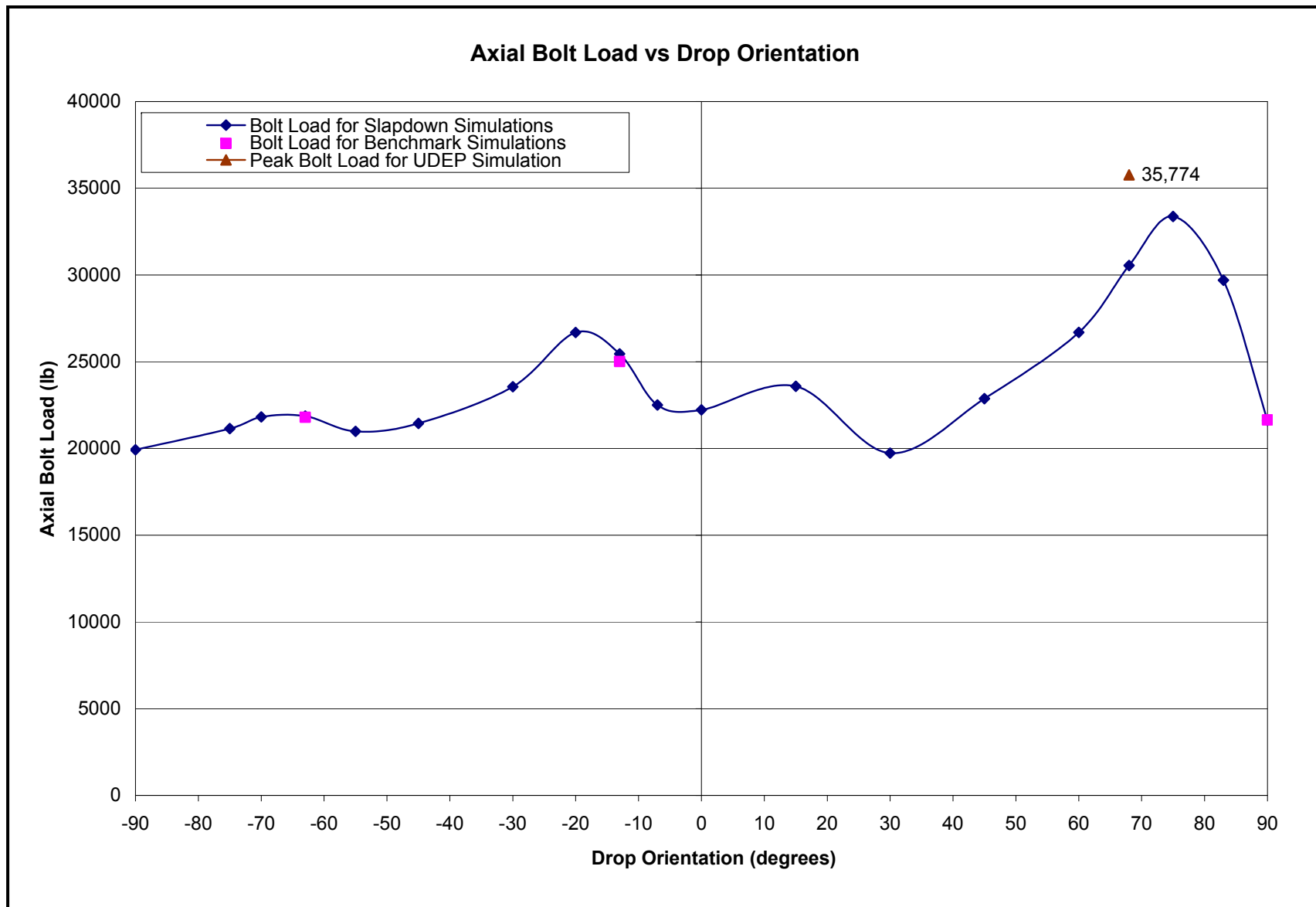


Figure 2.12.4-47 – Axial Bolt Load vs Drop Orientation

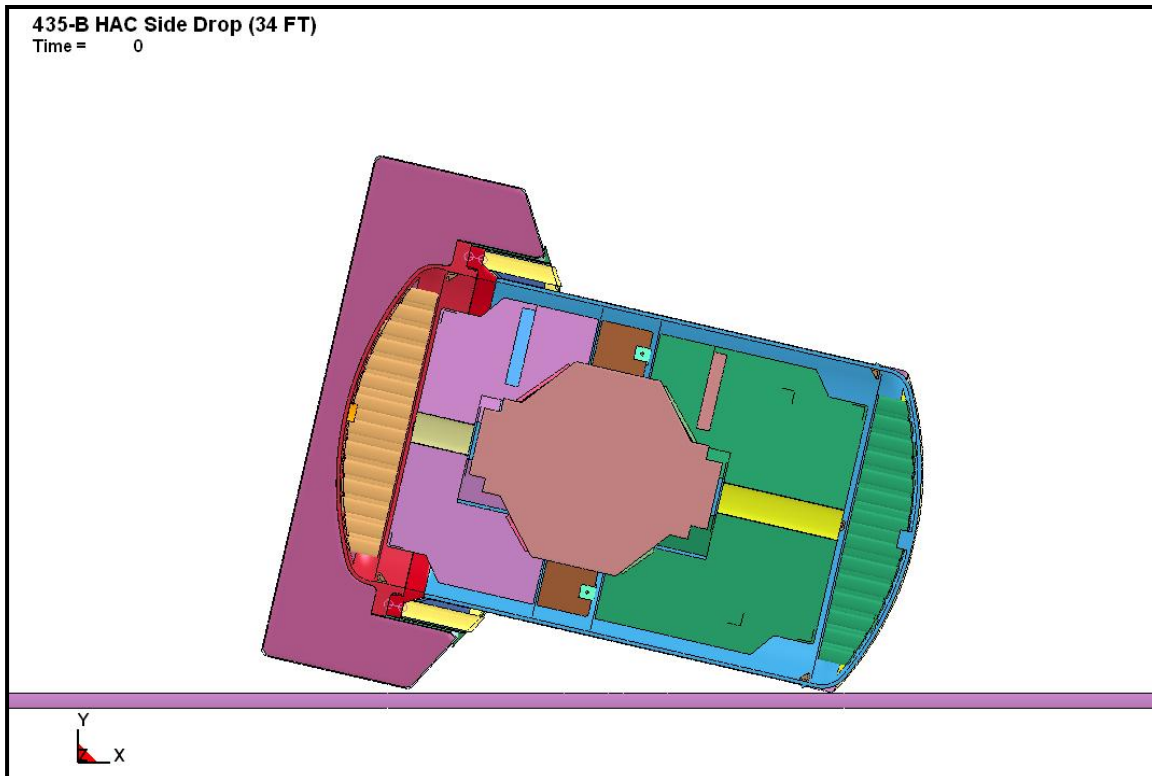


Figure 2.12.4-48 – Simultaneous Side Drop Initial State

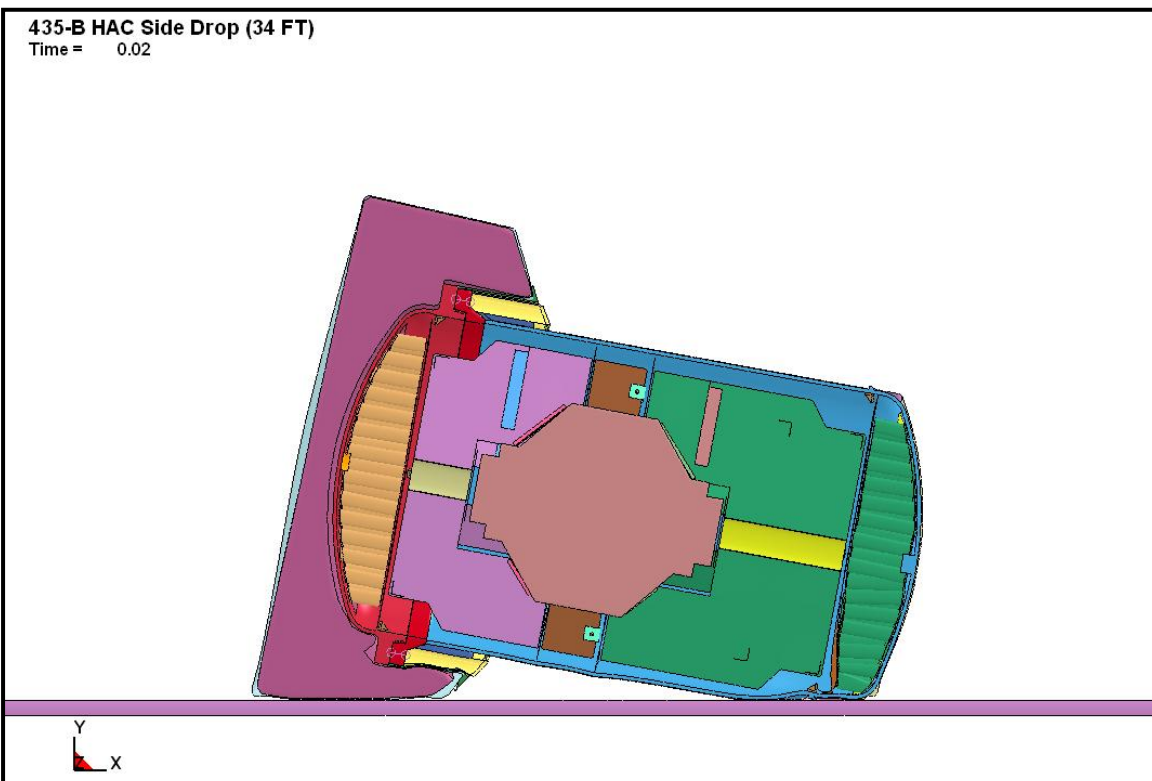


Figure 2.12.4-49 – Simultaneous Side Drop Final State

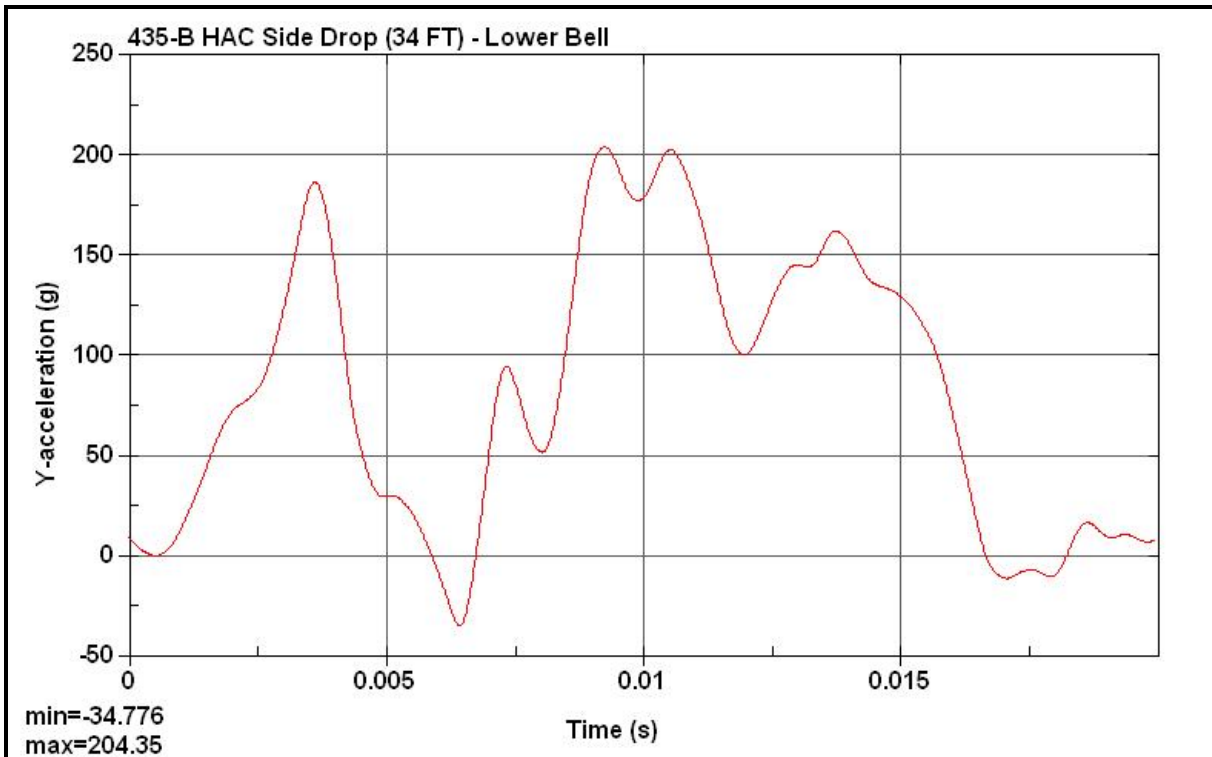


Figure 2.12.4-50 – Simultaneous Side Drop Lower Bell Acceleration

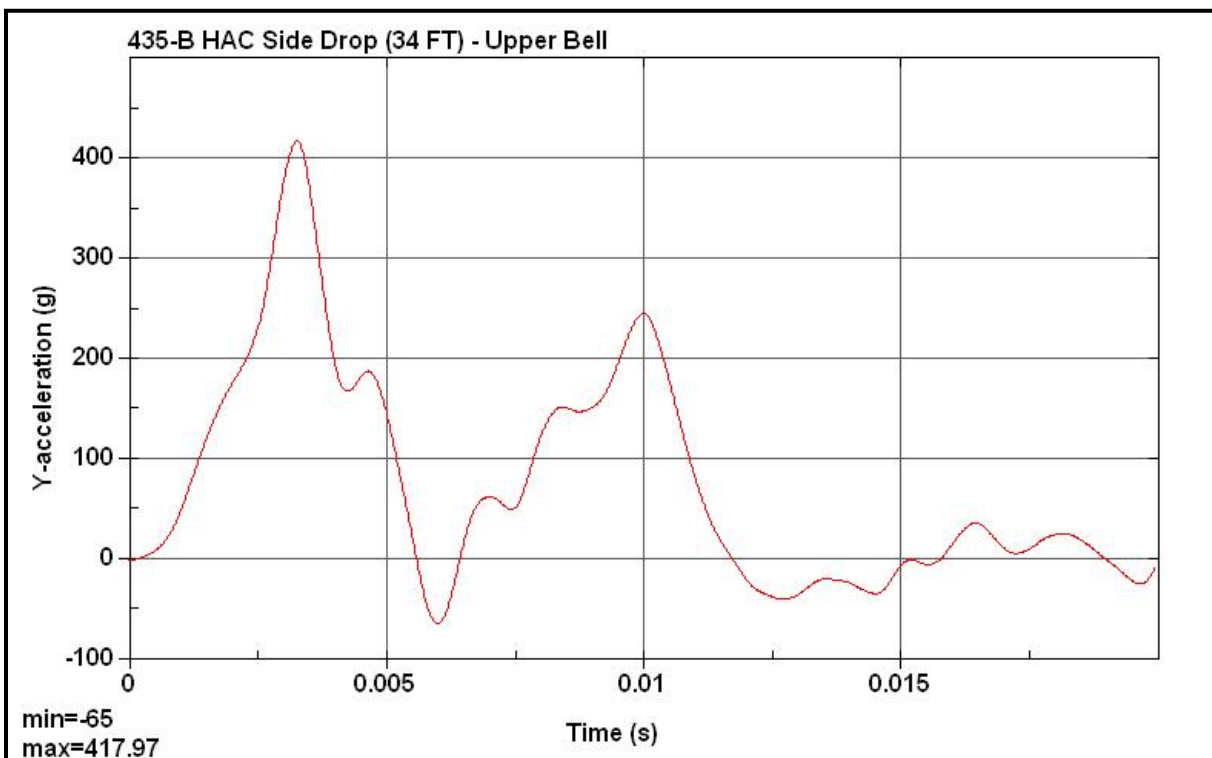


Figure 2.12.4-51 – Simultaneous Side Drop Upper Bell Acceleration

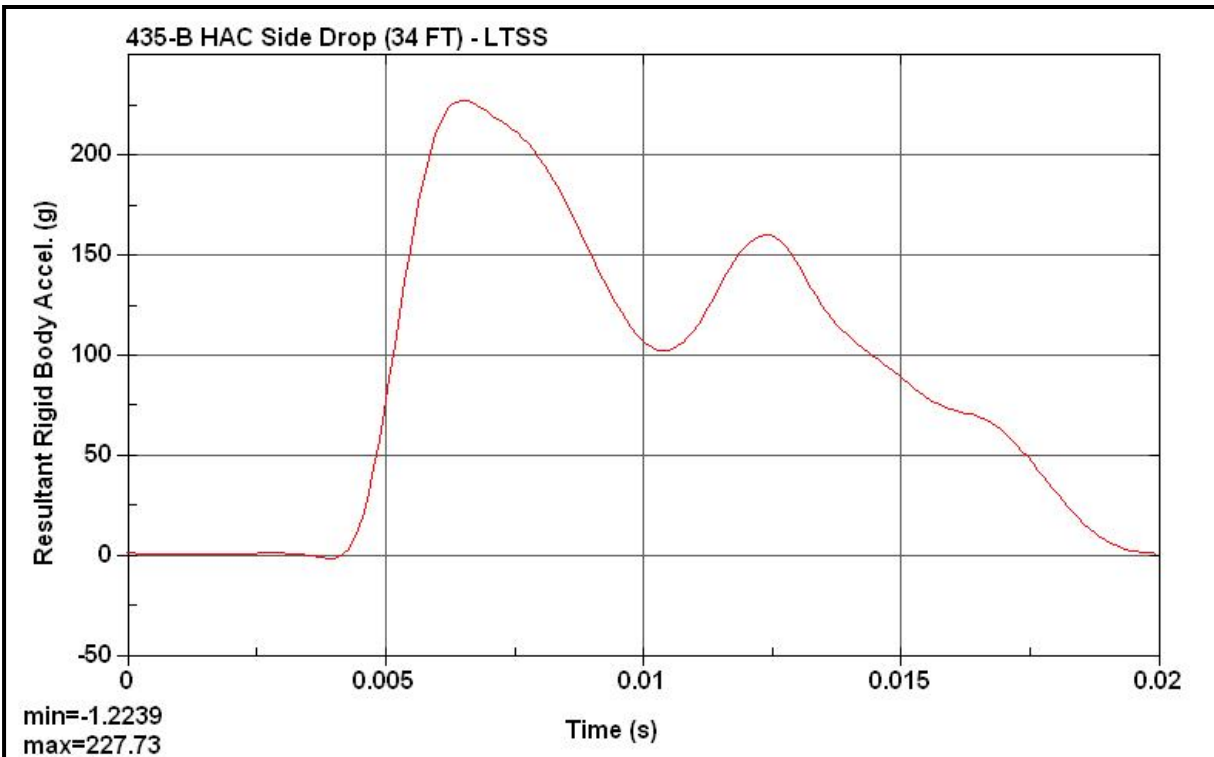


Figure 2.12.4-52 – Simultaneous Side Drop LTSS Acceleration

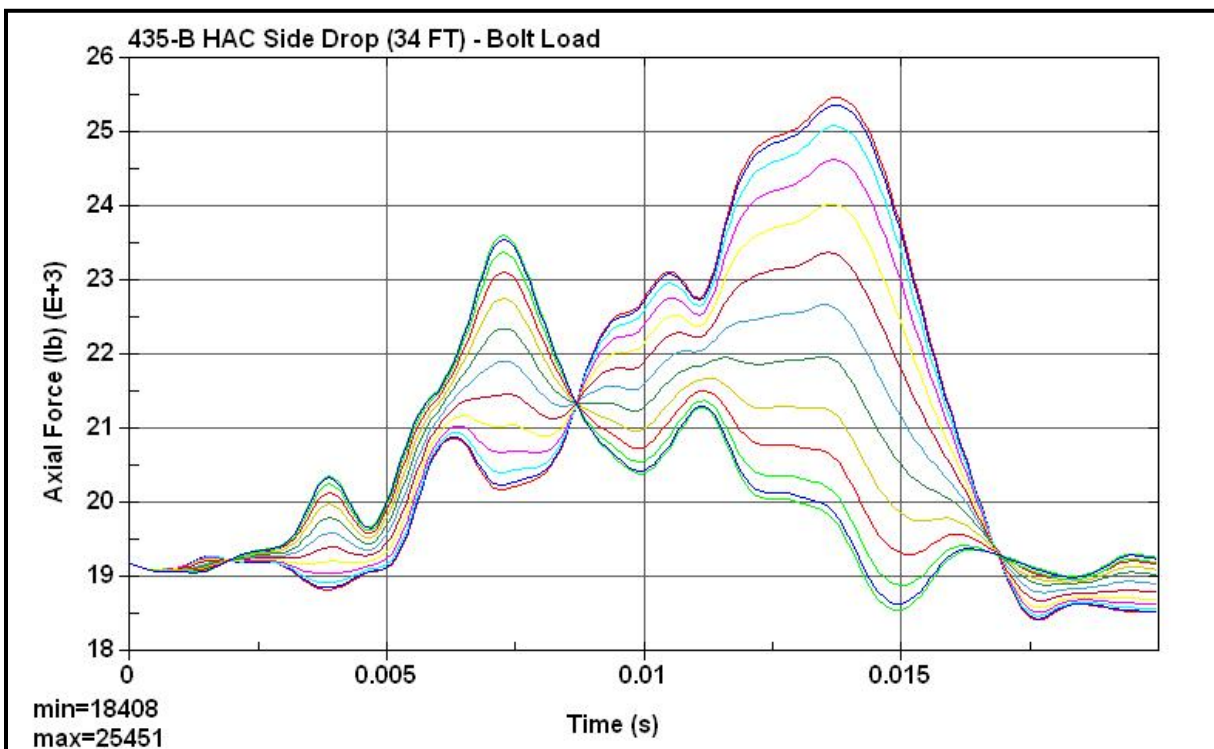


Figure 2.12.4-53 – Simultaneous Side Drop Axial Bolt Force

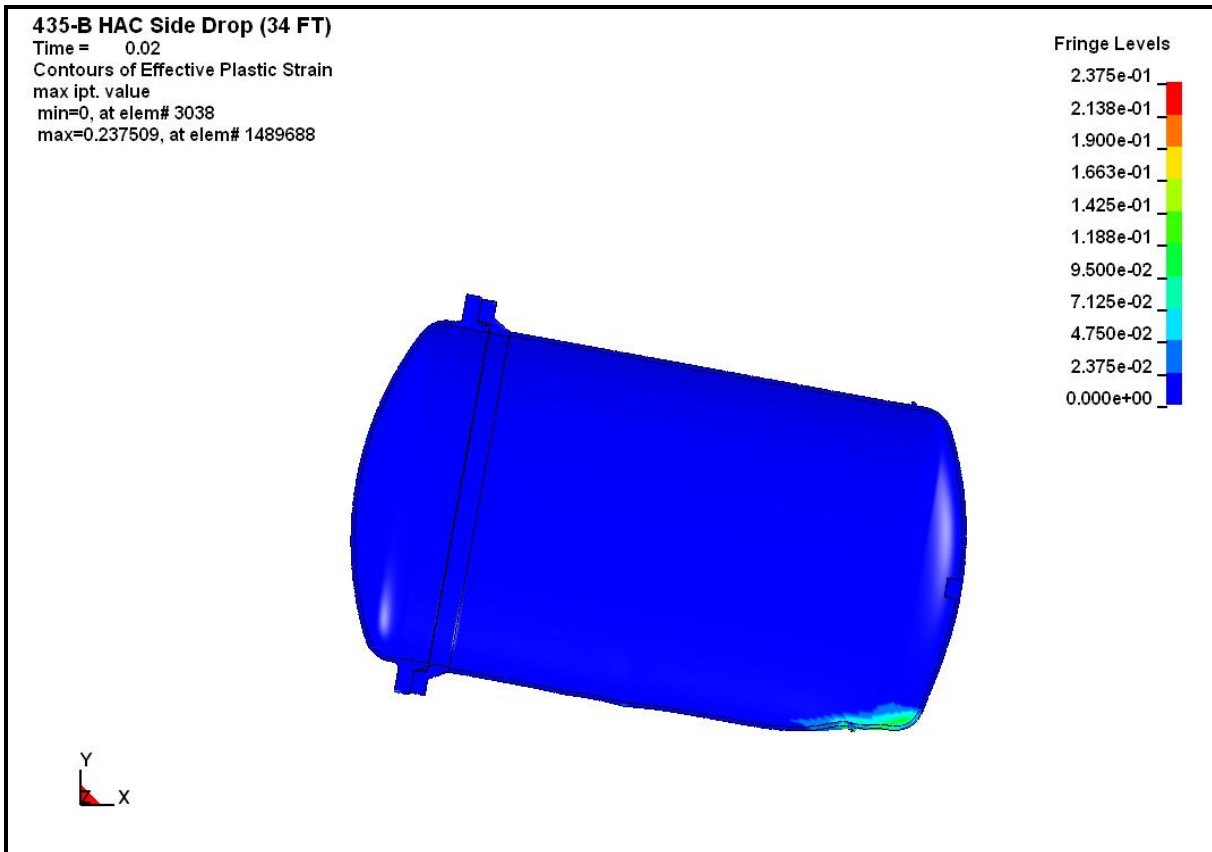
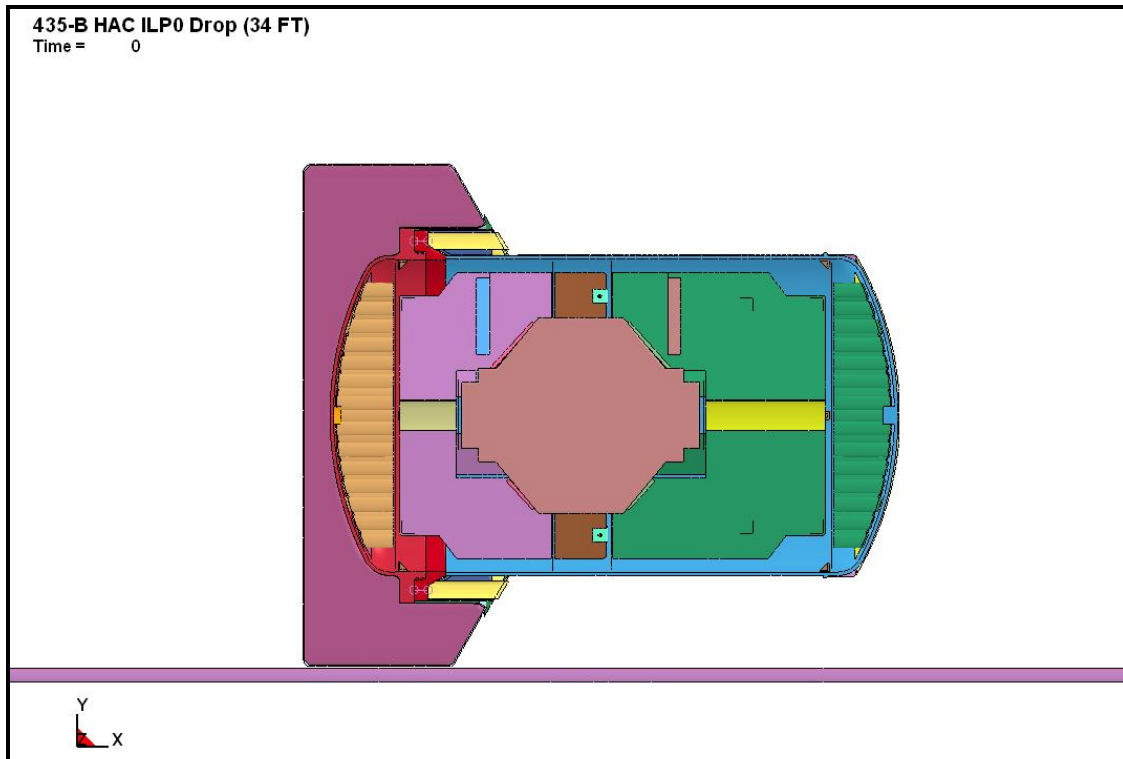
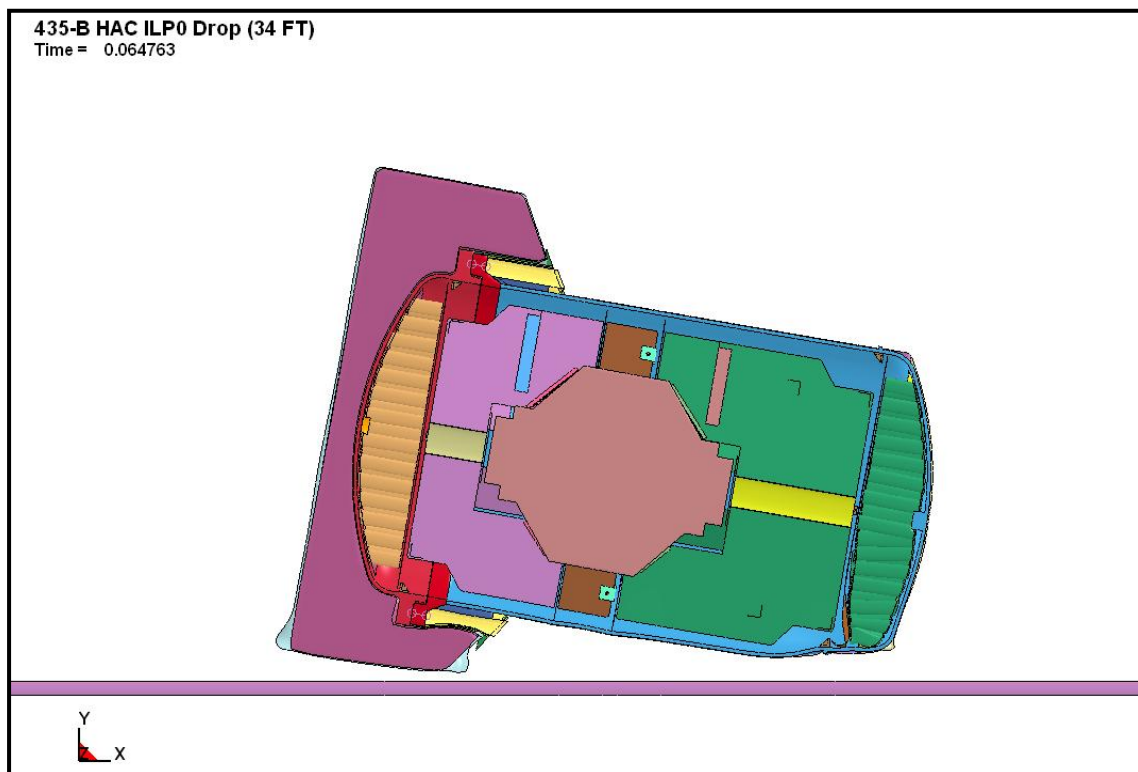
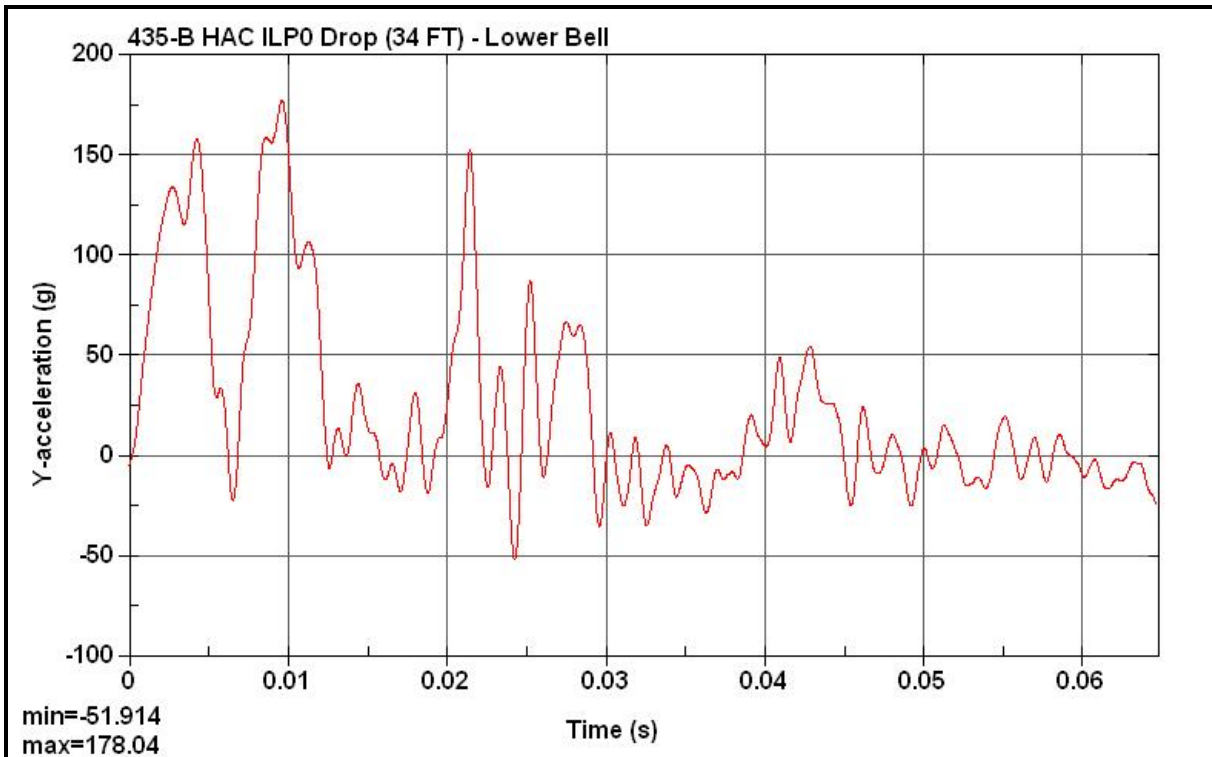
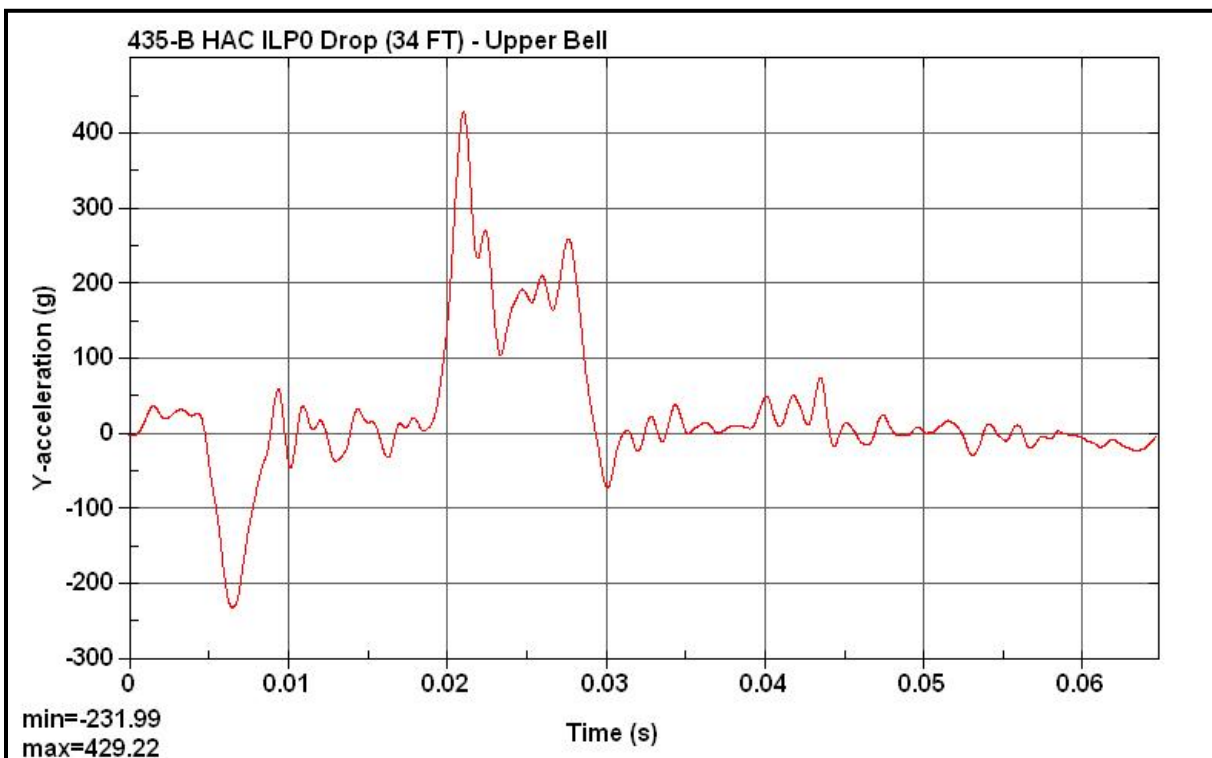
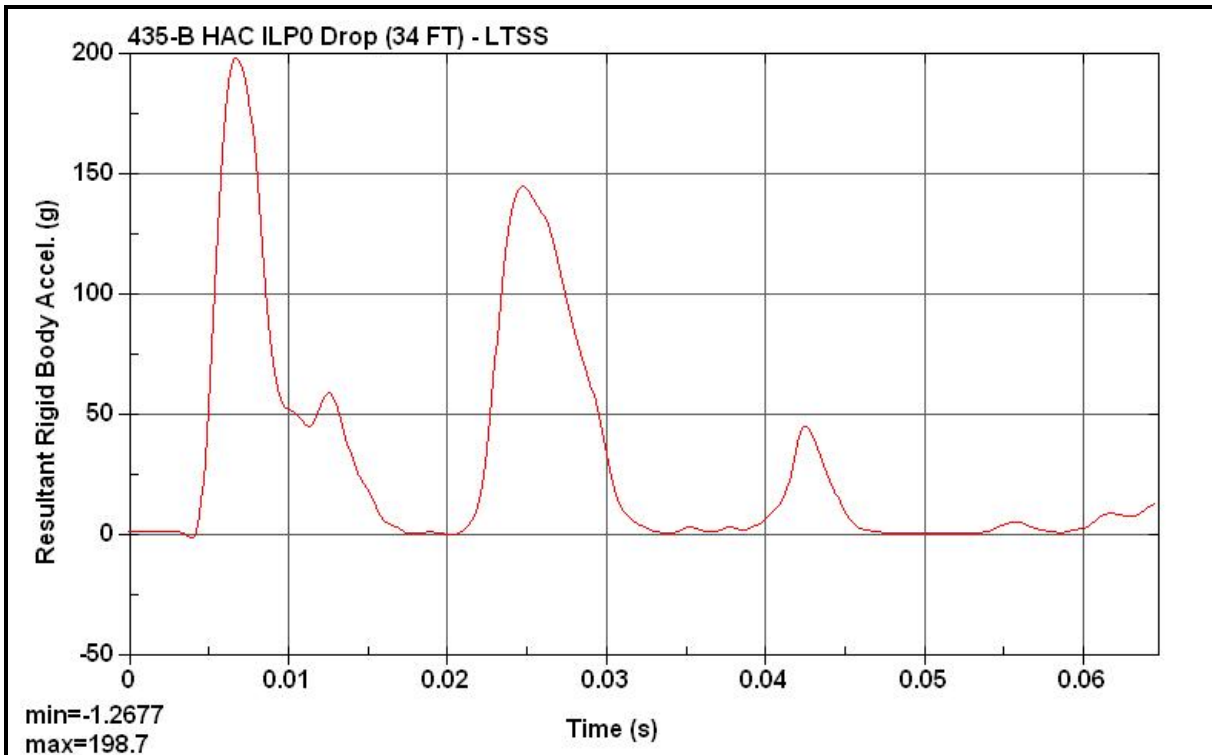
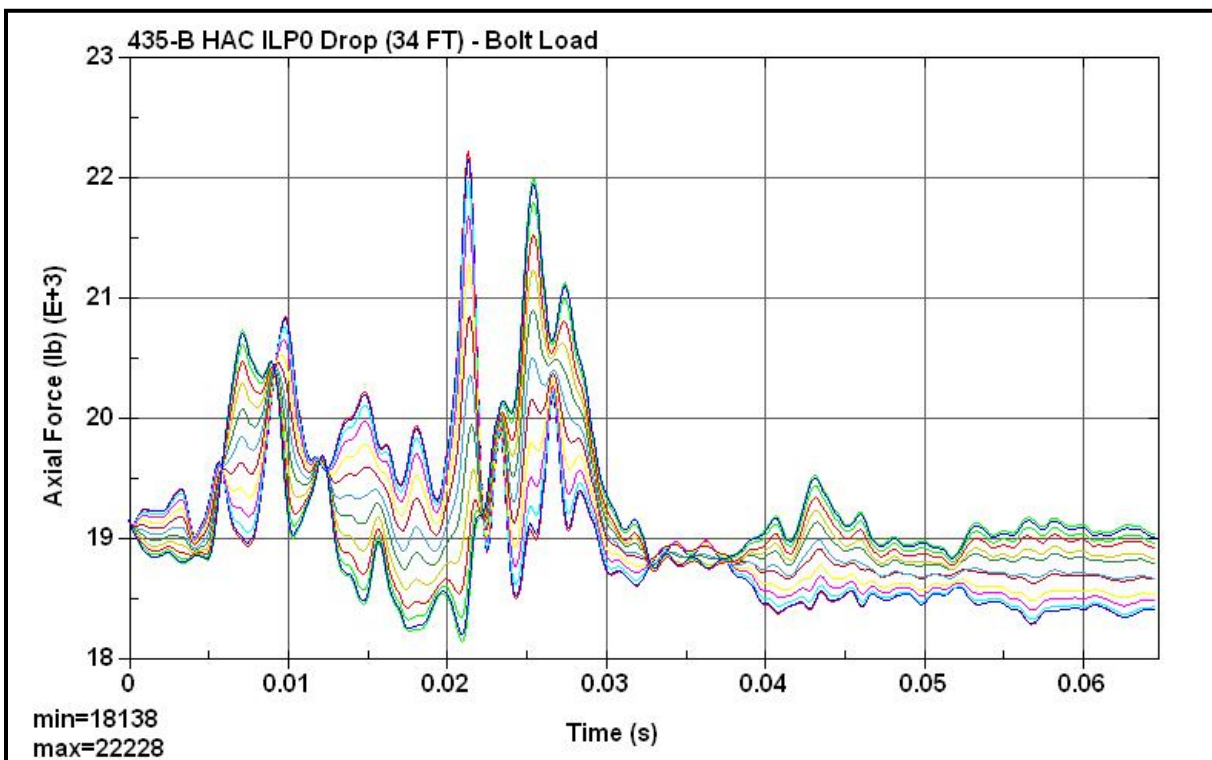


Figure 2.12.4-54 – Simultaneous Side Drop Containment Boundary Cumulative Effective Plastic Strain

**Figure 2.12.4-55 – ILP0 Initial State****Figure 2.12.4-56 – ILP0 Final State**

**Figure 2.12.4-57 – ILP0 Lower Bell Acceleration****Figure 2.12.4-58 – ILP0 Upper Bell Acceleration**

**Figure 2.12.4-59 – ILP0 LTSS Acceleration****Figure 2.12.4-60 – ILP0 Axial Bolt Force**

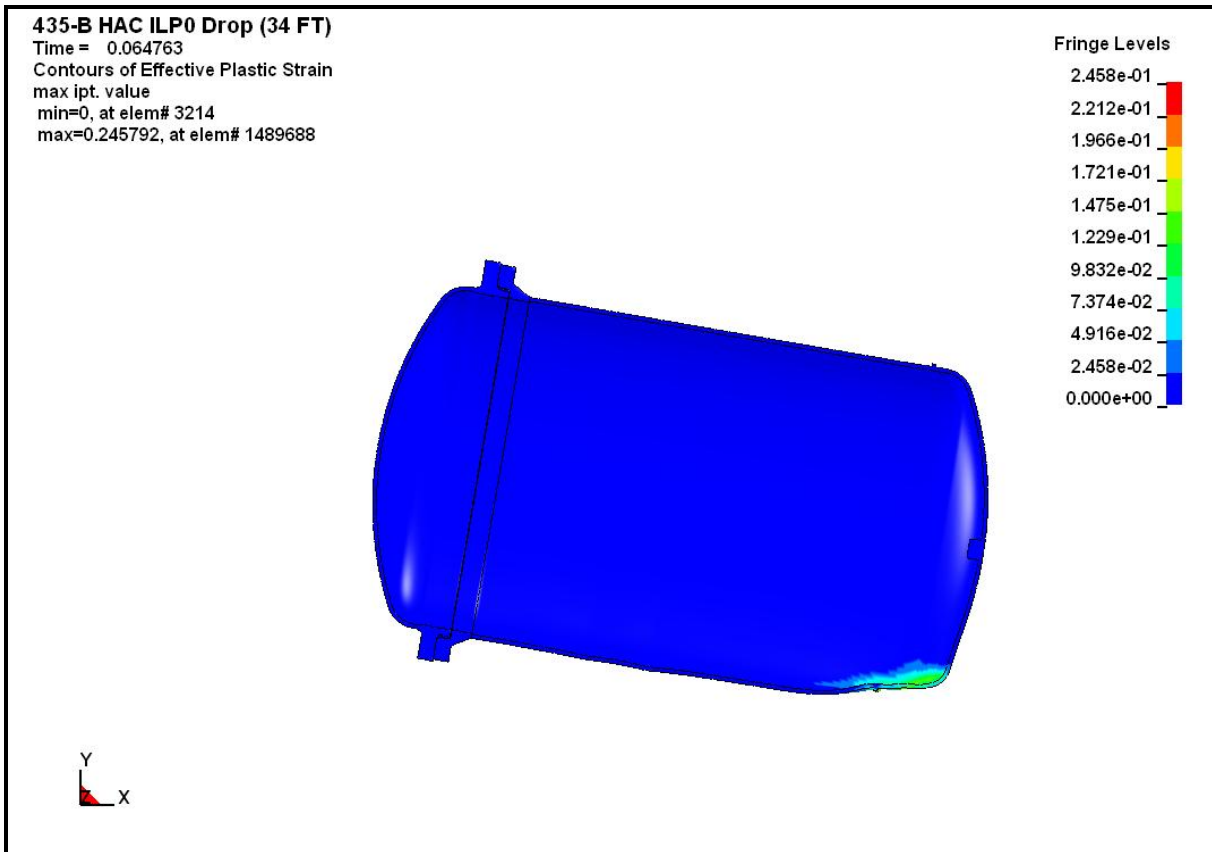


Figure 2.12.4-61 – ILP0 Containment Boundary Cumulative Effective Plastic Strain

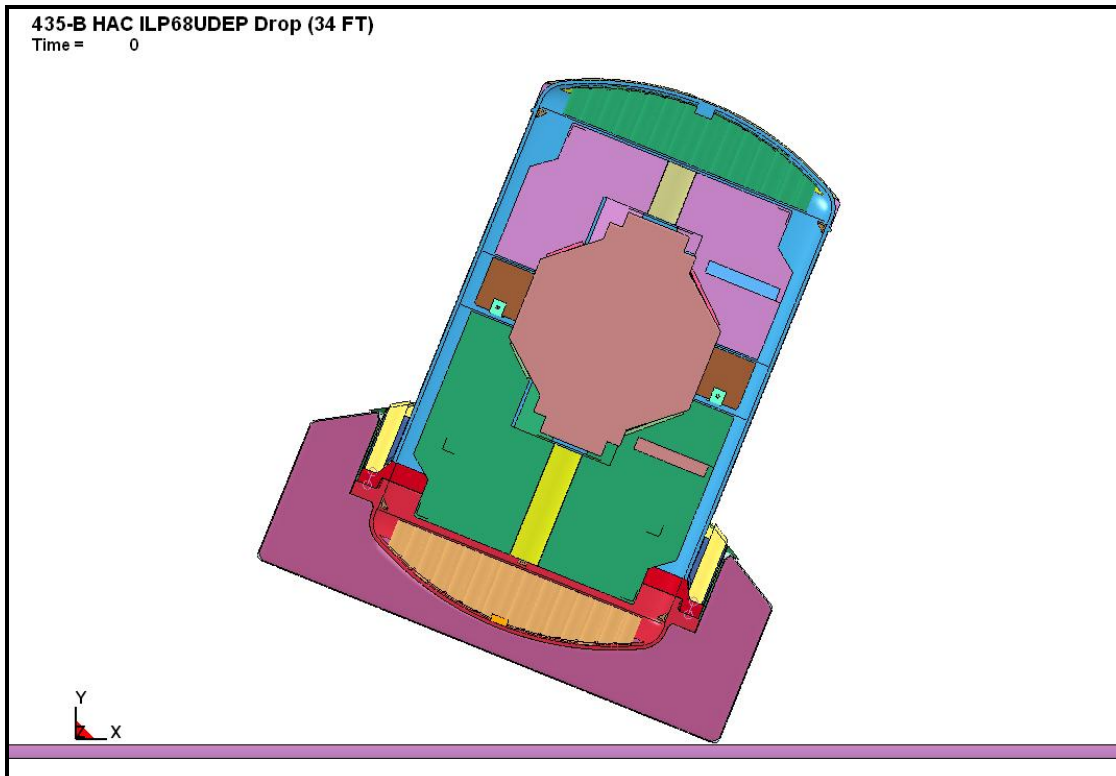


Figure 2.12.4-62 – ILP68UDEP Initial State

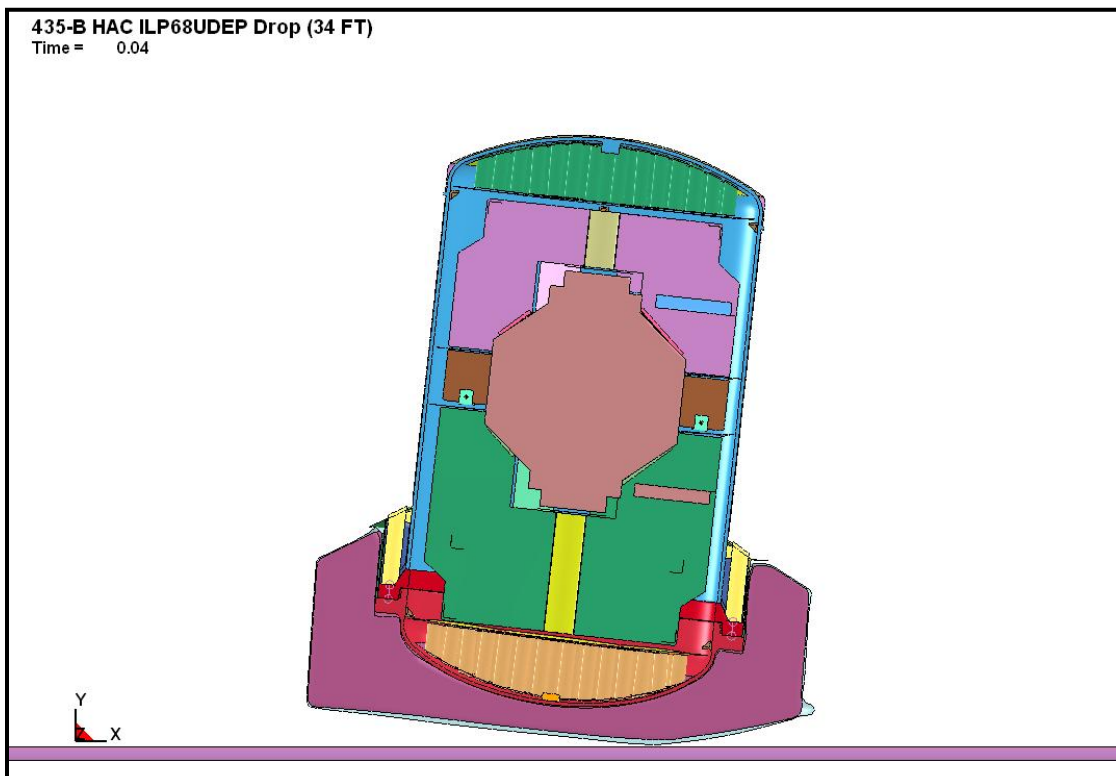
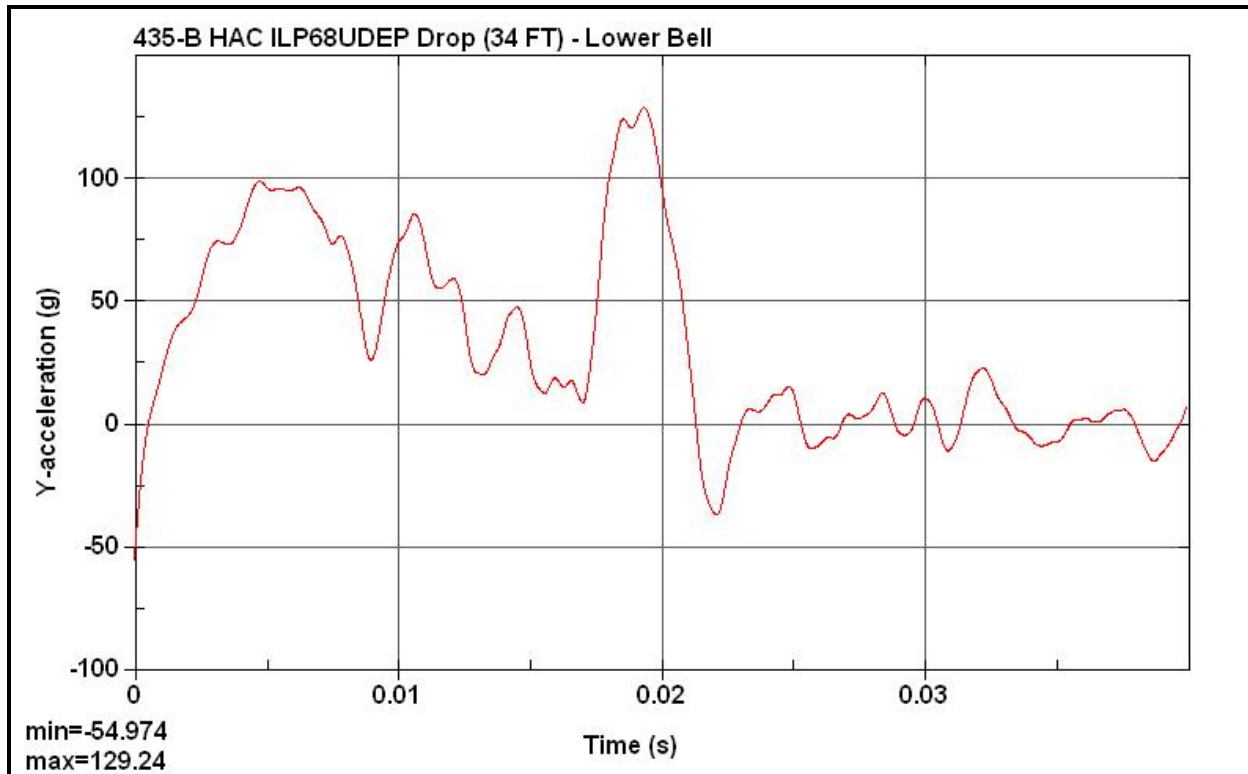
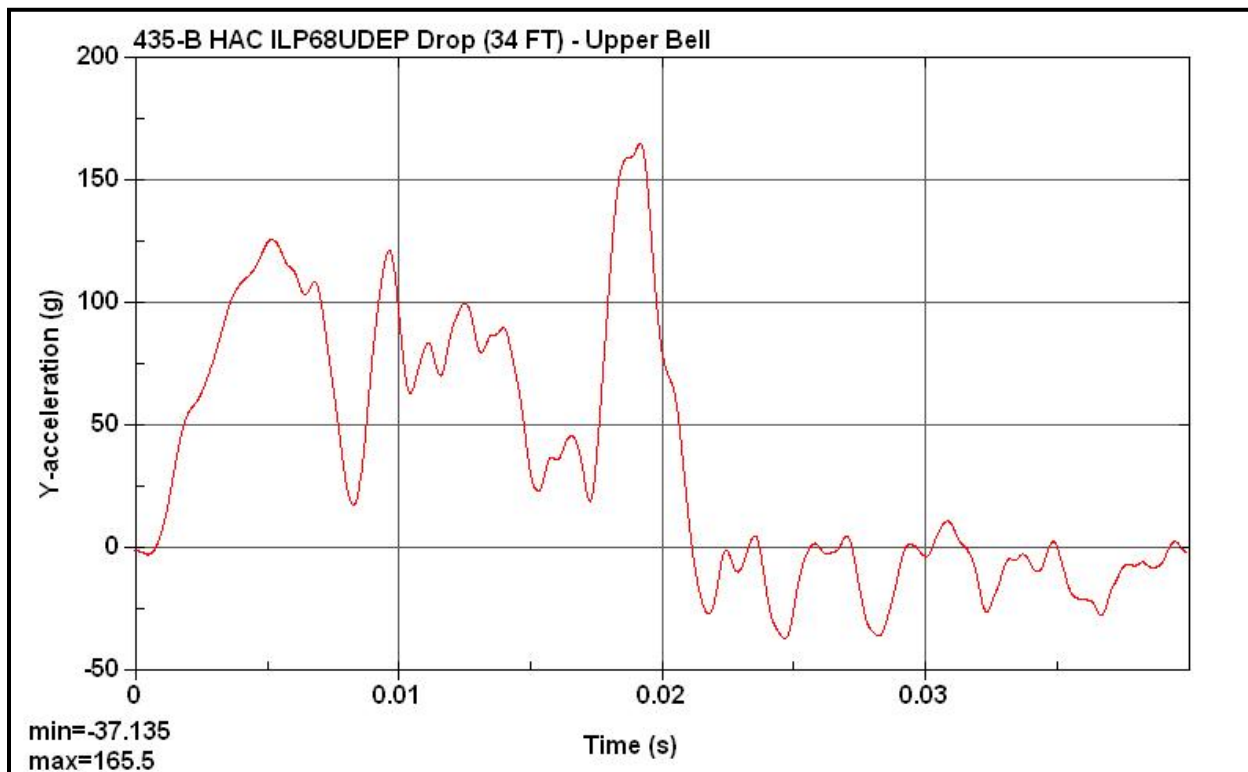
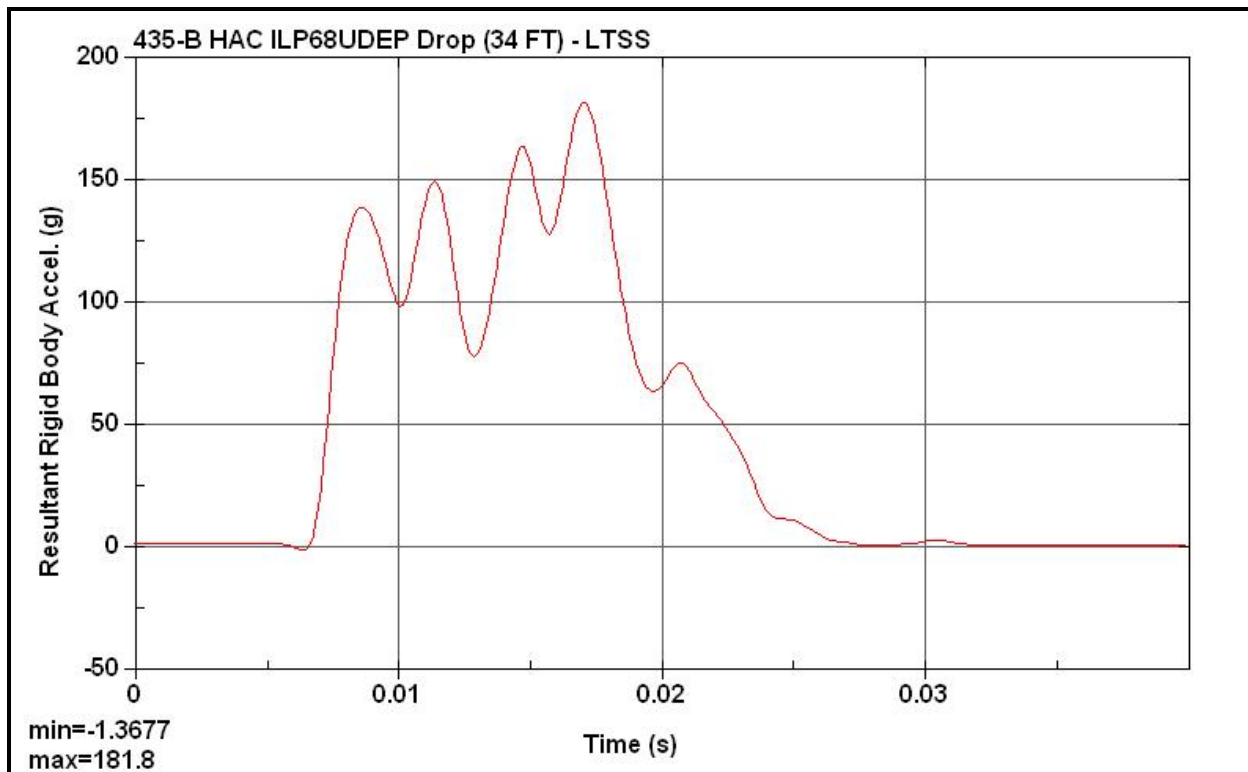
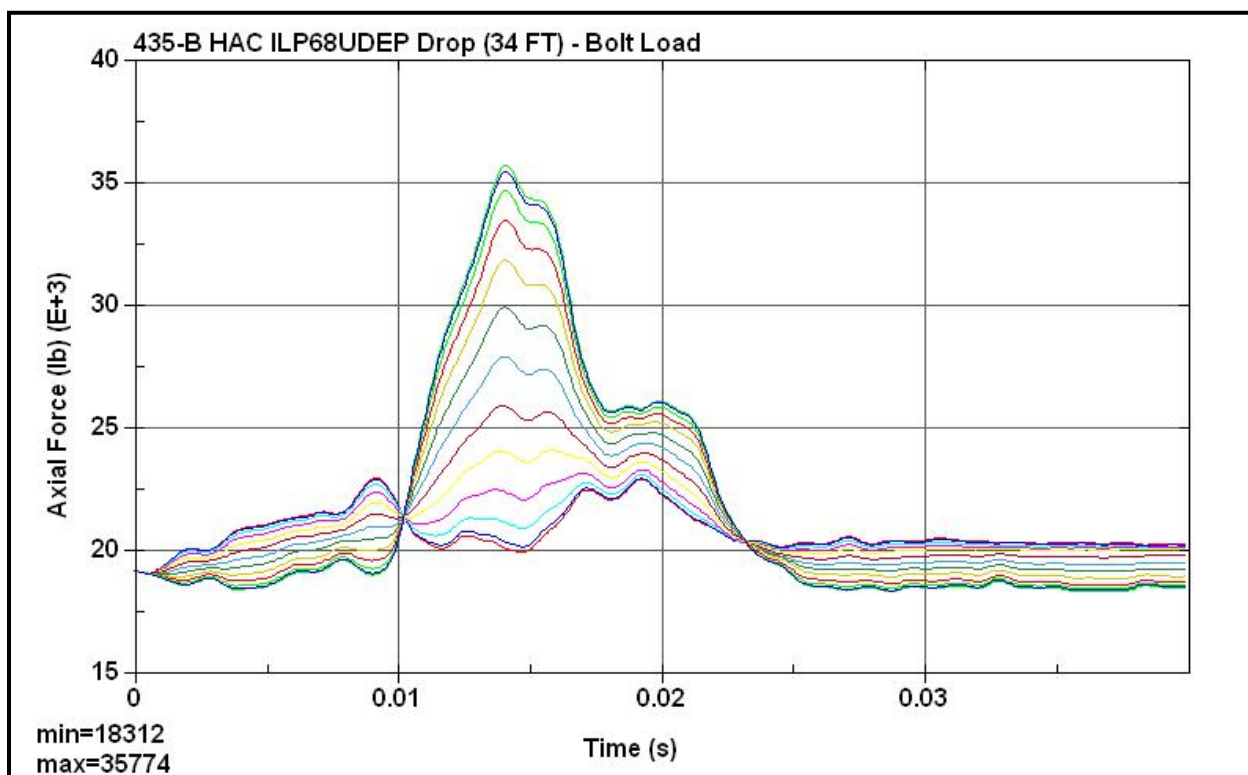


Figure 2.12.4-63 – ILP68UDEP Final State

**Figure 2.12.4-64 – ILP68UDEP Lower Bell Acceleration****Figure 2.12.4-65 – ILP68UDEP Upper Bell Acceleration**

**Figure 2.12.4-66 – ILP68UDEP LTSS Acceleration****Figure 2.12.4-67 – ILP68UDEP Axial Bolt Force**

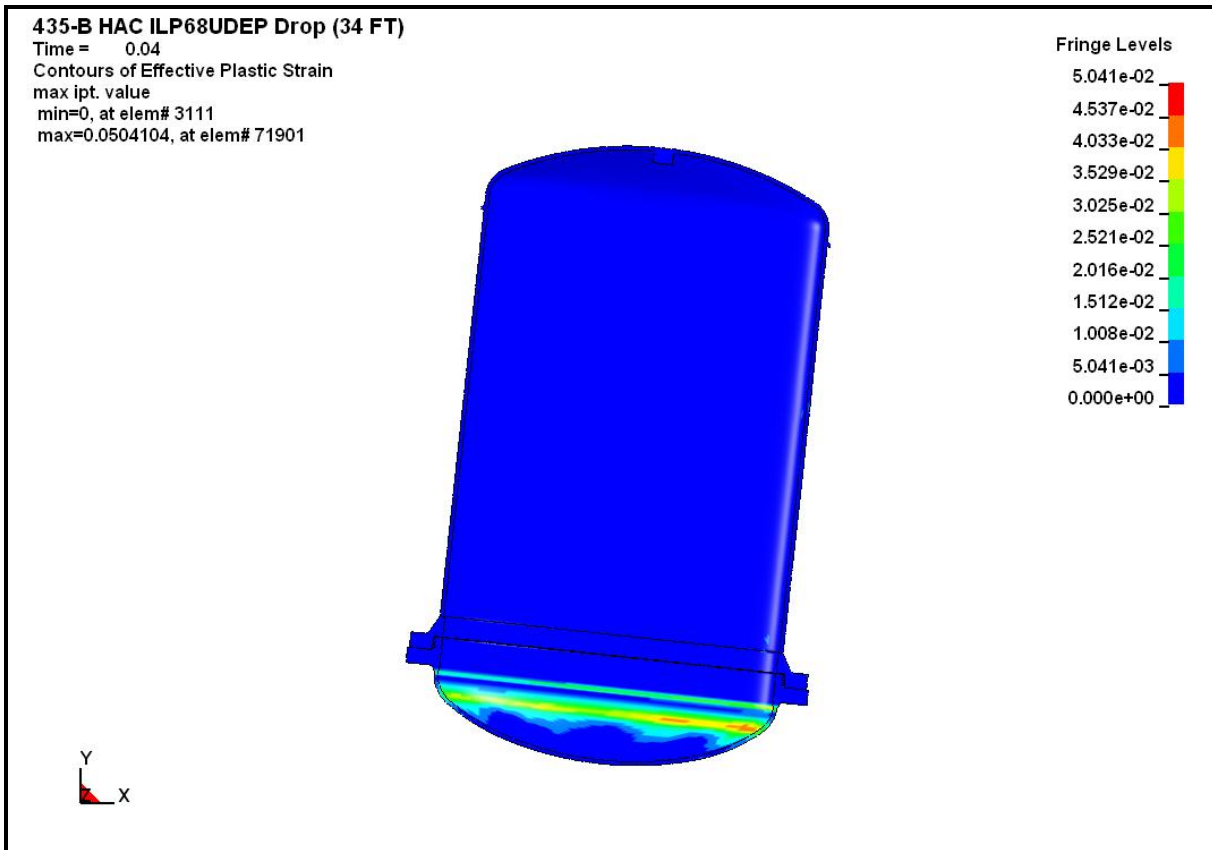


Figure 2.12.4-68 – ILP68UDEP Containment Boundary Cumulative Effective Plastic Strain

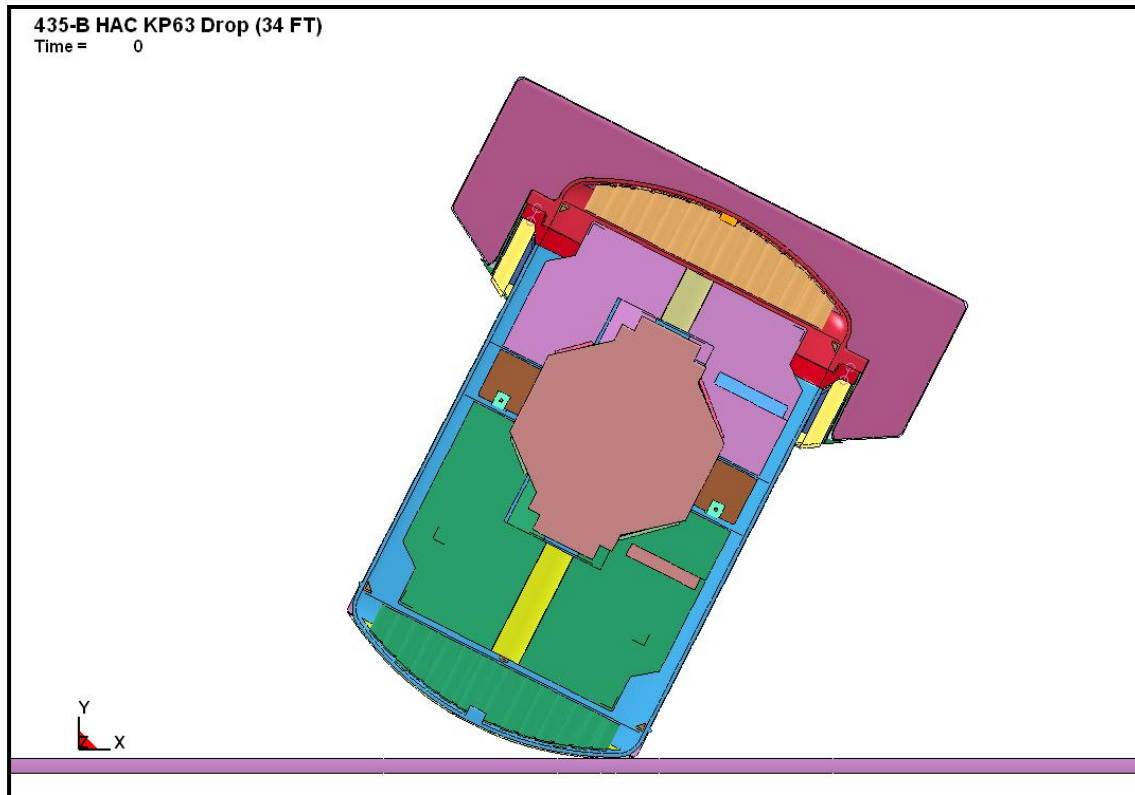


Figure 2.12.4-69 – KP63 (CG-over-Top Knuckle) Initial State

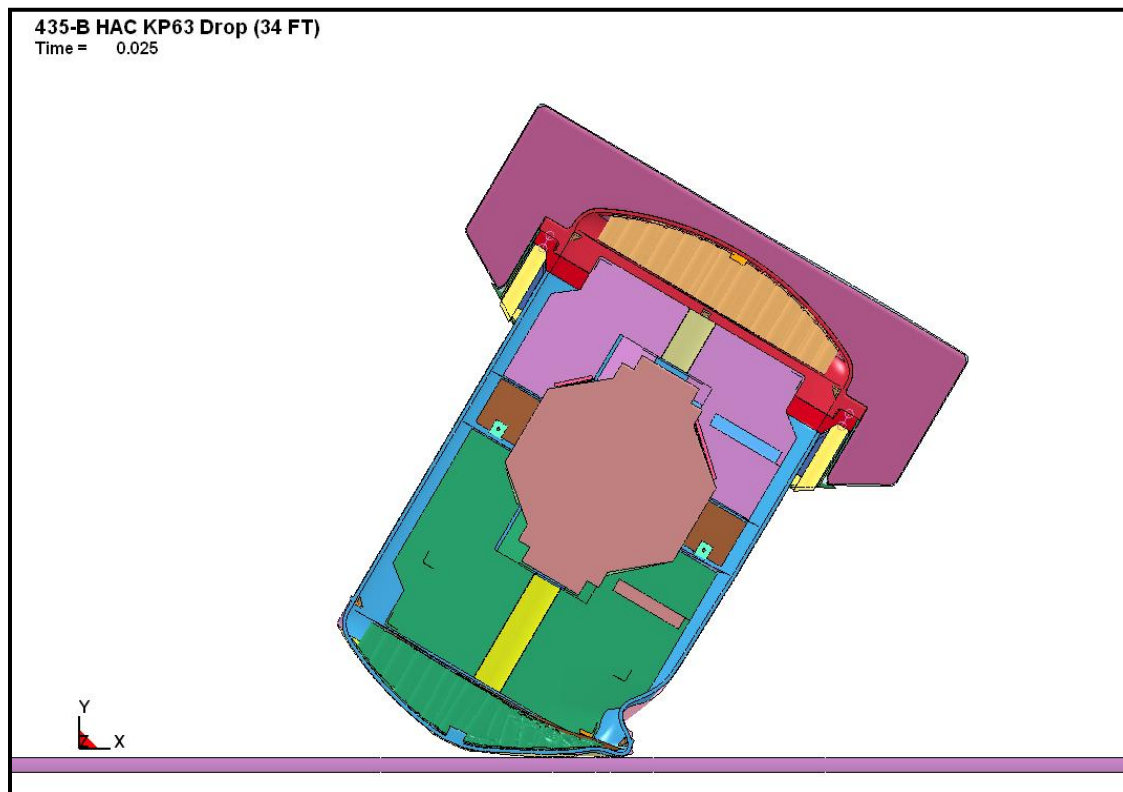
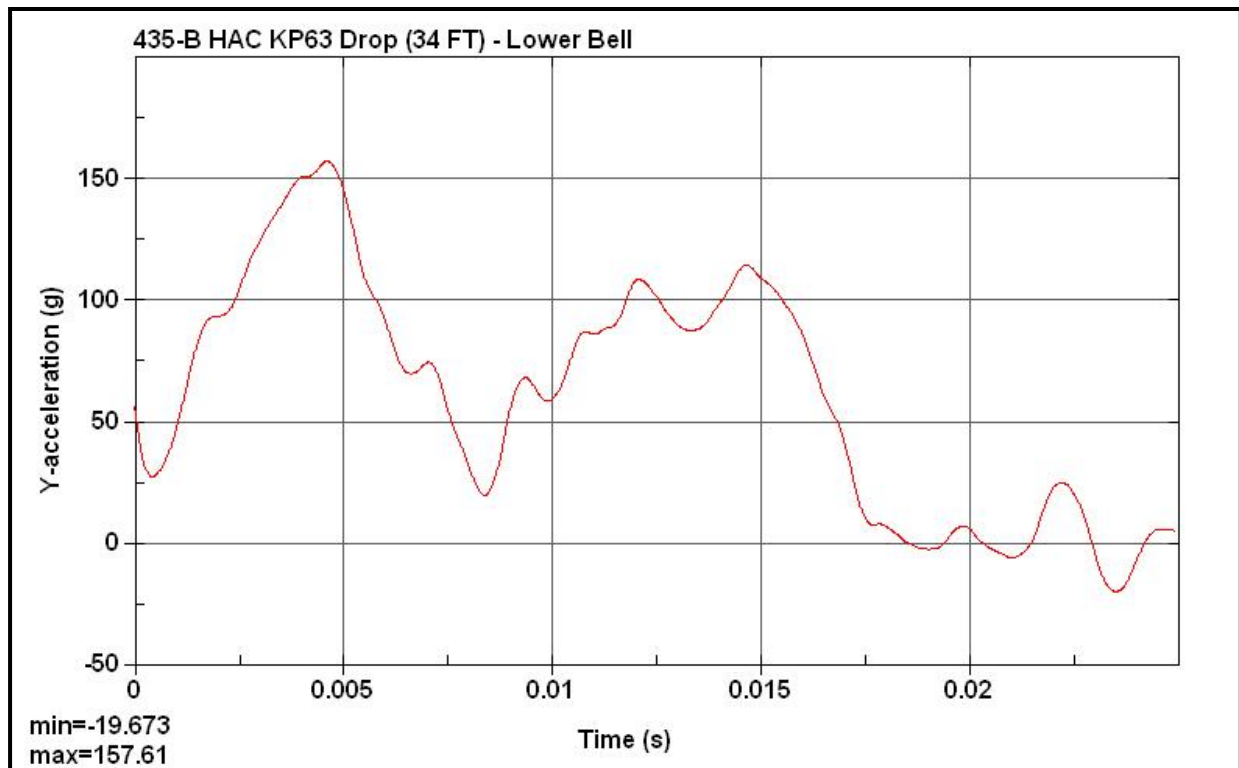
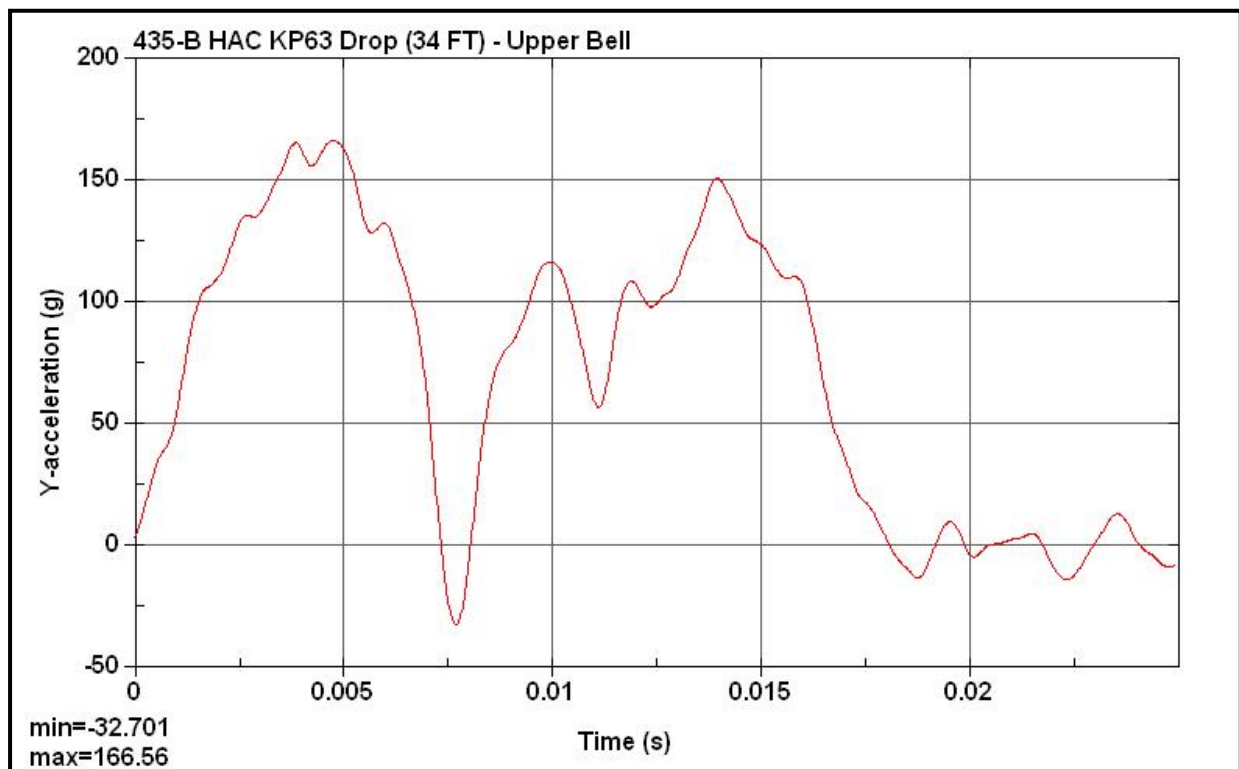
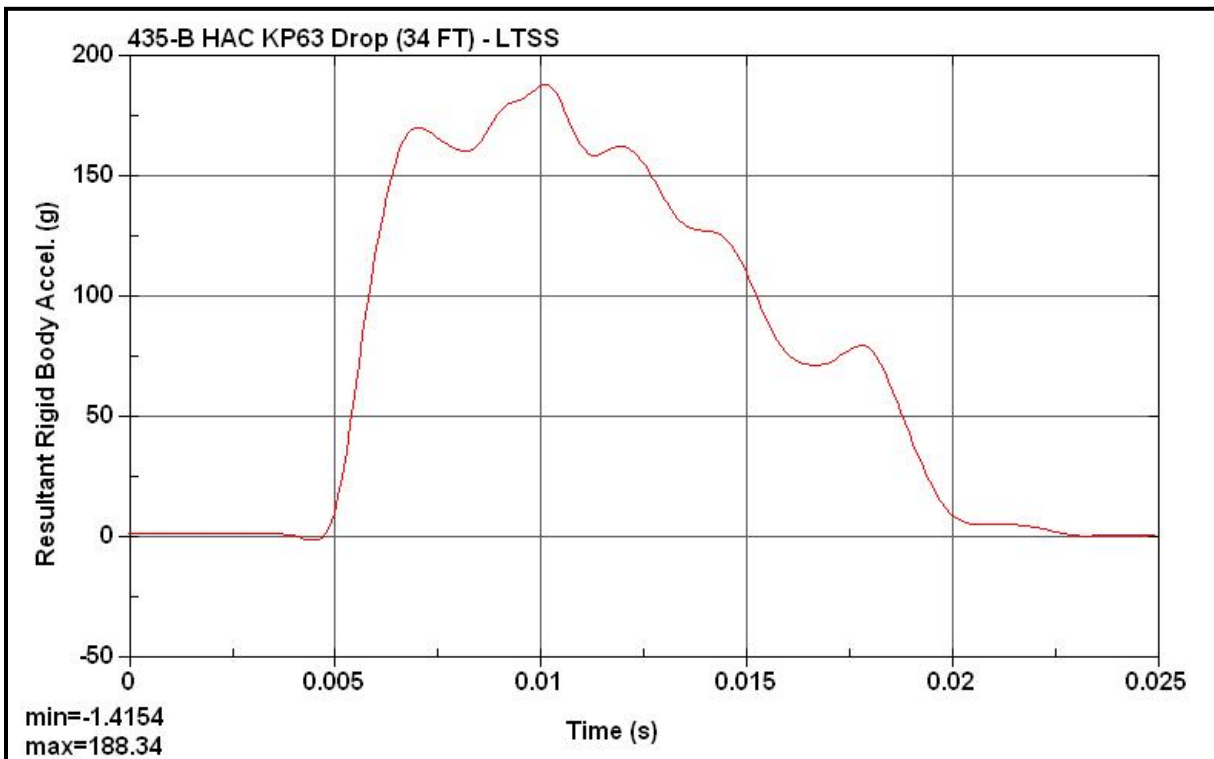
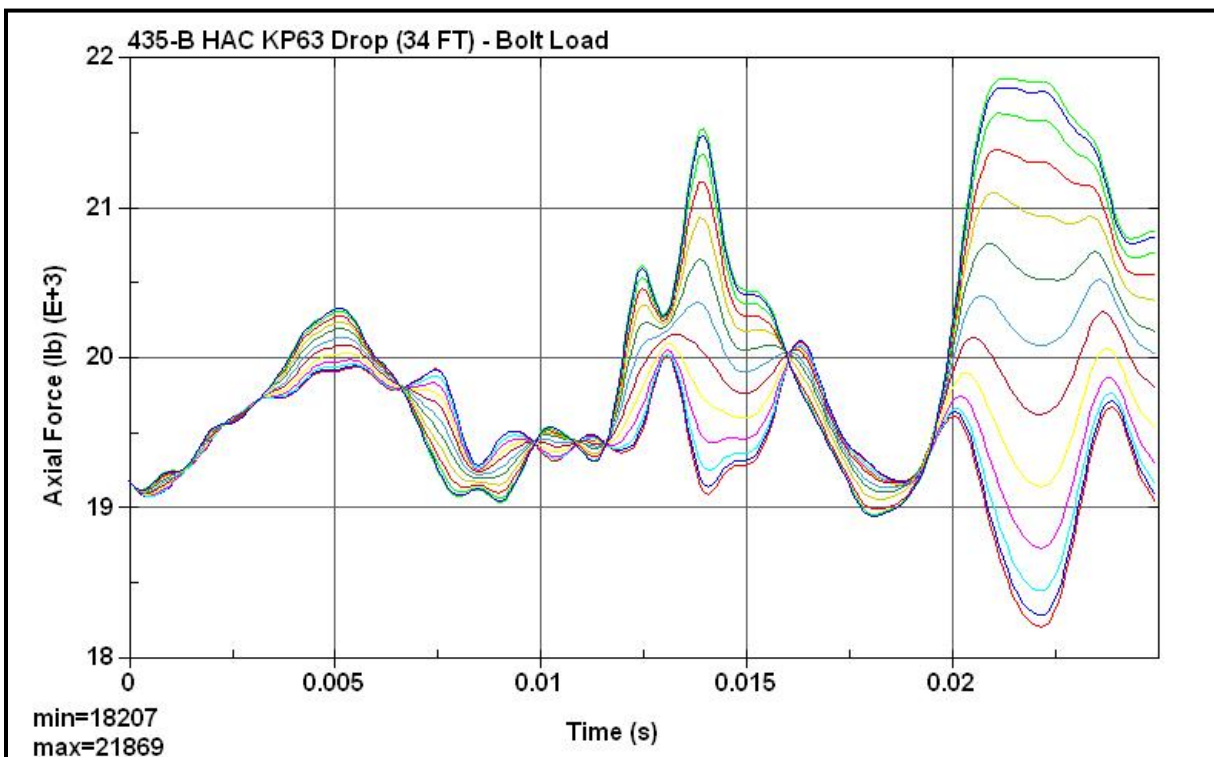


Figure 2.12.4-70 – KP63 (CG-over-Top Knuckle) Final State

**Figure 2.12.4-71 – KP63 Lower Bell Acceleration****Figure 2.12.4-72 – KP63 Upper Bell Acceleration**

**Figure 2.12.4-73 – KP63 LTSS Acceleration****Figure 2.12.4-74 – KP63 Axial Bolt Force**

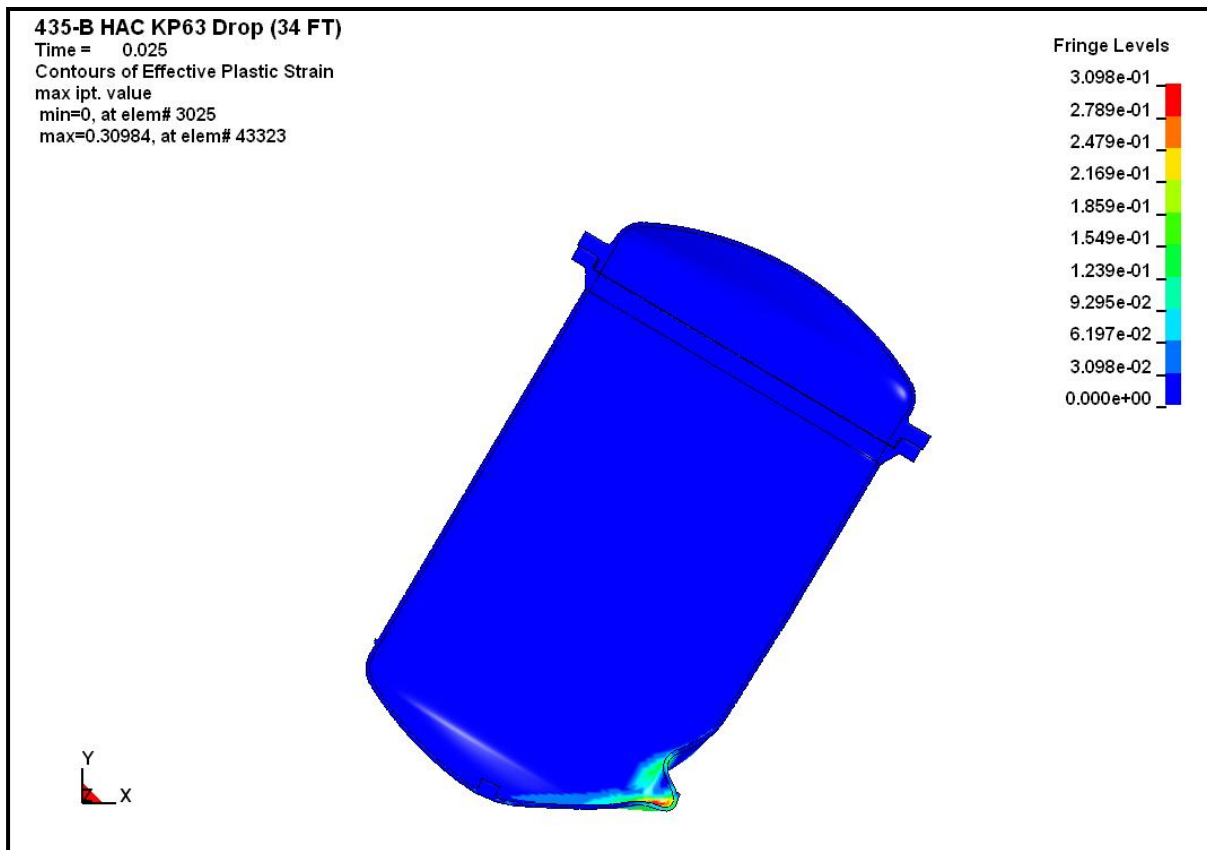


Figure 2.12.4-75 – KP63 Containment Boundary Cumulative Effective Plastic Strain

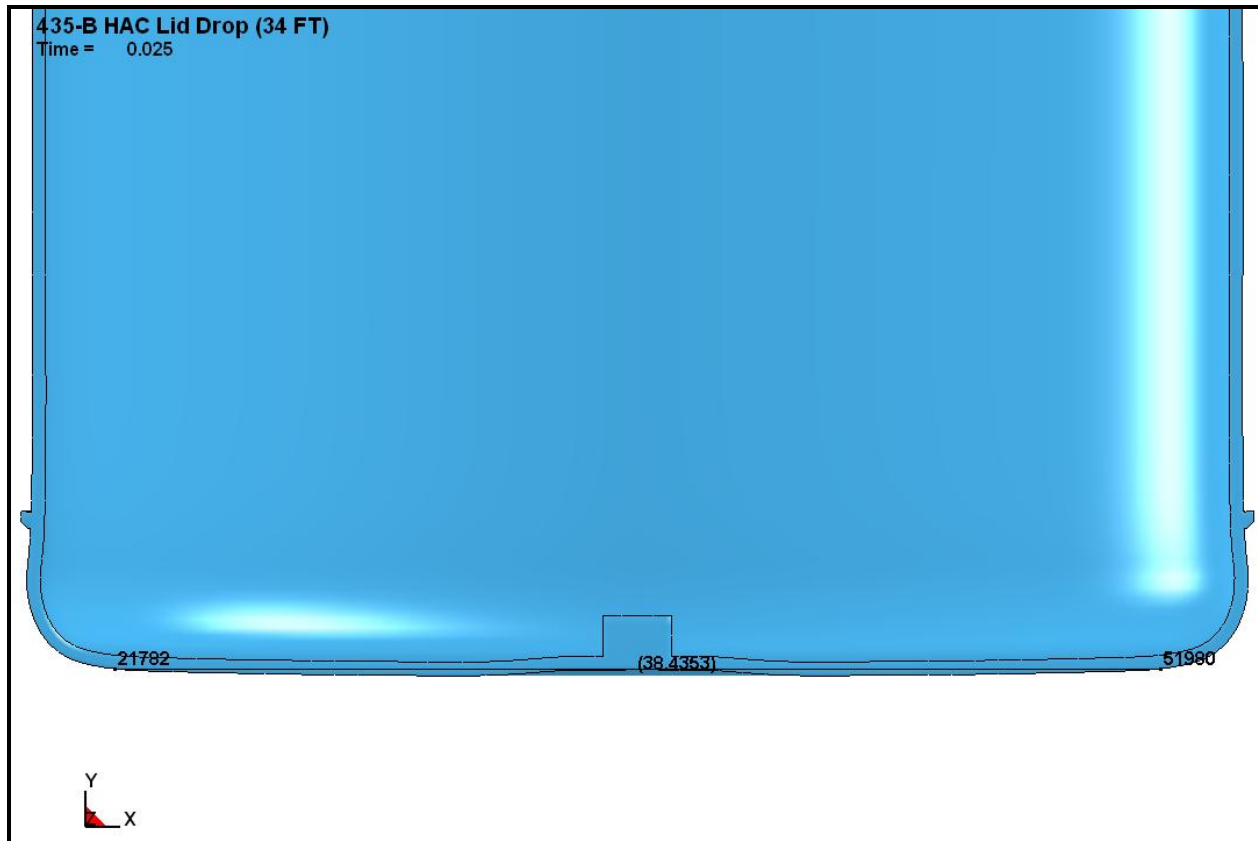


Figure 2.12.4-76 – Bell (Lid) Down Drop Flat Head Measurement

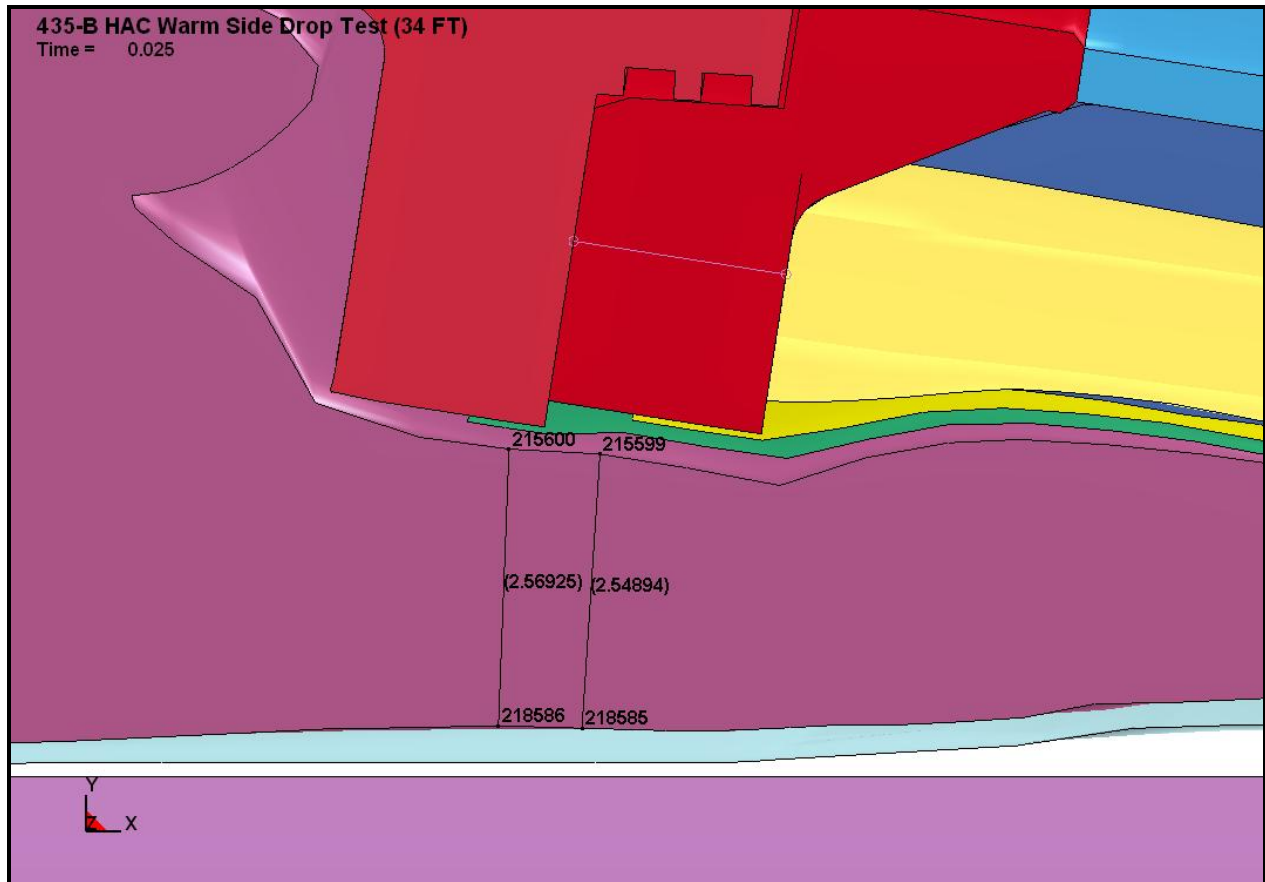


Figure 2.12.4-77 – Warm Side Drop Test Minimum Foam Thickness (14 pcf @ 117 °F)

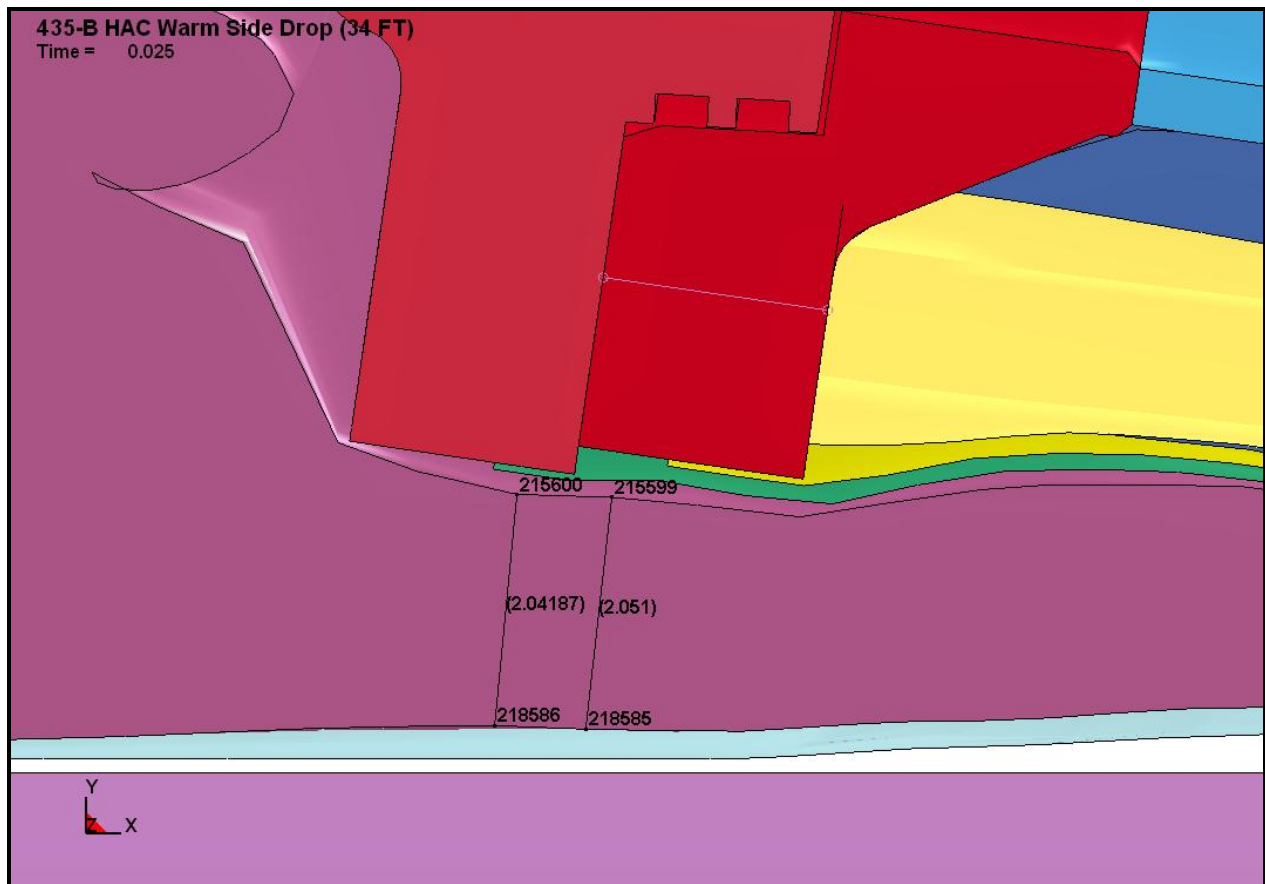


Figure 2.12.4-78 – Warm Side Drop Minimum Foam Thickness (15 pcf @ 150 °F)

2.12.4.7 References

1. Calculation 01916.01.C004.01-07, *435-B Drop Analysis*, Rev. 0, AFS.
2. Title 10, Code of Federal Regulations, Part 71 (10 CFR 71), *Packaging and Transportation of Radioactive Material*, 01-01-18 Edition.
3. International Atomic Energy Agency, *Regulations for the Safe Transport of Radioactive Material*, SSR-6, 2012 Edition.
4. ANSI N14.5–1997 *American National Standard for Radioactive Materials – Leakage Tests on Packages for Shipment*, American National Standards Institute (ANSI), Inc.
5. Sandia National Laboratories, *Reexamination of Spent Fuel Shipment Risk Estimates*, Main Report, NUREG/CR-6672, Vol. 1, US Nuclear Regulatory Commission, March 2000.
6. *LS-DYNA Keyword User's Manual Version 971*, May 2007, Livermore Software Technology Corp., Livermore, CA.
7. *Design Guide for use of Last-A-Foam® FR-3700 for Crash & Fire Protection of Radioactive Material Shipping Containers*, Issue 005, General Plastics Manufacturing Company, Tacoma, WA.
8. International Atomic Energy Agency, *Advisory Material for the IAEA Regulations for the Safe Transport of Radioactive Material*, SSG-26, 2012 Edition.
9. Avallone, E. A., and Baumeister, T, III., *Marks' Standard Handbook for Mechanical Engineers*, 10th Edition, 1996, McGraw-Hill, Inc.
10. Shigley, J.E., and Mischke, C.R., *Mechanical Engineering Design*, 5th Edition, 1989, McGraw-Hill, Inc.

2.12.5 Seal Performance Tests

This appendix contains descriptions of the performance tests which have been run on the butyl rubber compound used for the containment O-ring seal and sealing washers used in the 1105-SD package. The material is designated as Rainier Rubber R-0405-70. The performance tests which will be discussed have demonstrated the ability of this material to maintain a leaktight¹ containment boundary under minimum compression, minimum temperature, and maximum temperature conditions which are beyond those experienced in the 1105-SD package.

2.12.5.1 Performance Tests Associated with the TRUPACT-II Package

Two sets of butyl rubber performance tests have been done in support of the TRUPACT-II package certification (NRC Docket 71-9218). All relevant tests have used a bore-type fixture which is consistent with the configuration of the O-ring seals in the TRUPACT-II.

The test configuration and procedure was similar between the two tests and will now be briefly described. More details are available in Section 2.10.7.4 and Section 2.10.7.4A of [2]. Only the small test fixture is considered, since it was used in both sets of tests. The test fixture consists of an inner ring containing two O-ring grooves on its outer diameter and an outer ring which fits over the inner ring and provides compression of the two test O-rings. The cross-sectional diameter of the test O-rings was nominally 0.400 inches, which is essentially equivalent to the 0.375 nominal dimension of the 1105-SD package containment O-ring seal. To vary the O-ring compression in the test fixture, the radial position of the inner ring was controlled by jacking screws. When the inner ring was shifted to one side within the outer ring, a maximum compression was obtained on the side toward which the inner ring was shifted, and a minimum compression was obtained on the opposite side. The entire fixture could be placed in an environmental chamber and either cooled or heated for a set time. A helium leakage rate test was performed at various stages by testing the leakage rate between the outside of the fixture and the space between the two test O-rings.

The first set of tests was performed in 1989 and is documented in Section 2.10.7.4 of [2]. A typical test sequence consisted of the following steps:

1. Assemble the test fixture at ambient conditions.
2. Perform a leakage rate test with the inner ring centered in the outer ring.
3. Chill the fixture to -40 °F and perform a helium leakage rate test.
4. Allow the fixture to warm to -20 °F.
5. Shift the inner ring laterally within the outer ring to achieve maximum compression on one side and minimum compression on the other side.
6. Perform a helium leakage rate test with the fixture still at -20 °F.
7. Heat to an elevated temperature, maintaining the inner ring in the shifted position.

¹ Leaktight is defined as a maximum leakage rate of 1×10^{-7} ref-cc/sec, air, per [1].

8. Hold at temperature for 8 hours. Create a hard vacuum between the two test O-rings to confirm their integrity. A helium leakage rate test was not performed due to the tendency toward rapid saturation of the O-rings with helium at elevated temperature.
9. Chill the fixture to -20 °F, maintaining the inner ring in the shifted position.
10. Perform a final helium leakage rate test with the fixture still at -20 °F.

For each test, the maximum and minimum compressions were calculated using the dimensions of the fixture and of the test O-rings. The principal result of these tests was a demonstration that the subject rubber compound is capable of maintaining a leaktight condition at -20 °F with a minimum compression of 14.9% subsequent to an 8 hour soak at 400 °F. Details of the five small fixture tests are given in Table 2.12.5-1, adapted from Table 2.10.7-1 of [2]. Note that the term 'disk' in the table corresponds to the term 'inner ring' used in this description.

The second set of tests was performed in 1999, and are documented in Section 2.10.7.4A of [2]. These tests served to lower the minimum compression value at which a leaktight condition was demonstrated to be maintained. The tests used the same small test fixture, modified to allow it to achieve a lower minimum compression. The same test procedure was followed, except that all tests were run at a temperature of 400 °F. The principal result of these tests was a demonstration that the subject rubber compound is capable of maintaining a leaktight condition at -20 °F with a minimum compression of 11.9% subsequent to an 8 hour soak at 400 °F. Details of the three tests are given in Table 2.12.5-2, adapted from Table 2.10.7.4A-2 of [2].

2.12.5.2 Performance Tests Associated with the RTG Package

2.12.5.2.1 Face Seal Tests

O-ring tests were also performed in support of the Radioisotope Thermoelectric Generator (RTG) package certification (DOE Docket 94-6-9904). The results are reported in Section 2.10.6 of [3]. In these tests, a face-type fixture was used which permitted four different compressions to be tested at once. Unlike the TRUPACT-II testing, and consistent with the conditions in a face-type configuration, the O-rings were not mechanically moved or disturbed throughout the test. The fixture consisted of an inner plate having three concentric grooves on each side. Each groove had a different depth and contained an O-ring made from butyl compound R-0405-70 as described above. The inner and outer O-rings on each side were the test specimens; the center O-rings were used only to support leakage rate testing of the test specimens. The O-rings were compressed by outer plates which were set off from the inner plate by shims which, along with the groove depths, controlled the amount of compression of each test O-ring. The nominal test O-ring cross-sectional diameter was 0.275 inches. The minimum compression created by the fixture was 10%, which was uniform around the entire circumference of the fixture. Compressions of 12%, 14%, and 15.5% were tested at the same time. The dimensions of the fixture and of the test specimens, and the resulting compression values, are shown in Table 2.12.5-3.

The time/temperature sequence was as follows:

1. Assemble the test fixture at ambient conditions and perform a helium leakage rate test.
2. Chill the fixture to -40 °F and perform a helium leakage rate test.

3. Heat the fixture to 380 °F, and hold for 24 hours. Confirm integrity of the test O-rings by placing a hard vacuum on the test cavity (less than 0.2 mbar).
4. Allow the fixture to cool to 350 °F, and hold for 144 hours. The total time at elevated temperature is 168 hours, or one full week. Confirm integrity of the test O-rings by placing a hard vacuum on the test cavity (less than 0.2 mbar).
5. Cool the fixture to -20 °F and perform a final helium leakage rate test.

Each of the helium leakage rate tests demonstrated a leakage rate below the leaktight criterion of 1×10^{-7} ref-cc/sec, air, as defined by [1]. Of note, only the results from the outer O-ring tests (10% and 14% compression) were available at the time of publication of [3]. The successful completion of the inner O-ring tests (12% and 15.5% compression) was confirmed in [4].

2.12.5.2.2 Bore Seal Tests

Further O-ring tests were performed by Westinghouse Hanford Company in association with the RTG package, and documented in [5] and [6]². In these tests, the same bore-type fixture was used as that used for the TRUPACT-II tests described in Section 2.12.5.1, *Performance Tests Associated with the TRUPACT-II Package*. The procedure differed slightly in that a cold shift (step no. 5 from Section 2.12.5.1) was not performed. The test sequence was as follows:

1. Assemble the fixture at ambient conditions, and shift the inner ring fully to one side, generating minimum compression on one side and maximum on the other. Perform a helium leakage rate test.
2. Chill the fixture to -40 °F and perform a helium leakage rate test.
3. Heat to the specified elevated temperature and hold for the specified time. At the end of the hold time, perform a helium leakage rate test (saturation with helium at the high temperature was not reported to have had an effect on the helium leakage rate test).
4. Chill the fixture to -20 °F and perform the final helium leakage rate test.

For each test, the maximum and minimum compressions were calculated using the dimensions of the fixture and of the test O-rings. A number of different time/temperature tests were run, showing leaktight performance of the butyl material for 430 °F for one hour [6], 375 °F for 25 hours [6], and 350 °F for 168 hours [5]. Data is summarized in Table 2.12.5-4.

2.12.5.3 Long Term Performance of Butyl Rubber Seals

The tests of the Rainier Rubber R-0405-70 compound described in this appendix were performed at relatively high temperatures for relatively short times, consistent with the HAC fire event. Demonstration of the performance of the material at the lower temperature and longer duration associated with the NCT hot environment is made by extrapolation of this data.

Reference 7 uses thermogravimetric analysis to predict the relative lifetimes of some elastomers. One of the results of this study is to show that elastomer lifetime is linear when plotted on a log-lifetime (ordinate) vs. 1000/Temp (K) (abscissa) scales. This is shown in figure 3 of [7], which

² Note that some of the test reports refer to the material as 'RR-0405-70' while in some instances, 'R-0405-70' is used. Both refer to the same compound, where 'RR' is used for uncured material, and 'R' for a cured product form. All testing was performed on cured material.

is reproduced as Figure 2.12.5-1. The curve for butyl will not necessarily have the same slope or be placed in the same position relative to the scales as is shown in the figure. The position and slope for butyl will need to be established using the test data. Then, using linear extrapolation, its performance at longer lifetimes can be found. Note, since the abscissa is based on the inverse of temperature, temperature is actually decreasing along the abscissa towards the right, even though the values of $1000/\text{Temp (K)}$ are increasing. Consequently, the longest lifetimes correlate to the lowest temperature, as expected.

Figure 2.12.5-2 shows several time/temperature data points from the tests discussed above, along with the best-fit line through the data. For consistency, only data from the bore-type test fixture are considered. Note that this is not a locus of exact failure points (points defining the border between pass/fail), but of tests that passed (i.e., met the leaktight requirements of [1]). The possibility exists that some or all of these tests were "undertests", i.e., were not tested to the extreme limit of the material. Because the margin to failure may be different for each test, the actual locus of borderline results (zero-margin pass) may have a shallower slope than the best-fit curve to the data. If that curve were used to extrapolate upward to longer lifetimes, it might over predict the acceptable temperature (recall that temperature is decreasing to the right).

For the 1105-SD package, it is desired to determine the acceptable temperature for leaktight performance for a duration of one year (8,760 hours). The most conservative extrapolation (the lowest acceptable temperature) will be generated from the data curve fit having the shallowest (conservative) slope. To find the shallowest slope, a data point for a test failure (450 °F for 8 hours) is introduced, as shown in Figure 2.12.5-3. This is taken from the TRUPACT-II test results shown in Table 2.12.5-1. The straight line between this failure point and the longest-term successful data point (350 °F for 168 hours) has the shallowest slope which is consistent with the known data points. This can be concluded from the following observations:

1. The 450 °F/8 hour data point cannot be an undertest, since it is a known failure. Therefore, the actual zero-margin pass temperature must lie to the right of, but not to the left of, the test data point.
2. The 350 °F/168 hour data point is likely somewhat undertested. Therefore, the actual zero-margin pass temperature must lie to the left of, but not to the right of, the test data point.
3. Consequently, the actual locus of zero-margin performance could be steeper than, but could not be shallower than, the line formed by joining the 450 °F/8 hour and 350 °F/168 hour data points.

The equation of the line connecting these two data points is:

$$\text{Log}_{10}(\text{hrs}) = 5.396(1000/T(\text{K})) - 9.775$$

Using this expression, the maximum leak tight temperature for 8,760 hours (one year) is 249 °F. Therefore, the R-0405-70 butyl material can be held at at least 249 °F for one full year (constant temperature night/day) and is expected to be leak tight per ANSI N14.5. This is the most conservative extrapolation that can be made from the known data and is essentially equal to the long term limit for the butyl material of 250 °F which is stated in Section 3.2.2, *Technical Specification of Components*.

2.12.5.4 Summary

The butyl rubber compound used for the 1105-SD package containment seals was tested in both a bore-type and a face-type test fixture at low compression and elevated temperature. In the bore-type testing, the O-rings were demonstrated to be helium leaktight after a soak at 400 °F for 8 hours at a minimum compression of 11.9%. In the face-type testing, the O-rings were demonstrated to be helium leaktight after a soak at 380 °F for 24 hours followed by a soak at 350 °F for 144 hours at a minimum compression of 10%. In both types of test, the O-rings were shown to be helium leaktight at a temperature of -40 °F. These compression and temperature/time conditions exceed the severity of those experienced in the 1105-SD package. In addition, the seals are expected to be leaktight after one full year at a constant temperature of at least 249 °F. Because this value was conservatively obtained, the value of 250 °F used in Section 3.2.2, *Technical Specification of Components* is acceptable. The minimum compression of the 1105-SD package containment seal O-ring is calculated in Section 4.1.3, *Seals*, and the maximum temperature under NCT and HAC is discussed in Chapter 3, *Thermal Evaluation*.

Table 2.12.5-1 – TRUPACT–II O-ring Seal Performance Test Results (1989)⑦

Test Number	O-ring Seal Cross-Sectional Diameter (inches)				Stretch (%)		Maximum Gap (inches)		Minimum Compression (%)				Soak Temperature and Helium Leakage Rate Test Results ④				
	O-ring Seal No. 1		O-ring Seal No. 2		Min	Max	Disk Center	Disk Offset	Disk Centered		Disk Offset		Disk Centered		Disk Offset		
	Min	Max	Min	Max					Min	Max	Min	Max	Ambient	-40 °F	-20 °F	8 hrs⑤	-20 °F
1	0.387	0.397	0.387	0.396	2.0	4.1	0.026	③	22.1	25.6	14.9	20.0	Yes	Yes	Yes	350 °F	Yes
2	0.388	0.398	0.387	0.398	2.0	4.1	0.029	0.050	21.3	25.1	15.7	19.7	Yes	Yes	⑥	450 °F	No
3	0.387	0.397	0.387	0.399	2.0	4.1	0.027	0.052	21.9	25.8	15.2	19.4	Yes	Yes	Yes	400 °F	Yes
4	②	②	②	②	2.0	4.1	0.027	0.053	21.9	25.8	14.9	19.1	Yes	Yes	Yes	400 °F	Yes
5	②	②	②	②	2.0	4.1	0.026	0.050	22.1	26.0	15.7	19.9	Yes	Yes	Yes	400 °F	Yes

Notes:

- ① Material for all O-ring seal test specimens was butyl rubber compound R-0405-70, Rainier Rubber Co., Seattle, WA.
- ② Not measured; calculations assume the worst case range as taken from Tests Numbers 1 - 3 (i.e., Ø0.387 minimum to Ø0.399 maximum).
- ③ Range of values is 0.048 in. minimum to 0.053 in. maximum due to an indirect method of gap measurement (used for this test only).
- ④ A “Yes” response indicates that helium leakage rate testing demonstrated a leaktight condition as defined in [1], i.e., the leakage rate was less than or equal to 1×10^{-7} ref-cc/sec, air. In all cases, measured leak rates were less than or equal to 2.0×10^{-8} ref cc/s, helium, for tests with a “Yes” response.
- ⑤ No helium leakage rate tests were performed at elevated temperatures due to O-ring seal permeation and saturation by helium gas. The ability of the test fixture to establish a rapid, hard vacuum between the O-ring seals was used as the basis for leakage rate test acceptance at elevated temperatures. All tests rapidly developed a hard vacuum, with the exception of Test Number 2 at an elevated temperature of 450 °F, which slowly developed a vacuum.
- ⑥ Initial leakage rate of 1.0×10^{-5} ref cc/s, helium; became leaktight approximately one minute later.
- ⑦ Adapted from Table 2.10.7-1 of [2].

Table 2.12.5-2 – Supplementary TRUPACT–II O-ring Seal Performance Test Results (1999)④

Test No.	Disk Centered % Comp.		Disk Offset % Comp.		Helium Leak Tight②				
	O-ring #1	O-ring #2	O-ring #1	O-ring #2	Ambient Temp.	-40 °F	-20 °F (Disk Offset)	Hot Soak (Disk Offset)③	-20 °F (Disk Offset)
1	18.5	17.9	12.7	12.0	Yes	Yes	Yes	Held Vacuum	Yes
2	20.8	20.0	12.9	11.9	Yes	Yes	Yes	Held Vacuum	Yes
3	19.2	19.2	12.1	12.1	Yes	Yes	Yes	Held Vacuum	Yes

Notes:

- ① Material for all O-ring seal test specimens was butyl rubber compound R-0405-70, Rainier Rubber Co., Seattle, WA.
- ② Seal is considered to be leaktight if the actual leakage rate is less than or equal to 8×10^{-8} atm-cc/sec, He.
- ③ Hot soak was 8 hours at a uniform temperature of 400 °F.
- ④ Adapted from Table 2.10.7.4A-2 of [2].

Table 2.12.5-3 – RTG O-ring Face Seal Performance Test Parameters^③

Fixture Side	Outer groove depth, in.	Inner groove depth, in.	Shim Thickness, in.	Outer O-ring X- section, in.	Inner O-ring X- section, in.	Outer O-ring compression, %	Inner O-ring compression, %
Side A	0.2053	0.2000	0.044	0.2770	0.2773	10	12
Side B	0.2075	0.2033	0.031	0.2776	0.2774	14	15.5

Notes:

- ① Material for all O-ring seal test specimens was butyl rubber compound R-0405-70, Rainier Rubber Co., Seattle, WA.
- ② Each of the four test O-ring seals were leaktight per [1] when tested at a temperature of -20 °F following the time/temperature sequence of 380 °F for 24 hours followed by 350 °F for 144 hours.
- ③ Adapted from Appendix 2.10.6, Table 4.1-1 and Table 4.1-2, of [3].

Table 2.12.5-4 – RTG O-ring Bore Seal Performance Test Parameters

Test No.	Min Compression, %	Max Compression, %	Max Temperature, °F	Hold Time, hours	Data Source
4	17.5	30.5	350	168	Table 3 of [5]
4B	17.8	31.3	375	25	Table 3 of [6]
3	19.2	32.3	430	1	Table 3 of [6]

Notes:

- ① Material for all O-ring seal test specimens was butyl rubber compound R-0405-70, Rainier Rubber Co., Seattle, WA.
- ② O-ring seals were leaktight per [1] when tested initially at room temperature, at a temperature of -40 °F, again at the stated maximum temperature at the end of the hold time, and finally when chilled to -20 °F.

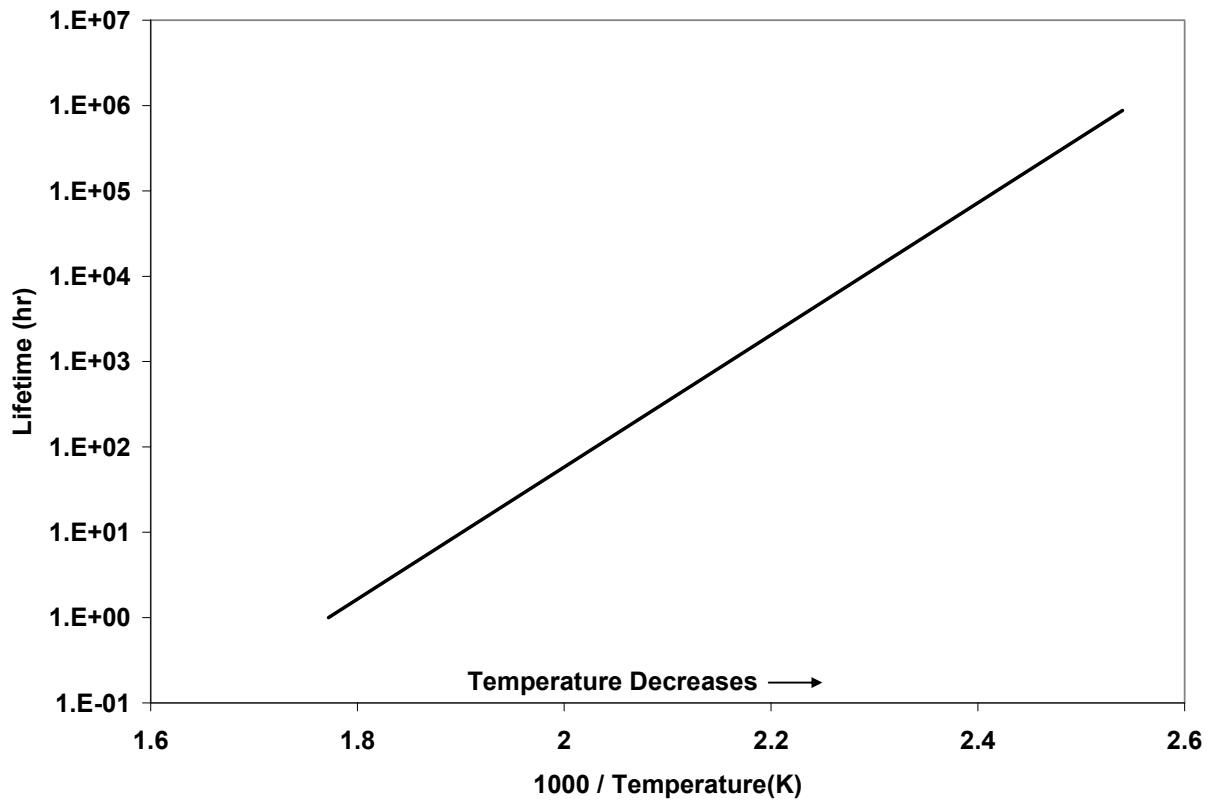


Figure 2.12.5-1 – Elastomer Time-Temperature Behavior (adapted from Figure 3 of [7])

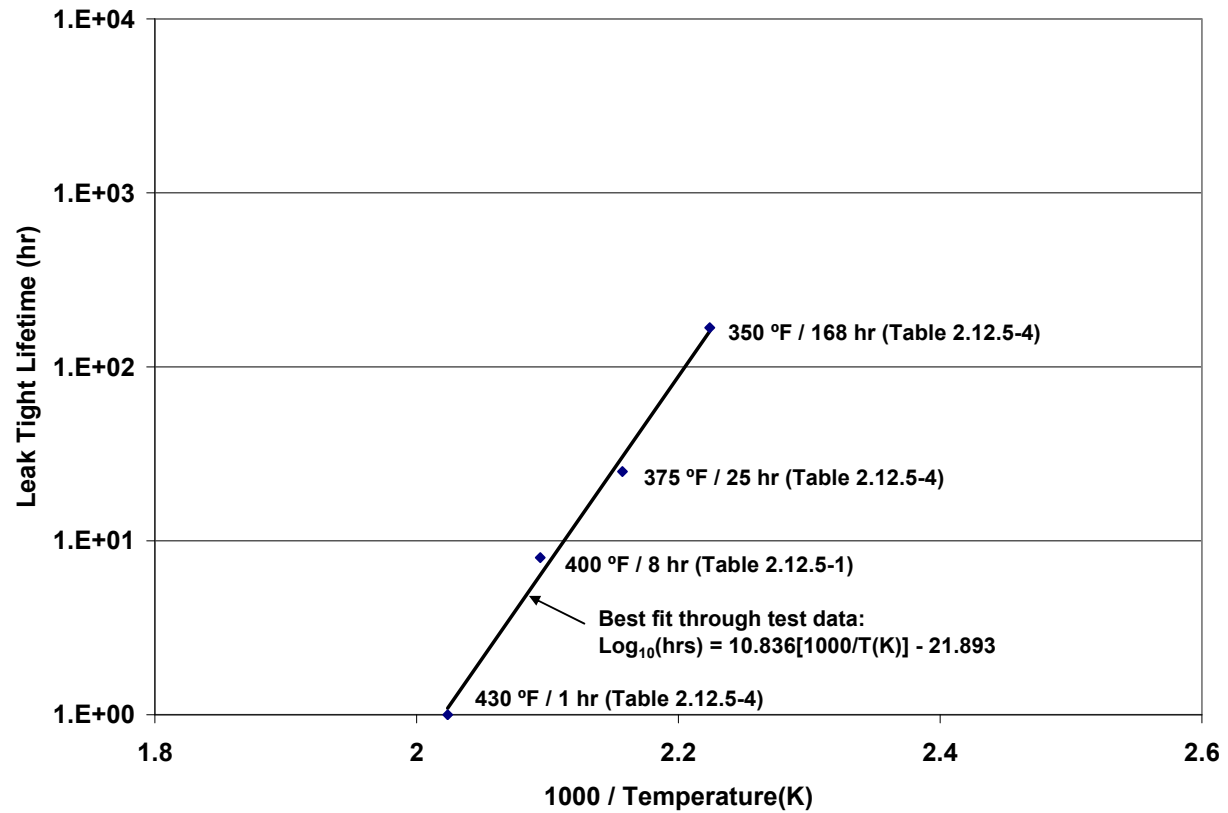


Figure 2.12.5-2 – R-0405-70 Test Data and Best Fit Curve

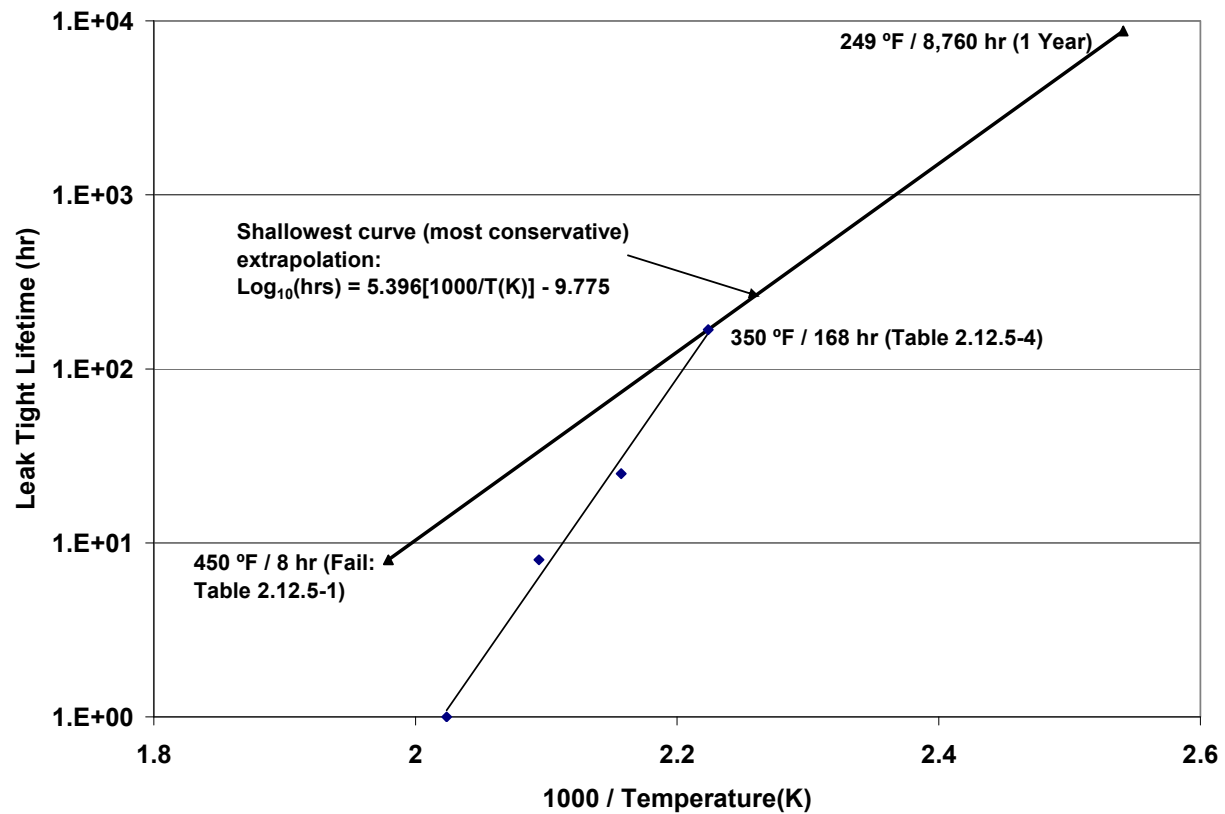


Figure 2.12.5-3 – Conservative Extrapolation to One Year

2.12.5.5 References

1. ANSI N14.5-1997, *American National Standard for Radioactive Materials – Leakage Tests on Packages for Shipment*, American National Standards Institute (ANSI), Inc.
2. USNRC Docket 71-9218, *Safety Analysis Report for the TRUPACT-II Shipping Package*, Revision 18, U.S. Department of Energy, Carlsbad Field Office, Carlsbad, New Mexico.
3. DOE Docket No. 94-6-9904, *Radioisotope Thermoelectric Generator Transportation System Safety Analysis Report for Packaging*, WHC-SD-RTG-SARP-001, prepared for the U.S. Department of Energy Office of Nuclear Energy under Contract No. DE-AC06-87RL10930 by Westinghouse Hanford Company, Richland, WA.
4. Westinghouse Hanford Company, *RTG Transportation System Packaging O-ring Material Thermal Validation Test Report for Face Seal Test Fixture*, WHC-SD-RTG-TRP-010, Rev 0.
5. Westinghouse Hanford Company, *Radioisotope Thermoelectric Generator (RTG) Transportation System Packaging O-ring Material Thermal Validation Test Report*, WHC-SD-RTG-TRP-001, Rev. 1.
6. Westinghouse Hanford Company, *Radioisotope Thermoelectric Generator (RTG) Transportation System Packaging O-ring Material Elevated Temperature Test Report*, WHC-SD-RTG-TRP-002, Rev. 0.
7. Nigrey, P. J., *Prediction of Packaging Seal Life Using Thermoanalytical Techniques*, Proceedings of the 12th International Conference on the Packaging and Transportation of Radioactive Materials, PATRAM 98, Vol. 4, p. 1730.

3.0 THERMAL EVALUATION

This chapter identifies and describes the principal thermal design aspects of the 1105-SD package. The 1105-SD package is used to transport radioactive sources in the Long Term Storage Shield (LTSS) or shielded devices containing their sources. The evaluations presented in this chapter demonstrate the compliance of the 1105-SD package¹ as a Type B(U)-96 shipping container with the thermal requirements of Title 10, Part 71 of the Code of Federal Regulations [1]. Further guidance for the evaluation is taken from NUREG-1609 [2] and Regulatory Guide 7.8 [4].

Specifically, all package components are shown to remain within their respective temperature limits under the normal conditions of transport (NCT). Further, per 10 CFR §71.43(g), the maximum temperature of the accessible package surfaces is demonstrated to be less than 122 °F for the maximum decay heat loading, an ambient temperature of 100 °F, and no insolation. Finally, the 1105-SD package is shown to retain sufficient thermal protection following the HAC free and puncture drop scenarios to maintain all package component temperatures within their respective short term limits during the regulatory fire event and subsequent package cool-down.

3.1 Description of Thermal Design

The principal components of the 1105-SD package are illustrated in Figure 1.2-1 through Figure 1.2-5 of Section 1.0, *General Information*. The principal components are: 1) a lower body assembly (or base), which includes a polyurethane foam filled impact limiter, 2) an upper body assembly (or bell) that bolts to the base, 3) and two internal impact limiter assemblies. The packaging is fabricated primarily of Type 304 austenitic stainless steel, polyurethane foam, and a small amount of 6061 aluminum. See Section 1.0, *General Information*, for more detail.

3.1.1 Design Features

The primary heat transfer mechanisms within the 1105-SD packaging are conduction, convection, and radiation. The principal heat transfer from the exterior of the packaging is via convection and radiation to the ambient environment. The 1105-SD transport packaging incorporates several thermal protection features intended to limit the peak package temperatures during the HAC fire event. These thermal protection features include the following:

- 1) dual thermal shields over the cylindrical body shell,
- 2) a single thermal shield over the upper torispherical head,
- 3) the inclusion of a closure bolt enclosure structure (see Figure 1.2-4) that provides distance separation and thermal protection for the closure bolt heads and upper surface of the upper body flange from the ambient conditions,
- 4) an impact limiter that surrounds and encompasses the lower portion of the upper body assembly as well as the package base, and

¹ The term 'packaging' refers to the assembly of components necessary to ensure compliance with the regulatory requirements, but does not include the payload. The term 'package' includes both the packaging components and the payload.

- 5) internal impact limiters that are configured to restrict heat flow between the payload and the torispherical heads.

The side of the package is thermally protected from the high heat fluxes generated during the HAC fire event via the use of dual thermal shields. The shields are located between the tube sheet and approximately the location of the weld between the torispherical head and cylindrical body shell. The dual thermal shield creates two thin, air-filled gaps between the cylindrical shell of the package and the ambient using two relatively thin stainless steel sheets. Figure 3.1-1 illustrates the layout of the dual shield arrangement. The inner sheet of the dual thermal shield is 0.060 inches thick and the outer sheet is 0.105 inches thick. The gaps are formed by a spiral wrap of stainless steel wire, 0.105 inches in nominal diameter, wrapped on a 3-inch pitch and tack welded in place. Small spacer strips at each end of the shield are welded in place to fully seal the gaps. To further thermally isolate the package side from the hot ambient conditions, the outer face of the cylindrical shell, both faces of the inner shield sheet, and the inside face of the outer shield sheet are brightened to an ASTM A480 type 3 or 4 finish to lower the emissivity and reduce heat transfer via radiation.

The upper torispherical head is covered by a similarly configured thermal shield, except that a single 0.105 inches thick stainless steel sheet is used. Again, spiral wrapped 0.105 inches diameter stainless steel wire on a 3-inch pitch is used to form the gap and the outer surface of the ½-inch torispherical head and the inner face of the head thermal shield are brightened to lower emissivity and reduce heat transfer via radiation.

Additional thermal protection is provided by the closure bolt enclosure structure depicted in Figure 1.2-4 of Section 1.0, *General Information*. The enclosure provides approximately 11 inches of spatial separation between the closure bolt heads and upper surface of the upper body flange from the ambient conditions. A rain shield prevents moisture from entering the individual bolt access tubes, but also serves as a radiation and convection shield during the HAC fire event. The integrity of the rain shield attachment was demonstrated from physical drop testing on the certification test units (CTUs) of the 1105-SD package (see Appendix 2.12.3, *Certification Test Results*) where, despite intentional attempts to dislodge it, the rain shield remained attached and functioning throughout the entire test program. The inclusion of blocks of 30 lb/ft³ polyurethane foam between the individual bolt access tubes and 0.5 inches of refractory insulation paper against the lower 8 inches of the cylindrical body shell provides further thermal protection.

Thermal and impact protection for the bottom and lower sides of the package is provided by the external impact limiter which is integral with and permanently connected to the lower body assembly. The 0.12 inches thick inner cylindrical shell of the impact limiter is welded to the outer edge of the lower flange. The outer shell (tapered top, outer cylinder, and flat bottom) is ¼ inches thick. The tapered top includes a short lead-in chamfer to guide the upper body assembly into place. The outer cylindrical shell is 70 inches in diameter and approximately 21 inches tall and features plastic melt-out plugs designed to relieve pressure generated by the thermal decomposition of the polyurethane foam during the HAC fire event. The inside surface of the bottom shell is covered with a ¼-inch thick layer of refractory insulation paper to reduce the thermal decomposition of the underlying polyurethane foam during the HAC fire event. The cavity of the limiter is filled with rigid, closed-cell polyurethane foam at a nominal density of 15 lb/ft³. The foam is poured in place.

Except for an approximately 0.30 inch gap between the head and the side thermal shields and a 3.5 inch diameter segment at the center of the upper torispherical head, the entire exterior surface of the containment boundary is shielded from direct exposure to the HAC generated temperature environment by the various thermal features described above. The lack of a thermal shield at the center of the upper torispherical head is partially offset by the presence of the upper body assembly lifting boss which effectively increases the local thickness of the head to 2 inches with an accompanying increase in the local thermal mass.

Heat transfer between the payload and the ends of the 1105-SD packaging is restricted by the presence of the internal impact limiters located at each end of the payload cavity (see Figures 1.2-2 and 1.2-5 in Section 1.0, *General Information*). The array of 130, 2-inch diameter \times 0.035-inch wall thickness, ASTM A249 or A269, Type TP304 stainless steel tubes greatly restricts the axial heat conduction between the payload and the torispherical heads via conduction. Likewise, the presence of the spherically curved stabilizer sheet and the low view factor down the length of the tubes effectively limits direct thermal radiation exchange between the torispherical heads and the aluminum base sheet of the internal impact limiters. The flat side of the impact limiters is made from a 1/2-inch thick, ASTM B209, 6061-T6 aluminum plate. The base of the tubes are anchored in shallow grooves machined into one side of the aluminum plate, while the other end is stabilized by passing through a 0.105-inch thick stainless steel tube stabilizer sheet which is spherically curved to match shape of the torispherical heads.

The void spaces within the packaging are filled with air nominally at 0 psig.

3.1.1.1 Design Features of LTSS Payload

The LTSS (Long Term Storage Shield) is one of the authorized payloads to be transported in the 1105-SD packaging. Figures 1.2-8 and 1.2-9, Section 1.0, *General Information*, provide an overview and a cross-section view of the LTSS. The LTSS consists of a central steel magazine, or barrel, surrounded by thick lead encased in a steel shell. All steel used in the LTSS is ASTM type 304 stainless steel. The barrel contains four longitudinal holes, each of which can accommodate one drawer assembly. Each end of the LTSS is closed using a lead-filled, hinged door. Except for minor exterior features, the LTSS exhibits quarter symmetry in the circumferential direction and half symmetry in the axial direction.

The LTSS can contain two types of drawer assemblies, each approximately 21.5 inches long and 2.5 inches in diameter. The Large Source Drawer (see Figure 1.2-10, Section 1.0, *General Information*) contains two end shields made of tungsten and a NLM-52 special form capsule made of stainless steel. The NLM-52 special form capsule is available in five different lengths, ranging from 74 mm to 325 mm. Each NLM-52 special form capsule may contain one or more sealed sources taken from shielded devices such as industrial irradiators, medical equipment, or research facilities. Other special form or non-special form capsules may be used that have the same length, diameter, and at least as much radiation attenuation as the NLM-52 capsule series, although the NLM 52 nomenclature is used elsewhere in this chapter for convenience. Typically the sealed source capsules are loaded and welded in an argon gas environment. Air is assumed to fill all other void volumes within the LTSS.

The other drawer type transported in the LTSS is the T80/T780. Like the Large Source Drawer, the T80 and T780 drawers are approximately 21.5 inches long and 2.5 inches in diameter. Instead of a special foam capsule, the T80/T780 drawers have a 1.1-inch diameter cross-drilled hole at the center which accepts a sealed source capsule. The T80/T780 drawers are made of

brass with a wall thickness of 0.2 inches and an end thickness of 0.8 inches. For the T80 drawer, the shielding on each side of the source is 9.2 inches of poured lead. For the T780 drawer, the shielding may be lead, tungsten, or depleted uranium. If tungsten or depleted uranium is used, the shielding would be in the form of machined bars. The lead filled T80/780 drawers are depicted in Figure 1.2-11, Section 1.0, *General Information*.

The position of the LTSS within the package payload cavity is maintained by the LTSS lodgment. The LTSS lodgment, depicted in Figure 1.2-6, Section 1.0, *General Information*, is a weldment made from ASTM B209, 6061-T6 aluminum alloy and is designed to support the LTSS with its axis vertical and its lower end approximately 8 inches above the bottom surface of the lodgment. The main structural components of the lodgment are 8 equally spaced 0.5-inch thick ribs running longitudinally and two 0.5-inch thick circumferential ribs going around the body of the LTSS. A "hub" made from 6061-T6, 4-inch, schedule 40 pipe is used to anchor the longitudinal ribs. Additional stiffening is provided by a number of $2 \times 2 \times \frac{1}{4}$ angles. The lodgment is constructed with an upper and lower half that are connected via 8 clevises and bolts in double shear. The LTSS rests on a $\frac{1}{2}$ -inch thick plate covered with a $\frac{1}{2}$ -inch thick layer of neoprene rubber, which is attached to the plate using four, $\frac{1}{4}$ -inch diameter screws. There is nominally no contact between lodgment ribs and the LTSS.

3.1.1.2 Design Features of Shielded Device Payload

The second type of authorized payload to be transported in the 1105-SD packaging are the Group 1 and 3 shielded devices. Shielded devices are units designed and manufactured to provide a safe radiation source for industrial, medical, or research purposes. Each such device includes a sealed source (or a group of sources), shielding lead, and a steel shell to surround the shielding material and provide structure. Figures 1.2-12 to 1.2-16, Section 1.0, *General Information*, illustrate a sampling of Group 1 and 3 shielded devices. Cabinets, stands, or unnecessary appurtenances attached to the devices are not transported. Prior to loading, movable sources are placed in the safe shipping position and the structural integrity is evaluated.

All Group 1 devices use Cs-137 as the radiation source and have a weight of approximately 3,300 lb. All of the devices are shielded with lead, which is contained within a thick steel shell weldment. Group 3 devices are similar and have a maximum weight is approximately 2,650 lb. While the general shape and size of devices in Group 1 and 3 are similar, the exact dimensions and shapes are varied. For that reason, dunnage will be used to block and brace the device into position within the inner container (IC). Acceptable blocking/dunnage materials are metallic structures or polyurethane foam as defined in Section 7.1.2.2, *Loading the Inner Container (IC) Into the 1105-SD*.

The IC is designed to hold and provide support for the shielded device and the blocking materials during transport. It is depicted in Figure 1.2-7, Section 1.0, *General Information*. The IC is 59.5 inches tall and 42.75 inches in outer diameter, with an interior cavity of 36.0 inches in diameter and 53.0 inches long. The IC is a weldment made from ASTM A240, Type 304 stainless steel. The shell, the base, and the inner sheet of the lid are made from $\frac{1}{4}$ -inch thick material; the bolting flanges, of $\frac{1}{2}$ -inch thick material; and the grid pattern of stiffening and energy absorbing ribs on the outside are made from $\frac{3}{16}$ -inch thick material. The base structure is 4.0 inches thick and is stiffened by 8 ribs made from $\frac{1}{4}$ -inch thick material. The lid, attached using bolts and nuts, is 2.5 inches deep, with three, $\frac{1}{4}$ -inch thick ribs and three threaded blocks near the outer diameter for lifting the entire IC. The open space in the lid is filled with eight layers of

1/4-inch thick refractory insulation paper. The top of the lid is sealed with 16 GA (0.06-inch thick) sheet metal.

3.1.2 Content's Decay Heat

As discussed in Section 1.2.2, *Contents*, the contents within the LTSS and shielded device payloads is limited by the isotope involved. The maximum decay heat loading in the LTSS is limited to 200W, which is conservatively assumed to occur within one, minimum-size sealed source located in one drawer (Large Source Drawer or T80/780 drawer) of the LTSS. This maximum heat dissipation is associated with Co-60 source material, which deposits a significant portion of its heat directly into the surrounding shielding material via gamma rays. A discussion of the modeling of the gamma heating is provided in Section 3.5.3.2, *LTSS and LTSS Lodgment Thermal Model*. The decay heat loading in the shielded devices is conservatively set at 30W, which is approximately 150% of the heat generated by the maximum device activity stated in Table 1.2-2. All of the heat dissipation for the shielded devices is conservatively assumed to originate within the sealed source.

3.1.3 Summary Tables of Temperatures

Table 3.1-1 and Table 3.1-2 provide summaries of the package component temperatures with the LTSS and shielded device payloads, respectively, under normal and accident conditions. The temperatures for normal conditions are based on an analytical model of the 1105-SD package with an ambient temperature of 100 °F and the 10 CFR §71.71(c)(1) prescribed insolation applied as a diurnal loading (i.e., *NCT Hot* condition). The temperatures for accident conditions are based on a transient simulation using an analytical model of a damaged 1105-SD package. The damage conditions represent the worst-case hypothetical pre-fire damage predicted from a combination of physical drop testing using full-scale CTUs and analytical structural evaluations.

The results for NCT conditions demonstrate that significant thermal margins exist for all package components. Further, the NCT evaluations demonstrate that the accessible surface temperatures will be below the maximum 122 °F permitted by 10 CFR §71.43(g) for non-exclusive use shipment when transported in a 100 °F environment with no insolation (i.e., *NCT Hot (no solar)* condition). The results for HAC conditions also demonstrate that the design of the 1105-SD package provides sufficient thermal protection to yield component temperatures that are significantly below the acceptable limits defined for each component. See Sections 3.2.2, *Component Specifications*, Section 3.3, *Thermal Evaluation for Normal Conditions of Transport*, and Section 3.4, *Thermal Evaluation for Hypothetical Accident Conditions*, for more discussion.

3.1.4 Summary Tables of Maximum Pressures

Table 3.1-3 presents a summary of the maximum pressures predicted under NCT and HAC conditions. The 1105-SD package has a design maximum pressure of 25 psig (39.7 psia). Based on an assumed fill gas temperature of 70 °F and one atmosphere, the maximum pressure rise under NCT will be 2.3 psig, while the maximum pressure rise under HAC conditions will be 9.4 psig. Based on the NCT pressure, the maximum normal operating pressure (MNOP) is set at a bounding level of 5 psig. The maximum HAC pressure is conservatively assumed to be 10 psig.

Table 3.1-1 – Maximum NCT and HAC Temperatures with LTSS Payload

Location / Component	NCT, °F	HAC, °F ^④	Allowable Temperature, °F ^③	
			Normal	Accident
Sealed Source Capsule ^①	882	908	1,100	1,100
NLM-52 Special Form Capsule	263	350	800	800
Large Source Drawer	218	308	800	800
LTSS Liner	190	283	800	800
LTSS Lead	185	279	620	620
LTSS Shell	176	270	800	800
Lodgment, Lower Half	157	464	400	1,100
Lodgment, Upper Half	152	415	400	1,100
Neoprene	157	361	200	500
Shell	152	1,164	800	1,300
Inner Thermal Shield	148	1,337	2,500	2,500
Outer Thermal Shield	148	1,422	2,500	2,500
Top Thermal Shield	192	1,438	2,500	2,500
Lower Internal Impact Limiter	155	266	400	1,100
Upper Internal Impact Limiter	164	1,062	400	1,100
Lower Torispherical Head	147	277	800	1,300
Upper Torispherical Head	183	1,274	800	1,300
Closure Seals	144	270	250	400
Vent Port Sealing Washer	144	274	250	400
Impact Limiter				
- Max. Foam	151	N/A	300	N/A
- Avg. Foam	132	N/A	300	N/A
- Shell	151	1,474	800	2,500
Max. Accessible Surface without Insolation	117 ^②	-	122	N/A
Cask Cavity Bulk Gas	152	366	N/A	N/A

Notes: ① Results assume smallest source capsule (i.e., assumed 1.45" length x 0.72" diameter) dissipating 200 W in shortest NLM-52 special form capsule filled with argon gas.

② Maximum temperature occurs for the narrow band at base of the side thermal shield. Bulk of accessible surfaces are at a lower temperature.

③ See Section 3.2.2, *Component Specifications*, for basis of listed temperature criterion.

④ Listed peak HAC temperatures represent the maximum from two separate damage scenarios, see Section 3.4.3, *Maximum Temperatures and Pressure*.

Table 3.1-2 – Maximum NCT and HAC Temperatures with Shielded Device Payload

Location / Component	NCT, °F	HAC, °F	Allowable Temperature, °F ^③	
			Normal	Accident
Sealed Source Capsule ^①	471	537 ^④	1,100	1,100
SD Drawer	192	293 ^④	800	800
SD Liner	153	259 ^④	800	800
SD Lead	152	259 ^④	620	620
SD Shell	152	260 ^④	800	800
Foam Dunnage	152	406	300	435
IC	134	977	800	2,500
Shell	146	1,150	800	1,300
Inner Thermal Shield	142	1,311	2,500	2,500
Outer Thermal Shield	142	1,420	2,500	2,500
Top Thermal Shield	191	1,437 ^④	2,500	2,500
Lower Internal Impact Limiter	127	224	400	1,100
Upper Internal Impact Limiter	157 ^②	848	400	1,100
Lower Torispherical Head	129	258	800	1,300
Upper Torispherical Head	180	1,086	800	1,300
Closure Seals	129	248	250	400
Vent Port Sealing Washer	129	251	250	400
Impact Limiter				
- Max. Foam	148	N/A	300	N/A
- Avg. Foam	124	N/A	300	N/A
- Shell	148	1,474 ^④	800	2,500
Max. Accessible Surface without Insolation	103 ^②	-	122	N/A
Cask Cavity Bulk Gas	134	352	N/A	N/A

Notes: ① Results assume smallest source capsule (i.e., assumed 1.7" length x 1.57" diameter) dissipating 30 W.

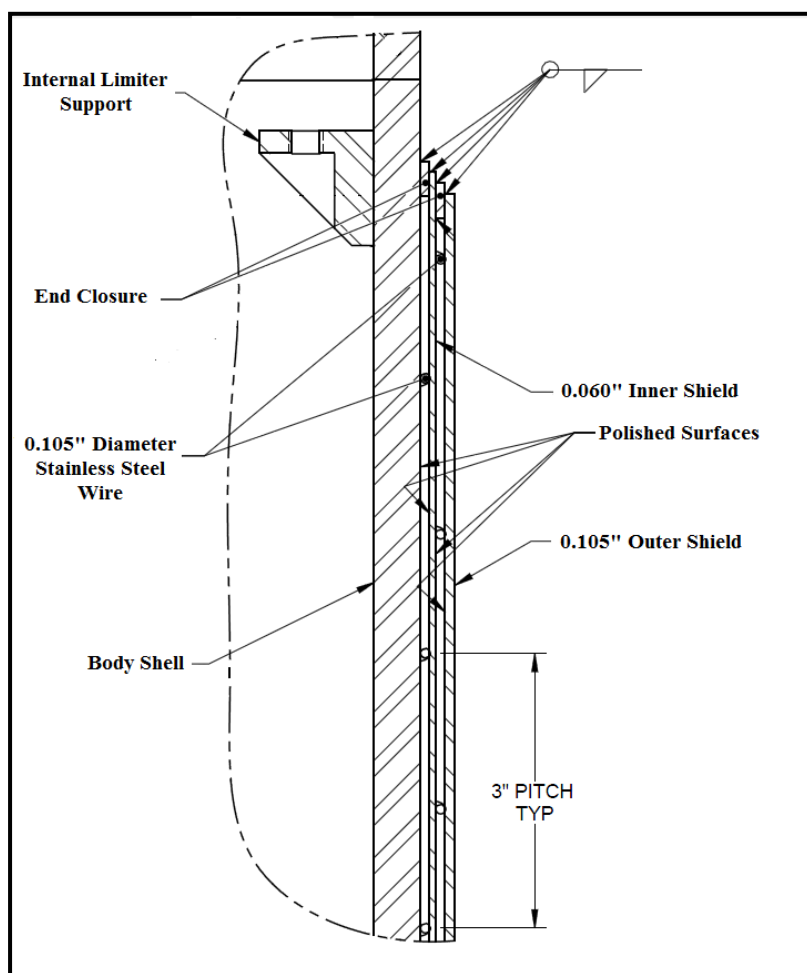
② Maximum temperature occurs for the narrow band at base of the side thermal shield. Bulk of accessible surfaces are at a lower temperature.

③ See Section 3.2.2, *Component Specifications*, for basis of listed temperature criterion.

④ Noted maximum temperature values are bounding when the shielded device is supported by metallic dunnage. All other temperatures are bounding when supported by polyurethane foam dunnage.

Table 3.1-3 – Summary of Maximum Pressures

Condition	Cask Cavity Pressure
NCT	2.3 psi gauge
HAC – LTSS Payload	8.2 psi gauge
HAC – Device Payload	9.4 psi gauge

**Figure 3.1-1: Dual Thermal Shield Layout**

3.2 Material Properties and Component Specifications

This section presents the thermal properties and specifications of the materials that affect heat transfer within the 1105-SD packaging and the LTSS, the shielded devices, and their support structures. Included are the gases (i.e., argon, and air) that may be present within the package and the gas (air) external to the package. The thermal absorptivities and emissivities appropriate for the package surface conditions for each thermal condition are identified.

3.2.1 Material Properties

The 1105-SD packaging is fabricated primarily of Type 304 austenitic stainless steel, polyurethane foam, and a small amount of 6061 aluminum. The closure bolts are fabricated from ASTM 320, Grade L43 alloy steel. ASTM 320, Grade L43 steel has approximately twice the thermal conductivity of Type 304 stainless steel at temperatures up to 800°F, while the specific heats of the two materials are similar at all temperature levels. The thermal model does not specifically model either the bolt's material or the bolt geometry. Justification for this modeling approach is provided in Appendix 3.5.3, *Analytical Thermal Model*.

The LTSS and shielded device payloads are fabricated primarily of Type 304 stainless steel and lead with minor amounts of tungsten and brass. The LTSS lodgment is fabricated of 6061-T6 aluminum, while the IC is fabricated of Type 304 stainless steel and refractory paper insulation. The dunnage/blocking used for the shielded devices is analyzed as either being entirely polyurethane foam or a metallic structure.

Table 3.2-1 presents the thermal properties of Type 304 stainless steel, 6061 aluminum, QQ-L-171E Grade A or C lead, tungsten, and brass. Properties for temperatures between the tabulated values are calculated via linear interpolation within the heat transfer code. The thermal properties for Type 304 stainless steel and 6061 aluminum are taken from the ASME material properties database [9] and the density is taken from an on-line materials database [8]. QQ-L-171E Grade A or C lead is 99.9% lead plus a small amount of copper (i.e., 0.04% to 0.08%) and other elements that are added for improved structural properties. The values listed in Table 3.2-1 are for ASTM B29 copperized lead [15] which has the same chemical makeup as QQ-L-171E Grade C lead. The nominal density for lead is 708 lbf/ft³ [8].

The emissivity of 'as-received' Type 304 stainless steel has been measured as 0.25 to 0.28 [18], while the emissivity of weathered Type 304 stainless steel has been measured as being between 0.36 to 0.44 [20]. An emissivity of 0.30 is assumed for the emittance from all non-brightened interior stainless steel surfaces based on a slightly weathered surface condition. A slightly lower emissivity of 0.25 is assumed for the mating surfaces at the closure seal due to the finer surface finish applied and maintained in that region. The outer face of the upper torispherical head and the cylindrical shell will receive a number 4 finish per ASTM A480, while both faces of the inner shield sheet, and the inside face of the outer shield sheet will receive a number 3 finish. The emissivity of a number 4 finish is 0.15, while the emissivity for a number 3 finish is 0.175 [21]. The emissivity of the outer faces of the package exposed to the ambient is 0.40 based on a weathered surface [20]. The solar absorptivity of Type 304/304L stainless steel for temperatures below 200°F is approximately 0.44 for the 'as-received' condition and 0.52 for the 'clean and smooth' condition [19]. A conservative value of 0.52 is used for normal conditions of transport.

The aluminum surfaces of the LTSS lodgment are assumed to have an emissivity of 0.20 based on an 'as-received' rough finish that has oxidized [19]. The emissivity for lead is not needed since the lead is assumed to be intimate contact with its surrounding surfaces and any radiative heat transfer is captured by the value assumed for the surface-to-surface contact. The intimate contact assumption reflects design experience that long term lead slump will yield an insignificant gap at the lead interface even if an initial gap is created following the lead pour process due to differential expansion.

Tungsten is used for shielding in the Large Source Drawers of the LTSS, while brass is used for the sleeves of the T80/780 source drawer for the LTSS and the source drawer for the Gammacell-40 shielded device. Thermal properties for tungsten are taken from [16] and for UNS C36000 brass from [8]. A temperature independent value for the thermal properties of brass is appropriate due to the limited extent of the material and the fact that temperature dependant properties for the material are not significant to the thermal results. Tungsten and brass are assumed to have emissivity values of 0.11 and 0.30, respectively, based on oxidized surfaces [19].

The polyurethane foam used in the impact limiter, the closure bolt enclosure structure, and dunnage/blocking for the shielded devices is based on a proprietary formulation that provides predictable impact-absorption performance under dynamic loading, while also providing an intumescent char layer that insulates and protects the underlying materials when exposed to HAC fire conditions. The thermal properties under NCT conditions are obtained from the manufacturer's website [5]. Because the website provides data at only a few specific densities and since the thermal conductivity of the material is tied to its density, interpolation is used to arrive at the listed material properties. Further, the manufacturing process for the poured in place foam can yield densities that are $\pm 15\%$ of the targeted value. As such, the calculation for 15 lb_m/ft³ (pcf) foam used in the impact limiter addresses the properties associated with both the low and high tolerance density foam (i.e., 12.75 and 17.25 pcf foam, see Table 3.2-2). Since the low tolerance foam yields a lower thermal conductivity, it is assumed for NCT operations, while the higher thermal conductivity of the high tolerance density foam is used for HAC evaluation to conservatively bound the heat flow into the package. The same process is not required for the 30 pcf foam used in closure bolt enclosure structure since it is formed from blocks with essentially zero deviation from the target density. The density of the dunnage/blocking foam used for the shielded devices is not important to safety since the level of heat transfer through the material is insignificant regardless of its density. The modeling assumes the properties of 15 pcf foam. The performance of polyurethane foam under HAC conditions is addressed in Appendix 3.5.4, '*Last-A-Foam*' Response under HAC Conditions. The potential for increased cavity pressure due to foam off-gassing addressed in Section 3.4.3.4, *Maximum HAC Pressures*, is conservatively based on the maximum foam dunnage weight permitted.

The refractory paper insulation used at the base of the impact limiter, the closure bolt enclosure structure, and the IC lid is a lightweight material processed from highly washed, spun, high purity alumina silica fibers that are formed into a highly flexible sheet. The material is easy to cut, wrap, or form, and it offers low thermal conductivity, low heat storage, and high heat reflectance. The material is resilient with excellent compression recovery. The thermal properties presented in Table 3.2-2 are based on the manufacturer's product brochure for LyTherm[®] 1530-L [17].

The thermal properties for neoprene synthetic rubber are also presented in Table 3.2-2. The properties, based on the *Polymer Data Handbook* [11], are assumed to be constant with

temperature. The density value assumed in the modeling is conservatively low for neoprene with a 85 Duro hardness.

The polyurethane foam and the LyTherm[®] refractory paper material have an assumed emissivity of approximately 0.90 [19] based on a combination of the material type and surface roughness. The same emissivity is assumed for the neoprene rubber.

The thermal properties for air, as derived from curve fits provided in [23], are presented in Table 3.2-3. Because the gas thermal conductivity varies significantly with temperature, the computer model calculates the thermal conductivity between the package and the ambient as a function of the mean film temperature. The calculation conservatively assumes argon as the backfill gas in the NLM-52 special form capsule used in the Large Source Drawers of the LTSS. Those properties, presented in Table 3.2-4, were also derived from curve fits provided in [23].

3.2.2 Component Specifications

The acceptance criteria for normal conditions is that the package components remain within their respective thermal limits and that the 1105-SD packaging maintains containment for the payload. Only a few materials used in the 1105-SD packaging are considered temperature sensitive. These are the butyl rubber compound used for the containment boundary and vent/test port seals, the polyurethane foam used in the impact limiters, and the 6061-T6 aluminum used in the internal impact limiters. The materials considered temperature sensitive for the payloads are the 6061-T6 aluminum used for the LTSS lodgment, the lead used for the radiological shielding of the sealed sources, the outer shell of the sealed sources, and the polyurethane foam used for dunnage/blocking of the shielded devices. The other materials either have temperature limits above the maximum expected temperatures or are not considered essential to the function of the package.

The butyl rubber compound used for the containment and vent/test port seals is fabricated from Rainier Rubber compound R0405-70. Butyl rubber has a long term temperature range of at least -40 °F to 250 °F and a short-term limit of 400 °F for 8 hours. See Section 2.12.5, *Seal Performance Tests*, for the basis of these temperature limits.

Below 250 °F the variation in the thermal properties with temperature for the proprietary polyurethane foam are slight and reversible. While small variations in the foam properties will occur between 250 and 500 °F, the observed changes in foam thermal conductivity, specific heat, and density are so slight that the same thermal properties used for temperatures below 250 °F may also be used to characterize the thermal performance of the foam between 250 and 500 °F. For conservatism, a long-term limit of 300 °F is assumed for the foam. There is no short term temperature limit for the foam used in the impact limiter as its decomposition under exposure to high temperatures is part of its mechanism for providing thermal protection during the HAC fire event. A short term temperature limit of 435 °F is assumed for foam used as dunnage/blocking for the shielded devices within the IC. This temperature limit is conservatively below 500 °F where significant weight loss due to thermal decomposition begins to occur for the material. A detailed description of the foam's behavior under elevated temperatures is presented in Appendix 3.5.4, *'Last-A-Foam' Response Under HAC Conditions*.

Aluminum has a melting point of approximately 1,100°F [8]; however for strength purposes the normal operational temperature is limited to 400 °F based on structural strength considerations for aluminum [9]. The limit under HAC conditions is 1,100 °F. Since the internal impact limiters are fabricated from a combination of stainless steel and aluminum, the lower temperature

limits for aluminum are conservatively assumed as the allowable temperature for the internal impact limiters.

Type 304 stainless steel has a melting point above 2,500 °F [8], but in compliance with ASME B&PV Code [10], its allowable temperature is limited to 800°F for structural components (e.g., the material's structural properties are relied on for loads postulated to occur in the respective operating mode or accidental free drop condition). As such, the appropriate upper temperature limit under normal conditions is 800 °F for stainless steel components that form the containment boundary or are used in the payload support. An allowable short term temperature limit of 1,300 °F is used for the torispherical heads of the package's containment boundary based on evaluations presented in Section 2.7.4.3, *Stress Calculations*. The same temperature limit will conservatively bound the short term limit for the cylindrical shell of the package's containment boundary. The IC does not have a structural role after the free drop. As such, the appropriate short-term temperature limit is the melting point for stainless steel (2,500 °F). The upper limit for all other stainless steel components is assumed to be 2,500 °F for both normal and accident conditions.

A neoprene (chloroprene) pad is attached to the lodgment using stainless steel screws to provide a cushion for the LTSS. Neoprene bumpers may also be used on dunnage in the IC. Properties of neoprene related to its potential thermal decomposition/combustion under elevated temperatures are as follows:

- a) chemical formulation [11]: $-\text{[CH}_2\text{-Cl-C=CH-CH}_2\text{]}_n-$,
- b) working temperature range [8]: -40 °F to 200 °F
- c) oxygen index [12]: 32-35% at atmospheric pressure,
- d) melting temperature: N/A - thermoset material
- e) temperature for initial decomposition [14]: 500 °F
- f) auto ignition temperature [12]: >700 °F in a 21% oxygen concentration environment

As a thermoset plastic, uncontrolled heating of neoprene will result in thermal decomposition and not melting. The high oxygen index demonstrates why neoprene can't support combustion without an external ignition source under normal atmospheric conditions. Based on the above information, the appropriate temperature range under normal conditions is -40 °F to 200 °F and 500 °F for accident conditions. Maintaining the neoprene below 500 °F will prevent significant off-gassing and eliminate any possibility for auto ignition of the material. The potential for thermal decomposition of payload materials under HAC is discussed in Section 3.4.3.5, *Behavior of Non-metallic Contents Materials Under HAC*.

The temperature sensitive material for the payloads include the 6061-T6 aluminum used for the LTSS lodgment, the lead used for the radiological shielding of the sealed sources, the outer shell of the sealed sources and the polyurethane foam used for dunnage/blocking of the shielded devices. The allowable temperature limits for the LTSS lodgment are the same as discussed for aluminum. The QQ-L-171E lead used for payload shielding serves no structural purpose but avoidance of lead melting is desirable because of possible shielding loss associated with the movement of the lead within the cavity. As such, the temperature limitation for either normal or accident conditions is the melting point for lead of approximately 620 °F [8].

The maximum allowable shell temperature for the source capsule is 1,100 °F (600 °C) [22]. The maximum accessible outside surface temperature of the package shall be less than 122 °F in

100 °F air temperature and in the shade [1]. The minimum allowable service temperature for all package components is below -40 °F.

Table 3.2-1 – Thermal Properties of Metallic Materials (2 pages)

Material	Temperature (°F)	Thermal Conductivity (Btu/hr-ft-°F)	Specific Heat (Btu/lb_m-°F)	Density (lb_m/in³)
Stainless Steel Type 304	-40 ^①	8.2	0.112	0.289
	70	8.6	0.114	
	100	8.7	0.115	
	200	9.3	0.119	
	300	9.8	0.123	
	400	10.4	0.126	
	500	10.9	0.129	
	600	11.3	0.130	
	700	11.8	0.132	
	800	12.3	0.134	
	1000	13.1	0.135	
	1200	14.0	0.138	
	1400	14.9	0.141	
	1500	15.3	0.142	
Aluminum Type 6061-T6	-40 ^①	93.2	0.208	0.0975
	70	96.1	0.214	
	100	96.9	0.216	
	150	98.0	0.220	
	200	99.0	0.222	
	250	99.8	0.224	
	300	100.6	0.227	
	350	101.3	0.230	
	400	101.9	0.231	
	600 ^①	104.3	0.236	
Copperized Lead (QQ-L-171E Grade A or C)	-58	21.7	0.030	0.410
	32	20.4	0.030	
	80.6	30.0	0.030	
	158	19.9	0.031	
	260.6	19.4	0.032	
	428	18.4	0.033	
	608	16.5	0.033	
	620.6	16.4	0.036	

Table 3.2-1 – Thermal Properties of Metallic Materials (2 pages)

Material	Temperature (°F)	Thermal Conductivity (Btu/hr-ft-°F)	Specific Heat (Btu/lb_m-°F)	Density (lb_m/in³)
Tungsten	80	100.5	0.032	0.697
	260	91.9	0.033	
	620	79.2	0.034	
	980	72.2	0.035	
Brass	-	66.5	0.091	0.307

Note: ① Properties values at indicated temperature based on linear extrapolation of other values

Table 3.2-2 – Thermal Properties of Non-Metallic Materials

Material	Temperature (°F)	Thermal Conductivity (Btu/hr-ft-°F)	Specific Heat (Btu/lb_m-°F)	Density (lb_m/ft³)
Polyurethane Foam	-	0.0262	0.353	17.25
	-	0.0213		12.75
	-	0.0398		30
LyTherm [®] Paper Insulation	100	0.020	0.136	7.5
	500	0.036	0.209	
	800	0.047	0.227	
	1300	0.069	0.245	
	1600	0.082	0.254	
Neoprene	-	0.110	0.522	76.8

Table 3.2-3 – Thermal Properties of Air

Temperature (°F)	Density (lb _m /in ³) ^①	Specific Heat (Btu/lb _m -°F)	Dynamic Viscosity (lb _m /ft-hr)	Thermal Conductivity (Btu/hr-ft-°F)	Prandtl Number ^②	Coef. Of Thermal Exp. (°R ⁻¹) ^③
-40	Use Ideal Gas Law w/ Molecular wt = 28.966	0.240	0.03673	0.0121	Compute as Pr = c _p μ / k	Compute as β = 1/(°F+459.67)
0		0.240	0.03953	0.0131		
50		0.240	0.04288	0.0143		
100		0.241	0.04607	0.0155		
200		0.242	0.05207	0.0178		
300		0.243	0.05764	0.0199		
400		0.245	0.06286	0.0220		
500		0.248	0.06778	0.0240		
600		0.251	0.07242	0.0259		
700		0.253	0.07680	0.0278		
800		0.256	0.08098	0.0297		
900		0.259	0.08500	0.0315		
1000		0.262	0.08887	0.0333		
1200		0.269	0.09620	0.0366		
1400		0.274	0.10306	0.0398		
1500		0.277	0.10633	0.0412		

Table Notes:

- ① Density computed from ideal gas law as $\rho = PM/RT$, where R= 1545.35 ft-lbf/lb-mole-R, T= temperature in °R, P= pressure in lbf/ft², and M= molecular weight of air. For example, at 100 °F and atmospheric pressure of 14.69lbf/in², $\rho = (14.69 \times 144 \text{ in}^2/\text{ft}^2 \times 28.966 \text{ lbm/lb-mole}) / (1545.35 \times (100 + 459.67)) = 0.071 \text{ lbm/ft}^3$.
- ② Prandtl number computed as $Pr = c_p \mu / k$, where c_p= specific heat, μ = dynamic viscosity, and k = thermal conductivity. For example, at 100 °F, $Pr = 0.241 \times 0.04607 / 0.0155 = 0.72$.
- ③ Coefficient of thermal expansion is computed as the inverse of the absolute temperature. For example, at 100 °F, $\beta = 1/(100 + 459.67) = 0.00179$.

Table 3.2-4 – Thermal Properties of Argon

Temperature (°F)	Density (lb _m /in ³) ^①	Specific Heat (Btu/lb _m -°F)	Dynamic Viscosity (lb _m /ft-hr)	Thermal Conductivity (Btu/hr-ft-°F)	Prandtl Number ^②	Coef. Of Thermal Exp. (°R ⁻¹) ^③
-40	Use Ideal Gas Law w/ Molecular wt = 39.948 g/mole	0.124	0.0444	0.0083	Compute as Pr = c _p μ / k	Compute as β = 1/(°F+459.67)
0			0.0480	0.0089		
50			0.0524	0.0097		
100			0.0566	0.0105		
200			0.0645	0.0120		
300			0.0718	0.0134		
400			0.0788	0.0148		
500			0.0853	0.0160		
600			0.0914	0.0172		
700			0.0972	0.0183		
800			0.1028	0.0194		
900			0.1081	0.0205		
1000			0.1133	0.0215		
1200			0.1230	0.0234		

Table Notes:

- ① Density computed from ideal gas law as $\rho = PM/RT$, where R= 1545.35 ft-lbf/lb-mole-R, T= temperature in °R, P= pressure in lbf/ft², and M= molecular weight of argon. For example, at 100 °F and atmospheric pressure of 14.69lbf/in², $\rho = (14.69 \times 144 \text{ in}^2/\text{ft}^2 \times 39.948 \text{ lbm/lb-mole}) / (1545.35 \times (100+459.67)) = 0.098 \text{ lbm/ft}^3$.
- ② Prandtl number computed as $Pr = c_p \mu / k$, where c_p= specific heat, μ = dynamic viscosity, and k = thermal conductivity. For example, at 100 °F, $Pr = 0.124 \times 0.0566 / 0.0105 = 0.67$.
- ③ Coefficient of thermal expansion is computed as the inverse of the absolute temperature. For example, at 100 °F, $\beta = 1/(100+459.67) = 0.00179$.

3.3 Thermal Evaluation for Normal Conditions of Transport

This section presents the thermal and gas generation evaluation of the 1105-SD package under normal conditions of transport (NCT). The package and payload configurations are assumed to be as described in Section 3.1, *Description of Thermal Design*. The thermal model used in the evaluation is described in Appendix 3.5.3, *Analytical Thermal Model*, while the thermal properties assumed for the various components are presented in Section 3.2.1, *Material Properties*. These evaluations establish the thermal and gas safety basis required to assess compliance with the 10CFR71 safety criteria [1] for the *NCT Hot*, *NCT Hot (no solar)*, and *NCT Cold* conditions. The safety basis for the *NCT Hot* ambient condition is evaluated using a diurnal cycle for insolation.

3.3.1 Heat and Cold

The NCT thermal performance is determined using three separate 3-D thermal models of the 1105-SD packaging with its various payloads. The modeling for all payloads is developed for use with the Thermal Desktop[®] [25 & 41] and SINDA/FLUINT [26 & 42] computer programs. Details of the thermal models and the analysis methodology are provided in Appendix 3.5.3, *Analytical Thermal Model*.

LTSS Payload

For the bounding LTSS payload, the model provides a full height, 180° representation of the system using approximately 32,600 thermal nodes, 11,000 solids, and 12,000 planar elements. The LTSS modeling conservatively assumes that only one Large Source Drawer in the LTSS is loaded with isotope material dissipating a maximum 200 W of decay heat. The temperatures and thermal gradients arising from this loading condition will bound those associated with the other loading scenarios.

Shielded Device Payload

The NCT thermal performance of the shielded device payload is determined using two 3-D thermal models of the 1105-SD package. One thermal model utilizes the maximum amount of insulating polyurethane foam blocking/dunnage allowed in the IC, while the other has no dunnage explicitly modeled. The first case represents the most restrictive case for heat transfer between the shielded device and the IC and analyzes the worst case for gas generation from the polyurethane foam dunnage. The second case represents the least-restrictive configuration.

The case including foam dunnage maximizes the thermal insulation of the dunnage supporting the shielded device. It utilizes a quarter symmetry representation, since the device is located on the package axis and has only a single drawer, so that potential asymmetric loading is not an issue. This model of the 1105-SD packaging with the shielded device payload uses approximately 20,000 thermal nodes, 5,300 solids, and 5,250 planar elements.

The case representing metallic dunnage maximizes the potential for heat transfer by increasing the available surface area for convection and radiation between the IC and the device. It is constructed using half symmetry in order to be consistent with the conservative modeling assumption used for HAC (see Section 3.4.3.3.2, *Side Drop Damage with Shielded Device Payload and Metallic Dunnage*). This model uses half symmetry representation of the package like the LTSS modeling. The second model uses approximately 35,000 thermal nodes, 10,500 solids, and 10,100 planar elements.

3.3.1.1 Maximum Temperatures

LTSS Payload

Table 3.3-1 presents the predicted 1105-SD package temperatures under NCT conditions for the transportation of the LTSS payload dissipating 200 W of decay heat. The analysis assumes the package is backfilled with air at atmospheric pressure at the time of loading. The results demonstrate that large thermal margins exist for all packaging and payload components. The minimum thermal margin of 106°F (i.e., 250 - 144°F), occurs for the cask closure seals. The large temperature rise between the special form capsule and the sealed source capsule in the Large Source Drawer is due to the conservative assumption of the 200 W loading occurring within a single, minimum size source capsule and no credit for direct contact between the source capsule and special form capsule sides. The relatively low temperatures seen for the other LTSS components reflects the effectiveness of the lead shielding to disperse the heat flux over the entire volume of the LTSS. The relatively large ratio of surface area of the 1105-SD package to the 200 W heat loading allows the package to dissipate the heat loading to the ambient conditions with only a small ΔT .

Per the discussion in Section 3.1.1.1, *Design Features of LTSS Payload*, neoprene rubber is used on the lower lodgment's support plate and rib edges. Since these surfaces are also in direct contact or close proximity with the LTSS payload, they also represent the hottest temperatures achieved by the lower lodgment under NCT. As seen from Table 3.3-1, the peak temperature of the neoprene rubber on these surfaces remains well below the allowable long term temperature limit for neoprene for all NCT conditions.

Figure 3.3-1 presents the predicted temperature distribution within the 1105-SD package for the NCT Hot condition and at the point in the diurnal insolation cycle where the solar heating on the package reaches its maximum. It is clearly evident from the temperature distribution that the majority of the temperature rise between the ambient and the source capsule occurs within the Large Source Drawer of the LTSS (note, for purposes of enhancing the clarity of the displayed temperature contours, the source capsule is not shown).

Since the use of the T80/780 drawer to house the sealed source capsule will result in a much smaller gap between the source capsule and the drawer and eliminate the added resistance posed by the presence of the NLM-52 special form capsule and the Large Source Drawer between the ends of the source capsule and the LTSS liner, the results for the Large Source Drawer above will bound those achieved with the T80/780 drawers regardless of whether lead, tungsten, or depleted uranium is used for shielding.

Evaluation of the package for an ambient air temperature of 100 °F without insolation loads demonstrates that the peak temperature for the accessible exterior surfaces of the packaging is below the maximum 122°F permitted by 10 CFR §71.43(g) for non-exclusive use shipments. As seen in Figure 3.3-2, the peak accessible surface temperature of 117°F occurs in a narrow band at the base of the side thermal shields where the closeout welds provide a direct thermal path to the package shell. Beyond this narrow region the accessible surface temperatures are significantly lower.

Shielded Device Payload

Table 3.3-2 presents the bounding predicted 1105-SD package temperatures of both models under NCT conditions for the transportation of a generic shielded device payload dissipating 30

W of decay heat. As with the LTSS model, both analyses assume the package is backfilled with air at atmospheric pressure at the time of loading.

Figure 3.3-3 presents the predicted temperature distribution within the 1105-SD package for the NCT Hot condition utilizing polyurethane foam blocking/dunnage at the point in the diurnal insolation cycle where the external thermal shield on the package reaches its maximum temperature. It is clearly evident from the temperature distribution that the majority of the temperature rise between the ambient and the source capsule occurs very near the source.

Figure 3.3-4 presents the predicted temperature distribution within the 1105-SD package with no dunnage explicitly modeled at the point in the diurnal insolation cycle where the external thermal shield on the package reaches its maximum temperature.

3.3.1.2 Minimum Temperatures

Table 3.3-1 presents the predicted package temperatures for the cold condition of transport (i.e., -20 °F, no solar, consistent with Regulatory Guide 7.8 [4]) with the LTSS payload. Since a portion of the heat transfer between the LTSS and the package shell is via radiation, the change in the temperature gradient between adjacent components of the packaging is larger for the cold ambient temperature versus the hot conditions. However, due to the relatively low decay heat loading, the differences are relatively small and not thermally significant.

Table 3.3-2 presents the cold condition results for the generic shielded device when supported by polyurethane foam dunnage. An explicit analysis of the shielded device when supported by metallic dunnage is not warranted because it has the same low decay heat loading, and thus can be expected to have the same thermally insignificant temperature gradients between adjacent components.

The minimum package temperature achieved for either payload will occur with a zero decay heat load and an ambient air temperature of -40 °F per 10 CFR §71.71(c)(2). The evaluation of this steady-state thermal condition requires no formal thermal calculation since all package components will eventually achieve the -40 °F temperature. As discussed in Section 3.2.2, *Component Specifications*, -40 °F is within the allowable operating temperature range for all package components.

3.3.2 Maximum Normal Operating Pressure

The package cavity is assumed to be filled with air at atmospheric pressure following loading procedure. None of the packaging components nor the LTSS or shielded devices contain material that is expected to decompose or outgas under the predicted NCT thermal conditions. As such, the pressurization of the package cavity will arise solely from ideal gas expansion.

The peak pressure developed within the package cavity under NCT conditions is estimated by assuming that the bulk average gas temperature at the time of loading is 70 °F. Combining this temperature with the predicted bulk gas temperature under the NCT Hot conditions and the ideal gas law yields:

$$\text{Cavity Pressure} = 14.7 \text{ psia} \frac{(152^\circ \text{F} + 460^\circ \text{F})}{(70^\circ \text{F} + 460^\circ \text{F})} - 14.7 \text{ psia}$$

$$\text{Cavity Pressure} = 2.3 \text{ psig}$$

Based on this same approach, the NCT pressures for the other transport conditions and for the shielded device payload are presented in Table 3.3-3. For conservatism, the maximum normal operating pressure (MNOP) within the package cavity is set at a bounding level of 5 psig.

Table 3.3-1 – NCT Temperatures for 1105-SD Packaging with LTSS Payload

Component	Temperature (°F)			
	NCT Hot (No Solar)	NCT Hot	NCT Cold	Allowable Temperature ^③
Sealed Source Capsule ^①	877	882	852	1,100
Special Form Capsule	246	263	143	800
Large Source Drawer	201	218	95	800
LTSS Liner	172	190	61	800
LTSS Lead	167	185	56	620
LTSS Shell	159	176	48	800
Lodgment, Lower Half	137	157	24	400
Lodgment, Upper Half	128	152	13	400
Neoprene	137	157	24	200
Shell	121	152	5	800
Inner Thermal Shield	117	148	0	2,500
Outer Thermal Shield	117	148	-1	2,500
Top Thermal Shield	112	192	-5	2,500
Lower Internal Impact Limiter	135	155	21	400
Upper Internal Impact Limiter	118	164	3	400
Lower Torispherical Head	126	147	8	800
Upper Torispherical Head	110	183	-7	800
Closure Seals	121	144	4	250
Vent Port Sealing Washer	120	144	3	250
Impact Limiter				
- Max. Foam	126	151	8	300
- Avg. Foam	110	132	-9	300
- Shell	118	151	0	800
Max. Accessible Surface	117 ^②	-	-	122
Cask Cavity Bulk Gas	128	152	13	N/A

Notes: ① Results assume smallest source capsule (i.e., assumed 1.45" length x 0.72" diameter) dissipating 200 W in shortest special form capsule filled with argon gas.

② Maximum temperature occurs for the narrow band at the base of the side thermal shield. Bulk of accessible surfaces are at a lower temperature.

③ See Section 3.2.2, *Component Specifications*, for basis of listed temperature criterion.

Table 3.3-2 – NCT Temperatures for 1105-SD Packaging with SD Payload

Component	Temperature (°F)			
	NCT Hot (No Solar)	NCT Hot	NCT Cold	Allowable Temperature ^③
Sealed Source Capsule ^①	461	471	399	1,100
SD Drawer	176	192	71	800
SD Liner	136	153	24	800
SD Lead	136	152	24	620
SD Shell	135	152	23	800
Foam Dunnage	135	152	23	300
IC	111	134	-7	800
Shell	105	146	-14	800
Inner Thermal Shield	104	142	-16	2,500
Outer Thermal Shield	103	142	-16	2,500
Top Thermal Shield	102 ^④	191	-19	2,500
Lower Internal Impact Limiter	104	127	-15	400
Upper Internal Impact Limiter	103 ^④	157 ^④	-18	400
Lower Torispherical Head	103	129	-16	800
Upper Torispherical Head	102 ^④	180	-19	800
Closure Seals	103	129	-17	250
Vent Port Sealing Washer	103	129	-17	250
Impact Limiter				
- Max. Foam	103	148	-16	300
- Avg. Foam	101	124	-18	300
- Shell	102	148	-17	800
Max. Accessible Surface	103 ^②	-	-	122
Cask Cavity Bulk Gas	108	134	-10	N/A

Note: ① Results assume smallest source capsule (i.e., assumed 1.7" length x 1.57" diameter) dissipating 30 W.

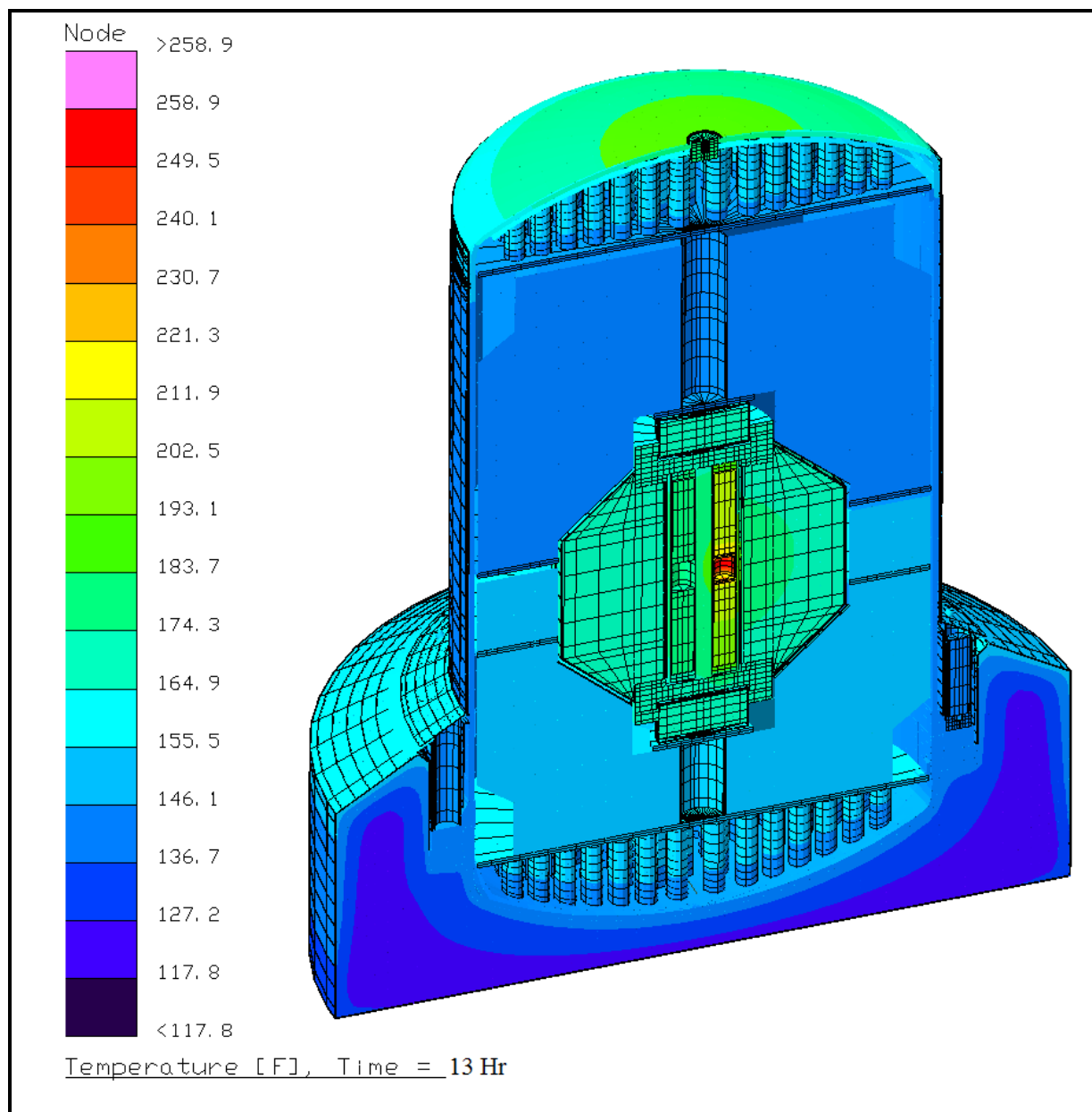
② Maximum temperature occurs for the narrow band at the base of the side thermal shield. Bulk of accessible surfaces are at a lower temperature.

③ See Section 3.2.2, *Component Specifications*, for basis of listed temperature criterion.

④ Noted maximum temperature values are bounding when the shielded device is supported by metallic dunnage. All other temperatures are bounding when supported by polyurethane foam dunnage.

Table 3.3-3 – NCT Pressures for 1105-SD Packaging

Condition	Package Cavity Pressure	
	LTSS Payload	Shielded Device Payload
NCT Hot (No Solar)	1.6 psi gauge	1.1 psi gauge
NCT Hot	2.3 psi gauge	1.8 psi gauge
NCT Cold	-1.6 psi gauge	-2.2 psi gauge



Note: For display clarity, the source capsule temperatures are not shown in the figure

Figure 3.3-1 – NCT Temperature Distribution for LTSS Payload¹

¹ Temperature distribution shown at point of peak solar heating during 24 hour diurnal cycle on insolation

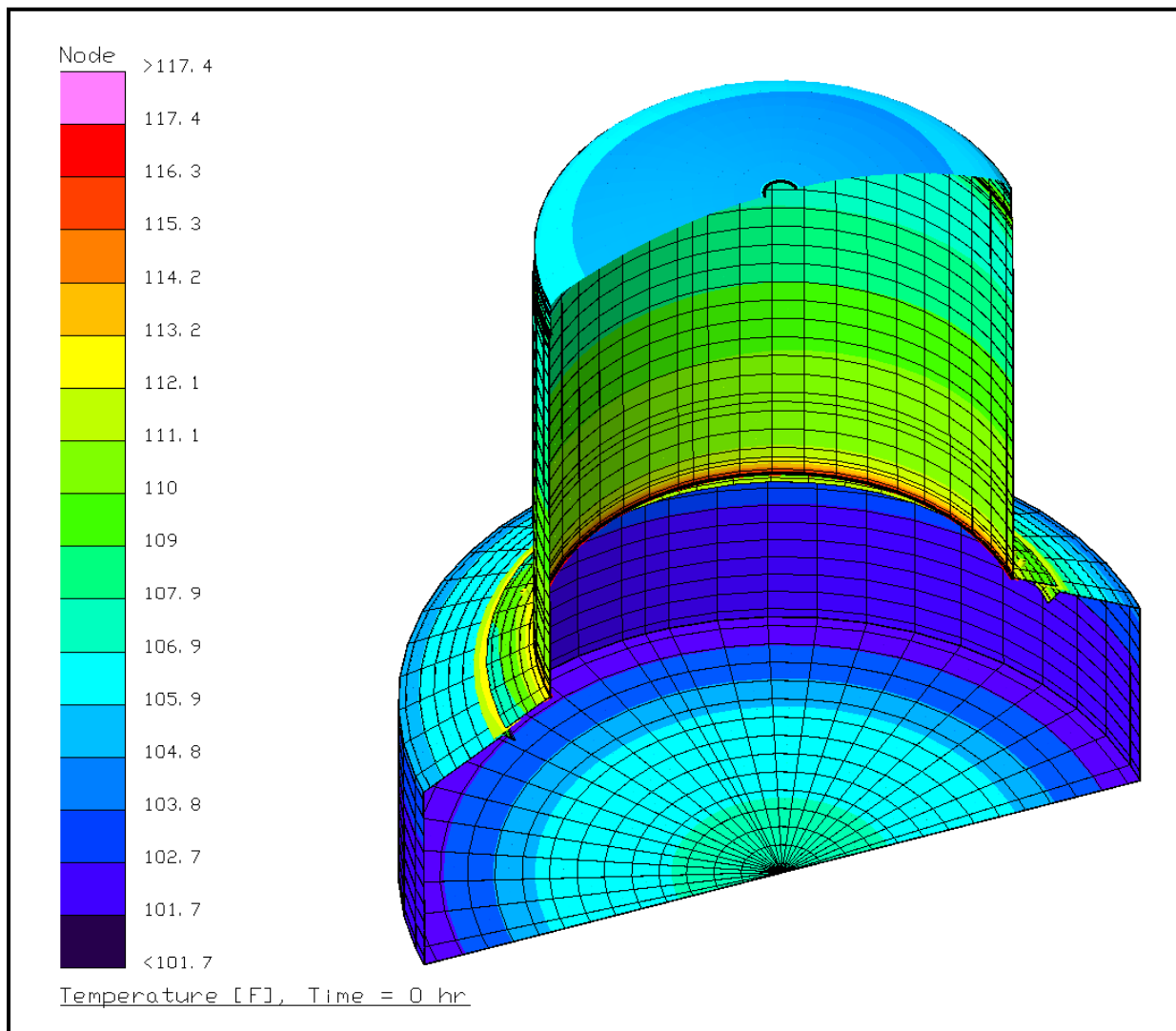
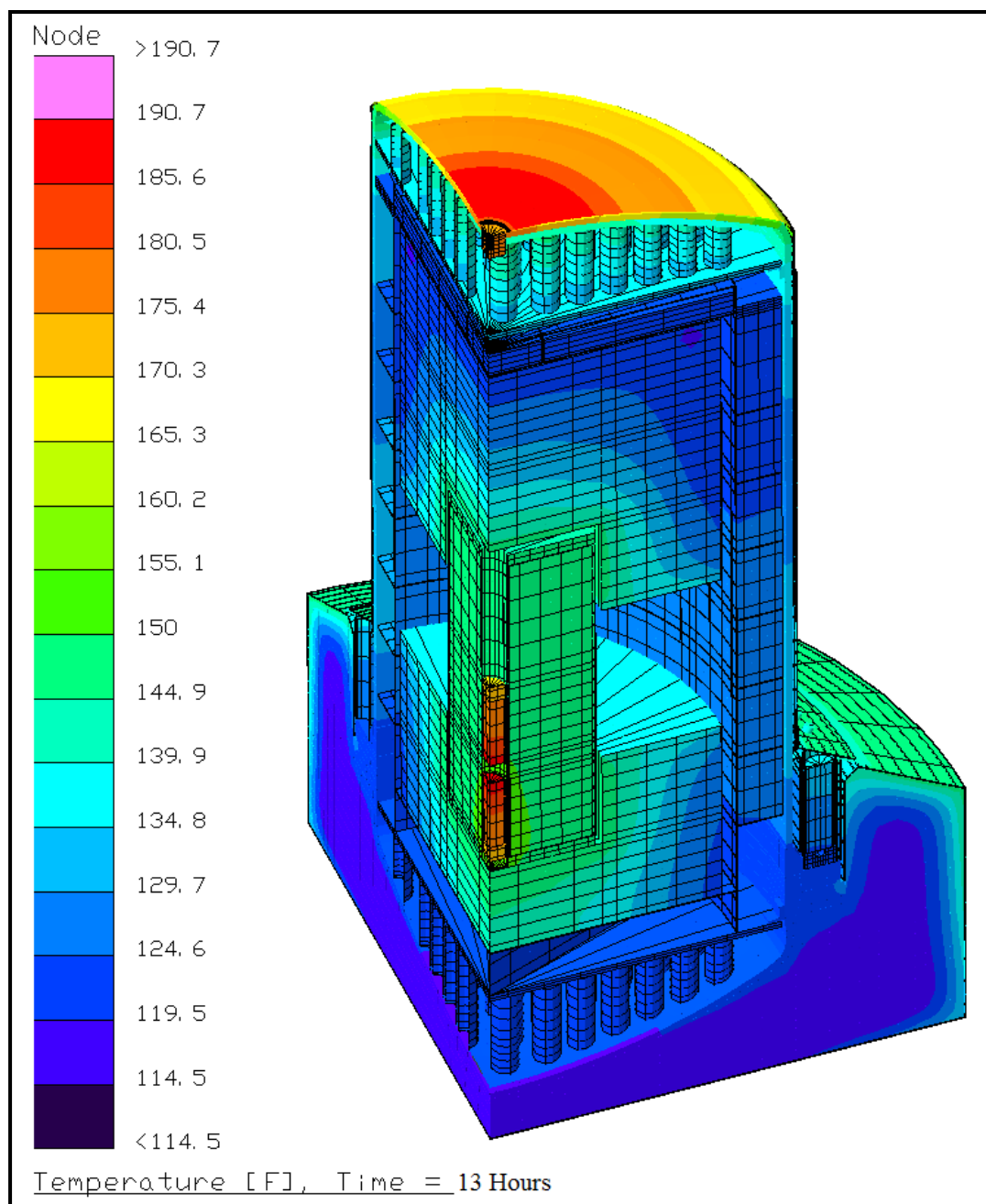


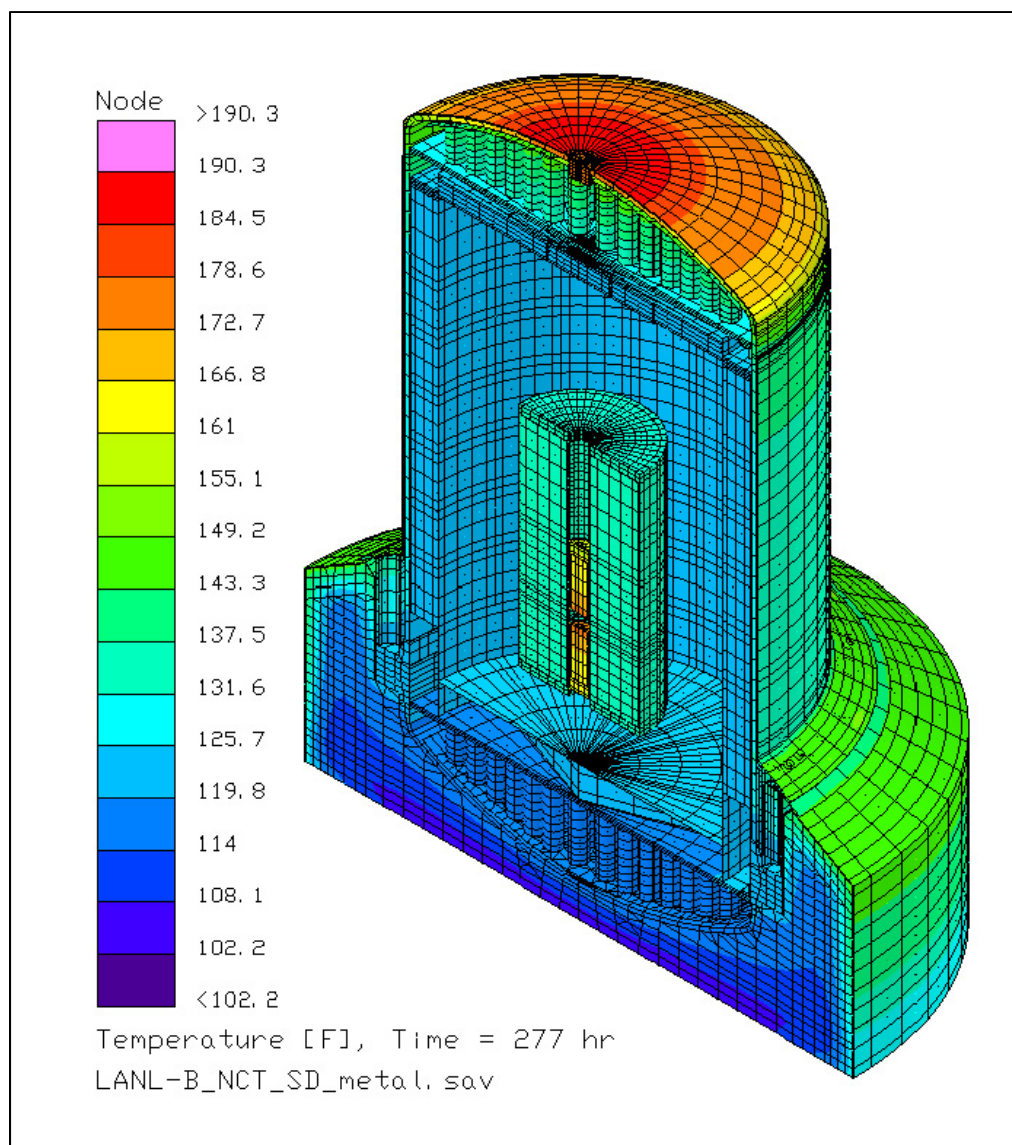
Figure 3.3-2 – Accessible Surface Temperature Distribution



Note: For display clarity, the source capsule temperatures are not shown in the figure

Figure 3.3-3 – NCT Temperature Distribution for Generic Shielded Device Supported by Polyurethane Foam Dunnage²

² Temperature distribution shown at point of peak solar heating during 24 hour diurnal cycle on insolation



Note: For display clarity, the source capsule temperatures are not shown in the figure

Figure 3.3-4 – NCT Temperature Distribution for Generic Shielded Device Supported by Metallic Dunnage³

³ Temperature distribution shown at point of peak solar heating during 24 hour diurnal cycle on insolation

3.4 Thermal Evaluation for Hypothetical Accident Conditions

This section presents the thermal evaluation of the 1105-SD package under the hypothetical accident condition (HAC) specified in 10 CFR §71.73(c)(4). The evaluation is based on modified versions of the analytical NCT thermal models for the 1105-SD package with the LTSS and shielded device payloads. Appendix 3.5.3.7, *Description of Thermal Model for HAC Conditions*, presents a description of the modifications made to the NCT model to reflect the HAC conditions.

Physical testing using prototypic full-scale certification test units (CTUs) is used to establish the expected level of damage sustained by the 1105-SD package from the 10 CFR 71.73 prescribed free and puncture drops preceding the HAC fire event. The configuration and initial conditions of the test article, the test facilities and instrumentation used, and the test results are documented in Section 2.12.3, *Certification Test Results*. An overview of the test results, the rationale for selecting the worst-case damage scenario, and the details of the thermal modeling used to simulate the package conditions during the HAC fire event are provided in Appendix 3.5.3.7, *Description of Thermal Model for HAC Conditions*.

3.4.1 Initial Conditions

The initial conditions assumed for the package prior to the HAC event are described below in terms of the modifications made to the NCT thermal model to simulate the assumed package conditions prior to and during the HAC event. These thermal model modifications are:

- simulated the expected damage arising from side or head down HAC free drops, determined in Appendix 3.5.3.7, *Description of Thermal Model for HAC Conditions*, to represent the worst case damage, and added the associated puncture drop damage,
- changed the package orientation from upright to horizontal to reflect the assumed position of the package following an HAC accident event and since this orientation maximizes the heat transfer between the shell of the package and the payloads,
- added heat transfer to and from the base of the package to simulate a fully engulfing fire event,
- increased the emissivity of all external surfaces to 0.8 and the solar absorptivity to 0.9 to account for possible oxidation and/or soot accumulation on the surfaces,
- increased the emissivity of the interior surface of the outer thermal shield from 0.175 to 0.225 to account for potential oxidization during the course of the HAC event,
- removed 1.8 to 2.8 inches of foam from the exterior portions of the impact limiter foam block and added heat transfer via radiation within the impact limiter enclosures with an emissivity of 0.95 to account for the loss of polyurethane foam from thermal decomposition. While this foam volume would be gradually lost over the course of the 30-minute fire event, the modeling conservatively assumes this foam volume is lost instantaneously at the start of the fire event.

- assumed an initial temperature distribution equivalent to the package's condition at the 14 hour point in the transient NCT analysis with a 100 °F ambient and diurnal insolation loading (see Section 3.5.3.5, *Insolation Loads*). This time point captures the peak shell temperatures achieved during the daily cycle in insolation loading.

Based on the CTU drop test results discussed in Section 2.12.3, *Certification Test Results*, the LTSS and shielded device payloads supported by polyurethane foam dunnage are predicted to remain intact and experience no significant damage or re-positioning as a result of the drop events. The shielded device supported by metallic dunnage is conservatively assumed to move to a position in contact with the hot wall of the IC. Since the packaging geometry is essentially axis-symmetrical, the thermal performance under HAC conditions is independent of the rotational orientation of the packaging.

3.4.2 Fire Test Conditions

The fire test conditions analyzed to address the 10 CFR §71.73(c) requirements are as follows:

- The initial pre-fire ambient conditions are assumed to be 100°F ambient with diurnal insolation loading,
- At time = 0, a fully engulfing fire environment consisting of a 1,475°F ambient with an effective emissivity of 1.0 is used to simulate the average flame temperature of the hydrocarbon fuel/air fire event. The assumption of an average flame emissivity coefficient of 1.0 conservatively bounds the minimum 0.9 flame emissivity specified by 10 CFR Part 71.73(c)(4).
- The convection heat transfer coefficients between the package and the ambient during the 30-minute fire event are based on an average gas velocity of 10 m/sec [28]. Following the 30-minute fire event the convection coefficients are based on still air.
- The ambient condition of 100 °F with insolation is assumed following the 30-minute fire event. A solar absorptivity of 0.9 is assumed for the exterior surfaces to account for potential soot accumulation on the package surfaces.

The transient analysis is continued for 8 hours after the end of the 30-minute fire to capture the peak package temperatures.

3.4.3 Maximum Temperatures and Pressure

3.4.3.1 Side Drop Damage with LTSS Payload

Table 3.4-1 presents the predicted peak temperature seen for the 1105-SD package with the LTSS payload under the side drop damage HAC conditions. The side drop damage scenario is predicted in Appendix 3.5.3.7, *Description of Thermal Model for HAC Conditions*, to yield the worst case damage to the package components that thermally protects the closure seals and the bottom portion of the package. As seen from the table, despite the damage sustained by the package under this drop scenario the thermal protection features incorporated into the package design limits the heat flux into the package resulting in significant thermal margins for all package components.

The closure and vent/test port seals remain approximately 126 °F below their maximum allowable short-term temperature limit due to a combination of the thermal shielding provided by the closure bolt enclosure structure and the amount of foam remaining. This temperature margin is significant, especially given the conservative assumptions used to model the loss of the protective polyurethane foam. In addition, the peak temperature predicted for the vent/test port seal assumes the worst case side drop impact limiter damage is assumed to align directly opposite the port location.

The large thermal mass of the LTSS payload effectively limits the temperature rise of the LTSS components during the fire event to approximately 100°F or less. The relatively cool mass of the LTSS payload also limits the rise of the bulk average package cavity gas temperature (and, thus the cavity pressure) to approximately 212 °F (i.e., resulting in a peak temperature of 364 °F). The lead used for shielding in the LTSS remains well below its melting point.

Figure 3.4-1 and Figure 3.4-2 illustrate the temperature response profiles for selected package components for the side drop damage scenario with the LTSS payload. Again, the low temperature rise seen for the LTSS payload and closure seals over the HAC event demonstrates the thermal protection afforded by the 1105-SD package design.

Figure 3.4-3 illustrates the temperature distribution within the 1105-SD package at the end of the 30-minute hypothetical fire. The fact that the high temperatures are limited to narrow regions on the exterior of the packaging temperature distribution demonstrates the thermal protection afforded to the package by the dual side thermal shields, the closure bolt enclosure structure, and the polyurethane filled impact limiter. The location of the damaged segments of the packaging is indicated by annotations in the figure. Although the modeling doesn't physically reflect the geometry realignment to the package exterior caused by the side drop damage, the thermal conductors used in the modeling have been modified to reflect the geometry realignment and associated effects of the damage. These modeling changes include higher conductance between the thermal shields to reflect potential contact from puncture bar damage, a narrowing of the air gap between the thermal shields and the package shell at the damaged area, and the crush of the polyurethane foam filled impact limiter and subsequent thermal decomposition under the HAC generated temperatures. See Appendix 3.5.3.7, *Description of Thermal Model for HAC Conditions*, for details of the HAC thermal modeling. The effect of the side crush on the loss of foam depth in the impact limiter can be seen by comparing the depiction of the foam boundary on the right and left sides of the figure.

Figure 3.4-4 depicts the package temperature distribution at 57 minutes (i.e., 27 minutes after the end of the fire event) when the bulk average gas temperature in the package cavity is predicted to reach its maximum. The exterior of the package has cooled dramatically by this point. The moderating effect of the LTSS thermal mass on the bulk average gas temperature can be clearly seen in the figure by its significantly lower temperature than its surrounding packaging components.

The temperature distribution within the LTSS lodgment at the point where it reaches its peak temperature is shown in Figure 3.4-5. The asymmetry of the temperature distribution is due to the assumption that the package is on its side following the HAC drop events and there is direct contact between the vertical ribs on one side of the lodgment and the package shell. The localized effect of the postulated puncture bar damage to the package side thermal shield and shell is clearly seen in the figure. See Appendix 3.5.3.7, *Description of Thermal Model for HAC*

Conditions, for details of the puncture bar damage modeling. As seen from Table 3.4-1 and Figure 3.4-5, the neoprene rubber used on the lower lodgment's support plate and rib edges remains well below the allowable short term temperature limit for neoprene of 500°F for HAC. As such, no contribution to package cavity pressurization will occur from material out-gassing nor is there any danger of auto ignition of the material.

3.4.3.2 Head Down Drop Damage with LTSS Payload

Table 3.4-2 presents the predicted peak temperature for the 1105-SD package with a LTSS payload under the head down drop HAC conditions. The head down damage scenario was selected for analysis (see Appendix 3.5.3.7, *Description of Thermal Model for HAC Conditions*) because of the resulting damage to the torispherical head and its protective top shield. As seen, except for the higher temperatures seen for the top torispherical head, the remaining peak package temperatures are similar to those seen for the side drop damage scenario. This is partially due to the fact that both damage scenarios assume that the package ends up on its side, but mostly reflects the thermal protection afforded by the package design despite the damage scenario.

Figure 3.4-6 and Figure 3.4-7 illustrate the temperature response profiles for selected package components for the head down drop damage scenario with the LTSS payload. The temperature trends are similar to those seen for the side drop damage scenario. Figure 3.4-8 illustrates the temperature distribution within the 1105-SD package at the end of the 30-minute hypothetical fire. Figure 3.4-9 illustrates the temperature distribution across the torispherical head at the end of the 30-minute hypothetical fire. The localized effect of the simulated puncture bar impact to the head is clearly seen in the figure. See Appendix 3.5.3.7, *Description of Thermal Model for HAC Conditions*, for details of the puncture bar damage modeling.

3.4.3.3 Side Drop Damage with Shielded Device Payload

The thermal performance of the 1105-SD packaging with the shielded device payload under HAC conditions is bounded by those achieved for the LTSS payload due to the higher decay loading of the LTSS payload. This bounding assumption applies to both the head down and the side drop damage scenarios. Further, as seen by the results for the LTSS payload, the side drop damage scenario results in the highest payload component temperatures over those achieved under the head down drop damage. As such, a separate analysis for the head down drop damage with the shielded device payload is not required to establish either the peak packaging or the peak shielded device payload temperatures under HAC.

Two separate HAC evaluations are conducted for the shielded device payload configuration in the side drop damage scenario to establish the expected peak shielded device payload component temperatures. The two evaluations assume two bounding conditions for any blocking/dunnage used. The two evaluations analyze the following configurations:

1. The shielded device is centered in the IC using the maximum amount polyurethane foam dunnage/blocking permitted. This configuration analyzes the worst case insulation of the shielded device decay heat during the HAC fire event. It also maximizes the amount of foam thermal decomposition and consequent gas generation as described below.
2. The second configuration is a model with metallic dunnage. It is conservatively assumed that the dunnage does not prevent the shielded device from coming in contact with the IC wall subsequent to the HAC free drop and puncture events. To maximize the heat

transfer from fire heat into the device, it is placed in intimate contact with the IC wall at the azimuth of the puncture damage to the thermal shield. This configuration will result in the maximum device temperatures.

3.4.3.3.1 Side Drop Damage with Shielded Device Payload and Foam Dunnage

As stated above, a principal objective of the first analysis is to ensure that if foam dunnage is used in the packaging, its temperature will remain below its thermal decomposition point during the fire event. The modeling is conducted using the same packaging model as used for the LTSS HAC side drop damage evaluation, except that a quarter symmetry representation of the package is used. This level of modeling will produce conservative results since it effectively over-predicts the impact of the concentrated drop damage. Further, the HAC evaluation for the shielded device uses an initial condition that captures the peak foam dunnage temperatures achieved during the diurnal insolation loading. This modeling approach maximizes the potential outgassing that could occur from the foam dunnage during an HAC event. Use of a time point that captures the peak shell temperatures achieved during the daily cycle in insolation loading was addressed by the HAC evaluation for the LTSS payload.

Table 3.4-3 presents the predicted peak temperature seen for the 1105-SD package with the shielded device payload under the side drop damage HAC conditions for both this load case and the load case described in Section 3.4.3.3.2, *Side Drop Damage with Shielded Device Payload and Metallic Dunnage*. As expected, the results for the 1105-SD packaging components are essentially the same as seen for the LTSS payload. The results for the shielded device components show that all remain within their associated short term temperature limits. In particular, the foam dunnage temperature remains below 435 °F, which is conservatively below 500 °F where significant weight loss due to thermal decomposition begins to occur for the material (see Appendix 3.5.4, *'Last-A-Foam' Response under HAC Conditions*) and well below the 570 to 670 °F level where the bulk of the thermal decomposition occurs. As such, thermal decomposition of the foam will not contribute to any significant package pressurization.

Figure 3.4-10 illustrates the temperature response profiles for selected payload components for the side drop damage scenario with the shielded device payload supported by polyurethane dunnage. The thermal response for the 1105-SD packaging components is similar to those depicted in Figure 3.4-1. Figure 3.4-12 illustrates the temperature distribution within the 1105-SD package at the 44-minute point in the fire event (i.e., when the foam dunnage is predicted to reach its maximum temperature point). As seen from the figure, the combination of the IC and the foam dunnage effectively thermally isolates the shielded device from the HAC heat flux.

The temperature distribution within the IC at the end of the 30-minute fire and at the point where the cylindrical shell of the IC reaches its peak temperature is shown in Figure 3.4-14. The asymmetry of the temperature distribution is due to the assumption that the package is on its side following the HAC drop events and there is direct contact between the vertical ribs on one side of the IC and the package shell. The localized effect of the postulated puncture bar damage to the package side thermal shield and shell is clearly seen in the figure wherein a short-term peak temperature of 977 °F is achieved for a short section of a the IC's rib. The majority of the IC remains well below its long-term temperature limit of 800 °F. The peak and average temperature of the IC's cylindrical shell at the end of the 30-minute fire is 388 °F and 200 °F, respectively.

The IC's cylindrical shell peak temperature of 445 °F is achieved after 43 minutes when the associated average of the cylindrical shell is 266 °F.

3.4.3.3.2 Side Drop Damage with Shielded Device Payload and Metallic Dunnage

The principle objective of this evaluation is to demonstrate that the shielded device remains below its allowable temperature limits if it comes in contact with the IC after a side drop and puncture damage scenario. Due to the offset of the shielded device from the cavity centerline the modeling is conducted using the same half symmetry packaging model as used for the LTSS HAC side drop damage evaluation. The thermal mass of the dunnage is conservatively neglected which maximizes the transient response of the package. The damaged configuration of the dunnage is also neglected which maximizes the radiation heat transfer directly from the IC wall. This approach neglects the conduction heat transfer of the dunnage to the shielded device. This is appropriate since it is negligible compared to the assumed direct intimate contact of the shielded device to the IC wall coincident with the puncture damage to the exterior thermal shield of the 1105-SD packaging.

As stated above, Table 3.4-3 presents the predicted peak temperature seen for the 1105-SD package with the shielded device payload under the side drop damage HAC conditions for both this load case and the load case described in Section 3.4.3.3.1. The shielded device remains below its allowable temperature limits even when in contact with the IC cylindrical wall during the worst case HAC fire scenario. Note that the only temperatures which are bounding for the metallic dunnage case are those of the shielded device itself, which is consistent with the conservative assumptions made in the analysis.

Figure 3.4-11 illustrates the temperature response profiles for selected payload components for the side drop damage scenario with the shielded device payload supported by metallic dunnage. Figure 3.4-13 illustrates the temperature distribution within the 1105-SD package when the shielded device skin reaches its maximum temperature of 260°F. This occurs 361 minutes after the start of the 30 minute fire event. Note that the peak shielded device skin temperature nearly matches the peak lead temperature (see Table 3.4-3), whose trace is shown in Figure 3.4-11.

3.4.3.4 Maximum HAC Pressures

LTSS Payload Case

Under the HAC condition, the maximum peak bulk average gas temperature achieved during the HAC transient for the LTSS payload case is 366 °F. Based on an assumed backfill gas temperature of 70 °F, the predicted maximum pressure within the cask cavity in the LTSS case is computed to be:

$$\text{Cavity Pressure} = 14.7 \text{ psia} \frac{(366^\circ \text{F} + 460^\circ \text{F})}{(70^\circ \text{F} + 460^\circ \text{F})} - 14.7 \text{ psia}$$

$$\text{Cavity Pressure} = 8.2 \text{ psig}$$

Shielded Device Payload Case with Metallic Dunnage

Under the HAC condition, the peak bulk average gas temperature achieved with the shielded device payload supported by metallic dunnage is 311 °F. Since there is no gas generation from the dunnage or other organics inside containment in this case (see Section 3.4.3.5, *Behavior of*

Non-metallic Contents Materials Under HAC), the pressurization of the package cavity will arise solely from ideal gas expansion and is therefore bounded by the LTSS payload case pressure.

Shielded Device Payload Case with Polyurethane Foam Dunnage

For the shielded device payloads, the only content material with any potential for off-gassing at the temperatures reached under HAC is the polyurethane foam dunnage that may be used with the shielded device payload. Foam decomposition evaluations using TGA (ThermoGravimetric Analysis) indicate a slight off-gassing will begin at foam temperatures above 325 °F. Based on the TGA curves [6], this initial off-gassing is limited to approximately a 2% weight loss for a temperature rise from 325 to 435 °F. Interpolating this curve yields a 0.45% weight loss for foam between 325 and 350 °F, 0.91% weight loss for foam between 325 and 375 °F, and 1.4% weight loss for foam between 325 and 400 °F.

A mass weighted averaging of the foam dunnage model used for the shielded device payload demonstrates that 3.9% of the total foam mass reached a temperature range of 325 to 350 °F during the HAC transient, 1.26% reached a temperature range of 350 to 375 °F, and 0.3% of the total foam mass reached a temperature in excess of 375 °F. The bulk average temperature of the foam dunnage remained below 180 °F throughout the HAC transient.

Since the foam dunnage model provides a quarter symmetry representation of the dunnage and since the package damage is centered on one of the symmetry planes, the total foam mass is computed by multiplying the modeled foam mass by a factor of 4. In contrast, the mass of the foam in each identified elevated temperature range is multiplied by a factor of 2 since the use of a factor of 4 would imply hot spots on diametrically opposite sides of the foam instead of just one side.

Given a maximum foam dunnage weight of 500 lb (Section 7.1.2.2, *Loading the Inner Container (IC) into the 1105-SD*) and the interpolated weight loss factors above, the maximum gas generation will be $500 \text{ lb} \times (0.039 \times 0.0045 + 0.0126 \times 0.0091 + 0.003 \times 0.014) = 0.166 \text{ lb}$. This weight loss occurs in the form of water vapor and/or the gas used for the foam blowing agent. As such, 0.166 lb of out gassing is equivalent to a maximum of 4.2 g-moles of gas generation, based on a molecular weight for water vapor of 18 g/g-mole. A lesser amount of gas generation would occur if the out gassing is in the form of the higher molecular weight foam blowing agent.

The interior volume of the containment is 106,238 in³ [29]. The displacement volume of both internal impact limiters is 2,012 in³ (assuming 72 lb of aluminum and 79 lb of Type 304 stainless steel for each limiter and densities from Section 2.2.1, *Material Properties and Specifications*). The displacement volume of the IC is 3,969 in³ (assuming 1,160 lb of Type 304 stainless steel), and the volume within the IC, which has an inner diameter of 36 inches and is 53 inches long, is 53,947 in³. For conservatism, the entire internal volume of the IC is assumed to be filled by either foam or the payload for the purposes of the pressure calculation.

The minimum net void volume within the package is therefore:

$$106,238 \text{ in}^3 - 2,012 \text{ in}^3 - 3,969 \text{ in}^3 - 53,947 \text{ in}^3 = 46,310 \text{ in}^3 \text{ (758.9 liters)}.$$

The minimum quantity of air required to fill the package's payload cavity to a pressure of 1 atmosphere at 70 °F (294 K) is determined via:

$$\begin{aligned} \text{g-moles fill gas} &= \text{Press} * \text{Volume} / [0.08206 \text{ L-atm}/(\text{g-mole-K}) * T(\text{K}) * 14.7 \text{ psia/L-atm}] \\ &= 14.7 * 758.9 / [0.08206 * 294 \text{ K} * 14.7] \end{aligned}$$

= 31.5 g-moles

Since the rise in the dunnage foam temperatures lag the peak bulk average cavity gas temperature, the actual peak foam off-gassing will not occur until 120 minutes after the cavity gas temperature peaks. This fact, illustrated in Figure 3.4-15, results in a lower ideal gas expansion effect and a lower associated cavity pressure. It should be noted that the "stair step" changes in the curve for the foam off-gassing quantity and, to a lesser degree, the curve for cavity pressure are due to the conservative analysis logic which assigns the entire gas generation quantity for each temperature range as soon as the minimum temperature level is exceeded and then assumes no further gas generation until the minimum temperature value of the next temperature range is exceeded.

The peak cavity pressure achieved under the HAC transient for the shielded device payload, computed as a combination of cavity gas quantity and temperature, is predicted to be 9.4 psig. This estimated pressure rise is conservative for the following reasons:

- 1) it is based on the maximum foam dunnage weight
- 2) it assumes a conservatively low void volume available to absorb the generated out-gas
- 3) it assumes the out-gas is entirely water vapor. Credit for at least a portion of the gas being CO₂ (i.e., the blowing agent) would raise the molecular weight from 18 to 44 and lower the quantity of gas generated
- 4) it ignores the potential for any generated water vapor to quickly re-condense on those surfaces of the IC and internal impact limiters that remain below 212 °F and, therefore, not contribute to an added pressure rise in the package cavity.

For conservatism, a peak HAC pressure of 10 psig is used for any payload configuration.

3.4.3.5 Behavior of Non-metallic Contents Materials Under HAC

Several non-metallic materials are present in association with the contents of the 1105-SD and are exposed to elevated temperatures during or after the HAC fire event. The discussion below (summarized in Table 3.4-4) lists each non-metallic material, its location within the package, its maximum temperature based on the calculated results taken from Table 3.4-1, Table 3.4-2, or Table 3.4-3, and the material's minimum thermal decomposition temperature based on published reference information. As shown, each non-metallic material has a significant margin of safety on its temperature limit, and gas generation from the thermal decomposition of these materials in association with the HAC fire event will not occur. Of note, none of these materials are important to safety, consequently their function under NCT or HAC is not required.

In the paragraphs below:

- *Lodgment maximum temperature* is equal to 464 °F from Table 3.4-1.
- *IC cylindrical shell maximum temperature* is equal to 445 °F from Table 3.4-3.
- *Shielded device shell maximum temperature* is equal to 260 °F, from Table 3.4-3.

Marking paint may be used on the lodgment or IC for alignment marks or identification. Paint may also be used on the dunnage. The temperature of paint on the lodgment is bounded by the lodgment maximum temperature, and the temperature of paint on the dunnage within the IC is bounded by the IC shell maximum temperature. Per drawings 3021718-SAR and 3021719-SAR

and Section 7.1.2.2, *Loading the Inner Container (IC) into the 1105-SD*, this paint must be rated for a temperature of at least 500 °F. Commercial high-temperature paints easily meet this standard. The minimum margin of safety is at least 36 °F.

Nitrile rubber is used for the O-ring dust seals on the LTSS end doors. The temperature of the dust seals is bounded by the maximum temperature of the LTSS shell of 270 °F given in Table 3.4-1. Figure 19 of [14] shows weight loss is negligible below approximately 300 °C (572 °F). The minimum margin of safety is 302 °F.

Nylon is present in the self-locking nuts used to attach the two halves of the lodgment together and on the fasteners attaching the neoprene pad (drawing 3021718-SAR, Items 11 and 16, respectively). Nylon may also be used on any fasteners used with dunnage in the IC. The temperature is bounded by the lodgment maximum temperature. Page 204 of [34] gives a thermal decomposition temperature for nylon of 578 K (581 °F). The minimum margin of safety is 117 °F.

Graphite is used in bushings in the GC-40 shielded device. Its temperature is bounded by the temperature of the shielded device drawer of 293°F from Table 3.4-3. Table II of [14] gives a temperature limit of 800 °C (1,472 °F). The minimum margin of safety is 1,179 °F.

Lifting slings are used to place the shielded device into the IC. As a convenience to the user, or if the device is resting on the slings, it may be necessary to leave the slings in place in the IC. Slings may be made from steel, nylon, polyester, or Kevlar®. The temperature of the slings is bounded by the IC shell maximum temperature. The temperature limit for nylon is given above as 581 °F. Figure 1(a) of [35] shows negligible decomposition for polyester below approximately 350 °C (662 °F). Page 155 of [34] gives a temperature limit for Kevlar® of 700 K (800 °F). The minimum margin of safety is 136 °F.

Silicone sealant may be used to seal crevices between the intermittent welds of the IC. The temperature of the sealant is bounded by the IC shell maximum temperature (except as noted below for sealant used in locations not adjacent to the IC shell). The chemical name for silicone materials is polydimethylsiloxane (PDMS). Table 3 of [36] lists the temperature of onset of thermal degradation (equivalent to a 1% mass loss) for several PDMS compounds in air. All of the temperatures exceed 300 °C (572 °F). Similarly, Figure 5 of [37] shows no significant mass loss for PDMS below 300 °C. Of note, this thermal decomposition temperature will be higher than the recommended maximum use temperature. The minimum margin of safety is 127 °F.

A small amount of silicone sealant may reach a temperature in excess of its decomposition temperature. However, this is shown to be negligible relative to pressure rise within the package. As shown on drawing 3021719-SAR, Sheet 2, Assembly A1, the external ribs of the IC consist of circumferentially continuous rings separated by vertical rib segments that are attached using intermittent welds (1" long on 2" centers). Each joint between a vertical rib and a circumferential ring has a radial dimension of 3 inches. (The vertical joints are adjacent to the shell as discussed above.) Thus the weld consists of two, one-inch long welds on either side of a one-inch long unwelded length, which may be sealed with a small bead of silicone sealant. Since the same weld exists on both sides of the vertical rib, there may be up to four, one-inch long segments of silicone sealant bead at each intersection of a vertical rib with a circumferential ring. The bead has the same nominal profile as the specified 1/8" fillet weld, and thus has a cross sectional area of $(0.125)^2/2 = 0.0078 \text{ in}^2$, or a volume of 0.0312 in^3 of sealant per rib intersection (four, one-inch long beads). As shown in Figure 3.4-14, the maximum temperature of the IC is

limited to a small region adjacent to the HAC puncture bar impact. The right side of the figure represents the temperature distribution at 43 minutes after the start of the HAC fire, and is the point at which the shell temperature reaches its maximum. As can be seen, the maximum size of the hot region of the ribs (i.e., where the temperature exceeds that of the IC shell) includes approximately two rib intersections. It is only at these intersections that any silicone sealant could exceed the temperature of the IC shell. Silicone sealant has a specific gravity essentially equal to unity, and the maximum credible gas which could result from the decomposition of the sealant would be the equivalent mass of water vapor. To calculate the maximum amount of sealant that could possibly decompose, it will be conservatively assumed that a total of six intersections (i.e., three times the number indicated by Figure 3.4-14) exceed the silicone sealant decomposition temperature of at least 572 °F. This volume is $6 \times 0.0312 = 0.1872 \text{ in}^3$, or an equivalent of 0.0068 lb of water (about 3 ml). The pressure that could result from the addition of 0.0068 lb of water vapor to the void volume of the 1105-SD (46,310 in³ per Section 3.4.3.4, *Maximum HAC Pressures*), is negligible.

Paint is used on the outer surfaces of most shielded devices. The temperature of the paint is bounded by the shielded device shell temperature. Thermogravimetric analysis (TGA) for various paint types show that significant degradation, measured as weight loss, does not occur below 200 °C to 300 °C (392 °F to 572 °F). See Figures 1 and 2 of [30], Figure 1a of [31], and Figure 1 of [32]. The minimum margin of safety is 132 °F.

Grease may be present in bearings or other mating parts of the shielded devices or as vacuum grease on the containment O-ring and vent port seal. The temperature of grease is bounded by the vent port sealing washer temperature of 274 °F from Table 3.4-1. Section 2.3 (with Figure 4) of [33] indicates that grease thickener begins to decompose at around 250 °C (482 °F). Of note, this thermal decomposition temperature will be higher than the recommended maximum use temperature. The minimum margin of safety is 208 °F.

Epoxy adhesive may be present on some devices. The temperature of epoxy is bounded by the shielded device shell temperature. The brand of epoxy adhesive used is 3M™ Scotch-Weld DP 100. The manufacturer's data sheet [38] shows a 5% weight loss at 318 °C (604 °F) in air. The minimum margin of safety is 344 °F. In these applications, a very small amount of thread locking compound may be used. Any gas that could be generated by the decomposition of this material will be negligible.

Acrylic plastic (PMMA or Lucite) or **Acetal plastic** (POM or Delrin) may be present on some devices. The temperature of these materials is bounded by the shielded device shell temperature. Figure 5(a) of [39] shows that thermal decomposition of PMMA (solid line) does not occur below at least 250 °C (482 °F). The MSDS for Delrin [40] states that thermal decomposition will not occur at the processing temperature of 210 – 220 °C (410 – 428 °F). The minimum margin of safety (based on Delrin at 410 °F) is 150 °F.

Thus, as discussed above and summarized in Table 3.4-4, gas generation due to the thermal decomposition of non-metallic materials which may be present within the containment of the 1105-SD, during or after the HAC fire event, is not of concern.

3.4.4 Maximum Thermal Stresses

The maximum thermal stresses under the HAC condition are addressed in Section 2.7.4, *Thermal*.

Table 3.4-1 – HAC Temperatures for Side Drop Damage with LTSS

Component	Temperature (°F)			
	End of Fire	Peak	Post-fire Steady State	Allowable ^②
Sealed Source Capsule ^①	881	908	887	1,100
Special Form Capsule	260	350	282	800
Large Source Drawer	215	308	238	800
LTSS Liner	191	283	210	800
LTSS Lead	191	279	205	620
LTSS Shell	195	270	197	800
Lodgment, Lower Half	460	464	177	1,100
Lodgment, Upper Half	327	415	167	1,100
Neoprene	321	361	177	500
Shell	1,132	1,132	170	1,300
Inner Thermal Shield	1,325	1,325	167	2,500
Outer Thermal Shield	1,421	1,421	166	2,500
Top Thermal Shield	1,438	1,438	152	2,500
Lower Internal Impact Limiter	184	266	175	1,100
Upper Internal Impact Limiter	905	905	154	1,100
Lower Torispherical Head	259	277	168	1,300
Upper Torispherical Head	1,101	1,101	149	1,300
Closure Seals	169	270	166	400
Vent Port Sealing Washer	185	274	166	400
Impact Limiter				
- Max. Foam	N/A	N/A	N/A	N/A
- Avg. Foam	N/A	N/A	N/A	N/A
- Shell	1,474	1,474	164	2,500
Cask Cavity Bulk Gas	319	364	167	N/A

Notes: ① Results assume smallest source capsule dissipating 200 W in shortest special form capsule filled with argon gas.

② See Section 3.2.2, *Component Specifications*, for basis of listed temperature criterion.

Table 3.4-2 – HAC Temperatures for Head Down Drop Damage with LTSS

Component	Temperature (°F)			
	End of Fire	Peak	Post-fire Steady State	Allowable ^②
Sealed Source Capsule ^①	881	907	887	1,100
Special Form Capsule	260	349	283	800
Large Source Drawer	215	307	239	800
LTSS Liner	191	282	211	800
LTSS Lead	189	277	206	620
LTSS Shell	193	269	198	800
Lodgment, Lower Half	336	386	179	1,100
Lodgment, Upper Half	325	413	168	1,100
Neoprene	255	325	179	500
Shell	1,164	1,164	172	1,300
Inner Thermal Shield	1,337	1,337	168	2,500
Outer Thermal Shield	1,422	1,422	167	2,500
Top Thermal Shield	1,431	1,431	149	2,500
Lower Internal Impact Limiter	174	260	177	1,100
Upper Internal Impact Limiter	1053	1,062	153	1,100
Lower Torispherical Head	255	273	174	1,300
Upper Torispherical Head	1,274	1,274	145	1,300
Closure Seals	169	268	168	400
Vent Port Sealing Washer	183	268	168	400
Impact Limiter				
- Max. Foam	N/A	N/A	N/A	N/A
- Avg. Foam	N/A	N/A	N/A	N/A
- Shell	1,474	1,474	166	2,500
Cask Cavity Bulk Gas	329	366	168	N/A

Notes: ① Results assume smallest source capsule dissipating 200 W in shortest special form capsule filled with argon gas.

② See Section 3.2.2, *Component Specifications*, for basis of listed temperature criterion.

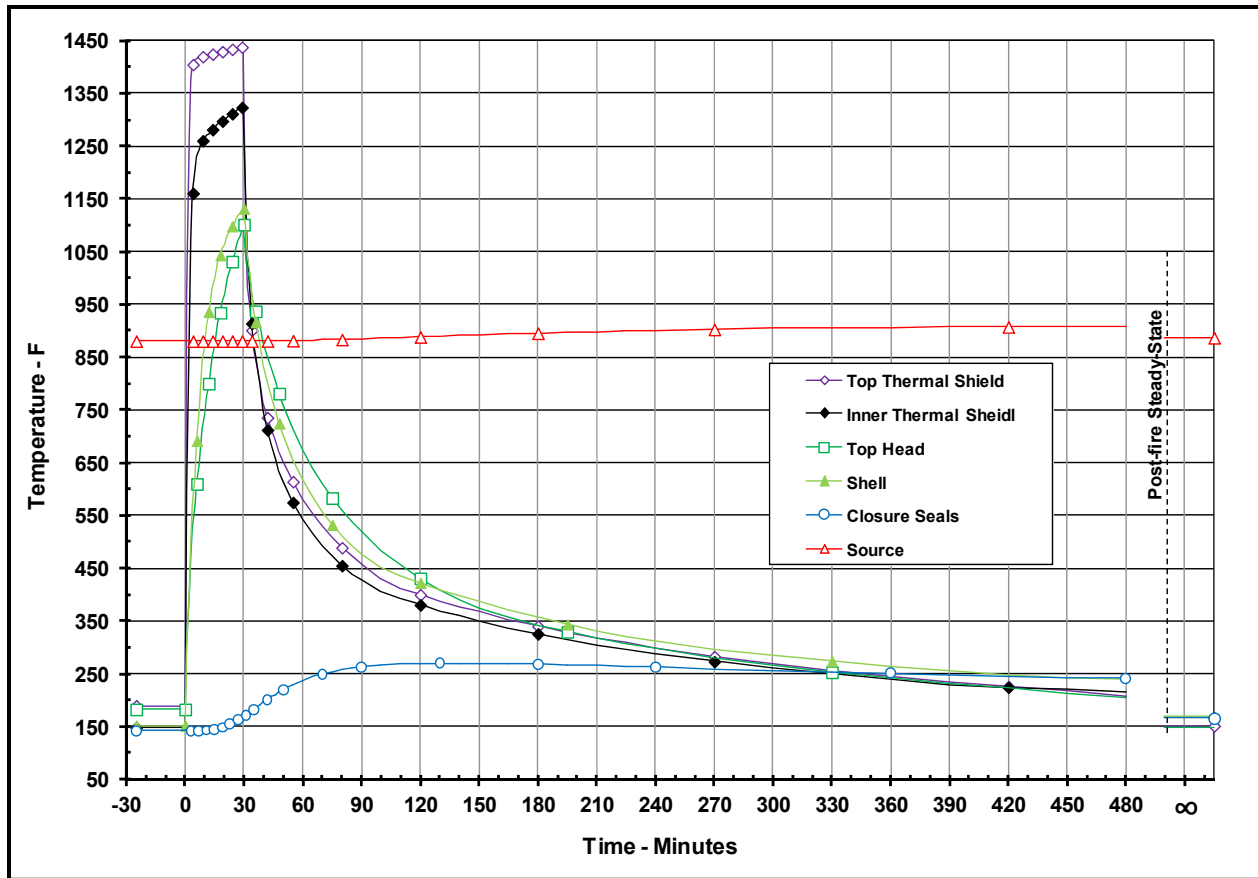
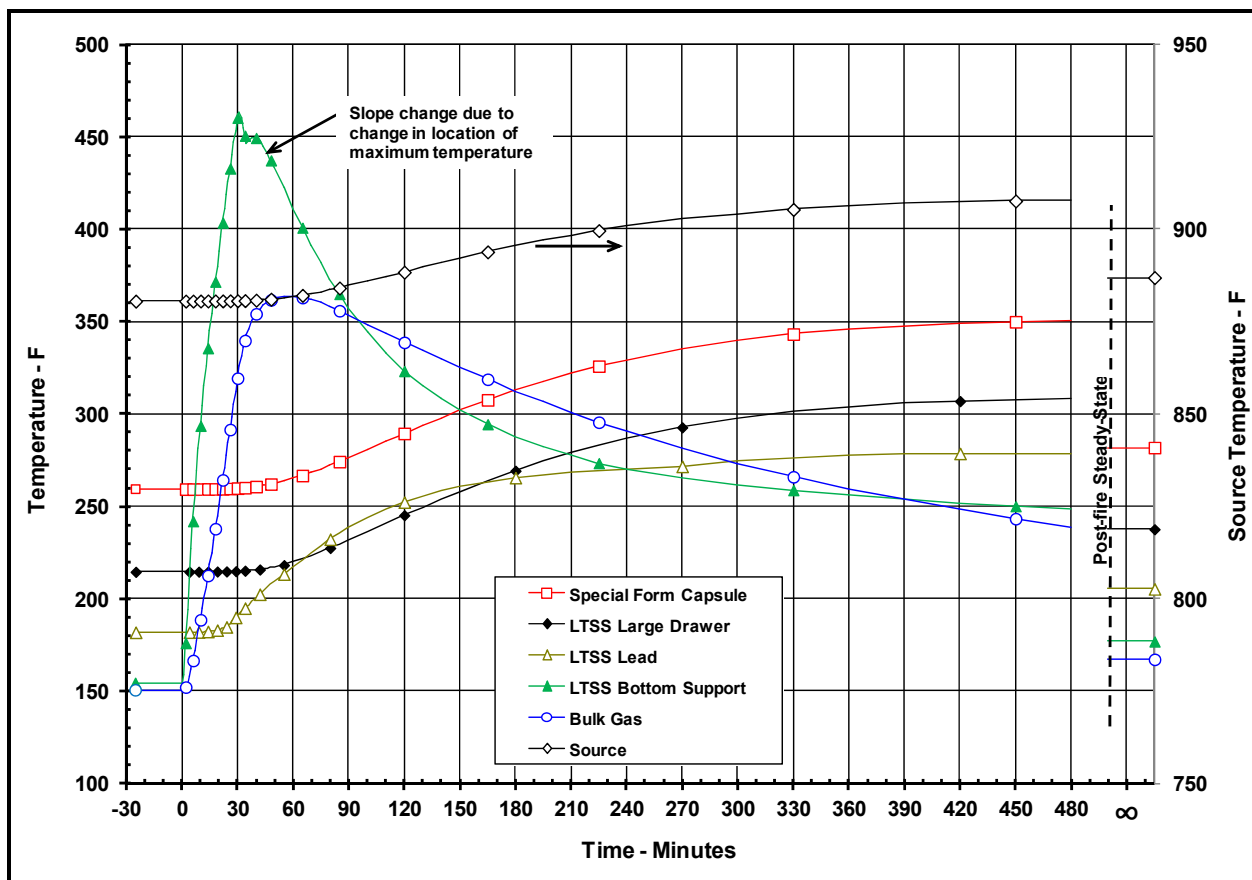


Figure 3.4-1 – Package HAC Temperature Response – Side Drop Damage with LTSS



Note: Scale for source temperature shown on right hand side

Figure 3.4-2 – LTSS HAC Temperature Response – Side Drop Damage

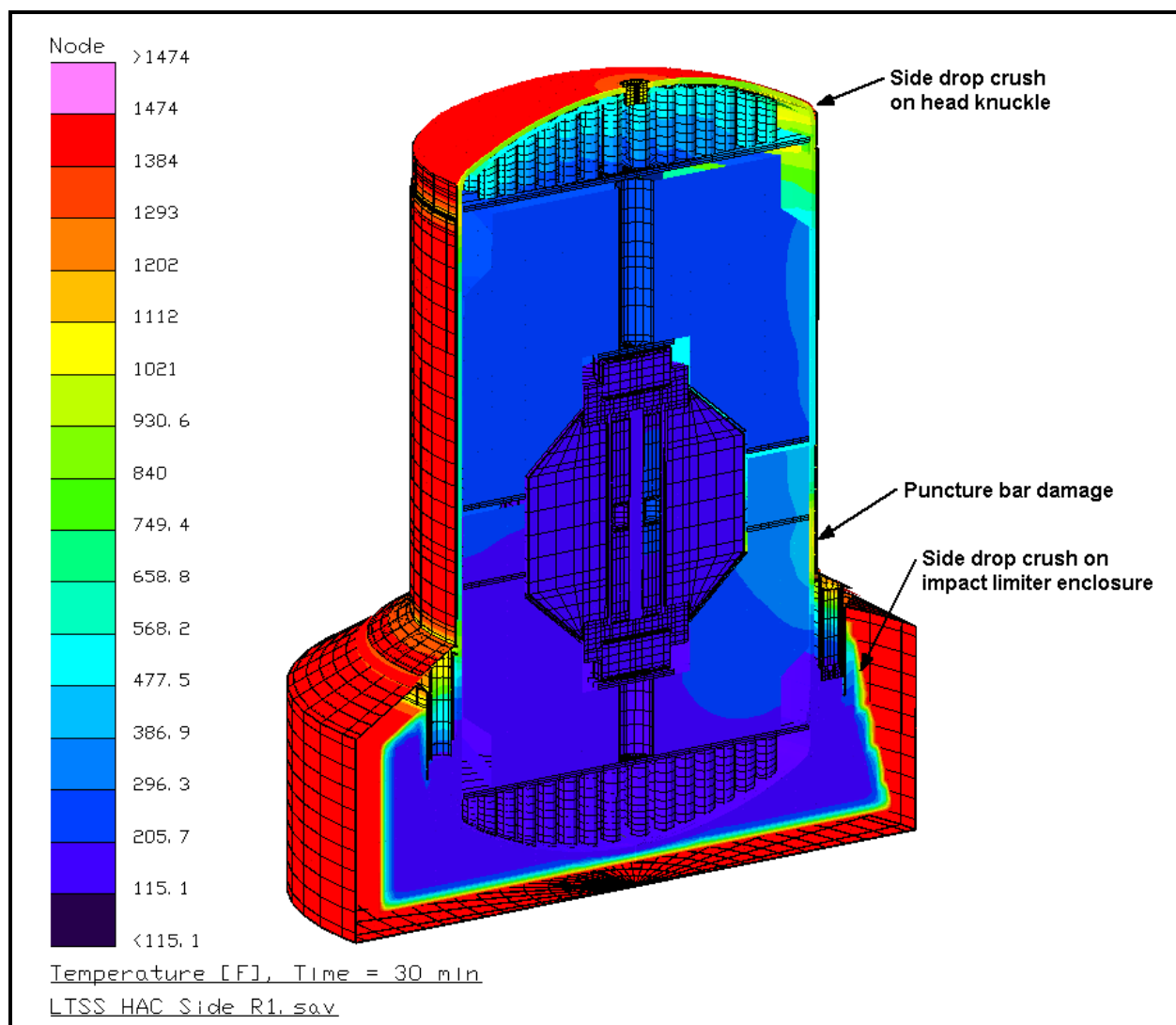


Figure 3.4-3 – Side Drop HAC Temperature Distribution with LTSS at End of 30 Minute Fire

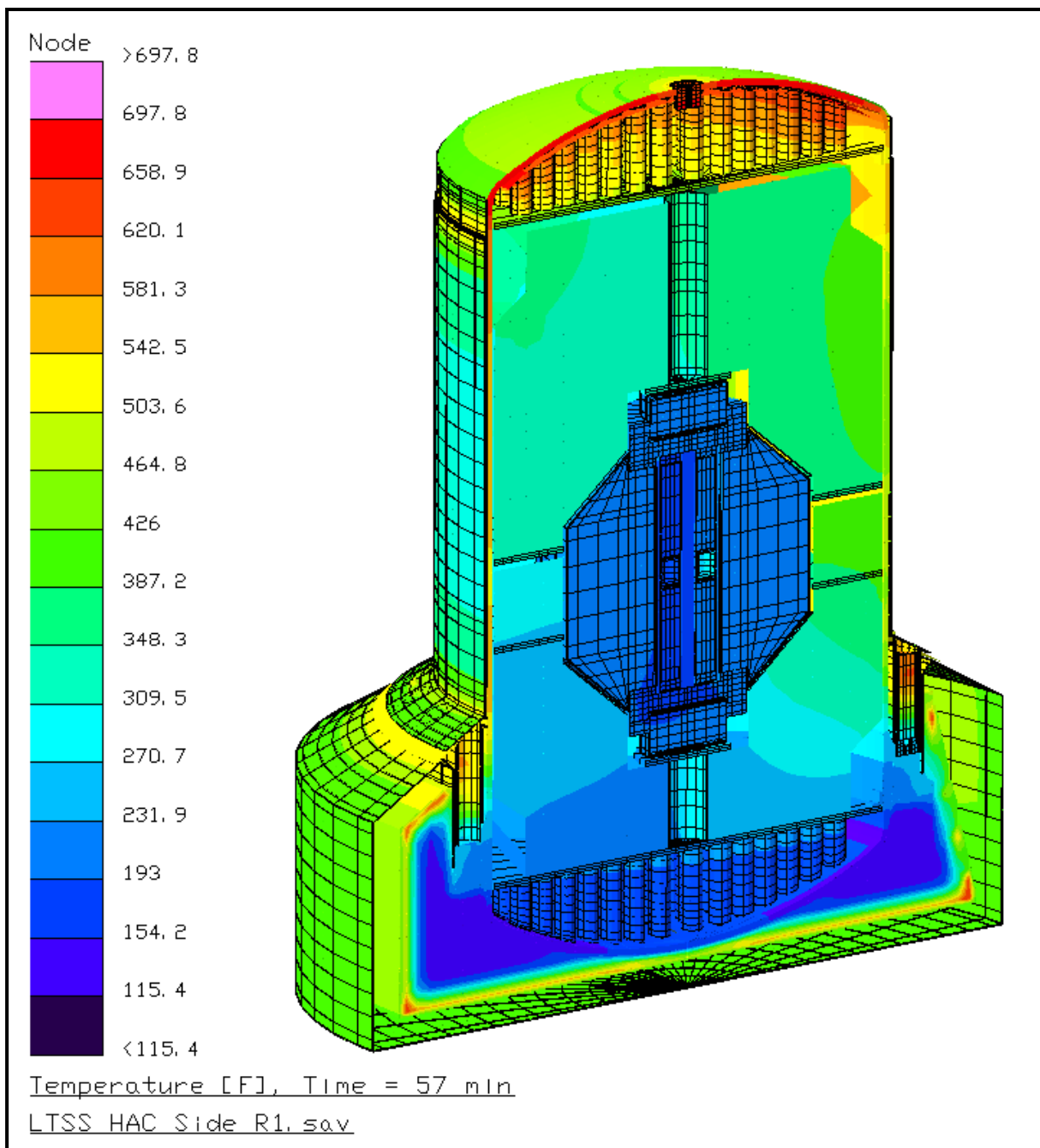


Figure 3.4-4 – Side Drop HAC Temperature Distribution with LTSS at 57 Minutes

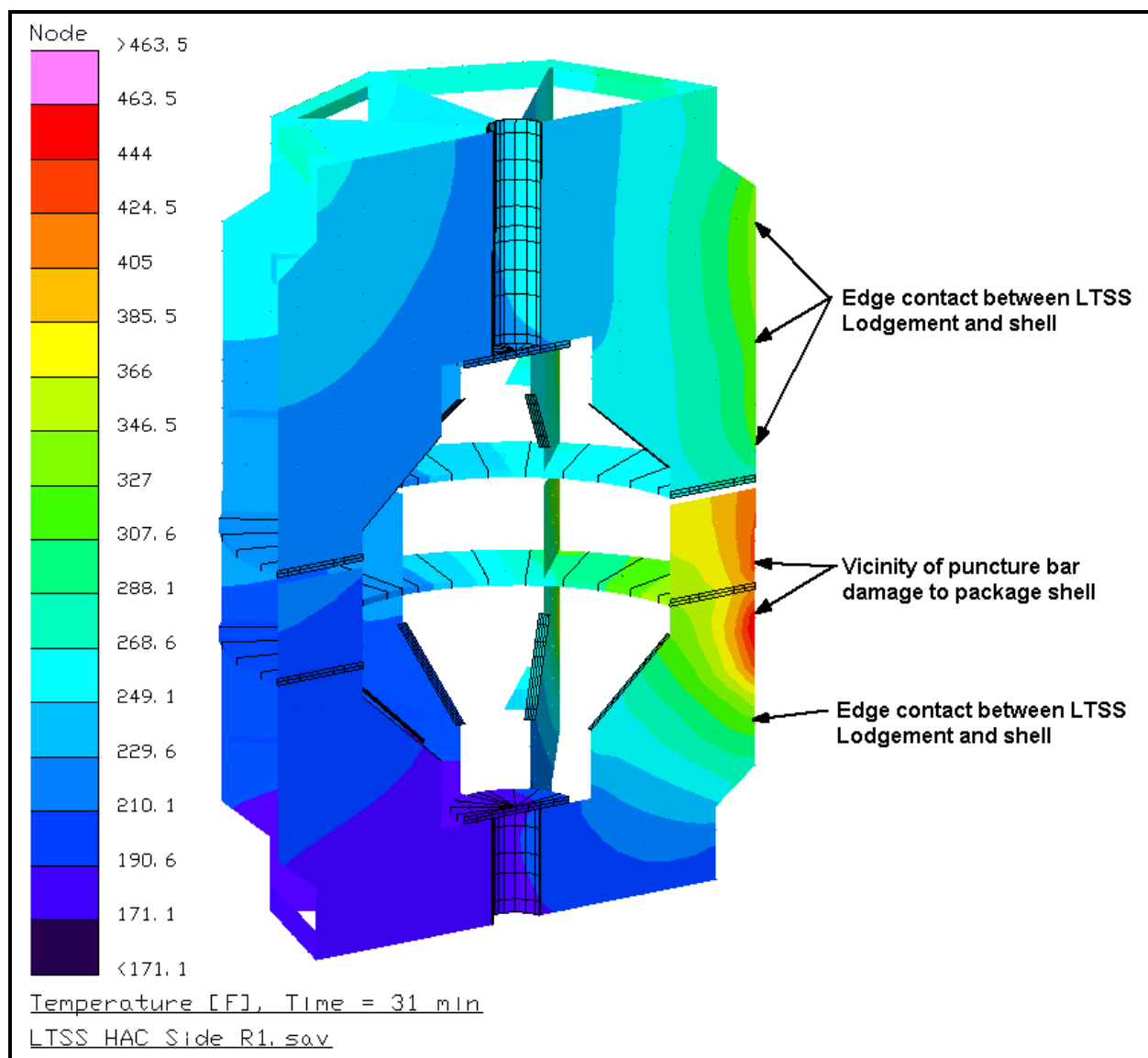


Figure 3.4-5 – Side Drop HAC Temperature Distribution for LTSS Lodgment at 31 Minutes

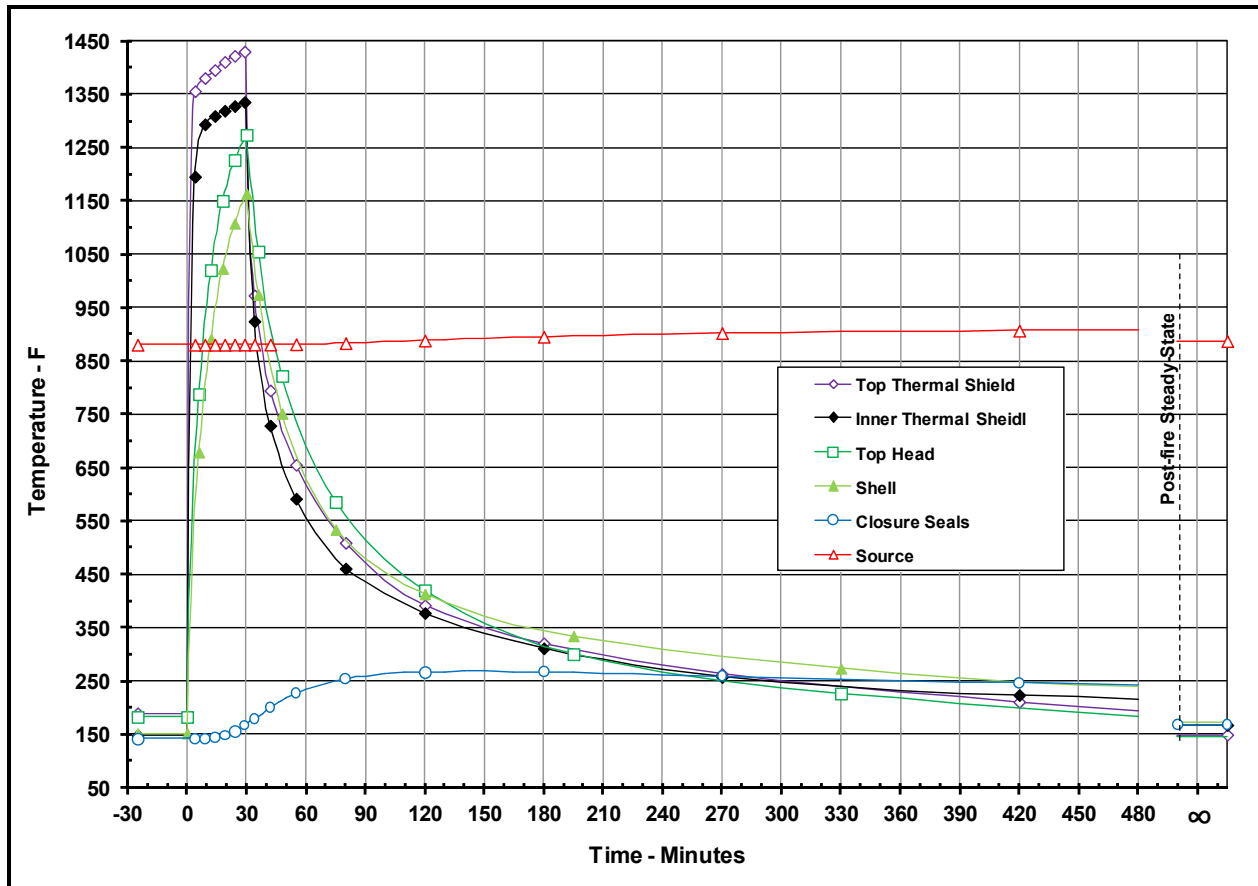
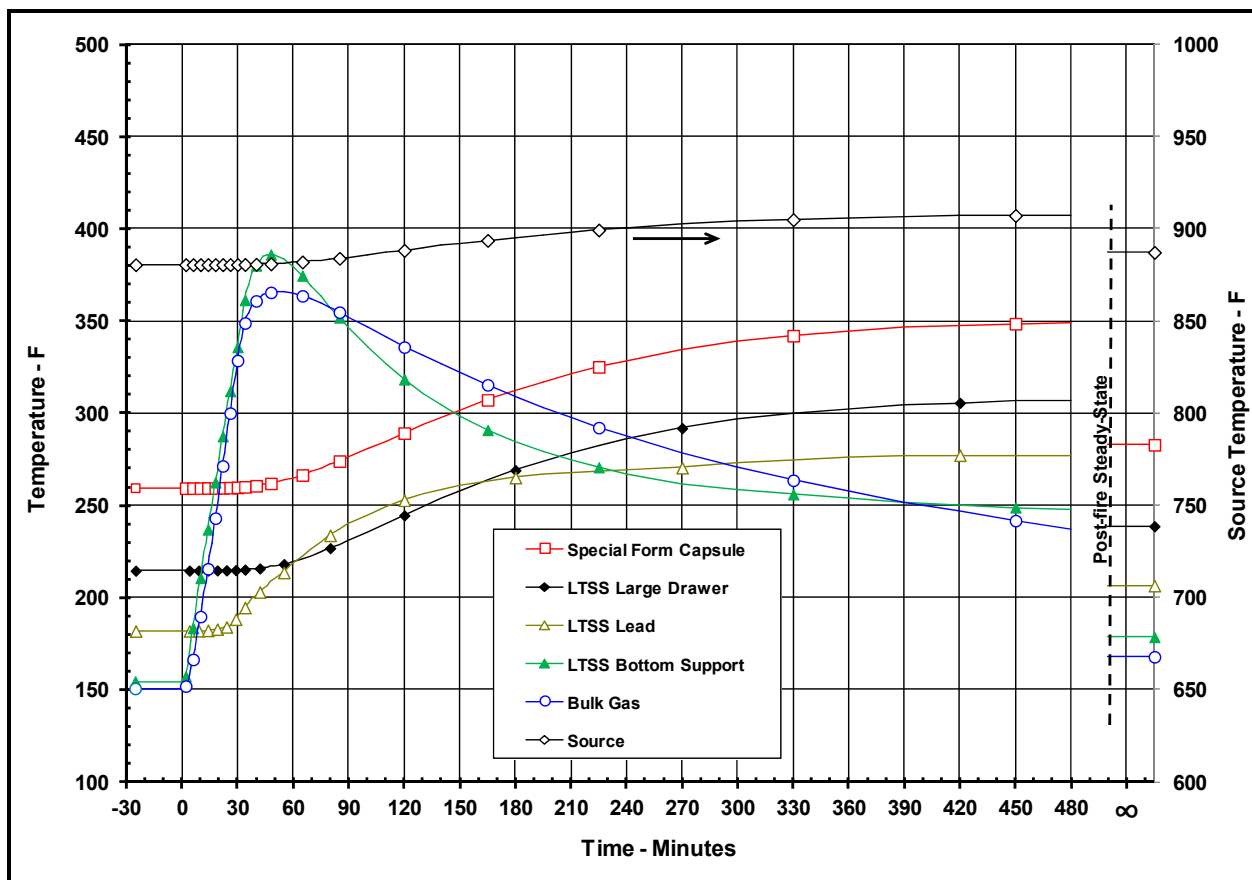


Figure 3.4-6 – Package HAC Temperature Response – Head Down Drop Damage with LTSS



Note: Scale for source temperature shown on right hand side

Figure 3.4-7 – LTSS HAC Temperature Response – Head Down Drop Damage

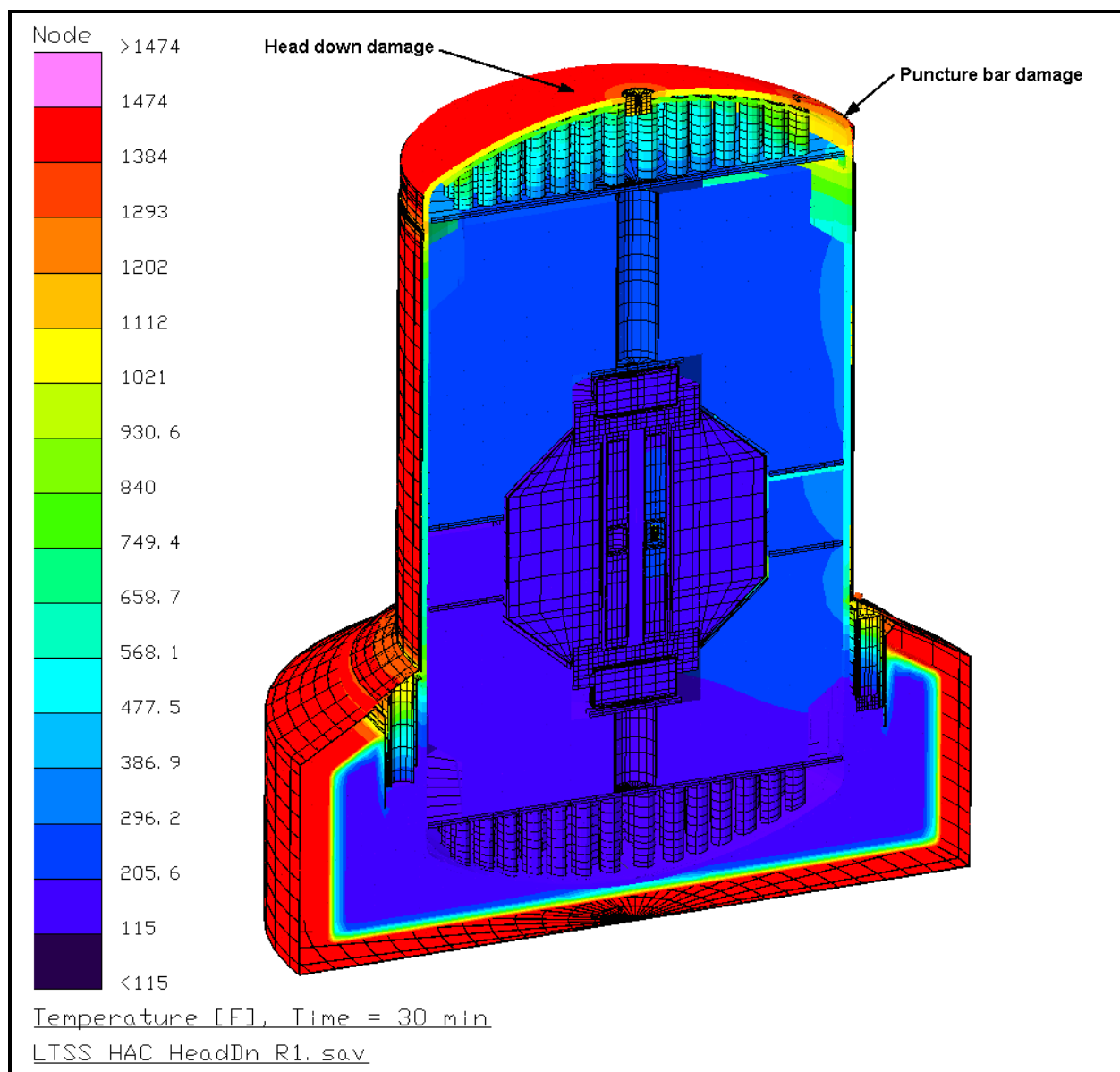


Figure 3.4-8 – Head Down Drop HAC Temperature Distribution with LTSS at End of 30 Minute Fire

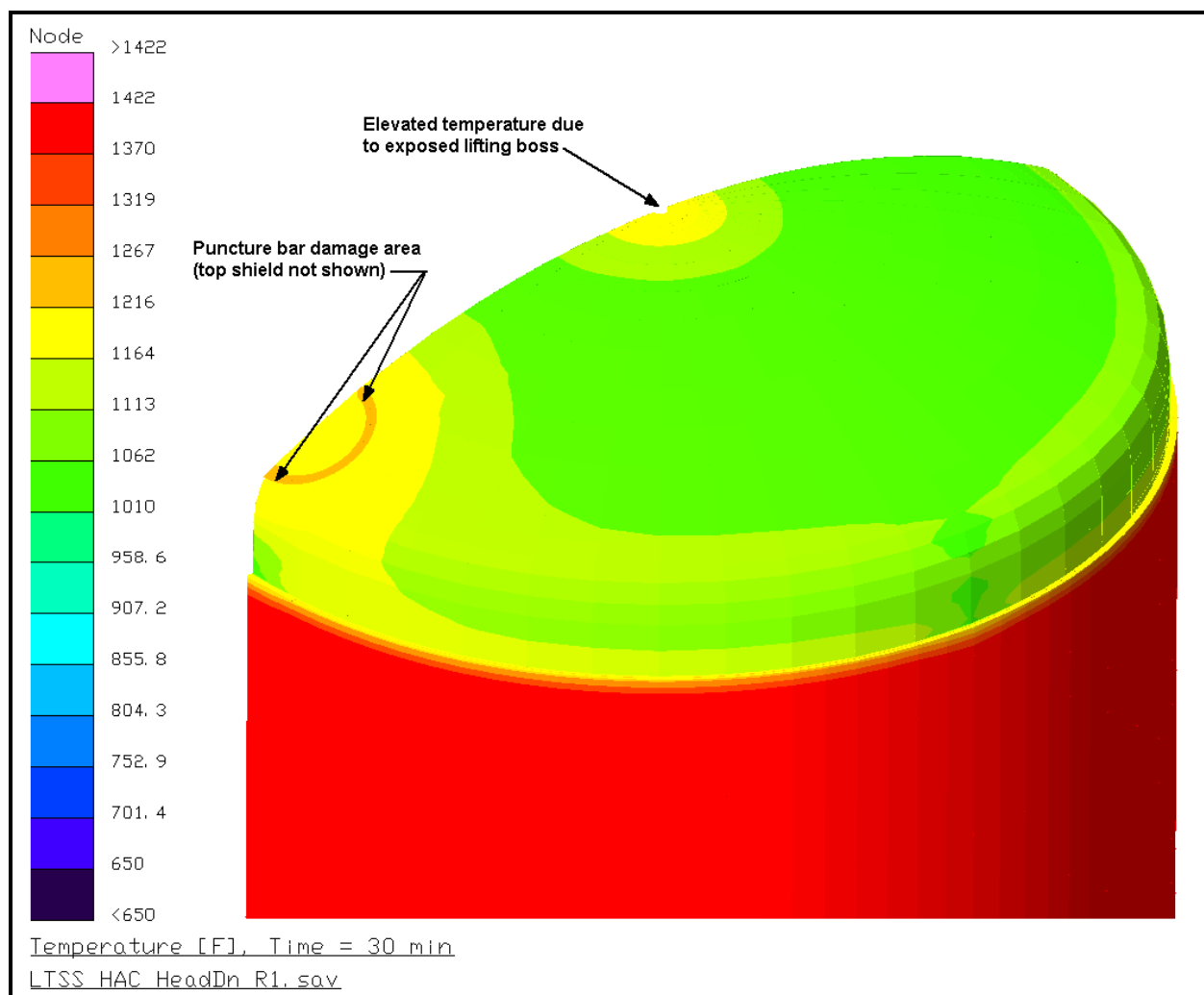


Figure 3.4-9 – Temperature Effect of Puncture Bar Damage for Head Down Drop

Table 3.4-3 – HAC Temperatures for Side Drop Damage with Shielded Device

Component	Temperature (°F)			
	End of Fire	Peak	Post-fire Steady State	Allowable ^②
Sealed Source Capsule ^①	471	537 ^③	487	1,100
SD Drawer	192	293 ^③	217	800
SD Liner	153	259 ^③	179	800
SD Lead	164 ^③	259 ^③	178	620
SD Shell	195 ^③	260 ^③	178	800
Foam Dunnage	354	406	178	435
IC	977	977	158	2,500
IC Cylindrical Wall	388	445	159	2,500
Shell	1,150	1,150	154	1,300
Inner Thermal Shield	1,311	1,311	153	2,500
Outer Thermal Shield	1,420	1,420	153	2,500
Top Thermal Shield	1,437 ^③	1,437 ^③	144	2,500
Lower Internal Impact Limiter	134	224	149	1,100
Upper Internal Impact Limiter	848	848	142	1,100
Lower Torispherical Head	241	258	149	1,300
Upper Torispherical Head	1,086	1,086	141	1,300
Closure Seals	149	248	150	400
Vent Port Sealing Washer	164	251	149	400
Impact Limiter				
- Max. Foam	N/A	N/A	N/A	N/A
- Avg. Foam	N/A	N/A	N/A	N/A
- Shell	1,474 ^③	1,474 ^③	151	2,500
Cask Cavity Bulk Gas	294	352	152	N/A

Notes: ① Results assume smallest source capsule (i.e., assumed 1.7" length x 1.57" diameter) dissipating 30 W.

② See Section 3.2.2, *Component Specifications*, for basis of listed temperature criterion.

③ Noted temperature values are from the metallic dunnage case. All other temperatures are from the polyurethane dunnage case. All temperature values are bounding for the shielded device payload.

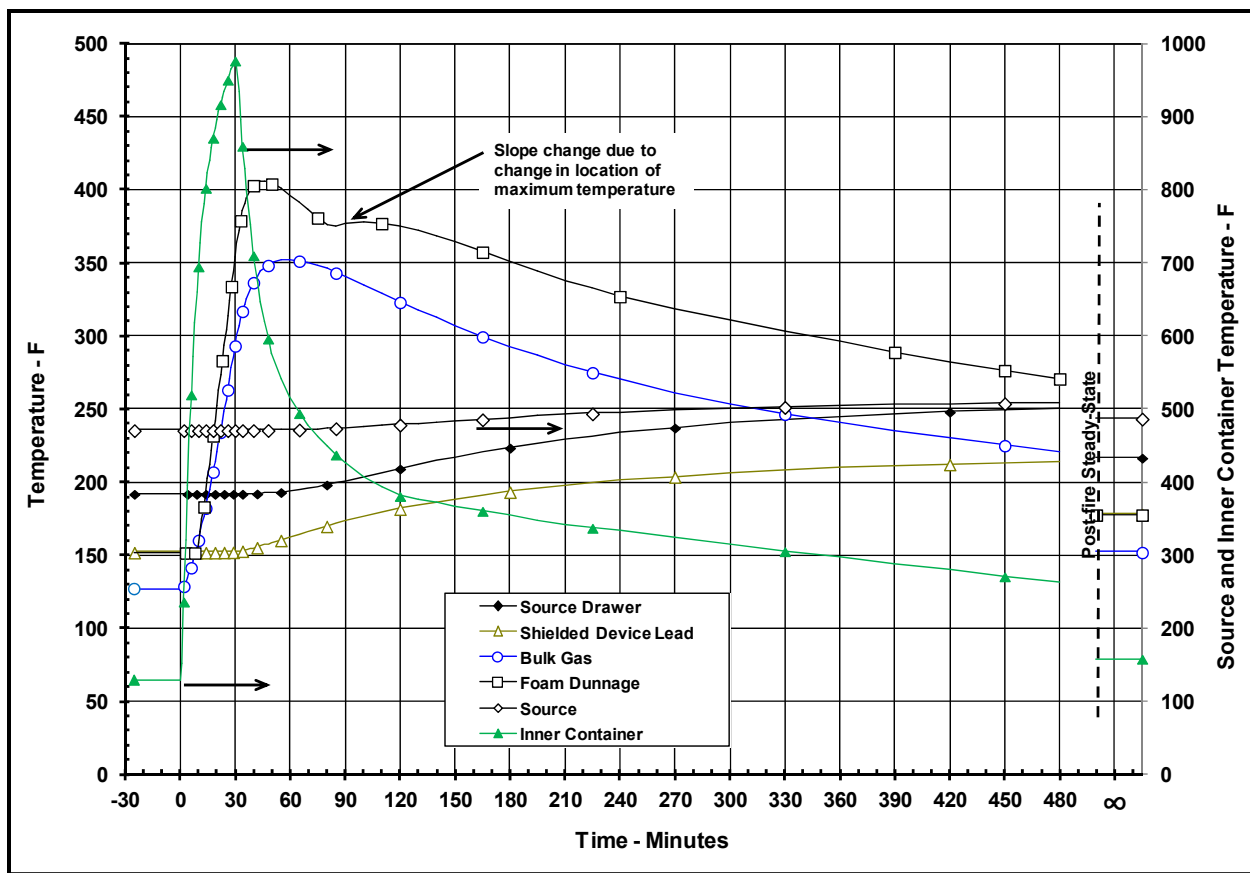
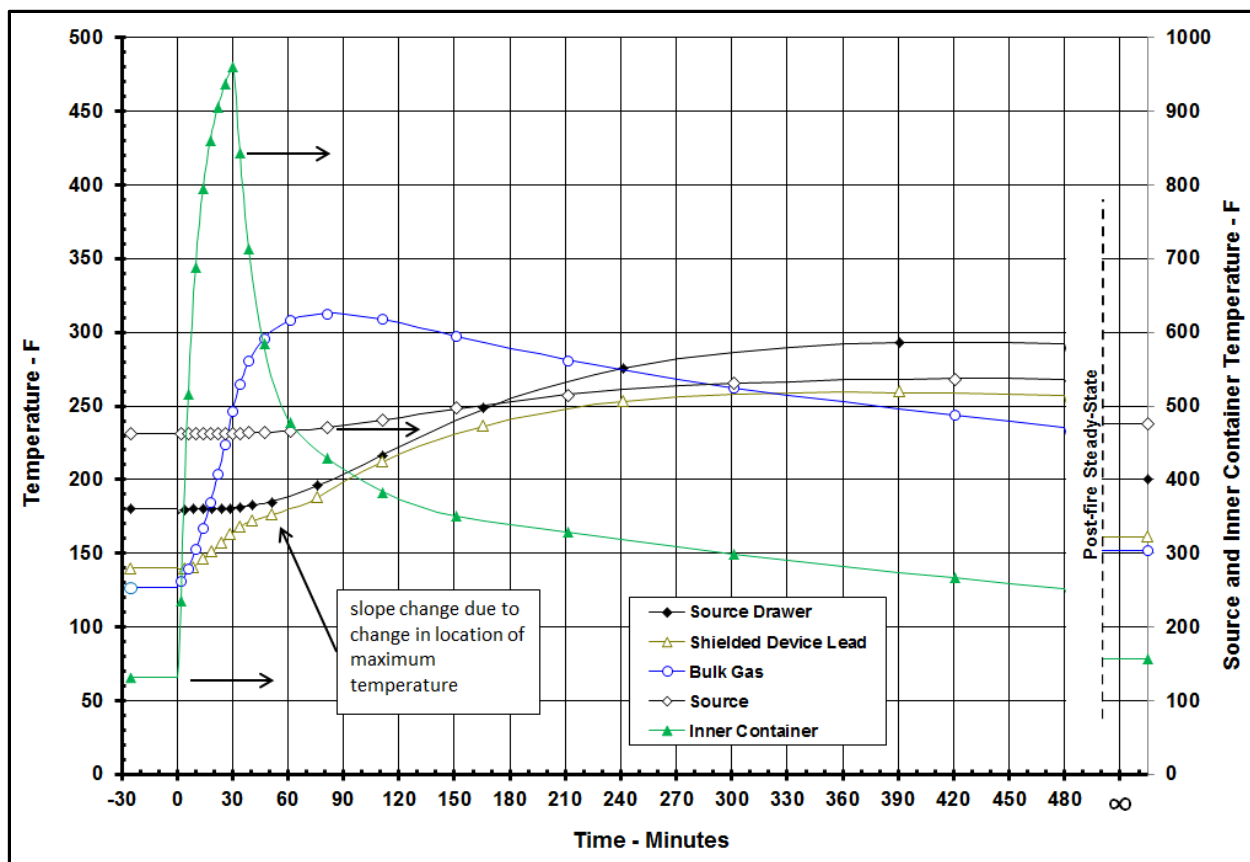


Figure 3.4-10 – Shielded Device HAC Temperature Response when Supported by Polyurethane Dunnage – Side Drop Damage



Note: Scale for source and IC temperatures shown on right hand side

Figure 3.4-11 –Shielded Device HAC Temperature Response when Supported by Metallic Dunnage – Side Drop Damage

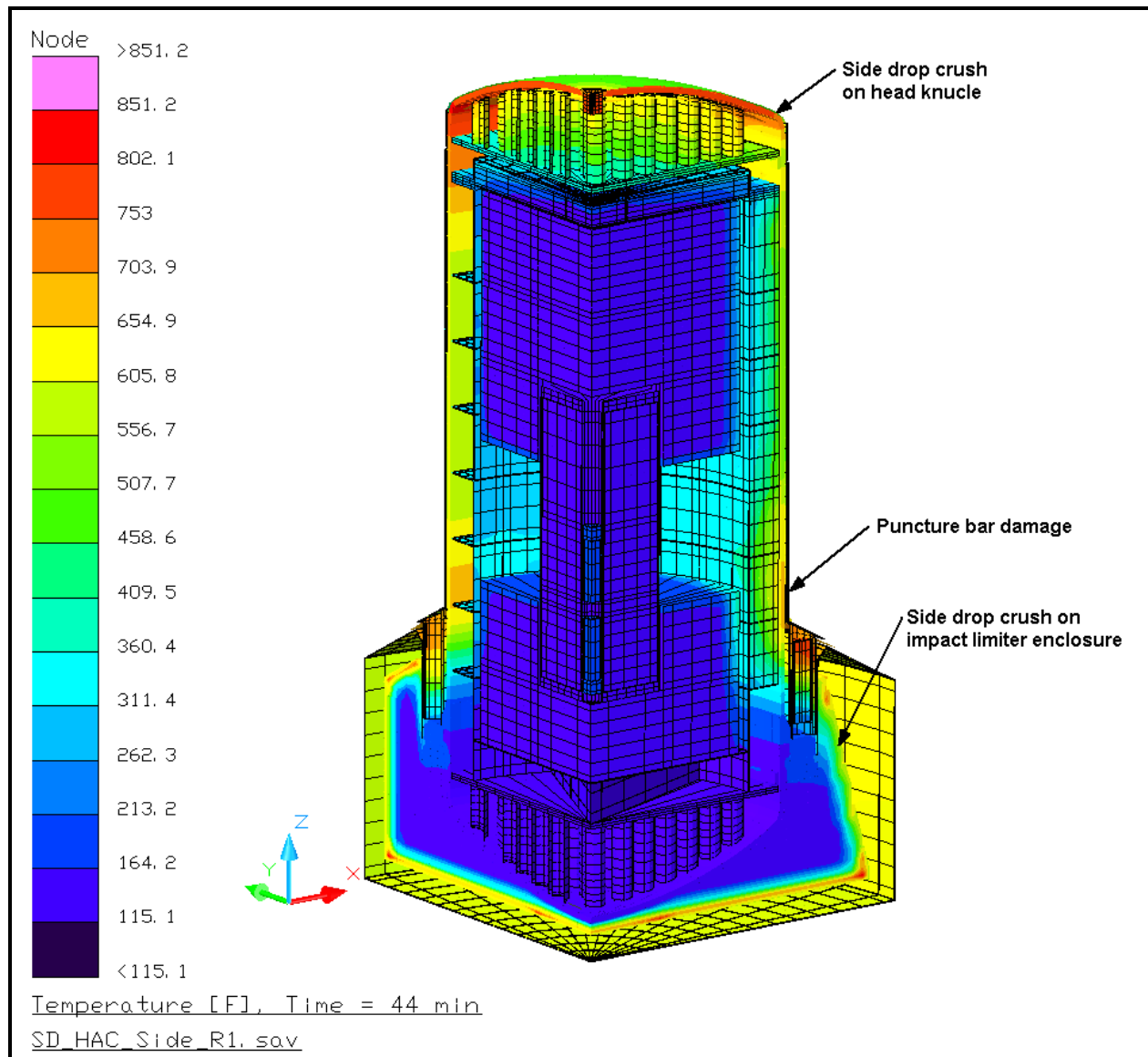


Figure 3.4-12 – Side Drop HAC Temperature Distribution with Shielded Device Supported by Polyurethane Foam Dunnage

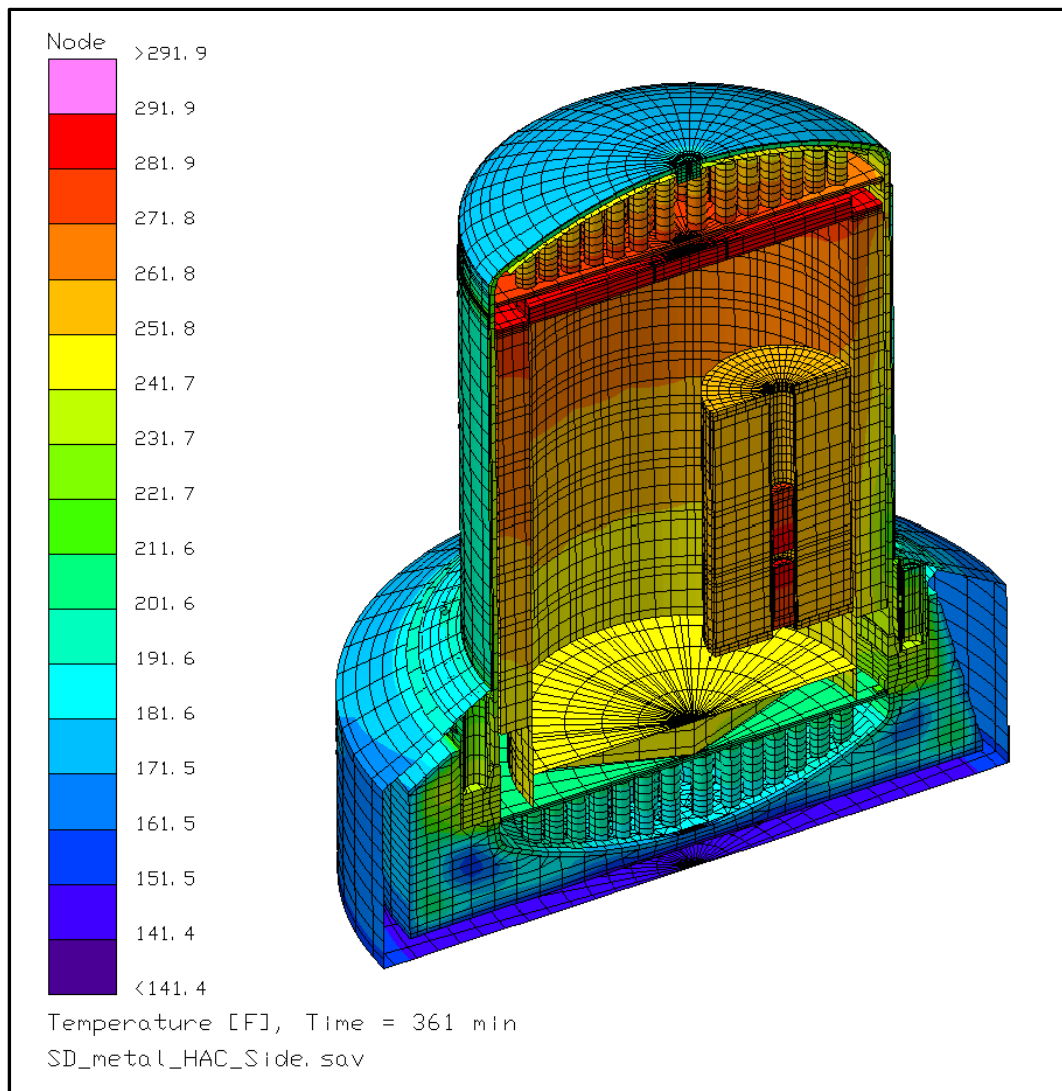


Figure 3.4-13 – Side Drop HAC Temperature Distribution with Shielded Device Supported by Metallic Dunnage

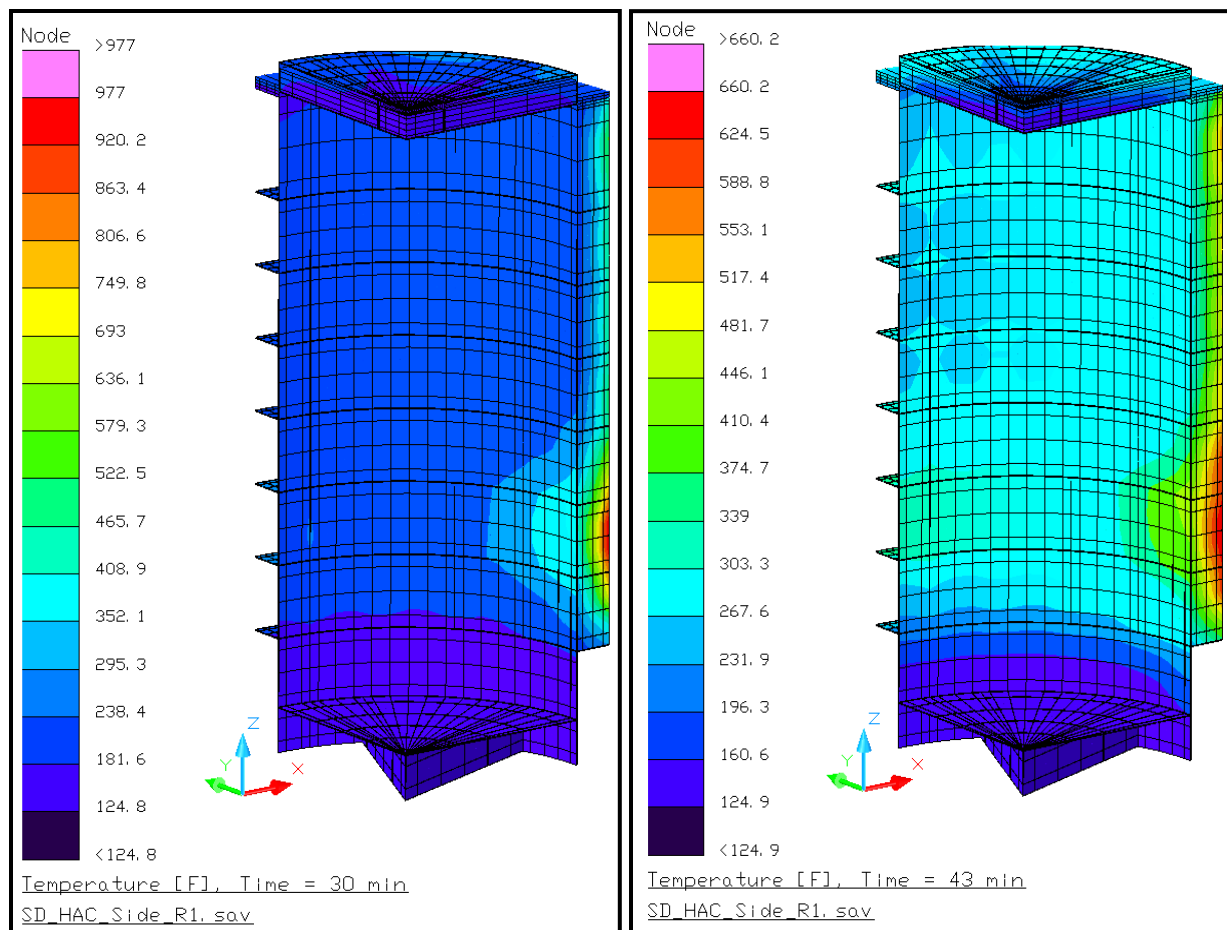
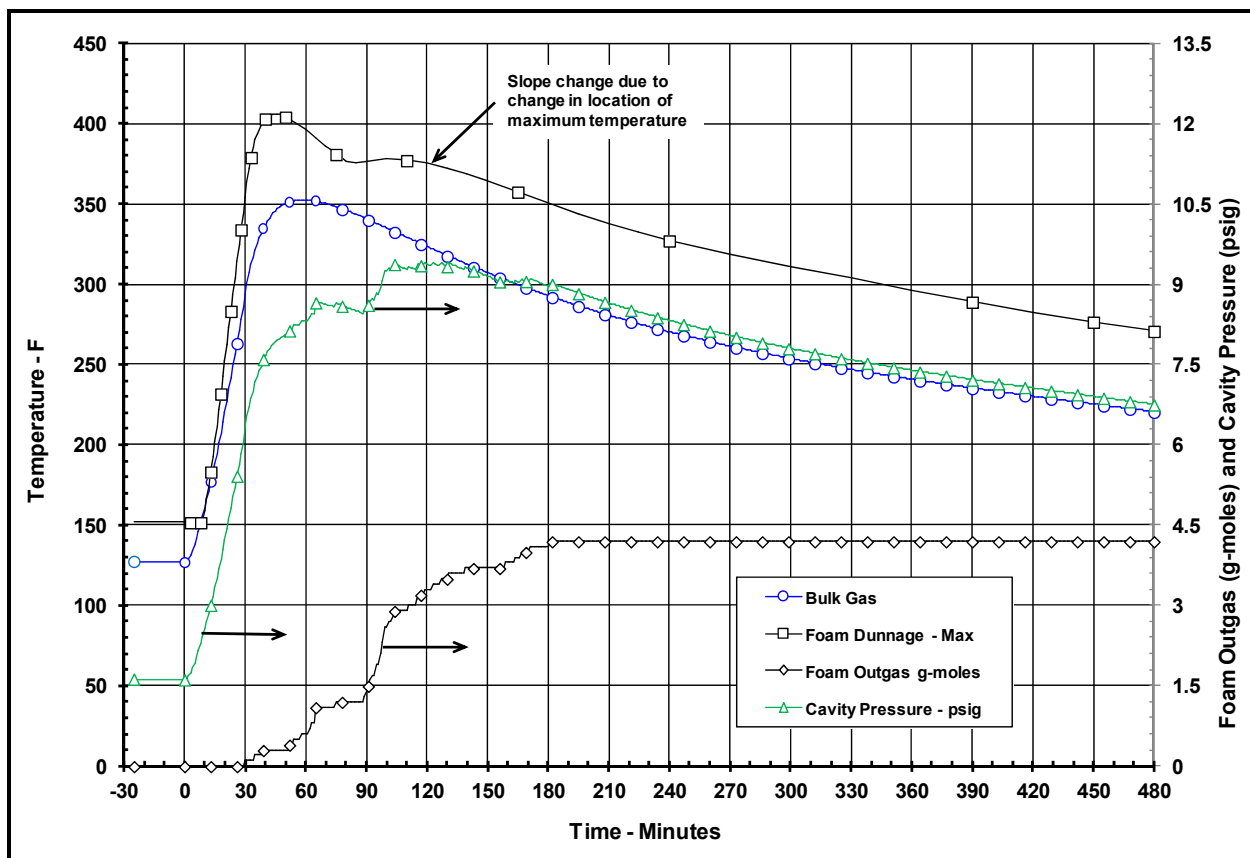


Figure 3.4-14 – Side Drop HAC Temperature Distribution in IC when Supported by Polyurethane Foam Dunnage



Note: Scale for cavity pressure and foam outgas quantity shown on right hand side

Figure 3.4-15 – Bounding Shielded Device HAC Cavity Pressure Response – Side Drop Damage

Table 3.4-4 – Non-metallic Contents Materials^①

Material	Location	Calculated Temperature, °F	Temperature Limit and Data Source
Marking paint & IC dunnage paint	Lodgment	Lodgment maximum ^②	High temperature paint (500 °F minimum use temperature) specified on SAR drawings and in Section 7.1.2.2.
	IC	IC shell maximum ^②	
Nitrile rubber	LTSS dust seals	270 °F (for LTSS shell, Table 3.4-1)	Figure 19 of [14] shows weight loss is negligible below approximately 300 °C (572 °F).
Nylon	Lodgment self-locking nuts	Bounded by Lodgment maximum ^②	578 K (581 °F) from pg. 204 of [34]
Graphite	GC-40 device bushings	293 °F (for shielded device drawer, Table 3.4-3)	800 °C (1,472 °F) from Table II of [14].
Lifting slings (Nylon)	IC	IC shell maximum ^②	578 K (581 °F) from pg. 204 of [34]
Lifting slings (polyester)	IC	IC shell maximum ^②	Figure 1(a) of [35] shows negligible decomposition below approximately 350 °C (662 °F).
Lifting slings (Kevlar®)	IC	IC shell maximum ^②	700 K (800 °F) from pg. 155 of [34]
Silicone sealant	IC	IC shell maximum ^②	Degradation does not occur below 300 °C (572 °F), from Table 3 of [36] and Figure 5 of [37].
Paint	On shielded device payload	Shielded device shell ^②	Significant degradation does not occur below 200 °C to 300 °C (392 °F to 572 °F), from Figure 1 and Figure 2 of [30], Figure 1a from [31], and Figure 1 of [32].
Grease	On shielded device payload	Shielded device shell ^②	Decomposition of the grease thickener begins at about 250 °C (482 °F), from Section 2.3 of [33].
Vacuum Grease	Vent port sealing washer	274 °F (Table 3.4-1)	
Epoxy adhesive	On shielded device payload	Shielded device shell ^②	Weight loss is less than 5% up to 318 °C (604 °F), per [38].
Acrylic or Acetal plastic	On shielded device payload	Shielded device shell ^②	Lower bound degradation (Acetal) does not occur below 210 °C (410 °F) [40].

Notes:

1. Neoprene rubber and polyurethane foam may also be present on the contents. These materials are discussed in Section 3.2.2. The butyl containment O-ring is discussed in Section 3.4.3.1.
2. Lodgment maximum temperature is 464 °F from Table 3.4-1. IC cylindrical shell maximum temperature (not including the external ribs) is 445 °F from Table 3.4-3. The shielded device maximum shell temperature is 260 °F from Table 3.4-3.

3.5 Appendices

- 3.5.1 References
- 3.5.2 Computer Analysis Results
- 3.5.3 Analytical Thermal Model
- 3.5.4 'Last-A-Foam' Response under HAC Conditions

3.5.1 References

1. Title 10, Code of Federal Regulations, Part 71 (10 CFR 71), Packaging and Transportation of Radioactive Material, United States Nuclear Regulatory Commission (USNRC), 01-01-18 Edition.
2. NUREG-1609, *Standard Review Plan for Transportation Packages for Radioactive Material*, Office of Nuclear Material Safety and Safeguards, U.S. Nuclear Regulatory Commission, Washington, DC 20555-0001, March 1999.
3. Safety Guide No. TS-G-1.1 (ST-2), *Advisory Material for the IAEA Regulations for the Safe Transport of Radioactive Material*, IAEA Safety Standards Series, International Atomic Energy Agency, Vienna, Austria, 2002.
4. U. S. Nuclear Regulatory Commission, Regulatory Guide 7.8, Load Combinations for the Structural Analysis of Shipping Casks for Radioactive Material, Revision 1, March 1989.
5. Last-A-Foam™ On-line Data Sheet, www.generalplastics.com, data sheet dated 4-7-2004.
6. Williamson, C., and Iams, Z., *Thermal Assault and Polyurethane Foam - Evaluating Protective Mechanisms for Transport Containers*, General Plastics Manufacturing Company, Tacoma, WA, Waste Management '05 Symposium, Tucson, AZ, 2005.
7. Williamson, C., and Iams, Z., *Thermal Assault and Polyurethane Foam - Evaluating Protective Mechanisms*, General Plastics Manufacturing Company, Tacoma, WA, presented at PATRAM International Symposium, Berlin, Germany, 2004.
8. Matweb, Online Material Data Sheets, www.matweb.com.
9. American Society of Mechanical Engineers (ASME) Boiler and Pressure Vessel (B&PV) Code, Section II, *Materials*, Part D, 2010.
10. American Society of Mechanical Engineers (ASME) Boiler & Pressure Vessel Code, Section III, *Rules for Construction of Nuclear Facility Components*, Division 1, Subsection NB, Class 1 Components, 2010 Edition.
11. Polymer Data Handbook, James E. Mark Editor, Oxford University Press, Inc., 1999.
12. Safe Use of Oxygen and Oxygen Systems, ASTM, 2nd Edition.
13. Product and MSDS sheets for 3M™ Spray 80 Neoprene Contact Adhesive or 3M™ Scotch-Weld Neoprene Contact Adhesive 1357.
14. Sircar, Anil K., *Analysis of Elastomer Vulcanizate Composition by TG-DTG Techniques*, Center for Basic and Applied Polymer Research, University of Dayton, 1991.
15. *Properties of Lead and Lead Alloys*, Booklet No. 5M-12-83, Lead Industries Association, Inc., New York, N.Y.
16. Incropera and DeWitt, Fundamentals of Heat and Mass Transfer, 5th Edition, John Wiley & Sons Publishers, 2002.
17. Grade 1530-L and 1535-L LyTherm® insulation, Lydall Industrial Thermal Solutions, Inc.

18. Frank, R., and Plagemann, W., *Emissivity Testing of Metal Specimens*, Boeing Analytical Engineering coordination sheet No. 2-3623-2-RF-C86-349, August 21, 1986. Testing accomplished in support of the TRUPACT-II design program.
19. Gubareff, G., Janssen, J., and Torborg, R., Thermal Radiation Properties Survey, 2nd Edition, Honeywell Research Center, 1960.
20. Azzazy, M., "Emissivity Measurements of 304 Stainless Steel", Report #ATI-2000-09-601, prepared for Southern California Edison, by Azzazy Technologies, Inc., September 6, 2000.
21. Touloukian, Y. S. and D. P. DeWitt, Thermophysical Properties of Matter, Volume 7 - Thermal Radiative Properties: Metallic Elements and Alloys, IFI/Plenum Publishers, New York, 1970.
22. ANSI/HPS N43.6-1997, *Sealed Radioactive Source - Classification*, American National Standards Institute, New York, NY, 10036.
23. Rohsenow, Hartnett, and Choi, Handbook of Heat Transfer, 3rd edition, McGraw-Hill Publishers, 1998.
24. Guyer, Eric, Handbook of Applied Thermal Design, McGraw-Hill, Inc., 1989.
25. Thermal Desktop[®], Version 5.3, Cullimore & Ring Technologies, Inc., Littleton, CO, 2010.
26. SINDA/FLUINT, Systems Improved Numerical Differencing Analyzer and Fluid Integrator, Version 5.3, Cullimore & Ring Technologies, Inc., Littleton, CO, 2010.
27. AFS Report AFS-TR-VV-013, Rev. 0, Thermal Desktop[®] and SINDA/FLUINT Testing and Acceptance Report, Version 5.3, AREVA Federal Services, LLC, 2010.
28. Schneider, M.E and Kent, L.A., *Measurements Of Gas Velocities And Temperatures In A Large Open Pool Fire, Heat and Mass Transfer in Fire - HTD Vol. 73*, 1987, ASME, New York, NY.
29. Jones, Dr, Daniel, *Computing Fluid Tank Volumes*, Chemical Processing, November, 2002, pp.46-50.
30. Debora Pugia, Liliana Manfredi, Analia Vazquez, and Jose Kenny, *Thermal degradation and fire resistance of epoxy-amine-phenolic blends*, Polymer Degradation and Stability 73, (2001).
31. Shahla Ataei, Rosiyah Yahya, and Seng Neon Gan, *Study of Thermal Decomposition Kinetics of Palm Oleic Acid-Based Alkyds and Effect of Oil Length on Thermal Stability*, Journal of Polymers and the Environment, June 2012.
32. Kelly Roberts, Matthew J. Almond, and John W. Bond, *Using Paint to Investigate fires: An ATR-IR Study of the Degradation of Paint Samples Upon Heating*, Journal of Forensic Sciences, March 2013, Vol. 58, No. 2.
33. Fumihiko Yokoyama, *Optimization of Grease Properties to Prolong the Life of Lubricating Greases*, Journal of Physical Science and Application, 4 (4) (2014).
34. Polymer Data Handbook, Oxford University Press, 1999.

35. K.S. Muralidhara and S. Sreenivasan, *Thermal Degradation Kinetic Data of Polyester, Cotton and Polyester-Cotton Blended Textile Material*, World Applied Sciences Journal, 11 (2): 2010.
36. Jelena D. Jovanovic, Milutin N. Govedarica, Petar R. Dvornic, & Ivanka G. Popovic, *The thermogravimetric analysis of some polysiloxanes*, Polymer Degradation and Stability 61 (1998), 87 – 93.
37. G. Camino, S.M. Lomakin, and M. Lazzari, *Polydimethylsiloxane thermal degradation Part I. Kinetic aspects*, Polymer 42 (2001), 2395 – 2402.
38. 3M Scotch-Weld™ Epoxy Adhesive DP100 Plus Clear Technical Datasheet, September 2016.
39. E. Dzunuzovic, et. al., *Influence of α -Fe₂O₃ nanorods on the thermal stability of poly(methyl methacrylate) synthesized by in situ bulk polymerisation of methyl methacrylate*, Polymer Degradation and Stability 93 (2008) 77 – 83.
40. DuPont Material Safety Data Sheet, "DELRIN" Acetal Resin/PTFE Blends All In Synonym List DEL012, Revised 20-APR-2007.
41. Thermal Desktop®, Version 5.8, Cullimore & Ring Technologies, Inc., Littleton, CO, 2015.
42. SINDA/FLUINT, Systems Improved Numerical Differencing Analyzer and Fluid Integrator, Version 5.8, Cullimore & Ring Technologies, Inc., Littleton, CO, 2015.

3.5.2 Computer Analysis Results

Due to the size and number of the output files associated with each analyzed condition, results from the computer analysis are provided on a CD-ROM.

3.5.3 Analytical Thermal Model

This section presents details of the thermal modeling used to simulate the 1105-SD packaging and its authorized payloads. The analytical model is developed for use with the Thermal Desktop[®] [25] and SINDA/FLUINT [26] computer programs. These programs work together to provide the functions needed to build, exercise, and post-process a thermal model. The codes are validated for generating safety basis calculations for nuclear related projects [27] and have been used for numerous other safety evaluations.

The Thermal Desktop[®] computer program provides graphical input and output display functions, as well as computing the thermal mass, conduction, and radiation exchange conductors for the defined geometry and thermal/optical properties. Thermal Desktop[®] is designed to run as an application module within the AutoCAD[™] design software. As such, all of the CAD tools available for generating geometry within AutoCAD[™] can be used for generating a thermal model. In addition, the use of the AutoCAD[™] layers tool presents a convenient means of segregating the thermal model into its various elements.

The SINDA/FLUINT computer program is a general purpose code that handles problems defined in finite difference (i.e., lumped parameter) and/or finite element terms and can be used to compute the steady-state and transient behavior of the modeled system. Although the code can be used to solve any physical problem governed by diffusion-type equations, specialized functions used to address the physics of heat transfer and fluid flow make the code primarily a thermal code.

Together, the Thermal Desktop[®] and SINDA/FLUINT codes provide the capability to simulate steady-state and transient temperatures using temperature dependent material properties and heat transfer via conduction, convection, and radiation. Complex algorithms may be programmed into the solution process for the purposes of computing heat transfer coefficients as a function of the local geometry, gas thermal properties as a function of species content, temperature, and pressure.

3.5.3.1 Description of 1105-SD Packaging Thermal Model for NCT Conditions

The 1105-SD packaging is represented by a 3-dimensional, half symmetry thermal model for the NCT evaluations. This modeling choice captures the full height of the packaging components and allows the incorporation of the varying insolation loads that will occur along the length of the package, the various degrees of symmetry within the payload, and the non-symmetry of the HAC free drop damage. The various packaging components are defined using a combination of planar and solid elements. Program features within the Thermal Desktop[®] computer program automatically compute the various areas, lengths, thermal conductors, and view factors involved in determining the individual elements that make up the thermal model of the complete assembly.

Figure 3.5-1 to Figure 3.5-5 illustrate various views of the 1105-SD packaging thermal model used for the NCT evaluations. The model is composed of solid and plate type elements

representing the various packaging components. Thermal communication between the various components is via conduction, radiation, and surface-to-surface contact. A total of approximately 26,400 nodes, 10,300 planar elements and surfaces, and 10,500 solid elements are used to simulate the modeled components. Twenty two of the solid elements are finite difference solids (i.e., FD solids), a Thermal Desktop[®] computer program feature that permits a group of solid elements to be represented by a single entity. As such, the number of individual solid 'bricks' utilized in the modeling is actually significantly larger than the 10,500 value indicated above. In addition, one boundary node is used to represent the ambient environment for convection and radiation purposes.

As seen from a comparison of Figure 3.5-1 with Figure 1.2-2, Section 1.0, *General Information*, the modeling accurately captures the geometry of the various components of the 1105-SD packaging, including the lower body assembly and its polyurethane foam filled impact limiter, the upper body assembly (or bell), and the two internal impact limiter assemblies. Also captured, but not easily seen due to the scale of the figure, are the side and top thermal shields. The maximum spatial resolution provided by the thermal modeling for the metallic package body components is approximately 1 inch in the radial direction, 2.25 inches in the axial direction, and every 7.5° in the circumferential direction. Greater spatial resolution (i.e., smaller radial and axial distances) is provided near the cask ends where larger thermal gradients are expected.

A lower radial resolution is provided for the polyurethane foam in the impact limiter since the low thermal conductivity of the foam will yield correspondingly low heat flows. Since the fabrication tolerance of the polyurethane foam used to fill the impact limiter can yield foam densities that are $\pm 15\%$ of the targeted 15 lb_m/ft³ (pcf) foam density and since the foam's conductivity is a function of its density, the thermal modeling conservatively assumes a low tolerance foam density (i.e., 15 pcf less 15% \approx 12.75 pcf) for NCT evaluations and a high tolerance foam density (i.e., 15 pcf plus 15% \approx 17.25 pcf) for HAC evaluations.

Figure 3.5-2 illustrates the thermal modeling used for the containment boundary of the 1105-SD packaging. As seen from the figure, the modeling captures much of the geometry detail in the upper and lower flanges, as well as the welded joint between the 1/2-inch thick plate of the lower torispherical head and the cylindrical shell and the thicker ends of the flange sections. The 24 closure bolts are not specifically modeled. Instead, the flange and bolt material are modeled as a homogenized region of Type 304 stainless steel. As pointed out in Section 3.2.1, *Material Properties*, the thermal conductivity of the ASTM 320, Grade L43 bolts is approximately twice that of the Type 304 stainless steel used for the flange, while the specific heat values are similar between the two materials. However, since the cross-section area of 1-1/4-7 UNC bolts represents only 62% of the flange area that is lost due to the presence of the 1.38 inch bolt holes, the net effect of ignoring the material property differences and treating the flange as a homogenous solid for conduction purposes drops from a factor of 2 to 1.25. This net effect drops to only about 1.02 when the localized enhanced conductivity represented by the closure bolts is smeared across the entire bolt flange area. The added surface area of the bolt heads doesn't have any significant effect since the bolts are enclosed by the tubes and shells which provide protection from HAC puncture bar impact or heat input from the HAC fire event. As such, the specific modeling of the closure bolts can be neglected without significantly impacting the accuracy of the predicted temperatures. The thermal model does include an enhanced conductivity between the upper and lower flanges to mimic the thermal conductance provided by the bolt shanks.

Figure 3.5-3 illustrates the thermal representation of the top and side thermal shields used in the modeling. The shields are modeled as surface elements since their relative thinness will yield essentially zero ΔT across their thickness. Heat transfer between each shield and its underlying surface is modeled as a combination of radiation and conduction across a 0.105-inch thick air gap and conduction through a 0.105-inch diameter stainless steel wire wrap on 3-inch centers. For conservatism under NCT condition, the conduction through the wire wrap is ignored for NCT.

A significant level of thermal protection to the thermally sensitive closure seals is provided by the closure bolt enclosure structure at the lower end of the upper body assembly. The closure bolt enclosure structure consists of tubes and shells which provides access to the closure bolts and the vent port and seal test port while also protecting these components from HAC puncture bar impact or excessive heat input from the HAC fire event. Figure 1.2-4, Section 1.0, *General Information*, illustrates the detail in this area, while Figure 3.5-4 illustrates the thermal representation used for the same region. As seen from a comparison of the two figures, the thermal modeling accurately captures the individual components and the complex geometry in this area. Included, but not seen in the figure, are the blocks of 30 pcf foam used between the individual bolt access tubes to thermally isolate the cylindrical shell from potentially high temperatures that may occur near the exterior of the enclosure structure during the HAC fire.

The thermal modeling of the internal impact limiters is illustrated in Figure 3.5-5. As seen, the modeling captures the individual stainless steel tubes and the 0.105-inch thick stainless steel tube stabilizer sheet which is spherically curved to match the shape of the torispherical heads. The Thermal Desktop[®] program automatically calculates the conduction and radiation between the various components of the internal impact limiters.

3.5.3.2 LTSS and LTSS Lodgment Thermal Model

Figure 3.5-6 illustrates the thermal modeling of the LTSS used for this evaluation. As with the 1105-SD packaging, the modeling represents a 3-dimensional, half symmetry thermal model. Approximately 4,200 nodes, 620 planar elements, and 600 solid elements are used to simulate the modeled components of the LTSS, the Large Source Drawer, and the source capsule. The modeling captures the individual components of the LTSS in a manner that the thermal properties of each significant component depicted in Figure 1.2-9, Section 1.0, *General Information*, and the gaps between the individual components are captured. Although the LTSS can accommodate 4 Large Source Drawers, the thermal modeling assumes that only one of the drawers is loaded with a source capsule dissipating the maximum 200 watts allowed for the entire LTSS. This assumption yields the worst case concentration of decay heat loading possible for the LTSS. The bounding 200 W heat load requires a Co-60 source which dissipates a significant amount of its energy in the form of gamma rays. Based on Monte Carlo N-Particle (MCNP) calculations using a source height of 1.45-in and diameter of 0.72-in, a Co-60 source will deposit approximately 20% of the decay heat within the source volume and the remaining 80% outside the source where the gamma rays emitted by the source are absorbed. While the gamma ray absorption will be distributed throughout the lead volume, the modeling conservatively assumes the entire absorption of this 80% portion occurs at the ends of the tungsten shielding in the Large Source Drawer and within a 6.75 inch high segment of the LTSS liner adjacent to the special form capsule. In reality, the heat deposition would occur over a much greater volume of the LTSS, thus lowering the effective heat flux at any point in the LTSS.

The LTSS is supported within the 1105-SD packaging by the LTSS lodgment. Thermal modeling of the lodgment (see Figure 3.5-7) is accomplished using approximately 2,000 nodes, 1,225 planar elements, and 12 finite-difference solids. Heat transfer between the LTSS and the lodgment is via radiation, convection, and conduction across the neoprene rubber covered ½-inch thick plate at the base of the lodgment and via the neoprene rubber covered pads on the tapered edges of the lower ribs.

The thermal modeling of convection for the safety evaluation is based on a combination of physics and conservatism. In some cases, a combination of package orientation and heat loading will physically prevent the formation of a convection cell, while in other cases ignoring the potential presence of convection will yield bounding package component temperatures.

Although convection heat transfer between the LTSS, the LTSS lodgment, and the interior of the 1105-SD packaging is assumed for NCT, the effect on the NCT temperatures is modest. A sensitivity analysis based on *NCT Hot No Solar* condition showed that completely ignoring convection or conduction through the airspace around the LTSS and LTSS lodgment raises the source capsule temperature by less than 10 °F and the LTSS lead shielding temperature by only 30 °F from the values presented in Section 3.3, *Thermal Evaluation for Normal Conditions of Transport*. These temperature increases are insignificant in comparison to the available margins for both components. Alternatively, ignoring convection will reduce the bulk gas temperature and payload temperatures under HAC conditions. As such, credit for convection heat transfer within the modeling is appropriate.

Examination of the sensitivity analysis results showed that the maximum allowable surface temperature without insolation during NCT did rise 4°F to 121°F. However, as pointed out in Section 3.3.1.1, *Maximum Temperatures*, the peak accessible surface temperature occurs in a very narrow band at the base of the side thermal shields where the closeout welds provide a direct thermal path to the package shell. Beyond this narrow band the accessible surface temperatures are significantly lower. Furthermore, the size of the open areas within the package payload cavity makes a 'no convection' situation a thermal impossibility.

The thermal modeling ignores convection heat transfer within the void volume encompassed by the containment's upper torispherical head during both NCT or HAC. This is done for two reasons: one, to most accurately model the real heat transfer in the head for a vertically oriented package, and two, to maximize payload temperatures under NCT and package shell temperatures under HAC. Peak NCT temperatures occur with the upper torispherical head hotter than either the bulk average gas temperature or the upper internal impact limiter. As such, there would be no buoyant force to drive convection. Under HAC, the potential contribution of convection within the containment's upper torispherical head void volume depends on the orientation of the package following the pre-fire drop event. However, the assumption of no convection within the containment's upper torispherical head void volume yields the peak temperature in either case. Inclusion of convection where it could occur would serve to accelerate heat removal from the torispherical head and lower the SAR predicted peak temperature with little to no change for the payload components.

Similarly, ignoring convection heat transfer within the void volume encompassed by the containment's lower torispherical head during both NCT or HAC reflects the reality of the thermal gradients that exist for a vertically oriented package under both NCT and HAC. Ignoring convection for other package orientations serves to conservatively bound the payload temperatures.

Figure 3.5-8 illustrates the combined modeling of 1105-SD packaging with the LTSS payload.

3.5.3.3 Shielded Device and Inner Containment Thermal Model Utilizing Polyurethane Foam Dunnage

As described in Section 1.0, *General Information*, the size and geometry of the Group 1 and 3 shielded devices vary. However, while the exact dimensions and shapes are varied, the general shape and size of devices in Group 1 and 3 are similar, especially after the cabinets, stands, or unnecessary appurtenances attached to the devices are removed prior to transportation. Given the variance in geometry, the modeling approach for the shielded devices was to develop a generic representation of a device that would thermally bound the Group 1 and 3 shielded devices. After considering the thermal features of the various Group 1 and 3 devices, the Gammacell-40 device was selected as the appropriate basis for developing a generic device whose thermal performance would bound the other devices. The 15.9 inch diameter and 28.7 inch length of the cylindrical body of the Gammacell-40 yields a surface area that is slightly less than that for the Gammator M38, and Gammacell 1000 and 3000 devices, while its weight is less than the Gammacell 1000 and 3000 devices and 18% higher than the Gammator M38. The smaller Group 1 devices, such as the Gammator 50B and B34 devices also have a significantly lower decay heat loading than the 30 W design basis used for the generic device. Further, the Gammacell-40 device uses a source capsule that is relatively compact, whereas the source for many of the other Group 1 and 3 devices uses elongated, pencil shaped sources. As such, a concentrated heat source based on the Gammacell-40 design will yield conservative source capsule temperatures.

The Group 1 and 3 generic device assumes 6 inches of lead shielding in a right cylinder geometry with a 15.9 inch diameter and 28.7 inch height. The source is assumed to be contained within a drawer assembly like that used for the Gammacell-40 device. Figure 3.5-9 illustrates the thermal model of the generic shielded device used for NCT evaluations. As seen, the modeling represents a 90° segment versus the 180° segment used for the LTSS modeling. A quarter symmetry model is appropriate for the shielded devices since a single source location within the device exists, thus asymmetric heat loading is not a factor as it was for the LTSS payload. Approximately 1,350 nodes, 11 planar elements, and 11 finite-difference solid elements are used to simulate the modeled components of the device. As previously explained, a finite-difference solid is a Thermal Desktop® computer program feature that permits a group of solid elements to be represented by a single entity. As such, the number of individual solid ‘bricks’ utilized in the modeling of the shielded device is actually significantly larger.

The modeling captures the off-center location of the source drawer (like that of the Gammacell-40 device) when it is in its storage location. This off-center location is significant when considering that the packaging dunnage is assumed to surround the ends of the device, thus restricting the heat transfer from the ends. The modeling also reflects the transport of a small source capsule (i.e., 1.7 inch long by 1.57 inch in diameter) versus the pencil shaped capsules used for many Group 1 and 3 devices. The smaller capsule yields a worst case heat concentration for the evaluation. The entire 30 W decay heat assumed for the shielded devices is conservatively assumed to be deposited within the source capsule.

Figure 3.5-10 illustrates alternate views of the Inner Container (IC) and the polyurethane foam blocking/dunnage used to support the shielded device in the IC. The IC is modeled using approximately 2,500 nodes, 80 planar elements, and 8 finite-difference solid elements. The

blocking/dunnage may consist of either a metallic framework or use a rigid polyurethane foam. Since solid blocking like rigid polyurethane foam restricts the heat transfer between the shielded device and the IC much more than would an open, metallic framework, the thermal modeling on this first configuration assumes the use of polyurethane foam. An additional 2,500 nodes and 16 finite-difference solid elements are used to model the foam dunnage. The foam dunnage is conservatively assumed to cover the ends and extend over the sides of the shielded device leaving only 50% or more of the side surface exposed to the IC interior.

As with the LTSS payload, convection heat transfer between the IC and the interior surfaces of the 1105-SD packaging and between the shielded device and the IC are assumed. Again, a sensitivity analysis showed that completely ignoring convection or conduction through the airspace raises the source capsule temperature by less than 10 °F. Since this temperature increase is insignificant in comparison to the available margins and since ignoring convection will reduce the bulk gas temperature and payload temperatures under HAC conditions, including credit for convection heat transfer within the modeling is appropriate.

Figure 3.5-11 illustrates the combined modeling of 1105-SD packaging with the generic shielded device payload.

3.5.3.4 Shielded Device and Inner Container NCT Thermal Model utilizing Metallic Dunnage

The thermal model of the shielded device and IC for the metallic dunnage evaluations is constructed using half symmetry in order to be consistent with the conservative modeling assumption used for HAC. No other changes are made to the shielded device and IC geometry from the description given in Section 3.5.3.3, *Shielded Device and Inner Container Thermal Model utilizing Polyurethane Foam Dunnage*.

The metallic dunnage material is not explicitly modeled, but the shielded device is positioned in the same location as the foam case. This modeling approach conservatively lowers the overall thermal mass of the package which maximizes the temperature response of the package during the transient solar loads. It also conservatively models the shielded device temperatures because the transfer of the decay heat from the shielded device to the IC is limited to convection and radiation.

3.5.3.5 Insolation Loads

The insolation loading on the 1105-SD package is based on the total 10CFR71.71(c)(1) specified insolation values over a 12-hour period [1]. Since the 1105-SD packaging is characterized by a thermally light upper body assembly, a lower body assembly encased by a foam filled impact limiter, and thermally massive interior payloads, the temperature response to diurnal changes in the insolation loading will vary significantly between the various packaging components and the payloads.

As such, the use of a time-averaged insolation loading based on the 10CFR71.71(c)(1) specified insolation over 12 hours will not accurately capture the peak component temperatures near the package's exterior under NCT conditions. Instead, the 10CFR71.71(c)(1) specified insolation values over a 12-hour period are converted to an equivalent diurnal insolation loading cycle. This analysis methodology follows the recommendations of IAEA Safety Guide TS-G-1.1

¶654.4 [3] which states that “the more precise way to model insolation is to use a time dependent sinusoidal heat flux”.

A sine wave model is used to simulate the variation in the applied insolation on the surfaces of the package over a 24-hour period, except that when the sine function is negative, the insolation level is set to zero. The timing of the sine wave is set to achieve its peak at 12 pm and the peak value of the curve is adjusted to ensure that the total energy delivered matched the 10CFR71.71(c)(1) specified values. As such, the total energy delivered in one day by the sine wave solar model is given by:

$$\int_{6\text{-hr}}^{18\text{-hr}} Q_{\text{peak}} \cdot \sin\left(\frac{\pi \cdot t}{12\text{-hr}} - \frac{\pi}{2}\right) dt = \left(\frac{24\text{-hr}}{\pi}\right) \cdot Q_{\text{peak}}$$

Using the expression above for the peak rate of insolation, the peak rates for insolation on horizontal flat and the vertical curved surfaces is calculated as follows:

$$Q_{\text{top}} = \left(800 \frac{\text{cal}}{\text{cm}^2}\right) \cdot \left(\frac{\pi}{24\text{ hr}}\right) \quad Q_{\text{top}} = 2.68 \frac{\text{Btu}}{\text{hr} \cdot \text{in}^2}$$

$$Q_{\text{side}} = \left(200 \frac{\text{cal}}{\text{cm}^2}\right) \cdot \left(\frac{\pi}{24\text{ hr}}\right) \quad Q_{\text{top}} = 0.67 \frac{\text{Btu}}{\text{hr} \cdot \text{in}^2}$$

Conversion factors of $1 \text{ cal/cm}^2\text{-hr} = 0.0256 \text{ Btu/hr-in}^2$ are used in the above calculations. These peak rates are multiplied by the sine function and the surface solar absorptivity to create the insolation values as a function of time of day. Figure 3.5-12 illustrates the level of insolation on flat horizontal, horizontal curved, and vertical surfaces versus time of day assumed for the evaluation of package performance under *NCT Hot* conditions. The diurnal cycle modeling approach results in a peak hourly insolation loading that is approximately 57% higher than the specified 10CFR71.71(c)(1) value averaged over 12 hours. However, the total insolation load applied to each surface of the package is the same as that specified by 10CFR71.71(c)(1).

3.5.3.6 Bulk Average Gas Temperature

The bulk average gas temperature is calculated for the LTSS and shielded device payloads on a volume weighted basis.

3.5.3.6.1 LTSS Payload Average Gas Temperature

For the LTSS payload, the package cavity is divided into 5 regions:

- 1) the upper internal impact limiter cavity volume,
- 2) the cavity volume beginning at the start of the taper above the cylindrical barrel on the LTSS payload and extending to the underside of the upper internal impact limiter,
- 3) the cavity volume opposite of the cylindrical barrel on the LTSS payload,
- 4) the cavity volume beginning at the start of the taper below the cylindrical barrel on the LTSS payload and extending to the topside of the lower internal impact limiter, and
- 5) the lower internal impact limiter cavity volume.

The void volume for each region is determined by subtracting the volume of the metallic components from the gross cavity volume. The resulting computed void volume for the 5

regions are 7,934.6 in³, 41,039.5 in³, 4,758.3 in³, 27,219.8 in³, and 7,934.6 in³, respectively. The bulk average gas temperature is computed by multiplying the computed mean gas temperature for each region by its associated void volume and then dividing the sum by the total void volume. Because of the complex arrangement of the internal impact limiters, the associated gas temperature for these regions is assumed to be equal to the average temperature of the nodes that represent the geometry of the limiters. This bulk average gas temperature is updated constantly within the thermal model as the model converges or proceeds through a transient event.

3.5.3.6.2 Shielded Device Average Gas Temperature when Supported by Polyurethane Foam Dunnage

The bulk average gas temperature is calculated for the shielded device payload using a similar method except the package cavity is divided into 4 regions:

- 1) the upper internal impact limiter cavity volume,
- 2) the cavity volume within the inner container (IC),
- 3) the cavity volume outside the IC and extending from the lower to the upper internal impact limiter, and
- 4) the lower internal impact limiter cavity volume.

The void volume for each region is determined by subtracting the volume of the metallic components from the gross cavity volume. The resulting computed void volume for the 4 regions are 7,934.6 in³, 15,806 in³ (equal to approximately 1/3 of the total empty void volume of the IC due to the presence of a shielded device and foam dunnage), 29,970 in³, and 7,934.6 in³, respectively. The bulk average gas temperature is then computed using a volume weighted average of the estimated mean gas temperature computed within each region. Again, the bulk average gas temperature is updated constantly within the thermal model as the model converges or proceeds through a transient event.

3.5.3.6.3 Shielded Device Average Gas Temperature when Supported by Metallic Dunnage

The bulk average gas temperature for the shielded device when supported by metallic dunnage is calculated using the same method as described above. The only exception is that the IC cavity volume is increased from 15,806 in³ to 48,248 in³ due to the reduction in the volume of the dunnage used.

3.5.3.7 Description of Thermal Model for HAC Conditions

The thermal evaluations for the hypothetical accident condition (HAC) are conducted using an analytical thermal model of the 1105-SD packaging loaded with the LTSS and shielded device payloads. The HAC thermal models are modified versions of the NCT models described above. The principal model modifications consist of simulating the expected package damage resulting from the drop events that precede the HAC fire, changing the package surface emissivities to reflect the assumed presence of soot and/or surface oxidization, and simulating the thermal performance of the polyurethane foam used in the impact limiter.

Physical testing using a series of prototypic full scale certification test units (CTUs) is used to establish the expected level of damage sustained by the 1105-SD packaging as a result of the 10 CFR 71.73 prescribed free and puncture drops that precede the HAC fire event. Documentation

of the configuration and initial conditions of the CTUs, a description of the test facility, CTU instrumentation, and the test results is presented in Appendix 2.12.3, *Certification Test Results*. The drop tests covered a range of hypothetical free drop orientations and puncture bar drops. An overview of the results of the drop tests is provided below.

- 1) Three free drop orientations were tested: a bottom end drop, a simultaneous side drop on the limiter and knuckle, and a C.G.-over-knuckle drop. Of these orientations, the worst case physical damage to the package occurs from the simultaneous side drop with elevated foam temperatures (i.e., test event D4). Overall, the resulting damage is thermally insignificant. The combined damage from both the NCT and HAC drops in this orientation resulted in flat regions on both the impact limiter and the knuckle of the package head. The impact limiter flat measured 25-1/2 inches long (along cask axis) and 33 inches wide (orthogonal). The knuckle flat was 11-1/2 inches long and 18-1/2 inches wide. The worst case radial crush distance of the polyurethane foam in the impact limiter was 4-13/16 inches, as measured from the cask body O.D. Since the impact occurred with the cask axis at an angle of approximately 13° to the ground, the crush in the direction of impact was $4\text{-}13/16 \times \cos(13) = 4.68$ inches. The depth of foam remaining, as measured perpendicular from the outer surface of the foam to the flange upper corner, was 5-1/8 inches. The crush at the knuckle was significantly less.
- 2) Two separate free drops in the bottom-down orientation (i.e., D1 and D5) resulted in a crush distance of only 5/16 inches or less. This level of damage is seen as negligible and no visible damage to the CTUs was seen.
- 3) The NCT and HAC C.G.-over-knuckle drops (i.e., test event D3) resulted in creation of a flat spot on the torispherical head, offset towards one side. The combined damage created a flat spot 21 inches long in the radial direction and 33-1/2 inches long in the circumferential direction. The internal impact limiter tubes located below the test D3 impact were crushed, and the plate of the upper internal limiter was buckled from both the D3 and D4 impacts. The deformation of the package head due to test event D3 is shown in Figure 2.12.3-45 and Figure 2.12.3-46 in Appendix 2.12.3, *Certification Test Results*, where the head thermal shield has been locally cut away to expose the containment boundary. The lower limiter had little damage. The lodgment showed some buckling of the radial plate adjacent to the impact of the D3 test, but little other damage (see Figure 2.12.3-47). The LTSS was supported in essentially its original position. Note that the LTSS was thoroughly tested in Test Series D1 and D2. The only additional damage to the LTSS from Test Series D3 and D4 was some shallow deformations (approximately 1/8 inches or less) due to support from the lodgment's circular plates in the side (D4) free drops.
- 4) With the exception of test event D3, no significant deformation of the LTSS lodgment or the IC was noted as a result of the other drop orientations.

No scaling of the noted crush dimensions are required since the CTUs are full scale representations of the 1105-SD package. However, the projected damage did need to be scaled to reflect the full effect of temperature on the polyurethane foam's structural properties since the warm drop test event D4 did not fully capture the peak foam NCT foam temperature and, thus, the worst case crush. This warm foam scaling added an estimated 0.5 inches to the expected crush depth, reducing the foam depth, as measured perpendicular from the outer surface of the

foam to the flange upper corner, from 5-1/8 inches to 4.63 inches, as discussed in Section 2.7.1.5.2, *Maximum Impact Limiter Crush Deformation*.

Based on a review of the above damage results, two damage events were selected to bound the worst-case scenarios for the 1105-SD package: 1) a simultaneous side drop on the limiter and knuckle and 2) a head down drop. The head down drop is used instead of the tested C.G.-over-knuckle drop since the head down drop damage affects the entire head versus the localized damage at the knuckle and because the simultaneous side drop on the limiter and knuckle already captured some of the effect of damage to the knuckle region of the package.

Figure 3.5-13 illustrates the assumed crush lines at the center of the impact zone for the side drop damage scenario. The modeled depth of the crush at the knuckle is approximately 2 inches. This crush depth yields a impact zone on the model that measures approximately 18.5 inches wide by 11.5 inches high, matching the measured knuckle flat observed from the CTU testing. Guidance for modeling the effect of the knuckle damage is taken from Figures 2.12.3-45 and 2.12.3-46 in Appendix 2.12.3, *Certification Test Results*. These figures illustrate a cutaway at the torispherical head following the C.G.-over-knuckle drop and demonstrate that the wire standoffs between the head and the top shield were left intact and, as evidenced by the lack of scuff marks on the head, that a direct contact between the top shield and the head did not occur. Based on this observation, the knuckle damage is simulated by conservatively assuming that the air gap separating the thermal shields is reduced by half and that direct contact between the shell and the aluminum plate of the upper internal impact limiter occurs over a 30 degree angle. Heat transfer via the wire wrap is also conservatively assumed everywhere.

Per Appendix 3.5.4, *'Last-A-Foam' Response under HAC Conditions*, approximately 2.5 inches of the nominal 15 pcf polyurethane foam will thermally decompose during a 30 minute HAC fire event. Since the HAC modeling assumes a conservatively low foam density of 12.75 pcf, the foam loss (or recession depth) is increased to 2.8 inches for this low end density. In the vicinity of crush damage the effective foam density will increase as a result of the crush, thus decreasing the local foam recession depth accordingly. Per the warm foam scaling discussed above, the foam depth at the package flange is reduced from approximately 8.75 inches to 4.63 inches, yielding an increase in the effective density of approximately 88% at the centerline of the damage. Based on an initial foam density of 12.75 pcf, an effective foam density of approximately 24 pcf will occur at the centerline of the damage, yielding an associated foam recession depth of approximately 1.5 inches. For conservatism, the modeling assumes a recession depth of 1.8 inches at the centerline of the impact limiter damage, increasing to 2.8 inches at the circumferential edges of the side drop damage.

Given a maximum foam recession depth of 2.8 inches, any foam depth remaining after the HAC drop events greater than approximately 3.25 inches will result in the underlying temperatures rising only marginally during the HAC fire event. Examination of Figure 3.5-13 demonstrates that, with the exception of the upper portion of the impact limiter, the side drop will leave sufficient foam everywhere to prevent any significant temperature rise on the backside of the remaining foam.

For modeling expediency, the physical geometry changes resulting from the drop event are not captured by the HAC modeling. Instead, the effect of the geometry realignment is captured by adjusting the conductors within the HAC model from the associated surface and any underlying component. For example, in the vicinity of the side crush, the gap between the outer edges of the

foam and the impact limiter shell at the end of the 30-minute fire is modeled as 1.8 inches (i.e., the foam recession depth) versus the variable distance indicated by the undamaged impact limiter shell geometry.

The controlling puncture bar damage for the side drop event is one that will enhance damage to the impact limiter and the underlying closure seals. Of the various CTU tested puncture bar scenarios to the lower end of the package, only the P7 orientation resulted in a thermally significant damage. The P1, P4, P5, and P6 scenarios did not result in damage that would significantly degrade the thermal resistance offered by the undamaged package geometry. While the P7 scenario is an oblique strike on side thermal shield through the C.G., the modeled damage location was shifted downward on the package to a point just above the rain shield in order to maximize the potential impact on the closure seals. In reality, since this location is not at the package C.G., the damage would be expected to be less severe than that noted from the P7 test.

Figures 2.12.3-30 and 2.12.3-36 in Appendix 2.12.3, *Certification Test Results*, illustrates the level of damage resulting from the P7 puncture bar attack. The modeling conservatively captures the observed damage by assuming direct contact over approximately a 6-inch diameter area between all layers of the dual thermal shield and the shell.

The head down drop damage scenario is depicted in Figure 3.5-14. The head crush line is assumed to be approximately 4 inches down from the top. Again, for modeling expediency, the physical geometry realignment resulting from the drop event is not captured by the HAC model, but is reflected in the adjusted conductors between the top shield and the underlying components. In this case, the thickness of the wire wrap and the associated air gap is reduced by 1/3 and the heat transfer via the wire wrap increased by a factor of approximately 2 to account for the assumed enhanced contact between the assumed flattened surfaces of the wire wrap and the adjacent thermal shield and torispherical head surfaces.

While the tubes of the upper internal impact limiter will be crushed as a result of the head down drop scenario, the effect on the radiation and conduction along the length of the tubes is limited since the expected folding in the tube walls will maintain the same total heat transfer length for conduction and increase the effective blockage of heat transfer via radiation. Although heat transfer via conduction through the fill gas along the length of the internal impact limiter will increase, this heat transfer mode represents an insignificant fraction of the total heat transfer. The nominal 0.6 inch gap between the tube stabilizer sheet of the internal impact limiter and the torispherical head is reduced to 0.1 inch to reflect the tube crushing and assumed shifting of the package internal components for the post-drop horizontal package orientation.

The associated puncture bar damage is taken to be the P3 orientation (i.e., C.G.-over-knuckle) from the CTU testing. Guidance for modeling the effect of a puncture bar attack in the knuckle region is taken from Figures 2.12.3-45 and 2.12.3-46 in Appendix 2.12.3, *Certification Test Results*. As previously explained, these figures illustrate a cutaway at the torispherical head following the C.G.-over-knuckle drop. A close examination of the figures demonstrate that puncture bar impact left an imprint around a portion of the bar's circumference, but the lack of a scuff mark would indicate that full area contact is not made. Based on this observation, the knuckle damage is simulated by conservatively assuming direct contact between the top thermal shield and the torispherical head in an 0.5-inch wide annular region around the circumference of the puncture bar. Heat transfer via the wire wrap is also conservatively assumed everywhere.

Beyond the specific modifications to simulate the HAC damage scenarios, the NCT thermal model for the package was modified for the HAC evaluations via the following steps:

- 1) Assume the package has been ejected from its transport support and is lying on its side for all damage scenarios. As such, the convective heat transfer from the package's exterior surfaces is based on a horizontal orientation. In addition, the adiabatic boundary condition assumed for selected surfaces of the lower impact limiter under NCT conditions are switched to active heat transfer surfaces.
- 2) The surface emissivity for all exterior surfaces is assumed to be 0.8 to account for potential oxidation and/or soot accumulation. The emissivity of all inside surfaces of the impact limiter exposed as the result of foam decomposition is assumed to be 0.95 to account for adherence of foam char.
- 3) Thermal conductance via the stand-off wire wrap under the thermal shields is assumed for the HAC condition. Thermal credit for the wire wrap was conservatively ignored for the NCT evaluations.
- 4) 1.8 to 2.8 inches of foam (see above) is removed from around the perimeter of the impact limiter at the start of the HAC evaluation. This change conservatively bounds the impact of the gradual decomposition of the foam over the 30 minute fire event.
- 5) Assume no significant damage to the LTSS, shielded device payload, or polyurethane foam dunnage but that the payloads have shifted to create edge contact between the LTSS lodgment and IC and the package bell. The orientation of the contacting surfaces is conservatively assumed to align with the location of the drop damage.
- 6) Assume that when the shielded device is supported by metallic dunnage that the metallic dunnage fails in such a way that the shielded device comes into intimate contact with the IC cylindrical wall. The contact area is conservatively modeled using a contact width of 1 inch the full length of the shielded device. This assumed contact area bounds the small amount of deformation observed on the IC wall due to the impact of the simulated shielded device during the D3 test (See Figure 2.12.3-37). In addition, the shielded device is conservatively arranged inside the IC such that the source is axially aligned with the P7 puncture damage to the thermal shield.
- 7) Assume that when the shielded device is supported by metallic dunnage that the failed metallic dunnage does not impede convection and radiation heat transfer to the surrounding IC surfaces.

3.5.3.8 Convection Coefficient Calculation

The 1105-SD package thermal model uses semi-empirical relationships to determine the level of convection heat transfer from the exterior package surfaces under both the regulatory NCT and HAC conditions. The convective heat transfer coefficient, h_c , has a form of:

$$h_c = \text{Nu} \frac{k}{L}$$

where k is the thermal conductivity of the gas at the mean film temperature and L is the characteristic length of the vertical or horizontal surface. The convection coefficient is correlated via semi-empirical relationships against the local Rayleigh number and the characteristic length. The Rayleigh number is defined as:

where
$$Ra_L = \frac{\rho^2 g_c \beta L^3 \Delta T}{\mu^2} \times Pr$$

g_c = gravitational acceleration, 32.174 ft/s² β = coefficient of thermal expansion, °R⁻¹
 ΔT = temperature difference, °F ρ = density of air at the film temperature, lb_m/ft³
 μ = dynamic viscosity, lb_m/ft-s Pr = Prandtl number = ($c_p \mu$) / k
 L = characteristic length, ft k = thermal conductivity at film temp., Btu/ft-hr-°F
 c_p = specific heat, Btu/ lb_m -°F Ra_L = Rayleigh #, based on length 'L'

Note that k , c_p , and μ are each a function of air temperature as taken from Table 3.2-3. Values for ρ are computed using the ideal gas law, β for an ideal gas is simply the inverse of the absolute temperature of the gas, and Pr is computed using the values for k , c_p , and μ from Table 3.2-3. Unit conversion factors are used as required to reconcile the units for the various properties used.

The natural convection from a discrete vertical surface is computed using Equations 3-19, 3-21 to 3-25 of reference [24], which is applicable over the range $1 < \text{Rayleigh number } (Ra) < 10^{12}$:

$$Nu^T = \bar{C}_L Ra^{1/4}$$

$$\bar{C}_L = \frac{0.671}{\left(1 + (0.492/Pr)^{9/16}\right)^{4/9}}$$

$$Nu_L = \frac{2.8}{\ln(1 + 2.8/Nu^T)}$$

$$Nu_t = C_t^V Ra^{1/3}$$

$$C_t^V = \frac{0.13 Pr^{0.22}}{\left(1 + 0.61 Pr^{0.81}\right)^{0.42}}$$

$$Nu = \frac{h_c L}{k} = \left[(Nu_L)^6 + (Nu_t)^6\right]^{1/6}$$

The natural convection from a vertical cylindrical surface is computed by applying a correction factor to the laminar Nusselt number (Nu_L) determined using the same methodology and Nu_t for a vertical plate (see above). The characteristic dimension, L , is the height of the vertical cylinder and D is the cylinder's diameter. The correction factor as defined by Equations 3-39 to 3-41 of reference [24] is:

$$Nu_{L-Cylinder} = \frac{\delta}{\ln(1 + \delta)} Nu_{L-Plate}$$

$$\delta = \frac{1.8 \times L/D}{Nu_{Plate}^T}$$

$$Nu_{Vert. Cylinder} = \frac{h_c L}{k} = \left[(Nu_{L-Cylinder})^6 + (Nu_{t-Plate})^6\right]^{1/6}$$

Natural convection from horizontal surfaces is computed from Equations 3-34 to 3-38 of reference [24], where the characteristic dimension (L) is equal to the plate surface area divided by the plate perimeter. For a heated surface facing upwards or a cooled surface facing downwards and $Ra > 1$:

$$Nu = \frac{h_c L}{k} = \left[(Nu_L)^{10} + (Nu_t)^{10} \right]^{1/10}$$

$$Nu_L = \frac{1.4}{\ln \left(1 + 1.4 / \left(0.835 \times \bar{C}_L Ra^{1/4} \right) \right)}$$

$$\bar{C}_L = \frac{0.671}{\left(1 + (0.492/Pr)^{9/16} \right)^{4/9}}$$

$$Nu_t = 0.14 \times Ra^{1/3}$$

For a heated surface facing downwards or a cooled surface facing upwards and $10^5 < Ra < 10^{10}$, the correlation is as follows:

$$Nu = Nu_L = \frac{0.527}{\left(1 + (1.9/Pr)^{9/10} \right)^{2/9}} Ra^{1/5}$$

Calculation of the convection coefficient from a horizontal cylindrical surface is computed using Equation 3-43, reference [24], where the characteristic length, D, is the outer diameter of the cylinder. This equation, applicable for $10^{-5} < Ra < 10^{12}$, is as follows:

$$Nu = \frac{h_c D}{k} = \left\{ 0.60 + \frac{0.387 Ra_D^{1/6}}{\left[1 + (0.559/Pr)^{9/16} \right]^{8/27}} \right\}^2$$

The convection heat transfer coefficients between the package and the ambient during the 30-minute fire event are based on an average gas velocity of 10 m/sec [28] and the Colburn relation for forced convection of:

$$Nu = 0.036 \times Pr^{1/3} \times Re^{0.8}$$

Given the turbulent nature of the 30-minute fire event, a characteristic length of 0.25 feet is conservatively used for all surfaces to define the probable limited distance for boundary growth. The resulting convection coefficient values exceed the 10 W/m²-°C suggested for large packages by IAEA advisory material [3].

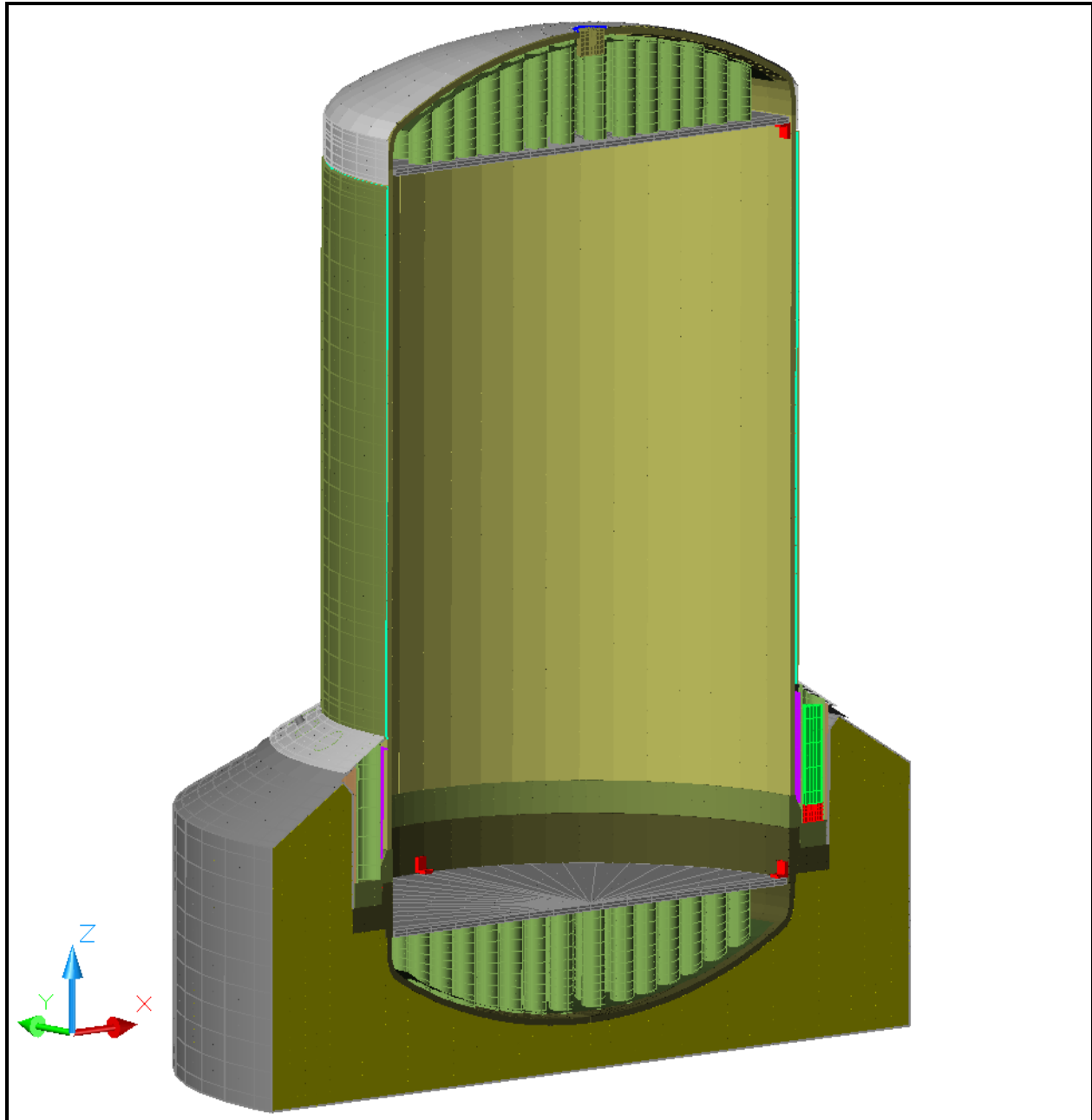


Figure 3.5-1 – Isometric View of ‘Solids’ Thermal Model for 1105-SD Packaging

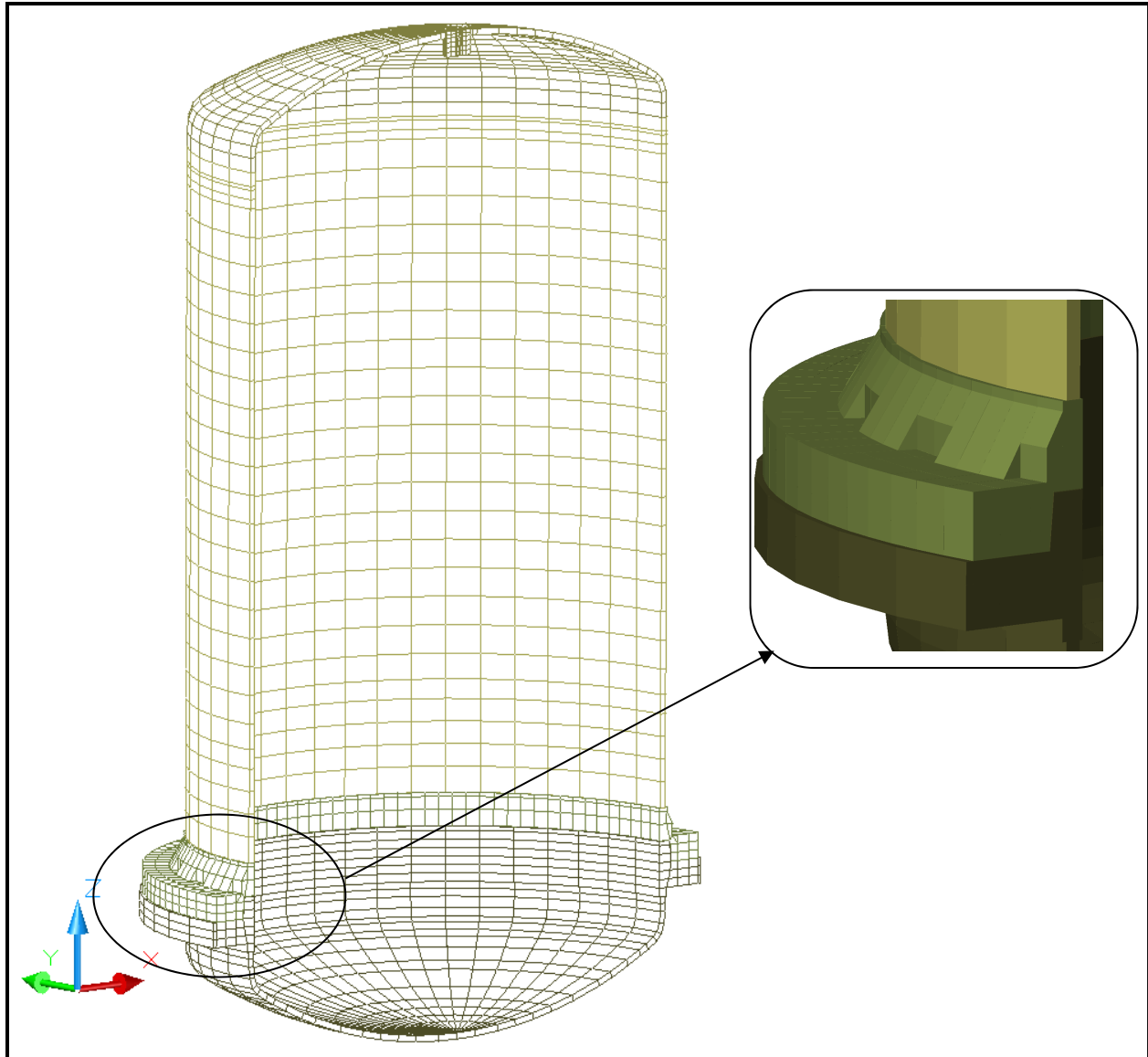


Figure 3.5-2 – Isometric View of ‘Solids’ Thermal Model for Containment Boundary

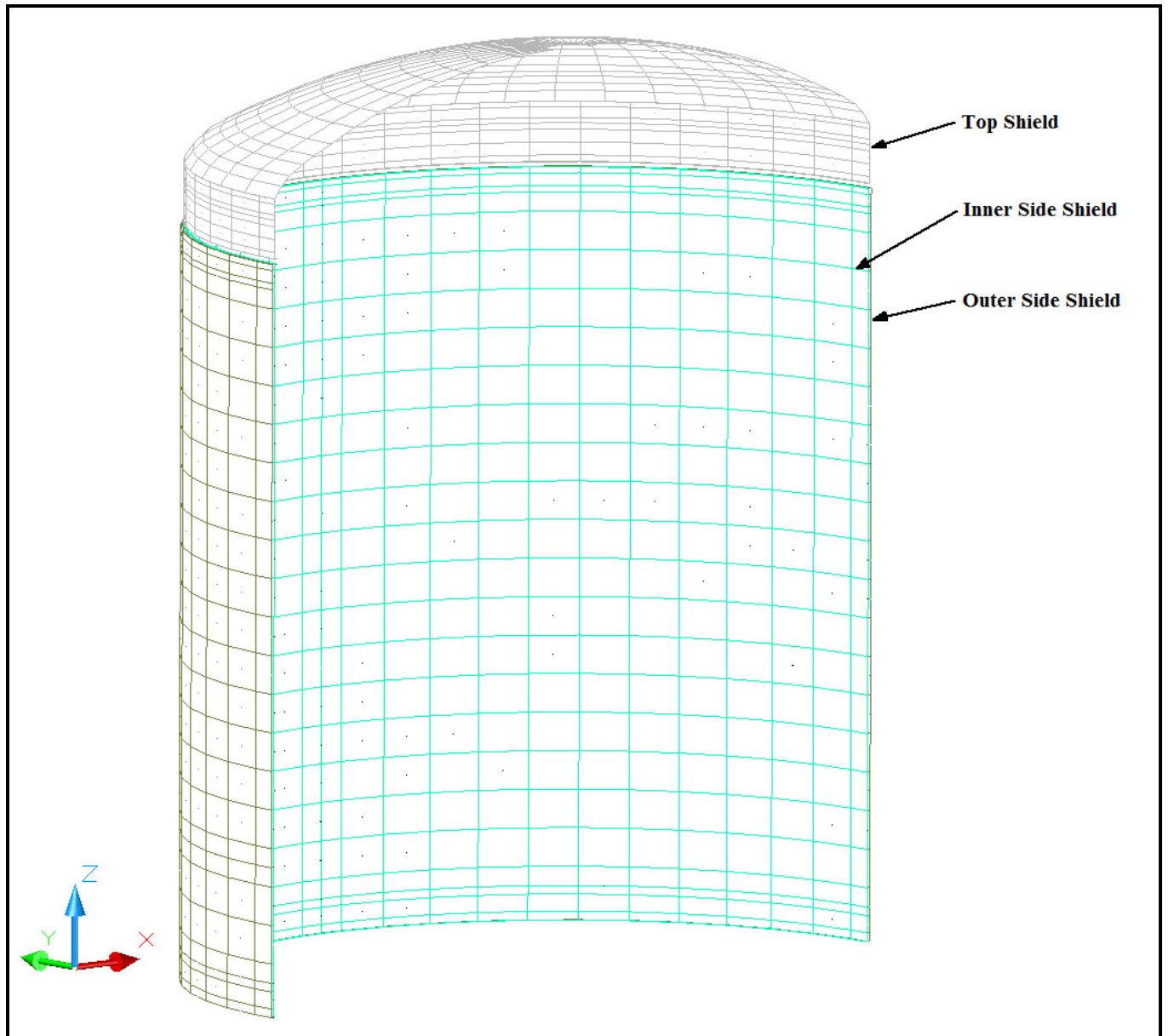


Figure 3.5-3 – Thermal Model for Top and Side Thermal Shields

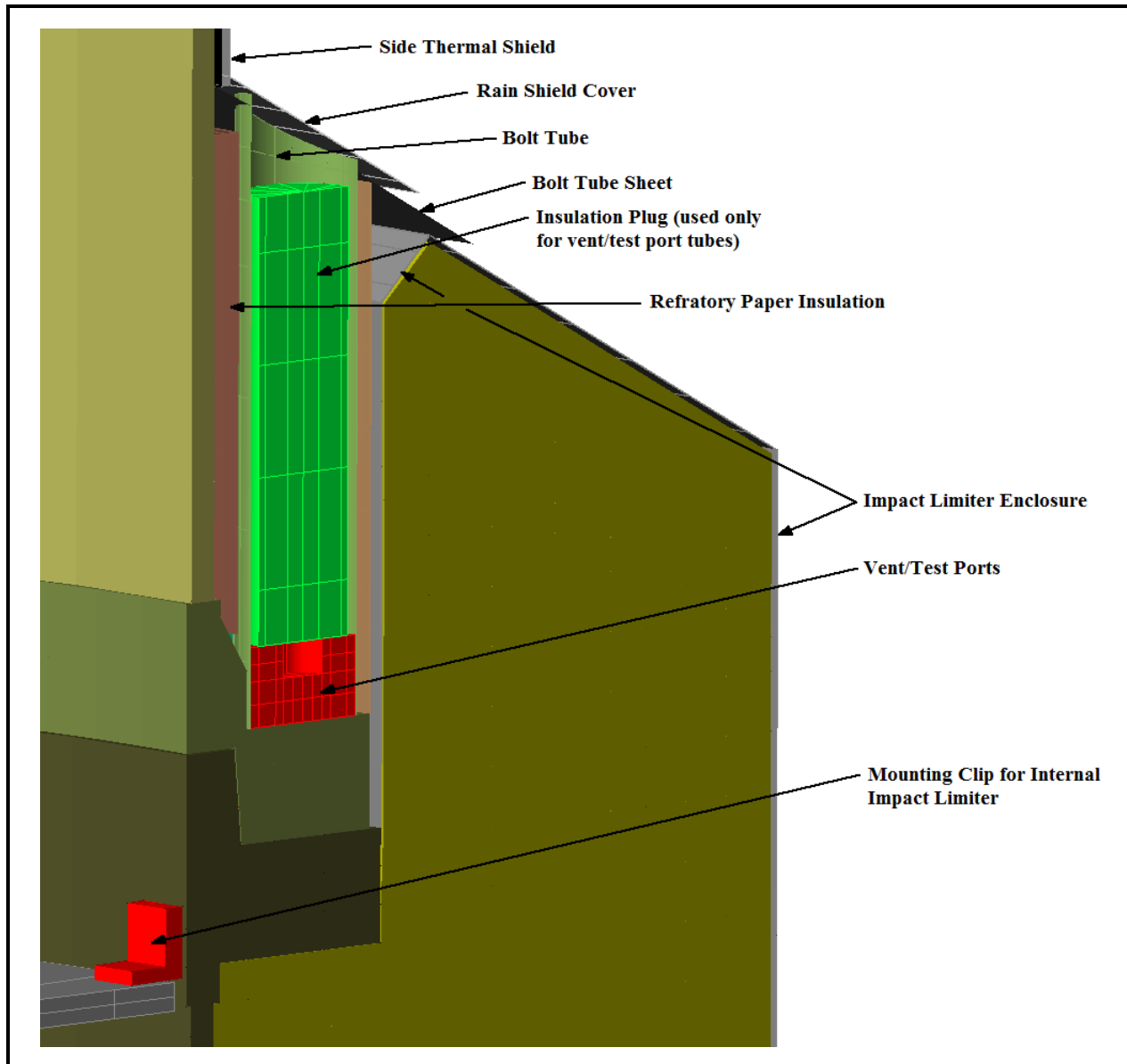


Figure 3.5-4 – Thermal Modeling at Closure Bolt Enclosure Structure

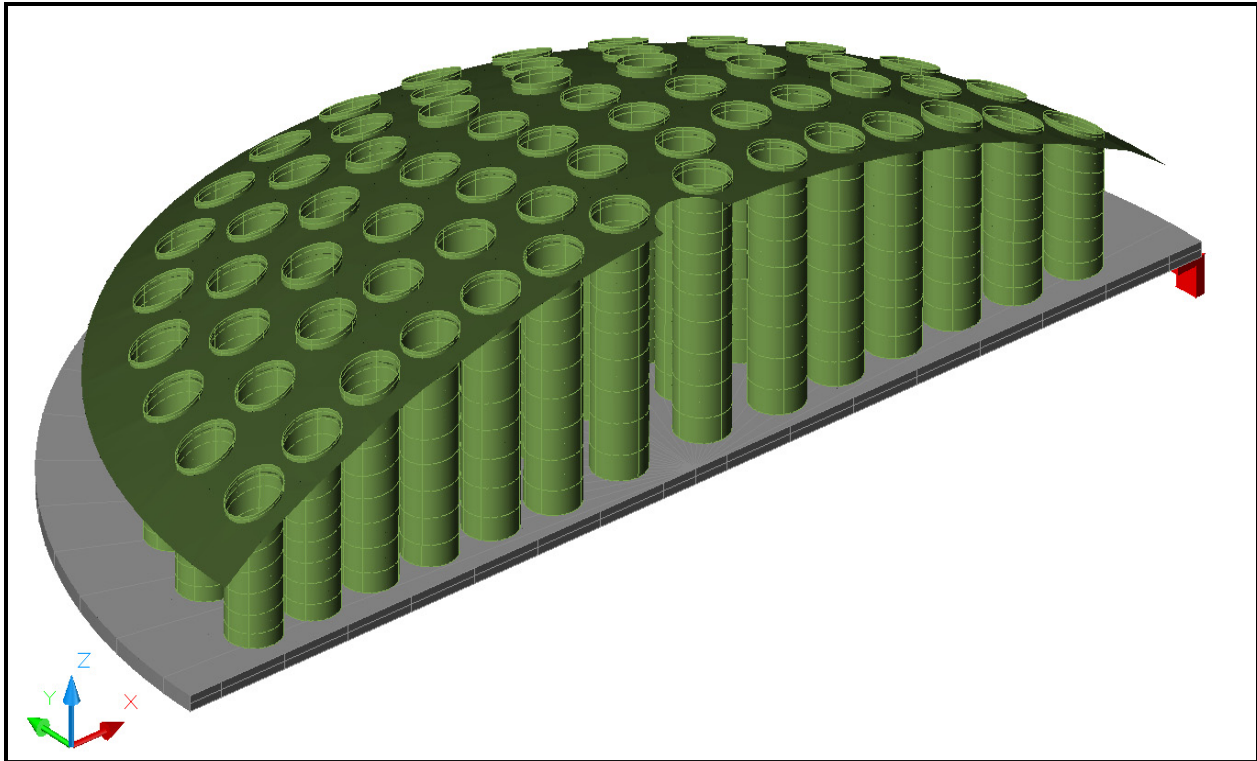


Figure 3.5-5 – Isometric View of Thermal Model for Internal Impact Limiters

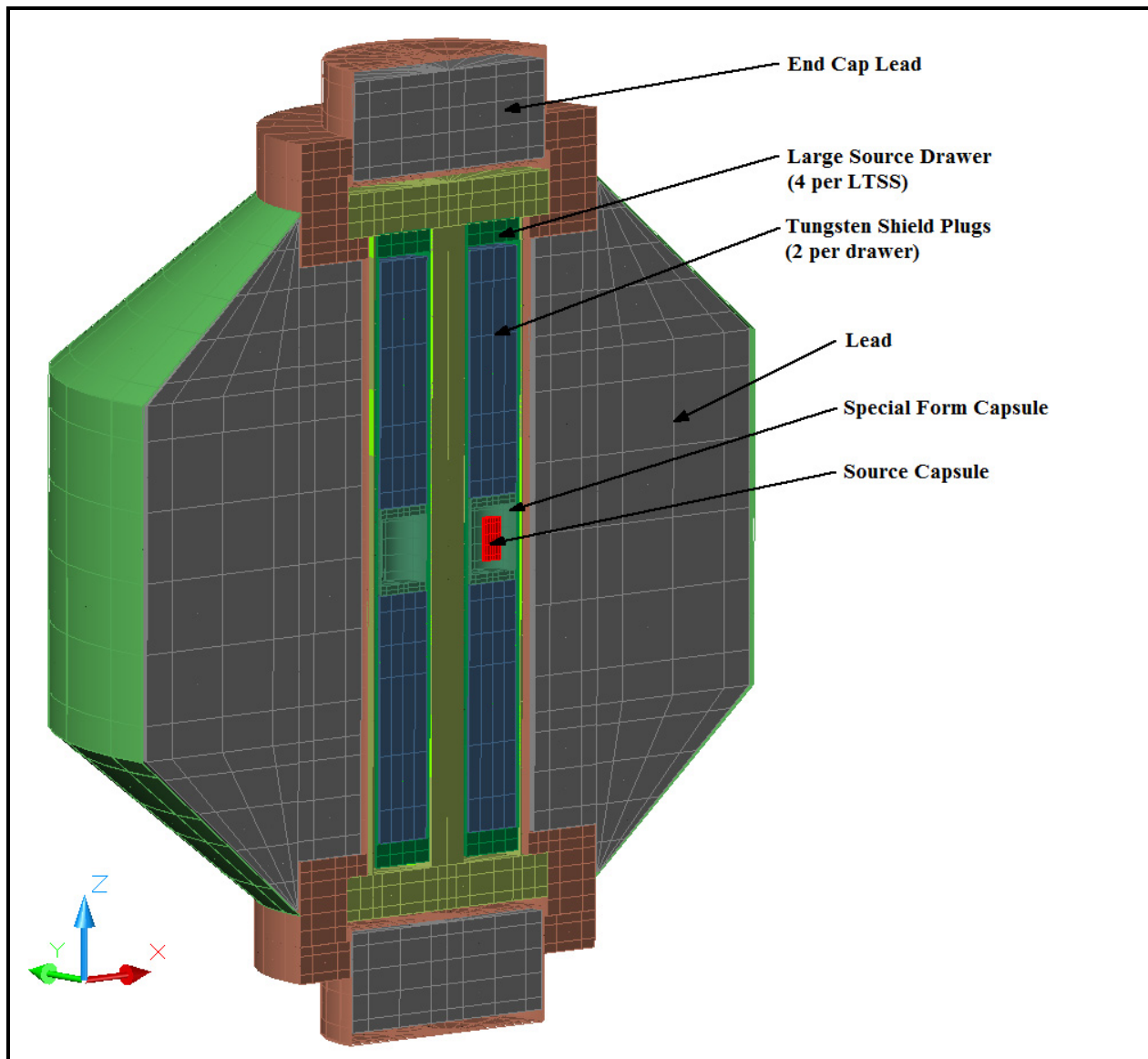


Figure 3.5-6 – Isometric View of Thermal Model for LTSS

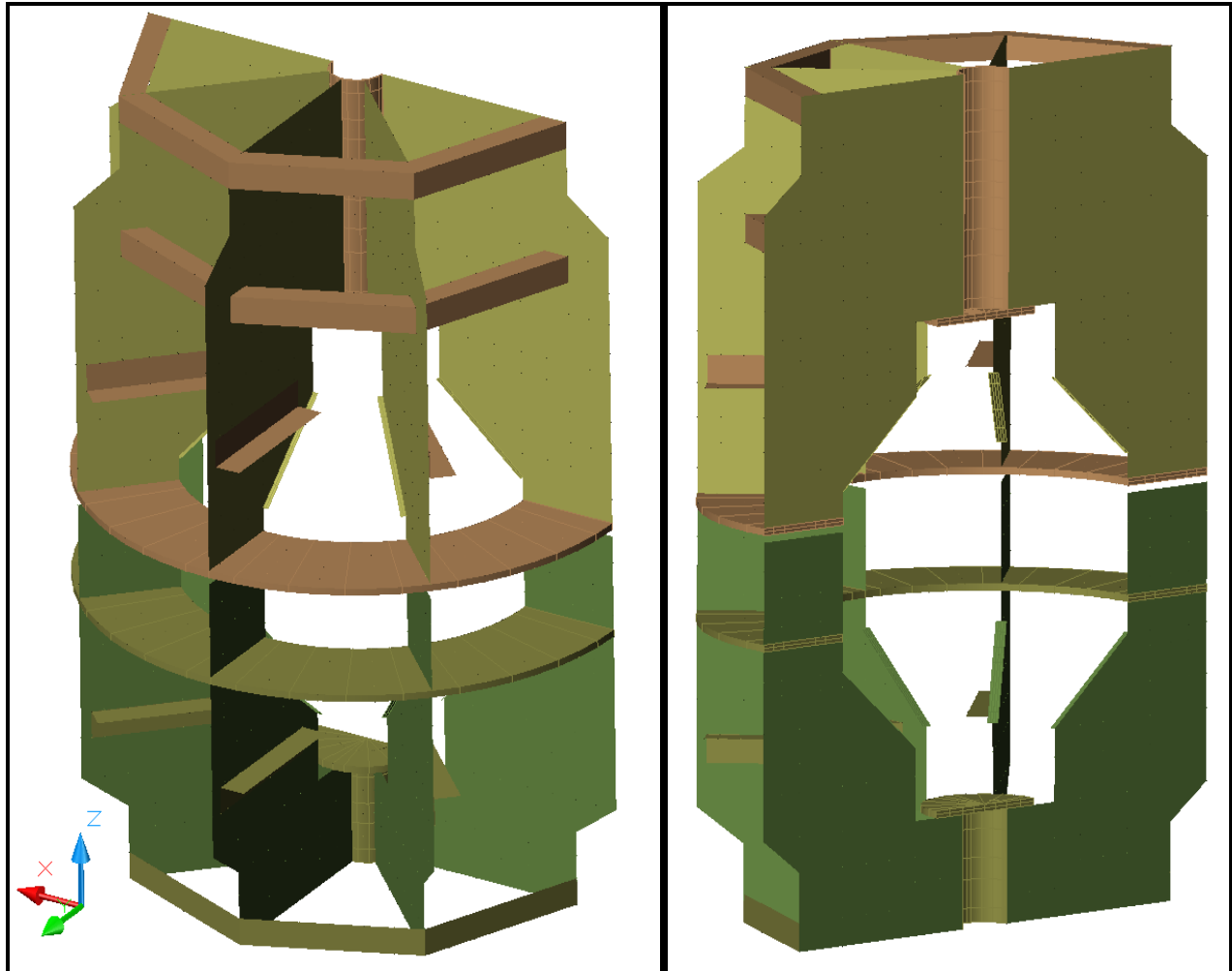


Figure 3.5-7 – Alternate Views of Thermal Model for LTSS Lodgment

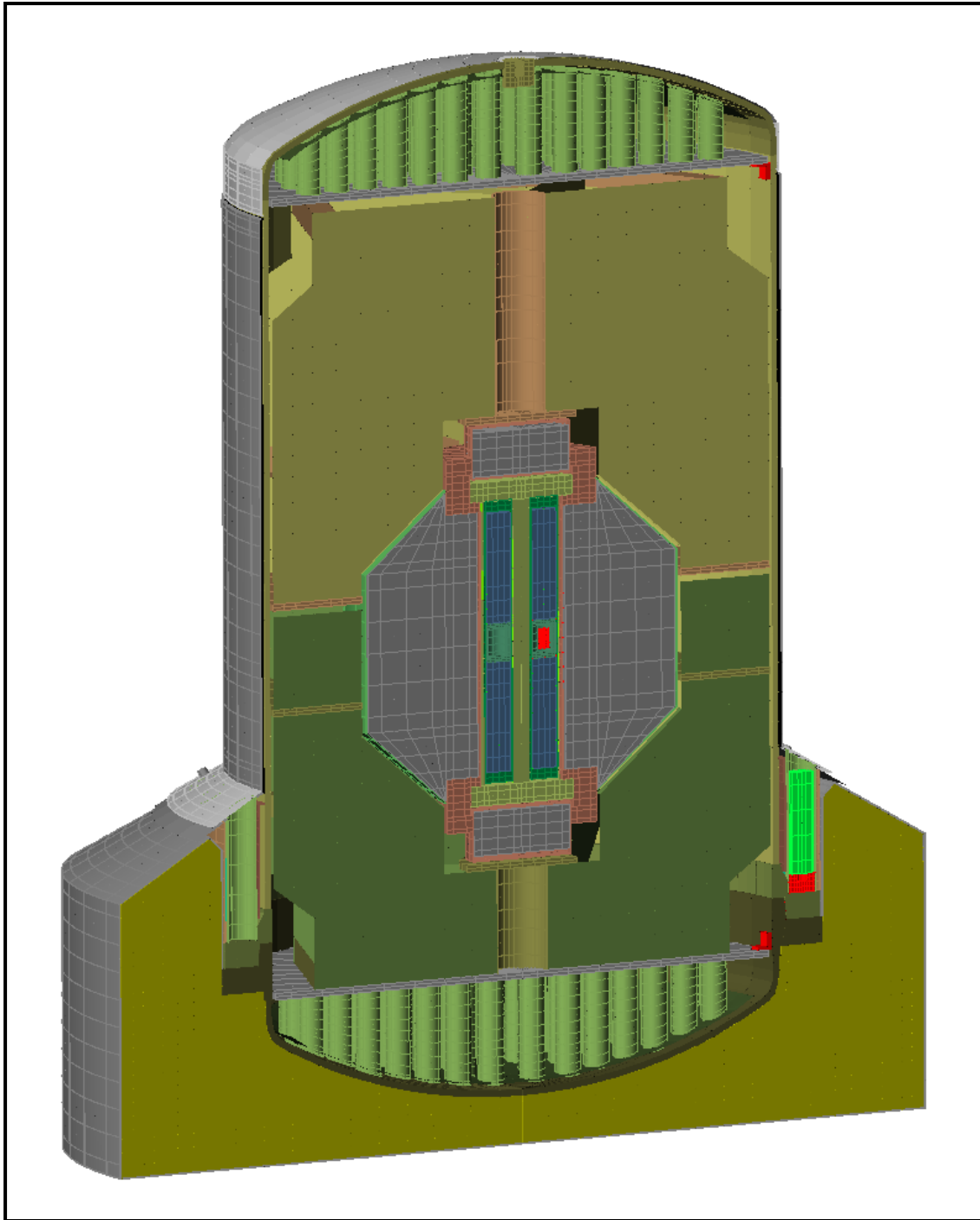


Figure 3.5-8 – Combined Modeling of 1105-SD Packaging with LTSS Payload

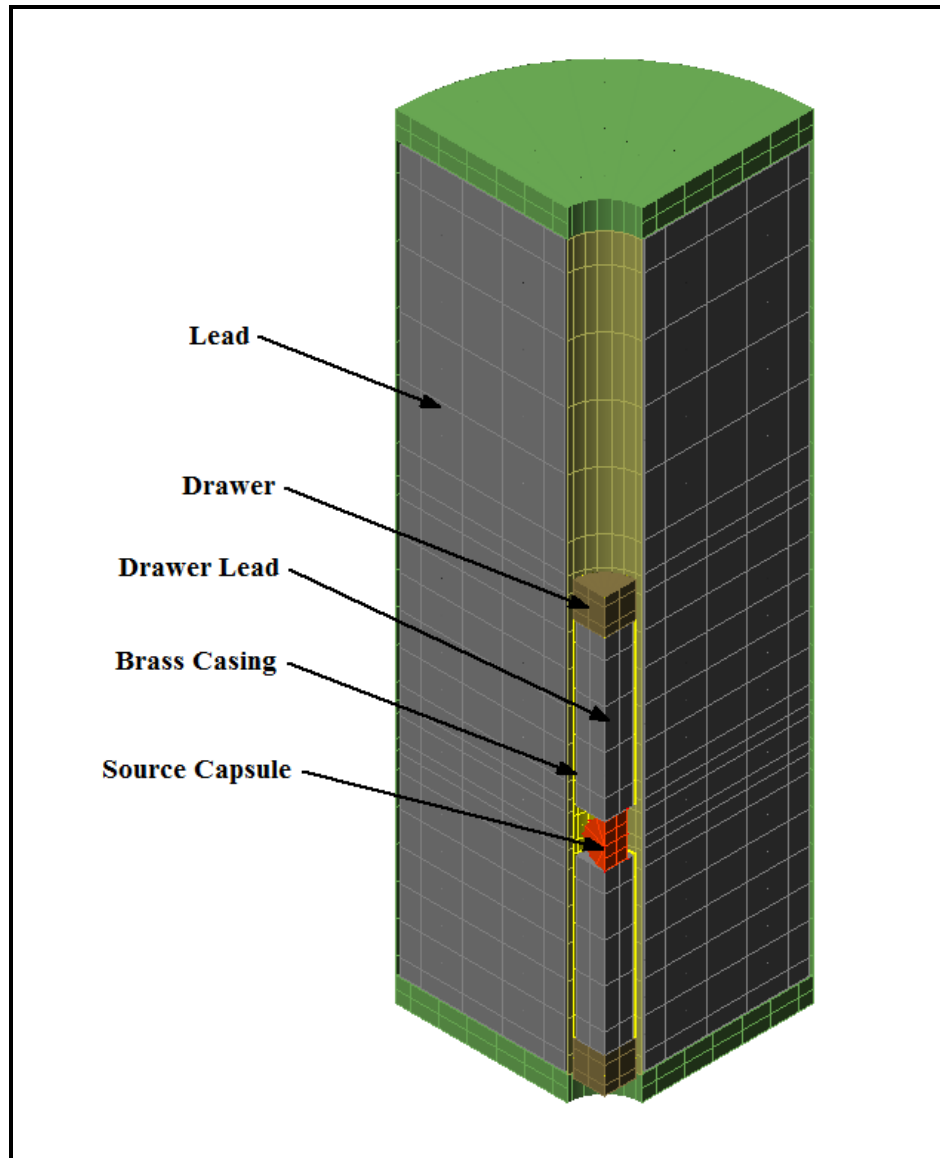


Figure 3.5-9 – Thermal Model for Generic Shielded Device

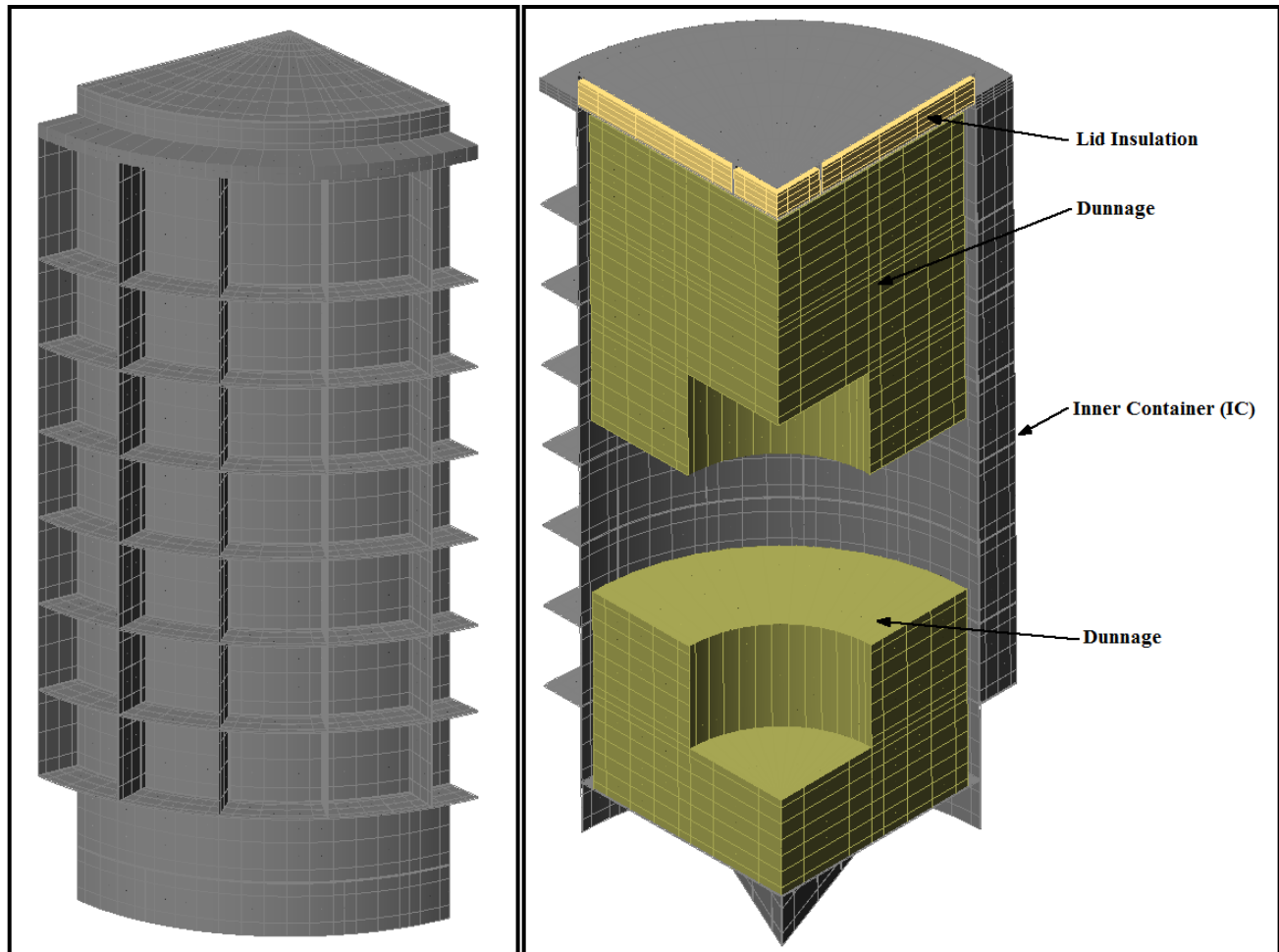


Figure 3.5-10 – Alternate Views of Thermal Model for Inner Container (IC) with Polyurethane Foam Dunnage

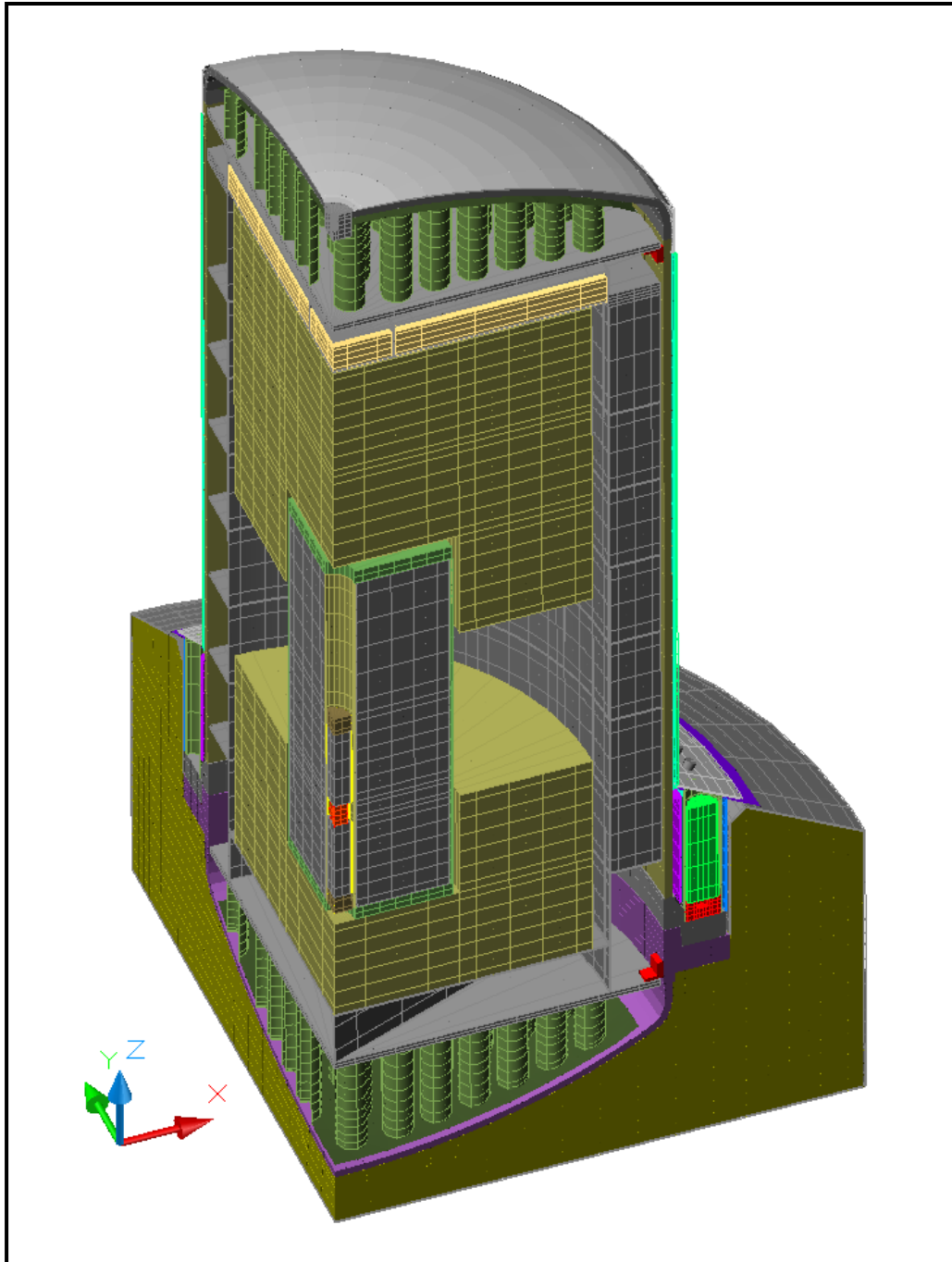


Figure 3.5-11 – Combined Modeling of 1105-SD Packaging with SD Payload Supported by Foam Dunnage

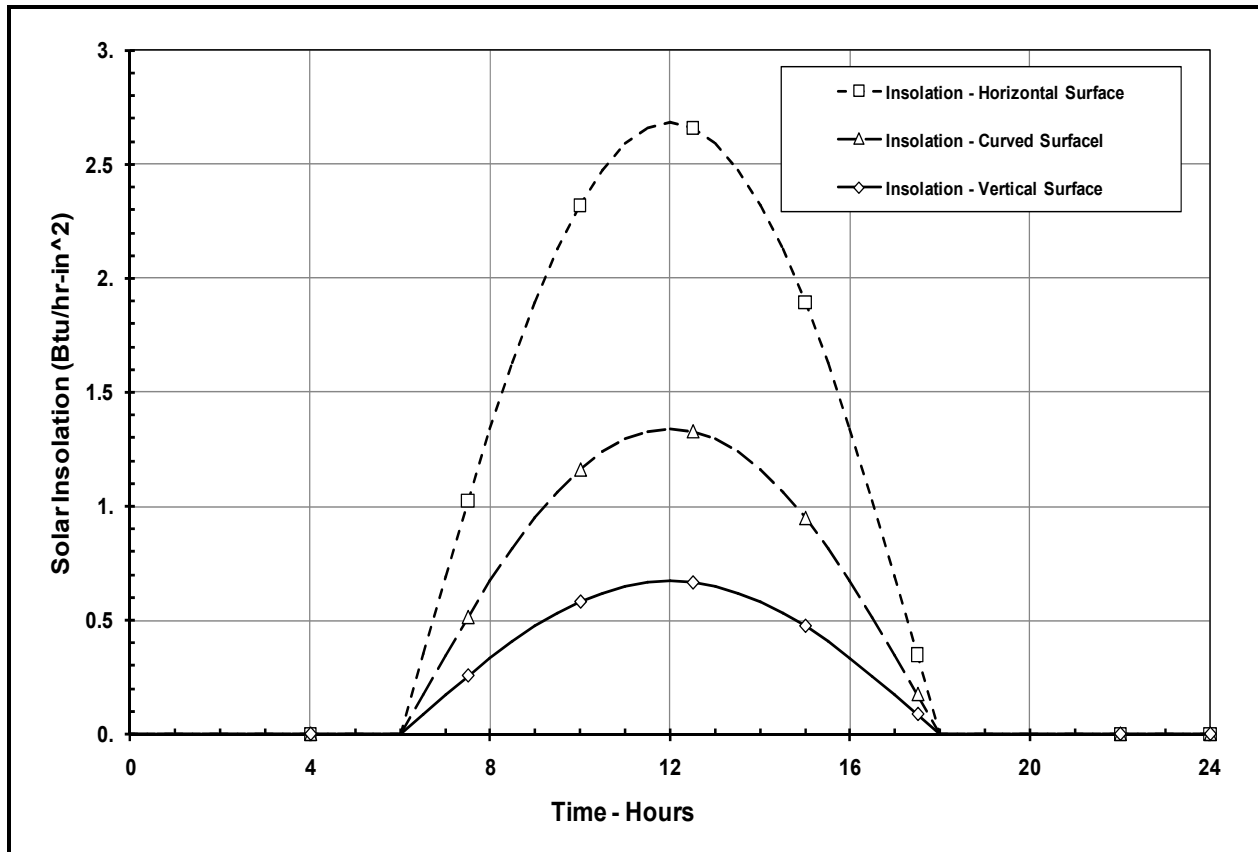


Figure 3.5-12 – Diurnal Cycle for Insolation

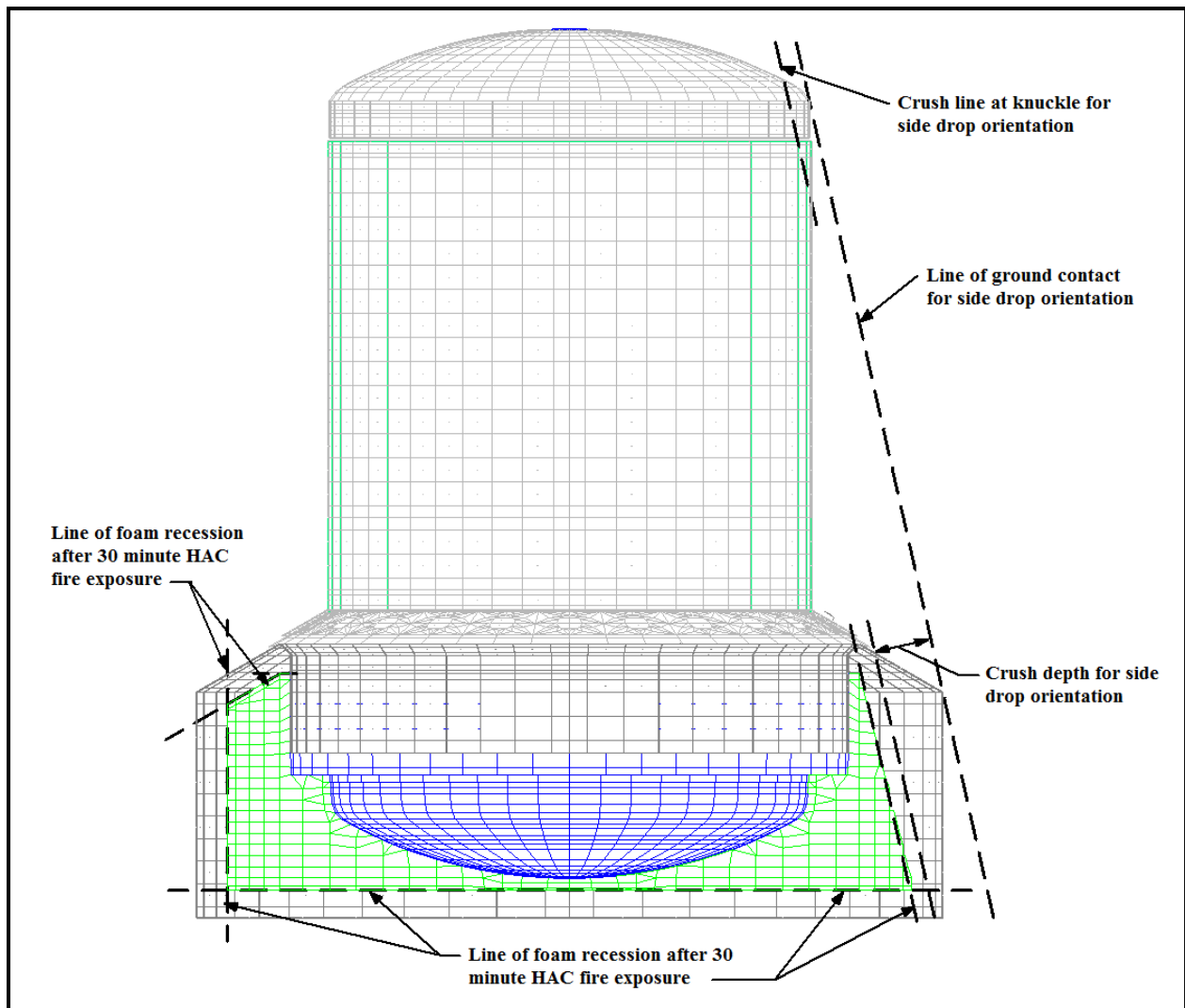


Figure 3.5-13 – HAC Side Drop Damage Modeling

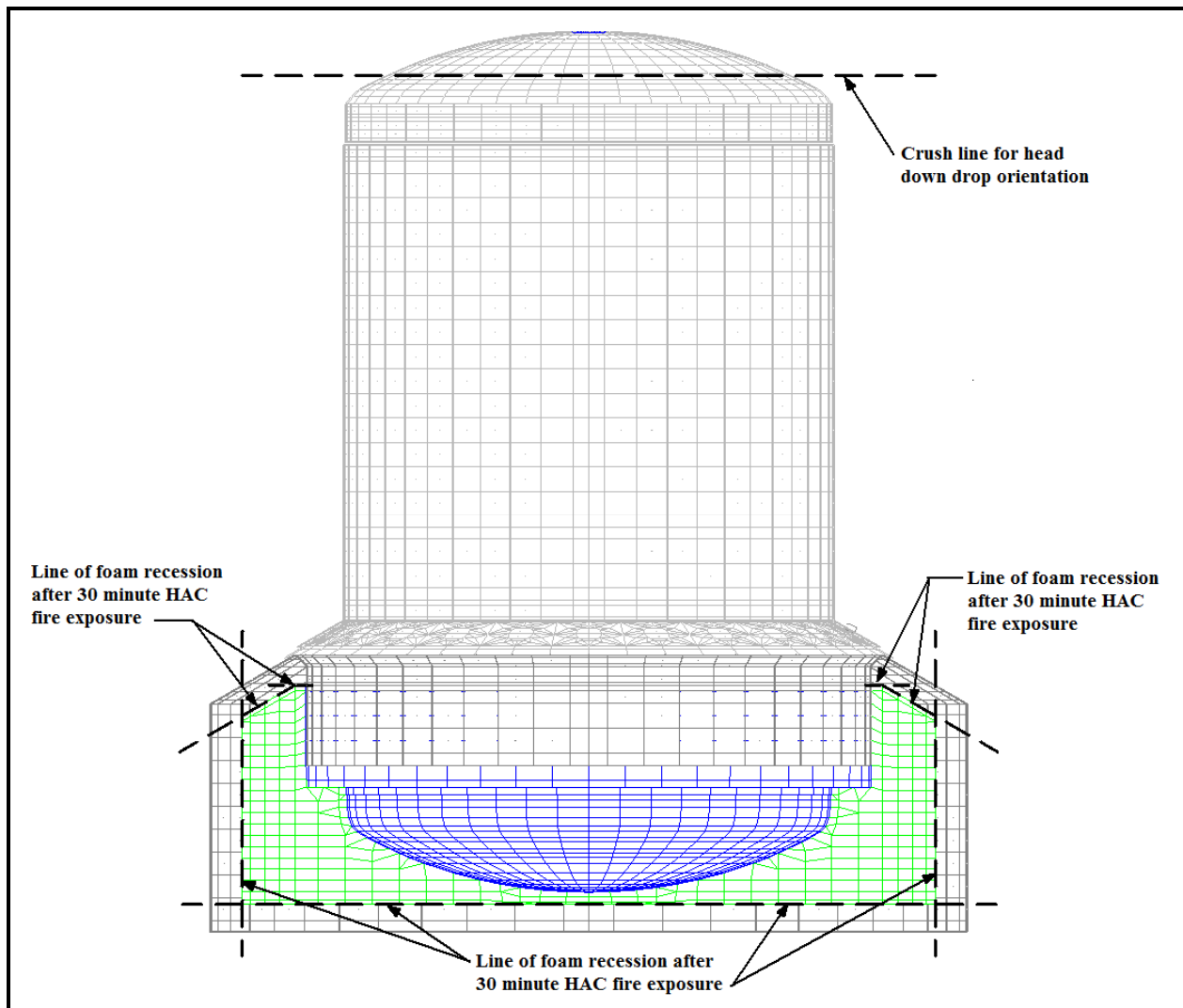


Figure 3.5-14 – HAC Head Down Drop Damage Modeling

3.5.4 'Last-A-Foam' Response under HAC Conditions

The General Plastics LAST-A-FOAM® FR-3700 rigid polyurethane foam [5] used in the impact limiters has been used for numerous transportation packages. The FR-3700 formulation is specially designed to allow predictable impact-absorption performance under dynamic loading, while also providing a significant level of thermal protection under the HAC conditions. Upon exposure to fire temperatures, this proprietary foam decomposes into an intumescent char that swells and tends to fill voids or gaps created by free drop or puncture bar damage. This thermal decomposition absorbs a significant amount of the heat transferred into the foam, which is then expelled from the impact limiters as a high temperature gas. Because the char has no appreciable structural capacity and will not develop unless there is space available, the char will not generate stresses within the adjacent package components. Without available space the pyrolysis gases developed as a result of the charring process will move excess char mass out through the vent ports and prevent its buildup. Only as the charring process continues and space becomes available will the char be retained, filling the available space and plugging holes at the surface of the impact limiters. The thermal decomposition process does not alter or cause a chemical reaction within the adjacent materials.

The mechanisms behind the observed variations in the thermal properties and behavior of the FR-3700 foam at elevated temperatures are varied and complex. A series of fire tests [6 and 7] conducted on 5-gallon cans filled with FR-3700 foam at densities from 6.7 to 25.8 lb/ft³ helped define the expected performance of the foam under fire accident conditions. Under the referenced fire tests, one end of the test article was subjected to an open diesel fueled burner flame at temperatures of 980 to 1,200°C (1,800 to 2,200 °F) for more than 30 minutes. A thermal shield prevented direct exposure to the burner flame on any surface of the test article other than the hot face. Each test article was instrumented with thermocouples located at various depths in the foam. In addition, samples of the foam were subjected to thermogravimetric analysis (TGA) to determine the thermal decomposition vs. temperature. The exposure temperatures for the TGA tests varied from 70 to 1,500 °F, and were conducted in both air and nitrogen atmospheres. The result for the nitrogen environment (see Figure 3.5-15) is more representative of the low oxygen environment existing within the impact limiter shells encasing the foam. These test results indicate that the following steps occur in the thermal breakdown of the foam under the level of elevated temperatures reached during the HAC fire event:

- Below 250 °F, the variation in foam thermal properties with temperature is slight and reversible. As such, fixed values for specific heat and thermal conductivity are appropriate.
- Between 250 and 500 °F, small variations in foam thermal properties occur. The observed changes are so slight that the same thermal properties used for temperatures below 250 °F may also be used to characterize the thermal performance of the foam between 250 and 500 °F.
- Between 325 and 435 °F, a foam weight reduction of approximately 2% (see Figure 3.5-15) will occur as water vapor and/or the gas used as the blowing agent is lost.
- Irreversible thermal decomposition of the foam begins as the temperature rises above 500 °F and increases non-linearly with temperature. Based on the TGA testing (see

Figure 3.5-15), approximately 2/3's of this decomposition occurs over a narrow temperature range centered about 670 °F.

- The decomposition is accompanied by vigorous out-gassing from the foam and an indeterminate amount of internal heat generation. The internal heat generation arises from the gases generated by the decomposition process that are combustible under piloted conditions. However, since the decomposition process is endothermic, the foam will not support combustion indefinitely. Further, the out-gassing process removes a significant amount of heat from the package via mass transport.
- The weight loss due to out-gassing not only has direct affect on the heat flux into the remaining virgin foam, but changes the composition of the resulting foam char since the foam constituents are lost at different rates. This change in composition affects both the specific heat and the thermal conductivity of the foam char layer.
- As temperature continues to rise, the developing char layer begins to take on the characteristics of a gas-filled cellular structure where radiative interchange from one cell surface to another becomes the dominant portion of the overall heat transfer mechanism. This change in heat transfer mechanisms causes the apparent heat conductivity to take on a highly non-linear relationship with temperature.
- Finally, at temperatures above 1,250 °F, the thermal breakdown of the foam is essentially completed and only about 5 to 10% of the original mass is left. In the absence of direct exposure to a flame or erosion by the channeling of the outgas products through the foam, the char layer will be the same or slightly thicker than the original foam depth. This char layer will continue to provide radiative shielding to the underlying foam material.

Since the thermal decomposition of the foam is an endothermic process, the foam is self-extinguishing and will not support a flame once the external flame source is removed. However, the gases generated by the decomposition process are combustible and will burn under piloted conditions. A portion of these generated gases can remain trapped within the charred layer of the foam after the cessation of the HAC fire event and continue to support further combustion, although at a much reduced level, until a sufficient time has passed for their depletion from the cell structure. This extended time period is typically from 15 to 45 minutes.

The sharp transition in the state of the foam noted in Figure 3.5-15 at or about 670 °F can be used to correlate the observed depth of the foam char following a burn test with the occurrence of this temperature level within the foam. The correlation between the foam recession depth and the foam density, as compiled from a series of tests, is expressed by the relation:

$$y = -0.94581 + 11.64 \times \log_{10}(x)$$

where y = the recession depth, cm

x = foam density (g/cm^3)

Based on this correlation, the recession depth expected for the nominal 15 pcf density foam used in the packaging is estimated to be 2.5 inches. The loss of foam could increase to a depth of approximately 2.8 inches for foam fabricated at the low end of the density tolerance (i.e., 12.75 pcf).

It should be noted that these results assume that the foam is enclosed within a steel shell with surface openings that are approximately 0.3 ft² or smaller. The presence of the steel enclosure helps shield the foam from the heat flux of a HAC fire event and helps contain the foam char that is generated. The same is true if a layer of 0.25" thick Lytherm paper is placed between the foam and the steel enclosure. Proprietary test results with and without a layer of Lytherm paper indicates that the foam loss for 8 pcf foam was reduced by approximately 11%.

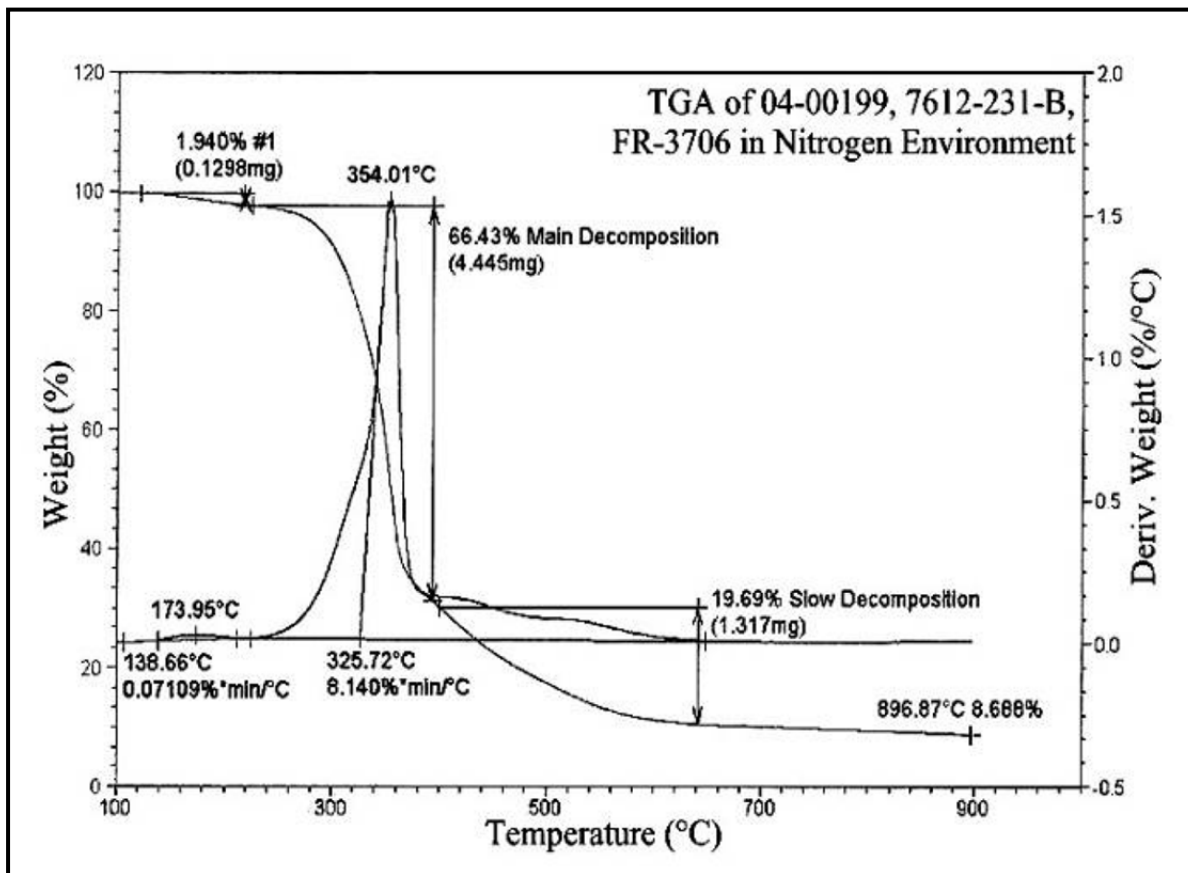


Figure 3.5-15 – TGA Analysis of Foam Decomposition in Nitrogen Environment

4.0 CONTAINMENT

4.1 Description of the Containment System

4.1.1 Containment Boundary

The 1105-SD package provides a single level of leaktight containment, defined as a leakage rate of less than 1×10^{-7} reference cubic centimeters per second (ref-cm³/s), air, per ANSI N14.5 [1]. The containment boundary of the 1105-SD package consists of the following elements. Unless noted, all elements are made of ASTM Type 304 stainless steel in various product forms. A full description of the packaging is given in Section 1.2.1, *Packaging*.

- The upper torispherical head and upper body assembly lifting boss
- The cylindrical side shell
- The upper flange (attached to the upper body assembly)
- The lower flange (attached to the lower body assembly)
- The lower torispherical head
- The containment elastomer O-ring seal
- The vent port block and brass vent port plug in the upper flange including elastomer sealing washer

The containment boundary is shown in Figure 4.1-1.

4.1.2 Containment Penetrations

The vent port is the only containment penetration. The vent port is located in a steel block welded to the upper flange, as shown in Figure 4.1-1. The vent port is designed and tested to ensure leaktight sealing integrity, i.e., a leakage rate not exceeding 1×10^{-7} ref-cm³/s, per ANSI N14.5.

4.1.3 Seals

The elastomeric portion of the containment boundary is comprised of a nominally 3/8-inch diameter, bore-type O-ring seal located in the upper groove in the lower flange, and a seal washer sealing element (an O-ring integrated with a stainless steel washer) for the vent port. The seals are made using a butyl elastomer compound suitable for continuous use between the temperatures of -65 °F and 250 °F [2], and capable of much higher temperatures during the HAC fire case transient. Further discussion of the thermal performance capabilities of the butyl rubber seals is provided in Appendix 2.12.5, *Containment Seal Performance Tests*.

Two O-ring seals are provided in the lower body flange: the upper seal is containment, and the lower forms an annular space for leakage rate testing of the containment seal. The leakage rate tests used for various purposes are summarized in Section 4.4, *Leakage Rate Tests for Type B Packages*, and described in detail in Chapter 8, *Acceptance Tests and Maintenance Program*.

The containment seal will retain adequate compression to afford a seal in the worst case condition. The nominal diameter of the containment seal (upper) groove is:

$$D_g = 45.74 - 2(1.2 \times \tan(5^\circ) + 0.265) = 45.0 \text{ inches}$$

where the flange outer diameter is 45.74 inches, the height of the upper groove centerline is 1.2 inches above the flange joint, the flange tapers at an angle of 5°, and the groove depth is 0.265 inches. See Detail G on drawing 3021717-SAR, sheet 4. The O-ring minimum length is 44.10 inches, minus 1%, or:

$$D_{OR} = 44.10 \times 0.99 = 43.66 \text{ inches}$$

The maximum stretch of the containment seal is therefore:

$$S = \frac{D_g - D_{OR}}{D_{OR}} \times 100 = 3.1 \%$$

The minimum stretch is 1%, using the O-ring maximum length of $44.10 \times 1.01 = 44.54$ inches. From the Parker O-ring Handbook [6], the observed cross-section reduction caused by this amount of stretch is 2.5% for the maximum stretch case, and 1.0% for the minimum stretch case. The O-ring diameters are:

$$d_{Min} = (0.375 - 0.007) \times (1 - 0.025) = 0.359 \text{ inches}$$

$$d_{Max} = (0.375 + 0.007) \times (1 - 0.010) = 0.378 \text{ inches}$$

where the O-ring cross section is 0.375 ± 0.007 inches.

The inner diameter of the mating surface of the upper body assembly is 45.765 ± 0.007 or 45.772 inches maximum. The corresponding diameter of the base flange component is 45.740 ± 0.007 , or 45.733 inches minimum. The maximum radial clearance between the two assembled flanges is therefore:

$$\text{gap}_{Max} = 45.772 - 45.733 = 0.039 \text{ inches.}$$

This assumes that the upper flange is shifted the maximum radial amount relative to the lower flange. The minimum gap, which occurs 180° away from the maximum gap, is equal to zero.

The depth of the groove which contains the seal is 0.265 ± 0.005 , or $g_{Max} = 0.270$ inches, and $g_{Min} = 0.260$ inches.

The compression range of the O-ring seal is:

$$C_{Min} = \frac{d_{Min} - g_{Max} - \text{gap}_{Max}}{d_{Min}} \times 100 = 13.9 \%$$

$$C_{Max} = \frac{d_{Max} - g_{Min}}{d_{Max}} \times 100 = 31.2 \%$$

Where C_{Max} and C_{Min} are the maximum and minimum compressions that the containment O-ring seal will experience. As shown in Appendix 2.12.5, *Seal Performance Tests*, the butyl rubber used in the 1105-SD has been successfully tested using compression values as low as 10%.

4.1.4 Welds

All butt welds used in the containment boundary (including any welds used to join plates prior to forming) are full penetration welds, and are radiograph and liquid penetrant inspected to ensure structural and containment integrity. Radiographic inspection is in accordance with the ASME Code, Subsection NB, Article NB-5000, and Section V, Article 2 [3] and liquid penetrant inspection on the final pass in accordance with the ASME Code, Subsection NB, Article NB-5000, and Section V, Article 6 [4]. The fillet weld between the vent port block and the lower flange and the full penetration groove weld which closes off the vent port machining access hole (see Section M-M on drawing 3021717-SAR, sheet 6) are liquid penetrant inspected on the final pass in accordance with the ASME Code, Subsection NB, Article 5000, and Section V, Article 6. All containment boundary welds are confirmed to be leaktight as discussed in Section 8.1.4, *Fabrication Leakage Rate Tests*.

4.1.5 Closure

The package closure is made using (24) 1-1/4-7 UNC socket head cap screws tightened to 300 ± 30 ft-lb. As shown in Chapter 2, *Structural Evaluation*, the closure lid cannot become detached by any internal pressure, NCT, or HAC events. The closure joint is protected by the impact limiter, which is integral with the lower body assembly. The bolt heads and the vent port are covered by the rain shield. Thus, the containment openings cannot be inadvertently opened.

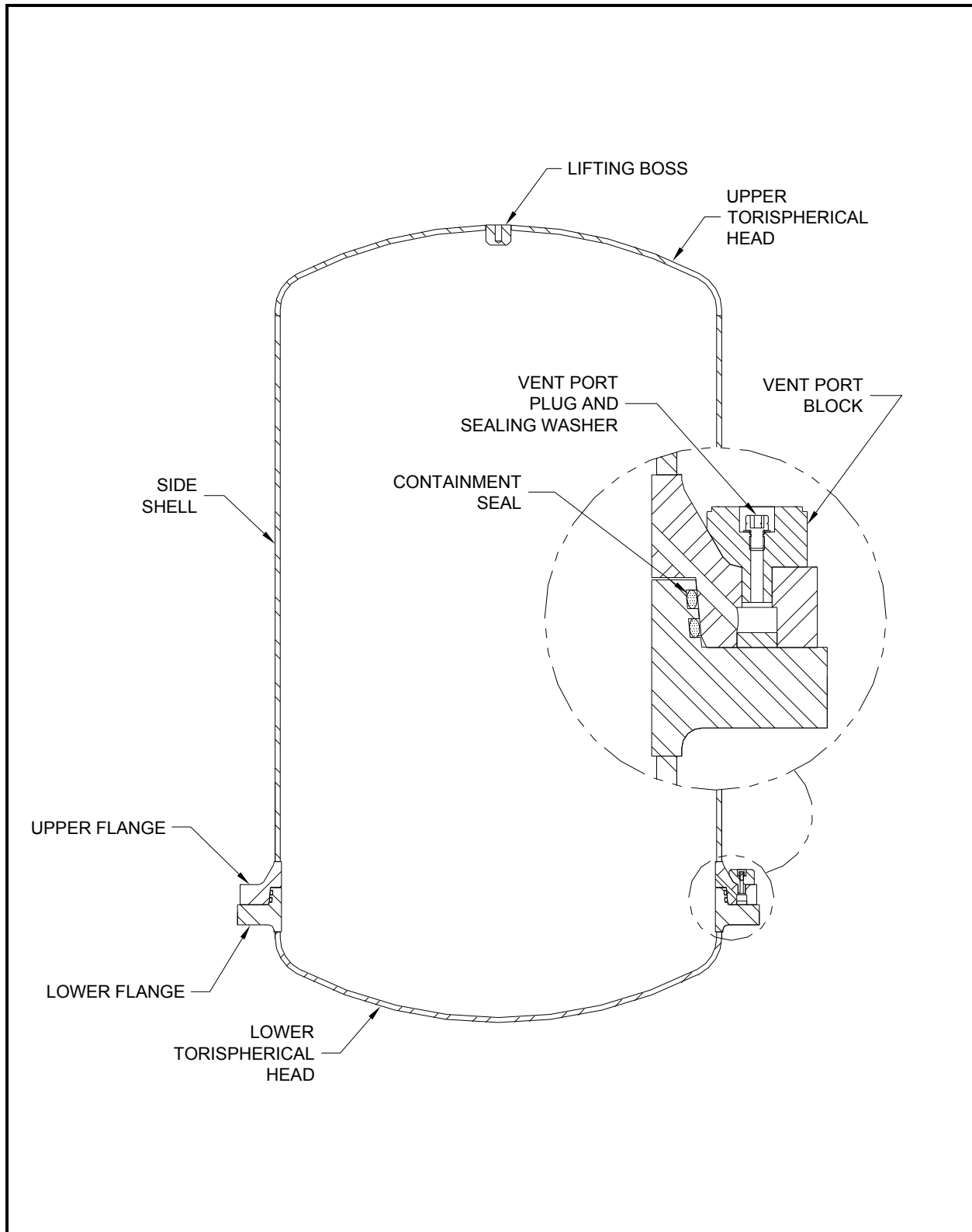


Figure 4.1-1 – 1105-SD Package Containment Boundary

4.2 Containment Under Normal Conditions of Transport

The results of the NCT structural and thermal evaluations presented in Sections 2.6, *Normal Conditions of Transport*, and 3.3, *Thermal Evaluation Under Normal Conditions of Transport*, respectively, demonstrate that there is no release of radioactive materials per the “leaktight” definition of ANSI N14.5 under any of the NCT tests described in 10 CFR §71.71 [5].

4.3 Containment Under Hypothetical Accident Conditions

The results of the HAC structural and thermal evaluations performed in Sections 2.7, *Hypothetical Accident Conditions*, and 3.4, *Thermal Evaluation Under Hypothetical Accident Conditions*, respectively, demonstrate that there is no release of radioactive materials per the “leaktight” definition of ANSI N14.5 under any of the hypothetical accident condition tests described in 10 CFR §71.73.

4.4 Leakage Rate Tests for Type B Packages

4.4.1 Fabrication Leakage Rate Tests

During fabrication, the containment boundary is leakage rate tested as described in Section 8.1.4, *Fabrication Leakage Rate Tests*. The fabrication leakage rate tests are consistent with the guidelines of Section 7.3 of ANSI N14.5. This leakage rate test verifies the containment integrity of the 1105-SD packaging to a leakage rate not to exceed 1×10^{-7} ref-cm³/s, air.

4.4.2 Maintenance/Periodic Leakage Rate Tests

In the 12-month period prior to shipment, or at the time of damaged containment seal replacement or sealing surface repair (whichever is sooner), the containment O-ring seal and the vent port sealing washer are leakage rate tested as described in Section 8.2.2, *Maintenance/Periodic Leakage Rate Tests*. The maintenance/periodic leakage rate tests are consistent with the guidelines of Section 7.4 of ANSI N14.5. This test verifies the sealing integrity of the containment seals to a leakage rate not to exceed 1×10^{-7} ref-cm³/s, air.

4.4.3 Preshipment Leakage Rate Tests

Prior to shipment of the loaded 1105-SD package, the containment O-ring seal and the vent port sealing washers are leakage rate tested per Section 7.4, *Preshipment Leakage Rate Test*. The preshipment leakage rate tests are consistent with the guidelines of Section 7.6 of ANSI N14.5. This test verifies the sealing integrity of the containment seals to a leakage rate sensitivity of 1×10^{-3} ref-cm³/s, air.

The maintenance/periodic leakage rate tests, described in Section 8.2.2, *Maintenance/Periodic Leakage Rate Tests*, may be performed as an option, in lieu of the preshipment leakage rate tests.

4.5 Appendix

4.5.1 References

1. ANSI N14.5–2014, *American National Standard for Radioactive Materials – Leakage Tests on Packages for Shipment*, American National Standards Institute (ANSI), Inc.
2. Rainier Rubber Company, Seattle, WA.
3. American Society of Mechanical Engineers (ASME) Boiler and Pressure Vessel Code, Section III, *Rules for Construction of Nuclear Facility Components*, Division 1 – Subsection NB, *Class 1 Components*, and Section V, *Nondestructive Examination*, Article 2, *Radiographic Examination*, 2010 Edition.
4. American Society of Mechanical Engineers (ASME) Boiler and Pressure Vessel Code, Section III, *Rules for Construction of Nuclear Facility Components*, Division 1 – Subsection NB, *Class 1 Components*, and Section V, *Nondestructive Examination*, Article 6, *Liquid Penetrant Examination*, 2010 Edition.
5. Title 10, Code of Federal Regulations, Part 71 (10 CFR 71), *Packaging and Transportation of Radioactive Material*, 01–01–18 Edition.
6. Parker O–ring Handbook, ORD–5700, Parker-Hannifin Corporation, Cleveland, OH, © 2007.

5.0 SHIELDING EVALUATION

The 1105-SD package is used to transport radioactive sources in the Long Term Storage Shield (LTSS) or shielded devices containing their sources (devices). The shielding analysis for the LTSS for a variety of source isotopes is presented in the main body of Chapter 5.0, *Shielding Evaluation*. The shielding analysis for the devices is presented in Appendix 5.5.3, *Shielded Device Evaluation*.

5.1 Description of Shielding Design

5.1.1 Design Features

The 1105-SD package itself offers little shielding. The outer shell of the 1105-SD is 0.5-in thick steel. The shielding is provided primarily by the LTSS, which features 85.8 mm lead shielding on the ends and 244 mm lead shielding on the sides. Sources are loaded into four recesses within the LTSS. The sources are sealed within one of five special form capsules of differing length. Each special form capsule is loaded into a large source drawer, which features tungsten shielding at each end. The large source drawer is 21.5-in long and 2.5-in in diameter. The length of the tungsten shielding is dependent upon the length of special form capsule utilized, and the tungsten length ranges between 88.5 and 214 mm.

In addition, the LTSS may be used with the T80/T780 drawer. The T80 and T780 drawers are physically identical. Like the large source drawer, they are 21.5-in long and 2.5-in in diameter. For the T80 drawer, the shielding on each side of the source is 9.2-in of lead. For the T780 drawer, the shielding may be either lead, tungsten, or depleted uranium.

As demonstrated by the certification testing documented in Appendix 2.12.3, *Certification Test Report*, the LTSS does not experience any significant damage which could reduce its effectiveness or which could lead to a release of the sources from the shield.

5.1.2 Summary Table of Maximum Radiation Levels

The number of possible LTSS loading scenarios can vary over a large range. Therefore, a simplified method is employed to compute dose rates for single isotopes, and then the dose rate from any arbitrary combination of isotopes may be calculated using a sum of fractions rule. Using this approach, the maximum surface and 1 m dose rates are conservatively limited to 190 mrem/hr and 9.5 mrem/hr, respectively, which are less than the normal condition of transport (NCT) limits for non-exclusive use transportation of 200 mrem/hr on the package surface and 10 mrem/hr at 1 m from the package surface. Therefore, the transport index (TI) will not exceed 9.5.

Under hypothetical accident conditions (HAC), there is no damage to the LTSS, LTSS lodgment, or 1105-SD package that affects dose rates. Because there is no change to the shielding under HAC, the HAC dose rates are the same as the NCT dose rates at 1 m, or 9.5 mrem/hr. This is significantly less than the limit of 1000 mrem/hr.

The LTSS loading methodology used to ensure compliance with the dose rate limits is summarized in Section 5.4.5, *LTSS Loading Methodology*.

5.2 Source Specification

Source terms are determined for a number of isotopes, which are summarized in Table 5.2-1. These isotopes may be either alpha or beta emitters, although from a shielding standpoint, only the corresponding gamma and neutron emissions contribute to the dose rate. The actinides may also be mixed with an (α ,n) target nucleus, such as beryllium. The decay heat of the 1105-SD package is limited to 200 watts. Therefore, each nuclide is also limited to 200 watts. In most cases, the gamma and neutron source terms are computed by the ORIGEN-S module of the SCALE6 code package [3].

5.2.1 Gamma Source

Co-60

Co-60 is a beta/gamma emitter. The decay of Co-60 is sufficiently simple to be treated explicitly. Each decay of Co-60 results in two gammas, with energies of 1.173 and 1.332 MeV [1]. The gamma source for 1 Ci of Co-60 is provided in Table 5.2-2.

An ORIGEN-S case is developed for 1 Ci of Co-60 in order to determine the decay heat. For 1 Ci of Co-60, the decay heat is 0.01542 watts. Therefore, the Co-60 activity is limited to 12,970 Ci for the maximum decay heat of 200 watts.

Cs-137

Cs-137 is a beta/gamma emitter. The decay of Cs-137 is sufficiently simple to be treated explicitly. The decay of Cs-137 emits a 0.662 MeV gamma with an 85% probability [1]. The gamma source for 1 Ci of Cs-137 is provided in Table 5.2-3.

Cs-137 quickly reaches equilibrium with its daughter product, Ba-137m. Therefore, to conservatively compute the decay heat, equal activities of both Cs-137 and Ba-137m are input to ORIGEN-S, and a maximum decay heat is computed at time zero. For 1 Ci of Cs-137/Ba-137m, the decay heat is 5.0400E-03 watts.

Sr-90

Sr-90 decays to Y-90, and both are beta/gamma emitters. Sr-90 reaches equilibrium with Y-90 after approximately 20 days. To conservatively compute the source term and decay heat, 1 Ci of both Sr-90 and Y-90 are input to ORIGEN-S. For 1 Ci of Sr-90/Y-90, the decay heat is 6.6980E-03 watts. The gamma source is extracted from the ORIGEN-S output and is provided in Table 5.2-4 for 1 Ci.

Ra-226

Ra-226 is an alpha/gamma emitter. The gamma source input files are developed using ORIGEN-S. The Ra-226 gamma source for a decay time from 0.1 to 10 years is provided in Table 5.2-5 for 1 Ci. The gamma sources for the energy groups that are primary contributors to the dose rate (0.6 to 2.5 MeV) peak at approximately 0.3 years of decay. The gamma source for the lower energy groups continue to increase slowly after 0.3 years, but these energy groups do not contribute to the dose rate. Therefore, the source at a decay time of 0.3 years is used in the shielding calculations.

The decay heat increases slowly with time and peaks after approximately 80 years of decay, with a maximum value of 0.1862 watts for 1 Ci.

The alpha radiation will lead to a neutron source when mixed with an (α ,n) target nucleus, such as beryllium. The neutron source is discussed in Section 5.2.2, *Neutron Source*.

Am-241

Am-241 is an alpha/gamma emitter and results in little gamma radiation. Am-241 sources are relatively pure, with an Am-241 content of approximately 0.997 g per gram of metal [5]. A representative distribution is provided in Table 5.2-6, taken from Table 16 of [5]. The maximum 1105-SD activity of 1,000 Ci Am-241 equates to 291.5 g. Based on the information in Table 5.2-6, for 291.5 g Am-241, the total plutonium mass is limited to approximately 0.98 g, which is significantly less than the fissile exemption limit of 15 g per 10 CFR 71.15(b).

The Am-241 gamma source is computed for pure Am-241 because the impurities are negligible. The gamma source for 1 Ci Am-241 listed in Table 5.2-7 is computed at time zero. The gamma source is quite weak at the energies that contribute to the dose rate. For 1 Ci of Am-241, the decay heat is 0.03337 watts.

The alpha radiation will lead to a neutron source when mixed with an (α ,n) target nucleus, such as beryllium. The neutron source is discussed in Section 5.2.2, *Neutron Source*.

Pu-238

Pu-238 is an alpha/gamma emitter and results in little gamma radiation. A Pu-238 sealed source is typically ~80% Pu-238 and ~20% other plutonium isotopes. The quantity of Pu-238 is limited for transport by the mass of fissile plutonium that may be present as an impurity. A representative distribution is provided in Table 5.2-8, taken from Table 4 of [5]. The fissile isotopes Pu-239, Pu-241, and U-235 are limited to a total of 15 g per 10 CFR 71.15(b). The total fissile mass per gram of plutonium is 0.168 g per Table 5.2-8. For the 1105-SD limit of 75 g Pu-238 (including impurities), the total fissile mass is $(75)(0.168) = 12.6 \text{ g} < 15 \text{ g}$.

The gamma source is computed using ORIGEN-S and is listed in Table 5.2-9 on a per gram basis. The plutonium impurities are neglected because the gamma source and decay heat are maximized for pure Pu-238, as the half-life of Pu-238 is relatively short. This source is computed at time zero. For 1 g of Pu-238, the decay heat is 0.56773 watts.

The alpha radiation will lead to a neutron source when mixed with an (α ,n) target nucleus, such as oxygen. The neutron source is discussed in Section 5.2.2, *Neutron Source*.

Pu-239

Pu-239 is an alpha/gamma emitter and results in little gamma radiation. The total mass of fissile isotopes is limited to 15 g per 10 CFR 71.15(b). However, sources containing Pu-239 will have other non-fissile plutonium impurities. Representative distributions for Pu-239 in sealed sources may be found in Table 10 of [5] and Table 2 (Reconciled Values) of [6]. These distributions are reproduced in Table 5.2-10 as isotopic sets #1 and #2. ORIGEN-S models are developed for both sets of isotopics. Because Pu-241 is a beta emitter and decays to Am-241, which is a minor gamma emitter, the Pu-241 is conservatively modeled as Am-241.

The gamma source computed using both sets of isotopics is provided in Table 5.2-11 on a per gram basis. Isotopic set #2 results in a larger gamma source, although the gamma source is small in either case. The gamma source for isotopic set #2 is used in the shielding calculations. The

source is computed at time zero. For 1 g of Pu-239 (including impurities), the decay heat is 0.00307 watts.

The alpha radiation will lead to a neutron source when mixed with an (α ,n) target nucleus, such as beryllium. The neutron source is discussed in Section 5.2.2, *Neutron Source*.

Ir-192

Ir-192 is a beta/gamma emitter. There is an error in the SCALE6/ORIGEN-S data libraries for Ir-192 and SCALE6/ORIGEN-S cannot be used to determine the gamma source for this isotope. Therefore, for this isotope only, SCALE44/ORIGEN-S [4] is used to compute the gamma source term. The gamma source is provided in Table 5.2-12 for 1 Ci and is computed at time zero. For 1 Ci of Ir-192, the decay heat is 0.00615 watts.

Se-75

Se-75 is a beta/gamma emitter. The gamma source term is computed using ORIGEN-S and is provided in Table 5.2-13 for 1 Ci Se-75. The source term is computed at time zero. For 1 Ci of Se-75, the decay heat is 0.00241 watts.

Decay Heat per Ci or Gram

The maximum decay heat for each source is listed in the individual sections above. However, it is useful to summarize the maximum decay heat for each isotope per either Ci or gram to facilitate the scenario in which different source isotopes are combined in the same LTSS. These data are presented in Table 5.2-14.

5.2.2 Neutron Source

Neutron sources are generated by Ra-226, Am-241, Pu-238, and Pu-239. These sources are generated by both (α ,n) reactions and spontaneous fission, although the spontaneous fission component is negligible compared to the (α ,n) component for the nuclides under consideration. Target nuclides that result in an (α ,n) source include oxygen, beryllium, and chlorine. The ORIGEN-S module of the SCALE6 code package is used to calculate the neutron sources. Quantities are input in grams rather than curies because the target nuclides are not radioactive.

Ra-226

Ra-226 sources exist either as a radium/beryllium mixture, or as radium with trace amounts of oxygen, carbon, sulfur, bromine, or chlorine (hydrous or anhydrous). Because the trace elements contain (α ,n) target nuclides, it is conservatively assumed that the trace elements are present as compounds RaSO_4 , RaBr_2 , RaCl_2 + water, RaCl_2 (anhydrous), RaCO_3 , or RaSO_3 . The masses of the target elements are computed based on the chemical formulas provided. For $\text{RaCl}_2 + \text{H}_2\text{O}$, the H_2O mass is arbitrarily selected as five times the RaCl_2 mass, although adding water simply decreases the neutron source magnitude. For the Ra/beryllium mixture, an infinitely dilute mixture is conservatively assumed (infinite dilution is defined as a beryllium mass 1000 times greater than the Ra-226 mass). Bromine is not an (α ,n) target isotope, so RaBr_2 does not generate neutrons.

The results for 1 Ci are summarized in Table 5.2-15. The maximum neutron source occurs for a decay time of 0.3 years. RaBe is by far the largest neutron source. Beryllium generates more neutrons than any other target material, and the infinite dilution assumption also increases the

beryllium neutron source. Of the non-Be target compounds, RaCl_2 (anhydrous) has the largest neutron source. Therefore, RaCl_2 (anhydrous) is used to bound all non-Be targets, and RaBe is treated separately.

Am-241

Am-241 sources exist either as an americium/beryllium mixture, or as americium with trace amounts of oxygen or chlorine. Because the trace elements contain (α, n) target nuclides, it is conservatively assumed that the trace elements are present as compounds AmO_2 or AmCl . The masses of the target elements are computed based on the chemical formulas provided. For the Am/beryllium mixture, an infinitely dilute mixture is conservatively assumed (infinite dilution is defined as a beryllium mass 1000 times greater than the Am-241 mass).

The neutron sources are summarized in Table 5.2-16 for a 1 Ci source. The sources are computed at time zero. AmO_2 and AmCl result in similar neutron sources, while the AmBe source is orders of magnitude larger. AmCl may be used to bound AmO_2 , and AmBe is treated separately.

Pu-238

Pu-238 sources exist as plutonium with a trace amount of oxygen. Because oxygen is an (α, n) target nuclide, it is conservatively assumed that the trace oxygen is present as the compound PuO_2 . Although a Pu-238 source contains other isotopes of plutonium, the total plutonium mass is conservatively modeled as pure Pu-238 for the neutron source calculation to maximize the activity. The Pu-238 source is provided in Table 5.2-17 for 1 g Pu-238. The source is computed at time zero.

Pu-239

Pu-239 sources exist as either PuBe_{13} or plutonium with a trace amount of oxygen. Because oxygen is an (α, n) target nuclide, it is conservatively assumed that the trace oxygen is present as the compound PuO_2 . The plutonium contains impurities with half-lives much shorter than Pu-239, and the neutron source strength is sensitive to the impurity content. Therefore, two different plutonium isotopic sets are used, as listed in Table 5.2-10. Pu-239 sources are treated as either PuO_2 or PuBe_{13} . The neutron sources for PuO_2 and PuBe_{13} for each of the two isotopic sets are presented in Table 5.2-18.

The Pu-241 impurity is a beta emitter and decays to Am-241, which is an alpha emitter. Therefore, the neutron source strength increases with time as the Am-241 concentration increases. To simplify the calculation, the Pu-241 impurity is conservatively input as Am-241, and the source is computed at time zero.

For both PuO_2 and PuBe_{13} , isotopic set #2 results in a more conservative neutron source than set #1 and is used in subsequent dose rate calculations. Because the PuBe_{13} neutron source is significantly larger than the PuO_2 neutron source, these compounds are treated separately in subsequent dose rate calculations.

Table 5.2-1 – Allowable Source Nuclides

Nuclide	Radiation Type	1105-SD Limit
Co-60	Gamma	12,970 Ci
Cs-137	Gamma	14,000 Ci
Sr-90	Gamma	1,000 Ci
Ra-226 (no Be)	Neutron and Gamma	20 Ci
Ra-226Be	Neutron and Gamma	1.3 Ci
Am-241 (no Be)	Neutron and Gamma	1000 Ci
Am-241Be	Neutron and Gamma	6.6 Ci
Pu-238 (no Be)	Neutron and Gamma	75 g plutonium
Pu-239 (no Be)	Neutron and Gamma	15 g plutonium
Pu-239Be	Neutron and Gamma	15 g plutonium
Ir-192	Gamma	200 Ci
Se-75	Gamma	80 Ci

Table 5.2-2 – Gamma Source, 1 Ci Co-60

Line Energy (MeV)	Gamma Source (γ/s)
1.173	3.7E+10
1.322	3.7E+10

Table 5.2-3 – Gamma Source, 1 Ci Cs-137

Line Energy (MeV)	Gamma Source (γ/s)
0.662	3.145E+10

Table 5.2-4 – Gamma Source, 1 Ci Sr-90

E_{upper} (MeV)	Gamma Source (γ/s)
5.00E-02	1.603E+10
1.00E-01	5.603E+09
2.00E-01	3.909E+09
3.00E-01	1.282E+09
4.00E-01	9.361E+08
6.00E-01	6.294E+08
8.00E-01	2.853E+08
1.00E+00	1.218E+08
1.33E+00	7.182E+07
1.66E+00	1.359E+07
2.00E+00	2.438E+06
2.50E+00	1.252E+05
Total	2.888E+10

Table 5.2-5 – Gamma Source (γ/s), 1 Ci Ra-226

E_{upper} (MeV)	0.1 y	0.3 y	0.5 y	0.7 y	1.0 y	3.0 y	5.0 y	10.0 y
5.00E-02	1.430E+10	1.439E+10	1.446E+10	1.453E+10	1.463E+10	1.529E+10	1.591E+10	1.729E+10
1.00E-01	1.356E+10	1.359E+10	1.360E+10	1.360E+10	1.362E+10	1.371E+10	1.379E+10	1.396E+10
2.00E-01	4.267E+09	4.277E+09	4.283E+09	4.289E+09	4.298E+09	4.354E+09	4.407E+09	4.524E+09
3.00E-01	1.229E+10	1.231E+10	1.231E+10	1.231E+10	1.231E+10	1.232E+10	1.232E+10	1.233E+10
4.00E-01	1.483E+10	1.485E+10	1.485E+10	1.484E+10	1.484E+10	1.484E+10	1.484E+10	1.482E+10
6.00E-01	1.353E+09	1.355E+09	1.356E+09	1.356E+09	1.356E+09	1.359E+09	1.362E+09	1.367E+09
8.00E-01	1.874E+10	1.877E+10	1.876E+10	1.876E+10	1.876E+10	1.874E+10	1.873E+10	1.869E+10
1.00E+00	2.222E+09	2.224E+09	2.224E+09	2.224E+09	2.224E+09	2.222E+09	2.220E+09	2.216E+09
1.33E+00	9.685E+09	9.695E+09	9.695E+09	9.695E+09	9.690E+09	9.685E+09	9.675E+09	9.655E+09
1.66E+00	4.921E+09	4.927E+09	4.926E+09	4.926E+09	4.925E+09	4.921E+09	4.917E+09	4.906E+09
2.00E+00	8.210E+09	8.220E+09	8.220E+09	8.220E+09	8.220E+09	8.210E+09	8.205E+09	8.185E+09
2.50E+00	3.136E+09	3.140E+09	3.140E+09	3.140E+09	3.139E+09	3.137E+09	3.134E+09	3.127E+09
3.00E+00	4.949E+07	4.955E+07	4.955E+07	4.954E+07	4.954E+07	4.949E+07	4.945E+07	4.934E+07
4.00E+00	1.183E+07	1.185E+07	1.185E+07	1.185E+07	1.185E+07	1.184E+07	1.183E+07	1.180E+07
5.00E+00	6.715E+00	6.720E+00	6.725E+00	6.735E+00	6.745E+00	6.835E+00	6.920E+00	7.140E+00
6.50E+00	1.935E+00	1.937E+00	1.938E+00	1.940E+00	1.943E+00	1.969E+00	1.994E+00	2.057E+00
8.00E+00	2.461E-01	2.464E-01	2.465E-01	2.468E-01	2.472E-01	2.504E-01	2.536E-01	2.616E-01
1.00E+01	3.284E-02	3.288E-02	3.290E-02	3.293E-02	3.299E-02	3.342E-02	3.385E-02	3.491E-02
Total	1.076E+11	1.078E+11	1.081E+11	1.089E+11	1.096E+11	1.099E+11	1.102E+11	1.106E+11

Table 5.2-6 – Representative Radionuclide Distribution for Am-241 Sealed Sources

Nuclide	Grams per Gram of Source Material
Am-241	9.97E-01
Pu-238	2.05E-06
Pu-239	2.75E-03
Pu-240	5.55E-04
Pu-241	3.97E-05
Pu-242	1.19E-05
U-234	1.14E-11
U-235	1.43E-09
U-238	5.71E-07
Cs-137	7.78E-10
Sr-90	4.46E-10

Table 5.2-7 – Gamma Source, 1 Ci Am-241

E_{upper} (MeV)	Gamma Source (γ/s)
5.00E-02	8.740E+09
1.00E-01	1.056E+10
2.00E-01	7.342E+06
3.00E-01	2.863E+05
4.00E-01	4.595E+05
6.00E-01	3.389E+04
8.00E-01	2.707E+05
1.00E+00	2.393E+03
1.33E+00	9.774E+01
1.66E+00	2.215E-35
2.00E+00	3.447E+01
2.50E+00	1.809E+01
3.00E+00	9.079E+00
4.00E+00	6.683E+00
5.00E+00	1.694E+00
6.50E+00	4.896E-01
8.00E+00	6.264E-02
1.00E+01	8.444E-03
Total	1.931E+10

Table 5.2-8 – Representative Radionuclide Distribution for Pu-238 Sealed Sources

Nuclide	Grams per Gram of Plutonium
Pu-238	8.03E-01
Pu-239	1.61E-01
Pu-240	2.63E-02
Pu-241	6.90E-03
Pu-242	2.33E-03
Am-241	2.84E-04
U-234	3.40E-09
U-235	4.25E-07
U-238	1.70E-04
Cs-137	2.31E-07
Sr-90	1.33E-07

Table 5.2-9 – Gamma Source, 1 g Pu-238

E_{upper} (MeV)	Gamma Source (γ/s)
5.00E-02	3.984E+10
1.00E-01	3.231E+07
2.00E-01	2.179E+07
3.00E-01	2.193E+04
4.00E-01	1.896E+02
6.00E-01	2.589E-03
8.00E-01	3.271E+05
1.00E+00	4.328E+04
1.33E+00	9.917E+03
1.66E+00	1.419E-13
2.00E+00	1.679E+03
2.50E+00	9.696E+02
3.00E+00	5.381E+02
4.00E+00	4.583E+02
5.00E+00	1.451E+02
6.50E+00	5.499E+01
8.00E+00	1.022E+01
1.00E+01	2.087E+00
Total	3.989E+10

Table 5.2-10 – Representative Radionuclide Distribution for Pu-239 Sealed Sources

Nuclide	Isotopic Set #1, Based on [5], Grams per Gram of Plutonium	Isotopic Set #2, Based on [6], Grams per Gram of Plutonium
Pu-238	1.48E-04	1.50E-04
Pu-239	9.32E-01	9.26E-01
Pu-240	6.50E-02	6.75E-02
Pu-241 ^⓪	2.44E-03	6.20E-03
Pu-242	3.62E-04	3.30E-04
Am-241	2.84E-04	2.50E-04
U-234	3.40E-09	-
U-235	4.25E-07	-
U-238	1.70E-04	-
Cs-137	2.31E-07	-
Sr-90	1.33E-07	-

^⓪Modeled as Am-241 in ORIGEN-S.

Table 5.2-11 – Gamma Source, 1 g Pu-239 (includes impurities)

E_{upper} (MeV)	Isotopic Set #1 Gamma Source (γ/s)	Isotopic Set #2 Gamma Source (γ/s)
5.00E-02	1.705E+08	2.831E+08
1.00E-01	9.933E+07	2.343E+08
2.00E-01	2.989E+05	3.925E+05
3.00E-01	1.764E+04	2.120E+04
4.00E-01	9.993E+04	1.051E+05
6.00E-01	3.337E+04	3.357E+04
8.00E-01	4.559E+03	8.013E+03
1.00E+00	5.455E+01	8.520E+01
1.33E+00	7.580E+01	7.933E+01
1.66E+00	1.961E-13	1.787E-13
2.00E+00	3.151E+01	3.295E+01
2.50E+00	1.887E+01	1.971E+01
3.00E+00	1.083E+01	1.129E+01
4.00E+00	9.600E+00	1.000E+01
5.00E+00	3.195E+00	3.322E+00
6.50E+00	1.266E+00	1.315E+00
8.00E+00	2.456E-01	2.547E-01
1.00E+01	5.175E-02	5.363E-02
Total	2.703E+08	5.179E+08

Table 5.2-12 – Gamma Source, 1 Ci Ir-192

E_{upper} (MeV)	Gamma Source (γ/s)
5.00E-02	1.994E+09
1.00E-01	3.602E+09
2.00E-01	3.023E+08
3.00E-01	1.271E+10
4.00E-01	3.736E+10
6.00E-01	2.055E+10
8.00E-01	3.031E+09
1.00E+00	1.095E+08
1.33E+00	1.926E+07
1.66E+00	4.233E+05
Total	7.969E+10

Table 5.2-13 – Gamma Source, 1 Ci Se-75

E_{upper} (MeV)	Gamma Source (γ/s)
5.00E-02	7.414E+09
1.00E-01	2.034E+09
2.00E-01	2.530E+10
3.00E-01	3.375E+10
4.00E-01	2.878E+09
6.00E-01	1.729E+09
8.00E-01	1.196E+06
1.00E+00	5.585E+04
Total	7.310E+10

Table 5.2-14 – Decay Heat per Ci or Gram

Isotope	Decay Heat	Unit
Co-60	1.5420E-02	Watts/Ci
Cs-137	5.0400E-03	Watts/Ci
Sr-90	6.6980E-03	Watts/Ci
Ra-226	1.8620E-01	Watts/Ci
Am-241	3.3370E-02	Watts/Ci
Pu-238	5.6773E-01	Watts/g
Pu-239	3.0873E-03	Watts/g
Ir-192	6.1500E-03	Watts/Ci
Se-75	2.4100E-03	Watts/Ci

Table 5.2-15 – Ra-226 Neutron Sources, 1 Ci Ra-226

Neutron Sources (n/s)						
E_{upper} (MeV)	RaSO₄	RaSO₃	RaCl₂	RaCl₂+H₂O	RaCO₃	RaBe
1.30E-06	9.865E-09	8.180E-09	0.000E+00	1.742E-08	9.015E-09	0.000E+00
1.86E-06	8.485E-07	7.040E-07	0.000E+00	1.498E-06	7.755E-07	0.000E+00
3.06E-06	1.839E-06	1.525E-06	7.775E-06	3.773E-06	1.681E-06	0.000E+00
1.07E-05	1.513E-05	1.255E-05	1.400E-04	3.609E-05	1.383E-05	0.000E+00
2.90E-05	1.094E-04	9.080E-05	7.920E-04	2.452E-04	1.769E-04	0.000E+00
1.01E-04	5.130E-04	4.259E-04	4.651E-03	1.212E-03	8.770E-04	0.000E+00
5.83E-04	6.440E-03	5.345E-03	7.085E-02	1.608E-02	1.528E-02	0.000E+00
3.04E-03	8.895E-02	7.385E-02	8.715E-01	2.147E-01	1.903E-01	8.645E-01
1.50E-02	1.058E+00	8.780E-01	9.855E+00	2.518E+00	2.137E+00	4.925E+01
1.11E-01	2.353E+01	1.953E+01	3.207E+02	6.280E+01	4.392E+01	2.243E+03
4.08E-01	1.168E+02	9.695E+01	2.676E+03	3.852E+02	2.193E+02	3.164E+04
9.07E-01	2.344E+02	1.945E+02	9.215E+03	1.034E+03	3.655E+02	2.966E+05
1.42E+00	3.638E+02	3.022E+02	1.024E+04	1.329E+03	3.947E+02	4.062E+05
1.83E+00	4.596E+02	3.819E+02	5.675E+03	1.186E+03	4.280E+02	2.484E+05
3.01E+00	2.224E+03	1.847E+03	2.197E+03	4.041E+03	2.040E+03	1.395E+06
6.38E+00	1.605E+03	1.331E+03	0.000E+00	2.832E+03	2.820E+03	6.640E+06
2.00E+01	3.004E-01	2.489E-01	0.000E+00	5.340E-01	3.805E+02	4.720E+06
Total	5.030E+03	4.174E+03	3.034E+04	1.087E+04	6.695E+03	1.374E+07

Table 5.2-16 – Am-241 Neutron Sources, 1 Ci Am-241

Neutron Sources (n/s)			
E_{upper} (MeV)	AmO₂	AmCl	AmBe
1.30E-06	3.953E-11	3.953E-11	3.953E-11
1.86E-06	1.426E-10	1.426E-10	1.426E-10
3.06E-06	3.831E-10	3.831E-10	3.831E-10
1.07E-05	3.985E-09	3.985E-09	3.985E-09
2.90E-05	1.635E-08	1.635E-08	1.635E-08
1.01E-04	1.678E-04	2.319E-04	1.161E-07
5.83E-04	1.741E-03	1.040E-02	1.755E-06
3.04E-03	1.723E-02	1.065E-01	6.515E-02
1.50E-02	2.166E-01	1.449E+00	3.304E+00
1.11E-01	4.277E+00	5.799E+01	1.470E+02
4.08E-01	2.018E+01	3.039E+02	5.816E+03
9.07E-01	4.156E+01	1.031E+03	7.359E+04
1.42E+00	5.809E+01	4.599E+02	1.002E+05
1.83E+00	7.920E+01	4.072E-02	5.915E+04
3.01E+00	4.075E+02	8.694E-02	3.323E+05
6.38E+00	2.036E+02	7.866E-02	1.497E+06
2.00E+01	8.728E-03	8.728E-03	8.535E+05
Total	8.146E+02	1.854E+03	2.922E+06

Table 5.2-17 – Pu-238 Neutron Source, 1 g Pu-238

E_{upper} (MeV)	Neutron Source (n/s)
1.30E-06	3.009E-07
1.86E-06	1.088E-06
3.06E-06	2.935E-06
1.07E-05	3.065E-05
2.90E-05	1.259E-04
1.01E-04	2.171E-03
5.83E-04	3.891E-02
3.04E-03	4.687E-01
1.50E-02	5.487E+00
1.11E-01	1.102E+02
4.08E-01	5.507E+02
9.07E-01	1.164E+03
1.42E+00	1.485E+03
1.83E+00	1.687E+03
3.01E+00	7.677E+03
6.38E+00	4.063E+03
2.00E+01	4.440E+01
Total	1.679E+04

Table 5.2-18 – Pu-239 Neutron Sources, 1 g Pu-239 (including impurities)

Neutron Sources (n/s)				
E_{upper} (MeV)	Isotopic Set #1 PuO₂	Isotopic Set #2 PuO₂	Isotopic Set #1 PuBe	Isotopic Set #2 PuBe
1.30E-06	2.467E-08	2.485E-08	8.267E-09	8.553E-09
1.86E-06	8.213E-08	8.280E-08	2.998E-08	3.102E-08
3.06E-06	1.941E-07	1.961E-07	8.107E-08	8.387E-08
1.07E-05	1.564E-06	1.589E-06	8.493E-07	8.787E-07
2.90E-05	5.215E-06	5.325E-06	3.493E-06	3.614E-06
1.01E-04	3.455E-05	3.752E-05	2.483E-05	2.569E-05
5.83E-04	4.706E-04	5.061E-04	3.755E-04	3.885E-04
3.04E-03	5.469E-03	5.846E-03	7.580E-03	8.267E-03
1.50E-02	6.155E-02	6.603E-02	2.260E-01	2.548E-01
1.11E-01	1.290E+00	1.379E+00	8.860E+00	1.010E+01
4.08E-01	7.207E+00	7.660E+00	3.141E+02	3.617E+02
9.07E-01	1.465E+01	1.561E+01	3.801E+03	4.398E+03
1.42E+00	1.626E+01	1.744E+01	4.684E+03	5.493E+03
1.83E+00	1.428E+01	1.559E+01	2.649E+03	3.127E+03
3.01E+00	4.755E+01	5.343E+01	1.685E+04	1.957E+04
6.38E+00	2.339E+01	2.647E+01	6.311E+04	7.520E+04
2.00E+01	9.047E-01	9.360E-01	3.687E+04	4.378E+04
Total	1.256E+02	1.386E+02	1.283E+05	1.519E+05

5.3 Shielding Model

5.3.1 Configuration of Source and Shielding

Models of the 1105-SD package and contents are developed in the MCNP5 computer program [2] for all allowable configurations of source and shielding. The objective is to determine the source activity for each nuclide within an LTSS that results in dose rates near the regulatory limit. Once these activity limits are known, the dose rate for any combination of different isotopes may be conservatively estimated using a sum of fractions rule. The details of the individual calculations and development of the sum of fractions rule is presented in Section 5.4, *Shielding Evaluation*. This section presents the geometry of the source and shielding that is common to the various models.

The LTSS is transported inside the LTSS lodgment, which is situated inside the 1105-SD cavity. The LTSS lodgment is not modeled explicitly in MCNP because it offers little axial or radial shielding, although credit is taken for the LTSS lodgment for axial placement of the LTSS within the package. The bottom of the LTSS is placed 8.5-in from the bottom of the package (8.0-in lodgment bottom piece plus 0.5-in lodgment support plate; the 0.5-in rubber pad is neglected). The 1105-SD is artificially shortened in the MCNP models so that the distance from the top of the LTSS to the inner top of the 1105-SD is 17.3-in (16.8-in for lodgment top piece plus 0.5-in lodgment top plate). Therefore, the LTSS is simultaneously modeled at both the bottom and top of the package, and no models are required in which the LTSS shifts axially.

The LTSS lodgment is transported inside the 1105-SD package. Key dimensions used in the MCNP model are listed in Table 5.3-1, and the model geometry is shown in Figure 5.3-1. As noted in the previous paragraph, the height of the 1105-SD is intentionally reduced in the model compared to the actual value. This is achieved by reducing the cavity length. The upper and lower internal impact limiters are conservatively modeled as void, although credit is taken for the 0.5-in impact limiter aluminum plates that form the top and bottom of the cavity. The outer shell of the package is stainless steel and includes the thermal shield below the torispherical head (the thermal shield on the torispherical head is neglected). Polyurethane foam fills the external impact limiter. Details of the flanges that connect the upper and lower package assemblies are conservatively ignored and modeled as foam.

The LTSS is the primary shield and is dimensioned on Figure 5.3-2. The key dimensions used to develop the LTSS models are listed in Table 5.3-2, and the model geometry is shown in Figure 5.3-3. The LTSS drawer barrel contains four recesses, and drawers containing sources are inserted into each recess. The drawer barrel rotates to facilitate source loading and is located inside the liner tube weldment. Steel cover plates are located on each end of the liner tube weldment. The ends of the liner tube weldment are covered with lead-shielded flanges. The LTSS also has thick lead shielding on the side between the liner tube and outer shell. The radial lead thickness is conservatively reduced by 7 mm to account for tolerances. The lead thickness in the shielded flange (both upper and lower) is conservatively reduced by the index cap penetration depth of 10 mm. This reduction is conservative because the index cap would be associated with only one drawer. Also, the index plate and index pivot plates contain a hole associated with only one drawer, although this hole is modeled with each drawer to maintain model symmetry. These modeling assumptions result in conservative dose rates.

The LTSS has two basic configurations: Large source drawers (LDs) and the T80/T780 drawer. The LD and T80/T780 drawer shall not be mixed within the same LTSS.

LD Configuration: Each of the four LTSS recesses shall be filled with either an LD or a shield drawer (no empty recesses). A shield drawer is a large source drawer body nominally filled with a tungsten shield plug. Five different LDs are available to accommodate the various sources. In general, the different LDs cannot be mixed within an LTSS because they do not provide equivalent shielding. The allowed combinations of LDs are defined in Table 5.3-3. For any of the allowed combinations, an LD may be replaced with a shield drawer because a shield drawer is more heavily shielded than an LD.

There are five LDs of various tungsten shielding lengths (LD-74, -150, -200, -250, and -325) and five NLM 52s special form capsules of various lengths to fit within the LDs (NLM 52-74, -150, -200, -250, and -325). Other special form or non-special form capsules may be used that have the same length, diameter, and at least as much radiation attenuation as the NLM-52 capsule series, although the NLM 52 nomenclature is used in the following discussion for convenience. The sources are located inside the NLM 52 special form capsules, and only one source nuclide type is allowed per NLM 52. In most cases, one NLM 52 is transported per LD, although two NLM 52-74s may be transported inside an LD-150.

Co-60 and Cs-137 may be either short cylinder (point) or pencil (line) sources, while the remaining source nuclides are point sources. Only point sources are allowed in the NLM 52-74, and only line sources are allowed in the NLM 52-250 and -325. The NLM 52-150 and -200 may contain either point or line sources. The allowable combinations of LDs, NLM 52s, and source types are summarized in Table 5.3-4.

MCNP models are developed for all allowable combinations of LDs and source nuclides. Each MCNP model contains either 1 Ci (or 1 g) of source nuclide in a single LD, while the three remaining LDs are modeled without sources. No credit is taken for self-shielding of the source or encapsulation material. Point sources are modeled as a sphere of radius 1 mm (to aid in visualization), and line sources are modeled as a cylinder of radius 1 mm with the lengths provided in Table 5.3-4.

Models are developed for different source locations within the capsules to maximize the dose rates due to streaming effects. Eight (x,y) source locations are utilized, as shown on Figure 5.3-4. The sources are placed either at the top or bottom of the capsule to maximize the dose rate through the ends of the LTSS. The source placement for the NLM 52-74 capsule is shown in Figure 5.3-5 for Location 1 at the top of the capsule.

Dimensions for the five NLM 52 capsules are provided in Table 5.3-5. The model geometry of a representative NLM 52 capsule is shown in Figure 5.3-6.

The LD features tungsten shielding at the ends. Dimensions of the LD and tungsten inserts are provided in Table 5.3-6. Small deviations of actual and as-modeled dimensions are noted in Table 5.3-6. These differences are small and may be neglected. The model geometry of a representative LD is shown in Figure 5.3-6.

T80/T780 Configuration: Each of the four LTSS recesses shall be filled with either a T80/T780 drawer or a shield drawer (no empty recesses). A shield drawer is a drawer body nominally filled with a tungsten shield plug. The T80/T780 contains a Co-60 point source with a maximum activity of 12,970 Ci. No other sources are authorized for this drawer. The dimensions of the

T80/T780 drawer are shown in Figure 5.3-7 and are determined by physically cutting a drawer in half and measuring the dimensions. The MCNP model geometry of the T80/T780 is consistent with this figure.

The T80 and T780 drawers are dimensionally identical. Like the large source drawer, they are 21.5-in long and 2.5-in in diameter. In the center is a 1.1-in diameter cross-drilled hole that accepts a source capsule. The drawers are made of brass with a wall thickness of 0.2-in and a stainless steel end thickness of 0.8-in. For the T80 drawer, the shielding on each side of the source is 9.2-in of lead. For the T780 drawer, the shielding may be either lead, tungsten, or depleted uranium, although this shielding is conservatively modeled as lead in MCNP.

5.3.2 Material Properties

Type 304 stainless steel with a density of 7.94 g/cm^3 is used for the 1105-SD shell, LTSS structural members, LD structure, and NLM 52 capsules. The Type 304 composition is provided in Table 5.3-7 and is obtained from the SCALE6 User's Manual [3].

Tungsten with a density of 17 g/cm^3 is used as a shield material in the LD. It is modeled as pure.

Lead with a density of 11.35 g/cm^3 is used as a shield material in the LTSS. It is modeled as pure.

Polyurethane foam with a density of 14 pounds per cubic foot (pcf) (0.224 g/cm^3) is modeled in the lower assembly of the 1105-SD. This bounds the actual density of 15 pcf. The foam composition utilized is provided in Table 5.3-8.

Aluminum with a density of 2.7 g/cm^3 is used in the 1105-SD internal impact limiter plates that form the top and bottom of the 1105-SD cavity. It is modeled as pure.

The T80 and T780 source drawers have the same dimensions. The T80 uses lead, while the T780 may use lead, tungsten, or depleted uranium. Since the density of tungsten (17 g/cm^3) and of depleted uranium (18.95 g/cm^3) are greater than the density of lead (11.35 g/cm^3), lead is conservatively used in the analysis. The T80/T780 drawer tube is modeled as brass with a density of 8.07 g/cm^3 , and the composition of brass is provided in Table 5.3-9 [7].

Table 5.3-1 – Key 1105-SD Dimensions

Component	Actual Dimension (in)	As-Modeled Dimension (in)
Shell inner diameter	43.5	Same
Shell thickness	0.5	Same
Side thermal shield thickness	0.165 (=0.06+0.105)	Same
Upper/Lower head thickness	0.5	Same
Upper/Lower head height	~9.0	Same
Cavity height	60.3	58.99
Overall package height	83.2	81.59
Upper/Lower internal impact limiter plate thickness	0.5	Same
Impact limiter outer diameter	70	Same
Impact limiter shell thickness	0.25	Same

Table 5.3-2 – Key LTSS Dimensions

Component	Actual Dimension (mm)	As-Modeled Dimension (mm)
Side lead thickness (max)	244 (=678/2-190/2)	237
Shielded flange lead thickness	85.8	76
Shielded flange lead outer diameter	216	Same
Shielded flange insert thickness	10	Same
Shielded flange thickness	32	Same
Side shell thickness	6	Same
Drawer inner diameter	64	Same
Drawer barrel outer diameter	169.75	Same
Liner tube outer diameter	190	Same
Liner tube inner diameter	171	Same
Liner tube assembly flange outer diameter	330	Same
Liner tube assembly flange thickness	74 (=19+55)	Same
Index pivot and pivot plate thickness	20	Same
Index pivot and pivot plate hole diameter	64	Same
Index pivot and pivot cover plate thickness	18	Same

Table 5.3-3 – Allowable LD Configurations

Configuration ^①	Recess 1	Recess 2	Recess 3	Recess 4
A	LD-74	LD-74	LD-74	LD-74
B	LD-150	LD-150	LD-150	LD-150
C	LD-200	LD-200	LD-200	LD-200
D	LD-250	LD-250	LD-250	LD-250
E	LD-325	LD-325	LD-325	LD-325
AB	LD-74	LD-150	LD-150	LD-150
BC	LD-150	LD-150	LD-200	LD-200
BD	LD-250	LD-150	LD-150	LD-150

①Any number of LDs may be replaced with a shield drawer.

Table 5.3-4 – Authorized Payload Special Form Capsule Sources and Nuclides

Drawer Model	Special Form Capsule Model	Authorized Source Geometry and Dimensions	Authorized Nuclides
LD-74	NLM 52-74	Point source	All nuclides in Table 5.2-1
LD-150	NLM 52-150	Point source	All nuclides in Table 5.2-1
		Line source, length ≥ 60 mm	Co-60 and Cs-137
LD-150	Two (2) NLM 52-74s	Point source	All nuclides in Table 5.2-1
LD-200	NLM 52-200	Point source	All nuclides in Table 5.2-1
		Line source, length ≥ 136 mm	Co-60 and Cs-137
LD-250	NLM 52-250	Line source, length ≥ 186 mm	Co-60 and Cs-137
LD-325	NLM 52-325	Line source, length ≥ 236 mm	Co-60 and Cs-137

Table 5.3-5 – NLM 52 Special Form Capsule Dimensions

Component	Actual Dimension (mm)	As-Modeled Dimension (mm)
Cylinder length NLM 52-74	74	Same
Cylinder length NLM 52-150	150	Same
Cylinder length NLM 52-200	200	Same
Cylinder length NLM 52-250	250	Same
Cylinder length NLM 52-325	325	Same
Outer diameter	52	Same
Inner diameter	47.3	Same
End cap thickness	8	Same

Table 5.3-6 – Large Source Drawer Dimensions

Component	Actual Dimension (mm)	As-Modeled Dimension (mm)
Tungsten length LD-74	214	Same
Tungsten length LD-150	176	Same
Tungsten length LD-200	151	Same
Tungsten length LD-250	126	Same
Tungsten length LD-325	88.5	Same
Tungsten outer diameter	51.85	53
Overall drawer length	547.80	548
Top end thickness	20	Same
Bottom end thickness	19.62 (=547.80-528.18)	20
Outer diameter	62.94	63
Inner diameter	54 (max)	53

Table 5.3-7 – SS304 Composition

Component	Wt. %
C	0.08
Si	1.0
P	0.045
Cr	19.0
Mn	2.0
Fe	68.375
Ni	9.5
Density = 7.94 g/cm ³	

Table 5.3-8 – Foam Composition

Component	Wt. %
C	60
O	24
N	12
H	4
Density = 0.224 g/cm ³	

Table 5.3-9 – Brass Composition

Component	Wt. %
Fe	0.0868
Cu	66.5381
Zn	32.5697
Sn	0.2672
Pb	0.5377
Density = 8.07 g/cm ³	

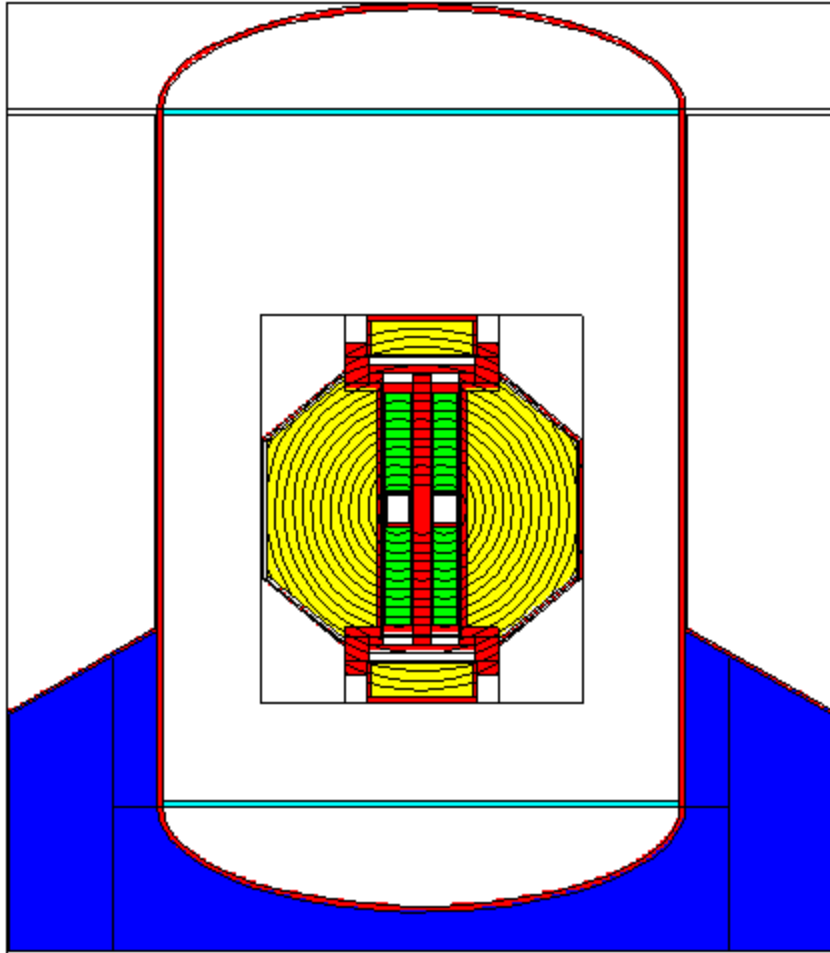


Figure 5.3-1 – 1105-SD with LTSS

**Security-Related Information
Figure Withheld Under
10 CFR 2.390**

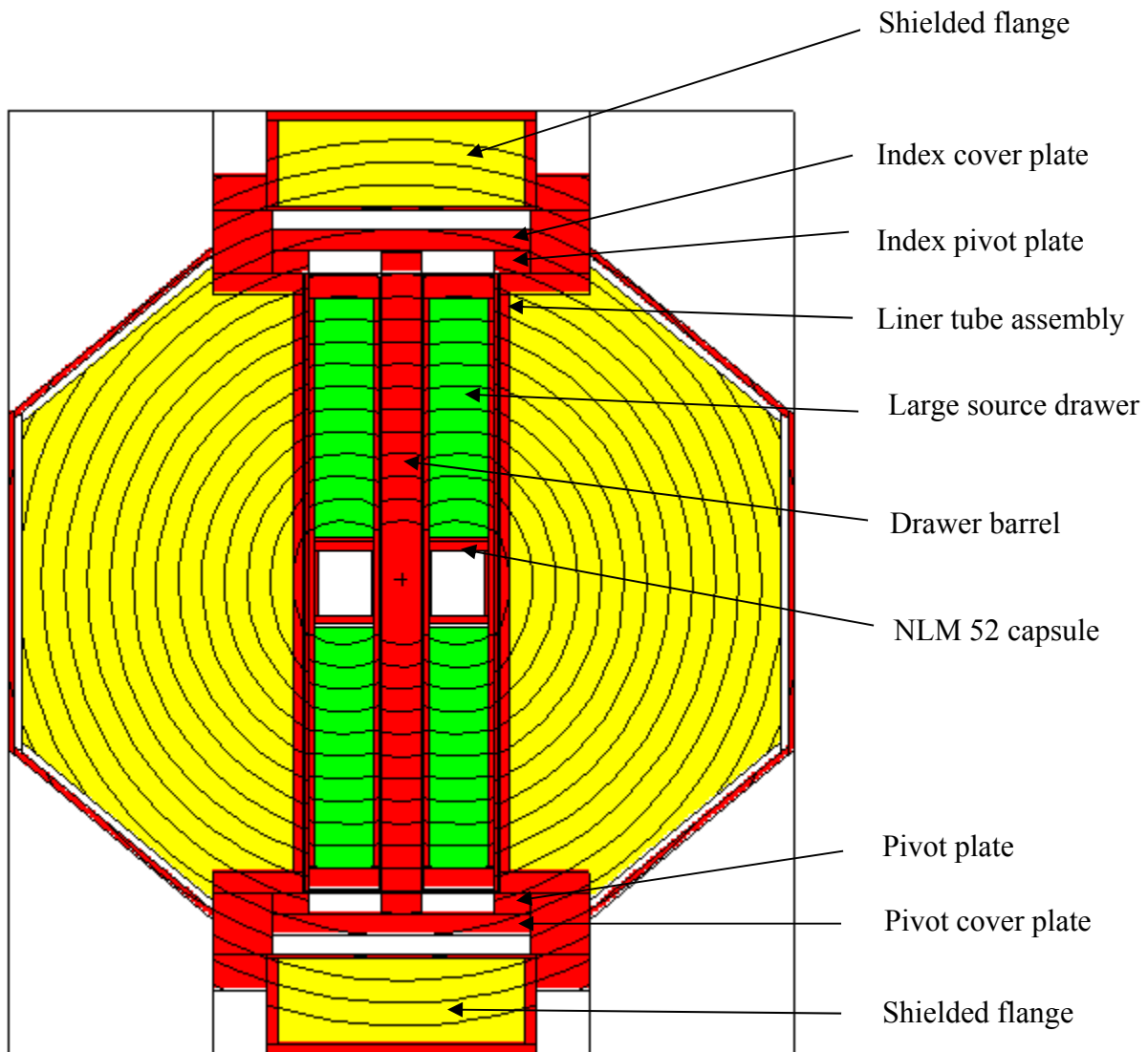


Figure 5.3-3 – LTSS with LD-74/NLM 52-74

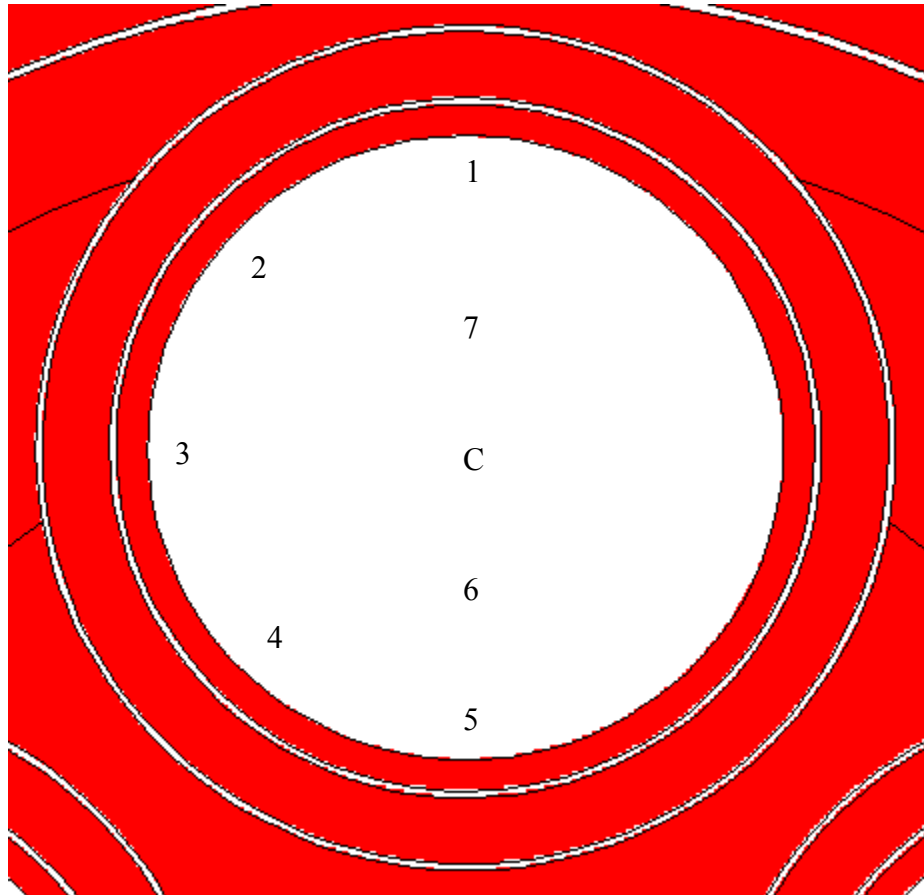


Figure 5.3-4 – Source Locations (x,y)

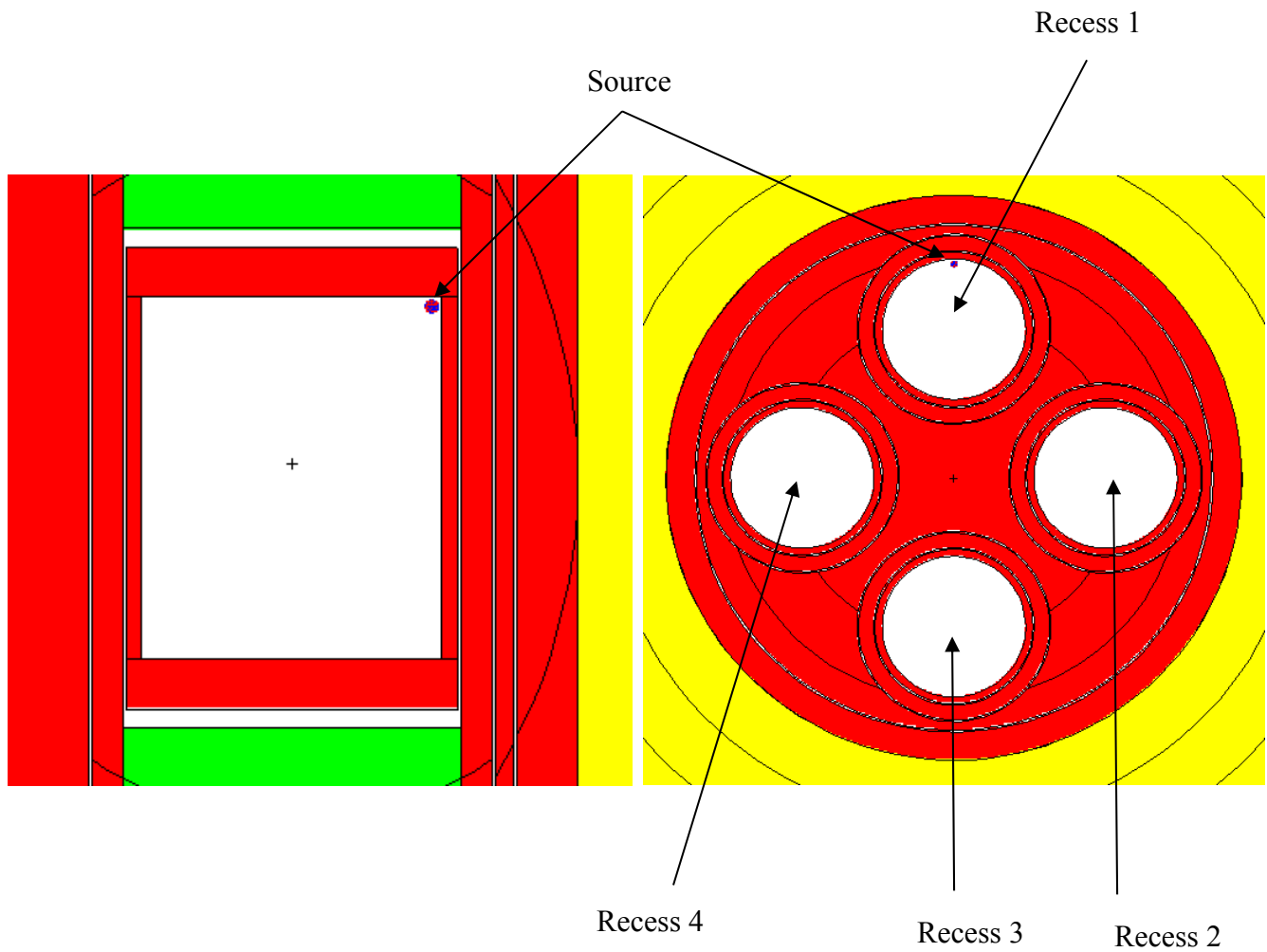


Figure 5.3-5 – Point Source in NLM 52-74 Capsule, Location 1, Top

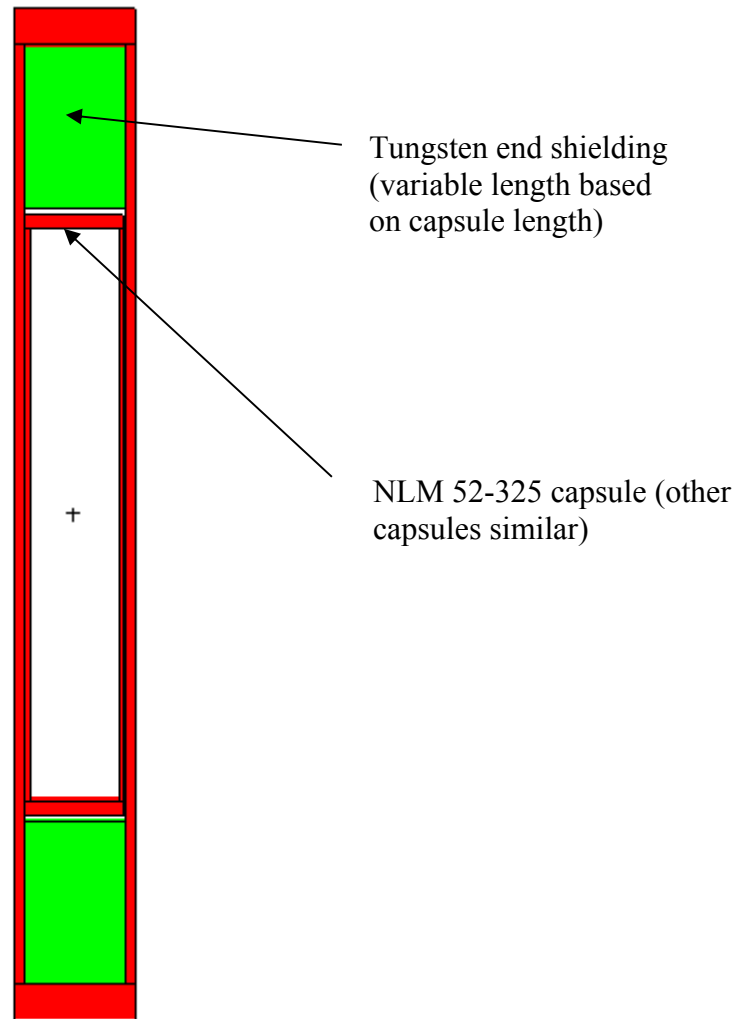
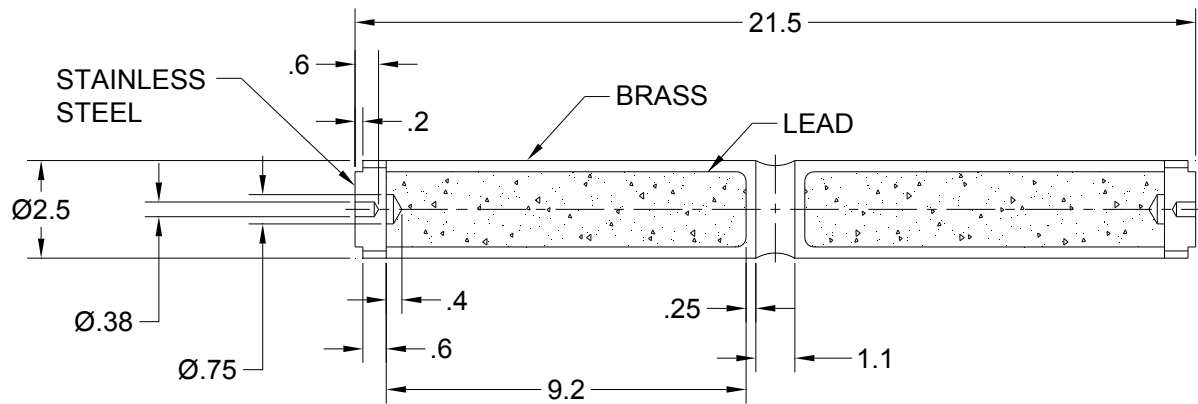


Figure 5.3-6 – Large Source Drawer with NLM 52-325 Capsule



Dimensions are in inches

Figure 5.3-7 – T80/T780 Drawer

5.4 Shielding Evaluation

5.4.1 Methods

MCNP5 v1.51 is used for the shielding analysis [2]. MCNP5 is a standard, well-accepted shielding program utilized to compute dose rates for shielding evaluations. A three-dimensional model is developed that captures all of the relevant design parameters of the 1105-SD package and contents. Dose rates are calculated by tallying the neutron and gamma fluxes over volumes of interest and converting these fluxes to dose rates.

In an actual LD shipping configuration, the LTSS may contain a different source isotope in each of the four recesses. For example, recess 1 could contain Co-60, recess 2 could contain Cs-137, recess 3 could contain Sr-90, and recess 4 could contain AmBe. Because an unlimited combination of sources and source activities within an LTSS is possible, it is not feasible to directly compute dose rates for all possible LTSS loading scenarios. Rather, a simplified approach is used in which each MCNP model is conservatively reduced to a single isotope in a single recess. The source is modeled with a strength of 1 Ci (or 1 g for the plutonium sources), and the dose rate is computed on the surface and 1 m from the surface of the 1105-SD.

Once the maximum dose rates from a 1 Ci source are known, the source activity is determined for each nuclide that results in dose rates near the regulatory limits. For non-exclusive use transportation, the dose rate is limited to 200 mrem/hr on the surface of the package and 10 mrem/hr at a distance of 1 m from the surface of the package. These limits are conservatively reduced to 190 mrem/hr and 9.5 mrem/hr at the surface and 1 m, respectively. The activities A_{surface} and $A_{1\text{m}}$ that result in dose rates near the regulatory limits are then:

$$A_{\text{surface}} = 190/D_{\text{max surface}}$$

$$A_{1\text{m}} = 9.5/D_{\text{max 1m}}$$

where $D_{\text{max surface}}$ is the maximum surface dose rate for a 1 Ci source, and $D_{\text{max 1m}}$ is the maximum 1 m dose rate for a 1 Ci source. The activity limit A_i for isotope i is then the lesser of A_{surface} and $A_{1\text{m}}$. For the 1105-SD, $A_{1\text{m}}$ always bounds A_{surface} . In many cases A_i violates heat load limits or administrative activity limits for the package. Therefore, the A_i value is simply a theoretical activity limit based *only* on shielding requirements.

A_i values are computed for each isotope in each of the allowed configurations of LD and source type, as defined in Table 5.3-3 and Table 5.3-4. Once the A_i values are known, the maximum possible dose rate for any arbitrary combination of nuclides in the LTSS may be determined by using a sum of fractions rule. Using a sum of fractions rule, the total dose rate may be estimated as the sum of the dose rate contribution from each individual source.

As a simple example, if $A_i = 5,000$ Ci results in a 1 m dose rate of 9.5 mrem/hr, then if 1,000 Ci of this isotope is present in each of the four recesses, the maximum total 1 m sum of fractions is $1000/5000 * 4 = 0.8$, or a dose rate of $(0.8)(9.5) = 7.6$ mrem/hr. *This 7.6 mrem/hr dose rate is conservative because the result is mathematically equivalent to placing all of the sources in the same LD, which is not possible.* In reality, each of the four sources would be in a different LD and a different recess, and the true maximum would be less than 7.6 mrem/hr at 1 m because the maximum dose rate from each source would not typically be at the same (x,y,z) location in space. Therefore, the sum of fractions method is inherently conservative.

The approach taken is to model each source isotope as a single point (or line, as applicable) in an LD. Also, models are developed with the sources in different locations within an NLM 52 to find the maximum dose rate, as the dose rate is sensitive to streaming effects for the gamma emitters. Mesh tallies are placed at the top, bottom, and side surfaces of the 1105-SD, as well as 1 m from these surfaces. Because the top surface of the 1105-SD is curved and the mesh tally is flat, the top surface mesh tally is placed as close to the top of the package as possible. The 1 m top tally is located 1 m from the axial center of the 9-in head (i.e., the axial center of the head is approximately 4.5-in below the top of the head) to bring this dose location closer to the package surface, as the 1 m top dose rate is often limiting. The bottom mesh tally is at the bottom surface of the impact limiter, and the 1 m bottom tally is located 1 m from this surface. The top and bottom mesh tallies are rectangular 32x32 grids, with mesh dimensions of 10 cm x 10 cm. Therefore, the top and bottom mesh tallies extend approximately 1 m from the side surface of the side thermal shield.

The side cylindrical mesh tally is located next to the side thermal shield. The dose rates beside the impact limiter surface are not tallied with a mesh because the dose rate will be lower here due to the larger distance from the source. The side surface mesh tally begins at the bottom of the side thermal shield and extends upward 140 cm axially in 10 cm increments. The mesh 1 m from the package side is located 0.95 m from the surface of the side thermal shield, and is conservatively brought 0.05 m closer to the package surface to account for potential non-concentricity of the package internals. The mesh tally 1 m from the side of the package begins 1 m below the bottom of the package and extends axially approximately 1 m above the top of the package in 10 cm increments. The side surface mesh tallies have 36 angular segments to capture the circumferential variation of the dose rate, since the dose rate is higher at the side of the package nearest where the source is placed.

For the neutron emitters, secondary gammas are not computed because there is no hydrogenous neutron shielding material that would lead to significant secondary gammas. The secondary gamma dose rate is at least two orders of magnitude less than the neutron dose rate, and this is demonstrated by comparing the neutron and secondary gamma dose rates for the RaCl_2 source. Also, the only neutron emitter that results in non-negligible primary gammas is Ra-226. The primary gammas for the other neutron emitters result in gamma dose rates many orders of magnitude below the neutron dose rate.

For the T80/T780 configuration, a similar approach is used, although the method is greatly simplified because there is only one type of drawer and only one source type (Co-60). Therefore, it is sufficient to develop only a single geometric model with the source in several locations within the drawer.

5.4.2 Input and Output Data

Sample ORIGEN-S and MCNP input files are provided in Appendix 5.5.2, *Sample Input Files for LTSS Evaluation*. A large number of input and output files are generated for this analysis due to the large number of configurations and sources.

Problem convergence is accelerated by dividing the LTSS into layers and splitting the particles as particles traverse outwardly through these layers. The Monte Carlo uncertainty associated with the limiting dose rate location is typically less than 5%. Ir-192 and Se-75 have rather poor statistics because the source energies are weak for the amount of shielding present, indicating

that there is essentially no dose rate from these isotopes. Therefore, the activity limits for Ir-192 and Se-75 are conservatively reduced by at least an order of magnitude from the calculated values.

5.4.3 Flux-to-Dose Rate Conversion

ANSI/ANS-6.1.1-1977 flux-to-dose rate conversion factors are used in this analysis. These are obtained from the MCNP User's Manual [2], Tables H.1 and H.2, although these values have been converted to provide results in mrem/hr rather than rem/hr. These conversion factors are provided in Table 5.4-1.

5.4.4 External Radiation Levels

NCT

NCT dose rates are computed at the surface and 1 m from the surface of the 1105-SD package for each of the sources listed in Table 5.2-1 and configurations listed in Table 5.3-3 and Table 5.3-4. Mesh tallies are used to determine the maximum dose rate for a unit source (1 Ci or 1 g), as described in Section 5.4.1, *Methods*.

In all cases, the 1 m dose rates are more limiting than the surface dose rates. Due to streaming effects, the gamma dose rate is sensitive to the location of the source within the LD. Therefore, cases are run with the source in several different locations within the LD to determine the limiting configuration. The A_i activity limit for each isotope, which is essentially the activity that results in a 1 m dose rate of 9.5 mrem/hr, is summarized in Table 5.4-6.

The limiting dose rate location for the gamma emitters is typically 1 m from the top of the package at an off-center location due to streaming through the steel structural members. The limiting dose rate location for the neutron emitters is 1 m from the side of the package next to the source because this is the shortest distance to the source. While the gamma emitter A_i values may change dramatically for the various LDs, the A_i values for the neutron emitters are relatively constant for the various LDs, as the LTSS contains no hydrogenous neutron shielding material.

Ir-192 and Se-75 result in essentially no dose rate due to the low gamma energies and large thickness of gamma shielding material. Therefore, the A_i values for Ir-192 and Se-75 are conservatively reduced by at least an order of magnitude from the computed values and are listed as constants in Table 5.4-6.

The T80/T780 analysis is performed only for a point source of Co-60 and is separate from the LD analysis presented above. The minimum $A_i = 39,339$ Ci for the T80/T780. This exceeds the Co-60 activity limit of the package of 12,970 Ci. Therefore, up to 12,970 Ci of Co-60 may be transported per 1105-SD and may be divided in any manner between the four T80/T780 drawers.

HAC

Drop testing, discussed in Section 2.12.3, *Certification Test Report*, showed negligible damage to the LTSS, LTSS lodgment, and 1105-SD package. Therefore, there is essentially no difference between the NCT and HAC shielding configurations. Because the methodology is developed to result in a 1 m dose rate of 9.5 mrem/hr, the HAC dose rate at 1 m will not exceed 9.5 mrem/hr. This is significantly less than the limit of 1000 mrem/hr.

5.4.5 LTSS Loading Methodology

The following is a concise summary of how to apply the results of this shielding evaluation when loading an LTSS. There are two allowable contents for the LTSS. Content 1 utilizes the T80/T780 source drawer and a Co-60 source. Content 2 utilizes the standard source drawer and the nuclides listed in Table 5.4-2. This summary is also provided in Chapter 7.0, *Package Operations*.

Limits for Content 1: The T80/T780 source drawer may contain up to the Table 5.4-2 limit of Co-60 (i.e., 12,970 Ci) in one to four drawers in any distribution. T80/T780 source drawers (Content 1) may not be mixed with large source drawers (Content 2) within the LTSS. Any of the four recesses in the LTSS that is not loaded with a T80/T780 drawer must be loaded with a shield drawer.

Limits for Content 2: There are seven steps in qualifying Content 2 for the LTSS.

1. **Basic Radionuclide Limits.** Verify that the total activity of each isotope to be transported in the LTSS does not exceed the basic radionuclide limits given in Table 5.4-2 or the limits specified in the special form capsule certificate, ZA/NLM52/S, or other special form capsules, if used.
2. **Fissile Mass Limit.** Verify that the total fissile mass within the LTSS does not exceed 15g. The fissile mass is equal to:

$$\text{Fissile mass (g)} = A + 0.2 \times B + 0.001 \times C$$

where:

A equals the total grams of plutonium in all Pu-239 sources

B equals the total grams of plutonium in all Pu-238 sources

C equals the curies of americium in all Am-241 sources

3. **Plutonium By Air Exclusion.** NO PLUTONIUM OR AMERICIUM SOURCES ARE PERMITTED FOR SHIPMENT OF THE 1105-SD BY AIR.
4. **Decay Heat Limit.** Verify that the total heat load is less than or equal to 200 watts. If only a single isotope is to be shipped in the LTSS, this is ensured by step 1 above. If multiple isotopes are to be transported, the total watts shall be calculated by multiplying the activity of each isotope by the heat generation rate found in Table 5.4-3.
5. **Physical Form Restrictions.** Verify that the source physical form and isotope comply with the requirements delineated in Table 5.4-4.
6. **Drawer Configuration Restrictions.** Verify that the drawer configuration to be transported is allowed per Table 5.4-5. NOTE: Any recesses in the LTSS that are not needed to carry sources must be given a shield drawer.
7. **Dose Rate Limits.** Verify the selected loading does not violate the dose rate limits using the following equation:

$$\sum_{i=1}^n \frac{S_i}{A_i} \leq 1 \quad (\leq 0.3 \text{ for commercial aircraft transport})$$

where:

S_i is the activity of each source in Ci (g Pu for Pu sources)

A_i is the appropriate value from Table 5.4-6 for each drawer for the configuration used (A – E, AB, BC, BD)

NOTE: ONLY ONE NUCLIDE TYPE MAY BE PLACED IN A SINGLE CAPSULE.

Examples are provided below.

Example 1:

Recess 1: LD-74 with 7,000 Ci Cs-137, point source

Recess 2: LD-74 with 5,000 Ci Cs-137, point source

Recess 3: LD-74 with 2,000 Ci Co-60, point source

Recess 4: LD-74 with 3,000 Ci Co-60, point source

Step 1: The total Cs-137 (12,000 Ci) and Co-60 (5,000 Ci) are less than the limits in Table 5.4-2.

Step 2: No plutonium or americium, does not apply.

Step 3: No plutonium or americium, air transport allowed.

Step 4: The total power is 138 watts \leq 200 watts based on Table 5.4-3.

Step 5: Physical form restrictions in Table 5.4-4 are met.

Step 6: The drawer configuration is consistent with Configuration A in Table 5.4-5.

Step 7: Table 5.4-6 Configuration A limits apply. The sum of fractions = $0.15 \leq 1.0$.

Therefore, this shipment is allowed by air (including commercial aircraft), land, or sea transport.

Example 2:

Recess 1: LD-150 with two NLM52-74 capsules. The first capsule has 1,000 Ci Co-60 and the second capsule has 1,000 Ci Sr-90

Recess 2: LD-150 with 5,000 Ci Cs-137, line source

Recess 3: LD-150 with 2,000 Ci Co-60, point source

Recess 4: LD-150 with 2 Ci AmBe

Step 1: The total Cs-137 (5,000 Ci), Co-60 (3,000 Ci), Sr-90 (1,000 Ci) and AmBe (2 Ci) are less than or equal to the limits in Table 5.4-2.

Step 2: Fissile mass = $0.001 * 2 = 0.002$ g \leq 15 g.

Step 3: Contains americium, air transport not allowed.

Step 4: The total power is 78 watts \leq 200 watts based on Table 5.4-3.

Step 5: Physical form restrictions in Table 5.4-4 are met.

Step 6: The drawer configuration is consistent with Configuration B in Table 5.4-5.

Step 7: Table 5.4-6 Configuration B limits apply. The sum of fractions = $0.83 \leq 1.0$.

Therefore, this shipment is allowed by land or water transport.

Example 3:

Recess 1: LD-74 with 15 g Pu in a Pu-238O₂ source

Recess 2: LD-74 with 15 g Pu in a Pu-238O₂ source

Recess 3: LD-74 with 2 g Pu in a Pu-239O₂ source

Recess 4: LD-74 with 2 g Pu in a Pu-239Be source

Step 1: The total Pu in the Pu-238 source (30 g) and total Pu in the Pu-239 source (4 g) are less than the limits in Table 5.4-2.

Step 2: The total fissile material in the package is $30 \text{ g} \times 0.2 + 4 \text{ g} = 10 \text{ g} \leq 15 \text{ g}$.

Step 3: Due to the presence of plutonium, air transport is not permitted.

Step 4: The total power is 17 watts \leq 200 watts based on Table 5.4-3.

Step 5: Physical form restrictions in Table 5.4-4 are met.

Step 6: The drawer configuration is consistent with Configuration A in Table 5.4-5.

Step 7: Table 5.4-6 Configuration A limits apply. The sum of fractions = $0.04 \leq 1.0$.

Therefore, this shipment is allowed by land or water transport.

Example 4:

Recess 1: LD-74 with 14,000 Ci Cs-137 point source

Recess 2: LD-150 with 5,000 Ci Co-60 line source

Recess 3: LD-150 with 1 Ci RaBe source

Recess 4: LD-150 with 2 Ci AmBe source

Step 1: The totals for each isotope are less than or equal to the limits in Table 5.4-2.

Step 2: Fissile mass = $0.001 \times 2 = 0.002 \text{ g} \leq 15 \text{ g}$.

Step 3: Contains americium, air transport not allowed.

Step 4: The total power is 148 watts \leq 200 watts based on Table 5.4-3.

Step 5: Physical form restrictions in Table 5.4-4 are met.

Step 6: The drawer configuration is consistent with Configuration AB in Table 5.4-5.

Step 7: Table 5.4-6 Configuration AB limits apply. The sum of fractions = $1.5 > 1.0$. Therefore, this shipment is **not** allowed.

This shipment is not allowed due to violation of the dose rate limit (Step 7).

Table 5.4-1 – Flux-to-Dose Rate Conversion Factors

E (MeV)	Neutron Factors (mrem/hr)/(n/cm²/s)	E (MeV)	Neutron Factors (mrem/hr)/(n/cm²/s)
2.50E-08	3.67E-03	0.5	9.26E-02
1.00E-07	3.67E-03	1.0	1.32E-01
1.00E-06	4.46E-03	2.5	1.25E-01
1.00E-05	4.54E-03	5.0	1.56E-01
1.00E-04	4.18E-03	7.0	1.47E-01
0.001	3.76E-03	10.0	1.47E-01
0.01	3.56E-03	14.0	2.08E-01
0.1	2.17E-02	20.0	2.27E-01
E (MeV)	Gamma Factors (mrem/hr)/(γ/cm²/s)	E (MeV)	Gamma Factors (mrem/hr)/(γ/cm²/s)
0.01	3.96E-03	1.4	2.51E-03
0.03	5.82E-04	1.8	2.99E-03
0.05	2.90E-04	2.2	3.42E-03
0.07	2.58E-04	2.6	3.82E-03
0.1	2.83E-04	2.8	4.01E-03
0.15	3.79E-04	3.25	4.41E-03
0.2	5.01E-04	3.75	4.83E-03
0.25	6.31E-04	4.25	5.23E-03
0.3	7.59E-04	4.75	5.60E-03
0.35	8.78E-04	5.0	5.80E-03
0.4	9.85E-04	5.25	6.01E-03
0.45	1.08E-03	5.75	6.37E-03
0.5	1.17E-03	6.25	6.74E-03
0.55	1.27E-03	6.75	7.11E-03
0.6	1.36E-03	7.5	7.66E-03
0.65	1.44E-03	9.0	8.77E-03
0.7	1.52E-03	11.0	1.03E-02
0.8	1.68E-03	13.0	1.18E-02
1.0	1.98E-03	15.0	1.33E-02

Table 5.4-2 – Basic 1105-SD Limits

Source	Maximum Quantity per 1105-SD
Co-60	12,970 Ci
Cs-137	14,000 Ci
Sr-90	1,000 Ci
Ra-226 (excluding Ra-226Be)①	20 Ci
Ra-226Be①	1.3 Ci
Am-241 (excluding Am-241Be)②	1000 Ci
Am-241Be②	6.6 Ci
Pu-238 (excluding Pu-238Be)③	75 g Pu
Pu-239 or Pu-239Be③	15 g Pu
Ir-192	200 Ci
Se-75	80 Ci

①Impurities may include oxygen, carbon, sulfur, bromine, and chlorine (hydrous or anhydrous).

②Impurities may include oxygen and chlorine.

③Impurities may include oxygen. The total fissile mass limit for the 1105-SD is 15 g.

Table 5.4-3 – Watts per Source Unit

Isotope	watts/unit
Co-60	1.5420E-02 watts/Ci
Cs-137①	5.0400E-03 watts/Ci
Sr-90②	6.6980E-03 watts/Ci
Ra-226③	1.8620E-01 watts/Ci
Am-241	3.3370E-02 watts/Ci
Pu-238	5.6773E-01 watts/g
Pu-239	3.0873E-03 watts/g
Ir-192	6.1500E-03 watts/Ci
Se-75	2.4100E-03 watts/Ci

①Includes Ba-137m.

②Includes Y-90.

③Includes decay products.

Table 5.4-4 – Authorized Payload Special Form Capsule Sources and Nuclides

Drawer Model	Special Form Capsule Model	Authorized Source Geometry and Dimensions	Authorized Nuclides
LD-74	NLM 52-74	Point source	All nuclides in Table 5.4-2
LD-150	NLM 52-150	Point source	All nuclides in Table 5.4-2
		Line source, length ≥ 60 mm	Co-60 and Cs-137
LD-150	Two (2) NLM 52-74s	Point source	All nuclides in Table 5.4-2
LD-200	NLM 52-200	Point source	All nuclides in Table 5.4-2
		Line source, length ≥ 136 mm	Co-60 and Cs-137
LD-250	NLM 52-250	Line source, length ≥ 186 mm	Co-60 and Cs-137
LD-325	NLM 52-325	Line source, length ≥ 236 mm	Co-60 and Cs-137

Table 5.4-5 – Allowable Drawer Configurations

Configuration^①	Recess 1	Recess 2	Recess 3	Recess 4
A	LD-74	LD-74	LD-74	LD-74
B	LD-150	LD-150	LD-150	LD-150
C	LD-200	LD-200	LD-200	LD-200
D	LD-250	LD-250	LD-250	LD-250
E	LD-325	LD-325	LD-325	LD-325
AB	LD-74	LD-150	LD-150	LD-150
BC	LD-150	LD-150	LD-200	LD-200
BD	LD-250	LD-150	LD-150	LD-150

①Any number of LDs may be replaced with a shield drawer.

Table 5.4-6 – A_i Activity Limits

	Cfg. A	Cfg. B	Cfg. C	Cfg. D	Cfg. E
Isotope	LD-74	LD-150	LD-200	LD-250	LD-325
Co-60 point (Ci)	34400	5800	1800	NA	NA
Co-60 line (Ci)	NA	11800	6500	2600	530
Cs-137 point (Ci)	3.50E+07	3.30E+06	6.40E+05	NA	NA
Cs-137 line (Ci)	NA	8.50E+06	3.90E+06	9.80E+05	1.00E+05
Sr-90 (Ci)	1.60E+07	3.20E+06	1.00E+06	NA	NA
Am-241 (no Be) (Ci)	14800	14200	14200	NA	NA
Am-241Be (Ci)	6.6	6.5	6.4	NA	NA
Ra-226 (no Be) (Ci)	720	680	530	NA	NA
Ra-226Be (Ci)	1.3	1.3	1.3	NA	NA
Pu-238 (no Be) (g Pu)	1300	1300	1300	NA	NA
Pu-239 (no Be) (g Pu)	1.60E+05	1.60E+05	1.50E+05	NA	NA
Pu-239Be (g Pu)	120	120	120	NA	NA
Ir-192 (Ci)	1.00E+05	1.00E+05	1.00E+05	NA	NA
Se-75 (Ci)	1.00E+05	1.00E+05	1.00E+05	NA	NA

	Cfg. AB		Cfg. BC		Cfg. BD	
Isotope	LD-74	LD-150	LD-150	LD-200	LD-150	LD-250
Co-60 point (Ci)	32700	Use Cfg. B Limits	5600	Use Cfg. C Limits	5600	Use Cfg. D Limits
Co-60 line (Ci)	NA		11800		10300	
Cs-137 point (Ci)	3.30E+07		3.30E+06		3.20E+06	
Cs-137 line (Ci)	NA		7.40E+06		6.90E+06	
Sr-90 (Ci)	1.60E+07		3.20E+06		3.10E+06	
Am-241 (no Be) (Ci)	14600		14100		14100	
Am-241Be (Ci)	6.6		6.4		6.4	
Ra-226 (no Be) (Ci)	720		680		680	
Ra-226Be (Ci)	1.3		1.3		1.3	
Pu-238 (no Be) (g Pu)	1200		1300		1300	
Pu-239 (no Be) (g Pu)	1.60E+05		1.60E+05		1.60E+05	
Pu-239Be (g Pu)	120		120		120	
Ir-192 (Ci)	1.00E+05		1.00E+05		1.00E+05	
Se-75 (Ci)	1.00E+05		1.00E+05		1.00E+05	

5.5 Appendices

5.5.1 References

5.5.2 Sample Input Files for LTSS Evaluation

5.5.3 Shielded Device Evaluation

5.5.1 References

1. Glenn F. Knoll, *Radiation Detection and Measurement*, Second Edition, John Wiley & Sons, 1989.
2. LA-UR-03-1987, *MCNP – A General Monte Carlo N-Particle Transport Code, Version 5*, Los Alamos National Laboratory, April 24, 2003 (Revised 2/1/2008).
3. *SCALE: A Modular Code System for Performing Standardized Computer Analyses for Licensing Evaluations*, ORNL/TM-2005/39, Version 6, Vols. I-III, January 2009.
4. SCALE4.4, *Modular Code System for Performing Standardized Computer Analyses for Licensing Evaluation for Workstations and Personal Computers*, Oak Ridge National Laboratory, September 1998.
5. *Radiological Characterization of Actinide Sealed Source Waste for Disposal at WIPP*, Los Alamos National Laboratory, 2005.
6. LA-UR-09-06701, *Radionuclide Distribution in Plutonium-239 Material Used for Sealed Source Production*, Los Alamos National Laboratory.
7. PNNL-15870, Rev. 1, *Compendium of Material Composition Data for Radiation Transport Modeling*.

5.5.2 Sample Input Files for LTSS Evaluation

Sample ORIGEN-S input file for AmBe neutron source:

```
'This SCALE input file was generated by
'OrigenArp Version 5.1.01 March 22, 2007
#origens
0$$$ a11 71 e t
Decay Case
3$$$ 21 1 1 27 a16 2 a33 18 e t
35$$$ 0 t
54$$$ a8 1 a11 2 e
56$$$ a2 7 a10 0 a13 2 a15 3 a17 2 e
57** 0 a3 1e-05 e
95$$$ 0 t
Case 1
0 MTU
60** 0.1 0.3 1 3 10 30 100
61** f0.05
65$$$
'Gram-Atoms      Grams      Curies      Watts-All      Watts-Gamma
3z  1  0  0  1 0 0  1 0 0  3z  6z
3z  1  0  0  1 0 0  1 0 0  3z  6z
3z  1  0  0  1 0 0  1 0 0  3z  6z
81$$$ 2 0 26 1 a7 200 e
82$$$ 2 2 2 2 2 2 2 e
83**
1.0000000e+07 8.0000000e+06 6.5000000e+06 5.0000000e+06 4.0000000e+06
3.0000000e+06 2.5000000e+06 2.0000000e+06 1.6000000e+06 1.3300000e+06
1.0000000e+06 8.0000000e+05 6.0000000e+05 4.0000000e+05 3.0000000e+05
2.0000000e+05 1.0000000e+05 5.0000000e+04 1.0000000e+04 e
84**
2.0000000e+07 6.3763000e+06 3.0119000e+06 1.8268000e+06
1.4227000e+06 9.0718000e+05 4.0762000e+05 1.1109000e+05 1.5034000e+04
3.0354000e+03 5.8295000e+02 1.0130000e+02 2.9023000e+01 1.0677000e+01
3.0590000e+00 1.8554000e+00 1.3000000e+00 1.1253000e+00 1.0000000e+00
8.0000000e-01 4.1399000e-01 3.2500000e-01 2.2500000e-01 1.0000000e-01
5.0000000e-02 3.0000000e-02 1.0000000e-02 1.0000000e-05 e
73$$$ 952410 40000
74** 291.5 3e5
75$$$ 2 4
t
56$$$ f0 t
end
```

Sample MCNP input file for LTSS evaluation, Co-60 point source, LD-074:

```
LANL-B
c
c      LANL-B Package
c
10      1 -7.94  10 -11 -35      imp:p=1.5e7 $ base sheet
11      1 -7.94  (60 -61 31 -35):(34 -35 11 -61) imp:p=1.5e7 $ cone sheet
12      0      -50 -12      imp:p=1.5e7 $ inside head
13      1 -7.94  50 -51 -12      imp:p=1.5e7 $ lower head
14      1 -7.94  30 -31 12 -17      imp:p=5.8e6 $ shell
15      5 -2.7   12 -13 -30      imp:p=1.5e7 $ bottom
```

```

16      2 -0.224 11 -12 51 -33      imp:p=1.5e7 $ foam
17      2 -0.224 31 -33 12 -60      imp:p=1.5e7 $ foam
18      2 -0.224 33 -34 11 -60      imp:p=1.5e7 $ foam
19      5 -2.7   16 -17 -30          imp:p=1.5e7 $ top plate
20      0          13 -16 -30 fill=3(0 0 97.014) imp:p=1 $ cavity
21      1 -7.94 61 -16 31 -32      imp:p=5.8e6 $ thermal shields
22      1 -7.94 52 -53 17          imp:p=1.5e7 $ top head
23      0          17 -52          imp:p=1 $ inside top
24      0          32 -35 61 -16    imp:p=1 $ side air
25      0          16 -17 31 -35    imp:p=1 $ side air sliver
26      0          17 -18 53 -35    imp:p=1 $ top air
27      0          (-10:18:35) 70 -71 -72      imp:p=1 $ 1m
28      0          (-70:71:72) 73 -74 -75      imp:p=1 $ 2m
99      0          -73:74:75        imp:p=0

c
c      Universe 1: Large Source Drawer
c
100     0          102 -103 -110      fill=2      u=1 imp:p=1 $ cavity
101     0          101 -102 -110      fill=6      u=1 imp:p=1 $ bottom W
102     0          103 -104 -110      fill=6      u=1 imp:p=1 $ top W
104     1 -7.94 100 -101 -111      fill=5      u=1 imp:p=1 $ bottom cap
105     1 -7.94 104 -105 -111      fill=5      u=1 imp:p=1 $ top cap
106     1 -7.94 101 -104 110 -111    fill=5      u=1 imp:p=1 $ cladding
107     0          -100:105:111      u=1 imp:p=1

c
c      Universe 2: NLM 52
c
200     0          201 -202 -210      u=2 imp:p=1 $ cavity
201     1 -7.94 201 -202 210 -211    fill=5      u=2 imp:p=1 $ cladding
202     1 -7.94 200 -201 -211      fill=5      u=2 imp:p=1 $ end cap
204     1 -7.94 202 -203 -211      fill=5      u=2 imp:p=1 $ end cap
205     0          -200:203:211      u=2 imp:p=1

c
c      Universe 3: LTSS
c
300     1 -7.94 300 -301 -302 303 304 305 306 fill=5 u=3 imp:p=1
301     0          300 -301 -303 fill=1(1)      u=3 imp:p=1 $ top drawer
302     0          300 -301 -304 fill=1(2)      u=3 imp:p=1 $ left drawer
303     0          300 -301 -305 fill=1(3)      u=3 imp:p=1 $ bottom drawer
304     0          300 -301 -306 fill=1(4)      u=3 imp:p=1 $ right drawer

c
305     0          (-300:301:302) 322 -325 -330 u=3 imp:p=1 $ gap to liner
306     1 -7.94 323 -324 330 -331 fill=5      u=3 imp:p=1 $ liner tube
307     1 -7.94 330 -333 322 -323 fill=5      u=3 imp:p=1 $ bottom liner
308     1 -7.94 332 -333 320 -322 fill=5      u=3 imp:p=1 $ bottom liner
309     1 -7.94 321 -322 -332 303 304 305 306 fill=5 u=3 imp:p=1 $ bottom
pivot
310     0          321 -322 -303      u=3 imp:p=1 $ bottom pivot
311     0          321 -322 -304      u=3 imp:p=1 $ bottom pivot
312     0          321 -322 -305      u=3 imp:p=1 $ bottom pivot
313     0          321 -322 -306      u=3 imp:p=1 $ bottom pivot
314     1 -7.94 328 -321 -332      fill=5      u=3 imp:p=1 $ bottom extra
315     0          320 -328 -332      u=3 imp:p=1 $ bottom air
316     1 -7.94 330 -333 324 -325 fill=5      u=3 imp:p=1 $ top liner
317     1 -7.94 332 -333 325 -327 fill=5      u=3 imp:p=1 $ top liner
318     1 -7.94 325 -326 -332 303 304 305 306 fill=5 u=3 imp:p=1 $ top pivot

```

1105-SD Package Safety Analysis Report

Docket No. 71-9379

Rev. 0, August 2018

319	0	325 -326 -303		u=3 imp:p=1 \$ top pivot
hole				
320	0	325 -326 -304		u=3 imp:p=1 \$ top pivot
hole				
321	0	325 -326 -305		u=3 imp:p=1 \$ top pivot
hole				
322	0	325 -326 -306		u=3 imp:p=1 \$ top pivot
hole				
323	1 -7.94	326 -329 -332	fill=5	u=3 imp:p=1 \$ top extra
324	0	329 -327 -332		u=3 imp:p=1 \$ top air
c				
330	1 -7.94	343 -320 -335	fill=5	u=3 imp:p=1 \$ bottom end
331	3 -11.35	341 -343 -334	fill=4	u=3 imp:p=1 \$ bottom end
332	1 -7.94	340 -341 -335	fill=5	u=3 imp:p=1 \$ bottom end
333	1 -7.94	341 -343 334 -335	fill=5	u=3 imp:p=1 \$ bottom end
334	1 -7.94	342 -320 335 -333	fill=5	u=3 imp:p=1 \$ bottom end
335	0	340 -342 335 -333		u=3 imp:p=1 \$ bottom end
336	1 -7.94	327 -344 -335	fill=5	u=3 imp:p=1 \$ top end
shield				
337	3 -11.35	344 -346 -334	fill=4	u=3 imp:p=1 \$ top end
shield				
338	1 -7.94	346 -347 -335	fill=5	u=3 imp:p=1 \$ top end
shield				
339	1 -7.94	344 -346 334 -335	fill=5	u=3 imp:p=1 \$ top end
shield				
340	1 -7.94	327 -345 335 -333	fill=5	u=3 imp:p=1 \$ top end
shield				
341	0	345 -347 335 -333		u=3 imp:p=1 \$ top end
c				
350	3 -11.35	(333 -354 -361 362 -363 -364):		
		(323 -324 331 -333) fill=4		u=3 imp:p=1 \$ side lead
351	0	354 -353 -355 -356 359 -360		u=3 imp:p=1 \$ side gap
352	0	333 -354 -355 359 361		u=3 imp:p=1 \$ bottom gap
353	0	333 -354 -356 -360 363		u=3 imp:p=1 \$ bottom gap
354	1 -7.94	333 -353 356 -351 -358	fill=5	u=3 imp:p=1 \$ side steel
top				
355	1 -7.94	353 -352 -350 -351 357 -358	fill=5	u=3 imp:p=1 \$ side steel
356	1 -7.94	333 -353 -350 355 357	fill=5	u=3 imp:p=1 \$ side steel
c				
360	0	-340:347:352		u=3 imp:p=1
361	0	333 -352 351 -347		u=3 imp:p=1
362	0	333 -352 350 340		u=3 imp:p=1
c				
c		Universe 4: Splitting universe for lead		
c				
400	3 -11.35	-400	u=4 imp:p=1	
401	3 -11.35	400 -401	u=4 imp:p=2.5	
402	3 -11.35	401 -402	u=4 imp:p=6.3	
403	3 -11.35	402 -403	u=4 imp:p=15.6	
404	3 -11.35	403 -404	u=4 imp:p=39.1	
405	3 -11.35	404 -405	u=4 imp:p=97.7	
406	3 -11.35	405 -406	u=4 imp:p=244	
407	3 -11.35	406 -407	u=4 imp:p=610	
408	3 -11.35	407 -408	u=4 imp:p=1525	
409	3 -11.35	408 -409	u=4 imp:p=3815	
410	3 -11.35	409 -410	u=4 imp:p=9537	
411	3 -11.35	410 -411	u=4 imp:p=2.4e4	

```

412  3 -11.35  411 -412 u=4 imp:p=6.0e4
413  3 -11.35  412 -413 u=4 imp:p=1.5e5
414  3 -11.35  413 -414 u=4 imp:p=3.7e5
415  3 -11.35  414 -415 u=4 imp:p=9.3e5
416  3 -11.35  415 -416 u=4 imp:p=2.3e6
417  3 -11.35  416 -417 u=4 imp:p=5.8e6
418  3 -11.35  417      u=4 imp:p=1.5e7

```

c

c Universe 5: Splitting universe for steel

c

```

500  1 -7.94  -400      u=5 imp:p=1
501  1 -7.94  400 -401 u=5 imp:p=2.5
502  1 -7.94  401 -402 u=5 imp:p=6.3
503  1 -7.94  402 -403 u=5 imp:p=15.6
504  1 -7.94  403 -404 u=5 imp:p=39.1
505  1 -7.94  404 -405 u=5 imp:p=97.7
506  1 -7.94  405 -406 u=5 imp:p=244
507  1 -7.94  406 -407 u=5 imp:p=610
508  1 -7.94  407 -408 u=5 imp:p=1525
509  1 -7.94  408 -409 u=5 imp:p=3815
510  1 -7.94  409 -410 u=5 imp:p=9537
511  1 -7.94  410 -411 u=5 imp:p=2.4e4
512  1 -7.94  411 -412 u=5 imp:p=6.0e4
513  1 -7.94  412 -413 u=5 imp:p=1.5e5
514  1 -7.94  413 -414 u=5 imp:p=3.7e5
515  1 -7.94  414 -415 u=5 imp:p=9.3e5
516  1 -7.94  415 -416 u=5 imp:p=2.3e6
517  1 -7.94  416 -417 u=5 imp:p=5.8e6
518  1 -7.94  417      u=5 imp:p=1.5e7

```

c

c Universe 6: Splitting universe for tungsten

c

```

600  4 -17.0  -400      u=6 imp:p=1
601  4 -17.0  400 -401 u=6 imp:p=2.5
602  4 -17.0  401 -402 u=6 imp:p=6.3
603  4 -17.0  402 -403 u=6 imp:p=15.6
604  4 -17.0  403 -404 u=6 imp:p=39.1
605  4 -17.0  404 -405 u=6 imp:p=97.7
606  4 -17.0  405 -406 u=6 imp:p=244
607  4 -17.0  406 -407 u=6 imp:p=610
608  4 -17.0  407 -408 u=6 imp:p=1525
609  4 -17.0  408 -409 u=6 imp:p=3815
610  4 -17.0  409 -410 u=6 imp:p=9537
611  4 -17.0  410 -411 u=6 imp:p=2.4e4
612  4 -17.0  411 -412 u=6 imp:p=6.0e4
613  4 -17.0  412 -413 u=6 imp:p=1.5e5
614  4 -17.0  413 -414 u=6 imp:p=3.7e5
615  4 -17.0  414 -415 u=6 imp:p=9.3e5
616  4 -17.0  415 -416 u=6 imp:p=2.3e6
617  4 -17.0  416 -417 u=6 imp:p=5.8e6
618  4 -17.0  417      u=6 imp:p=1.5e7

```

c

c Package

c

```

10  pz  0          $ bottom of package
11  pz  0.635      $ bottom plate

```


1105-SD Package Safety Analysis Report

```

12 pz 32.004 $ bottom of inner support
13 pz 33.274 $ bottom of cavity
16 pz 183.106 $ top of cavity
17 pz 184.376 $ top of top plate
18 pz 207.3 $ top of model
30 cz 55.245 $ shell inner
31 cz 56.515 $ shell outer
32 cz 56.9341 $ outer thermal shields
33 cz 66.04 $ foam interface
34 cz 88.265 $ base sheet inner
35 cz 88.9 $ base sheet outer
50 ell 0 0 32.004 0 0 21.59 -55.245 $ lower head inner
51 ell 0 0 32.004 0 0 22.86 -56.515 $ lower head outer
52 ell 0 0 184.376 0 0 21.59 -55.245 $ upper head inner
53 ell 0 0 184.376 0 0 22.86 -56.515 $ upper head outer
60 kz 103.0298 3.0 -1
61 kz 103.7630 3.0 -1
70 pz -100 $ bottom 1m
71 pz 295.8 $ top 1m (measured from the axial middle of the head)
72 cz 156.9341 $ side 1m
73 pz -200 $ bottom of model
74 pz 410 $ top of model
75 cz 256 $ side of model
c
c Large Source Drawer
c
100 pz -27.4 $ bottom of drawer
101 pz -25.4 $ bottom of lower tungsten
102 pz -4.0 $ top of lower tungsten
103 pz 4.0 $ bottom of upper tungsten
104 pz 25.4 $ top of upper tungsten
105 pz 27.4 $ top of drawer
110 cz 2.65 $ IR
111 cz 3.15 $ OR
c
c NLM 52
c
200 pz -3.7 $ bottom
201 pz -2.9 $ bottom cap
202 pz 2.9 $ top cap
203 pz 3.7 $ top
210 cz 2.365 $ IR
211 cz 2.6 $ OR
c
c LTSS
c
300 pz -27.575 $ bottom of drawer barrel
301 pz 27.575 $ top of drawer barrel
302 cz 8.4875 $ outer surface of drawer barrel
303 c/z 0 5.0 3.2 $ drawer 1
304 c/z -5.0 0 3.2 $ drawer 2
305 c/z 0 -5.0 3.2 $ drawer 3
306 c/z 5.0 0 3.2 $ drawer 4
320 pz -33.15 $ liner tube assembly bottom
321 pz -29.65 $ pivot flange
322 pz -27.65 $ liner tube assembly recess
323 pz -25.75 $ liner tube assembly

```

1105-SD Package Safety Analysis Report

324 pz 25.75 \$ liner tube assembly
325 pz 27.65 \$ liner tube assembly recess
326 pz 29.65 \$ pivot flange
327 pz 33.15 \$ liner tube assembly top
328 pz -31.45 \$ extra bottom plate
329 pz 31.45 \$ extra top plate
330 cz 8.55 \$ liner tube IR
331 cz 9.5 \$ liner tube OR
332 cz 11.25 \$ recess IR
333 cz 16.5 \$ liner tube assembly OR
334 cz 10.8 \$ end shield lead
335 cz 11.75 \$ end shield OR
340 pz -42.15 \$ bottom end shield
341 pz -41.15 \$ bottom end shield
342 pz -36.35 \$ bottom end flange
343 pz -33.55 \$ bottom end
344 pz 33.55 \$ top end
345 pz 36.35 \$ top end flange
346 pz 41.15 \$ top end shield
347 pz 42.15 \$ top end shield
350 kz -43.8489 1.4203 \$ bottom shell outer
351 kz 43.8489 1.4203 \$ top shell outer
352 cz 34.5 \$ side shell outer
353 cz 33.9 \$ side shell inner
354 cz 33.2 \$ gap in lead
355 kz -43.0666 1.4203 \$ bottom shell inner
356 kz 43.0666 1.4203 \$ top shell inner
357 pz -43.8489 \$ ambiguity surface for 350
358 pz 43.8489 \$ ambiguity surface for 351
359 pz -43.0666 \$ ambiguity surface for 355
360 pz 43.0666 \$ ambiguity surface for 356
361 kz -42.1528 1.4203 \$ bottom lead gap
362 pz -42.1528 \$ ambiguity surface for 361
363 kz 42.1528 1.4203 \$ top lead gap
364 pz 42.1528 \$ ambiguity surface for 363

c

c Splitting

c

400 so 5.5
401 so 7.5
402 so 9.5
403 so 11.5
404 so 13.5
405 so 15.5
406 so 17.5
407 so 19.5
408 so 21.5
409 so 23.5
410 so 25.5
411 so 27.5
412 so 29.5
413 so 31.5
414 so 33.5
415 so 35.5
416 so 37.5
417 so 39.5

c

c Tally surfaces

c

2000 cz 7.5
2001 cz 22.5
2002 cz 37.5
2003 cz 52.5
2004 cz 67.5
2005 cz 82.5
2006 cz 97.5
2007 cz 112.5
2008 cz 127.5
2009 cz 142.5

c

2050 pz -90.5
2051 pz -75.5
2052 pz -60.5
2053 pz -45.5
2054 pz -30.5
2055 pz -15.5
2056 pz -0.5
2057 pz 14.5
2058 pz 29.5
2059 pz 44.5
2060 pz 59.5
2061 pz 74.5
2062 pz 89.5
2063 pz 104.5
2064 pz 119.5
2065 pz 134.5
2066 pz 149.5
2067 pz 164.5
2068 pz 179.5
2069 pz 194.5
2070 pz 209.5
2071 pz 224.5
2072 pz 239.5
2073 pz 254.5
2074 pz 269.5
2075 pz 284.5

c

2100 pz 52.4

mode p

m1	6000	-0.08	\$ SS304
	14000	-1.0	
	15031	-0.045	
	24000	-19	
	25055	-2	
	26000	-68.375	
	28000	-9.5	
m2	6000	-0.6	\$ foam
	8000	-0.24	
	7000	-0.12	
	1000	-0.04	
m3	82000	1	\$ lead
m4	74000	1	\$ tungsten
m5	13027	1	\$ al

```

c
*tr1  0  5  0
*tr2 -5  0  0  90  0  90  180  90  90
*tr3  0 -5  0  180  90  90  90  180  90
*tr4  5  0  0  90  180  90  0  90  90
c
sdef cel=d1 pos=0 2.264 2.799 erg=d3 rad=0.1 wgt=7.4e10 $ 1 Ci Co-60
sil  L 20:301:100:200
spl  1
#    si3    sp3
    L      d
    1.173 0.5
    1.332 0.5
c
c    Tallies
c
c    ansi/ans-6.1.1-1977 flux-to-dose, photons (mrem/hr)/(p/cm**2/s)
de0    0.01  0.03  0.05  0.07  0.10  0.15  0.20  0.25  0.30
        0.35  0.40  0.45  0.50  0.55  0.60  0.65  0.70  0.80
        1.00  1.40  1.80  2.20  2.60  2.80  3.25  3.75  4.25
        4.75  5.00  5.25  5.75  6.25  6.75  7.50  9.00  11.0
        13.0  15.0
df0    3.96-3 5.82-4 2.90-4 2.58-4 2.83-4 3.79-4 5.01-4 6.31-4 7.59-4
        8.78-4 9.85-4 1.08-3 1.17-3 1.27-3 1.36-3 1.44-3 1.52-3 1.68-3
        1.98-3 2.51-3 2.99-3 3.42-3 3.82-3 4.01-3 4.41-3 4.83-3 5.23-3
        5.60-3 5.80-3 6.01-3 6.37-3 6.74-3 7.11-3 7.66-3 8.77-3 1.03-2
        1.18-2 1.33-2
c
fc12    Bottom Surface
f12:p    10
fs12    -2000 -2001 -2002 -2003 -2004 -2005
c
fc22    Top Surface
f22:p    53
fs22    -2000 -2001 -2002 -2003
c
fc32    Side surface (primary)
f32:p    32
fs32    -2061 -2062 -2063 -2064 -2065 -2066 -2067 -2068
c
fc42    Side surface (base) (last junk)
f42:p    35
fs42    -2057 -2058 -2059 -2100
c
fc52    Side surface (base conical)
f52:p    61
fs52    -2004 -2005
c
fc62    Bottom 1m Surface
f62:p    70
fs62    -2000 -2001 -2002 -2003 -2004 -2005 -2006 -2007 -2008 -2009
c
fc72    Top 1m Surface
f72:p    71
fs72    -2000 -2001 -2002 -2003 -2004 -2005 -2006 -2007 -2008 -2009
c
fc82    Side 1m surface

```

```
f82:p      72
fs82      -2050 -2051 -2052 -2053 -2054 -2055 -2056 -2057 -2058 -2059
          -2060 -2061 -2062 -2063 -2064 -2065 -2066 -2067 -2068 -2069
          -2070 -2071 -2072 -2073 -2074 -2075

c
c      A rectangular mesh tally is placed at the top surface.
c      The grid is 32x32, and each square is 10 cm x 10 cm
c
fmesh14:p geom=xyz origin=-160 -160 207.3
          imesh=160
          iints=32
          jmesh=160
          jints=32
          kmesh=208.3
          kints=1

c
c      A rectangular mesh tally is placed 1m from the top,
c      The 1 m location is measured from the center of the head.
c      The grid is 32x32, and each square is 10 cm x 10 cm
c
fmesh24:p geom=xyz origin=-160 -160 296.8
          imesh=160
          iints=32
          jmesh=160
          jints=32
          kmesh=298.8
          kints=1

c
c      A rectangular mesh tally is placed at the bottom surface.
c      The grid is 32x32, and each square is 10 cm x 10 cm
c
fmesh34:p geom=xyz origin=-160 -160 -1
          imesh=160
          iints=32
          jmesh=160
          jints=32
          kmesh=0
          kints=1

c
c      A rectangular mesh tally is placed 1m from the bottom surface.
c      The grid is 32x32, and each square is 10 cm x 10 cm
c
fmesh44:p geom=xyz origin=-160 -160 -101
          imesh=160
          iints=32
          jmesh=160
          jints=32
          kmesh=-99
          kints=1

c
c      A cylindrical mesh tally is placed around the package surface.
c      Circumferentially there are 36 segments,
c      each 10 degrees wide.  Theta=0 corresponds to the positive y-axis.
c      radius=i
c      axial=j
c      circumferential=k
c
```

```
fmesh54:p    geom=cyl origin=0 0 70 axs=0 0 1 vec=0 1 0
              imesh=56.94 57.94
              iints=1 1
              jmesh=140
              jints=14
              kmesh=1
              kints=36

c
c    A cylindrical mesh tally is placed around the package
c    0.95 m from the surface of the package.
c    Circumferentially there are 36 segments,
c    each 10 degrees wide.  Theta=0 corresponds to the positive y-axis.
c    radius=i
c    axial=j
c    circumferential=k
c
fmesh64:p    geom=cyl origin=0 0 -100 axs=0 0 1 vec=0 1 0
              imesh=150.9 152.9
              iints=1 1
              jmesh=400
              jints=40
              kmesh=1
              kints=36

c
prdmp      j j 1 2
ctme      2940 $ 60*7*7 for 7 CPUs
c nps      100
```

This page left intentionally blank.

5.5.3 Shielded Device Evaluation

The 1105-SD package has been designed to transport a variety of devices containing sources, including laboratory irradiators and teletherapy heads. These devices are further subdivided into Group 1 and Group 3, as defined in Chapter 1.0, *General Information*. The Gammacell 3000 (GC-3000) is selected to bound all Group 1 devices. The shielding analysis is performed on the GC-3000 since it has a smaller minimum shielding distance compared to the other types in Group 1. It is designed to use an external, removable auxiliary shielding component which is not shipped with the unit and not credited in the analysis. The Gammacell 40 (GC-40) is the only device in Group 3. The dose rates are shown to be below the regulatory limits for each device.

5.5.3.1 Description of Shielding Design

5.5.3.1.1 Design Features

The 1105-SD package itself offers little shielding. The outer shell of the 1105-SD is 0.5-in thick steel. The shielding is provided primarily by the devices and varies widely between devices. Two specific devices are addressed in this analysis, the GC-3000 and GC-40.

The GC-3000 is heavily shielded with lead. The lead thickness through the top lead plug is approximately 3-in. Additional shielding at the top is provided by a source holder that features approximately 2.35-in steel shielding. The minimum side lead thickness is approximately 4.5-in.

The GC-40 is also heavily shielded with lead. The GC-40 drawer provides approximately 5.75-in axial lead shielding and 1.3-in axial steel shielding. The GC-40 is highly asymmetrical in shape and in the transport position provides several inches of lead shielding.

As demonstrated by the certification testing documented in Appendix 2.12.3, *Certification Test Report*, and as supplemented by analyses in Section 2.7.1.6, *Structural Evaluation of the Shielded Devices*, the devices do not experience any significant damage which could reduce their effectiveness or which could lead to a release of the sources from the shields.

5.5.3.1.2 Summary Table of Maximum Radiation Levels

The dose rates are limited to 200 mrem/hr on the surface of the package and 10 mrem/hr at a distance of 1 m from the package for non-exclusive use transportation. Dose rates are computed for a Group 1 device (GC-3000) with a 3,840 Ci Cs-137 pencil source and for the Group 3 device (GC-40) with a 2,250 Ci Cs-137 point source. Normal condition of transport (NCT) dose rates are provided in Table 5.5.3-1 and Table 5.5.3-2 for the GC-3000 and GC-40, respectively.

Because the GC-3000 bounds the GC-40 under NCT based on the results in Table 5.5.3-1 and Table 5.5.3-2, hypothetical accident condition (HAC) dose rates are computed only for the GC-3000. The HAC dose rates are computed at a distance of 1 m from the surface of the package and are provided in Table 5.5.3-3. The HAC dose rates are negligible compared to the limit of 1000 mrem/hr.

Table 5.5.3-1 – GC-3000 NCT Dose Rates (Non-exclusive use)

	Package Surface (mrem/hr)			1 m from Package Surface (mrem/hr)		
	Top	Side	Bottom	Top	Side	Bottom
Gamma	6.7	18.6	0.4	0.8	1.6	0.04
Neutron	0	0	0	0	0	0
Total	6.7	18.6	0.4	0.8	1.6	0.04
Limit	200			10		

Table 5.5.3-2 – GC-40 NCT Dose Rates (Non-exclusive use)

	Package Surface (mrem/hr)			1 m from Package Surface (mrem/hr)		
	Top	Side	Bottom	Top	Side	Bottom
Gamma	0.3	1.4	0.4	0.04	0.1	0.06
Neutron	0	0	0	0	0	0
Total	0.3	1.4	0.4	0.04	0.1	0.06
Limit	200			10		

Table 5.5.3-3 – Bounding HAC Device Dose Rates

	1 m from Package Surface (mrem/hr)		
	Top	Side	Bottom
Gamma	0.8	2.6	0.04
Neutron	0	0	0
Total	0.8	2.6	0.04
Limit	1000		

5.5.3.2 Source specification

5.5.3.2.1 Gamma source

Sources contain only Cs-137. The decay of Cs-137 is sufficiently simple to be treated explicitly. The decay of Cs-137/Ba-137m emits a 0.662 MeV gamma with an 85% probability [1].

The activities for the GC-3000 and GC-40 are given in Table 1.2-2. The GC-3000 contains up to 3,048 Ci Cs-137, although the maximum activity for Group 1 is 3,840 Ci Cs-137 for both the Gammator M38 and GC-1000. Because the intent is to bound all Group 1 devices with the GC-3000 analysis, the larger 3,840 Ci activity is modeled in the GC-3000. Therefore, the as-modeled gamma source for the GC-3000 is $3840 \times 0.85 \times 3.7\text{E}+10 = 1.208\text{E}+14$ γ/s .

The GC-40 contains up to 4,200 Ci Cs-137. However, only the upper or lower module of a GC-40 will be transported within the 1105-SD, and the maximum activity within a module is

2,250 Ci. Therefore, the as-modeled gamma source for the GC-40 is $2250 \times 0.85 \times 3.7 \times 10^{10} = 7.076 \times 10^{13} \text{ } \gamma/\text{s}$.

5.5.3.2.2 Neutron source

No neutron sources are utilized.

5.5.3.3 Shielding Model

5.5.3.3.1 Configuration of Source and Shielding

The GC-3000 transports pencil sources. It is assumed in this calculation that the GC-3000 source has a radius of 0.5 cm and length of approximately 24 cm, which is the length of the source capsule cavity. The GC-40 transports non-pencil sources, which are modeled as a point (radius of 0.1 cm to aid visualization). No credit is taken for self-shielding within the source for either the GC-3000 or GC-40.

Models of the 1105-SD package, GC-3000 or GC-40 device, and GC-3000 or GC-40 drawer are developed in the MCNP5 computer program [2]. The geometries of the GC-3000 and GC-40 have been determined by physically cutting the devices in half and measuring the dimensions. These measurements are provided in Figure 5.5.3-1 through Figure 5.5.3-5. The dimensions used in the MCNP models are consistent with these dimensions. For convenience, all steel is modeled as stainless steel, although some items, such as the GC-3000 and GC-40 shells, are carbon steel. This simplification has no impact on the results.

Each device is transported inside the inner container (IC). The IC is not modeled explicitly in MCNP because it offers little axial or radial shielding, although credit is taken for radial placement of the device within the package. The devices are positioned within the IC using blocking, which will radially center the device within the package cavity during normal conditions. Because the blocking may place the source axial location up to the axial center of the package cavity, cases are conservatively developed with the devices at the top or bottom of the package cavity, which will bound the actual configuration. In the actual configuration, a device is offset from the top and bottom of the package cavity by several inches due to the IC lid and bottom structures.

The IC is transported inside the 1105-SD package. The 1105-SD MCNP model is described in Section 5.3.1, *Configuration of Source and Shielding*. The normal conditions of transport (NCT) MCNP models for the GC-3000 and GC-40 are shown in Figure 5.5.3-6 through Figure 5.5.3-9. The large cavity shown on the left side of the GC-3000 in Figure 5.5.3-1 is absent in the MCNP models because even with this feature, there is less lead on the right half of the device. Also, the ends of the GC-40 drawer are modeled as brass for simplicity, although the ends are stainless steel per Figure 5.5.3-5. This simplification has a negligible impact on the results.

Hypothetical accident condition (HAC) models are developed only for the GC-3000 and are shown in Figure 5.5.3-10. Under HAC, testing has shown negligible deformation of the 1105-SD package. Therefore, the dimensions of the 1105-SD in the HAC model are the same as the NCT model. The foam is conservatively modeled as void in the HAC models. Damage to the blocking, resulting from the HAC impact, is assumed to allow the device to relocate within the IC. Although the IC itself is not significantly damaged, any radial spacing provided by the IC is not credited, and the device is placed against the inner wall of the 1105-SD.

As shown in Section 2.7.1.6, *Structural Evaluation of the Shielded Devices*, the devices are not damaged under HAC, the sources remain secure in the shielded position, and that lead melt or lead displacement does not occur. Therefore, the devices are modeled as undamaged in the HAC models. Prior to transport, each device will be surveyed. Only devices with a surface dose rate of 200 mrem/hr, or less, and a dose rate at a distance of one meter from the surface of 10 mrem/hr, or less, will be transported.

5.5.3.3.2 Material Properties

Stainless steel 304 with a density of 7.94 g/cm^3 is modeled for the 1105-SD shell and device structural members. The stainless steel composition is provided in Section 5.3.2, *Material Properties*. Carbon steel items, such as the GC-3000 and GC-40 shells, are modeled as stainless steel for convenience. This has no effect on the results.

Lead with a density of 11.35 g/cm^3 is modeled as a shield material in the GC-3000 and GC-40. It is modeled as pure.

Polyurethane foam with a density of 14 pounds per cubic foot (pcf) (0.224 g/cm^3) is modeled in the lower assembly of the 1105-SD. This bounds the actual density of 15 pcf. The foam composition is provided in Section 5.3.2, *Material Properties*.

Aluminum with a density of 2.7 g/cm^3 is modeled in the 1105-SD internal impact limiter plates that form the top and bottom of the 1105-SD cavity. It is modeled as pure.

The cladding and ends of the GC-40 drawer is modeled as brass with a density of 8.07 g/cm^3 . The brass composition is provided in Section 5.3.2, *Material Properties*.

**Security-Related Information
Figure Withheld Under
10 CFR 2.39**

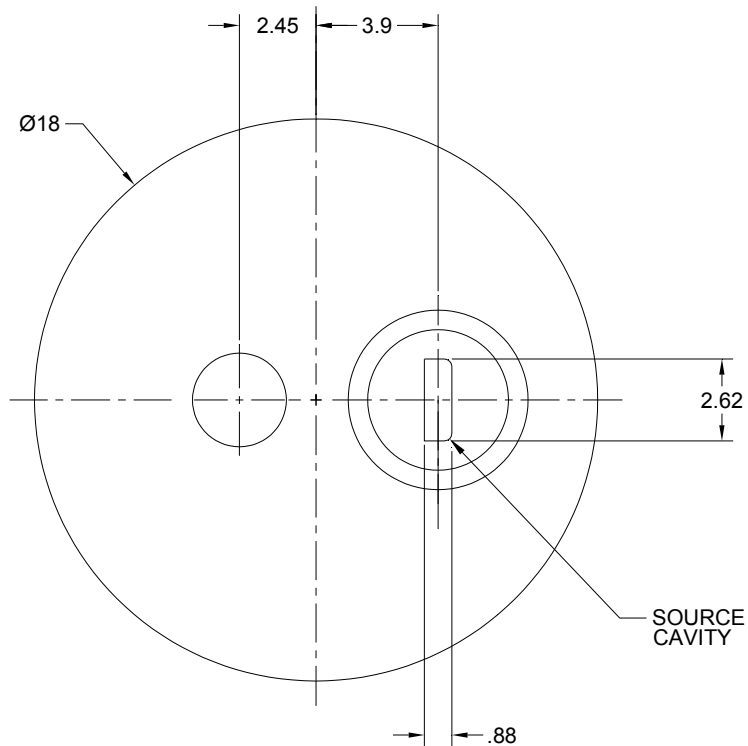


Figure 5.5.3-2 – GC-3000 (x-y view)

**Security-Related Information
Figure Withheld Under
10 CFR 2.390**

**Security-Related Information
Figure Withheld Under
10 CFR 2.390**

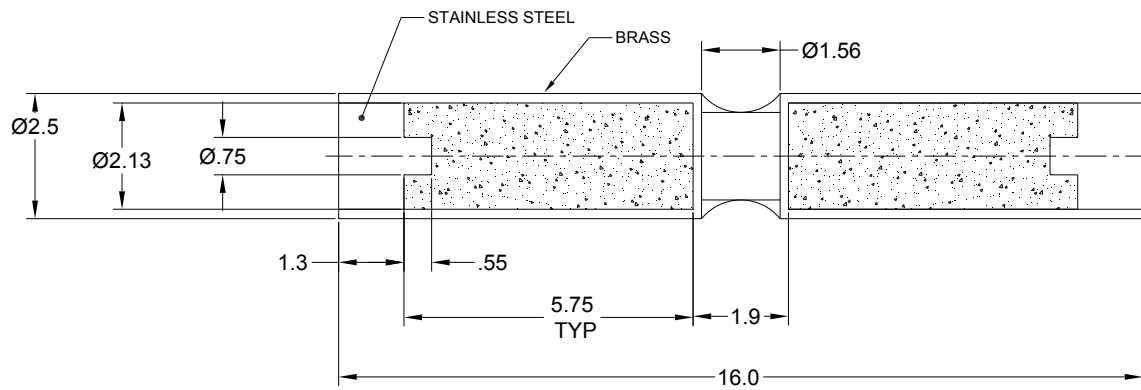


Figure 5.5.3-5 – GC-40 Drawer

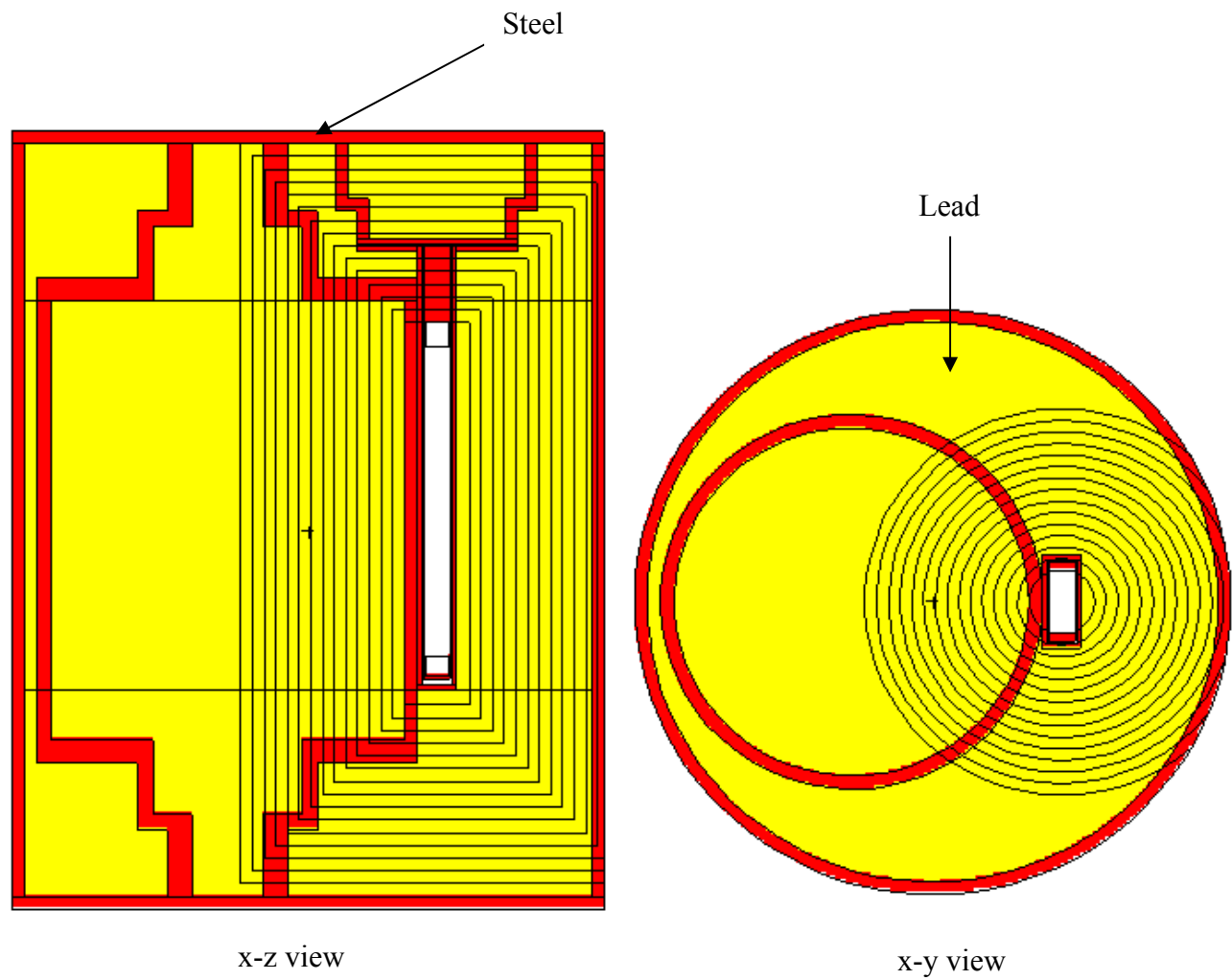


Figure 5.5.3-6 – GC-3000 MCNP Model

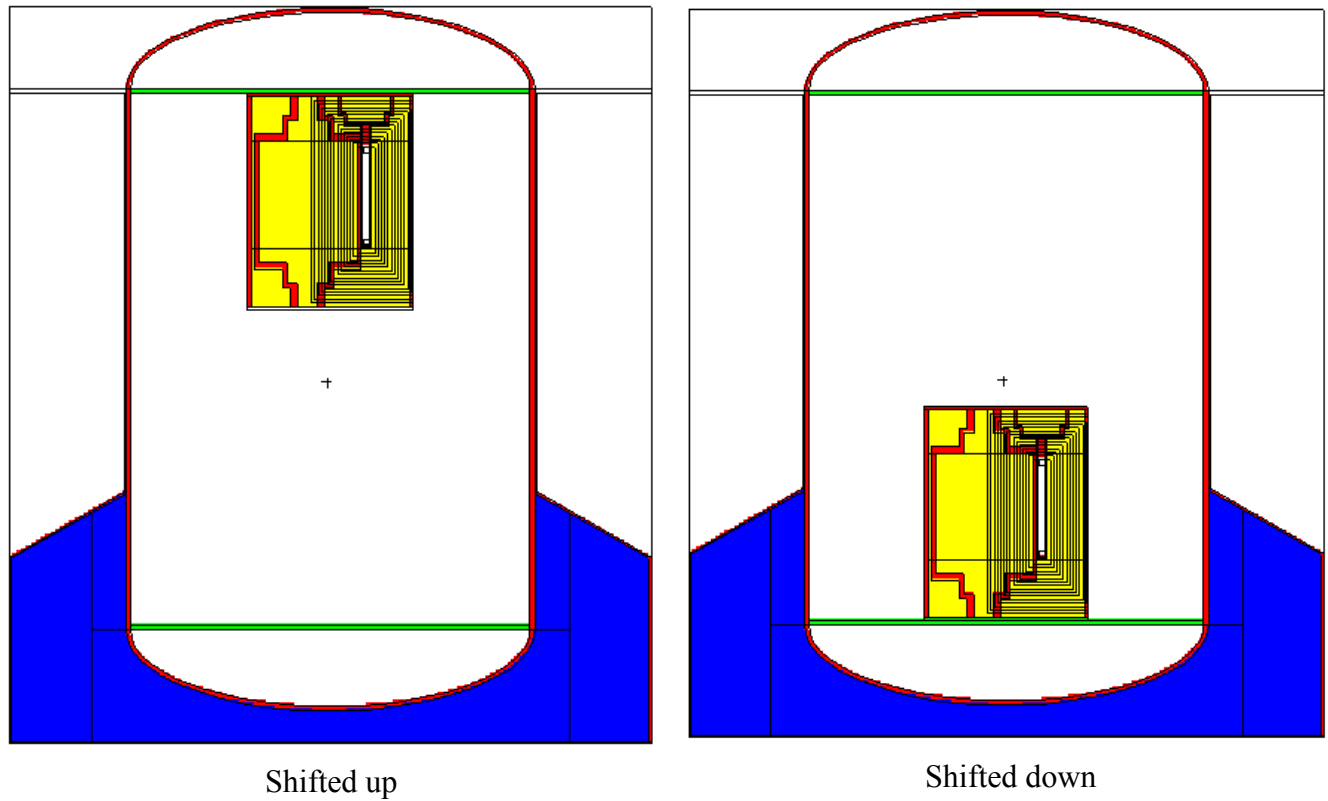


Figure 5.5.3-7 – NCT 1105-SD with GC-3000 MCNP Models

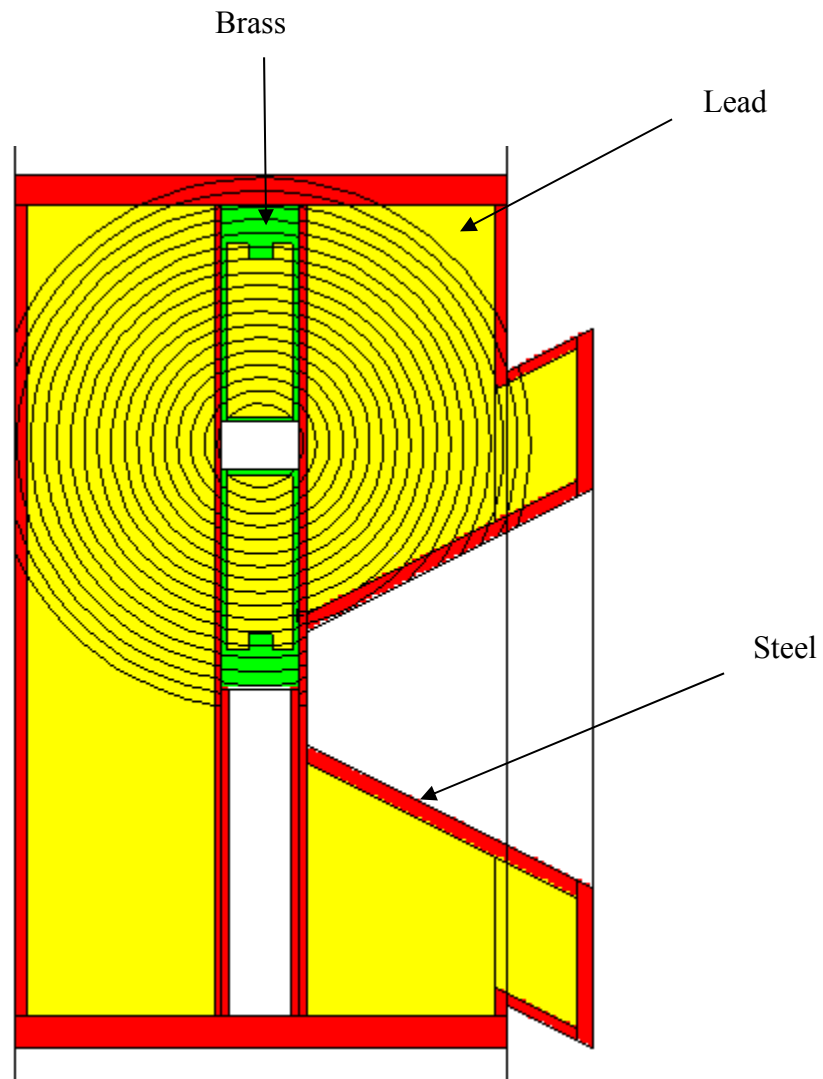


Figure 5.5.3-8 – GC-40 MCNP Model

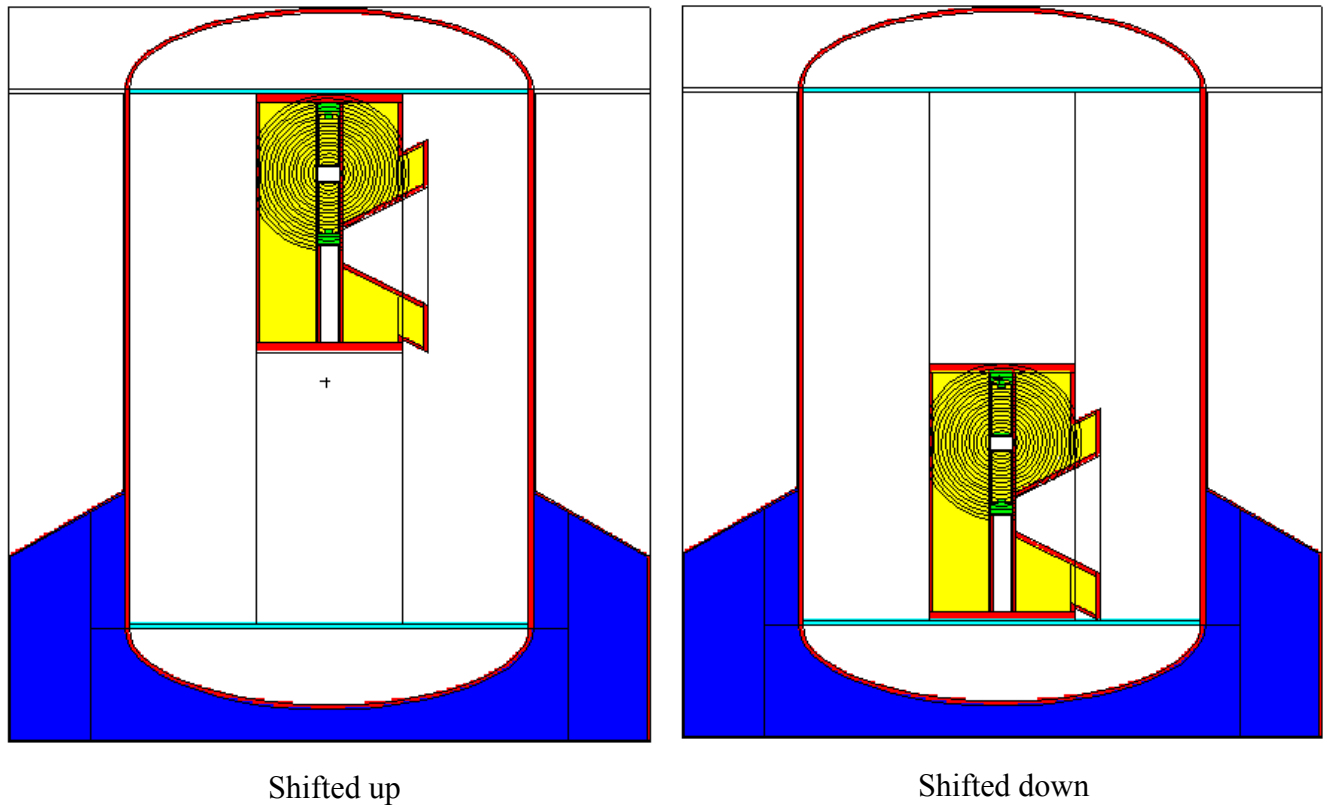


Figure 5.5.3-9 – NCT 1105-SD with GC-40 MCNP Models

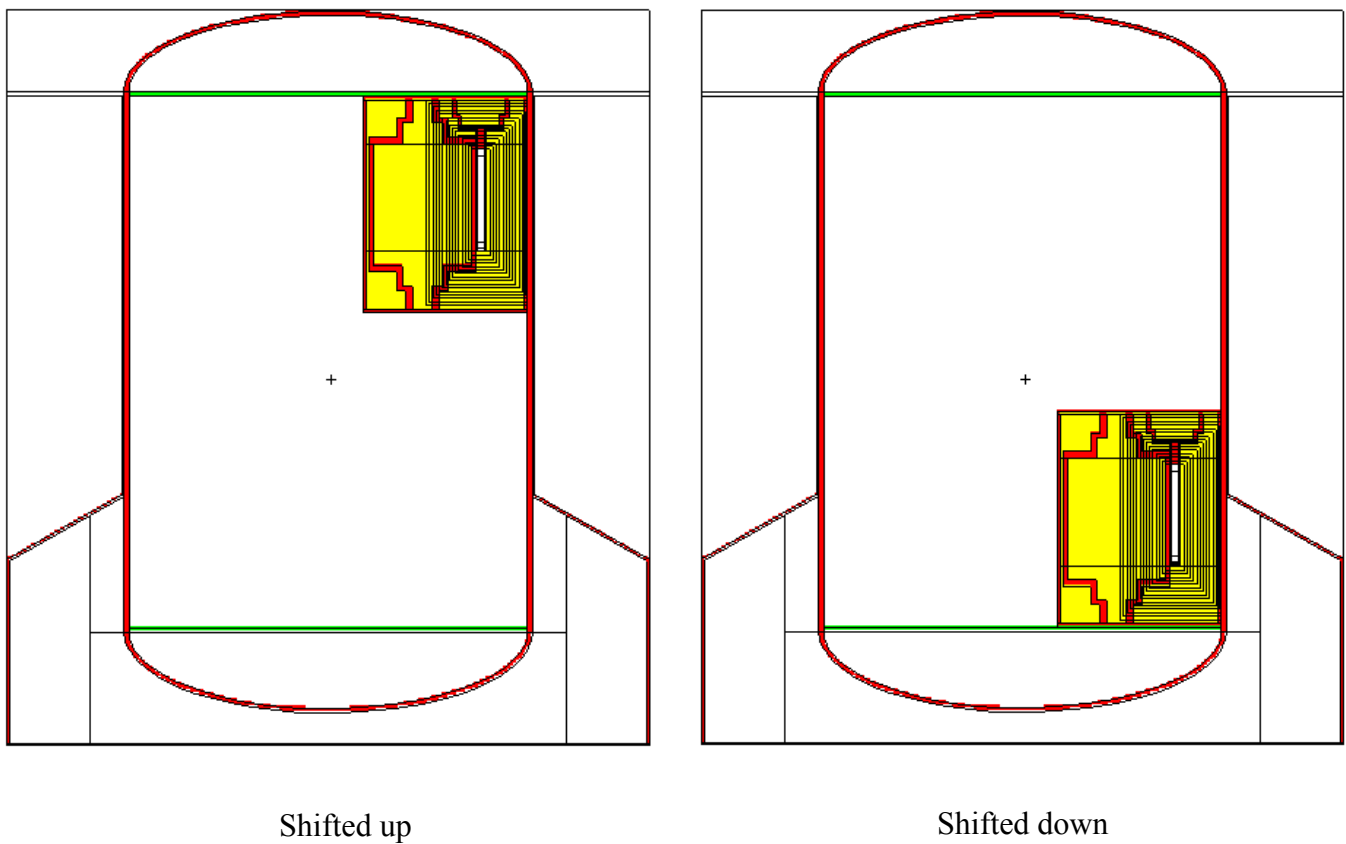


Figure 5.5.3-10 – HAC 1105-SD with GC-3000 MCNP Models

5.5.3.4 Shielding Evaluation

5.5.3.4.1 Methods

MCNP5 v1.51 is used for the shielding analysis [2]. MCNP5 is a standard, well-accepted shielding program utilized to compute dose rates for shielding licenses. A three-dimensional model is developed that captures all of the relevant design parameters of the 1105-SD package and contents. Dose rates are calculated by tallying the gamma fluxes over surfaces (or volumes) of interest and converting these fluxes to dose rates.

Mesh tallies are placed at the top, bottom, and side surfaces of the 1105-SD, as well as 1 m from these surfaces. Because the top surface of the 1105-SD is curved and the mesh tally is flat, the top surface mesh tally is placed as close to the top of the package as possible. The 1 m top tally is located 1 m from the axial center of the 9-in head (i.e., the axial center of the head is approximately 4.5-in below the top of the head) to bring this dose location closer to the package surface. The bottom mesh tally is at the bottom surface of the impact limiter, and the 1 m bottom tally is located 1 m from this surface. The top and bottom mesh tallies are rectangular 32x32 grids, with mesh dimensions of 10 cm x 10 cm. Therefore, the top and bottom mesh tallies extend approximately 1 m from the side surface of the side thermal shield.

The side cylindrical mesh tally is located next to the side thermal shield. The dose rates beside the impact limiter are not tallied with a mesh because the dose rate will be lower here due to the larger distance from the source. The side surface mesh tally begins at the bottom of the side thermal shield and extends 140 cm axially in 10 cm increments. The mesh 1 m from the package side is located 0.95 m from the surface of the side thermal shield, and is conservatively brought 0.05 m closer to the package surface to account for potential non-concentricity of the package internals. The mesh tally 1 m from the side of the package begins 1 m below the bottom of the package, and extends axially approximately 1 m above the top of the package in 10 cm increments. The side surface mesh tallies have 36 angular segments to capture the circumferential variation of the dose rate, since the dose rate is higher at the side of the package nearest where the source is placed.

5.5.3.4.2 Input and Output Data

A sample input file is provided in Appendix 5.5.3.5.2, *Sample Input File for Shielded Device*. Problem convergence is accelerated by dividing the device into layers and splitting the particles as particles traverse outwardly through these layers. The Monte Carlo uncertainty associated with the limiting dose rate location is less than 5%.

5.5.3.4.3 Flux-to-Dose Rate Conversion

Flux to dose rate conversion factors are defined in Section 5.4.3, *Flux-to-Dose Rate Conversion*.

5.5.3.4.4 External Radiation Levels

Dose rates are computed at the surface and 1 m from the surface of the 1105-SD package using mesh tallies, as described in Section 5.5.3.4.1, *Methods*. For non-exclusive use transportation, the dose rate is limited to 200 mrem/hr on the surface of the package and 10 mrem/hr at a distance of 1 m from the surface of the package.

The limiting dose rate results are summarized in Table 5.5.3-4 and Table 5.5.3-5 for the GC-3000 and GC-40, respectively. In all cases, the dose rates are far below the limits of 200 mrem/hr on the surface and 10 mrem/hr at a distance of 1 m from the surface.

It is apparent from the GC-3000 and GC-40 dose rates that the GC-3000 results in higher dose rates than the GC-40. Therefore, an HAC evaluation is performed only for the GC-3000. Dose rates at 1 m are computed using the same mesh tallies used in the NCT analysis. HAC results are provided in Table 5.5.3-6. Dose rates are negligible compared to the limit of 1000 mrem/hr.

Table 5.5.3-4 – NCT Dose Rate Results, GC-3000

Tally Location	GC-3000 Location	Dose Rate (mrem/hr)	σ	Limit (mrem/hr)
Top Surface	Shifted up	6.7	1.4%	200
Bottom Surface	Shifted down	0.4	7.1%	
Side Surface	Shifted up	18.6	2.6%	
Tally Location	GC-3000 Location	Dose Rate (mrem/hr)	σ	Limit (mrem/hr)
1m Top	Shifted up	0.8	2.9%	10
1m Bottom	Shifted down	0.04	5.7%	
1m Side	Shifted up	1.6	3.3%	

Table 5.5.3-5 – NCT Dose Rate Results, GC-40

Tally Location	GC-40 Location	Dose Rate (mrem/hr)	σ	Limit (mrem/hr)
Top Surface	Shifted up	0.3	1.1%	200
Bottom Surface	Shifted down	0.4	2.4%	
Side Surface	Shifted up	1.4	1.6%	
Tally Location	GC-40 Location	Dose Rate (mrem/hr)	σ	Limit (mrem/hr)
1m Top	Shifted up	0.04	2.5%	10
1m Bottom	Shifted down	0.06	5.6%	
1m Side	Shifted up	0.1	2.1%	

Table 5.5.3-6 – HAC Dose Rate Results, GC-3000

Tally Location	GC-3000 Location	Dose Rate (mrem/hr)	σ	Limit (mrem/hr)
1m Top	Shifted up	0.8	2.7%	1000
1m Bottom	Shifted down	0.04	4.3%	
1m Side	Shifted up	2.6	2.9%	

5.5.3.5 Appendices to Shielded Device Evaluation

5.5.3.5.1 References for Shielded Device Evaluation

1. Glenn F. Knoll, *Radiation Detection and Measurement*, Second Edition, John Wiley & Sons, 1989.
2. LA-UR-03-1987, *MCNP – A General Monte Carlo N-Particle Transport Code, Version 5*, Los Alamos National Laboratory, April 24, 2003 (Revised 2/1/2008).

5.5.3.5.2 Sample Input File for Shielded Device Evaluation

Sample case GC3000_UP1:

LANL-B

c

c LANL-B Package

c

```

10 1 -7.94 10 -11 -35 imp:p=1.5e7 $ base sheet
11 1 -7.94 (60 -61 31 -35):(34 -35 11 -61) imp:p=1.5e7 $ cone sheet
12 0 -50 -12 imp:p=1.5e7 $ inside head
13 1 -7.94 50 -51 -12 imp:p=1.5e7 $ lower head
14 1 -7.94 30 -31 12 -17 imp:p=5.8e6 $ shell
15 5 -2.7 12 -13 -30 imp:p=1.5e7 $ bottom
16 2 -0.224 11 -12 51 -33 imp:p=1.5e7 $ foam
17 2 -0.224 31 -33 12 -60 imp:p=1.5e7 $ foam
18 2 -0.224 33 -34 11 -60 imp:p=1.5e7 $ foam
19 5 -2.7 16 -17 -30 imp:p=1.5e7 $ top plate
20 0 13 -16 -30 fill=1(0 0 122.1) imp:p=1 $ cavity
21 1 -7.94 61 -16 31 -32 imp:p=5.8e6 $ thermal shields
22 1 -7.94 52 -53 17 imp:p=1.5e7 $ top head
23 0 17 -52 imp:p=1 $ inside top
24 0 32 -35 61 -16 imp:p=1 $ side air
25 0 16 -17 31 -35 imp:p=1 $ side air sliver
26 0 17 -18 53 -35 imp:p=1 $ top air
27 0 (-10:18:35) 70 -71 -72 imp:p=1 $ 1m
28 0 (-70:71:72) 73 -74 -75 imp:p=1 $ 2m
99 0 -73:74:75 imp:p=0

```

c

c Universe 1: GC-3000

c

```

100 0 103 -106 127 -128 131 -132 fill=2(9.906 0 18) u=1 imp:p=1
101 1 -7.94 100 -101 -151 fill=5 u=1 imp:p=1
102 1 -7.94 101 -112 150 -151 fill=5 u=1 imp:p=1
103 1 -7.94 112 -113 -151 fill=5 u=1 imp:p=1
104 3 -11.35 (111 -112 -122):(107 -111 -120) fill=4 u=1 imp:p=1
105 1 -7.94 102 -103 126 -129 130 -133 fill=5 u=1 imp:p=1
106 1 -7.94 103 -106 126 -129 130 -133 #100 fill=5 u=1 imp:p=1
107 1 -7.94 (107 -110 120 -121):
(110 -111 120 -123):(111 -112 122 -123) fill=5 u=1 imp:p=1
108 1 -7.94 106 -107 -121 fill=5 u=1 imp:p=1
109 1 -7.94 (-126:129:-130:133) 114 -106 -121 fill=5 u=1 imp:p=1
110 1 -7.94 (109 -112 140 -141):(108 -109 140 -143):
(105 -108 142 -143):(104 -105 142 -144) fill=5 u=1 imp:p=1
113 3 -11.35 (104 -108 -142):(108 -112 -140) fill=4 u=1 imp:p=1
114 3 -11.35 104 -112 -150 #100 #104 #106 #107 #108

```



```

#109 #110 #113 fill=4 u=1 imp:p=1
115 3 -11.35 101 -102 -150 #116 fill=4 u=1 imp:p=1
116 1 -7.94 (140 -141 101 -116):(141 -142 115 -116):
(142 -143 115 -118):(143 -144 117 -118):
(145 -144 118 -102) fill=5 u=1 imp:p=1
117 3 -11.35 (-126:129:-130:133) 102 -104 -150 #118 fill=4 u=1 imp:p=1
118 1 -7.94 102 -104 145 -144 fill=5 u=1 imp:p=1
199 0 -100:151:113 u=1 imp:p=1
c
c Universe 2: Pencil Holder
c
200 0 206 -207 201 -202 209 -210 u=2 imp:p=1 $ cavity
201 1 -7.94 205 -208 209 -210 212 -200 u=2 imp:p=1 $ bottom
202 0 200 -201 -211 u=2 imp:p=1 $ hole
203 0 202 -203 -211 u=2 imp:p=1 $ hole
204 1 -7.94 200 -201 205 -208 209 -210 211 u=2 imp:p=1 $ bottom w/ hole
205 1 -7.94 201 -202 205 -206 209 -210 u=2 imp:p=1 $ side
206 1 -7.94 201 -202 207 -208 209 -210 u=2 imp:p=1 $ side
207 1 -7.94 202 -203 205 -208 209 -210 211 u=2 imp:p=1 $ top w/ hole
208 1 -7.94 205 -208 203 -220 209 -210 u=2 imp:p=3 $ top
209 1 -7.94 205 -208 220 -221 209 -210 u=2 imp:p=9 $ top
210 1 -7.94 205 -208 221 -222 209 -210 u=2 imp:p=27 $ top
211 1 -7.94 205 -208 222 -223 209 -210 u=2 imp:p=81 $ top
212 1 -7.94 205 -208 223 -224 209 -210 u=2 imp:p=243 $ top
213 1 -7.94 205 -208 224 -204 209 -210 u=2 imp:p=729 $ top
214 0 -205:208:-212:204:-209:210 u=2 imp:p=1
c
c Universe 4: Splitting universe for lead
c
400 3 -11.35 -400 460 -430 u=4 imp:p=1
401 3 -11.35 (400:430:-460) -401 -431 461 u=4 imp:p=3
402 3 -11.35 (401:431:-461) -402 -432 462 u=4 imp:p=9
403 3 -11.35 (402:432:-462) -403 -433 463 u=4 imp:p=27
404 3 -11.35 (403:433:-463) -404 -434 464 u=4 imp:p=81
405 3 -11.35 (404:434:-464) -405 -435 465 u=4 imp:p=243
406 3 -11.35 (405:435:-465) -406 -436 466 u=4 imp:p=729
407 3 -11.35 (406:436:-466) -407 -437 467 u=4 imp:p=2187
408 3 -11.35 (407:437:-467) -408 -438 468 u=4 imp:p=6561
409 3 -11.35 (408:438:-468) -409 -439 469 u=4 imp:p=2e4
410 3 -11.35 (409:439:-469) -410 -440 470 u=4 imp:p=6e4
411 3 -11.35 (410:440:-470) -411 -441 471 u=4 imp:p=1.8e5
412 3 -11.35 (411:441:-471) -412 -442 472 u=4 imp:p=5.3e5
413 3 -11.35 (412:442:-472) -413 -443 473 u=4 imp:p=1.6e6
414 3 -11.35 (413:443:-473) -414 -444 474 u=4 imp:p=4.8e6
415 3 -11.35 (414:444:-474) u=4 imp:p=1.4e7
c
c Universe 5: Splitting universe for steel
c
500 1 -7.94 -400 460 -430 u=5 imp:p=1
501 1 -7.94 (400:430:-460) -401 -431 461 u=5 imp:p=3
502 1 -7.94 (401:431:-461) -402 -432 462 u=5 imp:p=9
503 1 -7.94 (402:432:-462) -403 -433 463 u=5 imp:p=27
504 1 -7.94 (403:433:-463) -404 -434 464 u=5 imp:p=81
505 1 -7.94 (404:434:-464) -405 -435 465 u=5 imp:p=243
506 1 -7.94 (405:435:-465) -406 -436 466 u=5 imp:p=729
507 1 -7.94 (406:436:-466) -407 -437 467 u=5 imp:p=2187
508 1 -7.94 (407:437:-467) -408 -438 468 u=5 imp:p=6561

```

```

509 1 -7.94 (408:438:-468) -409 -439 469 u=5 imp:p=2e4
510 1 -7.94 (409:439:-469) -410 -440 470 u=5 imp:p=6e4
511 1 -7.94 (410:440:-470) -411 -441 471 u=5 imp:p=1.8e5
512 1 -7.94 (411:441:-471) -412 -442 472 u=5 imp:p=5.3e5
513 1 -7.94 (412:442:-472) -413 -443 473 u=5 imp:p=1.6e6
514 1 -7.94 (413:443:-473) -414 -444 474 u=5 imp:p=4.8e6
515 1 -7.94 (414:444:-474) u=5 imp:p=1.4e7

```

c

c Package

c

```

10 pz 0 $ bottom of package
11 pz 0.635 $ bottom plate
12 pz 32.004 $ bottom of inner support
13 pz 33.274 $ bottom of cavity
16 pz 183.106 $ top of cavity
17 pz 184.376 $ top of top plate
18 pz 207.3 $ top of model
30 cz 55.245 $ shell inner
31 cz 56.515 $ shell outer
32 cz 56.9341 $ outer thermal shields
33 cz 66.04 $ foam interface
34 cz 88.265 $ base sheet inner
35 cz 88.9 $ base sheet outer
50 ell 0 0 32.004 0 0 21.59 -55.245 $ lower head inner
51 ell 0 0 32.004 0 0 22.86 -56.515 $ lower head outer
52 ell 0 0 184.376 0 0 21.59 -55.245 $ upper head inner
53 ell 0 0 184.376 0 0 22.86 -56.515 $ upper head outer
60 kz 103.0298 3.0 -1
61 kz 103.7630 3.0 -1
70 pz -100 $ bottom 1m
71 pz 295.8 $ top 1m (measured from the axial middle of the head)
72 cz 156.9341 $ side 1m
73 pz -200 $ bottom of model
74 pz 410 $ top of model
75 cz 256 $ side of model

```

c

c GC-3000

c

```

100 pz 0.0001 $ bottom of GC3000
101 pz 0.9652
102 pz 17.1958
103 pz 17.526
104 pz 47.625
105 pz 49.53
106 pz 52.07
107 pz 52.5272
108 pz 53.467
109 pz 54.737
110 pz 54.7878
111 pz 55.7022
112 pz 59.9948
113 pz 60.96 $ top of GC3000
114 pz 51.6128
115 pz 6.223
116 pz 7.493
117 pz 11.43

```

```
118 pz 13.335
c
120 c/z 9.906 0 5.2578 $ source side
121 c/z 9.906 0 6.1722
122 c/z 9.906 0 6.8453
123 c/z 9.906 0 7.7597
126 px 8.4328          $ source slot
127 px 8.763
128 px 11.049
129 px 11.3792
130 py -3.6322
131 py -3.302
132 py 3.302
133 py 3.6322
c
140 c/z -6.223 0 2.7178 $ chamber side
141 c/z -6.223 0 4.6482
142 c/z -6.223 0 5.715
143 c/z -6.223 0 6.985
144 c/z -6.223 0 14.6553
145 c/z -6.223 0 13.5856
c
150 cz 21.8948
151 cz 22.86
c
c Holder
c
200 pz 0.3302
201 pz 1.8542
202 pz 26.1112
203 pz 28.0162
204 pz 33.9852 $ top
205 py -3.175
206 py -2.413
207 py 2.413
208 py 3.175
209 px -1.0478
210 px 1.0478
211 cz 0.889 $ hole
212 pz 0.0002
220 pz 29
221 pz 30
222 pz 31
223 pz 32
224 pz 33
c
c Splitting
c
400 c/z 9.906 0 2.5
401 c/z 9.906 0 3.4
402 c/z 9.906 0 4.3
403 c/z 9.906 0 5.2
404 c/z 9.906 0 6.1
405 c/z 9.906 0 7.0
406 c/z 9.906 0 7.9
407 c/z 9.906 0 8.8
408 c/z 9.906 0 9.7
```

409 c/z 9.906 0 10.6
410 c/z 9.906 0 11.5
411 c/z 9.906 0 12.4
412 c/z 9.906 0 13.3
413 c/z 9.906 0 14.2
414 c/z 9.906 0 15.1
c 415 c/z 9.906 0 17.5
c 416 c/z 9.906 0 18.5
c 417 c/z 9.906 0 19.5
c
430 pz 46
431 pz 47
432 pz 48
433 pz 49
434 pz 50
435 pz 51
436 pz 52
437 pz 53
438 pz 54
439 pz 55
440 pz 56
441 pz 57
442 pz 58
443 pz 59
444 pz 60
c
460 pz 16
461 pz 15
462 pz 14
463 pz 13
464 pz 12
465 pz 11
466 pz 10
467 pz 9
468 pz 8
469 pz 7
470 pz 6
471 pz 5
472 pz 4
473 pz 3
474 pz 2
c
c Tally surfaces
c
2000 cz 7.5
2001 cz 22.5
2002 cz 37.5
2003 cz 52.5
2004 cz 67.5
2005 cz 82.5
2006 cz 97.5
2007 cz 112.5
2008 cz 127.5
2009 cz 142.5
c
2050 pz -90.5
2051 pz -75.5

2052 pz -60.5
 2053 pz -45.5
 2054 pz -30.5
 2055 pz -15.5
 2056 pz -0.5
 2057 pz 14.5
 2058 pz 29.5
 2059 pz 44.5
 2060 pz 59.5
 2061 pz 74.5
 2062 pz 89.5
 2063 pz 104.5
 2064 pz 119.5
 2065 pz 134.5
 2066 pz 149.5
 2067 pz 164.5
 2068 pz 179.5
 2069 pz 194.5
 2070 pz 209.5
 2071 pz 224.5
 2072 pz 239.5
 2073 pz 254.5
 2074 pz 269.5
 2075 pz 284.5
 c
 2100 pz 52.4

mode p

m1 6000 -0.08 \$ SS304
 14000 -1.0
 15031 -0.045
 24000 -19
 25055 -2
 26000 -68.375
 28000 -9.5
 m2 6000 -0.6 \$ foam
 8000 -0.24
 7000 -0.12
 1000 -0.04
 m3 82000 1 \$ lead
 m5 13027 1 \$ al

c

sdef cel=d1 pos=0 0 13.9827 erg=d3 rad=d2 ext=d4 axs=0 0 1 wgt=1.208e14 \$ 3840 Ci Cs-137

si1 L 20:100:200

sp1 1

si2 0.5

si4 12.1

si3 sp3

L d

0.662 1

c

c Tallies

c

c ansi/ans-6.1.1-1977 flux-to-dose, photons (mrem/hr) / (p/cm**2/s)

de0	0.01	0.03	0.05	0.07	0.10	0.15	0.20	0.25	0.30
	0.35	0.40	0.45	0.50	0.55	0.60	0.65	0.70	0.80
	1.00	1.40	1.80	2.20	2.60	2.80	3.25	3.75	4.25

	4.75	5.00	5.25	5.75	6.25	6.75	7.50	9.00	11.0
	13.0	15.0							
df0	3.96-3	5.82-4	2.90-4	2.58-4	2.83-4	3.79-4	5.01-4	6.31-4	7.59-4
	8.78-4	9.85-4	1.08-3	1.17-3	1.27-3	1.36-3	1.44-3	1.52-3	1.68-3
	1.98-3	2.51-3	2.99-3	3.42-3	3.82-3	4.01-3	4.41-3	4.83-3	5.23-3
	5.60-3	5.80-3	6.01-3	6.37-3	6.74-3	7.11-3	7.66-3	8.77-3	1.03-2
	1.18-2	1.33-2							

c

fc12 Bottom Surface

f12:p 10

fs12 -2000 -2001 -2002 -2003 -2004 -2005

c

fc22 Top Surface (last junk)

f22:p 53

fs22 -2000 -2001 -2002 -2003

c

fc32 Side surface (primary)

f32:p 32

fs32 -2061 -2062 -2063 -2064 -2065 -2066 -2067 -2068

c

fc42 Side surface (base) (last junk)

f42:p 35

fs42 -2057 -2058 -2059 -2100

c

fc52 Side surface (base conical)

f52:p 61

fs52 -2004 -2005

c

fc62 Bottom 1m Surface

f62:p 70

fs62 -2000 -2001 -2002 -2003 -2004 -2005 -2006 -2007 -2008 -2009

c

fc72 Top 1m Surface

f72:p 71

fs72 -2000 -2001 -2002 -2003 -2004 -2005 -2006 -2007 -2008 -2009

c

fc82 Side 1m surface

f82:p 72

fs82 -2050 -2051 -2052 -2053 -2054 -2055 -2056 -2057 -2058 -2059
-2060 -2061 -2062 -2063 -2064 -2065 -2066 -2067 -2068 -2069
-2070 -2071 -2072 -2073 -2074 -2075

c

c A rectangular mesh tally is placed at the top surface.

c The grid is 32x32, and each square is 10 cm x 10 cm

c

fmesh14:p geom=xyz origin=-160 -160 207.3

imesh=160

iints=32

jmesh=160

jints=32

kmesh=208.3

kints=1

c

c A rectangular mesh tally is placed 1m from the top,

c The 1 m location is measured from the center of the head.

c The grid is 32x32, and each square is 10 cm x 10 cm

c

```
fmesh24:p geom=xyz origin=-160 -160 296.8
          imesh=160
          iints=32
          jmesh=160
          jints=32
          kmesh=298.8
          kints=1

c
c      A rectangular mesh tally is placed at the bottom surface.
c      The grid is 32x32, and each square is 10 cm x 10 cm
c
fmesh34:p geom=xyz origin=-160 -160 -1
          imesh=160
          iints=32
          jmesh=160
          jints=32
          kmesh=0
          kints=1

c
c      A rectangular mesh tally is placed 1m from the bottom surface.
c      The grid is 32x32, and each square is 10 cm x 10 cm
c
fmesh44:p geom=xyz origin=-160 -160 -101
          imesh=160
          iints=32
          jmesh=160
          jints=32
          kmesh=-99
          kints=1

c
c      A cylindrical mesh tally is placed around the package surface.
c      Circumferentially there are 36 segments,
c      each 10 degrees wide.  Theta=0 corresponds to the positive y-axis.
c      radius=i
c      axial=j
c      circumferential=k
c
fmesh54:p  geom=cyl origin=0 0 70 axs=0 0 1 vec=0 1 0
          imesh=56.94 57.94
          iints=1 1
          jmesh=140
          jints=14
          kmesh=1
          kints=36

c
c      A cylindrical mesh tally is placed around the package
c      0.95 m from the surface of the package.
c      Circumferentially there are 36 segments,
c      each 10 degrees wide.  Theta=0 corresponds to the positive y-axis.
c      radius=i
c      axial=j
c      circumferential=k
c
fmesh64:p  geom=cyl origin=0 0 -100 axs=0 0 1 vec=0 1 0
          imesh=150.9 152.9
          iints=1 1
          jmesh=400
```

```
jints=40
kmesh=1
kints=36

c
prtmp  j j 1 2
ctme   2940
```


This page left intentionally blank.

6.0 CRITICALITY EVALUATION

Based on the provisions of 10 CFR 71.15(b) [1], the 1105-SD package contents are exempt from classification as fissile material. The maximum content of fissile material in the 1105-SD is 15g. There is an adequate mass of steel in the packaging, neglecting any other materials, to satisfy the requirements of 10 CFR 71.15(b). Therefore, a criticality evaluation is not required.

6.1 References

1. Title 10, Code of Federal Regulations, Part 71 (10 CFR 71), *Packaging and Transportation of Radioactive Material*, 01-01-18 Edition.

This page left intentionally blank.

7.0 PACKAGE OPERATIONS

The 1105-SD packaging consists of four major components: the Lower Body Assembly, or base (3021717-SAR, Assembly A2), the Upper Body Assembly, or bell (3021717-SAR, Assembly A3), the Lodgment (3021718-SAR), and the Inner Container, or IC (3021719-SAR). Both the bell and the base include an Internal Impact Limiter Assembly (3021717-SAR, Assembly A4), which are not removed during normal operation. The single external impact limiter is part of the base and is not separable. Reference to specific 1105-SD packaging components may be found in Appendix 1.3.3, *Packaging General Arrangement Drawings*.

7.1 Procedures for Loading the Package

This section delineates the procedures for loading a payload into the 1105-SD packaging.

7.1.1 General Lifting and Handling

1. The 1105-SD package is lifted only from the bottom using a pallet. The threaded hole in the top of the bell is not to be used for lifting the package.
2. After the 24 closure bolts have been removed, the bell is lifted off of the base using the 3/4-10 UNC threaded hole in the top of the bell.
3. The bell must be set down on a smooth, clean surface free of grit, such as paper or plastic sheet.
4. With the bell removed, the base may be moved either using the pallet, or by making use of the threaded closure bolt holes. The maximum depth of penetration into the threaded holes from the flange surface must not exceed 2.5 inches. Use caution not to damage the machined flange surface or the O-rings, if installed, and do not apply any loads to the vertical portion of the flange that contains the O-ring grooves.
5. Perform all operations in a clean work area. Before lifting the payload or the bell over the base, ensure that the lower surfaces are free of debris.

7.1.2 Loading of Contents

The 1105-SD payload consists either of the Long Term Storage Shield (LTSS), transported using the lodgment (see drawing 3021718-SAR) or any of the devices listed in Table 1.2-2 using the Inner Container (IC) (see drawing 3021719-SAR). NOTE: The visual inspections of packaging components delineated in the following steps may be performed at any time during the loading sequence.

7.1.2.1 Loading the LTSS into the 1105-SD

1. Remove the 5, 1/2-13UNC socket head cap screws (SHCS) from each half of the rain shield (total of 10 bolts).
2. Remove the vent port insulation cylinder and seal test port insulation cylinder from the vent port and seal test port access tubes, respectively.

3. Remove the 24, 1-1/4-7UNC socket head cap screws from the bell flange. The bolt heads feature holes that may be used with wire hooks to lift the bolts out of the tubes.
4. Using the lift point at the top, remove the bell.
5. Ensure that the LTSS has been loaded according to the procedure delineated in Section 7.1.4, *Loading and Preparing the LTSS for Transport*.
6. The LTSS may be loaded into the lodgment before placing it in the 1105-SD packaging. Optionally, the LTSS may be loaded into the lodgment with the lodgment in place in the packaging.
7. Remove the 8, 1/2-13UNC bolts which connect the upper and lower halves of the lodgment.
8. Lift off the upper lodgment half. For convenience, lifting shackles may optionally be retained in storage locations found near the lifting holes.
9. Remove the LTSS from its storage base and upright it so that its longitudinal axis is essentially vertical.
10. Lift the LTSS using hoist rings or equivalent mounted in the two M16 threaded holes located in the LTSS lifting blocks.
11. Place the LTSS into the lodgment lower half, taking care to align the hinge on the LTSS with the associated clearance cutouts in the ribs in the lower half. Ensure that the lower end of the LTSS is approximately centrally placed and seated on the thick rubber pad at the bottom of the lodgment.
12. Remove the lifting load from the LTSS. Temporary spacers or equivalent may be used between the LTSS and the lodgment, if necessary, in order to keep the LTSS essentially vertical after removal of the lifting load. The two hoist rings may be left in place in the LTSS.
13. Lower the upper half of the lodgment over the LTSS using the index marks to align the ribs in the correct orientation. Ensure that the three toggle clamps are open, and that they pass freely over the top end of the LTSS.
14. Install the 8, 1/2-13UNC bolts in the clevises which connect the lodgment upper half and lower half. Tighten the hex locknuts only to contact with the clevises.
15. Close each of the three toggle clamps. Adjust each clamp as necessary so that a similar clamping force is applied by each clamp. If used, remove temporary spacers.
16. Using the lifting holes provided in two opposite ribs of the upper lodgment, lift the loaded lodgment assembly over the package base. Before passing over the base, ensure that the bottom of the lodgment is free of loose debris.
17. Using the centering guides located on the lower internal impact limiter, lower the lodgment into position on the base. Ensure that the lower surface of the lodgment is resting flat on the base.
18. Visually inspect both main containment O-ring seals and the mating surfaces on the bell. If damage is present that is sufficient to impair containment integrity (e.g., cuts, tears, and/or joint separation in the O-ring, or scratches or dents in the sealing surfaces), replace the seals

and/or repair the damaged surfaces per Section 8.2.3.2, *Sealing Area Routine Inspection and Repair*.

19. As an option, remove and sparingly apply vacuum grease to the O-ring seals and/or sealing surfaces, and reinstall the O-rings into the grooves in the base flange. NOTE: If the O-rings are removed, perform a visual surface finish inspection of the O-ring grooves for scratches or dents that could impair containment integrity. If necessary, repair the damaged surfaces per Section 8.2.3.2, *Sealing Area Routine Inspection and Repair*.
20. Remove and visually inspect the vent port and seal test port plugs and associated sealing washers and mating surfaces on the flange. If damage is present that is sufficient to impair containment integrity (e.g., cuts, tears, and/or separation of the O-ring from the metal washer, or scratches or dents in the sealing surfaces), replace the seals and/or repair the damaged surfaces per Section 8.2.3.2, *Sealing Area Routine Inspection and Repair*.
21. Reinstall the vent port and seal test port plugs and sealing washers. Do not tighten at this time.
22. If not already present, install seal surface protector(s) on the bell, and optionally, install seal protector(s) on the base.
23. Verify that no foreign material has entered the packaging cavity during loading.
24. Lower the bell over the lodgment. When the bell bottom edge is several inches below the widest part of the lodgment, remove the bell seal surface protector(s) and base seal protector(s), if used. Continue to lower the bell into position on the base, using the alignment marks and the alignment pins. Before losing sight of the base O-ring seals, visually determine that no debris is present on the O-ring seals.
25. Coat closure bolt threads and washer surfaces with a low-halogen, nickel based nuclear grade lubricant prior to assembly. Re-coating is not required if an adequate coat exists. Install the 24 closure bolts, and using a crossing pattern, tighten to 270 – 330 ft-lb torque.
26. Preshipment leakage rate testing of the main containment O-ring seal and vent port sealing washer shall be performed according to the following criteria:
 - a. If the main containment (upper) O-ring seal has been replaced or the corresponding sealing surface repaired, or if the vent port plug or sealing washer has been replaced or the mating sealing surface repaired, the leakage rate tests shall be performed according to Section 8.2.2, *Maintenance/Periodic Leakage Rate Tests*.
 - b. If the criteria of step (a) above do not apply, as an option, preshipment leakage rate testing may be performed according to Section 7.4, *Preshipment Leakage Rate Test*.
27. After preshipment leakage rate testing is complete and associated equipment has been removed, ensure that the vent port plug and seal test port plug are tightened to 48 – 60 in-lb torque.
28. Install a port insulation cylinder in the vent port access tube and in the seal test port access tube. Note that both cylinders are identical.
29. Install the two halves of the rain shield using 5 each, 1/2-13UNC bolts, tightened to 22 – 28 ft-lb torque. Optionally, a weather seal may be used with the rain shield, or nuclear-grade duct tape may be used to cover the rain shield or tube sheet-to-impact limiter joints.

30. Install tamper-indicating lockwire in two adjacent rain shield bolts. Both bolts must be located on the same rain shield half.

7.1.2.2 Loading the Inner Container (IC) into the 1105-SD

1. Remove the 5, 1/2-13UNC socket head cap screws (SHCS) from each half of the rain shield (total of 10 bolts).
2. Remove the vent port insulation cylinder and seal test port insulation cylinder from the vent port and seal test port access tubes, respectively.
3. Remove the 24, 1-1/4-7UNC socket head cap screws from the bell flange. The bolt heads feature holes that may be used with wire hooks to lift the bolts out of the tubes.
4. Using the lift point at the top, remove the bell.
5. Prepare a shielded device for transport per the procedural steps in Section 7.1.2.2.1, *Preparing Group 1 Devices for Transport*, or Section 7.1.2.2.2, *Preparing Group 3 Devices for Transport*.
6. Remove the six, 1-8UNC bolts holding the lid to the IC, and remove the lid using the three, 1/2-13UNC lifting holes located near the perimeter of the lid top surface.
7. Load the shielded device into the IC.
 - a. Prepare the blocking/dunnage. Dunnage shall be structural metal such as aluminum, stainless steel, or carbon steel in a welded or bolted configuration, which may include neoprene bumpers, or it may be made from blocks of Series FR3700 polyurethane foam, manufactured by General Plastics Manufacturing Company, Tacoma, WA. Polyurethane foam dunnage shall be rigid, closed-cell, and have a decomposition temperature greater than or equal to 435 °F. The total weight of all dunnage material must be less than or equal to 500 lb. Any paint used on blocking/dunnage components shall be rated for 500 °F minimum.
 - b. Ensure that the cavity of the IC is clean and dry and free of foreign material. Protect from entry of precipitation.
 - c. Place the lower dunnage, as needed, into the bottom of the IC.
 - d. Place the shielded device into the IC with its axis vertical.
 - i. The dunnage shall be configured to locate the axis of the device approximately along the axis of the IC.
 - ii. The CG of the device (alternately, the center of the device) must be placed at or below the mid-height of the IC (i.e., no more than 26.5 inches from the bottom floor of the IC).
 - iii. If using polyurethane foam as dunnage, ensure that at least 50% of the side axial height of the device is not covered by dunnage material. This restriction does not apply to metallic dunnage.
 - iv. As an option, lifting slings made of steel, nylon, polyester, or Kevlar® may be left inside the IC during transport.
 - e. Place the upper dunnage, as needed, into the IC.

- f. As an option, the device may be assembled together with the dunnage and lowered into the IC as a unit.
8. Replace the IC lid and install the six, 1-8UNC bolts, flat washers, and nuts, applying a torque of 170 to 210 ft-lb. Since the bolts are zinc plated, lubrication of the threads is optional.
9. Using the three, ½-13UNC lifting holes in the IC lid, lift the IC over the package base. Before passing over the base, ensure that the bottom of the IC is free of loose debris.
10. Using the centering guides located on the lower internal impact limiter, lower the IC into position on the base. Ensure that the lower surface of the IC is resting flat on the base.
11. Visually inspect both main containment O-ring seals and the mating surfaces on the bell. If damage is present that is sufficient to impair containment integrity (e.g., cuts, tears, and/or joint separation in the O-ring, or scratches or dents in the sealing surfaces), replace the seals and/or repair the damaged surfaces per Section 8.2.3.2, *Sealing Area Routine Inspection and Repair*.
12. As an option, remove and sparingly apply vacuum grease to the O-ring seals and/or sealing surfaces, and reinstall the O-rings into the grooves in the base flange.
13. Remove and visually inspect the vent port and seal test port plugs and associated sealing washers and mating surfaces on the flange. If damage is present that is sufficient to impair containment integrity (e.g., cuts, tears, and/or separation of the O-ring from the metal washer, or scratches or dents in the sealing surfaces), replace the seals and/or repair the damaged surfaces per Section 8.2.3.2, *Sealing Area Routine Inspection and Repair*.
14. Reinstall the vent port and seal test port plugs and sealing washers. Do not tighten at this time.
15. If not already present, install seal surface protector(s) on the bell, and optionally, install seal protector(s) on the base.
16. Verify that no foreign material has entered the packaging cavity during loading.
17. Lower the bell over the IC. When the bell bottom edge is several inches below the IC top, remove the bell seal surface protector(s) and base seal protector(s), if used. Continue to lower the bell into position on the base, using the alignment marks and the alignment pins. Before losing sight of the base O-ring seals, visually determine that no debris is present on the O-ring seals.
18. Coat closure bolt threads and washer surfaces with a low-halogen, nickel based nuclear grade lubricant prior to assembly. Re-coating is not required if an adequate coat exists. Install the 24 closure bolts, and using a crossing pattern, tighten to 270 – 330 ft-lb torque.
19. Preshipment leakage rate testing of the main containment O-ring seal and vent port sealing washer shall be performed according to the following criteria:
 - a. If the main containment (upper) O-ring seal has been replaced or the corresponding sealing surface repaired, or if the vent port plug or sealing washer has been replaced or the mating sealing surface repaired, the leakage rate tests shall be performed according to Section 8.2.2, *Maintenance/Periodic Leakage Rate Tests*.

- b. If the criteria of step (a) above do not apply, as an option, preshipment leakage rate testing may be performed according to Section 7.4, *Preshipment Leakage Rate Test*.
- 20. After preshipment leakage rate testing is complete and associated equipment has been removed, ensure that the vent port plug and seal test port plug are tightened to 48 – 60 in-lb torque.
- 21. Install a port insulation cylinder in the vent port access tube and in the seal test port access tube. Note that both cylinders are identical.
- 22. Install the two halves of the rain shield using 5 each, 1/2-13UNC bolts, tightened to 22 – 28 ft-lb torque. Optionally, a weather seal may be used with the rain shield, or nuclear-grade duct tape may be used to cover the rain shield or tube sheet-to-impact limiter joints.
- 23. Install tamper-indicating lockwire in two adjacent rain shield bolts. Both bolts must be located on the same rain shield half.

7.1.2.2.1 Preparing Group 1 Devices for Transport

- 1. Identify the shielded device and ensure that the model number matches one of the model numbers listed under Group 1 in Table 1.2-2.
- 2. Remove all components that are not necessary to the shielding function or to the source retention function, such as stands, cabinets, enclosures, electrical components including wires and insulation, turntable motors, beaker rotation sensors, or any other auxiliary or unnecessary equipment. Remove non-metallic labels, tape, and adhesive. Remove the auxiliary (external) shield components from the GC-3000. Lifting loops may be left intact.
- 3. The maximum weight of the device must be less than or equal to 3,500 lb.
- 4. The rotating sample chamber (aka the rotor) must be mechanically fixed in position with the sample chamber facing outward.
- 5. Inspect the device for damage to the body assembly and to structural components that contain the lead shielding or retain the source in a safe position. Visually inspect the weld that retains the shield plug. Any cracks, voids, damage, corrosion that is significantly deeper than the surface, or other defects that could significantly reduce the structural or shielding integrity of the device disqualifies the device for transport.
- 6. Perform a radiation survey of the entire device surface. The dose rate must be less than 200 mrem/hr on the surface and less than 10 mrem/hr at a distance of one meter from the surface. Failure to meet this requirement disqualifies the device for transport.
- 7. The Group 1 device is now ready for placement in the inner container.

7.1.2.2.2 Preparing Group 3 Devices for Transport

- 1. The only Group 3 device defined and eligible for transport in the 1105-SD is the Gammacell-40, also known as the Exactor, or as the GC-40.
- 2. Remove all components that are not necessary to the shielding function or to the source retention function, such as stands, cabinets, enclosures, electrical components including wires and insulation, or any other auxiliary or unnecessary equipment. Remove non-metallic labels, tape, and adhesive.

3. The maximum weight must be less than or equal to 3,500 lb.
4. A fully configured GC-40 contains two separate shielded devices, the upper head and the lower head. Only one device shall be transported at a time.

To prepare the upper head:

5. Disassemble the upper head from the sample chamber. Inspect the device for damage to the body assembly and to structural components that contain the lead shielding or retain the source in a safe position. Any cracks, voids, damage, corrosion that is significantly deeper than the surface, or other defects that could significantly reduce the structural or shielding integrity of the device disqualifies the device for transport.
6. The source must be located in the storage position and held in place by a shipping fixture placed in the drawer opening.
7. A retaining plate must be fastened to each end of the head using four socket head cap screws meeting the tensile strength requirements of ASTM F837 (stainless steel) or ASTM A574 (alloy steel) or better.
8. Perform a radiation survey of the entire device surface. The dose rate must be less than 200 mrem/hr on the surface and less than 10 mrem/hr at a distance of one meter from the surface. Failure to meet this requirement disqualifies the device for transport.
9. The upper head is now ready for placement in the inner container.

To prepare the lower head:

10. Disassemble the sample chamber from the top of the lower head. Remove the lower head from any base to which it may be attached.
11. Using appropriate equipment, cut off the steel framework which is welded to the lower head. Leave approximately one to two inches of the plate material still attached. Do not damage the shell of the head.
12. The maximum weight must be less than or equal to 3,500 lb.
13. Inspect the device for damage to the body assembly and to structural components that contain the lead shielding or retain the source in a safe position. Any cracks, voids, damage, corrosion that is significantly deeper than the surface, or other defects that could significantly reduce the structural or shielding integrity of the device disqualifies the device for transport.
14. The source must be located in the storage position and held in place by a shipping fixture placed in the drawer opening.
15. A retaining plate must be fastened to each end of the head using four socket head cap screws meeting the tensile strength requirements of ASTM F837 (stainless steel) or ASTM A574 (alloy steel) or better.
16. Perform a radiation survey of the entire device surface. The dose rate must be less than 200 mrem/hr on the surface and less than 10 mrem/hr at a distance of one meter from the surface. Failure to meet this requirement disqualifies the device for transport.
17. The lower head is now ready for placement in the inner container.

7.1.3 Preparation of the 1105-SD Package for Transport

1. Cover the threaded hole in the top of the bell by mechanical means, such as a bolt, per drawing 3021717-SAR.
2. Place the 1105-SD package and pallet onto the conveyance.
3. Install the tie-down assembly over the top of the impact limiter, and secure to the conveyance. Ensure that chocks (horizontal restraints) are properly installed on the conveyance.
4. Monitor external radiation for the package per the requirements of 49 CFR §173.441 [2].
5. Determine that surface contamination levels for the package is per the requirements of 10 CFR §71.87(i) [1] and 49 CFR §173.443 [2].
6. Determine the transport index for the package per the requirements of 49 CFR §173.403 [2].
7. Complete all necessary shipping papers in accordance with Subpart C of 49 CFR 172 [3].
8. 1105-SD package marking shall be in accordance with 10 CFR §71.85(c) [1] and Subpart D of 49 CFR 172 [3]. Package labeling shall be in accordance with Subpart E of 49 CFR 172. Package placarding shall be in accordance with Subpart F of 49 CFR 172.

7.1.4 Loading and Preparing the LTSS for Transport

The LTSS is loaded and prepared for transport in the 1105-SD package in three steps: 1) Qualifying a payload for transport (Section 7.1.4.1), 2) Preparing large source drawers (Section 7.1.4.2), and 3) Loading drawers into the LTSS (Section 7.1.4.3).

7.1.4.1 Qualifying a Payload for Transport

INTRODUCTORY INFORMATION

The LTSS may transport two content types: *Content 1* is the T80/T780 source drawer containing a Co-60 source.

Content 2 (the subject of the following paragraphs) is the large source drawer containing end shield plugs and a capsule, which, in turn, contains a radioactive source. Content 2 sources must be placed in capsules for loading into the LTSS. There are five different special form capsules that may be used, differing only in length: NLM 52-74, NLM 52-150, NLM 52-200, NLM 52-250, or NLM 52-325, which are 74 mm, 150 mm, 200 mm, 250 mm, and 325 mm long, respectively. The special form capsule is certified by the South African Competent Authority under certificate number ZA/NLM52/S. Other special form or non-special form capsules may be used that have the same length, diameter, and at least as much radiation attenuation as the NLM-52 capsule series. The NLM 52 nomenclature is used in the following discussion for convenience. When loaded with a special form capsule, the large source drawer is designated accordingly. For example, a large source drawer loaded with a NLM 52-250 special form capsule is designated the large source drawer 250, or LD-250. With the exception of the LD-150, a large source drawer contains a single special form capsule, centered between two equal-length tungsten end shield plugs. The LD-150 may contain either a NLM 52-150 or two NLM 52-74s. The longer the capsule, the shorter the end shield plugs. The end shield plugs nominally fill the space not taken by the special form capsule.

Sources are differentiated into two physical forms: pencil and short cylinder. All pencil sources are allowed to contain only one of two isotopes: Co-60 or Cs-137. Short cylinder sources may contain any of the isotopes in Table 7.1-1. The special form capsules must contain only the isotopes and physical form combinations delineated in Table 7.1-3. Each capsule must contain only one isotope type, but may contain multiple sources having the same isotope. Any of the four recesses in the LTSS that is not loaded with a large source drawer must be loaded with a shield drawer. An empty recess is not permitted.

There are eight configurations of large source drawers that are permitted in the LTSS, depending on the contents of the drawer and the arrangement of the drawers in the four recesses in the LTSS. These configurations are designated A, B, C, D, E, AB, BC, and BD. All of the single-letter designations specify a single large source drawer type in each of the four recesses. For example, configuration C is for an LD-200 in each recess. All of the two-letter designations specify a certain combination of drawers in the four recesses. For example, configuration BC specifies an LD-150 in recesses 1 and 2, and an LD-200 in recesses 3 and 4. The configurations are completely defined in Table 7.1-4. Note that a shield drawer may be substituted for any loaded drawer in any of the configurations. Note: a shield drawer is a large source drawer nominally filled with a tungsten plug.

The following procedure identifies the activity that may be transported in the LTSS and its distribution among the four recesses in the LTSS. At the conclusion of this process, it will be established:

- a. The configuration of each drawer (LD-xx) in each recess (configurations A – E, AB, BC, BD)
- b. The isotope and form of each source to be placed in each special form capsule (pencil, short cylinder, Co-60, Cs-137, etc.)
- c. The activity in each capsule and the total in the LTSS.

Examples of acceptable source loadings in the LTSS are given in Appendix 7.5.1, *LTSS Loading Examples*.

PROCEDURAL REQUIREMENTS

Limits for Content 1: The T80/T780 source drawer may contain up to the Table 7.1-1 limit of Co-60 (i.e., 12,970 Ci) in one to four drawers in any distribution. T80/T780 source drawers (Content 1) may not be mixed with large source drawers (Content 2) within the LTSS. Any of the four recesses in the LTSS that is not loaded with a T80/T780 drawer must be loaded with a shield drawer.

Limits for Content 2: There are seven steps in qualifying Content 2 for the LTSS.

1. **Basic Radionuclide Limits.** Verify that the total activity of each isotope to be transported in the LTSS does not exceed the basic radionuclide limits given in Table 7.1-1 or the limits specified in the special form capsule certificate, ZA/NLM52/S, or other special form capsules, if used.
2. **Fissile Mass Limit.** Verify that the total fissile mass within the LTSS does not exceed 15g. The fissile mass is equal to:

$$\text{Fissile mass (g)} = A + 0.2 \times B + 0.001 \times C$$

where:

A equals the total grams of plutonium in all Pu-239 sources

B equals the total grams of plutonium in all Pu-238 sources

C equals the curies of americium in all Am-241 sources

3. **Plutonium By Air Exclusion.** NO PLUTONIUM OR AMERICIUM SOURCES ARE PERMITTED FOR SHIPMENT OF THE 1105-SD BY AIR.
4. **Decay Heat Limit.** Verify that the total heat load is less than or equal to 200 watts. If only a single isotope is to be shipped in the LTSS, this is ensured by step 1 above. If multiple isotopes are to be transported, the total watts shall be calculated by multiplying the activity of each isotope by the heat generation rate found in Table 7.1-2.
5. **Physical Form Restrictions.** Verify that the source physical form and isotope comply with the requirements delineated in Table 7.1-3.
6. **Drawer Configuration Restrictions.** Verify that the drawer configuration to be transported is allowed per Table 7.1-4. NOTE: Any recesses in the LTSS that are not needed to carry sources must be given a shield drawer.
7. **Dose Rate Limits.** Verify the selected loading does not violate the dose rate limits using the following equation:

$$\sum_{i=1}^n \frac{S_i}{A_i} \leq 1 \quad (\leq 0.3 \text{ for commercial aircraft transport})$$

where:

S_i is the activity of each source in Ci (g Pu for Pu sources)

A_i is the appropriate value from Table 7.1-5 for each drawer for the configuration used (A – E, AB, BC, BD)

NOTE: ONLY ONE NUCLIDE TYPE MAY BE PLACED IN A SINGLE CAPSULE.

7.1.4.2 Preparing Large Source Drawers

Large source drawers shall be prepared for loading as follows. Operations shall take place in a hot cell or equivalent, consistent with site ALARA rules.

1. The capsule to be placed into the large source drawer must be either the NLM 52 special form capsule or another special form or non-special form capsule that has the same length, diameter, and at least as much radiation attenuation as the NLM-52 capsule series. Verify that the capsule has been closed and prepared for shipping in accordance with a written procedure.
2. Verify that only source material that conforms to all of the limits, restrictions, and controls specified in Section 7.1.4.1, *Qualifying a Payload for Transport*, have been placed into the capsule.
3. Place the special form capsule into a large source drawer. The special form capsule shall be centrally located between two tungsten shield plugs. The tungsten end shield plug lengths shall be utilized according to Table 7.1-3. Note: when using two NLM 52-74s in lieu of one NLM 52-150, use the end shield plugs for the NLM 52-150.

4. Thread in the end cap of the large source drawer until fully seated and secure with a set screw. The large source drawer is now designated a LD-xx, where xx corresponds to the length of the special form capsule that was placed inside, e.g., LD-250.
5. Alternately, the end cap of the large source drawer may be threaded in and secured after the drawer body has been placed into the LTSS.
6. Proceed to Section 7.1.4.3, *Loading Drawers into the LTSS*.

7.1.4.3 Loading Drawers into the LTSS

The LTSS may be loaded either inside a hot cell, mated to the outside of a hot cell, mated to another LTSS, or mated to a shielded device containing a loaded drawer(s). The order of the steps below may be altered in accordance with site safety requirements.

1. Prepare the LTSS to receive a source drawer by opening the end doors and removing the security plates.
2. Place the LTSS in a hot cell. Alternately, mate it to a hot cell, to another LTSS, or to another device containing a loaded drawer.
3. Rotate the barrel to place a recess in the load/unload position.
4. Place a loaded drawer (LD-xx or T80/T780 drawer) into the recess in the LTSS.
 - a. The contents of the drawer must be in accordance with Section 7.1.4.1, *Qualifying a Payload for Transport*, and the drawer must be prepared in accordance with Section 7.1.4.2, *Preparing Large Source Drawers*.
 - b. Do not mix LD-xx drawers with T80/T780 drawers.
 - c. If not already done, thread in the drawer end cap and secure with a set screw.
5. Rotate the barrel to the next recess and repeat with the next drawer or shield drawer.
6. Repeat until all the cavities of the LTSS are filled with either loaded drawers or shield drawers.
7. Separate the LTSS from any other equipment, if mated.
8. Install security plates on each end of the LTSS.
9. Close the end doors and fasten to the LTSS with eight, M16 socket head cap screws, tightened to 60 – 70 N-m (44 – 52 ft-lb) as shown in Figure 7.1-1.

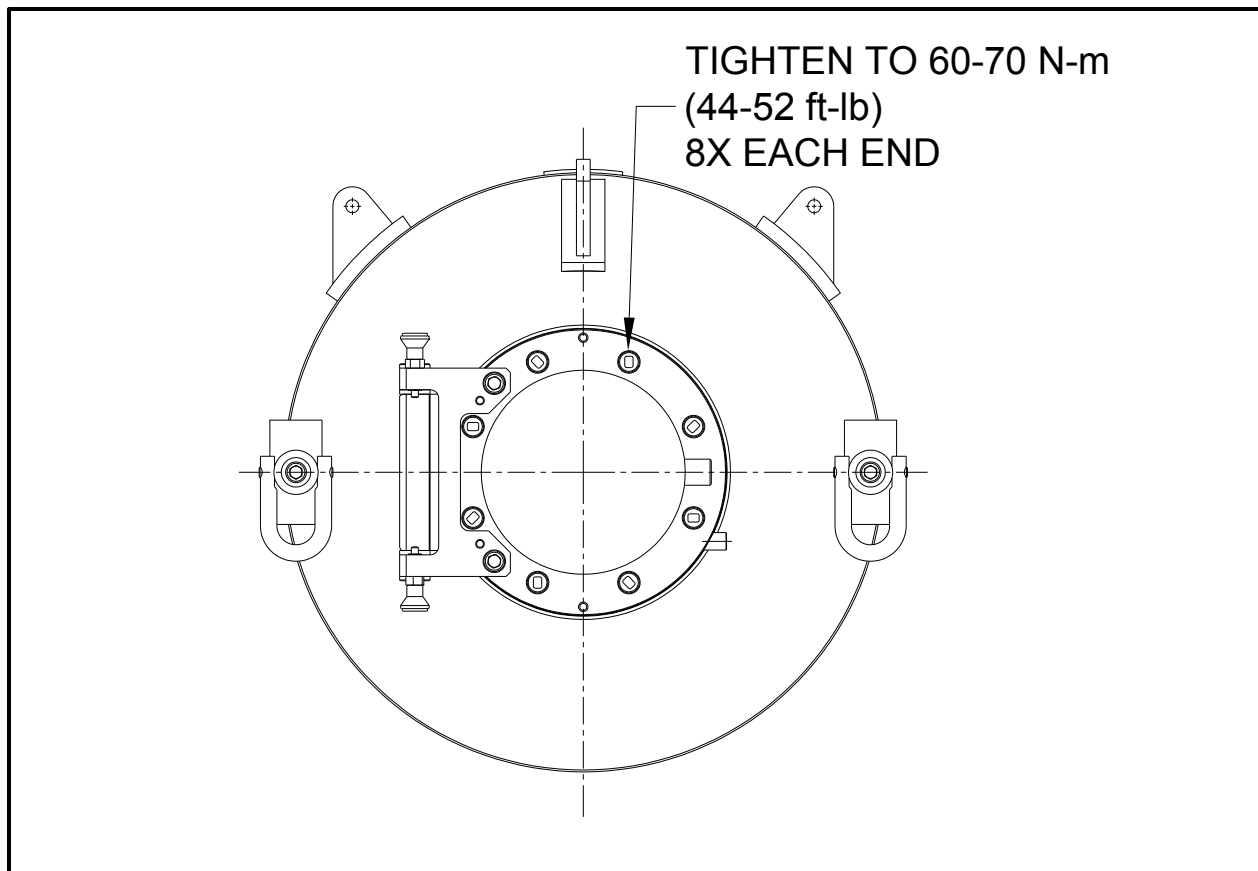


Figure 7.1-1 – Tightening Torque of LTSS End Door Fasteners

Table 7.1-1 – Basic 1105-SD Limits

Source	Maximum Quantity per 1105-SD
Co-60	12,970 Ci
Cs-137	14,000 Ci
Sr-90	1,000 Ci
Am-241 (excluding Am-241Be)②	1000 Ci
Am-241Be②	6.6 Ci
Pu-238 (excluding Pu-238Be)③	75 g Pu
Pu-239 or Pu-239Be③	15 g Pu
Ir-192	200 Ci
Se-75	80 Ci

①Not used.

②Impurities may include oxygen and chlorine.

③Impurities may include oxygen. The total fissile mass limit for the 1105-SD is 15 g.

Table 7.1-2 – Watts Per Source Unit

Isotope	watts/unit
Co-60	1.5420E-02 watts/Ci
Cs-137①	5.0400E-03 watts/Ci
Sr-90②	6.6980E-03 watts/Ci
Am-241	3.3370E-02 watts/Ci
Pu-238	5.6773E-01 watts/g
Pu-239	3.0873E-03 watts/g
Ir-192	6.1500E-03 watts/Ci
Se-75	2.4100E-03 watts/Ci

①Includes Ba-137m.

②Includes Y-90.

③Not used.

Table 7.1-3 – Authorized Payload Special Form Capsule Sources and Nuclides

Drawer Model	End Shield Length, mm	Special Form Capsule Model	Authorized Source Shape and Dimensions	Authorized Nuclides
LD-74	214	NLM 52-74	Short cylinder	All nuclides in Table 7.1-1
LD-150	176	NLM 52-150	Short cylinder	All nuclides in Table 7.1-1
			Pencil source, len. ≥ 60 mm	Co-60 and Cs-137
LD-150	176	Two NLM 52-74s	Short cylinder	All nuclides in Table 7.1-1
LD-200	151	NLM 52-200	Short cylinder	All nuclides in Table 7.1-1
			Pencil source, len. ≥ 136 mm	Co-60 and Cs-137
LD-250	126	NLM 52-250	Pencil source, len. ≥ 186 mm	Co-60 and Cs-137
LD-325	88.5	NLM 52-325	Pencil source, len. ≥ 236 mm	Co-60 and Cs-137

Table 7.1-4 – Allowable Drawer Configurations

Configuration ^①	Recess 1	Recess 2	Recess 3	Recess 4
A	LD-74	LD-74	LD-74	LD-74
B	LD-150	LD-150	LD-150	LD-150
C	LD-200	LD-200	LD-200	LD-200
D	LD-250	LD-250	LD-250	LD-250
E	LD-325	LD-325	LD-325	LD-325
AB	LD-74	LD-150	LD-150	LD-150
BC	LD-150	LD-150	LD-200	LD-200
BD	LD-250	LD-150	LD-150	LD-150

^①Any number of LDs may be replaced with a shield drawer.

Table 7.1-5 – A_i Activity Limits

	Cfg. A	Cfg. B	Cfg. C	Cfg. D	Cfg. E
Isotope	LD-74	LD-150	LD-200	LD-250	LD-325
Co-60 point (Ci)	34400	5800	1800	NA	NA
Co-60 line (Ci)	NA	11800	6500	2600	530
Cs-137 point (Ci)	3.50E+07	3.30E+06	6.40E+05	NA	NA
Cs-137 line (Ci)	NA	8.50E+06	3.90E+06	9.80E+05	1.00E+05
Sr-90 (Ci)	1.60E+07	3.20E+06	1.00E+06	NA	NA
Am-241 (Ci) (no Be)	14800	14200	14200	NA	NA
Am-241Be (Ci)	6.6	6.5	6.4	NA	NA
Pu-238 (g Pu) (no Be)	1300	1300	1300	NA	NA
Pu-239 (g Pu) (no Be)	1.60E+05	1.60E+05	1.50E+05	NA	NA
Pu-239Be (g Pu)	120	120	120	NA	NA
Ir-192 (Ci)	1.00E+05	1.00E+05	1.00E+05	NA	NA
Se-75 (Ci)	1.00E+05	1.00E+05	1.00E+05	NA	NA

	Cfg. AB		Cfg. BC		Cfg. BD	
Isotope	LD-74	LD-150	LD-150	LD-200	LD-150	LD-250
Co-60 point (Ci)	32700	Use Cfg. B Limits	5600	Use Cfg. C Limits	5600	Use Cfg. D Limits
Co-60 line (Ci)	NA		11800		10300	
Cs-137 point (Ci)	3.30E+07		3.30E+06		3.20E+06	
Cs-137 line (Ci)	NA		7.40E+06		6.90E+06	
Sr-90 (Ci)	1.60E+07		3.20E+06		3.10E+06	
Am-241 (Ci) (no Be)	14600		14100		14100	
Am-241Be (Ci)	6.6		6.4		6.4	
Pu-238 (g Pu) (no Be)	1200		1300		1300	
Pu-239 (g Pu) (no Be)	1.60E+05		1.60E+05		1.60E+05	
Pu-239Be (g Pu)	120		120		120	
Ir-192 (Ci)	1.00E+05		1.00E+05		1.00E+05	
Se-75 (Ci)	1.00E+05		1.00E+05		1.00E+05	

7.2 Procedures for Unloading the Package

This section delineates the procedures for unloading a payload from the 1105-SD packaging. The requirements in Section 7.1.1, *General Lifting and Handling*, must be observed when unloading the packaging.

7.2.1 Removal of Contents

7.2.1.1 Unloading the LTSS

1. Disconnect the 1105-SD package tie-downs and remove them from the package.
2. Record the condition of the tamper-indicating lockwires, then remove them.
3. Remove the 5, 1/2-13UNC socket head cap screws (SHCS) from each half of the rain shield (total of 10 bolts).
4. Remove the vent port insulation cylinder and seal test port insulation cylinder from the vent port and seal test port access tubes, respectively.
5. Connect a vent port tool to the vent port.
6. Using the vent port tool, loosen and remove the vent port plug.
7. Vent the cavity to atmosphere to equalize cavity pressure.
8. Remove the 24, 1-1/4-7UNC socket head cap screws from the bell flange. The bolt heads feature holes that may be used with wire hooks to lift the bolts out of the tubes.
9. Using the lift point at the top, remove the bell. Use care not to allow contact of the bell sealing surface with any object capable of scratching the surface, or use a seal surface protector before lifting the bell above the LTSS.
10. The lodgment with the LTSS may be removed from the package base for unloading, or may be unloaded without removing it from the package base.
11. Remove the 8, 1/2-13UNC bolts which connect the upper and lower halves of the lodgment.
12. Release the three toggle clamps. Temporary spacers or equivalent may be used between the LTSS and the lodgment, if necessary, to control the position of the LTSS after release of the toggle clamps.
13. Lift off the lodgment upper half, ensuring that the toggle clamps clear the LTSS.
14. Lift the LTSS out of the lodgment lower half using hoist rings or equivalent mounted in the two M16 threaded holes located in the LTSS lifting blocks. Ensure that the LTSS clears the lodgment lower half as it is being lifted.
15. Replace the upper half of the lodgment using the index marks to align the ribs in the correct orientation.
16. Install the 8, 1/2-13UNC bolts in the clevises which connect the lodgment upper half and lower half. Tighten the hex locknuts only to contact with the clevises.
17. If the lodgment was removed from the package base, replace it using the lifting holes provided in two opposite ribs of the upper lodgment. Using the centering guides located on the lower

internal impact limiter, lower the lodgment into position on the base. Before passing over the base, ensure that the bottom of the lodgment is free of loose debris.

18. Lower the bell into position on the base, using the alignment marks and the alignment pins.
19. Coat closure bolt threads and washer surfaces with a low-halogen, nickel based nuclear grade lubricant prior to assembly. Re-coating is not required if an adequate coat exists. Install the 24 closure bolts, and using a crossing pattern, tighten to at least 150 ft-lb torque, but not more than 330 ft-lb torque.
20. Install and tighten the vent port plug to 48 – 60 in-lb torque.
21. Install the vent port insulation cylinder in the vent port access tube and the seal test port insulation cylinder in the seal test port access tube. Note that both cylinders are identical.
22. Install the two halves of the rain shield using 5 each, 1/2-13UNC bolts, tightened to 22 – 28 ft-lb torque. Optionally, a weather seal may be used with the rain shield, or nuclear-grade duct tape may be used to cover the rain shield or tube sheet-to-impact limiter joints.
23. Place the 1105-SD package and pallet onto the conveyance.
24. Cover the threaded hole in the top of the bell by mechanical means, such as a bolt, per drawing 3021717-SAR.
25. Install the tie-down assembly over the top of the impact limiter, and secure to the conveyance. Ensure that chocks (horizontal restraints) are properly installed on the conveyance.

7.2.1.2 Unloading the Inner Container (IC)

1. Disconnect the 1105-SD package tie-downs and remove them from the package.
2. Record the condition of the tamper-indicating lockwires, then remove them.
3. Remove the 5, 1/2-13UNC socket head cap screws (SHCS) from each half of the rain shield (total of 10 bolts).
4. Remove the vent port insulation cylinder and seal test port insulation cylinder from the vent port and seal test port access tubes, respectively.
5. Connect a vent port tool to the vent port.
6. Using the vent port tool, loosen and remove the vent port plug.
7. Vent the cavity to atmosphere to equalize cavity pressure.
8. Remove the 24, 1-1/4-7UNC socket head cap screws from the bell flange. The bolt heads feature holes that may be used with wire hooks to lift the bolts out of the tubes.
9. Using the lift point at the top, remove the bell. Use care not to allow contact of the bell sealing surface with any object capable of scratching the surface, or use a seal surface protector before lifting the bell above the IC.
10. Using the three, 1/2-13 UNC holes in the lid of the inner container, lift the IC off from the package base.
11. Remove the six, 1-8UNC bolts from the lid of the inner container, and remove the lid.
12. Remove the blocking/dunnage and the shielded device from the inner container.

13. Optionally, replace the blocking/dunnage for the return shipment.
14. Replace the lid on the IC and tighten the six, 1-8UNC bolts to a torque of at least 100 ft-lb torque, but not more than 210 ft-lb.
15. Using the three, ½-13 UNC holes in the lid of the inner container, replace the IC on the package base. Using the centering guides located on the lower internal impact limiter, lower the IC into position on the base. Before passing over the base, ensure that the bottom of the IC is free of loose debris.
16. Lower the bell into position on the base, using the alignment marks and the alignment pins.
17. Coat closure bolt threads and washer surfaces with a low-halogen, nickel based nuclear grade lubricant prior to assembly. Re-coating is not required if an adequate coat exists. Install the 24 closure bolts, and using a crossing pattern, tighten to at least 150 ft-lb torque, but not more than 330 ft-lb torque.
18. Install and tighten the vent port plug to 48 – 60 in-lb torque.
19. Install the vent port insulation cylinder in the vent port access tube and the seal test port insulation cylinder in the seal test port access tube. Note that both cylinders are identical.
20. Install the two halves of the rain shield using 5 each, 1/2-13UNC bolts, tightened to 22 – 28 ft-lb torque. Optionally, a weather seal may be used with the rain shield, or nuclear-grade duct tape may be used to cover the rain shield or tube sheet-to-impact limiter joints.
21. Cover the threaded hole in the top of the bell by mechanical means, such as a bolt, per drawing 3021717-SAR.
22. Place the 1105-SD package and pallet onto the conveyance.
23. Install the tie-down assembly over the top of the impact limiter, and secure to the conveyance. Ensure that chocks (horizontal restraints) are properly installed on the conveyance.

7.3 Preparation of an Empty Package for Transport

Previously used and empty 1105-SD packagings shall be prepared and transported per the requirements of 49 CFR §173.428 [2].

7.4 Preshipment Leakage Rate Test

After the 1105-SD package is assembled and prior to shipment, leakage rate testing shall be performed to confirm proper assembly of the package following the guidelines of Section 7.6, *Preshipment Leakage Rate Test*, and Appendix A.5.2, *Gas Pressure Rise*, of ANSI N14.5 [4].

7.4.1 Gas Pressure Rise Leakage Rate Test Acceptance Criteria

In order to demonstrate containment integrity in preparation for shipment, no leakage shall be detected when tested to a sensitivity of 1×10^{-3} reference cubic centimeters per second (ref-cm³/s) air, or less, per Section 7.6 of ANSI N14.5, *Preshipment Leakage Rate Test*.

7.4.2 Determining the Test Volume and Test Time

1. Assemble a leakage rate test apparatus that consists of, at a minimum, the components illustrated in Figure 7.4–1, using a calibrated volume with a range of 6 – 31 cubic inches, and a calibrated pressure transducer with a minimum sensitivity of 100 millitorr. Connect the test apparatus to the test volume (i.e., the seal test port, or vent port insert, as appropriate).
2. Set the indicated sensitivity on the digital readout of the calibrated pressure transducer, ΔP , to, at a minimum, the resolution (i.e., sensitivity) of the calibrated pressure transducer (e.g., $\Delta P = 1, 10, \text{ or } 100$ millitorr sensitivity).
3. Open all valves (i.e., the vent valve, calibration valve, and vacuum pump isolation valve), and record ambient atmospheric pressure, P_{atm} .
4. Isolate the calibrated volume by closing the vent and calibration valves.
5. Evacuate the test volume to a pressure less than the indicated sensitivity on the digital readout of the calibrated pressure transducer or 1.0 torr, whichever is less.
6. Isolate the vacuum pump from the test volume by closing the vacuum pump isolation valve. Allow the test volume pressure to stabilize and record the test volume pressure, P_{test} (e.g., $P_{\text{test}} < 1$ millitorr for an indicated sensitivity of 1 millitorr).
7. Open the calibration valve and, after allowing the system to stabilize, record the total volume pressure, P_{total} .
8. Knowing the calibrated volume, V_c , calculate and record the test volume, V_t , using the following equation:

$$V_t = V_c \left(\frac{P_{\text{atm}} - P_{\text{total}}}{P_{\text{total}} - P_{\text{test}}} \right)$$

9. Knowing the indicated sensitivity on the digital readout of the calibrated pressure transducer, ΔP , calculate and record the test time, t , using the following equation:

$$t = \Delta P(1.32)V_t$$

7.4.3 Performing the Gas Pressure Rise Leakage Rate Test

1. Isolate the calibrated volume by closing the calibration valve.

2. Open the vacuum pump isolation valve and evacuate the test volume to a pressure less than the test volume pressure, P_{test} , determined in Step 6 of Section 7.4.2, *Determining the Test Volume and Test Time*.
3. Isolate the vacuum pump from the test volume by closing the vacuum pump isolation valve. Allow the test volume pressure to stabilize and record the beginning test pressure, P_1 . After a period of time equal to “t” seconds, determined in Step 9 of Section 7.4.2, *Determining the Test Volume and Test Time*, record the ending test pressure, P_2 . To be acceptable, there shall be no difference between the final and initial pressures such that the requirements of Section 7.4.1, *Gas Pressure Rise Leakage Rate Test Acceptance Criteria*, are met.
4. If, after repeated attempts, the O-ring seal fails to pass the leakage rate test, replace the damaged seal and/or repair the damaged sealing surfaces per Section 8.2.3.2, *Sealing Area Routine Inspection and Repair*. Perform verification leakage rate test per the applicable procedure delineated in Section 8.2.2, *Maintenance/Periodic Leakage Rate Tests*.

7.4.4 Optional Preshipment Leakage Rate Test

As an option to Section 7.4.3, *Performing the Gas Pressure Rise Leakage Rate Test*, Section 8.2.2, *Maintenance/Periodic Leakage Rate Tests*, may be performed.

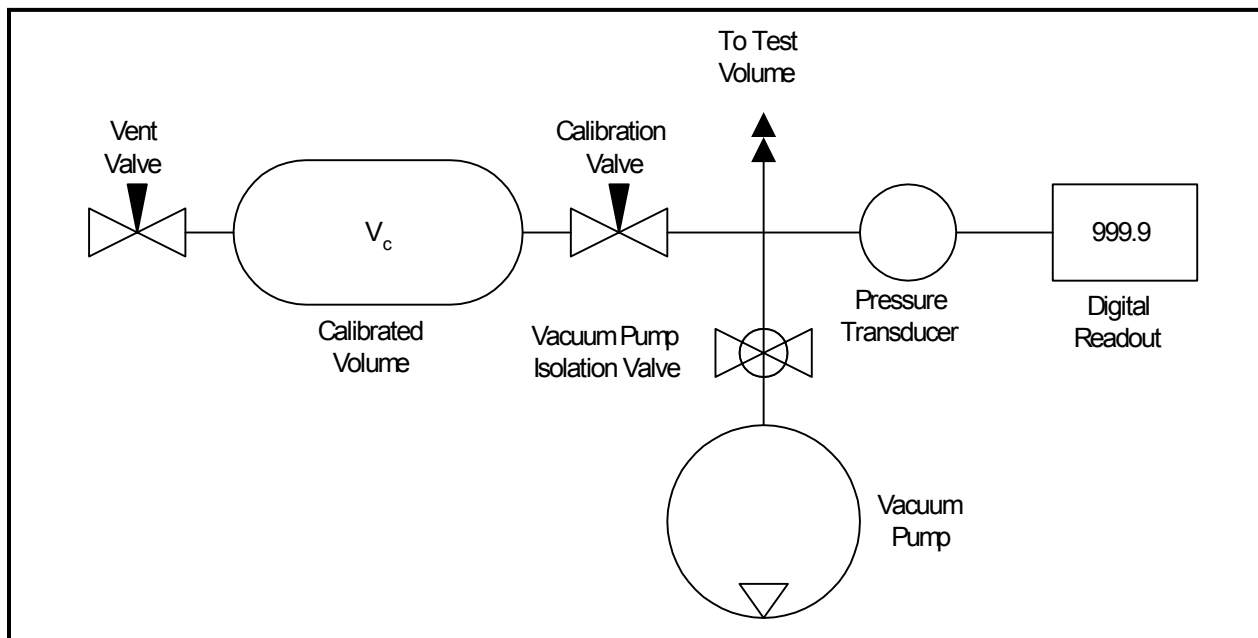


Figure 7.4-1 – Pressure Rise Leakage Rate Test Schematic

7.5 Appendix

7.5.1 LTSS Loading Examples

Example 1:

Recess 1: LD-74 with 7,000 Ci Cs-137, point source
Recess 2: LD-74 with 5,000 Ci Cs-137, point source
Recess 3: LD-74 with 2,000 Ci Co-60, point source
Recess 4: LD-74 with 3,000 Ci Co-60, point source

Step 1: The total Cs-137 (12,000 Ci) and Co-60 (5,000 Ci) are less than the limits in Table 7.1-1.
Step 2: No plutonium or americium, does not apply.
Step 3: No plutonium or americium, air transport allowed.
Step 4: The total power is 138 watts \leq 200 watts based on Table 7.1-2.
Step 5: Physical form restrictions in Table 7.1-3 are met.
Step 6: The drawer configuration is consistent with Configuration A in Table 7.1-4.
Step 7: Table 7.1-5 Configuration A limits apply. The sum of fractions = $0.15 \leq 1.0$.

Therefore, this shipment is allowed by air (including commercial aircraft), land, or sea transport.

Example 2:

Recess 1: LD-150 with two NLM52-74 capsules. The first capsule has 1,000 Ci Co-60 and the second capsule has 1,000 Ci Sr-90
Recess 2: LD-150 with 5,000 Ci Cs-137, line source
Recess 3: LD-150 with 2,000 Ci Co-60, point source
Recess 4: LD-150 with 2 Ci AmBe

Step 1: The total Cs-137 (5,000 Ci), Co-60 (3,000 Ci), Sr-90 (1,000 Ci) and AmBe (2 Ci) are less than or equal to the limits in Table 7.1-1.
Step 2: Fissile mass = $0.001 * 2 = 0.002 \text{ g} \leq 15 \text{ g}$.
Step 3: Contains americium, air transport not allowed.
Step 4: The total power is 78 watts \leq 200 watts based on Table 7.1-2.
Step 5: Physical form restrictions in Table 7.1-3 are met.
Step 6: The drawer configuration is consistent with Configuration B in Table 7.1-4.
Step 7: Table 7.1-5 Configuration B limits apply. The sum of fractions = $0.83 \leq 1.0$.

Therefore, this shipment is allowed by land or sea transport.

Example 3:

Recess 1: LD-74 with 15 g Pu in a Pu-238O₂ source
Recess 2: LD-74 with 15 g Pu in a Pu-238O₂ source
Recess 3: LD-74 with 2 g Pu in a Pu-239O₂ source
Recess 4: LD-74 with 2 g Pu in a Pu-239Be source

Step 1: The total Pu in the Pu-238 source (30 g) and total Pu in the Pu-239 source (4 g) are less than the limits in Table 7.1-1.

Step 2: The total fissile material in the package is $30 \text{ g} \cdot 0.2 + 4 \text{ g} = 10 \text{ g} \leq 15 \text{ g}$.

Step 3: Due to the presence of plutonium sources, air transport is not permitted.

Step 4: The total power is 17 watts \leq 200 watts based on Table 7.1-2.

Step 5: Physical form restrictions in Table 7.1-3 are met.

Step 6: The drawer configuration is consistent with Configuration A in Table 7.1-4.

Step 7: Table 7.1-5 Configuration A limits apply. The sum of fractions = $0.04 \leq 1.0$.

Therefore, this shipment is allowed by land or sea transport.

7.5.2 References

1. Title 10, Code of Federal Regulations, Part 71 (10 CFR 71), *Packaging and Transportation of Radioactive Material*, 01–01–18 Edition.
2. Title 49, Code of Federal Regulations, Part 173 (49 CFR 173), *Shippers–General Requirements for Shipments and Packagings*, 10–01–18 Edition
3. Title 49, Code of Federal Regulations, Part 172 (49 CFR 172), *Hazardous Materials Tables and Hazardous Communications Regulations*, 10–01–18 Edition.
4. ANSI N14.5–2014, *American National Standard for Radioactive Materials – Leakage Tests on Packages for Shipment*, American National Standards Institute (ANSI), Inc.

This page left intentionally blank.

8.0 ACCEPTANCE TESTS AND MAINTENANCE PROGRAM

This section describes the acceptance tests and the maintenance program that shall be used on the 1105-SD package in compliance with Subpart G of 10 CFR 71 [1].

8.1 Acceptance Tests

Per the requirements of 10 CFR §71.85, this section discusses the inspections and tests to be performed prior to first use of the 1105-SD packaging. Successful completion of these tests will ensure that the requirements of 10 CFR §71.85(a) have been met. Acceptance criteria for all inspections and tests are found either on the drawings in Appendix 1.3.3, *Packaging General Arrangement Drawings*, or in the sections that follow. Deviations from requirements will be recorded and dispositioned in accordance with the cognizant quality assurance program.

8.1.1 Visual Inspection and Measurements

Each 1105-SD packaging will be visually inspected and measured to ensure that all of the requirements delineated on the drawings in Appendix 1.3.3, *Packaging General Arrangement Drawings*, are satisfied. This includes but is not limited to such items as materials, physical arrangement of components, quantities, dimensions, welds, and measurements.

8.1.2 Weld Examinations

The locations, types, and sizes of all welds will be identified and recorded to ensure compliance with the drawings in Appendix 1.3.3, *Packaging General Arrangement Drawings*. All welds are subject to visual examination per AWS D1.6 [2] or AWS D1.2 for aluminum [18]. All containment boundary welds (those joining the torispherical heads, cylindrical shell, and flanges, including the bell lifting boss and any axial joints) are examined by radiographic inspection in accordance with the ASME Code, Subsection NB, Article NB-5000, and Section V, Article 2 [3]. Containment boundary welds associated with the vent port and all welds subject to radiographic inspection are liquid penetrant inspected on the final pass in accordance with the ASME Code, Subsection NB, Article NB-5000, and Section V, Article 6 [4]. All other welds on the 1105-SD package, except seal, tack, and intermittent welds, are liquid penetrant inspected on the final pass in accordance with the ASME Code, Subsection NF, Article NF-5000, and Section V, Article 6 [5].

8.1.3 Structural and Pressure Tests

8.1.3.1 Lifting Device Load Testing

The 1105-SD package is lifted and handled using a pallet, and thus does not contain any lifting devices that require load testing.

8.1.3.2 Containment Boundary Pressure Testing

Since the MNOP equals 5 psig, no pressure test is required by 10 CFR 71.85(b). The 1105-SD package containment boundary is pressure tested to 125% of the design pressure of 25 psig per the requirements of ASME Code, Subsection NB, Article NB-6220 [6], or a test pressure of 31.25 psig.

Following pressure testing of the containment boundary, welds directly related to the pressure testing and accessible base material adjacent to the welds shall be visually inspected for plastic deformation or cracking in accordance with AWS D1.6, and liquid penetrant inspected per ASME Code, Subsection NB, Article NB-5000, and Section V, Article 6, as delineated on the drawings in Appendix 1.3.3, *Packaging General Arrangement Drawings*. Indications of cracking or distortion shall be recorded and evaluated in accordance with the cognizant quality assurance program.

Leakage rate testing per Section 8.1.4, *Fabrication Leakage Rate Tests*, shall be performed after completion of pressure testing to verify package configuration and performance to design criteria.

8.1.4 Fabrication Leakage Rate Tests

This section provides the generalized procedure for fabrication leakage rate testing of the containment vessel boundary and vent port penetration during fabrication. Fabrication leakage rate testing shall follow the guidelines of Section 7.3, *Fabrication Leakage Rate Test*, of ANSI N14.5 [7]. Three separate tests comprise the series. Each test shall meet the acceptance criteria delineated in Section 8.1.4.1, *Fabrication Leakage Rate Test Acceptance Criteria*.

8.1.4.1 Fabrication Leakage Rate Test Acceptance Criteria

1. To be acceptable, each leakage rate test shall demonstrate a “leaktight” leakage rate of 1×10^{-7} reference cubic centimeters per second (ref-cm³/s), air, or less, per Section 6.3, *Application of Reference Air Leakage Rate (L_R)*, of ANSI N14.5.
2. In order to demonstrate the leaktight leakage rate, the sensitivity of the leakage rate test procedure shall be 5×10^{-8} cm³/s, air, or less, per Section 8.4, *Sensitivity*, of ANSI N14.5.
3. Failure to meet the stated leakage rate shall be recorded and evaluated in accordance with the cognizant quality assurance program.

8.1.4.2 Helium Leakage Rate Testing the Containment Structure Integrity

This leakage rate test verifies the leak tightness of the containment boundary structures, including the lower torispherical head, lower flange, upper torispherical head, cylindrical body, upper flange, and connecting welds.

1. The fabrication leakage rate test shall be performed following the guidelines of Section A.5.3, *Gas Filled Envelope – Gas Detector*, of ANSI N14.5.
2. The upper and lower halves of the containment boundary shall be assembled together for the test. The stage of completion of the 1105-SD packaging shall be sufficient to support the test.
3. Connect a port tool to the vent port in the upper flange.
4. Install a helium mass spectrometer leak detector (MSLD) to the port tool. Evacuate through the port until the vacuum is sufficient to operate the MSLD.
5. Surround the outer surface of the containment body with an envelope filled with helium gas (99% purity or better) to a minimum concentration of 50%, and to a pressure slightly greater than atmospheric pressure. The final leakage rate shall be adjusted for the helium concentration in the envelope.

6. Perform the helium leakage rate test to the requirements of Section 8.1.4.1, *Fabrication Leakage Rate Test Acceptance Criteria*. If, after repeated attempts, the containment structure fails to pass the leakage rate test, isolate the leak path and, prior to repairing the leak path and repeating the leakage rate test, record on a nonconformance report and disposition prior to final acceptance in accordance with the cognizant quality assurance program.

8.1.4.3 Helium Leakage Rate Testing the Containment O–ring Seal

1. The fabrication leakage rate test of the 1105-SD package containment O–ring seal integrity shall be performed following the guidelines of Section A.5.4, *Evacuated Envelope – Gas Detector*, of ANSI N14.5.
2. Assemble the 1105-SD package with the two O–ring seals installed in the lower flange and the closure bolts tightened. Ensure the vent and seal test ports are installed with their associated sealing washers. Assembly information is given in Appendix 1.3.3, *Packaging General Arrangement Drawings*.
3. Utilizing a port tool, attach a vacuum pump and a source of helium gas, in parallel, to the vent port.
4. Close the valve to the source of helium gas and open the valve to the vacuum pump.
5. Utilizing a port tool, rotate the vent port plug to the open position.
6. Evacuate the system to a 90% vacuum or better ($\leq 10\%$ ambient atmospheric pressure). Isolate the vacuum pump from the system.
7. Provide a helium atmosphere inside the evacuated cavity by backfilling with helium gas (99% purity or better) to ambient atmospheric pressure (+1 psi, -0 psi).
8. Utilizing the port tool, rotate the vent port plug to the closed position, and remove the helium–contaminated port tool from the vent port.
9. Install a clean (helium–free) port tool into the seal test port.
10. Attach a helium MSLD to the port tool.
11. Utilizing the port tool, rotate the seal test port plug to the open position.
12. Evacuate the cavity between the containment O–ring seal and the test O–ring seal until the vacuum is sufficient to operate the leak detector per the manufacturer’s recommendations.
13. Perform the helium leakage rate test to the requirements of Section 8.1.4.1, *Fabrication Leakage Rate Test Acceptance Criteria*. If, after repeated attempts, the 1105-SD package containment O–ring seal fails to pass the leakage rate test, isolate the leak path and, prior to repairing the leak path and repeating the leak test, record on a nonconformance report and disposition prior to final acceptance in accordance with the cognizant quality assurance program.

8.1.4.4 Helium Leakage Rate Testing the Vent Port Sealing Washer

1. The fabrication leakage rate test of the vent port plug sealing washer integrity shall be performed following the guidelines of Section A.5.4, *Evacuated Envelope – Gas Detector*, of ANSI N14.5.
2. Assemble the 1105-SD package with the two O–ring seals installed in the lower flange and the closure bolts tightened. Ensure the vent and seal test ports are installed with their

associated sealing washers. Assembly information is given in Appendix 1.3.3, *Packaging General Arrangement Drawings*.

3. Verify the presence of a helium atmosphere below the vent port plug sealing washer, as specified above in Steps 3 – 8 of Section 8.1.4.3, *Helium Leakage Rate Testing the Containment O-ring Seal*. Alternatively, perform this test immediately after the containment O-ring seal test.
4. Install a clean (helium-free) port tool into the vent port.
5. Attach a helium MSLD to the port tool.
6. Evacuate the cavity above the vent port plug sealing washer until the vacuum is sufficient to operate the leak detector per the manufacturer's recommendations.
7. Perform the helium leakage rate test to the requirements of Section 8.1.4.1, *Fabrication Leakage Rate Test Acceptance Criteria*. If, after repeated attempts, the vent port plug sealing washer fails to pass the leakage rate test, isolate the leak path and, prior to repairing the leak path and repeating the leak test, record on a nonconformance report and disposition prior to final acceptance in accordance with the cognizant quality assurance program.

8.1.5 Component and Material Tests

8.1.5.1 Polyurethane Foam

This section establishes the requirements and acceptance criteria for installation, inspection, and testing of the rigid, closed-cell polyurethane foam utilized within the 1105-SD packaging impact limiter. These requirements apply only to the nominally 15 lb/ft³ foam used in the external impact limiter, since the performance of this material is important to the structural and thermal evaluations of the packaging. These requirements do not apply to the nominally 30 lb/ft³ foam blocks used in the upper body assembly, because these components are used primarily as spacing material, and their structural and thermal performance is not critical.

8.1.5.1.1 Introduction and General Requirements

The polyurethane foam used within the 1105-SD packaging is comprised of a specific “formulation” of foam constituents that, when properly apportioned, mixed, and reacted, produce a polyurethane foam material with physical characteristics consistent with the requirements given in Section 8.1.5.1.2, *Physical Characteristics*. In practice, the chemical constituents are batched into multiple parts (e.g., parts A and B) for later mixing in accordance with a formulation. Therefore, a foam “batch” is considered to be a specific grouping and apportionment of chemical constituents into separate and controlled vats or bins for each foam formulation part. Portions from each batch part are combined in accordance with the foam formulation requirements to produce the liquid foam material for pouring into a component or box. Thus, a foam “pour” is defined as apportioning and mixing the batch parts into a desired quantity for subsequent installation (pouring). Finally, all contiguous pours into a single mold are termed a “bun”.

The following sections describe the general requirements for constituent storage, and foam pour and test data records. The major chemical constituents of the foam are: carbon, 50% - 70%, oxygen, 14% - 34%, nitrogen, 4% - 12%, and hydrogen, 4% - 10%.

8.1.5.1.1.1 Polyurethane Foam Constituent Storage

The foam supplier shall certify that the polyurethane foam constituents have been properly stored prior to use, and that the polyurethane foam constituents have been used within their shelf life.

8.1.5.1.1.2 Polyurethane Foam Installation

The foam shall be installed while the longitudinal axis of the impact limiter shell is vertical. The walls of the shell where the liquid foam material is to be installed shall be between 55 °F and 95 °F prior to foam installation. Measure and record the shell temperature to an accuracy of ± 2 °F.

In the case of multiple pours into a single impact limiter, the cured level of each pour shall be measured and recorded to an accuracy of ± 1 inch.

Measure and record the weight of liquid foam material installed during each pour to an accuracy of ± 10 pounds.

All test samples shall be poured into disposable containers at the same time as the actual pour it represents, clearly marking the test sample container with the pour date and a unique pour identification number. All test samples shall be cut from a larger block to obtain freshly cut faces. Prior to physical testing, each test sample shall be cleaned of superfluous foam dust.

8.1.5.1.1.3 Polyurethane Foam Pour and Test Data Records

A production pour and testing record shall be compiled by the foam supplier during the foam pouring operation and subsequent physical testing. Upon completion of production and testing, the foam supplier shall issue a certification referencing the production record data and test data pertaining to each foamed component. At a minimum, relevant pour and test data shall include:

- formulation, batch, and pour numbers, with foam material traceability, and pour date,
- instrumentation description, serial number, and calibration due date,
- pour and test data (e.g., date, temperature, dimensional, and/or weight measurements, compressive stress, etc., as applicable), and
- technician and Quality Assurance/Quality Control (QA/QC) sign-off.

8.1.5.1.2 Physical Characteristics

The following subsections define the required physical characteristics of the polyurethane foam material.

Testing for the various polyurethane foam physical characteristics is based on a “formulation”, “batch”, or “pour”, as appropriate, as defined in Section 8.1.5.1.1, *Introduction and General Requirements*. The physical characteristics determined for a specific foam formulation are relatively insensitive to small variations in chemical constituents and/or environmental conditions, and therefore include physical testing only for leachable chlorides, thermal conductivity, and specific heat. Similarly, the physical characteristics determined for a batch are only slightly sensitive to small changes in formulation and/or environmental conditions during batch mixing, and therefore include physical testing only for flame retardancy. Finally, the physical characteristics determined for a pour are also only slightly sensitive to small changes in formulation and slightly more sensitive to variations in environmental conditions during pour mixing, and therefore include physical testing for density and compressive stress.

8.1.5.1.2.1 Physical Characteristics Determined for a Foam Formulation

8.1.5.1.2.1.1 Leachable Chlorides

The leachable chloride physical characteristic shall be determined once for a particular foam formulation. If multiple components are to utilize a specific foam formulation, then additional physical testing, as defined below, need not be performed.

1. The leachable chlorides test shall be performed using an ion chromatograph (IC) apparatus. The IC measures inorganic anions of interest (i.e., chlorides) in water. Description of a typical IC is provided in EPA Method 300.0 [8]. The IC shall be calibrated against a traceable reference specimen per the IC manufacturer's operating instructions.
2. One test sample shall be taken from a pour for each foam formulation. The test sample shall be a cube with dimensions of 2.00 ± 0.06 in.
3. Place the test sample in a room (ambient) temperature environment (i.e., 65 °F to 85 °F) for sufficient time to thermally stabilize the test sample. Measure and record the room temperature to an accuracy of ± 2 °F.
4. Obtain a minimum of 550 mL of distilled or de-ionized water for testing. The test water shall be from a single source to ensure consistent anionic properties for testing control.
5. Obtain a 400 mL, or larger, contaminant free container that is capable of being sealed. Fill the container with 262 ± 3 mL of test water. Fully immerse the test sample inside the container for a duration of 72 ± 3 hours. If necessary, use an inert standoff to ensure the test sample is completely immersed for the full test duration. Seal the container prior to the 72-hour duration.
6. Obtain a second, identical container to use as a "control". Fill the control container with 262 ± 3 mL of the same test water. Seal the control container prior to the 72-hour duration.
7. At the end of the test period, measure and record the leachable chlorides in the test water per the IC manufacturer's operating instructions. The leachable chlorides in the test water shall not exceed one part per million (1 ppm).
8. Should leachable chlorides in the test water exceed 1 ppm, measure and record the leachable chlorides in the test water from the "control" container. The difference in leachable chlorides from the test water and "control" water sample shall not exceed 1 ppm.

8.1.5.1.2.1.2 Thermal Conductivity

1. The thermal conductivity test shall be performed using a heat flow meter (HFM) apparatus. The HFM establishes steady state unidirectional heat flux through a test specimen between two parallel plates at constant but different temperatures. By measurement of the plate temperatures and plate separation, Fourier's law of heat conduction is used by the HFM to automatically calculate thermal conductivity. Description of a typical HFM test method is provided in ASTM C518 [9]. The HFM shall be calibrated against a traceable reference specimen per the HFM manufacturer's operating instructions.
2. Three test samples shall be taken from the sample pour. Each test sample shall be of sufficient size to enable testing per the HFM manufacturer's operating instructions.

3. Place the test samples in a room (ambient) temperature environment (i.e., 65 °F to 85 °F) for sufficient time to thermally stabilize the test samples.
4. Measure and record the necessary test sample parameters as input data to the HFM apparatus per the HFM manufacturer's operating instructions.
5. Perform thermal conductivity testing and record the measured thermal conductivity for each test sample following the HFM manufacturer's operating instructions.
6. Determine and record the average thermal conductivity of the three test samples. The numerically averaged thermal conductivity of the three test samples shall be within the range between 0.22 and 0.34 (BTU-in)/(hr-ft²-°F).

8.1.5.1.2.1.3 Specific Heat

1. The specific heat test shall be performed using a differential scanning calorimeter (DSC) apparatus. The DSC establishes a constant heating rate and measures the differential heat flow into both a test specimen and a reference specimen. Description of a typical DSC is provided in ASTM E1269 [10]. The DSC shall be calibrated against a traceable reference specimen per the DSC manufacturer's operating instructions.
2. Three test samples shall be taken from the sample pour. Each test sample shall be of sufficient size to enable testing per the DSC manufacturer's operating instructions.
3. Place the test samples in a room (ambient) temperature environment (i.e., 65 °F to 85 °F) for sufficient time to thermally stabilize the test samples.
4. Measure and record the necessary test sample parameters as input data to the DSC per the DSC manufacturer's operating instructions.
5. Perform specific heat testing and record the measured specific heat for each test sample following the DSC manufacturer's operating instructions.
6. Determine and record the average specific heat of the three test specimens. The numerically averaged specific heat of the three test samples shall be within the range between 0.28 and 0.42 Btu/lb_m-°F.

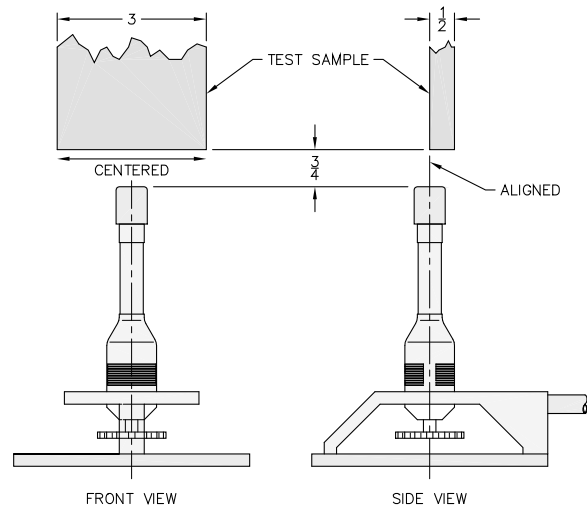
8.1.5.1.2.2 Physical Characteristics Determined for a Foam Batch

Polyurethane foam material physical characteristics for flame retardancy shall be determined once for a particular foam batch based on the batch definition in Section 8.1.5.1.1, *Introduction and General Requirements*. If single or multiple components are to utilize a single foam batch, then additional flame retardancy testing, as defined below, need not be performed for each foam pour.

Polyurethane foam shall be tested for flame retardancy as follows:

1. Three test samples shall be taken from a pour from each foam batch. Each test sample shall be a rectangular prism with nominal dimensions of 0.5 inches thick, 3.0 inches wide, and a minimum length of 8.0 inches. In addition, individual sample lengths must not be less than the total burn length observed for the sample when tested.
2. Place the test samples in a room (ambient) temperature environment (i.e., 65 °F to 85 °F) for sufficient time to thermally stabilize the test samples. Measure and record the room temperature to an accuracy of ±2 °F.

3. Install an approximately 3/8-inch, or larger, Bunsen or Tirrill burner inside an enclosure of sufficient size to perform flame retardancy testing. Adjust the burner flame height to $1\frac{1}{2} \pm 1/4$ inch. Verify that the burner flame temperature is 1,550 °F, minimum.
4. Support the test sample with the long axis oriented vertically within the enclosure such that the test sample's bottom edge will be $3/4 \pm 1/8$ inch (see adjacent figure) above the top edge of the burner.
5. Move the burner flame under the test sample for an elapsed time of 60 ± 2 seconds. As illustrated, align the burner flame with the front edge of the test sample thickness and the center of the test sample width.
6. Immediately after removal of the test sample from the burner flame, measure and record the following data:
 - a. Measure and record, to the nearest second, the elapsed time until flames from the test sample extinguish.
 - b. Measure and record, to the nearest second, the elapsed time from the occurrence of drips, if any, until drips from the test sample extinguish.
 - c. Measure and record, to the nearest 0.15 inch, the burn length following cessation of all visible burning and smoking.
7. Flame retardancy testing acceptance is based on the following criteria:
 - a. The numerically averaged flame extinguishment time of the three test samples shall not exceed fifteen seconds.
 - b. The numerically averaged flame extinguishment time of drips from the three test samples shall not exceed three seconds.
 - c. The numerically averaged burn length of the three test samples shall not exceed 6.0 in.



8.1.5.1.2.3 Physical Characteristics Determined for a Foam Pour

8.1.5.1.2.3.1 Density

Polyurethane foam material physical characteristic for density shall be determined for each foam pour based on the pour definition in Section 8.1.5.1.1, *Introduction and General Requirements*.

1. Three test samples shall be taken from the foam pour. Each test sample shall be a rectangular prism with minimum nominal dimensions of 1.0 inch thick (T) \times 2.0 inch wide (W) \times 2.0 inch long (L).
2. Place the test samples in a room (ambient) temperature environment (i.e., 65 °F to 85 °F) for sufficient time to thermally stabilize the test samples. Measure and record the room temperature to an accuracy of ± 2 °F.
3. Measure and record the weight of each test sample to an accuracy of ± 1 gram.

4. Measure and record the thickness, width, and length of each test sample to an accuracy of ± 0.03 in.
5. Determine and record the room temperature density of each test sample utilizing the following formula:

$$\rho_{foam} = \frac{\text{Weight, g}}{453.6 \text{ g/lb}_m} \times \frac{1,728 \text{ in}^3/\text{ft}^3}{T \times W \times L, \text{ in}^3}, \text{ lb}_m/\text{ft}^3$$

6. Determine and record the average density of the three test samples. The numerically averaged density of the three test samples shall be within $\pm 15\%$ of the specified nominal foam density, i.e., within the range of 12.7 to 17.3 lb_m/ft^3 for a nominal 15 lb_m/ft^3 foam.

8.1.5.1.2.3.2 Compressive Stress

1. Three test samples shall be taken from each foam pour. Each test sample shall be a rectangular prism with minimum nominal dimensions of 1.0 inch thick (T) \times 2.0 inch wide (W) \times 2.0 inch long (L). The thickness dimension shall be the parallel-to-rise direction (for the perpendicular-to-rise direction, see below).
2. Place the test samples in a room (ambient) temperature environment (i.e., 65 °F to 85 °F) for sufficient time to thermally stabilize the test samples. Measure and record the room temperature to an accuracy of ± 2 °F.
3. Measure and record the thickness, width, and length of each test sample to an accuracy of ± 0.03 inch.
4. Compute and record the surface area of each test sample by multiplying the width by the length (i.e., $W \times L$).
5. Place a test sample in a Universal Testing Machine. Lower the machine's crosshead until it touches the test sample. Set the machine's parameters for the thickness of the test sample.
6. Determine and record the average parallel-to-rise compressive stress of the three test samples from each batch pour for each foam density. As shown in Table 8.1-1, the average parallel-to-rise compressive stress for each foam pour shall be the nominal compressive stress $\pm 15\%$ at strains of 10%, 40%, and 70%.
7. Determine and record the average parallel-to-rise compressive stress of all test samples from each foamed component. As shown in Table 8.1-1, the average parallel-to-rise compressive stress for all foam pours used in a single bun shall be the nominal compressive stress $\pm 10\%$ at strains of 10%, 40%, and 70%.
8. Data for compressive stress in the perpendicular-to-rise direction shall be obtained in an identical manner, using three additional test samples, except that the thickness dimension of the test samples shall be perpendicular to the foam rise direction. As shown in Table 8.1-2, the average perpendicular-to-rise compressive stress for each foam pour shall be the nominal compressive stress $\pm 15\%$ at strains of 10%, 40%, and 70%. As further shown in Table 8.1-2, the average perpendicular-to-rise compressive stress for all foam pours used in a single bun shall be the nominal compressive stress $\pm 10\%$ at strains of 10%, 40%, and 70%.

8.1.5.2 Butyl Rubber O-rings

Physical characteristics of the butyl rubber containment O-ring seals and sealing washers for the following parameters shall be determined for each lot based on the following acceptance tests. All material shall conform to the following ASTM D2000 [11] designation:

M4AA710 A13 B13 F17 F48 Z Trace Element.

8.1.5.2.1 Durometer

The durometer of each lot of the butyl rubber material shall be determined in accordance with ASTM D2240 [12]. Each lot of butyl rubber material shall have a hardness of 70 ± 5 Shore A durometer (i.e., within the range of 65 to 75 Shore A durometer).

8.1.5.2.2 Tensile Strength and Elongation

The tensile strength of each lot of the butyl rubber material shall be determined in accordance with ASTM D412 [13]. Each lot of butyl rubber material shall have a minimum tensile strength of 10 MPa and a minimum elongation of 250%.

8.1.5.2.3 Heat Resistance

The heat resistance of each lot of the butyl rubber material shall be determined in accordance with ASTM D573 [14]. Each lot of butyl rubber material shall experience a maximum 10 Shore A durometer hardness increase, a maximum reduction in tensile strength of 25%, and a maximum reduction in ultimate elongation of 25%, when tested at 70 °C.

8.1.5.2.4 Compression Set

The compression set of each lot of the butyl rubber material shall be determined in accordance with Method B of ASTM D395 [15]. After 22 hours at 70 °C, each lot of butyl rubber material shall have a maximum compression set of 25%.

8.1.5.2.5 Cold Temperature Resistance

The cold temperature resistance of each lot of the butyl rubber material shall be determined in accordance with Method A, 9.3.2 of ASTM D2137 [16]. After 3 minutes at -40 °C, each lot of butyl rubber material shall be non-brittle.

8.1.5.2.6 Cold Temperature Resiliency

The cold temperature resiliency of each lot of the butyl rubber material shall be determined in accordance with the TR-10 test of ASTM D1329 [17]. Each lot of butyl rubber material shall be resilient at a test temperature of -50 °C or less.

8.1.6 Shielding Integrity Tests

The 1105-SD does not include any components whose primary purpose is shielding. Therefore, tests to demonstrate the integrity of shielding components are not required.

8.1.7 Thermal Tests

Tests to demonstrate the heat transfer capability of the packaging are not required because the thermal evaluations presented in Chapter 3, *Thermal Evaluation*, are based on well established heat transfer properties and methodologies and demonstrate relatively large thermal margins for all components. As such, the uncertainties in the predicted temperature levels are small. Further, since the thermal modeling incorporates several conservative assumptions, it is expected that the peak temperatures achieved will be less than predicted. See Chapter 3, *Thermal Evaluation*, for further discussions.

Table 8.1-1 – Compressive Strength (psi) Parallel-to-Foam Rise at 65°F to 85°F

Strain	Minimum		Nominal	Maximum	
	Nom. –15%	Nom. –10%		Nom. +10%	Nom. +15%
10%	535	566	629	692	723
40%	641	679	754	829	867
70%	2,248	2,381	2,645	2,910	3,042

Table 8.1-2 – Compressive Strength (psi) Perpendicular-to-Foam Rise at 65°F to 85°F

Strain	Minimum		Nominal	Maximum	
	Nom. –15%	Nom. –10%		Nom. +10%	Nom. +15%
10%	513	543	603	663	693
40%	654	692	769	846	884
70%	2,287	2,422	2,691	2,960	3,095

8.2 Maintenance Program

This section describes the maintenance program used to ensure continued performance of the 1105-SD packaging.

8.2.1 Structural and Pressure Tests

No structural or pressure tests are necessary to ensure continued performance of the packaging.

8.2.2 Maintenance/Periodic Leakage Rate Tests

This section provides the generalized procedure for maintenance/periodic leakage rate testing of the containment boundary penetrations during routine maintenance, or at the time of seal replacement or sealing area repair. Maintenance leakage rate testing shall follow the guidelines of Section 7.4, *Maintenance Leakage Rate Test*, and Section 7.5, *Periodic Leakage Rate Test*, of ANSI N14.5.

Maintenance/periodic leakage rate testing shall be performed on the main O-ring seal and the vent port sealing washer in accordance with Section 8.2.2.1, *Helium Leakage Rate Testing the Containment O-ring Seal* and 8.2.2.2, *Helium Leakage Rate Testing the Vent Port Sealing Washer*. Each leakage rate test shall meet the acceptance criteria delineated in Section 8.1.4.1, *Fabrication Leakage Rate Test Acceptance Criteria*.

8.2.2.1 Helium Leakage Rate Testing the Containment O-ring Seal

1. The maintenance/periodic leakage rate test of the 1105-SD package containment O-ring seal integrity shall be performed following the guidelines of Section A.5.4, *Evacuated Envelope – Gas Detector*, of ANSI N14.5.
2. Assemble the 1105-SD package with the two O-ring seals installed in the lower flange and the closure bolts tightened. Ensure the vent and seal test ports are installed with their associated sealing washers. Assembly information is given in Appendix 1.3.3, *Packaging General Arrangement Drawings*.
3. Utilizing a port tool, attach a vacuum pump and a source of helium gas, in parallel, to the vent port.
4. Close the valve to the source of helium gas and open the valve to the vacuum pump.
5. Utilizing a port tool, rotate the vent port plug to the open position.
6. Evacuate the system to a 90% vacuum or better ($\leq 10\%$ ambient atmospheric pressure). Isolate the vacuum pump from the system.
7. Provide a helium atmosphere inside the evacuated cavity by backfilling with helium gas (99% purity or better) to ambient atmospheric pressure (+1 psi, -0 psi).
8. Utilizing the port tool, rotate the vent port plug to the closed position, and remove the helium-contaminated port tool from the vent port.
9. Install a clean (helium-free) port tool into the seal test port.
10. Attach a helium MSLD to the port tool.
11. Utilizing the port tool, rotate the seal test port plug to the open position.

12. Evacuate the cavity between the containment O-ring seal and the test O-ring seal until the vacuum is sufficient to operate the leak detector per the manufacturer's recommendations.
13. Perform the helium leakage rate test to the requirements of Section 8.1.4.1, *Fabrication Leakage Rate Test Acceptance Criteria*. If, after repeated attempts, the 1105-SD package containment O-ring seal fails to pass the leakage rate test, isolate the leak path and, prior to repairing the leak path and repeating the leak test, record on a nonconformance report and disposition prior to final acceptance in accordance with the cognizant quality assurance program.

8.2.2.2 Helium Leakage Rate Testing the Vent Port Sealing Washer

1. The maintenance/periodic leakage rate test of the vent port plug sealing washer integrity shall be performed following the guidelines of Section A.5.4, *Evacuated Envelope – Gas Detector*, of ANSI N14.5.
2. Assemble the 1105-SD package with the two O-ring seals installed in the lower flange and the closure bolts tightened. Ensure the vent and seal test ports are installed with their associated sealing washers. Assembly information is given in Appendix 1.3.3, *Packaging General Arrangement Drawings*.
3. Verify the presence of a helium atmosphere below the vent port plug sealing washer, as specified above in Steps 3 – 8 of Section 8.2.2.1, *Helium Leakage Rate Testing the Containment O-ring Seal*. Alternatively, perform this test immediately after the containment O-ring seal test.
4. Install a clean (helium-free) port tool into the vent port.
5. Attach a helium MSLD to the port tool.
6. Evacuate the cavity above the vent port plug sealing washer until the vacuum is sufficient to operate the leak detector per the manufacturer's recommendations.
7. Perform the helium leakage rate test to the requirements of Section 8.1.4.1, *Fabrication Leakage Rate Test Acceptance Criteria*. If, after repeated attempts, the vent port plug sealing washer fails to pass the leakage rate test, isolate the leak path and, prior to repairing the leak path and repeating the leak test, record on a nonconformance report and disposition prior to final acceptance in accordance with the cognizant quality assurance program.

8.2.3 Component and Material Tests

8.2.3.1 Fasteners

All threaded components shall be visually inspected before installation for deformed or stripped threads. Damaged threaded components shall be repaired or replaced prior to further use. The threaded components to be visually inspected include the closure bolts, vent port plug, the test port plug, and the rain shield attachment bolts.

8.2.3.2 Sealing Area Routine Inspection and Repair

At the time of seal removal or replacement, containment sealing surfaces shall be visually inspected for damage that could impair the sealing capabilities of the packaging. Perform visual surface finish inspections for the base O-ring grooves, the mating sealing area on the bell, and

the surfaces that mate with the sealing washer in the vent port. Damage shall be repaired prior to further use (e.g., using emery cloth or other surface finishing techniques) to restore the sealing surfaces to the value specified on the drawings in Appendix 1.3.3, *Packaging General Arrangement Drawings*.

Upon completion of any surface finish repairs, perform a leakage rate test per Section 8.2.2, *Maintenance/Periodic Leakage Rate Tests*.

8.2.3.3 Impact Limiter

Before each use, the external impact limiter shell shall be inspected for tears or perforations and for the presence of the fire-consumable plastic plugs. The lower internal impact limiter shall be inspected for proper installation and to ensure that the 3/8-16 UNC SHCS are intact and tightened to the value specified in drawing 3021717-SAR, flag note 34. Any damage shall be repaired prior to further use.

Once per year, the upper internal impact limiter shall be inspected for proper installation and to ensure that the 3/8-16 UNC SHCS are intact and tightened to the value specified in drawing 3021717-SAR, Flag Note 34. Any damage shall be repaired prior to further use.

8.2.3.4 Seals

The containment boundary O-ring seal and the vent port sealing washer shall be replaced within the 12-month period prior to shipment or when damaged (whichever is sooner), per the size and material requirements delineated on the drawings in Appendix 1.3.3, *Packaging General Arrangement Drawings*. Following seal replacement and prior to a loaded shipment, the new seals shall be leakage rate tested to the requirements of Section 8.2.2, *Maintenance/Periodic Leakage Rate Tests*.

8.2.4 Thermal Tests

No thermal tests are necessary to ensure continued performance of the 1105-SD packaging.

8.3 Appendix

8.3.1 References

1. Title 10, Code of Federal Regulations, Part 71 (10 CFR 71), *Packaging and Transportation of Radioactive Material*, 01–01–18 Edition.
2. ANSI/AWS D1.6/D1.6M:2007, *Structural Welding Code–Stainless Steel*, American Welding Society (AWS).
3. American Society of Mechanical Engineers (ASME) Boiler and Pressure Vessel Code, Section III, *Rules for Construction of Nuclear Facility Components*, Division 1 – Subsection NB, *Class 1 Components*, and Section V, *Nondestructive Examination*, Article 2, *Radiographic Examination*, 2010 Edition.
4. American Society of Mechanical Engineers (ASME) Boiler and Pressure Vessel Code, Section III, *Rules for Construction of Nuclear Facility Components*, Division 1 – Subsection NB, *Class 1 Components*, and Section V, *Nondestructive Examination*, Article 6, *Liquid Penetrant Examination*, 2010 Edition.
5. American Society of Mechanical Engineers (ASME) Boiler and Pressure Vessel Code, Section III, *Rules for Construction of Nuclear Facility Components*, Division 1 – Subsection NF, *Supports*, and Section V, *Nondestructive Examination*, Article 6, *Liquid Penetrant Examination*, 2010 Edition.
6. American Society of Mechanical Engineers (ASME) Boiler and Pressure Vessel Code, Section III, *Rules for Construction of Nuclear Facility Components*, Division 1 – Subsection NB, *Class 1 Components*, Article NB–6220, 2010 Edition.
7. ANSI N14.5–2014, *American National Standard for Radioactive Materials – Leakage Tests on Packages for Shipment*, American National Standards Institute (ANSI), Inc.
8. EPA Method 300.0, Revision 2.2 (October 1999), *Determination of Inorganic Anions by Ion Chromatography*, U.S. Environmental Protection Agency.
9. ASTM C518–04, *Standard Test Method for Steady–State Thermal Transmission Properties by Means of the Heat Flow Meter Apparatus*, American Society for Testing and Materials (ASTM).
10. ASTM E1269, *Standard Test Method for Determining Specific Heat Capacity by Differential Scanning Calorimetry*, American Society for Testing and Materials (ASTM).
11. ASTM D2000–05, *Standard Classification System for Rubber Products in Automotive Applications*, American Society for Testing and Materials (ASTM).
12. ASTM D2240–05, *Standard Test Method for Rubber Property – Durometer Hardness*, American Society for Testing and Materials (ASTM).
13. ASTM D412–98a(2002)e1, *Standard Test Methods for Vulcanized Rubber and Thermoplastic Rubbers and Thermoplastic Elastomers – Tension*, American Society for Testing and Materials (ASTM).
14. ASTM D573–04, *Standard Test Method for Rubber – Deterioration in an Air Oven*, American Society for Testing and Materials (ASTM).

15. ASTM D395–03, *Standard Test Methods for Rubber Property – Compression Set*, American Society for Testing and Materials (ASTM).
16. ASTM D2137–94(2000), *Standard Test Methods for Rubber Property – Brittleness Point of Flexible Polymers and Coated Fabrics*, American Society for Testing and Materials (ASTM).
17. ASTM D1329–02, *Standard Test Method for Evaluating Rubber Property – Retraction at Lower Temperatures (TR Test)*, American Society for Testing and Materials (ASTM).
18. ANSI/AWS D1.2/D1.2M:2008, *Structural Welding Code–Aluminum*, American Welding Society (AWS).